



HAL
open science

Biosensors for open and closed-loop glycemia control

Emilie Puginier

► **To cite this version:**

Emilie Puginier. Biosensors for open and closed-loop glycemia control. Cellular Biology. Université de Bordeaux, 2022. English. NNT : 2022BORD0136 . tel-03689283

HAL Id: tel-03689283

<https://theses.hal.science/tel-03689283v1>

Submitted on 7 Jun 2022

HAL is a multi-disciplinary open access archive for the deposit and dissemination of scientific research documents, whether they are published or not. The documents may come from teaching and research institutions in France or abroad, or from public or private research centers.

L'archive ouverte pluridisciplinaire **HAL**, est destinée au dépôt et à la diffusion de documents scientifiques de niveau recherche, publiés ou non, émanant des établissements d'enseignement et de recherche français ou étrangers, des laboratoires publics ou privés.

THÈSE PRÉSENTÉE
POUR OBTENIR LE GRADE DE

DOCTEUR DE
L'UNIVERSITÉ DE BORDEAUX

ÉCOLE DOCTORALE : Sciences de la vie et de la santé
SPÉCIALITÉ : Biologie cellulaire et physiopathologie

Par Emilie PUGINIER PINET

**CAPTEURS BIO-ÉLECTRONIQUES POUR LE CONTRÔLE
DE LA GLYCÉMIE EN BOUCLE OUVERTE ET FERMÉE**

Sous la direction de : Jochen LANG

Soutenu le 31 Mars 2022

Membres du jury :

M. DALLE Stéphane , Directeur de Recherche, Université de Montpellier	Président
Mme. WOJTUSCISZYN Anne , Professeure associée, Université de Lausanne	Rapporteur
M. DALLE Stéphane , Directeur de Recherche, Université de Montpellier	Rapporteur
M. BENHAMOU Pierre Yves , Professeur, Université de Grenoble	Examineur
M. CHARLOT Benoit , Maître de Conférences, Université de Montpellier	Examineur
M. LANG Jochen , Professeur, Université de Bordeaux	Directeur de thèse
Mme. RENAUD Sylvie , Professeure, Université de Bordeaux	Invitée
M. RAOUX Matthieu , Maître de Conférences, Université de Bordeaux	Invité

A tous ceux qui ont contribué à ce travail.

Remerciements :

Ce travail de thèse a été réalisé au sein de l'institut de Chimie et Biologie des Membranes et Nanoobjets (CBMN, UMR CNRS 5248) dirigé par Sophie Lecomte que je souhaite remercier. Je remercie les membres de mon jury de thèse d'avoir accepté d'évaluer mon travail. J'adresse tout d'abord mes remerciements à Mme. Anne Wojtuszczyk et à M. Stéphane Dalle, pour votre temps et votre expertise en tant que rapporteurs de ma thèse. Je remercie également mes examinateurs, M. Pierre Yves Benhamou et M. Benoit Charlot. Mme Sylvie Renaud et M. Matthieu Raoux, merci d'avoir accepté de faire partie de mon jury en tant que membres invités. Merci à M. Marc Landry, d'avoir accepté de présider ce jury de thèse, c'est un honneur de vous compter parmi ce comité.

J'adresse mes sincères et chaleureux remerciements à mon directeur de thèse, Jochen. Il y a maintenant plus de trois ans, je me souviens du courriel que vous m'aviez adressé en octobre afin de me présenter le projet de thèse proposé par l'équipe. A la première lecture de celui-ci je me suis demandée si je pouvais être capable de passer des neurosciences à la physiologie des ilots, puis au grès de nos échanges je me suis dit que ce projet allait être un fabuleux challenge. Je vous remercie d'avoir eu confiance en moi pour ce projet, même lorsque j'ai pu douter. J'ai beaucoup apprécié, au fil de ces années, que vous n'ayez jamais eu peur de mes idées et de mes bricolages parfois ... extravagants, que vous m'avez toujours encouragé dans la construction de mon propre parcours. Formation à la bio impression ? Formation au développement et montage d'entreprise ? Des formations pourtant fortes éloignées de l'électrophysiologie ou de la physiologie des ilots mais pour lesquelles vous m'avez encouragée. Je vous remercie également pour la manière dont vous m'avez encadrée, vous avez toujours été disponible quand j'en ai eu besoin et vous avez toujours pris le temps de me conseiller.

Suite à votre prise de contact en Octobre 2018, je me souviens avoir effectué des recherches sur la thématique et sur l'équipe. Ce qui m'a marqué, aux travers de celles-ci, c'est la notion de groupe. Jochen, dans les différentes présentations de l'équipe sur les pages de l'Université ou de CBMN, vous mettez toujours en avant le fait que les travaux sont le fruit de la cohésion

de l'équipe et d'une force collective de travail. J'ai été très sensible à cette valorisation que vous faites de votre équipe et à l'importance de chaque collaborateur.

C'est dans cet esprit que je souhaite continuer ces remerciements et remercier maintenant de manière générale le Groupe Lang. Merci à l'équipe qui a su m'accueillir, apprivoiser ma timidité et me transmettre le meilleur de leurs connaissances et de leur rigueur de travail. Je vous serai toujours reconnaissante de l'opportunité que vous m'avez offerte en m'accueillant parmi vous et du soutien que vous m'avez apporté dans l'exaltation des beaux résultats mais aussi dans les passages à vide où rien ne marche.

Il faut maintenant prendre le temps de remercier chacun de vous de manière particulière, car sans vous, il n'y aurait pas ce manuscrit aujourd'hui. Je ne fais pas de hiérarchie dans les remerciements qui suivent, ils viennent au gré de la plume.

Un immense merci à Julien, ou plutôt devrais-je dire, à Magic Julien, comme nous l'avons récemment renommé avec les doctorantes. Tu es TOUJOURS disponible pour nous aider à faire avancer les projets. Toujours prêt à donner un coup de main et à prendre le temps de nous expliquer même si ça fait trois fois que l'on te pose la même question. Certes parfois tu t'énerves un peu ... mais c'est toujours passager et en plus maintenant tu nous préviens quand tu es peut-être un peu moins bien luné. Derrière ce caractère de Bélier, tu es donc le meilleur soutien que l'on puisse espérer pour avancer techniquement et la manière dont tu nous formes à la culture cellulaire reste gravée. D'ailleurs je ne te remercie pas pour les nombreux tocs que j'ai pu attraper, impossible de me concentrer sous le PSM si le DASRI à pipette n'a pas toutes les pipettes parfaitement alignées pour optimiser l'espace. Je te remercie pour ces trois années à travailler avec toi.

Matthieu, après les remerciements très formels adressés à l'invité du jury que tu es, je tiens à t'adresser également mes chaleureux remerciements pour tous les conseils et discussions que nous avons pu échanger durant cette thèse. En plus de nous apporter ton expertise scientifique, tu apportes beaucoup de convivialité au sein de l'équipe et les échanges sont toujours positifs et constructifs. Par contre, je te soupçonne de vouloir créer une cohorte de diabétiques au sein de l'équipe avec les nombreux Kouign-amann que tu amènes ... quand je regarde la recette de cette chose je vois du beurre, du sucre, du beurre, du sucre, non ce n'est

pas possible ! Maintenant qu'il n'y a plus de bretons dans l'équipe je pense que l'on peut passer au régime crétois et ainsi éviter de se poser des CGMs. Plus sérieusement je ne sais pas quoi dire d'autre sans que ce soit interminable, donc merci infiniment.

Alexandra, merci également pour tout. Tu es un élément clé du bon fonctionnement du groupe. Ton organisation nous permet à tous de fonctionner de manière optimale sur nos projets. Je tenais à te présenter mes excuses pour mon écriture mi tordue, mi hiéroglyphique sur le tableau des commandes, je pense que je t'ai mené la vie dure à devoir déchiffrer mes lignes et à faire des commandes souvent hors marché comme tout le matériel d'impression 3D. Merci pour ces trois ans et ton aide précieuse !

Pier, merci pour ta présence bienveillante dans l'équipe. Même si nos projets sont très éloignés j'ai toujours apprécié ton intérêt pour l'avancée du projet et tes suggestions notamment pour le projet Connexine 36. Ton expertise en immunofluorescence et tes nombreux conseils ont été un véritable plus pour gagner la guerre contre les anticorps anti Cx36 qui nous menaient la vie dure dans l'élaboration de notre protocole. Merci pour tout.

Après les remerciements adressés à Jochen et aux 4 fantastiques de l'équipe, je souhaiterai maintenant adresser mes remerciements aux doctorantes et docteurs avec qui j'ai eu la chance de travailler.

Par ordre chronologique, je tiens tout d'abord à remercier les M&Ms, plus connues sous le nom de Manon et Myriam, docteurs en biologie cellulaire et physiopathologie de leur état. Merci de m'avoir accueillie et intégrée dans l'équipe. Manon, merci pour tes connaissances sur l'art des MEAs et ta redoutable rigueur, je pense que j'avais plus peur de toi que de Julien si jamais j'oubliais de ranger un instrument en post isolation des ilots. Nous avons eu beaucoup de manip extrêmes en commun et cela soude, merci pour ton soutien et tes conseils. Myriam, grand maître des OECTs, merci pour ta bonne humeur et ta gentillesse cela a été également un plaisir de travailler avec toi. Vous noterez toutes les deux que je ne m'éternise pas... Ce qui se passe dans l'open space restera dans l'open space !

Aux nouvelles doctorantes, les Mariezzz (à mon avis il y a quand même un bais de recrutement avec la première lettre du prénom, je me demande comment j'ai atterri là), également un immense merci. Merci pour les bons moments passés ensemble même si je ne suis pas beaucoup sortie ces derniers mois, les manips en communs et les afterworks ont vraiment été très agréables. Merci pour votre gentillesse et bienveillance.

Karen, je ne pourrais pas formuler ces remerciements sans t'inclure également. Merci tout d'abord pour tes cahiers de manip dont j'ai hérité quand je suis arrivée pour le projet sphéroïde. Ils m'ont grandement aidée à me familiariser avec le projet, c'est par eux que j'ai commencé à te connaître un peu. Comme tu es une familière de l'équipe j'ai pu te rencontrer en personne lors des stages que tu es venue effectuer lors du master et ainsi mieux te connaître. Merci pour ta gentillesse, ta grande disponibilité, ton efficacité et tes bons conseils. Je te souhaite le meilleur dans ta nouvelle vie en Suisse et aurai grand plaisir, si jamais l'occasion se présente, à retravailler avec toi.

Après avoir fait le tour de notre équipe, je tiens à remercier chaleureusement l'équipe de Sylvie Renaud à l'IMS sans qui les projets et la vie scientifique de notre groupe ne serait pas la même. Ce qui m'a également attirée lorsque j'ai accepté mon projet de thèse est l'aspect interdisciplinaire de celui-ci. L'interaction directe avec l'équipe de bioélectronique entraîne une richesse immense dans les échanges et un cadre de travail particulièrement stimulant.

Je commence donc cette deuxième partie de remerciement en commençant par vous remercier Sylvie, là encore ces remerciements peuvent sembler faire doublon, comme pour Matthieu, mais ils sont pourtant essentiels. Je vous remercie pour les échanges que nous avons eus, ceux-ci ont toujours été bienveillants et très instructifs, aussi bien sur le plan professionnel qu'humain. J'ai toujours été très sensible également à la manière dont vous valorisez les travaux des étudiants lors des réunions ANR. Cela permet de s'épanouir et de prendre confiance au grès des réunions. Merci beaucoup pour tout cela.

Antoine, je pense qu'il y aurait trop de choses à écrire dans les remerciements. Que dire ? Par où commencer ? Tu as subi toutes mes caractérisations de circuits microfluidiques, simulé toutes les géométries de puce les plus farfelues, regardé des vidéos de cages thoraciques de

rat en boucle pour en extraire la fréquence respiratoire, bref tu as été essentiel à la réussite de ce projet. Ta gentillesse, ton humour, ta patience et ta curiosité scientifique ont été un plaisir lors des manip interminables, donnant souvent lieu à des réflexions existentielles et philosophiques devant l'incubateur qui nous a fait tant de misères. Je te remercie pour tout et aurai plaisir à retravailler avec toi (je garde en tête de te faire une proposition en cas de développement de start up...).

Florence, Annabelle, un immense merci à toutes les deux pour ces deux ans de manip que nous avons faits ensemble. Cela serait un doux euphémisme de dire que ces expériences ont été ardues. Des effluves d'isofluranes woodstockiennes au compresseur qui explose, je n'oublierai jamais mes jeudis à l'animalerie à mettre au point ces expériences nouvelles. Merci pour les soins apportés aux animaux, pour votre disponibilité à toute épreuve et pour votre soutien.

Je remercie enfin les collaborateurs avec qui je n'ai pas travaillé directement mais qui ont participé au projet, Yannick, Gilles, Loïc et je remercie également au sein de l'IMS l'équipe ARIA qui a également contribué à la richesse des échanges lors des réunions ANR.

Arrive maintenant la partie la plus délicate des remerciements, la plus difficile à mettre sur papier.

Après ce passage professionnel, je ne saurais faire l'impasse sur les gens qui m'accompagnent depuis longtemps, dans tous les moments de la vie.

Je remercie tout d'abord ma famille, en tant que groupe uni, qui m'a soutenu et aidé à avancer dans les bons les mauvais moments. Je remercie également mes beaux-parents qui m'ont également beaucoup soutenu depuis maintenant 7 ans.

Même s'ils ne sont plus là aujourd'hui, je tenais, par le biais de ces quelques mots à adresser des remerciements à mes grands-parents. Cela fait maintenant respectivement 6 ans et 5 ans que vous êtes partis. Vous me manquez doucement, silencieusement, tous les jours. Ce travail scientifique ne serait pas là aujourd'hui si vous n'aviez pas eu un rôle aussi important dans ma

vie. Papi, à toi le scientifique de la famille, un million de fois merci, pour tous les moments passés derrière le microscope et la binoculaire à observer microorganismes et minéraux, pour m'avoir appris à monter une lame mince alors que d'autres faisaient de la pâte à modeler. Même après ces années qui passent, le réflexe de composer votre numéro lors de la réussite d'une expérience ou même de l'explosion du fameux compresseur ne m'a pas quittée. Un million de fois merci pour ce que vous m'avez apporté et j'espère que vous auriez été fier de ce travail.

Je remercie mes parents pour tout leur amour qui m'a permis d'arriver là aujourd'hui. Vous m'avez toujours soutenue et encouragée dans mon travail mais aussi dans ma vie. Vous n'avez jamais douté de moi et vous avez toujours été présents. Je suis très fière de vous et j'espère que vous serez également fier de ce travail. Vous savez tout ce que je pense de vous et toute ma reconnaissance, je ne m'étalerai donc pas d'avantage, restons pudiques !

Enfin, the last but not the least, Clément. Toi qui auras le plus vécu cette thèse, mon soutien le plus précieux. Je te remercie infiniment pour ton amour, ta patience (beaucoup de patience), ton calme (beaucoup de calme) et tout ce que tu m'apportes au quotidien. Je te remercie également pour ta créativité, ton esprit scientifique, ta curiosité, notre atelier/labo clandestin à la maison, bref pour tout ce que tu es. Cela fait 7 ans que tu es à mes côtés, que tu m'accompagnes et me soutiens. Je ne serais pas là aujourd'hui si tu ne m'avais pas apporté autant d'amour. Pour tous les moments merveilleux passés et pour ceux à venir, je t'aime. Cette thèse c'est notre thèse à tous les deux...bon et peut être un peu au chat !

Table of contents

Introduction.....	16
1 Physiology and pathophysiology of glucose regulation.....	18
1.1 Glucose homeostasis.....	18
Macronutrient repartition for a healthy diet:.....	18
Glucose metabolism:.....	19
Main glucose metabolic pathways:.....	19
Specificity of glucose metabolism in β cells of pancreatic islets:.....	21
Glucose storage:.....	22
Glycemia, uses and distribution of glucose by the body:.....	23
Postprandial period:.....	24
Interprandial or post-absorptive period:.....	25
Physiological fasting at night:.....	26
1.2 Organs involved in glucose homeostasis.....	27
The nervous system:.....	29
1.3 Regulation of glucose maintenance: Sensors and Actuators.....	32
Actuators of glucose maintenance: Insulin and glucagon:.....	34
1.4 The different phases of food intake:.....	35
Cephalic phase.....	35
Gastro-enteric phase.....	36
Islet phase.....	36
2. The islet of Langerhans, the main glucose sensor.....	38
2.1: The endocrine pancreas.....	38
2.2: Cellular architecture of the islets of Langerhans.....	40
β -cells.....	41
The insulin-secreting β -cell: an electrogenic cell.....	41
Resting potential and initiation of the depolarization.....	42
Action potentials.....	43
Membrane potential oscillations and continuous action potential activity.....	45
Ion channels in the β -cell responsible for stimulus-secretion coupling.....	46
K_{ATP} channel.....	46
Voltage-dependent channels.....	47
Calcium channels.....	47
Sodium channels.....	48

Potassium channels.....	49
Coupling between B cells: role of Cx 36.....	49
Multicellular signals: slow potentials.....	51
Encoding nutrient concentration into an electrical signal.....	53
Stimulus and secretion coupling.....	54
α cell.....	54
δ-cell.....	55
γ cell.....	56
ε cell.....	57
2.3 interaction between the different cell types:.....	58
2.4 Innervation:.....	59
2.5 Vascularization:.....	59
3 Diabetes Mellitus.....	60
3.1 The different types of diabetes:.....	61
3.2 History of type 1 diabetes:.....	62
3.3 Type I diabetes: a complex autoimmune disease:.....	64
3.4 Complications of type 1 Diabetes:.....	68
3.5 The different therapies in management of T1DM:.....	69
Continuous Glucose Monitoring:.....	70
Islet/pancreas transplants:.....	71
New therapies of T1DM:.....	72
Cellular engineering:.....	73
Artificial Pancreas:.....	74
4 Methods of functional investigation of islets.....	76
4.1 Optical means for the study of islets.....	76
4.2 Techniques for studying the secretory function of islets:.....	77
4.3 Methods for electrophysiological studies of islets.....	78
Intracellular electrophysiology:.....	79
Sharp micro-electrode.....	79
Patch clamp.....	79
Extracellular electrophysiology:.....	81
Multi electrodes array.....	81
OECTs.....	83
Conclusion.....	85
5 From CGM to a new islet-based biosensor.....	86
5.1 Analysis of the CGM concept: Strengths and weaknesses.....	86

General principle of CGM:.....	86
The development of CGMs.....	88
Weaknesses of CGM systems.....	91
5.2 Non-invasive glucomonitoring	92
5.3 A new islets-based biosensor:.....	94
Where to measure glucose?.....	95
How to measure glucose?	98
5.4 Microfluidics: the flow management solution for the islets on chip biosensor.....	103
Organ-On-Chip (OOC):.....	105
Islets-on-chip:	106
Production of the chip:.....	109
5.5 Sensor, which biological substrate to use?	112
Rodent cell lines	112
Human cell lines	113
Limitations of stem cells and cell lines	114
Studies and Manuscripts	117
Biological substrate characterisation :Manuscript n°1	118
Development of an islets on chip microfluidic device : Manuscript n°2.....	142
Proof of concept of the islet-based biosensor in rodents: Manuscript n°3	167
Evolution and development of microfluidics during the thesis	194
Validation of a homemade acquisition system SYAM: Manuscript n°4.....	207
Design of a simple microfluidic chip adapted to OECTs: Manuscript n°5	222
Acquisition of biological data for in silico simulation: Manuscript n°6.....	253
Conclusion and perspectives:.....	284
Oral presentations:.....	291
Previous works:	291
Annexes	293
Annexe 1: Table 1	294
Annexe 2: table 2.....	295
Annexe 3: table 3.....	296
References:.....	298

Introduction

Introduction

Diabetes is a serious, debilitating and currently incurable disease with a significant psychological burden and societal cost. Type 1 diabetes is caused by the destruction of the β -cells of the pancreas resulting in absolute insulin deficiency. It accounts for 5-10% of the estimated 443 million cases of diabetes worldwide, and numbers are expected to increase to 700 million by 2045 (« IDF Atlas 9th Edition and Other Resources » s. d.). In the treatment of diabetes mellitus, continuous glucose monitoring (CGM) systems, linked to insulin delivery, provides a major advance (Brown et al. 2019)

CGMs measure subcutaneous glucose via electrochemical electrodes and use algorithms to predict insulin dosing (Kovatchev 2019). Although CGMs represent a major breakthrough, current CGMs are biased by their ability to capture only glucose, but no other nutrients such as lipids and amino acids. In addition, there are limitations in the algorithms used, especially in the face of unexpected events such as snacking or physical activity. For these reasons, CGMs alone cannot sufficiently control insulin delivery, as they require patient intervention for calibration of the CGM, fine-tuning of pump settings or carbohydrates counting and adaptation to physical activity.

In contrast to CGMs, the pancreatic islets are the endogenous sensors that have been optimally formed over 0.5 billion years of evolution (Falkmer 1979; Youson et Al-Mahrouki 1999). They integrate at each moment nutritional information but also the physiological situation of the whole organism via hormonal regulations (incretins, adrenalin etc.)(Rorsman and Huisling 2018) and also peripheral nervous system. Islets possess endogenous algorithms that encode physiologically essential kinetics such as biphasic insulin secretion for optimal insulin delivery or glucose hysteresis protecting against hypoglycaemia (Lebreton et al. 2015; Keenan et al. 2012), a potentially lethal risk poorly accounted for in CGM. Moreover, islet β -cell regulation is also influenced by the other cell types in islets, such as α , δ or γ (Noguchi et Huisling 2019), and thus represents a fare more complex and sophisticated nutrient sensor than CGMs.

Islet β -cells are excitable cells (Rorsman and Ashcroft 2018a) and their electrical behaviour integrates signals from nutrients and different hormones. Complex sequential activations and inactivations of ion channels on the surface of the plasma membrane leads to ionic fluxes responsible for the electrical activity of β -cells. In collaboration with the IMS group (S Renaud,

UMR 5218, Bordeaux) the team has developed the real-time detection, analysis and decoding of their specific electrical signature using microelectrode arrays (MEAs) (Pirog and al. 2018; Perrier and al. 2018). The group validated, in an Food and Drug Administration recognised in silico model of diabetic patients (Dalla Man et al. 2007) , that these signals could optimally drive an insulin pump to regulate blood glucose in 24h realistic scenarii (Olcomendy et al. 2020).

The aim of my thesis is to develop a therapeutic device, the Dia^βSENSOR (Fig. 1: Biosensor scheme), using the natural sensors of the human body, namely a few islets of exogenous source, in a bioelectronic module analysing in real time their electrical signals.

To address this problematic, I worked on 3 essential points which will be developed in this manuscript in the form of various studies:

First, the development of the most suitable biological substrate to serve as a sensor in the device, second the development of a microfluidic and micro-osmotic system allowing the maintenance of the biological material (a few islets) of the sensor in a small dead volume during few days, and finally the establishment of the proof of concept of the open loop in animals and in humans.

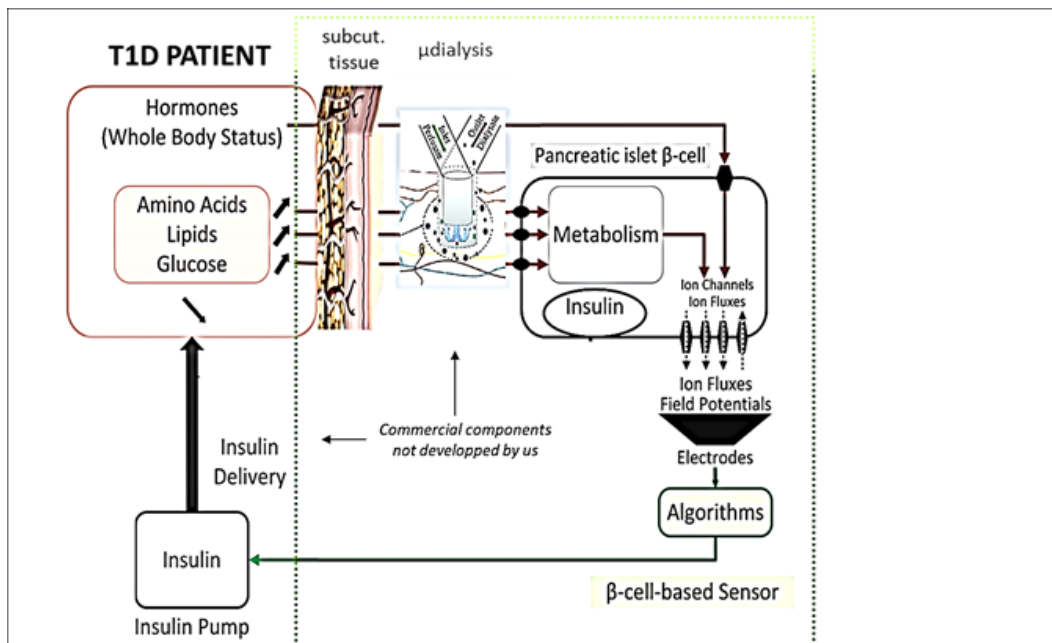


Figure 1: Scheme of the islet-based biosensor. The electrochemical electrodes used in current CGMs respond only to glucose, whereas the islets of Langerhans in a biosensor detect other nutrients in addition to glucose and hormonal variations (e.g. incretins, adrenaline) that better reflect the patient's actual insulin requirement. The native electrical response of β -cells (field potentials related to ionic flows) is then detected by extracellular electrodes. Subsequently, processing algorithms are used to control the delivery of the required amount of insulin via the insulin pump. Adapted from Renaud et al., 2014.

1 Physiology and pathophysiology of glucose regulation.

1.1 Glucose homeostasis

Macronutrient repartition for a healthy diet:

Cells need energy for function and this energy is supplied to the body through food. Nutrients, once digested, are transported to all the cells by the bloodstream to be used either as metabolic source of energy, or as anabolic material (for protein synthesis or membrane renewal, for example), or are stored for later use. Each macronutrient has the capacity to produce a certain amount of energy in the form of ATP (adenosine triphosphate) synthesis or other high-energy storage molecules. A healthy diet is one in which macronutrients and micronutrients are consumed in appropriate proportions to support physiological needs without excess intake (Stipanuk et Caudill 2018).

Diets around the world have evolved over time. Two characteristics have changed considerably: the quantities consumed and the contribution of the different macronutrients (carbohydrates, lipids and proteins) to the total calorie intake. This has occurred in all developed countries at different rates linked to the timing and vagaries of economic growth (Cépède et Langellé 1964). The quantitative satisfaction of needs was sought first and foremost through the consumption of the cheapest foods such as cereals and tubers, which were gradually supplemented by more expensive foods such as fats, sugar, then meat, as the standard of living rises. These more expensive foods replace the formers as soon as overall satiety is reached, thus accelerating the evolution of the structure of the food ration.

Nowadays, according to current Food and Agriculture Organization (FAO) recommendations, a balanced diet consists of: (i) 40 to 55% of calories (kcal) in the form of carbohydrates (previously 50 to 55%); (ii) 35 to 40 % of calories (kcal) in the form of lipids (previously 30 to 35 %), i.e. fats; (iii) 10 to 20 % of calories (kcal) in the form of proteins (replaces the previous 11 to 15 %), whether animal or vegetable (Cena et Calder 2020).

Glucose metabolism:

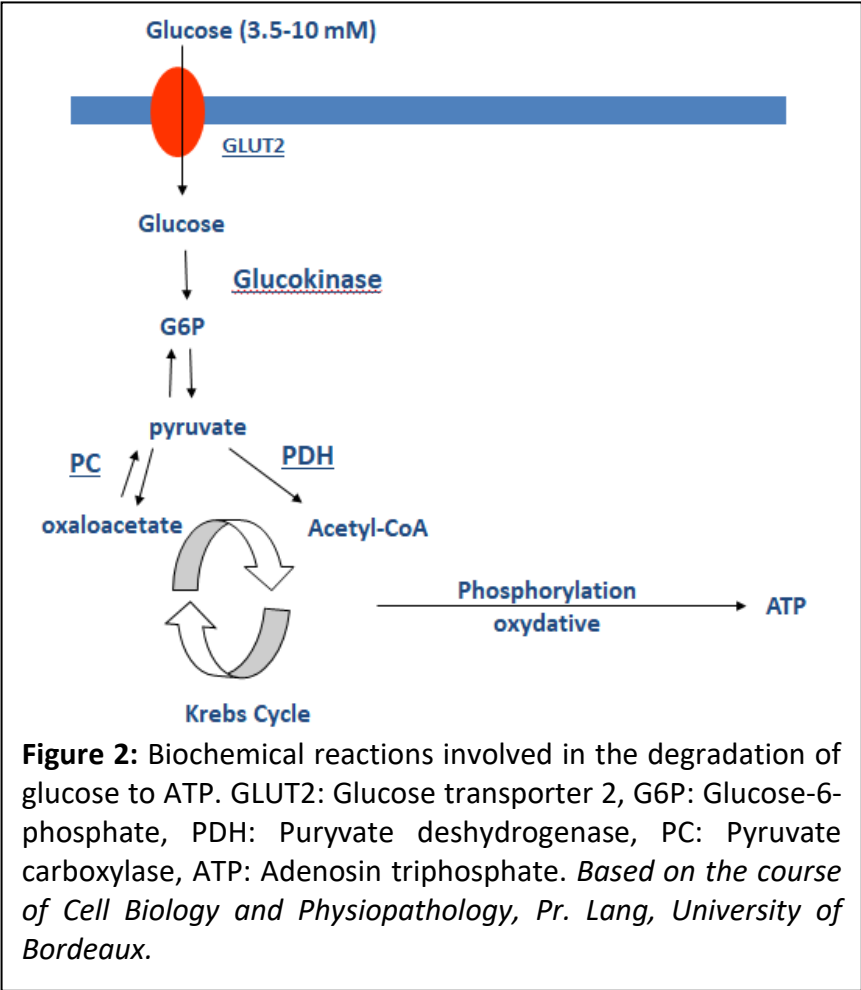
Carbohydrates, proteins and lipids arrive in the digestive tract and are cleaved into their constituents, sugars, amino acids and fatty acids. Glucose as a main source of calories is a simple carbohydrate that can be metabolized by almost all known organisms, either anaerobically by fermentation reactions, or aerobically by involving glycolysis, the Krebs cycle and finally oxidative respiration in the mitochondria. Some organs, such as the brain and kidneys, use glucose (along with ketone bodies) almost exclusively as an energy source. Therefore, the concentration of glucose in the blood must be kept constant in order to guarantee the energy supply of all organs and thus their proper functioning (Wémeau 2014). The catabolism of glucose is simpler and faster than that of other nutrients, so it is the basic energy unit for most living entities (Randle 1964). Glucose passes into the circulation to the liver cells or hepatocytes and to muscles, where it is stored. It can also be used directly by the body's cells in need of energy (Berg et al. 2002). In fact, glucose is broken down in the cytosol and then in the mitochondria in the presence of oxygen into CO₂ and H₂O to generate ATP and other energy rich molecules. If too much sugar is taken in, the liver will be saturated, forcing the body to metabolize sugars to fat and store it in the adipose tissue and, depending on the overload, also in most other tissues. About 20-30% of ingested glucose is metabolised in the liver (Adeva-Andany et al. 2016). Later, when the body needs them again for energy extraction, the liver will either release sugars from glycogen or providing glucose from other molecules and metabolic intermediates, a process termed neoglucogenesis.

Main glucose metabolic pathways:

All cells express specific glucose transporters on their surface for facilitated or for sodium-linked glucose transport (Navale et Paranjape 2016). The various glucose transporters that allow for facilitated diffusion constitute the GLUT (glucose transporter) family. Their common structure is characterised by the presence of 12 transmembrane segments of a single polypeptide chain of about 500 residues. Depending on the function of each cell, each type of transporter has varying affinities for glucose and the expression of these isoforms has a certain tissue specificity. There are ubiquitous isoforms (GLUT 1 and 3), i.e. present in all tissues, and specific isoforms (GLUT 2 and 4): GLUT1 and GLUT3, with low affinity for glucose ($K_m = 1 \text{ mM}$),

on the surface of neurons and red blood cells, which consistently take up glucose throughout the fasting and postprandial blood glucose range. In mice, the β -cell expresses the glucose transporter Glut2, which has a low affinity for glucose but a high transport capacity (Thorens et al. 2015) allowing a rapid balance of glucose between the intra- and extracellular environment. The human β -cell, on the other hand, mainly expresses the glucose transporters GLUT1 and GLUT3 (Berger et Zdzieblo 2020). They possess a higher affinity for glucose compared to Glut2 (McCulloch et al. 2011) which may partly explain why insulin secretion is triggered at lower glucose concentrations in humans (3 mM) than in mice (6 mM) (Rodriguez-Diaz et al. 2018). Whether in human or rodent β -cells, glucose uptake is not a limiting step for glucose metabolism (Lenzen 2014). Finally, GLUT4, with a low K_m for glucose (5 mM), is subject to regulation by insulin and is therefore found in so-called insulin-sensitive cells such as skeletal muscle and adipose tissue (Thorens et Mueckler 2010).

Carbohydrate catabolism represents the breakdown of glucose molecules to form energy-rich molecules. Glycolysis is the first chain of events in carbohydrate catabolism and is carried out in the cytosol by soluble enzymes also in anaerobic conditions. Its function is the synthesis of energy-rich molecules and the formation of pyruvate, which has several uses. Glycolysis consists of ten steps; however it can be summarised in three main parts: Activation of glucose with energy consumption, formation



of glyceraldehyde and finally synthesis of pyruvate and formation of energy-rich molecules providing finally 6 molecules of ATP/molecule of glucose

Subsequent metabolism of pyruvate in the mitochondria will result in approximately 36 mols of ATP/mol of glucose.

Specificity of glucose metabolism in β cells of pancreatic islets:

Glucose metabolism in the β -cell is particular and different from other cells, giving it unique properties as a direct sensor of glucose levels and the ability to adjust blood glucose levels through its insulin secretion (Nolan et Prentki 2008). Pancreatic β -cells have to respond to rising blood glucose concentration by increasing oxidative metabolism, leading to an increased ATP/ADP ratio in the cytosol with a subsequent action on ATP-sensitive potassium channels, membrane depolarisation, opening of voltage sensitive calcium channels and secretion of insulin. The mechanisms of glucose sensing in the pancreatic β -cell is the result of the coupling of cytoplasmic and mitochondrial processes (Fridlyand et Philipson 2011). One may say that such a sensor has to count each carbon to exactly sense the fuel level. β -cells are endowed with unique metabolic properties that adapt to ambient glucose levels and thus control insulin secretion (Ainscow et Brand 1999) as we will detailed below.

Subsequent to glucose entry into the β -cell via GLUT transporters, glucose is phosphorylated by a hexokinase isoenzyme, glucokinase, which is also present in liver cells. Unlike hexokinase, glucokinase is not inhibited by the product of its reaction, glucose-6-phosphate (G6P), and its affinity for glucose is high ($K_m = 4$ to 8 mM, compared with a K_m of 1 mM for hexokinase). It can therefore metabolise glucose under all circumstances in direct relation to the ambient glucose level and accurately determine the appropriate insulin secretion. GLUT and glucokinase together contribute to glucose metabolism in the β -cell in a manner that is directly dependent on increasing glucose concentration (Matschinsky et Wilson 2019).

Biochemical mechanisms couple an intracellular glucose concentration increase to insulin secretion in pancreatic β -cells. Increased glucose levels lead to an increase in the glycolytic flux and an acceleration of mitochondrial NADH production. Oxidation of NADH increases mitochondrial membrane potential and ATP synthesis, decreasing ADP concentration. The

ensuing increase in cytoplasmic ATP/ADP ratio causes closure of ATP-sensitive K^+ (K_{ATP}) channels resulting in depolarization of the β -cell plasma membrane. This increase in β -cell membrane potential opens voltage-dependent Ca^{2+} channels (VDCCs) and allows Ca^{2+} influx, raising the intracellular free calcium concentration, a key signal in the initiation of insulin secretion along with release of Ca^{2+} from intracellular stores (Brissova et Powers 2008). In the β -cell, little glucose is metabolised to lactate as lactate dehydrogenase and the lactate monocarboxylate transporter (carrying lactate produced in muscle fibres during exercise) are very poorly expressed (Sekine et al. 1994). This absence is necessary to prevent insulin secretion during exercise: indeed, expression of the lactate monocarboxylate transporter in human β -cells will lead to hypoglycaemia during exercise (Ishihara et al. 1999) .

In conclusion, at the level of the β -cell, the complete oxidation of glucose by glycolysis and by the Krebs cycle to produce ATP allows for the transmission of accurate information about the body's need for insulin. This ensures that the rate of insulin secretion corresponds to the level of ambient glucose levels (Berger et Zdziebło 2020). Although we have discussed here solely sugar metabolism, the same applies for lipids as well as amino acids. The latter may lead to depolarisation through metabolism and corresponding changes in ATP/ADP ratios or via changes in ion concentrations through sodium cotransport. Note that in the course of the metabolism secretion coupling factors other than ATP may play a role, such as glutamate, malonate and others but in general their role is less well understood (Seino et al. 2017). Moreover, increased ATP/ADP ratios are not only necessary for the closure of K_{ATP} channels, but also for several energy consuming steps during secretion (exocytosis) itself (Hastoy et al. 2017).

Glucose storage:

Glucose itself is not a form of energy reserve, but it can be stored in a highly branched structure as glycogen, an osmotically far more economic form, mainly in liver, and muscles but also islets. Glucose from these stores is used for systemic purposes (from the liver) or locally (muscle) in the post-absorptive phase or at the beginning of fasting. In islets, glycogen is primarily localized in granulated β cells; degranulated β cells also contain glycogen, though in smaller amounts (Graf et Klessen 1981). In the liver, glucose is taken up via GLUT2 and

phosphorylated to glucose-6-phosphate (G6P) by a glucokinase, before being used for glycogen synthesis by isomerisation under the action of a glycogen synthase. The stimulation of glycogen synthase by insulin and other polypeptide growth factors results in the dephosphorylation and activation of glycogen synthase (Chan et al. 1987; Yamamoto-Honda et al. 1995) followed by glycogen synthesis, which occurs in the postprandial phase (Corssmit and al.2001) .

Hypoglycaemia initiates hepatic glycogenolysis. After a cascade of debranching enzymatic reactions (glycogen phosphorylase and phosphoglucomutase), the hydrolysis of G6P produces “free” glucose which passes into the extracellular space via GLUT2 to maintain glucose homeostasis. Glycogenesis and glycogenolysis are tightly regulated by allosteric control and covalent modifications. The latter are under hormonal control: insulin stimulates glycogenosynthesis, glucagon and adrenaline stimulate glycogenolysis (Petersen et al. 1996). Lipogenesis from glucose is another storage modeBut hepatic lipogenesis occurs mainly in the case of a high carbohydrate diet and/or hyperinsulinism (Sanders et Griffin 2016) . It results from the oxidative decarboxylation of pyruvate which produces, like certain amino acids and fatty acids subject to beta-oxidation, acetyl-CoA which is a substrate for the synthesis of palmitic acid and other fatty acids.

Glycemia, uses and distribution of glucose by the body:

The supply of glucose to the cells is directly dependent on its circulating concentration as we have seen above. Regardless of nutritional status, the level of glucose in the bloodstream, known as glycaemia, is maintained within narrow limits of 4 to 6 mmol/L or 72 to 108 mg/dL in human in the fasting state (Mathew et Tadi 2021). This narrow concentration range defines a very important concept, called normoglycemia, and is the result of the balance between energy expenditure and intake. This also implies that a human being has only about 3 to 5 g of glucose in the bloodstream at any given moment, which corresponds just to about a third or the half of a French horn. As already basal activity requires glucose, and even more physical activity, a considerable flux of glucose is required to maintain and replenish these narrow levels.

In fasting situation, below 4 mmol/L a human being is in hypoglycaemia, above 6 mmol/L in hyperglycaemia. Hypoglycaemia presents an immediate and potentially lethal danger for the subject (Bastos 1989). Hyperglycaemia, on the other hand, will present a danger if it is chronic, as in the case of diabetes. Indeed, prolonged hyperglycaemia favours glycation of proteins, lipids and nucleic acids, i.e. non-enzymatic glycosylations via the ketose forms of glucose (Sebeková et Somoza 2007). Moreover, increased glucose levels lead to a change in gene expression in glucose-sensitive tissues (Ottooson-Laakso et al. 2017). In a future chapter we will discuss the consequences of chronic hyperglycaemia in type 1 diabetes.

The glucose requirement and availability are not constant as every day we have to deal with various physiological states, linked to our level of physical activity, our stress situation and even simply to the time of day. In fact, we alternate between periods of fasting and periods of eating (Berg et al. 2002). To respond to the different situations, a quartet of four hormones will come into play. Two of these hormones are synthesized in the islets of Langerhans. These are insulin, the body's only hypoglycaemic hormone, secreted by the β -cells, and glucagon, an antagonistic hyperglycaemic hormone secreted by the α -cells. Two other hyperglycaemic hormones also have a key role in maintaining glucose homeostasis, that is cortisol and adrenaline. Glucocorticoids preserve plasma glucose during stress by generally counteracting insulin action (Kuo et al. 2015) and adrenalin plays a major role in the counterregulatory response to hypoglycaemia, often blunted in T1DM (Verberne et al. 2016). We can examine different cases encountered in the course of a day or a lifetime to illustrate the functioning of the different actors involved in maintaining normoglycemia.

Postprandial period:

During the postprandial period, which is characterised by the arrival of considerable amounts of nutrients in the blood stream, insulin rises. Glucagon also increases shortly, probably linked to the handling of amino acids, before decreasing. The increase in insulin and decrease in glucagon allows nutrients to be stored in the form of glycogen and triglycerides. Overall, about 50% of ingested glucose is stored, which limits postprandial hyperglycaemia. The combination of inhibition of endogenous glucose production and stimulation of plasma glucose entry, utilisation and storage limits excursions in blood glucose levels (Wémeau 2014).

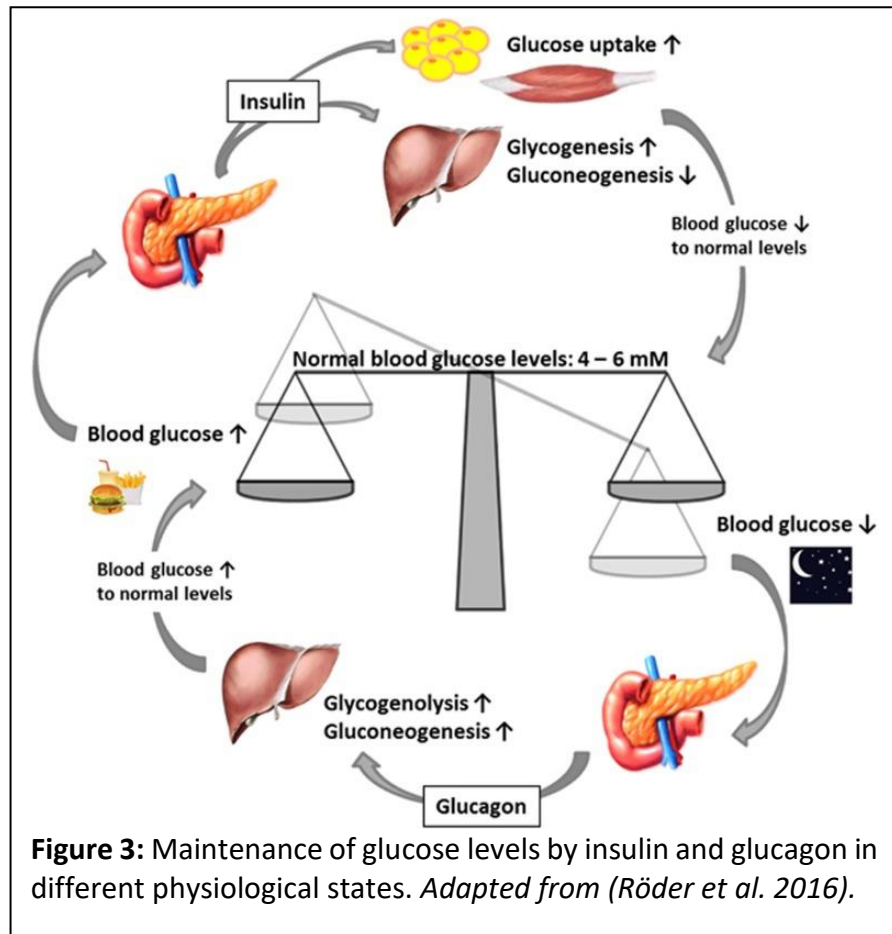
Interprandial or post-absorptive period:

This period starts as soon as the digestion of dinner is completed in the late evening. It is characterised by a decrease in the insulin/glucagon ratio where increased glucagon secretion will allow us to cope with the decrease in glucose levels (Berg et al. 2002). Glucagon signals the fasting state. Its main target is the liver, to trigger glycogenolysis and de novo glucose synthesis to maintain blood glucose levels. Glycogen synthesis and glycolysis are inhibited, as well as fatty acid synthesis. The liver can also use fatty acids from adipose tissue for its own metabolism if it needs an energy source, as can the muscle. Glucose released by the liver from glycogen will be able to reach the muscle and fat tissues, in order to respond to the decrease in insulin levels, even if they are not very energy consuming at this time. Towards the end of the night, still in order to maintain normoglycemia, the fatty acids previously stored will be used as energy donors and cortisol will be secreted to stimulate neoglucogenesis. Proteins, at least a fraction of them, will release glucogenic amino acids in order to have a possibility of glucose formation by pyruvate or oxaloacetate (Röder et al. 2016).

Physiological fasting at night:

During night-time fasting, glucose homeostasis is ensured by hepatic glucose production through glycogen breakdown and, to a lesser degree, by gluconeogenesis. The glucose produced is used primarily by the glucose dependant organs (brain) (Maughan, Fallah, et Coyle 2010). Peripheral glucose utilisation is reduced in proportion to the decrease in insulin which reduces the synthesis

and translocation of GLUT4, the only hormone-regulated GLUT that is mostly expressed in muscle and adipocytes. This results in a reduced capacity for glucose utilisation by muscles and adipose tissue. The increase in fatty acids levels induces the production of ketone bodies by the liver, which can be used by the brain,



results in a decrease of insulin sensitivity of target tissues and therefore a reduction in glucose storage (Boujard, Anselme, et Cullin 2015). As fasting continues, gluconeogenesis intensifies to compensate for the loss of glycogen reserves. Ketogenesis from Acetyl-CoA, due to the decrease in the insulin/glucagon ratio, provides a substitute for glucose. The substrates of gluconeogenesis come from lipolysis (glycerol), lactates and muscular amino acids. The substrates of ketogenesis are above all beta-oxidised fatty acids from lipolysis (Berg et al. 2002).

1.2 Organs involved in glucose homeostasis

As glucose homeostasis is a balance between glucose intake and expenditure in the body, all organs are to some extent involved in its regulation due to their own energy consumption. For example, central nervous system and skeletal muscles are the biggest consumers of glucose. However, certain organs play a more important role in maintaining homeostasis by playing a very specific regulatory role.

The pancreas:

The pancreas has two distinct parts: the exocrine pancreas which intervenes in the digestion process by releasing pancreatic juices into the duodenum, and the endocrine pancreas which produces and secretes two essential hormones directly involved in glycaemia control.

Insulin is the only hypoglycaemic hormone in the body. It is synthesised, stored and then secreted by the β cells of the pancreatic islets when blood sugar levels rise (Magnan et Ktorza 2005). Released into the bloodstream, insulin acts at its targets to lower blood sugar levels: overall, it inhibits glucose production (whether glycogenolysis or neoglucogenesis) in the liver, muscles and kidneys, and stimulates glucose uptake in muscles and adipose tissue, as well as glycolysis and glycogen synthesis. In addition, it has an anabolic effect by increasing the uptake of amino acids in the muscles and liver, as well as an antilipolytic action (inhibition of the lipases responsible for lipolysis) on adipocytes, where it promotes the formation of glycerol-phosphate (Cheatham et Kahn 1995) . At the central level, insulin acts at the hypothalamic level by modulating dietary behaviour: it inhibits food intake by suppressing the expression of neuropeptide Y (NPY), an orexigenic neuropeptide. Its action at the hypothalamic level also interferes with the counter-regulation of hypoglycaemia and indirectly regulates the endogenous production of glucose by the liver (Obici et Martins 2010). Thus, by promoting the consumption and storage of glucose and inhibiting endogenous glucose production, insulin fulfils its hypoglycaemic function. We will see in a next chapter, the details of the functioning of the pancreas.

The liver:

Is one of the main sources of glucose in the body outside of food intake. Indeed, when nutrients are supplied through food, the liver stores glucose in a polymerised form, glycogen,

and supplies other organs with glucose between food intakes. In the postprandial state, which is the period necessary for the total assimilation of nutrients from a meal (lasting about 5 to 6 hours), the glucose in the bloodstream no longer comes from liver production but from intestinal absorption of nutrients. In this case, the liver stops producing glucose and becomes a consumer of glucose (~45% of circulating glucose) by producing glycogen (Shrayyef et Gerich 2010). Because of its function of endogenous glucose production, the liver is one of the main targets of the mechanisms that regulate blood glucose levels, notably insulin and glucagon. This change pre/post is induced by insulin; insulin resistance (T2D), high glucose output from liver even at postprandial state

When glucose levels are high, glucose utilization by the liver increases, stimulated by insulin, and glucose serves as a substrate for glycogenogenesis (Polakof, Mommsen, et Soengas 2011). As the blood glucose level in the postabsorptive state is about 5 mM (i.e. once the nutrients in a meal have been fully absorbed by the body; usually measured after a 12-hour fast, such as in the morning upon waking), 50% of the glucose entering the circulation comes from glycogenolysis by the liver.

The kidneys:

Are endogenous producers of glucose. Although it has low glycogen reserves, it is not able to produce glucose by glycogenolysis due to the absence of glucose-6-phosphatase in glycogen-containing kidney cells. The kidney's production of glucose therefore stems entirely from neoglucogenesis (Gerich et al. 2001). During the postabsorptive phase, renal glucose production corresponds to a quarter of the hepatic glucose release, however renal involvement increases as fasting is prolonged. During the postprandial phase, the kidney also uses glucose (~10% of circulating glucose) as energy. The renal system acts as a filter, and its multiple transporters often require large amounts of ATP. Finally, in addition of its glucose production by neoglucogenesis and of its own use of glucose, the kidney may also influence glucose homeostasis by reabsorbing glucose (Gerich 2013).

The nervous system:

Is one of the organs with the highest energy requirements, especially glucose. The brain lacks fuel stores and hence requires a continuous supply of glucose. It consumes about 120 g daily, which corresponds to an energy input of about 420 kcal (1760 kJ), accounting for some 60% of the utilization of glucose by the whole body in the resting state (Mergenthaler et al. 2013). Much of the energy, estimates suggest from 60% to 70%, is used to power transport mechanisms that maintain the $\text{Na}^+\text{-K}^+$ membrane potential gradients required for the transmission of the nerve impulses. The brain must also synthesize neurotransmitters and their receptors to propagate nerve impulses. Overall, glucose metabolism remains unchanged during mental activity, although local increases are detected when a subject performs certain tasks (Berg et al. 2002).

Glucose is transported into brain cells by the glucose transporter GLUT3. This transporter has a low value of K_m for glucose (1.6 mM), which means that it is saturated under most conditions. Thus, the brain is usually provided with a constant supply of glucose (Jurcovicova 2014). Fatty acids do not serve as fuel for the brain, because they are bound to albumin in plasma and thus do not traverse the blood-brain barrier. During starvation, ketone bodies generated by the liver partly replace glucose as fuel for the brain (Berg et al. 2002).

The nervous system therefore influences blood sugar levels through its use of glucose but also through regulatory mechanisms operating at various levels. The central autonomic nervous system acts directly on the hormonal secretion of the pancreas through sympathetic and parasympathetic nerve projections (Yoshimatsu et al. 1984). In rats, lesions of the ventromedial nucleus of the hypothalamus, involved in food intake, have been shown to induce hypersecretion of insulin at elevated glucose and increased glucagon levels upon stimulation with the amino acid arginine (Rohner-Jeanrenaud et Jeanrenaud 1980). In addition, the presence of glucose-sensitive neurons in the central nervous system will produce rapid and adaptive responses from effector organs involved in glucose homeostasis (Levin et al. 2011). Insulin can also act directly on its receptors which are expressed in the central nervous system, including the brain, hypothalamus, cerebral cortex and cerebellum (Hopkins et Williams 1997). As a result, insulin can regulate food intake and appetite by decreasing the expression of neuropeptide Y (NPY which is orexigenic, or by increasing the expression of pro-opiomelanocortin (POMC) which is anorexigenic (Schwartz et al. 2000).

Skeletal muscles:

The major fuels for muscle are glucose, fatty acids, and ketone bodies. Muscle differs from the brain in having a large store of glycogen (1200 kcal, or 5000 kJ). In fact, about three-fourths of all the glycogen in the body is stored in muscle (Berg et al. 2002) . However, unlike the liver, muscles are not able to release glucose into the circulation. Their glycogen reserve is therefore used by the muscles themselves as a source of energy to perform their locomotor function. This glycogen is readily converted into glucose 6-phosphate for use within muscle cells. Muscle, like the brain, lacks glucose 6-phosphatase, and so is therefore unable to export glucose. As a consequence, muscle retains glucose, its preferred fuel for bursts of activity. In actively contracting skeletal muscle, the rate of glycolysis far exceeds that of the citric acid cycle, and much of the pyruvate formed is reduced to lactate, some of which flows to the liver, where it is converted into glucose (Severinsen et Pedersen 2020).

In addition, myocytes also secrete cytokines called myokines that regulate carbohydrate and fat metabolism (Severinsen et Pedersen 2020). One of the best known in this regulation is interleukin-6 (IL-6): it increases glucose uptake via the glucose transporter GLUT4 (Zisman et al. 2000) and promotes lipid oxidation (Carey et al. 2006). It thus acts on postprandial blood glucose by delaying gastric emptying (Lehrsokov et al. 2018). IL-6 also finely controls the endocrine function of the pancreas by stimulating the proliferation of α -cells, secretors of glucagon and the expression of pro-glucagon messenger ribonucleic acid (mRNA) (Carey et al. 2006).

On the other hand, the ability of muscle tissue to rapidly increase its glucose utilisation makes it an important player in the regulation of blood sugar levels, especially just after a meal. This organ is in fact a major user of glucose in the postprandial period (~30% of circulating glucose) just second to the liver (Yang 2014) . The glucose captured by the muscles is then either used immediately or used as a substrate for glycogenogenesis to maintain its energy reserves. Finally, skeletal muscle plays an additional role in the regulation of blood glucose levels by releasing amino acids into the bloodstream which will be used by the liver for gluconeogenesis (Spargo, Pratt, et Daniel 1979).

White adipose tissue:

This tissues plays a role in stockage and after a meal, the adipose tissue harvests 10-15% of the glucose ingested, which further metabolized to triglycerides (Rosen et Spiegelman 2006).

When energy consumption exceeds energy expenditure, the unspent lipids are stored as triacylglycerol in the adipose tissue cells, the adipocytes. The latter secrete fatty acids (produced by the breakdown of triacylglycerols) into the circulation when glucose availability is limited, so that other organs can use them as an energy source (Berg et al. 2002). In situations when, hepatic gluconeogenesis is necessary (depletion of glycogen stores), the adipose tissue releases free fatty acids and glycerol into the bloodstream which will be used by the liver as a substrate for glucose production. In addition, white adipose tissue plays an important endocrine role, secretes proteins, more particularly cytokines (cell signalling proteins) called adipokines. The first adipokine discovered in 1994 was leptin, which is the most studied adipokine and the one that has a considerable role in fat regulation (Friedman, 2002); it inhibits hunger at the central level and stimulates energy expenditure. Leptin acts directly on insulin secretion by inhibiting it (Kieffer et Habener 2000). It also exerts its anti-hyperglycaemic action in the muscles and liver where it increases insulin sensitivity (Kamohara et al. 1997).

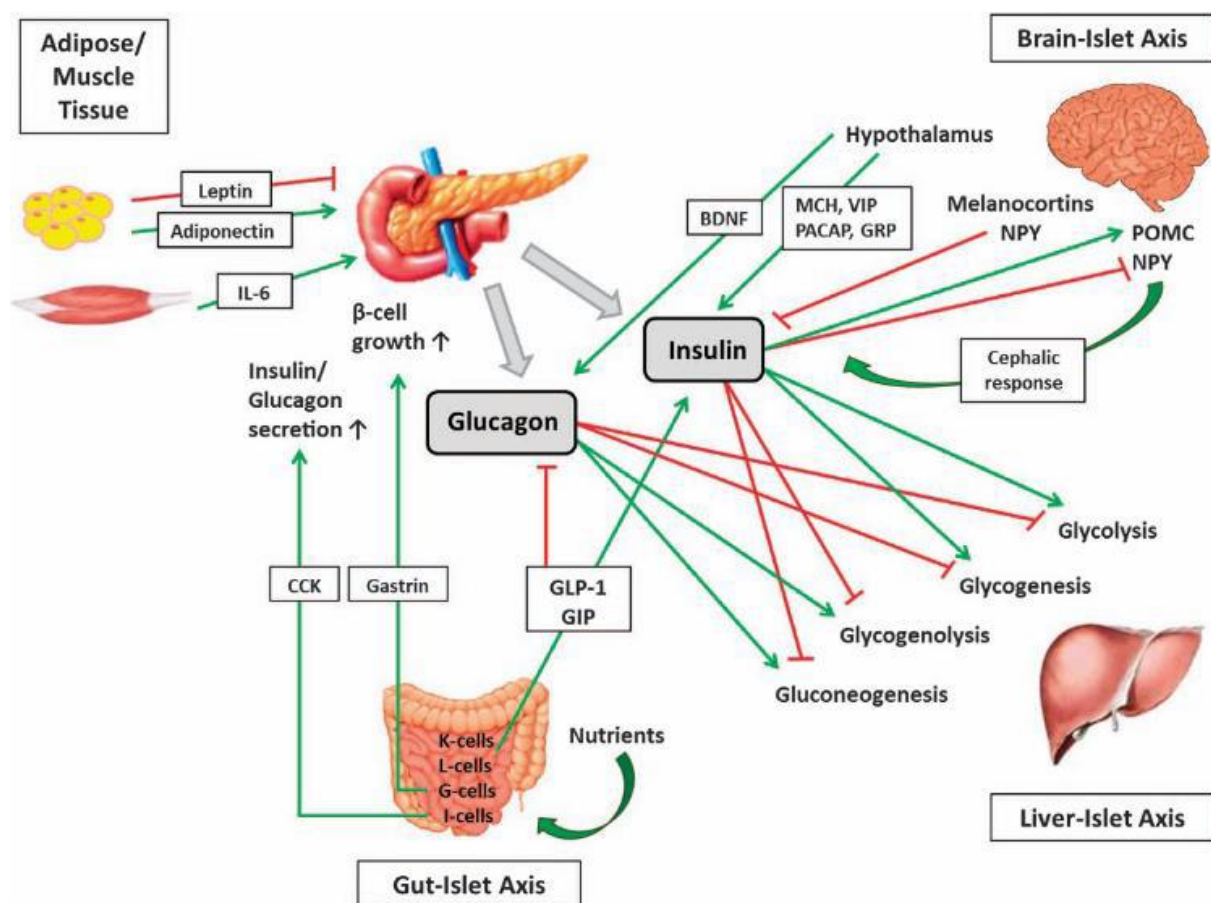


Figure 4: Interaction of the pancreas with the nervous system, liver, small intestine, white adipose tissue and skeletal muscle via a network involving hormones and neurotransmitters. BDNF, brain-derived neurotrophic factor; CCK, cholecystokinin; GIP, glucose-dependent

insulinotropic peptide; GLP-1, glucagon-like peptide 1; GRP, gastrin-releasing peptide; IL-6, Interleukin 6; MCH, melanin concentrating hormone; NPY, neuropeptide Y; PACAP, pituitary adenylate cyclase-activating polypeptide; POMC, pro-opiomelanocortin; VIP, vasoactive intestinal peptide. *Adapted from (Röder et al. 2016)*

1.3 Regulation of glucose maintenance: Sensors and Actuators.

The maintenance of blood glucose within a defined narrow range, during periods of intake and of consumption, requires a precise and reliable control mechanism. Such a mechanism requires first precise detection of the entity to be regulated by a sensor, second regulators, also called actuators, of glucose levels and finally feed-back loops to keep the system constant.

The different glucose sensors of the body

A sensor is commonly defined as a device that detects and responds to some type of input from the physical environment. In our body, we have different biosensors that are able to detect changes in nutrients, be it glucose, amino acids (Thorens et Mueckler 2010) or lipids in the form of free fatty acids (Moullé et al. 2014), and whose response is a function of the levels of the detected nutrients. This response or actuators therefore constitutes a signal that is transmitted, via hormonal, neuronal or intercellular signals to the effector organs so that they adapt their use or production of glucose and fatty acids to the ambient blood levels of glucose and lipids, thus contributing to the proper maintenance of energy homeostasis. Both types of sensors (glucose, fatty acid or also amino acids) are involved in the regulation of blood glucose levels, given the influence that these nutrients have on each other in their metabolism and the interconnections of biochemical pathways. Here we will only deal with glucose sensors, although some of them may be modulated by fatty acids and amino acids.

The body's most important glucose detectors are contained in the islets of Langerhans, and are none other than the cells β and the α cells, which directly influence blood glucose levels through the hormones they secrete, while being regulated by blood glucose levels (their secretory activity being a function of extracellular glucose concentrations). Like neurons, these cells are said to be excitable because they generate electrical activity. While β cells are activated by increases in glucose concentrations, α cells are sensitive to glucose variations at low concentrations (Thorens 2008). We will discuss in details in a next chapter the architecture

and the functioning of this specific glucose detector which has the principal role in our biosensor.

However, glucose levels are also measured at various strategic points in the body by the bias of gluco-sensitive neurons, i.e. whose electrical activity is modified when blood sugar levels vary. In the periphery, these neurons are found in the autonomic nervous system, in the digestive tract. They intervene in the regulation of food intake by influencing intestinal motility, digestion speed and gastric emptying (Browning 2013; Mithieux et Gautier-Stein 2014) .

In the central nervous system, glucose-sensitive neurons become more sensitive to glucose and are found in several cerebral areas mostly in the hypothalamic area. The best-known circuits are those involved in the regulation of energy homeostasis. These neurons are divided into two categories: glucose-excited (GE) neurons, just like pancreatic β cells, are activated when blood glucose levels rise, during which their discharge frequency increases, whereas glucose-inhibited (GI) neurons, on the other hand, will be more active if the blood sugar level drops, as it does for pancreatic α cells. These neurons are particularly present in the hypothalamus (Oomura et al. 1975; Routh et al. 2014) which integrates nervous, metabolic and hormonal information from the periphery to regulate eating behaviour and energy expenditure according to changes in homeostasis. Sensors located at the central level, notably the GI, are also involved in the counter-regulation of hypoglycaemia (Levin et al. 2011) . Finally, the carotid body contains sensors to signal hypoglycaemia (Prabhakar et Joyner 2015).

At the level of the digestive tract and the portal vein, the first blood passage of digested nutrients, several sensors are positioned at these early points of nutrient income. The hepatic portal vein constitutes a key site in the detection of glucose being since it collects the blood flow from the entire digestive tract and thus the nutrients from food. The hepato-portal glucose detector is used to control the intake of glucose (Thorens 2004). When the blood sugar levels increase in the portal vein, this sensor reduces the electrical tone of the nerve afferents passing through the vagus nerve and the spinal cord projecting on the nerve centres (Niiijima, Torii, et Uneyama 2005). Within the GIT, enteric neurons are capable to sense glucose levels and provide afferent signals (Raybould 2007) . Two other kind of sensors, L cells and K cells, dispersed throughout the GIT, are able to detect glucose during nutrient passage and provide corresponding hormones to tune the islet system (Ezcurra et al. 2013).

The carotid body is looked at as a multipurpose sensor for blood gases, blood pH, and several hormones. The matter of glucose sensing by the carotid body has been debated for several years in the literature, and these days there is a consensus that carotid body activity is modified by metabolic factors that contribute to glucose homeostasis (Conde, Sacramento, et Guarino 2018).

Interestingly these anatomically very different sensors, from islets to liver, GIT, carotid and brain, are using a certain set of common molecular tools that have initially been described for β -cells. Indeed, these cellular glucose sensors express and use typically the glucose transporter GLUT2 (in rodents), glucokinase, and an ATP-sensitive potassium channel (K_{ATP}) that allows the triggering of electrical activity when glucose is metabolised by the cell (Schuit et al. 2001; Thorens et al. 2015; Liu, Seino, et Kirchgessner 1999).

These multiple sensors and their interactions via hormones and nerves led to the concepts of gut-brain axes, brain-liver axis etc (Thorens et al. 2015), that provide pathways for the coordinated read-out of changes in nutrient status within an organism.

Actuators of glucose maintenance: Insulin and glucagon:

The “balance” between insulin and glucagon secreted by the endocrine pancreas is essential to blood sugar regulation by acting on the different organs presented above. Insulin is secreted by the β -cells of the islets in response to an increase in blood glucose, in combination with other nutrients. Its main targets are the liver, adipose tissue and muscle as well as the islets themselves (Petersen et Shulman 2018). Thus, insulin increases glucose uptake by these insulin-sensitive cells. As detailed above, some of the glucose is used as an energy source, while the rest enters the anabolic pathways leading to the conversion of glucose to glycogen and fat. Insulin also inhibits glucose production (glycogenolysis and gluconeogenesis) in the liver, muscle, kidney and intestine (Pocock et Richards 2006). Finally, insulin stimulates lipogenesis by increasing the synthesis of fatty acids from glucose and thus increases triglyceride synthesis and very low-density lipoprotein production in the liver (Pocock et al., 2019). In contrast, although there are several hyperglycaemic hormones, the most potent is

glucagon, and many of its actions are directly opposed to insulin (Scott et Bloom 2018). Glucagon is secreted by α -cells following a decrease in blood glucose. The main target of glucagon is the liver, where it increases hepatic glucose production via the stimulation of glycogenolysis and gluconeogenesis. Glucagon also has a significant lipolytic effect by mobilising fatty acids and glycerol from adipose tissue (Pocock et al., 2019).

1.4 The different phases of food intake:

The simple view or even thought of a meal already prepares the body for digestion (Power et Schulkin 2011) . During food intake, three phases are involved in regulating blood glucose levels. The cephalic phase involves the central and peripheral nervous system and begins before the nutrients are ingested to prepare the body. The gut phase is the release of incretin hormones (GLP-1 and GIP), stimulated by the passage of nutrients through the gut. These hormones prepare the β -cells for the arrival of glucose and then potentiate insulin secretion. Finally, the islet phase corresponds to the arrival and action of glucose on the islets (Rorsman et Ashcroft 2018a) .

Cephalic phase

In the cephalic phase , the anticipation of food prepares the body for digestion, absorption and use of nutrients in food (Power et Schulkin 2011). The sensory aspect of food, such as sight and smell, influences eating behaviour. For example, the smell of a favourite dish can set the stage for overeating. The sensation of food in the mouth or thoughts related to food send signals to the spinal cord via the vagus nerve to stimulate the release of gastric chemicals, pepsin and hydrochloric acid, which play a role in the breakdown of food (Wiedemann et al. 2020). The parasympathetic nervous system thus releases an excitatory neurotransmitter within the islets, acetylcholine (ACh). It has also multiple and complex effects on β -cells that are mainly mediated through the activation of M3 muscarinic receptors(Molina et al. 2014) . At a cellular level such a signal promotes translocation of secretory granules to the plasma membrane in β -cells and thus enhances their readiness for release (Niwa et al. 1998). Non-cholinergic mechanisms also participate in the cephalic phase. For example, parasympathetic nerves contain several neuropeptides in addition to ACh: VIP (Vasoactive intestinal peptide), PACAP (Pituitary adenylate cyclase-activating polypeptide) and GRP (Gastrin releasing

peptide). These neuropeptides are released after activation of the vagal nerve of the pancreas and stimulate insulin secretion (Ahrén 2000). This phase therefore prepares the β -cell and the body to take handle glucose. It is crucial for the regulation of postprandial blood glucose. Due to readily cephalic phase a high concentration of insulin is released during food intake and its digestion, thus allowing a better uptake of absorbed glucose (Teff 2011). In mice, the nerve terminations extend into the islets to be in direct contact with the endocrine cells (Lundquist et Ericson 1978). In contrast, human islets are less innervated. Indeed, the nerve endings are rather in contact with the smooth muscles of the blood vessels than with the endocrine cells (Rodriguez-Diaz, Abdulreda, et al. 2011). Thus, the nervous regulation of human islets seems to be mainly indirect via the control of blood flow.

Gastro-enteric phase

Its food arrives in in the stomach , the vago-vagal reflex communicates that nutrients are present (Faris et al. 2008) Based on the feedback, the required levels of digestive chemicals are released. After the gastric phase, the "enteric phase", or "intestinal phase", comes into play. Indeed, oral administration of glucose leads to a greater stimulation of insulin secretion than intravenous or intraperitoneal administration, despite similar plasma glucose levels (Elrick et al. 1964). This phenomenon is called the "incretin effect". It is caused by a release of incretin hormones, stimulated by the passage of the food bolus through the gut which potentiates insulin secretion by β -cells in response to glucose. Two peptides synthesised and released by the entero-endocrine cells of the gut have been identified as incretin hormones. The first is glucose-dependent insulinotropic polypeptide (GIP), which is released from K-cells located in the duodenum and upper jejunum (Buchan et al. 1978) . The second is glucagon-like peptide-1 (GLP-1), and its secretion by L-cells, located mainly in the ileum and colon, is stimulated by GIP released from more proximal K-cells (Baggio et Drucker 2007; Holst 2006; Meier et Nauck 2005). This "incretin effect" accounts for about 65% of the total insulin secretory response (Nauck et al. 1986) .

Islet phase

As glucose reaches the β -cells, the islet phase begins. Islet insulin secretion has two characteristic phases, a peak phase and a plateau phase with oscillations, as will be detailed

in a next chapter. Together, the cephalic, gastro-enteric and islets phases ensure the maintenance of normoglycaemia before, during and after meals in the healthy subject and any disruption of this system results in major metabolic disorders.

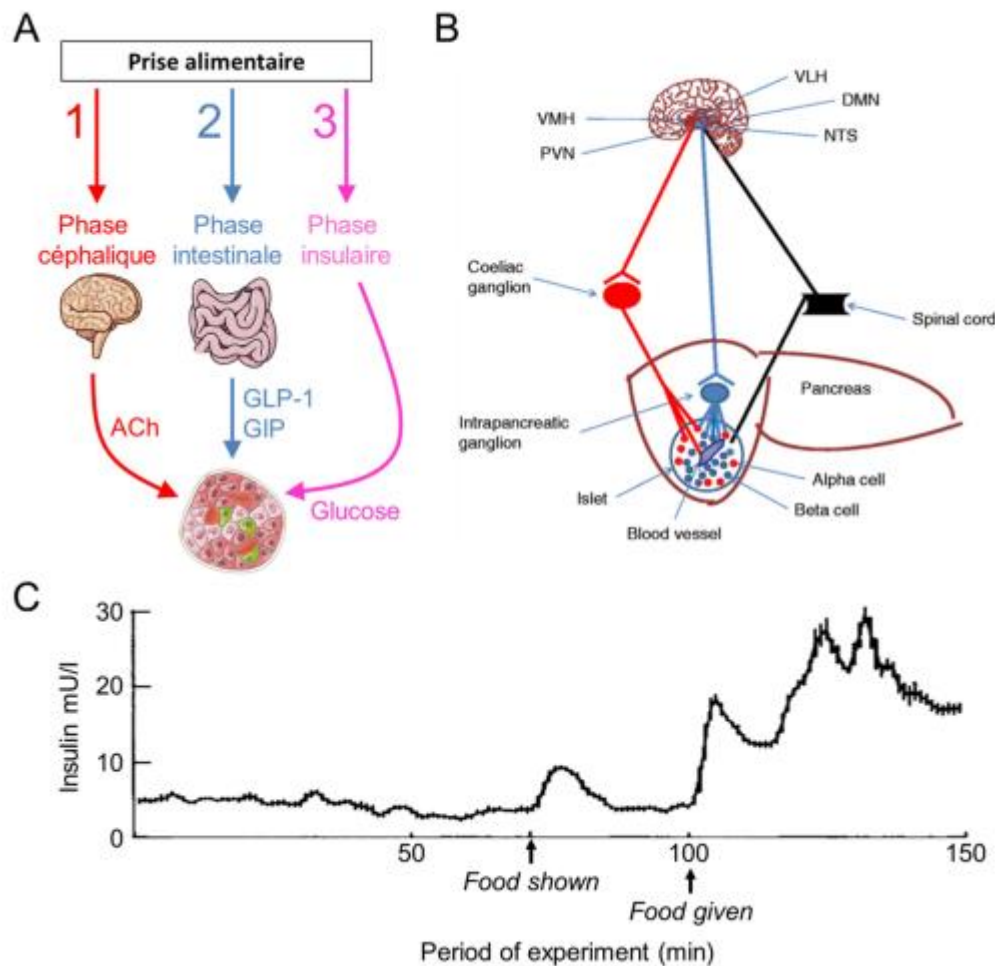


Figure 5: Successive phases of blood sugar regulation during food intake. (A) During food intake, three phases are involved in regulating blood glucose levels. The cephalic phase involves the nervous system and begins before the nutrients are ingested to prepare the body. The gut phase is the release of incretin hormones (GLP-1 and GIP), stimulated by the passage of nutrients through the gut. These hormones prepare the β -cells for the arrival of glucose and then potentiate insulin secretion. Finally, the islet phase corresponds to the arrival and action of glucose on the islets (A panel: Jaffredo 2021 thesis). (B) Diagram of the innervation of the islets and the three branches of the autonomic nervous system, namely the sympathetic nerves (red, Noradrenaline), the parasympathetic nerves (blue, Acetylcholine) and the sensory nerves (black). The different nuclei of the hypothalamus are indicated (VLH, VMH, PVN, DMN, NTS). From Ahrén (2012). (C) Cephalic phase demonstrated in conscious sheep. Portal venous insulin concentration is measured after showing food (at 70 min) and after ingestion (at 100 min). Adapted from Matthew & Clarke (1987)

2. The islet of Langerhans, the main glucose sensor.

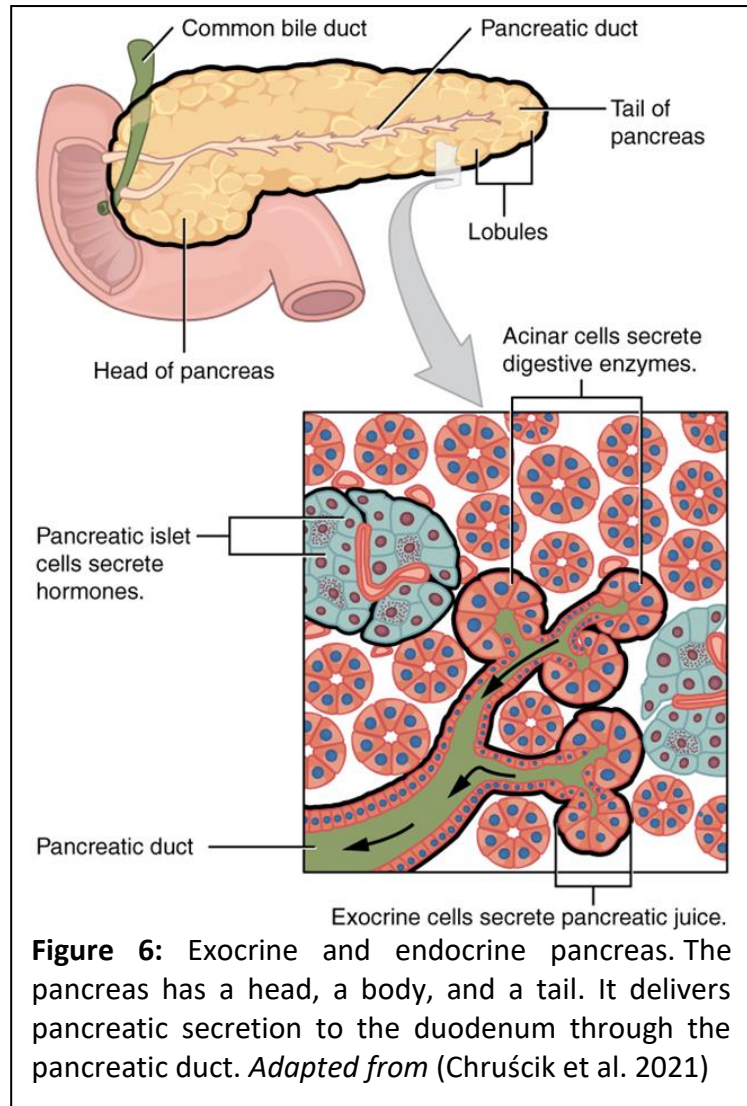
The pancreas plays a key role in the regulation of digestion and carbohydrate homeostasis through the release of digestive enzymes and pancreatic hormones. Due to its retroperitoneal

location, the pancreas has been a little-known organ for long time and it

is divided into 3 parts: the head, the body and the tail. This organ consists of acinar (or exocrine) cells that secrete pancreatic juice containing digestive enzymes (e.g. amylase, pancreatic lipase, trypsinogen) into the bile duct.

These enzymes then flow into the duodenum and small intestine to break down fats, proteins and carbohydrates (Chruścik et al. 2021). Pancreatic islet hormones, on the other hand, are released endocrine, i.e. directly into the bloodstream, to regulate blood sugar (Röder et al. 2016) . It is on

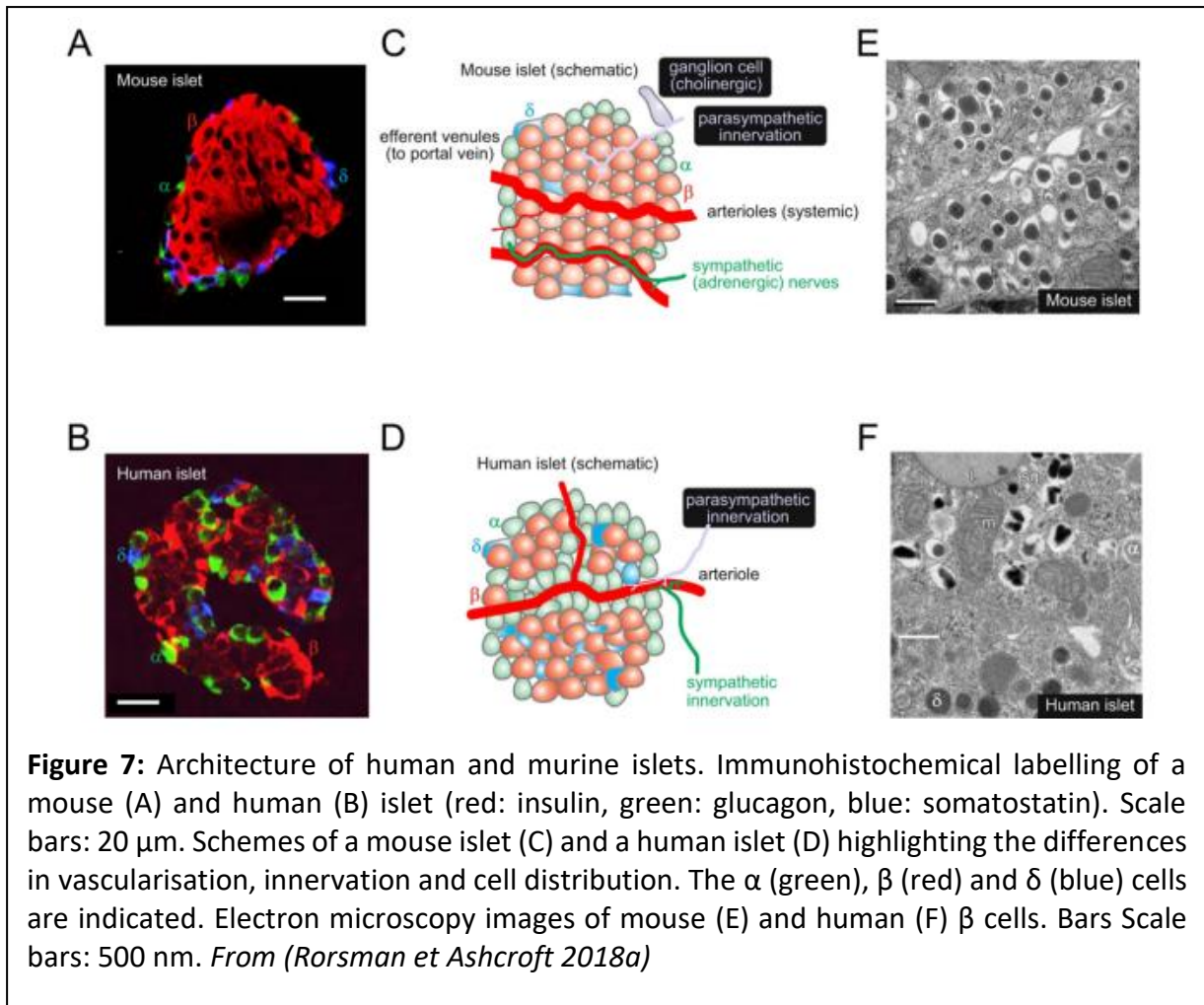
this last point that we will focus.



2.1: The endocrine pancreas.

In contrast to the massive exocrine portion of the pancreas, the endocrine portion represents only 1–4% of the total mass of the organ. Despite this minority, islet cells mediate indispensable functions in glucose homeostasis. The pancreatic islets of Langerhans,

discovered in 1869 by Paul Langerhans (Langerhans 1869), are microorganisms embedded in the exocrine parenchyma of the pancreas. They are dispersed throughout the organ, with a higher density in the tail region. Using optical methods, it was shown that the pancreas of an 8-week-old mouse contained about 1,100 pancreatic islets and that a mouse islet was composed of an average of 80 cells, with an average diameter of 60 μm . A human pancreas, on the other hand, contains about 1 million islets, with a diameter of 130 μm corresponding to about 200 β cells per islet on average (Rorsman et Ashcroft 2018a). A pancreatic islet is composed of several endocrine cell types and their relative contribution varies among species (Barbieux et al. 2016) and location of islets, within the pancreas. Thus, even within a given species such as man, there is hardly a “standard islet” (Dybala et Hara 2019) although some conserved principles emerge (Hoang et al. 2014). The predominant islet cell types are insulin-secreting β -cells (~50% in humans, ~75% in mice), glucagon-releasing α -cells (35-40% in humans, 15-20% in mice) and somatostatin-secreting δ -cells, an inhibitor of glucagon and insulin secretion (10% in humans, ~5% in mice) (Rorsman et Huisling 2018). There are also two rarer cell types: the PP-releasing γ -cells and the ghrelin-secreting ϵ -cells (Aamodt et Powers 2017). One of the major differences between rodent and human islets is therefore the ratio of β to α cells. Interspecies differences also exist in the arrangements of the different cell types in relation to each other. This optimal arrangement is driven by the need for interaction between cell types and would allow human β -cells to respond more to low glucose levels compared to mouse β -cells (Klemen et al. 2017; Cabrera et al. 2006). The unique position of β -cells among the different cell types is underscored by the fact, that all other cell types are also found in the gastrointestinal tract or hypothalamus, whereas the β -cells is unique to islets.



Next, we will discuss in detail the different cell types of these pancreatic islets, and try to understand why islet of Langerhans constitute a suitable sensor for the maintenance of glycaemia and a well-adapted substrate for the development of our biosensor.

2.2: Cellular architecture of the islets of Langerhans.

Langerhans islets are made up of different cell types, from α to ε -cells. These cell populations share common characteristics even if they have different functions. These cells are all electrogenic and have K_{ATP} channels on their surface making them sensitive to metabolic variations. Finally, they all secrete hormones via vesicles. We look at the specificities of each of these cell types.

β -cells

β -cells are the principal component of the pancreatic islets. They are polygonal cells, with an average diameter of 13–18 μm (Göpel et al. 1999) that possess around 10,000 secretory granules (Olofsson et al. 2007), each containing up to 8–9 fg of insulin (1.6–1.8 amol insulin) (Rorsman et al. 2018a).

The main stimulus for insulin secretion by the β -cell is glucose, both in humans and in mice, since it is the most common component found in our diet and enters the bloodstream directly after digestion of the meal. When blood glucose levels exceed the threshold of 3 mM for human or 5 mM in mice, the β -cell will secrete insulin (Klemen et al. 2017; Rodriguez-Diaz et al. 2018). Insulin is expressed in pancreatic β -cells from a single *INS* gene in humans, whereas in rodents two genes exist, *INS1* and *INS2*. Transcription of the *INS* gene leads to pre-pro-insulin mRNA, which is then translated into pre-pro-insulin peptide. Glucose regulates gene expression and mRNA stability, and thus the insulin content of the cell (Evans-Molina et al. 2007; Leibiger et al. 1998). The pre-pro-insulin peptide passes into the endoplasmic reticulum with concomitant processing to pro-insulin followed by transport to the Golgi apparatus and is packaged there into secretory vesicles where maturation to insulin takes place. If we look at the ultrastructure of the β -cell, we find secretory granules of two types: granules with a compact core, containing immature pro-insulin, and granules with a crystalline core containing so-called mature insulin, arranged in hexamers around two zinc molecules (Folli et al. 2018; Orci, Vassalli, and Perrelet 1988). Mature insulin is preferentially secreted around the β -cell and subsequently reaches the liver via the portal circulation. The hepatocytes use 50% of the insulin; the rest is transported to the heart via the venous circulation, which can then distribute it to the rest of the body via the arterial circulation (Tokarz, MacDonald and Klip 2018). Insulin will be able to stimulate GLUT4 translocation to the plasma membrane and thus enhances glucose uptake by muscle cells and adipocytes. At the end of this process, the remaining circulating insulin is degraded by the kidney (El, Capozzi, and Campbell 2020).

The insulin-secreting β -cell: an electrogenic cell

As in all endocrine cells, the secretory activity of β -cells is finely controlled by ion channels. These channels control potassium, sodium, calcium and chloride fluxes that generate changes

in β -cell membrane potential (Rorsman et Ashcroft 2018a). This electrical coding has several advantages. First, a threshold effect: insulin is a very potent hormone with potentially lethal effects if secretion is continuous or excessive. Ion channels, especially voltage-gated ones, open and close in a very controlled manner, with thresholds for activation and inactivation. Secondly, ions are small, highly mobile charged elements that do not consume any energy when passing through the channels in a passive manner along a gradient. Although ion transporters are implicated in later steps, the energetic cost has only to be paid only afterwards. Finally, the kinetics of channel opening and inactivation/closing are very fast (a few ms), allowing very precise electrical coding. β -cells express ~30 families of channels that can be regulated at different levels: transcription, translation, post-translational modifications (e.g. phosphorylations and dephosphorylations), intracellular trafficking, associations with regulatory subunits and partner proteins. This allows the β -cell to respond to extra- and intracellular signals to refine this electrical code and thus secretion.

The biochemical mechanism of stimulus-secretion coupling whereby glucose initiates electrical activity to induce insulin secretion was described in Chapter 1. It is important to add that the electrical activity of the β -cell is stimulated by glucose, but can be modulated by amino acids (Henquin et Meissner 1981), neurotransmitters (such as acetylcholine) (Hermans, Schmeer, et Henquin 1987) and hormones (such as GLP-1) (Leech et al. 2011). All these molecules require glucose to initiate membrane depolarisation. Having carried out my thesis work on mouse islets, I will detail the ionic events responsible for the stimulus-secretion coupling found in this animal model. Let us first look at the sequence of events before detailing the behaviour and characteristics of the different types of channels.

Resting potential and initiation of the depolarization

At low glucose concentration and consequently low metabolic activity, the intracellular ATP/ADP ratio in the β -cell is low. The membrane of the insulin-secreting cell is hyperpolarised its membrane potential between -70 and -80 mV and without electrical activity (Rorsman et Ashcroft 2018a), whether in humans or mice. This resting potential is maintained by the K_{ATP} channel, the opening of which induces an outflow of K^+ ions and thus an excess of negative

charges in the intracellular medium. From 5 mM glucose onwards, the ATP/ADP ratio increases, more K_{ATP} channels are closing, the membrane depolarises and reaches -60 mV but without initiation of electrical activity. It is only above 6 mM glucose that K_{ATP} channels are completely inhibited, the membrane potential reaches a threshold sufficient to initiate the electrical activity i.e. between -60 mV and -50 mV.

Action potentials

The decrease in potassium outward currents alone does not sufficiently depolarise the membrane. The closure of K_{ATP} channels strongly increases the input resistance of the membrane. This phenomenon is combined with the presence of background depolarising inward currents. Indeed, once the membrane input resistance increases, the impact of these background depolarising currents on the membrane potential strongly increases ($V=R \cdot I$, and R increases), which leads to the rapid membrane depolarisation. However, the identity of these background currents is not yet clear, eventually involving cationic TRP channels (Gall et al. 1999). Recently osmo-regulated chloride channels, activated by glucose entry and its metabolism, have been shown to contribute to this initial depolarisation (Kang et al., 2018; Stuhlmann et al., 2018). The membrane depolarises at around -50 mV, which initiates the regenerative electrical activity by opening the VDCCs (Göpel et al. 2004). The L-type calcium channels contribute to >60% of calcium currents. These channels contribute to the exocytosis of insulin-containing secretory granules, but are not the only depolarising currents involved. Voltage-gated sodium channels as well as P/Q-type calcium channels (15-25% of calcium currents) contribute to the final rise (from -30 to ~0 mV) of the action potential (Rorsman, Braun, et Zhang 2012). Once calcium and sodium channels are inactivated, voltage-gated (mainly in mouse) and calcium-activated (mainly in human) potassium channels contribute to the membrane repolarisation. These K^+ channels already open a little during the upstroke of the action potential, but given their very slow opening rate, their impact on the membrane potential is delayed compared to depolarizing channels (Rorsman et Huising 2018).

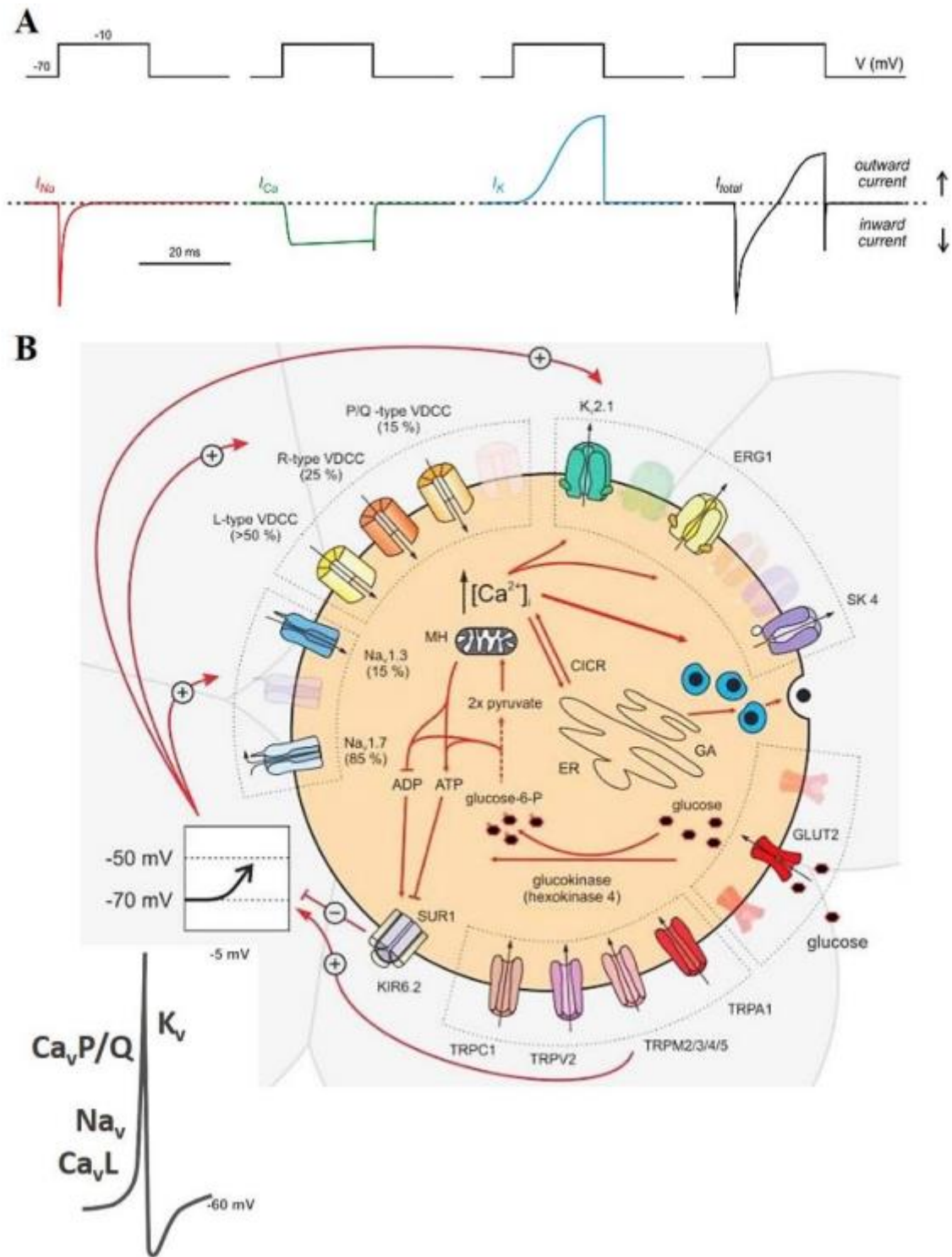


Figure 8: The ionic currents involved in the action potential of the β -cell. (A) Schematic representation under voltage imposed of the sodium (I_{Na}), calcium (I_{Ca}), potassium (I_K) and total membrane current (I_{total}) involved in depolarisation. (B) Sodium, calcium and potassium ion channels responsible for the generation of the action potential in the β -cell. Note that other channels, notably TRPs, modulate the electrical activity. Adapted from (Klemen et al. 2017; Rorsman et Ashcroft 2018a).

Membrane potential oscillations and continuous action potential activity

After an action potential, the repolarisation of the membrane is not complete as there is a membrane potential plateau between -50 mV and -40 mV. This is due, among other, to the rectifying K^+ channels that remain open after membrane repolarisation and maintain the plateau in order to maintain a temporal period between successive action potentials (Rorsman et Trube 1986). In addition, a decrease in the amplitude and frequency of action potentials is observed over time, which is thought to be due to the inactivation of calcium channels (Rorsman et al. 2011). In mice, electrical activity is presented by alternating active phases of membrane depolarisation with bursts of action potentials and silent phases of membrane repolarisation. At 10 mM glucose, for example, the active phases last 5-10 s, with 2-4 bursts/min, and the inactive phases last 10-20 s. These membrane potential oscillations then convert to continuous action potential activity with the progressive increase in glucose, a reduction in silent phases, to reach at 20 mM glucose a discharge pattern where only active phases persist (Henquin et Meissner 1984). Note that the K_{ATP} channel activity is involved in these switches between active and inactive phases (Fig. 9).

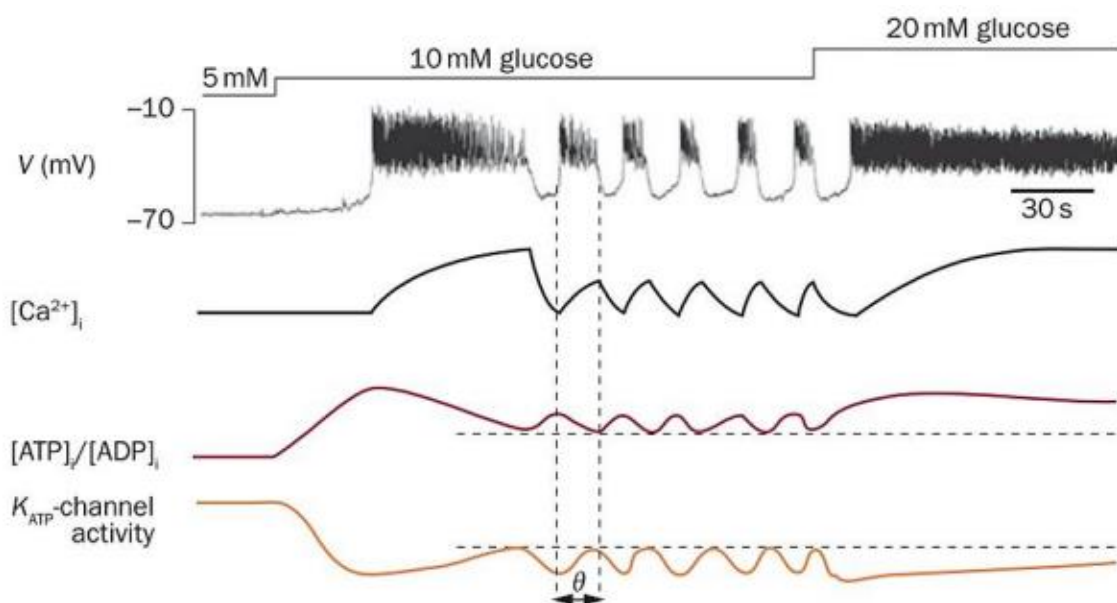


Figure 9: Effect of glucose on β -cell electrical activity. Changes in membrane potential, intracellular calcium concentration, intracellular ATP concentration and concentration and K_{ATP} channel activity at 5, 10 and 20 mM glucose. Oscillations in intracellular ATP concentration are in antiphase (θ) with K_{ATP} channel activity, calcium oscillations and electrical activity. According to (Ashcroft et Rorsman 2013).

Ion channels in the β -cell responsible for stimulus-secretion coupling

Having described the general sequence of events, we will have a look at the molecular identities. The β -cell contains more than 50 different ion channels on its plasma membrane surface (Ashcroft et Rorsman 1989; Rorsman et al. 2011). Only the main ion channels responsible for the ionic events involved in stimulus-secretion coupling will be discussed.

K_{ATP} channel

The ATP-sensitive potassium channel is the main ion channel that opens at the resting potential in insulin-secreting cells of all species. However, even in the absence of glucose, a large proportion of the K_{ATP} channels are already closed, with channel conductance around 7% and falling to 3% when glucose is increased to 10 mM. The slightest change in channel conductance induces marked changes in membrane potential. This is physiologically important and advantageous for glucose regulation to prevent random opening of a single channel which would hyperpolarise the membrane at high glucose and thus inhibit insulin secretion (Rorsman et Ashcroft 2018). Opening the K_{ATP} channel clamps the β -cell membrane to low potentials, while closing it induces depolarisation as explained above. The concentration of ATP in the β -cell is low at low glucose, leaving the K_{ATP} channel open allowing potassium efflux, membrane hyperpolarisation and lack of insulin secretion. When the concentration of glucose increases and the K_{ATP} channel closes and depolarises the cell. The kinetic properties of the β -cell K_{ATP} channel are qualitatively similar in mice and humans.

The β -cell K_{ATP} channel hetero-octamer is formed by two proteins: the sulphonylurea receptor and regulator type 1 (SUR1), unique to β -cells, and the channel pore-forming protein for the rectifying inward potassium current, Kir6.2 (Islam 2020). SUR1 is a target of the class of antidiabetic agents called sulphonylureas that block the K_{ATP} channel and thus insulin secretion. The K_{ATP} channel is composed of 8 subunits, 4 Kir6.2 proteins surrounded by 4 SUR1 proteins. Inhibition of β -cell K_{ATP} channel activity is induced by ATP binding to Kir6.2. However, ATP inhibits the Kir6.2 subunit only with an IC_{50} of 100-200 μ M and the presence of SUR1 significantly increases the affinity to the nucleotide ($IC_{50} = 5-10 \mu$ M) (Koster et al. 2005). The role of this channel in insulin secretion is central since mutations in the K_{ATP} channel subunits alter its biophysical properties and cause hypo- or hyperglycaemia (Gloyn et al. 2004). New concepts have emerged in recent years showing that depolarisation following glucose surge

does not rely solely on the closure of the K_{ATP} channel. Indeed, β -cells deficient for the gene coding for Kir6.2 respond to glucose stimulation (Ravier et al. 2009). Depolarising currents, so-called background, and surely of composite nature (chloride out, cation in), currents are always present even at low glucose explaining why the resting potential of the cells is not the K^+ reversal potential (-120 mV) but somewhat more depolarised (-80 to -70 mV) (Patrik Rorsman et Ashcroft 2018a). To date, these currents have yet to be identified. In addition, glucose entry and metabolism in the β -cell increases intracellular osmolarity sufficiently to activate, along with K_{ATP} channel closure, anion channels (such as leucine-rich repeat-containing protein 8 or LRRC8/SWELL1, volume regulatory anion current or VRAC,) (Kang et al. 2018; Stuhlmann, Planells-Cases, et Jentsch 2018).

Voltage-dependent channels

Calcium channels

Calcium currents are implicated in membrane potential, as well as calcium signals for secretion and for gene expression. Different molecular entities may form the base for these calcium currents and the situation is even a bit more complex as different entities may be responsible for depolarisation and for calcium influx linked to exocytosis.

When the membrane potential reaches -50 mV, the probability of opening the VDCCs/ Ca_v potential-dependent calcium channels increases. As already discussed above, calcium currents are mostly (about 50-60%) due to L-type VDCCs ($Ca_v1.2$) in mice (Klemen et al. 2017). In contrast, in humans, P/Q-type potential-dependent calcium channels are involved to the same extent as L-type channels (Rorsman et Braun 2013). As we will see later, insulin secretion by the β -cell follows a biphasic pattern, with two phases of secretion. Inhibition or deletion of L-type VDCCs in mice causes a reduction in both phases of insulin secretion (Rorsman, Braun, et Zhang 2012). However, not only L-type VDCCs play a role in stimulus-secretion coupling as 25% of calcium currents are attributed to R-type VDCCs ($Ca_v2.3$), which are more involved in the second phase than in the first phase of insulin secretion (Jing et al. 2005). P/Q-type VDCCs ($Ca_v2.1$) are responsible for 15-25% of the remaining calcium currents. VDCCs have different biophysical properties and pharmacology permitting their differentiation (Jing et al. 2005) (Rorsman et Ashcroft 2018). L-type (long duration) channels have longer kinetics than P/Q-type (intermediate-long duration) channels. While L-type VDCCs can be blocked by

dihydropyridines (e.g. nifedipine), P/Q-type VDCCs are insensitive to them, but can be blocked by agatoxin IVA. R-type (intermediate duration) calcium channels have intermediate opening kinetics and can be inhibited by the toxin SNX-482.

In contrast to mice, human and rat β -cells express T-type calcium channels that induce a transient calcium current (Barnett, Pressel, and Mislner 1995) that activates at low thresholds, i.e. when the membrane is weakly depolarised (about -60 mV) and are therefore the first to activate. These channels undergo rapid voltage-dependent inactivation from -50 mV, i.e. this inactivation accelerates at increasingly depolarised membrane potentials. These channels may have pacemaker activity in human β -cells, particularly when the membrane potential is close to the threshold for triggering PAs.

Sodium channels

In most excitable cells, calcium and sodium channels are responsible for the depolarisation phase and the rise of the action potential. The use of specific sodium channel inhibitors such as tetrodotoxin (TTX) reduces the amplitude of β -cell action potentials, demonstrating the contribution of these channels in the generation of electrical activity (Göpel et al. 1999). Voltage-dependent sodium channels (Na_v s) in the β -cell include $Na_v1.3$ (Scn3a), $Na_v1.6$ (Scn8a) and $Na_v1.7$ (Scn9a), of which the latter are quantitatively more important as deletion of these $Na_v1.7$ channels leads to a loss of more than 85% of sodium current (Zhang et al. 2014). However, deletion of $Na_v1.3$ decreases insulin secretion in contrast to deletion of $Na_v1.7$ which has no effect on insulin secretion. Furthermore, the $Na_v1.7$ -governed current is inactivated by half at -105 mV while the $Na_v1.3$ current is inactivated by half at -50 mV demonstrating the role of these channels in action potential initiation and rise (Klemen et al. 2017). $Na_v1.3$ are functionally the most important sodium channel subtypes in the β -cell. Sodium current probably more involved in the AP of human beta cells than in mouse. Probably not in all beta cells in mouse contrary to human.

Potassium channels

Mouse β -cell action potentials have a long duration as discussed above, 30-40 ms up to 90 ms (Jacobson et al. 2007; Rorsman et al. 2011). In addition, invalidation of genes encoding $K_v2.1$ channels induces an increase in the amplitude and duration of action potentials. The action of GLP-1 on the increase of insulin secretion could be, among others effects, through K_v currents (Shigeto et al. 2015): GLP-1 would reduce K_v currents which would prolong action potentials and increase the entry of Ca^{2+} ions into the β -cell through VDCCs (Islam 2020). K^+ channels called ERGs ($K_v11.1$ and $K_v11.2$) modulate the frequency of action potentials. These channels allow little current to flow during the action potential but when the membrane is repolarised, they allow an outward current to flow, called the tail (or end) current, which lasts for some time and is thought to increase the interval times between successive action potentials slowing down the frequency of signals (Rorsman et Braun 2013). Inhibition of these channels increases calcium influx and insulin secretion in mice, and action potential frequency in humans (Rosati et al. 2000). In addition, these ERG channels are found in cardiac muscle cells; mutations in the genes encoding these channels are responsible for long QT syndrome, which is a cardiac rhythm abnormality and episodes of hypoglycaemia, hypokalaemia, which increases the risk of cardiac arrhythmias and therefore death (Torekov et al. 2014).

Coupling between B cells: role of Cx 36

Cells can communicate through contact between cells via connexins (Hervé et Derangeon 2013). Communicating junctions between β -cells were identified about 50 years ago using electron microscopy (Orsi, Vassalli, et Perrelet 1988) and their function was first studied by recordings with two electrodes showing waves of synchronised electrical activity induced by glucose in different cells of the same islet (Palti et al. 1996). Connexins consist of nonglycosylated proteins that oligomerise into hexamers to form connexons. These structures are concentrated in domains of membrane junctions where the intercellular space is closed to 2-3 nm wide. Connexons from one cell bind to connexons from another cell to create an intercellular hydrophilic channel for the rapid exchange of several types of cytosolic molecules such as ions and metabolites up to about 1 kD in size.

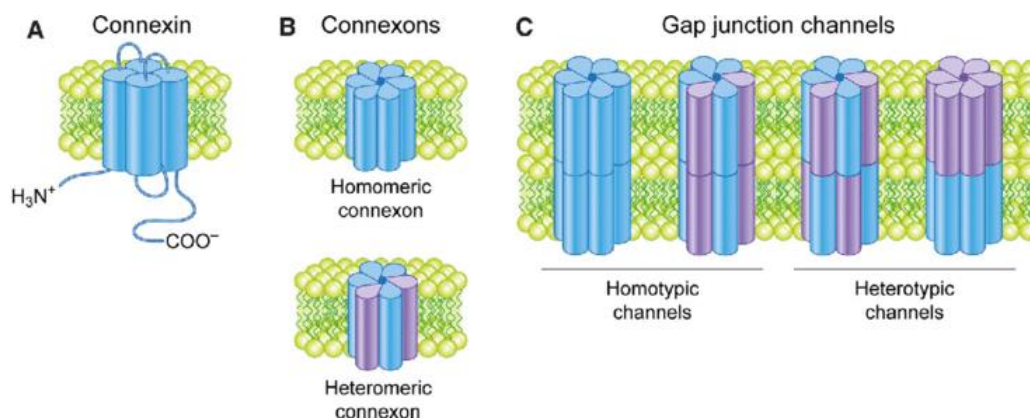


Figure 10: Structure of gap junctions. Connexins are non-glycosylated proteins with four transmembrane domains and intracellular NH₂ and COOH terminals (left). Six connexins oligomerise to form a hemi-channel, also called a connexon, which inserts into the membrane (middle). The assembly of a connexon from one cell with that of a neighbouring cell forms a channel of a communicating junction through the extracellular space allowing the bidirectional diffusion of cytosolic molecules. *Adapted from (Totland et al. 2020).*

In humans, 22 different connexins have been identified, compared to 19 in mice (Willecke et al. 2002). In the context of the study of β -cells, we are particularly interested in connexin 36 (Cx36) because their junction is composed exclusively of this type of connexin (Serre-Beinier et al. 2009). Cx36 is encoded by the gene *gjd2* which encodes a 321 amino acids protein containing a long cytoplasmic loop with 10 glycine residues and a small cytoplasmic C-terminal region containing recognition sites for protein kinases (Berchtold et al. 2017). Cx36 function can be regulated by phosphorylation (Alev et al. 2008) and this phosphorylation tends to reduce conductance (Farnsworth et al. 2016). Channels formed with Cx36 are permeable to small cationic molecules (Charpantier, Cancela, et Meda 2007) although they also allow the passage of negatively charged metabolites such as glucose metabolites or nucleotides (Meda et al. 1981). The best-known role of Cx36 in β -cells is the calcium and electrical coupling leading to synchronisation between β -cells upon glucose stimulation (Benninger et al. 2011). However, they are also thought to play a role when glucose concentration is low, by acting as a 'brake'. In fact, they reduce the spontaneous calcium responses of β -cells, which would be more reactive, thus limiting basal insulin secretion (Benninger et al. 2011). Several studies conducted on pre-diabetic mouse models suggest that Cx 36 is involved in the pathophysiology of diabetes, as a strong decrease in Cx 36 expression has been noted in pre-diabetic animals (Carvalho et al. 2012). Note that islet cells also express pannexins which may contribute to coupling (Berchtold et al. 2017).

Multicellular signals: slow potentials

Electrical coupling between the cells via connexin in a specific electrical signature called slow potential. This signal corresponds to the summation of synchronized slow depolarizations and repolarizations of coupled β cells within the islet (Jaffredo et al. 2021). SPs are distinct from APs. They correspond to the summation of slow Ca^{2+} waves that we can record intracellularly (Jaffredo et al. 2021). Slow Ca^{2+} waves are synchronized between beta cells, but not APs. Note that δ -cells are also electrically coupled to β -cells (Briant et al. 2018; Miranda et al. 2021) and may contribute to the signal. Precisely, SPs correspond to slow extracellular field potentials triggered by glucose in the islets, but also sulphonylureas or Leucine (Lebreton et al. 2015; Jaffredo et al. 2021). These field potentials result from complex spatiotemporal summations of ionic flows in the vicinity of the electrodes (Buzsáki, Anastassiou, et Koch 2012). In contrast to APs, which are single-cell signals, SPs are inhibited by pharmacological inhibitors of communicating junctions (connexions and pannexins) and are also absent from islets of Cx36 knockout mouse models.

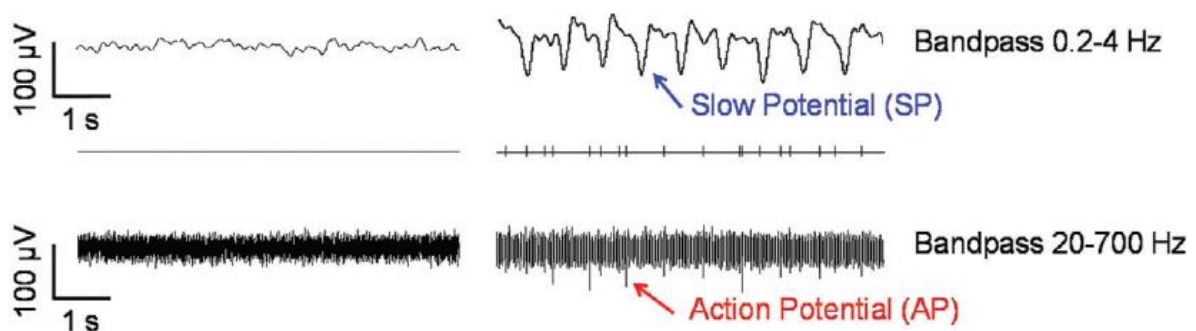


Figure 11: Representative raw and filtered recordings of islets at low glucose (non-stimulatory, 3mM) and high glucose (stimulatory, 11mM) in physiological buffered ion solution. The different time scales are shown as well as non-filtered and bandpass filtered traces (0.2–4Hz, 20–700Hz). The presence of slow potentials reflecting islet β -cell coupling are indicated. Adapted from (Abarkan et al. 2022).

A ~60% decrease in Cx36 expression specifically in β -cells is sufficient to prevent the occurrence of SPs (Lebreton et al. 2015). These signals are characterised by 3 parameters, their frequency, amplitude and shape, the latter being very difficult to characterize. The frequency of SPs is directly dependent on glucose concentration. Since they are also triggered by the closure of K_{ATP} channels by glibenclamide, their genesis may be independent of coupling factors other than ATP. SPs also involve the activation of L-type calcium channels, given their

inhibition by nifedipine. Finally, their frequency is significantly decreased by adrenaline and increased by GLP-1 with an EC_{50} (5 pM) close to physiological levels (Lebreton et al. 2015).

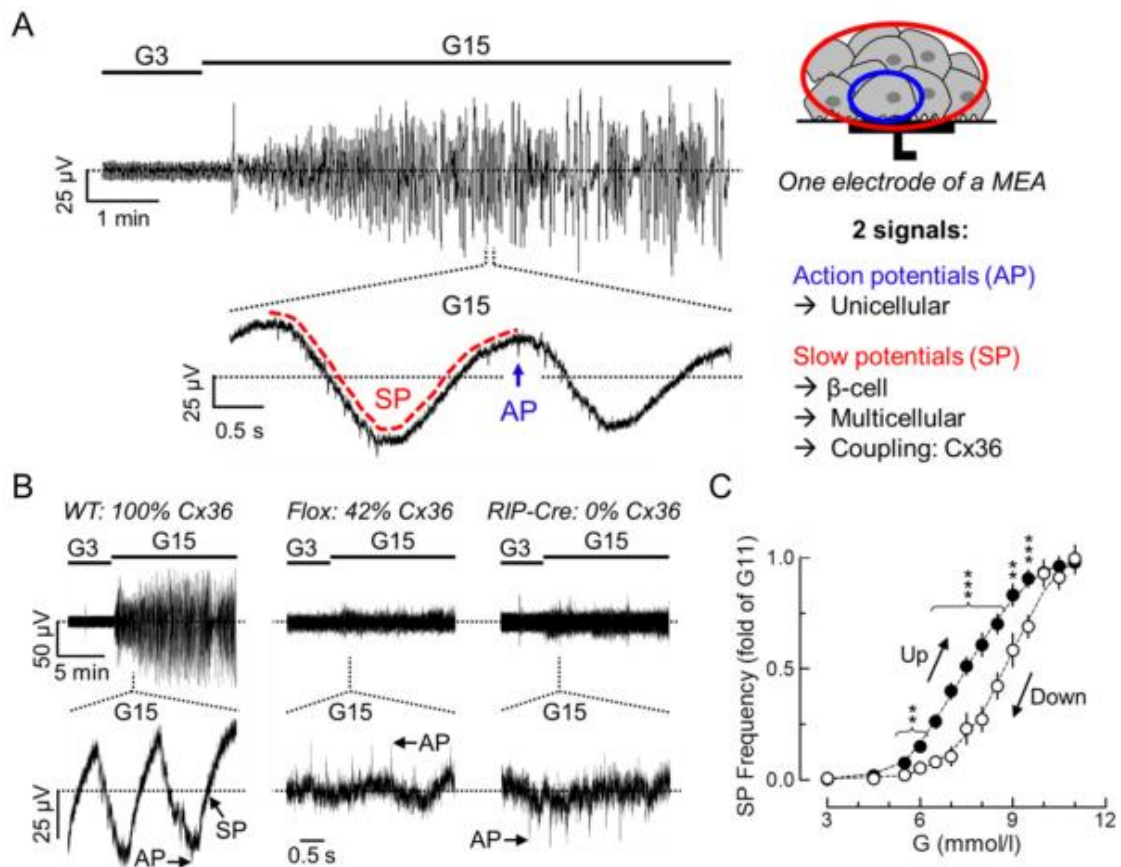


Figure 12: Slow Potentials: multicellular signals due to couplings between β -cells. (A) On the left is an extracellular recording obtained on an MEA electrode of glucose-triggered electrical activity in a mouse islet. Islets generate two types of electrical signals: APs (blue) and Slow Potentials (SPs, red). Right: APs are single-cell signals generated by the cells closest to the electrode, while SPs originate from a set of cells on and around the electrode. (B) SPs are dependent on GAP junctions formed by the Cx36. Electrical activity triggered by 15 mM glucose (G15) in islets from wild-type mice (WT, 100% Cx36) is not observed in islets from Flox (42% Cx36) and RIP-Cre (0% Cx36) mouse islets, in contrast to the WT islets which have both signals. High time resolution plots (bottom panel) show the presence of APs but no SPs in Flox and RIP-Cre mouse islets. (C) Hysteresis of SPs in response to glucose. The glucose dependence curves of the SPs frequency are not the same for increasing and decreasing glucose. The EC_{50} is shifted from 7.5 mM (on the way up) to 8.7 mM (on the way down) thus providing protection against hypoglycaemia. Adapted from (Lebreton et al. 2015).

Encoding nutrient concentration into an electrical signal

The electrical activity of β -cells is accompanied by variations in cytosolic calcium concentration required for the secretion of insulin-containing exocytosis granules. The initial calcium response to glucose starts with a small decrease due to cation uptake into the endoplasmic reticulum, followed by a peak and finally a plateau characterised by calcium oscillations (Rorsman, Braun, et Zhang 2012). Due to the coupling between cells within the islet, changes in intracellular calcium concentration will propagate throughout the islet. Even though each β -cell is more or less capable of responding to glucose, the propagation of these calcium oscillations allows for an extensive recruitment and synchronization of the insulin-secreting cells of the pancreatic islet. After a meal, blood glucose levels raise from a basal concentration of 5 mM to 8 mM in about 30 min in humans (Frayn 2013). This increase in glucose induces insulin secretion within a few minutes according to a particular profile that can be described as biphasic (Nunemaker et al. 2006) and is clearly detectable in vivo. This biphasic insulin secretion profile consists of an initial transient peak (5-15 min) followed by a decrease in secretion called the nadir, and then a second continuous phase of secretion or plateau phase, which is lower than the peak of the first phase but still 10 times higher than the basal secretion (Henquin et al. 2006). During this second plateau phase, oscillations in insulin secretion occur at a rate of about every 5 min (Nunemaker et al. 2006). In vivo insulin reaches the liver via the portal vein during the first phase, allowing an immediate reduction in blood glucose levels, notably by inhibiting hepatic glucose production. When the liver is saturated with insulin (it takes up 2/3 of it), the second phase targets more distant tissues such as muscle or adipocytes as long as blood glucose remains high (Tokarz, MacDonald, et Klip 2018). Pulsatile insulin secretion avoids a loss of insulin sensitivity of the target tissues in the liver, and ultimately the development of insulin resistance. This biphasic secretion profile persists ex vivo in perfused pancreas and isolated islets (Henquin et al. 2006) proving that the origin of these kinetics lies in the micro-organ itself. Both phases of insulin secretion can be induced by glucose, while sulphonylureas or potassium chloride (KCl) only induce a monophasic secretion profile (Henquin 2000). The biphasic profile tends to disappear when the glucose concentration increases too sharply, e.g. 2 mM to 25 mM glucose, with at best only a minor first phase (Del Prato 2003; Huang et al. 1995). The loss of a biphasic profile is observed in diabetic patients, particularly in type 2 diabetes, who show an almost complete absence of the first phase of

insulin secretion, with a decrease in the second phase (Groop et al. 1991). This change can even be observed very early in T2D.

Stimulus and secretion coupling

Glucose-stimulated insulin secretion proceeds through several steps, including glucose entry into the β -cell, metabolism, production of coupling factors such as ATP, activation of ion channels, Ca^{2+} entry and finally exocytosis of insulin granules. The increase in cytosolic calcium subsequently triggers the exocytosis of large, dense-core vesicles containing insulin and the hormone enters the bloodstream to its target organs in order to lower blood glucose levels. As a result, a feedback control takes place: glucose entry into the β -cell decreases, thereby reducing glucose metabolism having the effect of reopening K_{ATP} channels and inhibiting insulin secretion (Rorsman et Ashcroft 2018a).

α cell

α -cells are electrically active, like the beta cell but at low glucose (Lebreton et al. 2015) and their action potentials promote the secretion of glucagon (Rorsman et Braun 2013). The resting potential of α -cells is very low, with the initiation of action potentials starting at -60 mV at low glucose (Quesada et al. 2008; Ramracheya et al. 2010)

The α -cells also contain the K_{ATP} channel as others glucose sensitive cells, such as β - and δ -cells (MacDonald et al. 2007). Pharmacological experiments (K_{ATP} channel inhibitor tolbutamide and K_{ATP} channel activator diazoxide) have shown that glucagon secretion is inhibited by glucose, as it completely closes K_{ATP} channels (similar to the effect of tolbutamide on K_{ATP} channels) (Bokvist et al. 1999). Maximum inhibition of glucagon secretion by glucose is observed at a glucose level of 6 mmol/l (Ramracheya et al. 2010). At low glucose, membrane depolarisation will activate Ca_vs , which are responsible for the intracellular calcium oscillations required for exocytosis of glucagon granules (Barg et al. 2000). The action potentials of the α -cell also depend on Na_v activation. The use of TTX (Na_v channel blocker) strongly inhibits glucagon secretion. The Na_v channels are involved in the rising phase of the action potential and are rapidly inactivated (1-10 ms) as soon as the membrane potential falls to -60 mV

(MacDonald et al. 2007). Note that the physiological inhibition of α -cells by glucose seems to result from a cellular mechanism and from an inhibitory input via somatostatin, whose secretion is stimulated by elevated glucose (Gylfe et Gilon 2014).

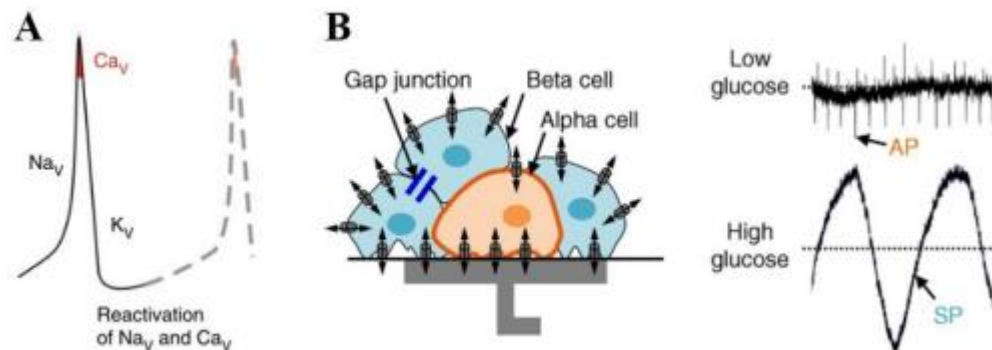


Figure 13: (A) Sequential opening of action potential-dependent ion channels in the glucagon-secreting cell. (B) The α -cell is electrically active at low glucose and generates rapid action potential (AP) signals. It is silent at high glucose (absence of APs) compared to β -cells which exhibit slow potentials (SPs). According to (Rorsman et Braun 2013; Lebreton et al. 2015).

For the other potassium channels which are, unlike the K_{ATP} channel, voltage dependent (K_v), the α -cell also expresses them (Craig, Ashcroft, et Proks 2008). They activate following depolarisation of the membrane, during the action potential, and allow repolarisation of the membrane potential.

δ -cell

Pancreatic δ -cells mainly release somatostatin, a hormone that is also released in a small amount from cells in the pylorus and duodenum (Arimura et al. 1975) and especially in the hypothalamus (Hökfelt et al. 1975). There are two types of somatostatin: somatostatin-14 and somatostatin-28. Both forms of somatostatin are derived from the precursor pre-prosomatostatin (116 amino acids) which is cleaved into prosomatostatin (92 amino acids). Prosomatostatin undergoes C-terminal post-translational processing to generate somatostatin-14 and somatostatin-28. Both peptides are very short-lived and have a half-life of 1min in circulation. While somatostatin-28 is the dominant isoform elsewhere in systemic secretion, the pancreatic δ -cells secrete somatostatin-14, which is stored in secretory granules (Breton et al. 2015) and released by Ca^{2+} -dependent exocytosis.

Therefore δ -cell secretion does not contribute to levels of circulating somatostatin but plays an important paracrine role on β -cell and α -cell secretory activity (Rorsman et Huising 2018).

Morphologically, δ cells extend projections that can be more than 20 μm long allowing them to form a large paracrine network (Brereton et al. 2015). Although they represent only 5% of the endocrine cell population within the islet, these projections allow them to establish contacts with each other, but also with a number of other endocrine cells in the islet.

The δ -cells are excitable cells like the α - and β -cells and their mode of secretion of somatostatin has much in common with that of insulin by the β -cells. This can be explained by their common origin, as they both derive from the same progenitor cell (Sosa-Pineda et al. 1997). δ cells are equipped with ATP-sensitive potassium channels (K_{ATP}) (Zhang et al. 2007). Glucose also stimulates somatostatin secretion by mechanisms independent of K_{ATP} channels.

The electrical activity of δ cells is coupled to that of β cells (Briant et al. 2018). Moreover, factors released from neighbouring β cells (such as GABA and urocortin-3) amplify the glucose-induced effects on δ cell electrical activity/somatostatin secretion.

As an important paracrine regulator within the islet somatostatin controls and coordinates insulin and glucagon secretion rates, exerting an inhibitory action on α and β cells (Rorsman et Huising 2018; Hauge-Evans et al. 2009). The effects of somatostatin are mediated by the activation of somatostatin receptors that are coupled to the inhibitory G protein and lead to the suppression of electrical activity and exocytosis of α - and β -cells (Gromada et al. 2001). Interestingly somatostatin is secreted already at lower glucose concentrations as compared to β -cell insulin, i.e. as early as 3 mM glucose (Del Guercio et al. 1976) and this secretion increases in a linear and dose-dependent manner, up to 20mM glucose. Moreover, somatostatin secretion evoked by a square pulse of insulin (20 mM) is slightly delayed as compared to insulin secretion (Strowski et al. 2000).. This suggests a tonic role throughout physiological glucose levels and a kind of feedback that may be compared to inhibitory interneurons in the spinal cord.

γ cell

γ -cells secrete pancreatic polypeptide (PP) and are the least studied. PP secretion by γ -cells plays an important part in the pancreas-gut-central nervous system regulatory axis (Holzer, Reichmann, et Farzi 2012). The peptide secreted after a meal is regulated by the vagus nerve and enteric nervous system (acetylcholine and adrenaline (Field, Chaudhri, et Bloom 2010; Schwartz et al. 2000) and stimulated by incretins (such as GIP) (Chia et al. 2014) lipids and

amino acids (Field, Chaudhri, et Bloom 2010). In rodents and humans, PP acts as an anorectic hormone: it inhibits stomach and intestinal motility to slow down the digestive process, thus regulating satiety by reducing appetite and food intake (Batterham et al. 2003).

PP cells express potential-dependent calcium channels, as well as the K_{ATP} channel. Work measuring intracellular calcium levels in isolated mouse islets has shown that glucose activates γ cells (Liu, Seino, et Kirchgessner 1999). At low glucose, PP directly inhibits α cells via its PPYR1 receptors, and indirectly inhibits β and δ cells (Aragón et al. 2015) demonstrating that PP cells participate in intra-islet regulation.

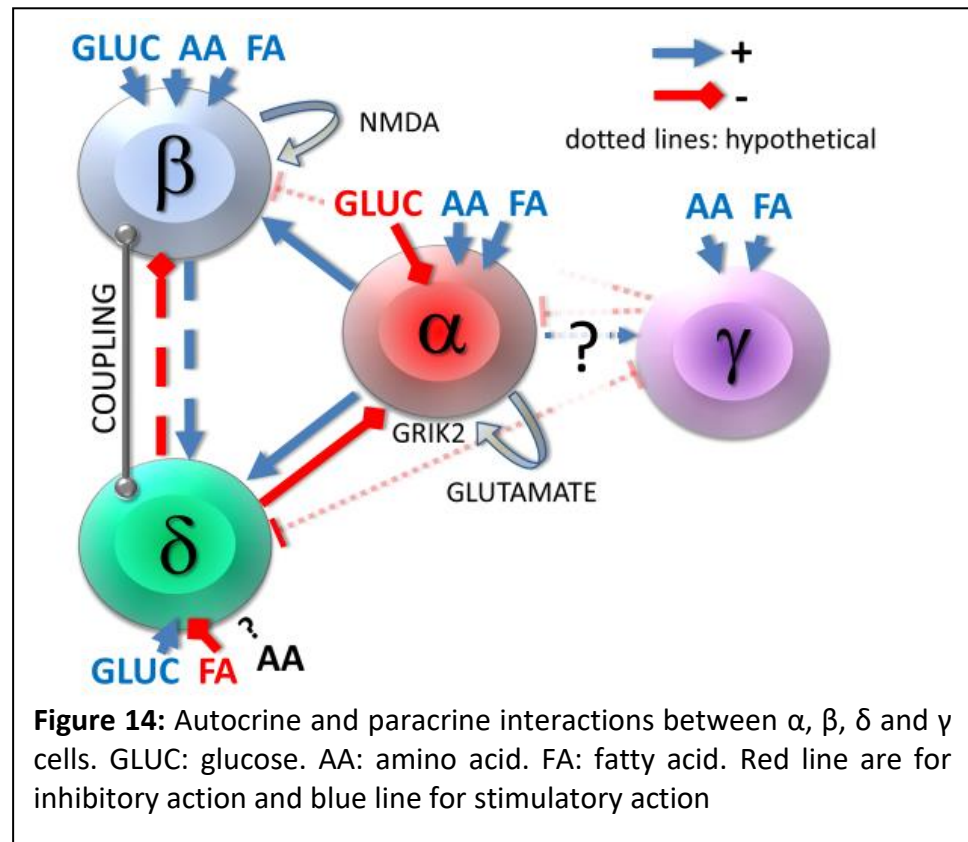
ϵ cell

The last endocrine cell type corresponds to the ϵ cells which play a role mainly during development since they are found in very small numbers within mature islets (maximally about 1/islet) (Andralojc et al. 2009) and many islets are devoid of them. However, in-utero, for human, they represent 30% of the islet mass, and this percentage will decrease to 5% after birth (Andralojc et al. 2009). They secrete the hunger hormone ghrelin, which is also found in the cells of the gastrointestinal tract (Date et al. 2000). Although the role of ϵ -cells in islets in adults has yet to be studied, it has been shown from a comparison of healthy and type 2 diabetic human islets that this hormone decreases insulin secretion, and that ghrelin expression in islets is reduced in diabetics (Lindqvist et al. 2020).

2.3 interaction between the different cell types:

The pancreatic islet is a complex micro-organ formed by a network of sensor capable of interacting

together dynamically to maintain glucose homeostasis (Gosak et al. 2018). Islets truly act as a systemic glucostat since they impose depending on the different stimuli received, normoglycemia (4 to 6 mmol)



(Rodriguez-Diaz et al. 2018). Studies on islets in-vitro have allowed the identification of regulatory mechanisms existing within the micro organ, involving ions, hormones and communications between the different cell types (Briant et al. 2017; Cadwell et al. 2017; DiGruccio et al. 2016; Rorsman et al. 2011). Each cell type receives a multitude of endocrine, paracrine, neural and nutrient stimuli, but despite their same embryonic origin during development (duodenum), their sensitivity to these stimuli is different (Noguchi et Huising 2019). The arrangement of these different endocrine cells within the islet, with each other and with other non-endocrine cells is crucial to both receive external and paracrine stimuli, but also to efficiently deliver their own signals in return (Henquin 2021; Koh, Cho, et Chen 2012). The interaction pathways can be direct between cell types or indirect via another cell type. For the physiological functioning of the micro-organ, different positive and negative loops are necessary. These fine interactions in the islet allow an optimal adapted physiological response.

2.4 Innervation:

The islets are controlled by the central nervous system, which plays a role in the hormonal secretion of the islets during the stress phase or when a meal is taken (Rodriguez-Diaz et Caicedo 2014; Rodriguez-Diaz et al. 2018). Sympathetic stimulation, responsible for metabolic/physiological responses during an immediate reaction or stress state ("fight or flight"), will lead to increased glucagon secretion and decreased insulin and somatostatin secretion through the presence of distinct adrenoreceptor isoforms on endocrine cells (Rodriguez-Diaz et Caicedo 2014; Brunicardi, Shavelle, et Andersen 1995). The parasympathetic innervation, on the other hand, will be mobilised for digestion for example ("rest and digest") by secreting acetylcholine which will potentiate insulin secretion but also glucagon and inhibit somatostatin secretion (Alvarsson et al. 2020).

Innervation of the islets seems not to be the same across the different species although the questions has not been completely settled. Indeed, studies have shown that mouse islets are much more innervated than human islets (Rodriguez-Diaz, Dando, et al. 2011), whereas other work has reposted that human islets exhibit much greater autonomic innervation (Tang et al. 2018). However, it is well established that in mice, α -cells and blood vessel smooth muscle cells are innervated by sympathetic fibres (Chiu et al. 2012), while parasympathetic fibres innervate all pancreatic endocrine cells. In humans, parasympathetic fibres innervate not only endocrine but also exocrine cells, and sympathetic fibres make contact only with smooth muscle cells (Dolenšek, Rupnik, et Stožer 2015). Acetylcholine, whether of neuronal (mouse) or paracrine (human) origin potentiates insulin secretion via the $G_{\alpha q}$ -coupled muscarinic type 3 cholinergic receptor (CHRM3) present on β -cells (Gautam et al. 2006).

2.5 Vascularization:

The islets of Langerhans are highly vascularised, which enables them to detect variations in blood sugar levels according to nutritional status and to deliver into the bloodstream the various pancreatic hormones that will then act on the various tissues. They are more vascularised than the exocrine pancreas and have a 5-10 times higher blood flow, not least because they have their own arterioles, thus a separate circulation from the exocrine pancreas

(Jansson et Carlsson 2019). The vascularisation of the islet has an important role throughout the life of the individual but also during development in utero. Indeed, the interactions between endothelial cells and the developing pancreatic epithelium are critical to establish optimal islet vascularisation and maintain a mass of β -cells. Endothelial cells provide signals necessary for differentiation into β -cells (Lammert, Cleaver, et Melton 2001). In addition, they regulate the expression of transcription factors involved in pancreas development, which are necessary to maintain the multipotent progenitor population and induce differentiation (Yoshitomi et Zaret 2004).

Blood arrives via the splenic artery and the islets are exposed to systemic glucose concentration. It is drained by the splanchnic veins which empty into the hepatic portal vein. The intra-islet vascular system allows for remote cellular interactions. The direction of flow is important for regulating hormone secretion in the islets. It has been shown that a specific direction of perfusion exists in rats and humans, namely: β -cells first, then α -cells and finally δ -cells (Samols et al. 1988; Samols et Stagner 1988).

Intra-islet capillaries are fenestrated and thick, denser than capillaries in exocrine tissue (Murakami et al. 1997). The β -cells communicate directly with these capillaries, allowing a rapid response to increases in blood glucose by secreting insulin directly into the bloodstream (Bonner-Weir et Orci 1982). Intra-islet capillaries also connect to endocrine cells for gas exchange, nutrient supply and elimination of cellular waste. In addition, blood vessels play an important role in providing non-nutritional signals to the islets, creating a vascular niche for optimal β -cell development and function (Nikolova, Strilic, et Lammert 2007).

Islet blood flow is subject to variation due to endothelial mediators that will affect vessel status, but also the nervous system and gastrointestinal hormones such as incretins and adipokines (Dolenšek, Rupnik, et Stožer 2015). The degree of vascularity appears to alter the ability of cells to secrete insulin, with rich vascularity allowing for better β -cell function as well as greater metabolic activity (Ullsten, Lau, et Carlsson 2015).

3 Diabetes Mellitus

The demographic transition that has affected all human populations for about half a century has resulted in an epidemiological transition characterised by an increase in the incidence of chronic diseases, such as cancers or cardiovascular diseases, and their risk factors (Yach,

Kellogg, et Voute 2005). For the past 10 to 20 years, the phenomenon of "globalisation" has also contributed to the standardisation of lifestyles in a way that which favours the increase of obesity and sedentary lifestyle (Popkin et Gordon-Larsen 2004). In this context, the incidence of diabetes is rising sharply in all countries of the world, even taking the form of an epidemic of diabetes (Zimmet 2000). The global prevalence of diabetes is steadily increasing with an estimated 578 million diabetics in 2030 (« IDF Atlas 9th Edition and Other Resources » s. d.). Diabetes is a serious chronic disease with a heavy human and economic burden that is responsible for 4.6 million deaths per year worldwide, it represents 1 death every 7 seconds and an economic cost of US\$ 612 million per day in the United States (« IDF Atlas 9th Edition and Other Resources » s. d.).

3.1 The different types of diabetes:

The term "diabetes" refers to "a group of metabolic diseases characterised by hyperglycaemia resulting from defects in the secretion or action of insulin, or both combined" (*definition by the American Diabetes Association*). This hyperglycaemia is associated, to varying degrees, with long-term complications, particularly affecting the eyes, kidneys, nerves, heart and arteries (Sladek 2018). It is a disease with a very heterogeneous clinical presentation existing in several forms. The two main forms are based on the absence (type 2) or presence (type 1) of antibodies directed against insulin-secreting cells. More recently a discussion has been raised whether there are really two distinct subtypes or different situations in a kind of continuum (Prasad et al. 2022; Ahlqvist, Prasad, et Groop 2020; Pigeyre et al. 2022). A series of publications were able to identify 4 subgroups, There are also other forms of diabetes or diabetic conditions, such as gestational diabetes, which is usually transient but can sometimes persist after pregnancy or iatrogenic diabetes (due to certain medications, pancreatitis, haemochromatosis, etc.) (Redondo, Steck, et Pugliese 2018).

If we look at the profile of patients affected by diabetes mellitus, 60% are over 65 years of age and we can identify few risks factors such as overweight or family history of diabetes (IDF diabetes atlas). Type 1 diabetes is rarer than type 2 diabetes, around 10 % of the total cases of diabetes mellitus. In contrast to type 2 diabetes, it is recognised by clinical signs that are often intense (polyuria, polydipsia, weight loss), and occurs preferentially in childhood and

adolescence or in young adults (IDF Diabetes atlas 2019). Although it accounts for 5-10% of all diabetes cases, type 1 diabetes has a particularly high economic and social as lifelong care is required and the disease occurs during the working age.

The management of type I diabetes involves rigorous life management, the administration of insulin and self-monitoring of the patient's blood glucose levels with the help of various technologies. Concerning the latter two elements it is important to underline that the cost of insulin has increased by 117% in 10 years in the United States (Simeone et al. 2020) . More broadly, in a 2020 study by Sussman and colleagues, it was noted that in the USA, there was an \$813 billion difference in health care costs between patients with type 1 diabetes and those with other forms of diabetes. This represents a high burden, requiring new management solutions to reduce these costs and improve patients' quality of life. In this thesis, I will developed only type 1 because I have worked on a new sensor for T1DM patients.

3.2 History of type 1 diabetes:

Type 1 diabetes is a disease that has affected populations throughout History, and whose characteristics have been brought to light as human knowledge has progressed.

As early as 3000 BC, in Egypt, we find, annotated by a scribe on the famous Ebers papyrus, the first descriptions of the main clinical characteristics of type 1 diabetes (Metwaly et al. 2021) . Indeed, it is mentioned that some people suddenly began to drink and urinate abundantly. About 100 years before our era, the name diabetes was first uttered by Aretaeus of Cappadocia. The term diabetes, which comes from the Greek word “διαβήτης”, "to pass through", was intended to characterise people with a disease that led to rapid death in young people (Ahmed 2002), the form of diabetes we now call T1D. It was not until 1500 AD that Paracelsus discovered a substance in the urine of diabetics that appeared as a white powder. At that time, this substance, which was glucose, was mistaken for salt. One hundred years later (1600 AD), it was discovered that the urine of diabetics tasted sweet. The term diabetes mellitus was first used. It took another 100 years (1700 AD) for Thomas Cawley to discover that the substance found in abundance in the urine of diabetics was a sugar (King et Rubin 2003). In 1869 AD, Langerhans discovered the pancreatic islets (Langerhans 1869), and the French physician Edouard Laguesse proposed to name them after him. At the time of the discovery of these small tissue structures with a total mass of no more than 2 g, equivalent to

the volume of half a thimble. It was not until several decades later that von Mering and Minkowski demonstrated that total removal of the pancreas led to diabetes (v. Mering et Minkowski 1890). In 1902, Eugene Opie discovered that diabetics have a degeneration of the pancreatic islets (Opie 1901). From this date onwards, the pace of discoveries continued to accelerate, initially without general success such as the first isolation of a pancreatic insulin-containing extract by Zülzer in Berlin in 1908, named and patented with Schering as a comatol (which lead to hypoglycemia) (Zueler, 1908), the isolation and use of extracts by Paulescu in Bucarest (1916), whose publications were retarded by the first World War, to the work of Kleiner in the US (Kleiner 1919) and finally the isolation of insulin in 1921 by Banting, Best and Collip (« Banting FG, Best CH, Collip JB, Campell WR, Fletcher AA (1922) » 2010) to the elucidation of its amino-acid sequence by Sanger as the first protein fully sequenced (Sanger et Thompson 1953) , its crystal structure by Dorothy Hodgkin (Blundell & Cutfield, 1971) which paved the way for the first recombinant drug in 1972 by Boyer and Goeddel at Genentech and in the 1990s the production of short-acting and then long-acting insulin analogues (Monnier et Colette, 2019). Directly or indirectly 4 Nobel prizes had been attributed to insulin.

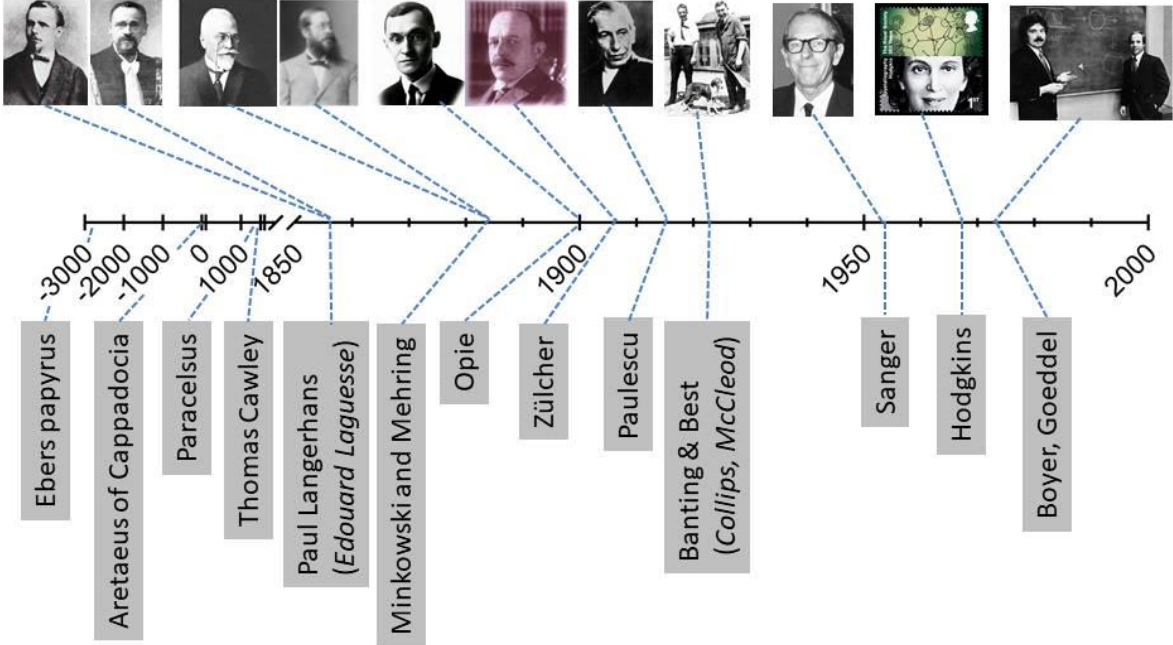
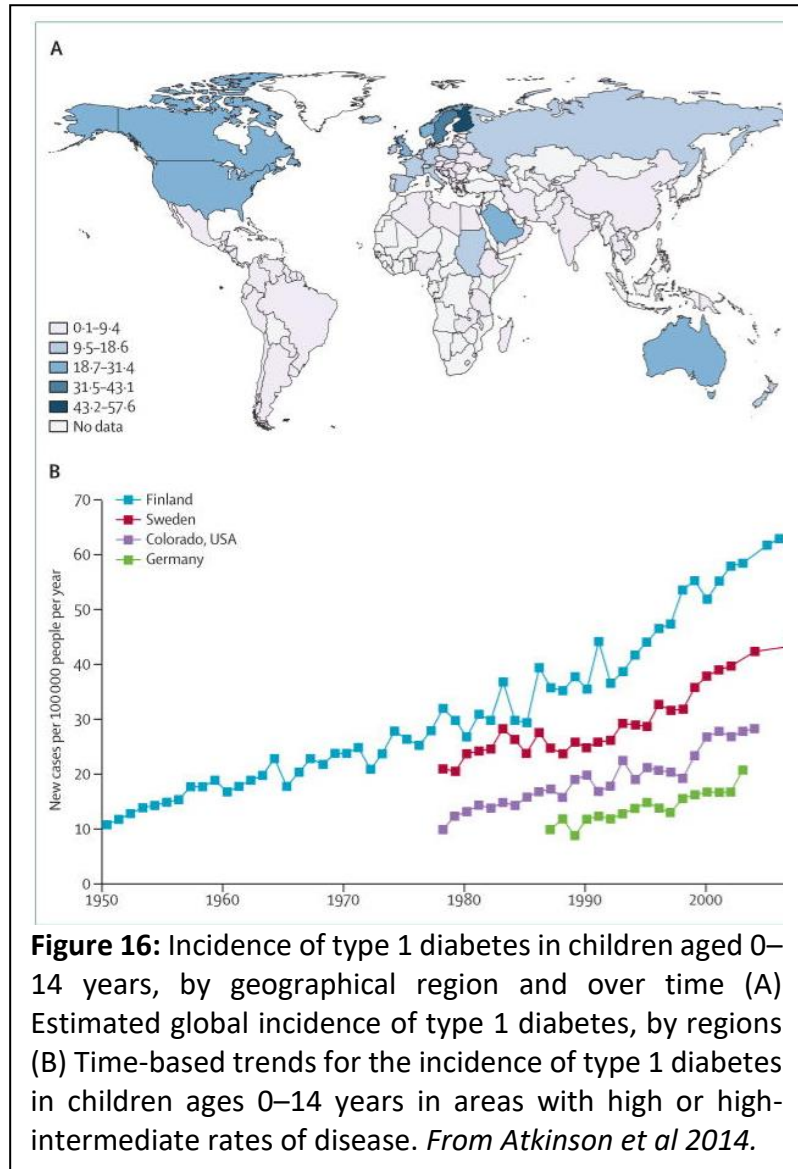


Figure 15: Time line of the diabetes discoveries, from Ebers Papyrus to Boyer and Goeddel. Adapted from a course of Pr Jochen Lang, University of Bordeaux

3.3 Type I diabetes: a complex autoimmune disease:

T1D is a metabolic disorder with autoimmunity targeting insulin-producing β cells in the pancreas, leading to a severe paucity of endogenous insulin and subsequent hyperglycemia (Atkinson, Eisenbarth, et Michels 2014). T1D was initially recognized as a chronic disease among children and young adolescents but over time it has become apparent that T1D can occur at any age (Atkinson, Eisenbarth, et Michels 2014). The incidence of childhood T1D has been growing globally since the past few decades though stagnation has also been observed in a small number of regions around the world (Berhan et al. 2011; Bruno et al. 2013; Haynes et al. 2015).



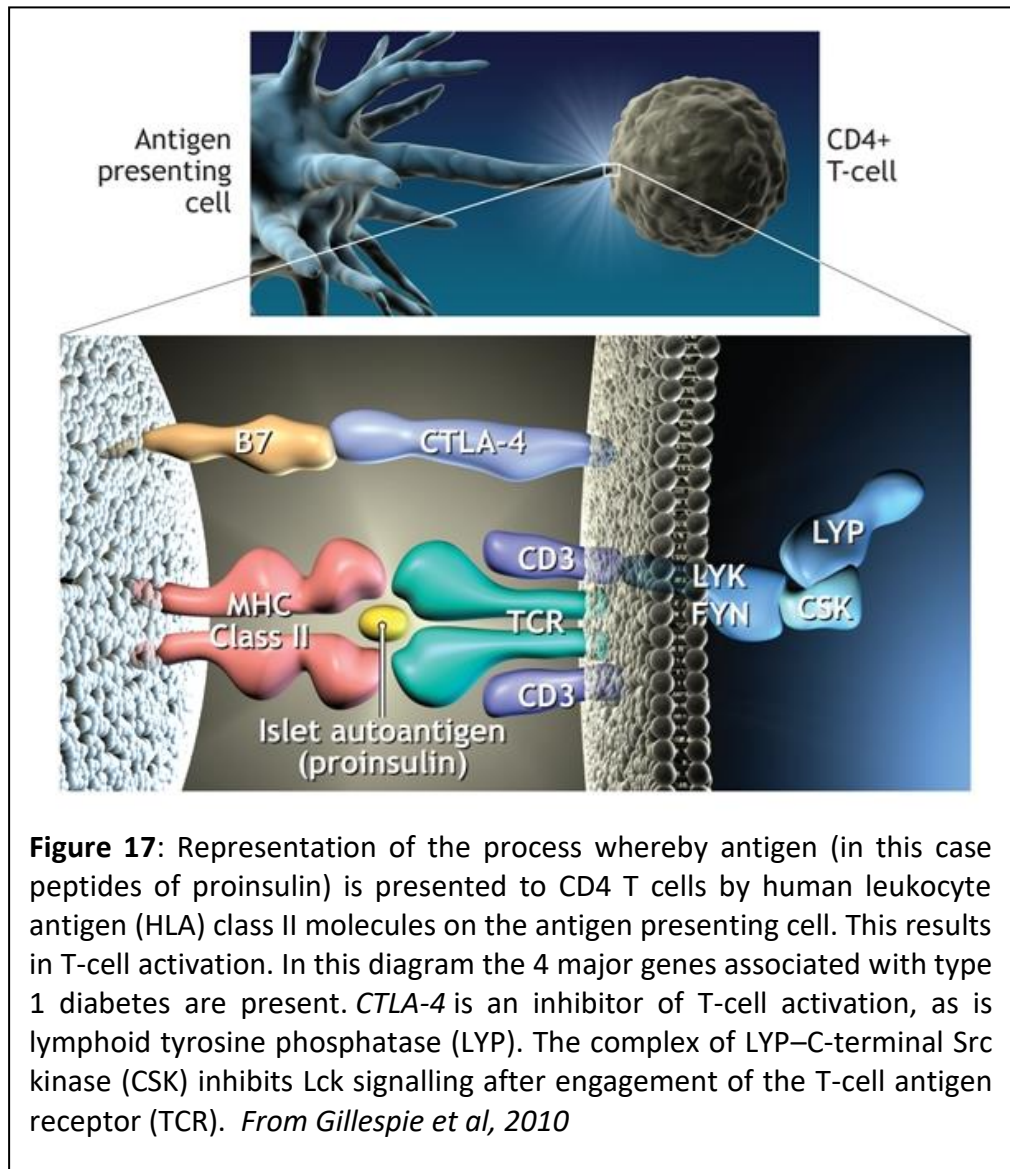
Type 1 diabetes is characterized by autoimmune destruction of insulin-producing β cells in the pancreas by CD4+ and CD8+ T cells and macrophages infiltrating the islets (Foulis, McGill, et Farquharson 1991). The causes of T1D are not fully understood although they received increased attention during the last two decades. The disease appears to result from an

interplay between genetic predisposition, environmental factors and microbiome, and individual characteristics (DiMeglio, Evans-Molina, et Oram 2018).

Like other organ-specific autoimmune diseases, type 1 diabetes has human leukocyte antigen (HLA) associations. The HLA on chromosome 6 was the first locus shown to be associated with the disease by candidate gene studies (Cudworth et Woodrow 1975; Nerup et al. 1974) and is considered to

contribute about half of the familial basis of type 1 diabetes (Todd 1995; Risch 1987). Two combinations of HLA genes (or haplotypes) are of particular importance:

DR4-DQ8 and DR3-DQ2 are present in 90% of children with type 1

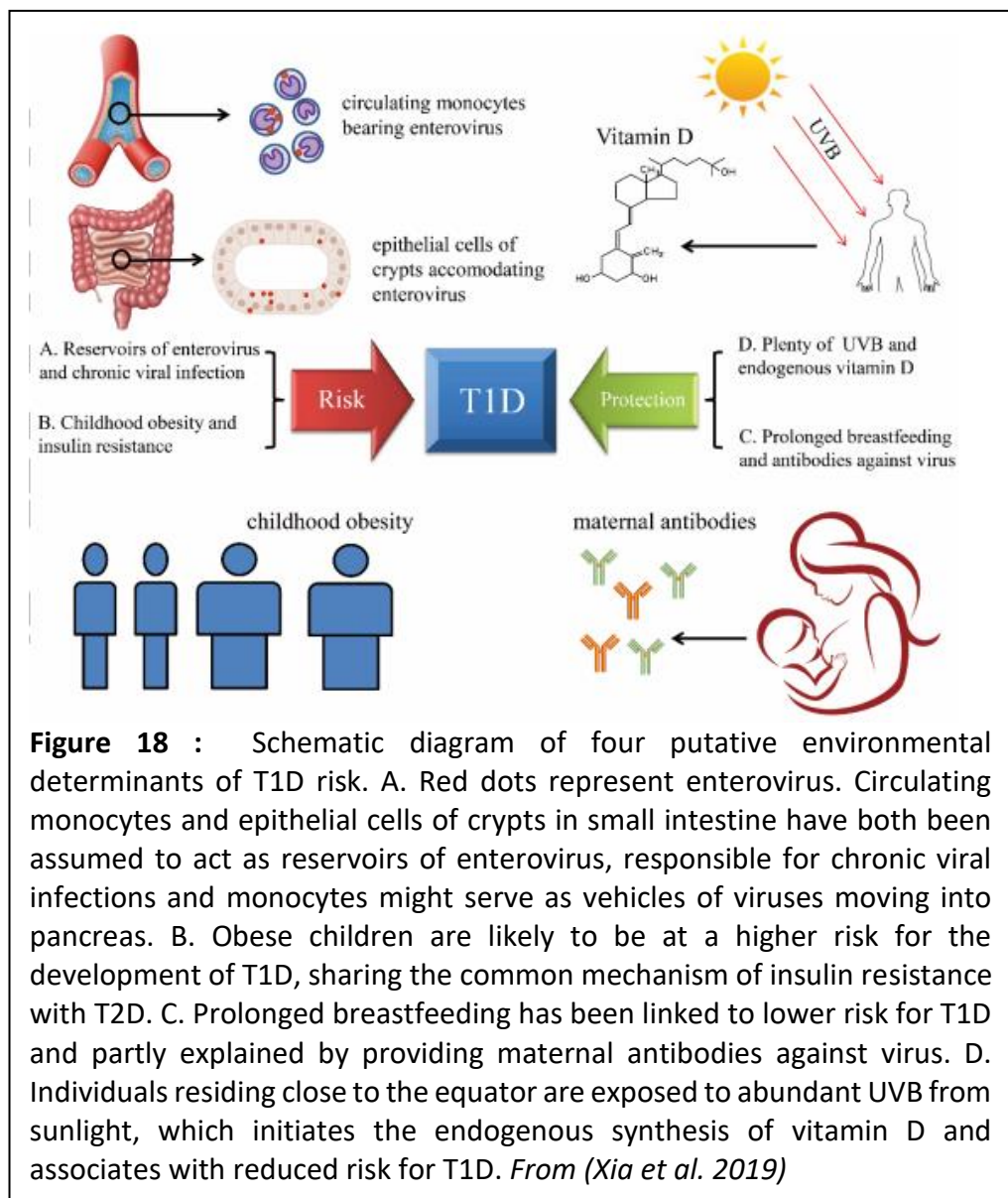


diabetes (Devendra et Eisenbarth 2003). The genotype combining the 2 susceptibility haplotypes (DR4-DQ8/DR3-DQ2) contributes the greatest risk of the disease and is most common in children in whom the disease develops very early in life (Caillat-Zucman et al. 1992).

Candidate gene studies also identified the insulin gene on chromosome 11 as the second most important genetic susceptibility factor, contributing 10% of genetic susceptibility to type 1 diabetes (Bell, Horita, et Karam 1984). Shorter forms of a variable number tandem repeat in the insulin promoter are associated with susceptibility to the disease, whereas longer forms are associated with protection (Bennett et al. 1995). Demonstration of increased expression of insulin (mRNA) in the thymus of people with “long” or protective repeats — which suggests more efficient deletion of insulin-specific T cells during induction of central tolerance — provides an attractive potential mechanism for the role of the insulin gene in type 1 diabetes (Vafiadis et al. 1997; Pugliese et al. 1997).

Genetic studies have highlighted the importance of large, well-characterized populations in the identification of susceptibility genes for type 1 diabetes. Some genes will have a relatively

minor individual impact on susceptibility to disease but could nevertheless provide more clues to future preventive therapies. The genes for intercellular adhesion molecule (ICAM) and vitamin D are candidates.. Some epidemiologic



observations support a protective role for vitamin D in type 1 diabetes. Maternal intake of vitamin D in pregnancy and high doses of vitamin D supplements early in life have been shown to protect against islet autoimmunity in offspring, (Fronczak et al. 2003; Hyppönen et al. 2001) whereas children with a diagnosis of rickets in the first year of life have been found to have a 3-fold increased risk of type 1 diabetes later in life (Mathieu et Badenhoop 2005).

Studies in most populations confirm an increase in the incidence of type 1 diabetes (Xia et al. 2019), these changes are too rapid to be caused by alterations in the genetic background and are likely the result of environmental changes.

Despite that genetic susceptibility represents a major determinant of T1D risk, genetics alone can not afford a satisfactory explanation for the dramatic changes in T1D incidence. Moreover, the rising tide of incidence has been accompanied by a lower percentage of human leukocyte antigen (HLA) genotype DR3/DR4 which confers the greatest risk for T1D and a higher percentage of moderate-risk genotypes (Fourlanos et al. 2008) compared to those detected decades ago, implying a less important role for genetic predisposition but an amplifying environmental pressure.(Hermann et al. 2003; Gillespie et al. 2004).

Identification of the potential environmental factors proved to be difficult. The most advocated candidates are viruses, with enteroviruses, (Hyöty 2002) rotavirus (Honeyman et al. 2000) and rubella virus being the usual suspects. In Western cultures, the developing immune system of the infant is no longer exposed to widespread infection, which may contribute to the current increases in incidence observed in atopic and autoimmune disease.

Large studies are required to address the role of environmental factors in susceptibility to type 1 diabetes. An international consortium — the Environmental Determinants of Diabetes in the Young (TEDDY) — has been established to follow several thousand babies with high-risk HLA genotypes from birth until adolescence to identify infectious agents, dietary factors or other environmental factors that trigger islet autoimmunity in genetically susceptible people.

More than 30 years ago, it was recognized that antibodies in sera from patients with type 1 diabetes could bind to sections of pancreatic islets. These antibodies were termed islet cell antibodies. The 3 principal autoantigens identified are islets or even b-cell specific proteins, namely glutamic acid decarboxylase (GAD 65),(Baekkeskov et al. 1989) a protein tyrosine

phosphatase-like molecule (IA-2)(Lan et al. 1996) and insulin (Palmer 1987). Studies involving first-degree relatives gave insight into the potential usefulness of islet cell antibodies as predictors of future disease, but the immunofluorescence assay proved difficult to standardize. About 90% of people with newly diagnosed type 1 diabetes have autoantibodies to at least 1 of these 3 antigens. It is in the pre-diabetes phase that islet autoantibodies have been most useful. They appear to be already present in most cases of future diabetes by the age of 5 years (Ziegler et al. 1999) This indicates that the autoimmune process “smoulders” subclinically for many years in the majority of patients and that clinical symptoms do not appear until up to 80% of β cells have been destroyed (Gillespie 2006).

A way for intervention strategies to delay or slow the autoimmune process has been given by the observations that islet cell autoantibodies predict autoimmune diabetes in first-degree relatives (Bingley, Williams, et Gale 1999), that the presence of 2 or more autoantibodies in people in the general population is highly predictive of future disease (Bingley et al. 1997) and that persons who have IA-2 antibodies are at very high risk (Decochez et al. 2005; Achenbach et al. 2004).

Prevention of the disease process before the appearance of islet cell autoantibodies would be ideal, but the accuracy of prediction based on the presence of genes associated with type 1 diabetes is limited (Gillespie et al. 2004).

3.4 Complications of type 1 Diabetes:

The glycaemic disorders of type I diabetics can be considered according to two components: chronic sustained hyperglycaemia leading to long-term complications and glycaemic variability which has consequences in the daily life of patients (Bunn et al. 1975; Sacks et al. 2012).

They will gradually set in, insidiously, silently, and only a regular and appropriate follow-up will allow their detection. The likelihood of developing long-term complications depends on many factors: quality of blood glucose control, genetic predisposition, gender, dietary balance, regular physical activity, smoking, etc (Sun et al. 2011). These complications are mainly due to damage of the endothelium of the blood vessels. Most common complications in TD1 patients are retinopathy which can lead to blindness (Monson et al. 1986), cardiopathy

(Colom et al. 2021), nephropathy (Wheelock et al. 2017) and the so-called “diabetic foot” due to mixed damage to the nerves and arteries of the lower limbs. Over time, deformities and injuries can occur (Lauri et al. 2020). This loss of sensation and reduced blood flow can lead to poor healing of wounds on the feet of diabetic patients and eventually necessitate amputation of the affected limb (Hicks et al. 2016). Diabetes is the leading cause of non-traumatic amputation worldwide (IDF, Diabetes Atlas 2019).

In non-diabetic subjects, fasting blood glucose appears to be around 5.5 mmol/L, with postprandial glucose peaks rarely exceeding 7.7 mmol/L. The blood glucose level of a non-diabetic individual should never exceed 9.9 mmol/L, which is the glycosuric threshold in a normal individual (Polonsky et al. 1988). In type 1 diabetics, blood glucose profiles are profoundly disturbed with alternating "peaks" and "troughs" that are more or less intense. The peaks correspond to the postprandial periods but they can also occur unexpectedly without any food intake (Leiter et al. 2005). The "troughs", which can lead to more or less severe hypoglycaemia, generally occur between meals: in the middle of the night, before lunch or dinner (Monnier et Colette 2019). The occurrence of these dips is sometimes unpredictable. In some cases, hypoglycaemia occurs in the period following food intake as a kind of rebound effect. This lack of a "quiet" blood glucose profile is due to the lack of endogenous insulin secretion (Monnier et al. 2007). The subject is totally dependent on the resorption of injected or infused insulins and life events such as emotions, annoyances, meals and physical activity are no longer compensated by the adaptation of insulin secretion. The various therapeutic strategies employed in the management of type 1 diabetes are therefore aimed at a blood glucose profile close to normal.

3.5 The different therapies in management of T1DM:

Upon diagnosis of type 1 diabetes, the patient should receive extensive therapeutic education, as the management of type 1 diabetes relies mainly on the patient himself, as well as on relatives who are also involved in order to be able to accompany and react to potentially critical situations such as the occurrence of severe hypoglycaemia (OMS).

Different types of exogenous insulin have been developed, with increasingly rapid actions, and are administered daily by injection. Patients have to measure their blood sugar levels, usually by picking their finger, to determine the dose of insulin to be administered.

The different types of insulin allow the patient to cope with different situations in everyday life in the most appropriate way. The ultra-rapid acting analogues (insulin lispro and aspart) come into action 10 to 15 minutes after injection, reach their peak in 30 to 60 minutes and last for about four hours (Evans et al. 2019). These characteristics make them to cope with meals and enabling the diabetic to cope with sudden and unexpected changes in lifestyle. Rapid acting (or normal) insulin has a half-hour latency, peaks in two to four hours and disappears after four to eight hours. It is used before meals to control hyperglycaemia after eating and to lower blood glucose levels quickly when they rise too high. Nph (neutral protamine Hagedorn) insulin contains a substance (protamine) that slows down its action so that the latency is two to four hours, the peak is produced six to eight hours after the injection and the total duration is 12 to 15 hours (Lau et al. 2019). Two injections per day usually provide sufficient blood glucose control. Slow acting insulin, which contains zinc, has the same characteristics as Nph: a latency of two hours, a peak of 6 to 12 hours and a duration of 18 to 24 hours. Like Nph, it theoretically provides satisfactory blood sugar control with only two daily injections. Ultra-slow acting insulin contains more zinc, which further delays its action. Thus, the latency is four to six hours and the maximum eight to fifteen hours, while the effect disappears after 18 to 24 hours (Turner, Phillips, et Ward 1983). For this reason, one injection per day is sufficient, in combination with small doses of rapid insulin (e.g. before meals).

Unfortunately, insulin carries a significant risk of hypoglycaemia, which is a major obstacle when used as a monotherapy. Research into non-insulin therapies has progressively emerged that reduce insulin requirements and associated risks (Heptulla et al. 2005; Kuhadiya et al. 2016; Pettus, Price, et Edelman 2015) . They are mainly aimed at reducing gluconeogenesis (e.g. amylin, liraglutide, glucagon receptor blockers) or increasing glucose excretion (e.g. SGLT2 inhibitors).

Continuous Glucose Monitoring:

In order to improve the daily monitoring of blood glucose and the daily burden of this monitoring on the patient, a new technology called CGM for “Continuous Glucose Monitoring”, was developed in the 1970s in Germany and Japan (Kropff et DeVries 2016). It was initially reserved for use by health professionals. It took many years before it was available to patients directly (Kravarusic et Aleppo 2020). A CGM consists of a meter and a sensor that

must be placed on the skin and replaced every week. CGM systems measure glucose levels continuously in the interstitial fluid; most systems use an enzymatic re-action with glucose oxidase as a substrate, whereas the implantable Eversense system from Senseonics (Germantown, MA) uses a fluorescence-sensing technology (O'Connor et al. 2020). They can display blood glucose values in real time (real-time CGM) or on-demand ('flash' blood glucose monitoring). Real-time CGMs also use alarms when sensor glucose levels reach predefined thresholds of hypo- and hyperglycaemia and during rapid glucose excursions (Tauschmann et Hovorka 2018). We will discuss more in details of CGMs technic in the last part of this introduction, and see what are the benefit and the limits of it.

Islet/pancreas transplants:

Islets can be transplanted either alone, or as a whole pancreas, or as pancreas/kidney transplantation. Each approach has its advantages and disadvantages, and islet only transplantation represents the least surgical risk. Islet/pancreas transplantation is one option that provides an alternative for patients with severe glycaemic instability despite optimised insulin treatment (Rickels et al. 2018). Depending on the patient's profile, a choice has to be made between islet or whole pancreas transplantation. This choice is made on several criteria as the age of the patient but more particularly on his health status from a renal and cardiovascular point of view. Indeed, islet transplantation is proposed in cases of insulin-deficient diabetes without declared renal insufficiency. When renal insufficiency is present, a kidney/pancreas transplantation will be preferred (Vantyghem et al. 2019; Wojtusciszyn et al. 2018).

Islet transplantation aims to restore an appropriate hormonal secretion of insulin and glucagon. Islets are isolated from cadaveric donors and are then injected via the portal vein into the liver under immunosuppressive treatment (Vantyghem et al. 2019; Shapiro, Pokrywczynska, et Ricordi 2017). Human cadaveric donor islets are isolated using a technique based on enzymatic and mechanical digestion followed by density gradient purification (Varhue et al. 2017).

Islet transplantation, while attractive on paper, has limiting points that need to be addressed. First of all, the use of cadaveric donors limits the number of patients that can be transplanted. Indeed, two to three donors are needed for one transplantation and there is a real shortage

of organs available (Matsumoto 2010). Secondly, a part of the cells dies quickly after transplantation due to an inflammatory reaction and ischaemia. Therefore, despite the use of 2 to 3 donors for each recipient, full insulin independence is not yet achieved and a second islet infusion is generally required (Lablanche et al. 2017; 2015). Furthermore, the functional quality of islets varies greatly between donors, and rapid and efficient methods of assessing islet functionality before transplantation are currently lacking. Finally, the continued use of immunosuppressants to prevent rejection is difficult to tolerate for most patients (Shapiro, Pokrywczynska, et Ricordi 2017) and the intervention is not without risk of thrombosis of the portal vein (Kawahara et al. 2011). The use of an encapsulation system as a physical barrier could avoid the use of immunosuppressants (Desai et Shea 2017). An ideal islet encapsulation device should provide sufficient blood supply to maintain islet survival and function, be biocompatible and non-fibrotic, and provide a protected environment against autoimmune reactions and thus prevent rejection (Sneddon et al. 2018).

New therapies of TDIM:

These therapeutic approaches are constantly evolving in order to improve the quality of life of patients with T1DM and to reduce the daily burden of managing this disease. From these stem new therapeutic strategies and we are now going to focus on two of them in particular: Cellular engineering techniques through which we will discuss the use of stem cells and cell conversion methods. The concept of an artificial pancreas, which is at the centre of my thesis.

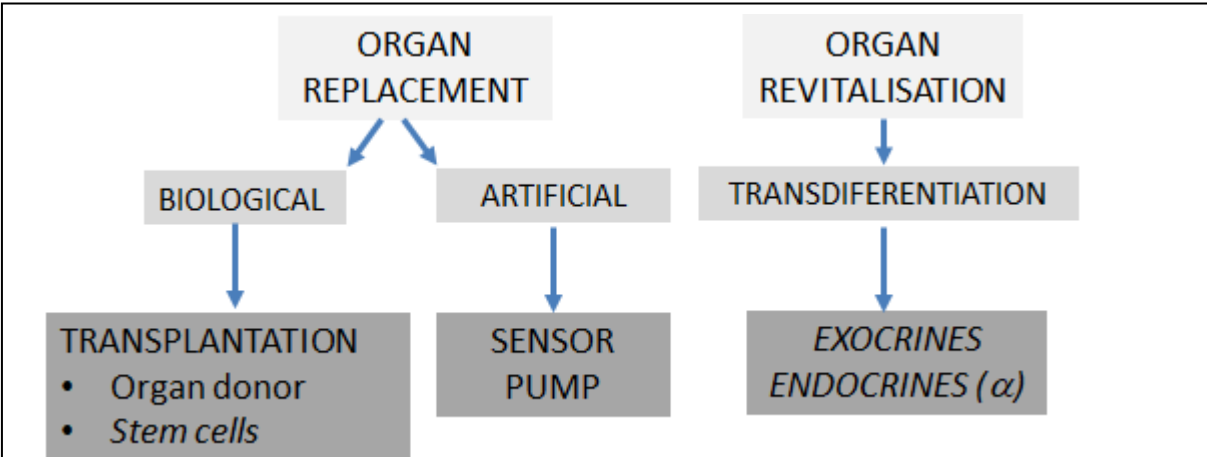


Figure 19: Therapies in TDIM. Therapies arising from a strategy to replace the failed organ. Therapies arising from a strategy of revitalisation of the failed organ

Cellular engineering:

In order to compensate for the loss of β -cell mass in the islets, to restore insulin secreting function in the patient and to find an alternative to cadaveric donor islets new avenues have been explored, including reconstituting the β -cell mass in T1DM patients from stem cells. Numerous studies of pancreatic development in different animal species have provided insight into the key steps to β -cell formation (Murtaugh et Melton 2003; Arda, Benitez, et Kim 2013). This understanding of pancreatic development has been useful in the field of regenerative medicine and more specifically for the use of human embryonic stem (hES) cells (Thomson et al. 1998). The hES cells represent a promising source for β -cell replacement in transplantation, non-limited by donor availability (Pagliuca et al. 2014; Chetty et al. 2013). Human induced pluripotent stem cells (iPSCs) were developed (Takahashi et al., 2007). These cells are generated from patient somatic cells (e.g. skin fibroblasts or peripheral blood mononuclear cells) reprogrammed with cocktails of transcription factors (OCT4, SOX2, etc...) (Teo et al. 2013). In the first studies of differentiation of hES cells into pancreatic endocrine cells, a stepwise protocol was designed. This protocol is based on the use of different cocktails of factors to induce the differentiation of hES cells through 4 successive steps: definitive endoderm, pancreatic epithelium, endocrine progenitors and " β -like" cells. These initial differentiation assays generated populations of cells with mixed hormonal expression but no mature β -cells (D'Amour et al. 2006). More complex protocols were therefore developed with additional steps, new factor cocktails and culture in organoids and/or microfluidics. Transplanting these in-vivo generated cells then induces further functional maturation allowing remission of diabetes in mouse models (Pagliuca et al. 2014; Rezanian et al. 2014) but transposition to humans still remains a challenge with important risks, notably the presence of poorly differentiated cells that can be a source of tumours due to their pluripotency, but also autoimmune reactions generated by the transplantation (Helman et Melton 2021; Nair, Tzanakakis, et Hebrok 2020).

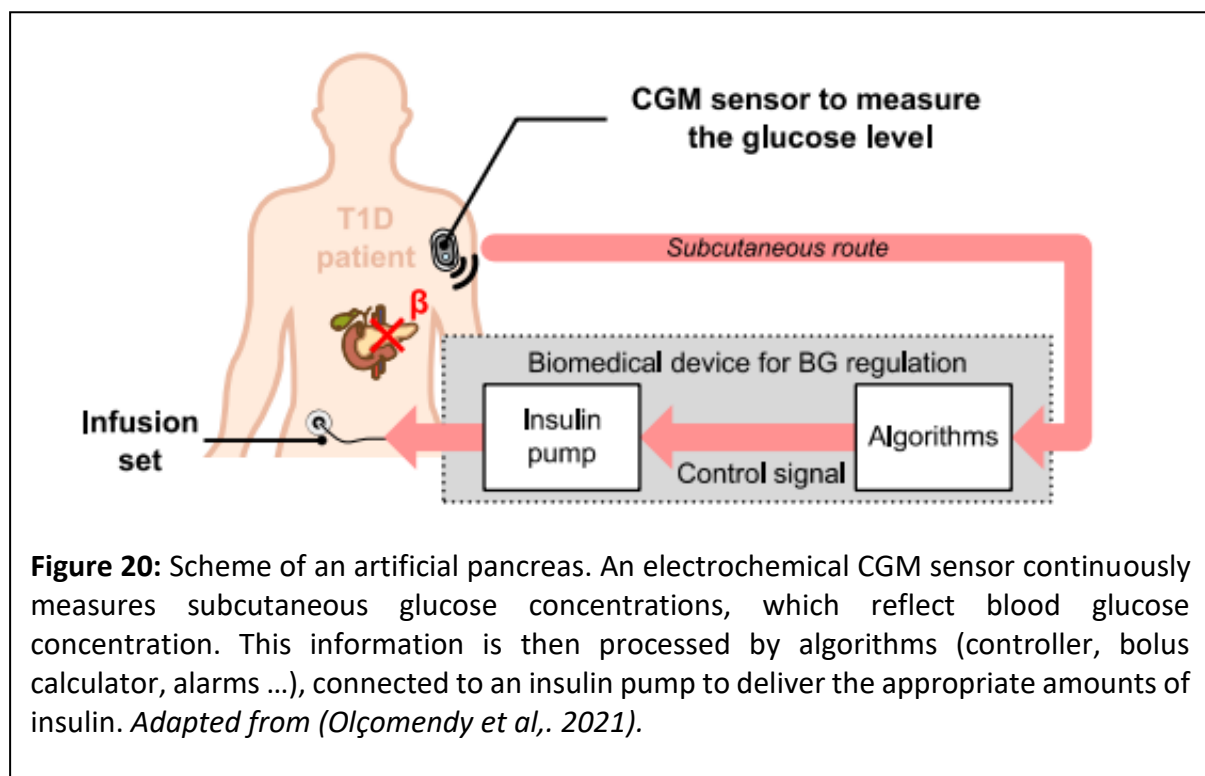
Another way for cell engineering is the reconstitution of a β -cell pool by stimulating the proliferation of endogenous β -cells or reprogramming non- β -cells into β -cells (Zhou et Melton 2018). Pancreatic islet hyperplasia is observed at certain times of life in humans, during the first year of life, during pregnancy or in cases of obesity (Zhou et Melton 2018). Following this observation, the idea of stimulating β -cell proliferation seems to be a solution to replace the

β -cell mass. Many growth factors and mitogenic agents promote β -cell proliferation in animal models (Schulz et al. 2016) but they fail to stimulate human β -cell proliferation. Therefore, there has been great interest in using key regulators of β -cell development to convert non- β cells into insulin-secreting cells. Insulin expression and secretion can be induced in non- β cells but these cells do not take on the morphological, molecular and functional properties of β cells (Baeyens et al. 2005; Kaneto et al. 2005). Alternatively, extreme β -cell loss can trigger a spontaneous conversion of α and δ cells to β -cells (Chera et al. 2014). Although the molecular mechanisms behind this conversion remain unknown, forced expression of PDX1 (Pancreatic and duodenal homeobox factor 1) and PAX4, two regulators of β -cell development, allows for the conversion of α -cells to β -cells in mouse models (Yang 2014). This plasticity in human islets remains still to be explored.

Artificial Pancreas:

Technological advances, while not restoring normoglycaemia for the majority of diabetics, have nevertheless improved the quality of life of patients and automated blood glucose control. Monitoring blood glucose levels on a daily basis requires a great deal of commitment from the patient, representing a significant physical and moral burden. For example, in order to monitor blood glucose levels, a type 1 diabetic patient pricks his or her fingertip more than 1,800 times on average in one year, an act that is harmless when performed occasionally, but therefore becomes a painful habit (Ascaso et Huerva 2016). Moreover, people who develop type 1 diabetes are often young and it is difficult for a child to fully take control of his or her blood sugar levels. Indeed, despite therapeutic education, not having the same carefree attitude at a birthday party or during a simple game in the playground is problematic for the patient and his entourage. They live in perpetual anxiety about the occurrence of a hypoglycaemic crisis, which can have serious consequences if it is not managed quickly and optimally. These considerations were the driving force behind the development of the concept of the artificial pancreas (Kadish 1963), in order to bring together the different technologies used up to now separately and thus move towards a more or less complete automation of the daily care process. Abusively called "artificial pancreas", it is not a physical organ that has been transplanted, but the conjunction of several systems that communicate with each other and thus form an interaction loop.

The three players in this loop are a device for continuous measurement of interstitial glucose (CGM); an external insulin pump; and a terminal that hosts algorithms that calculate the optimal amount of insulin to be administered according to current, and sometimes future, meal and exercise predictions and control their delivery autonomously via the insulin pump. The management of the algorithms can be physically separate (smartphone or connected tablet) or integrated into the pump. This interaction loop is still mostly an open loop, i.e. with patient intervention. The ultimate goal is to succeed in closing this loop and thus free the patient from the constraint of permanent monitoring in which he is locked.



In current systems, the user enters various information such as meal announcements and physical activity. Some improvements are currently being developed in recent years, such as linking insulin control to heart rate in order to avoid hypoglycaemia during physical effort (Rothberg et al. 2016). Given the importance of coordinated action between insulin and glucagon, there are now also bi-hormonal systems where glucagon delivery is triggered when hypoglycaemia is imminent or predicted (Haidar et al. 2016). However, these systems have significant flaws, which effectively prevent the loop from being closed. Due to a lack of insulin release during the cephalic phase, delayed absorption of insulin due to its subcutaneous administration, and the lack of an incretin effect CGMs only detect glucose°, these systems require basal insulin plus a bolus at mealtime (Latres et al. 2019). They therefore do not

reproduce physiological insulin kinetics, nor do they consider non-carbohydrate nutrients such as amino acids and lipids. It is therefore in relation to this observation that the development of a new approach using biosensors such as the islets of Langerhans as sensors is justified. The deciphering of the electrical signature of the islets could thus allow the development of new algorithms that would be as close as possible to the patient's insulin requirements, thanks to the inclusion in the analysed signal of glucose but also of non-carbohydrate elements that also play a key role, as we saw at the beginning of this section, in maintaining glucose homeostasis.

Following this presentation of the physiological and pathological functioning of the maintenance of glucose homeostasis in the context of type 1 diabetes, we will now carry out a state of the art of the technologies implemented during this thesis to establish the proof of concept of this new biosensor.

4 Methods of functional investigation of islets

4.1 Optical means for the study of islets.

Chemical and genetic approaches have enabled the creation of sensors capable of better understanding cell signalling through imaging (Poenie et al. 1986; Tsien et Hladky 1978). Chemical approaches have been developed to study the temporal relationship that exists between membrane potential and calcium fluxes, in order to learn more about the dynamics within the β -cell and other islet cells (Frank et al. 2018). Organic fluorescent probes and optical means can be used to dynamically study islet cells. They can be used in cell lines and primary cells without genetic manipulation. Particularly common and easy to use are single-excitation/single-emission calcium probes and their ratiometric variants. They are numerous (Fura2, Fura8, Fluo3, Fluo4, Fluo8, etc.) (Tsien 1989) and they differ according to their affinity for Ca^{2+} and their spectra (Paredes et al. 2008). Insulin secretion can also be monitored using zinc-sensitive probes (ZIMIR) (Li et al. 2011) which is co-secreted with insulin. However, these measurements are limited by photobleaching.

Another type of sensor, based on genetic techniques, has been developed. Recombinant sensors for ions or second messengers (eg. cAMP) have been developed. Corresponding

minigenes with specific promotor are introduced into cells using techniques such as transfection, viral transduction or genome editing including the generation of specific mice strains. Genetically encoded calcium sensors have been used in several studies on β -cells (van der Meulen et al. 2017). There are also genetic sensors for nucleotides (e.g. ATP and ADP, NAD^+ and NADH, NADP^+ and cAMP) as well as for small molecules such as glutamate (Brun et al. 2012; Cambronne et al. 2016).

Among the major limitations common to both genetic and chemical optical approaches is the issue of accessibility of probes to the cells at the center of the islet. Indeed, as a three-dimensional structure, only the peripheral layers of the islet will be in contact with the probes (Dolenšek, Rupnik, et Stožer 2015). The probes or genes therefore penetrate the surface of the islet but not the deeper layers. The read-out of optical measurements allows measurements of function and signalling, but provides little information on the characteristics of specific ion currents, which provide rapid and detailed information on β -cell activity (Dunlop et al. 2008). The frequency resolution is limited since the acquisition frequency is around 1 Hz and the frequencies of β -cell signals are in the range of 0.2-2 Hz for slow potentials and 3-700 Hz for action potentials. Furthermore, the pancreatic micro organ is a set of cells arranged in 3D (micro organ diameter equal to about 100 μm) which reduces the acquisition time and therefore the frequency if we want to report this 3D volume. In addition, the photobleaching of fluorescent probes is also a constraint when using optical tools.

4.2 Techniques for studying the secretory function of islets:

One of the central questions in the study of the islets of Langerhans is the study of the hormone secretion. The primary objective of the β -cell is to participate in the maintenance of normoglycaemia through the storage and release of insulin in the appropriate amount.

A first method used in *in vivo* experiments is the study of the proinsulin/insulin ratio in the plasma. An abnormal ratio can be a marker of a possible β -cell dysfunction (Cersosimo et al. 2014). The concentration of insulin measured in the blood differs from the total amount of insulin secreted, as a large portion of the secreted insulin is extracted by the liver before reaching the general circulation. To evaluate total insulin secretion *in vivo* it is therefore appropriate to focus on C-peptide, which is present in an equivalent quantity to insulin but which is totally extracted unlike insulin. The determination of plasma C-peptide

concentrations is therefore a good indicator for assessing the amount of insulin secreted in vivo. However, although useful for quantification, this method does not tell us the proportion of biologically active circulating insulin (Cersosimo et al. 2014).

Ex vivo several models are used with differences in the preservation of the normal environment. The perfused pancreas technique allows the study, in situ, of the secretion of hormones released by the islets (Bonnie-Nielsen, Steffes, et Lernmark 1981) . Surgery is performed on a freshly prebleached pancreas to create a closed system with only one entrance, the celiac artery and one exit, the hepatic portal vein (Sussman, Vaughan, et Timmer 1966). All the rest of the organ's vascular network is ligated. An oxygenated solution is then perfused through the pancreas and secretagogues are introduced to stimulate the secretion of various hormones (Wargent 2009). The difficulty of implementing this type of procedure must be emphasised, as it is complex and time-consuming to set up in order to obtain a perfectly sealed circuit (Bonnie-Nielsen, Steffes, et Lernmark 1981).

It is therefore simpler to study the secretory function of islets using isolated whole islets. Whole islets maintain native cell contacts and paracrine signalling between α , β and δ cells. Islets from mice and rats are routinely isolated according to established protocols, either through the use of gradients (O'Dowd 2009) or manual handpick as we practice in the laboratory (Lebreton et al. 2015; Jaffredo et al. 2021). Isolated islets can be cultured for several weeks however, as the culture progresses, cells degranulate and changes in cell function appear after a long period in culture (Gilon, Jonas, et Henquin 1994). In addition, there is heterogeneity in the fate in culture between islets isolated from the same pancreas. For example, small islets will show less necrosis markers following hypoxia than larger islets (Muthyala et al. 2017).

4.3 Methods for electrophysiological studies of islets

The β -beta cell is an electrogenic cell with characteristic electrical signals. These signals are an important parameter allowing the functional study of islets through their electrical response to glucose and their electrical properties depending on their different ion channels (Kravets et Benninger 2020; Rorsman et Ashcroft 2018).

We have already seen that islets can be studied using optical approaches via fluorescent probes, however these techniques only offer low temporal resolution. Compared to optical

approaches, electrophysiology allows a better monitoring of ionic flows within cells, which can reach several thousand measurements per second.

The methods of electrophysiological study of islets can be classified into two broad categories, intracellular and extracellular. Annexe 1, table 1.

Intracellular electrophysiology:

Sharp micro-electrode

Membrane potential recordings were initially performed in the 1970s in pancreatic islets using intracellular microelectrodes called sharp electrodes with a very thin diameter and an electrical resistance between 100-300 M Ω . With this technique, it is possible to monitor electrical activity and changes in membrane potential. By sending a current pulse, the associated voltage changes can be recorded at the cell level (Atwater, Ribalet, et Rojas 1978). This technique can also be used in vivo (Sánchez-Andrés, Gomis, et Valdeolmillos 1995). A major disadvantage of this technique is that the electrodes have a high impedance, so the speed of current injection is limited and the kinetics of the membrane currents responsible for action potentials cannot be reliably analysed (Rorsman et Ashcroft 2018).

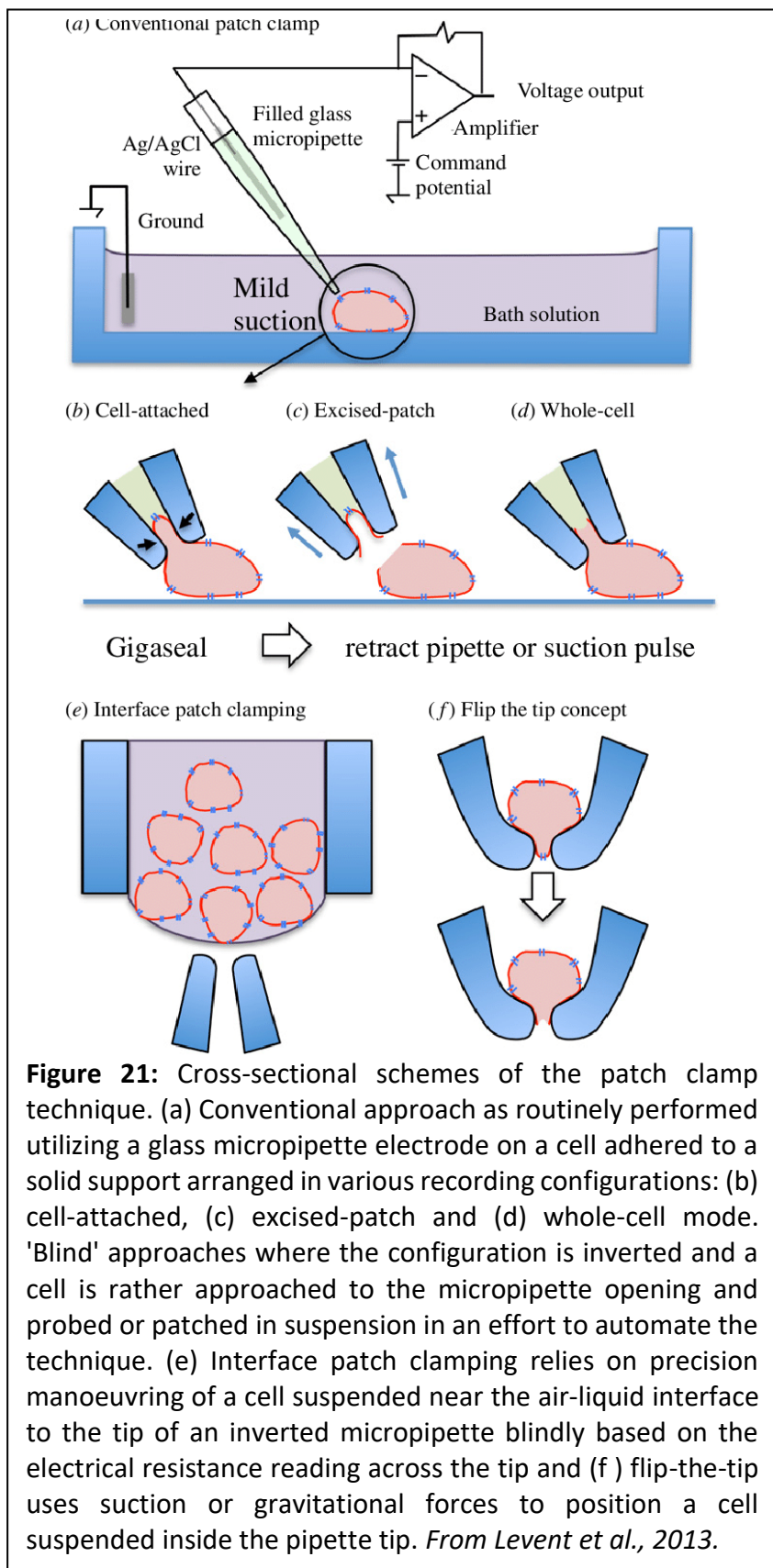
Patch clamp

In contrast to the sharp method, the patch clamp involves larger electrodes ($R > 1 \text{ G}\Omega$). The patch clamp is a method that was developed by E. Neher and B. Sakmann, Nobel Prize laureates in Medicine and Physiology, in 1991 (Neher et Sakmann 1976).

The patch clamp allows quantifying the involvement and contribution of ion channels in the activity of electrogenic cells and particularly β -cells (Düfer 2012). Several patch-clamp configurations (attached cell, whole cell or single channel with or without intracellular medium bathing in the pipette) can be performed on intact pancreatic microorgans (Rorsman & Ashcroft, 2018). The patch is most commonly used on dispersed islet cells, but extrapolating results obtained on dispersed cells to an islet can lead to bias in the analysis. Indeed, culture and dispersion can induce changes in ion channel properties or density, not to mention the

suppression of electrical couplings which play a major functional role (Rorsman & Ashcroft, 2018).

When performing a whole islet patch clamp experiment, the islet is held by a fairly large glass pipette and the target patch electrode on the opposite side of a cell (Göpel et al. 2000). Although the patch clamp is ideal for biophysical studies of ion channels and fluxes due to its high resolution, it is a technique that requires great dexterity (Fridlyand, Jacobson, et Philipson 2013). In addition, the cytosol, a key cellular compartment in carrying out β -cell glycolysis, is diluted in the large volume of the patch pipette, which poses a problem for the regulation of cytosolic metabolic pathways when studying channel ion activity. It is still possible to preserve the internal cell environment by



switching to the perforated patch configuration from the attached cell (Mason et al. 2005). Perforation of the membrane can be achieved by adding ionophores to the pipette that will introduce monovalent ion permeable pores into the membrane, allowing us electrical access to the interior of the cell. In patch clamp, ion channel agonists/antagonists are delivered by external perfusion or through the patch pipette allowing the isolation and characterisation of specific channels.

In conclusion, intracellular electrophysiology, although having multiple advantages for the functional study of the islets, is invasive and only allows recordings lasting a few tens of minutes. The implementation of these techniques is complex and requires a great deal of expertise on the part of the experimenter. Finally, the recordings are made on the scale of a single cell and do not provide information on the behaviour of the entire microorganism that is the islet.

Extracellular electrophysiology:

Extracellular recording techniques have been explored since the eighteenth century with experiments such as those conducted by Galvani on frogs to quantify "animal electricity". Closer to home, during the 1970s, these techniques were mainly used in neuroscience or cardiology to study neurons or cardiomyocytes, the most studied electrogenic cells at that time. It was only recently, in the 1990s, that these approaches were applied to the study of Langerhans islets.

Multi electrodes array

Palti and colleagues performed electrophysiological studies on islets initially using only two electrodes (Palti et al. 1996). Since then the number of electrodes used to conduct these non-invasive studies has increased and we now speak of microelectrode arrays (MEAs) fabricated by electrochemical deposition. Our team has greatly contributed to the study of signals from β -cells cultured on MEAs (Raoux et al. 2012b; Bornat et al. 2010), whose amplitude is much lower than those of signals observed in neurons or cardiomyocytes (10-50 μ V for PAs, 50-350

μV peak-to-peak for PLs) (Lebreton et al. 2015). Pancreatic SPs show an amplitude in the microvolt range, whereas other electrogenic cells in the body show signals in the mV range. Murine or human pancreatic islets can be cultured on MEAs for days to monitor their electrical activity (Jaffredo et al. 2021; Pedraza et al. 2015; Perrier 2018; Raoux et al. 2012b). This approach allows us to study non-invasively and in real time the different signals (APs and SPs) of the pancreatic islet cells and to inform us in detail about islet activity (Lebreton et al. 2015;

Renaud, Catargi, et Lang 2014).

Conventional MEAs consist of culture chambers

containing 59 titanium recording

electrodes of $30\ \mu\text{m}$ diameter, spaced at

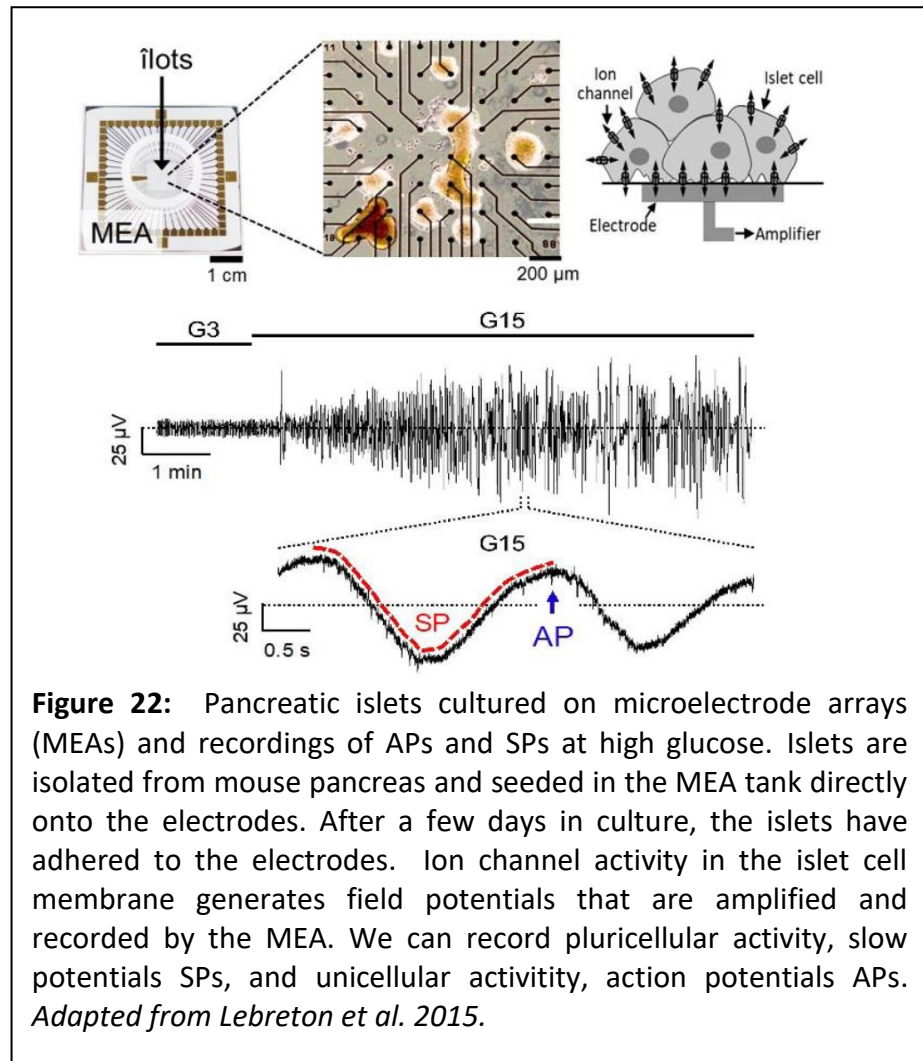
$200\ \mu\text{m}$. Their sensitivity is further

improved by coverage with the

conducting polymer PEDOT: PSS,

especially in the high frequency

range (Koutsouras 2017). This



configuration provides high temporal resolution, but spatial resolution is very limited when considering the diameter of an islet endocrine cell of approximately $10\ \mu\text{m}$. Spatial resolution can be increased by denser arrangement of electrodes in high density MEAs (HD-MEAs).

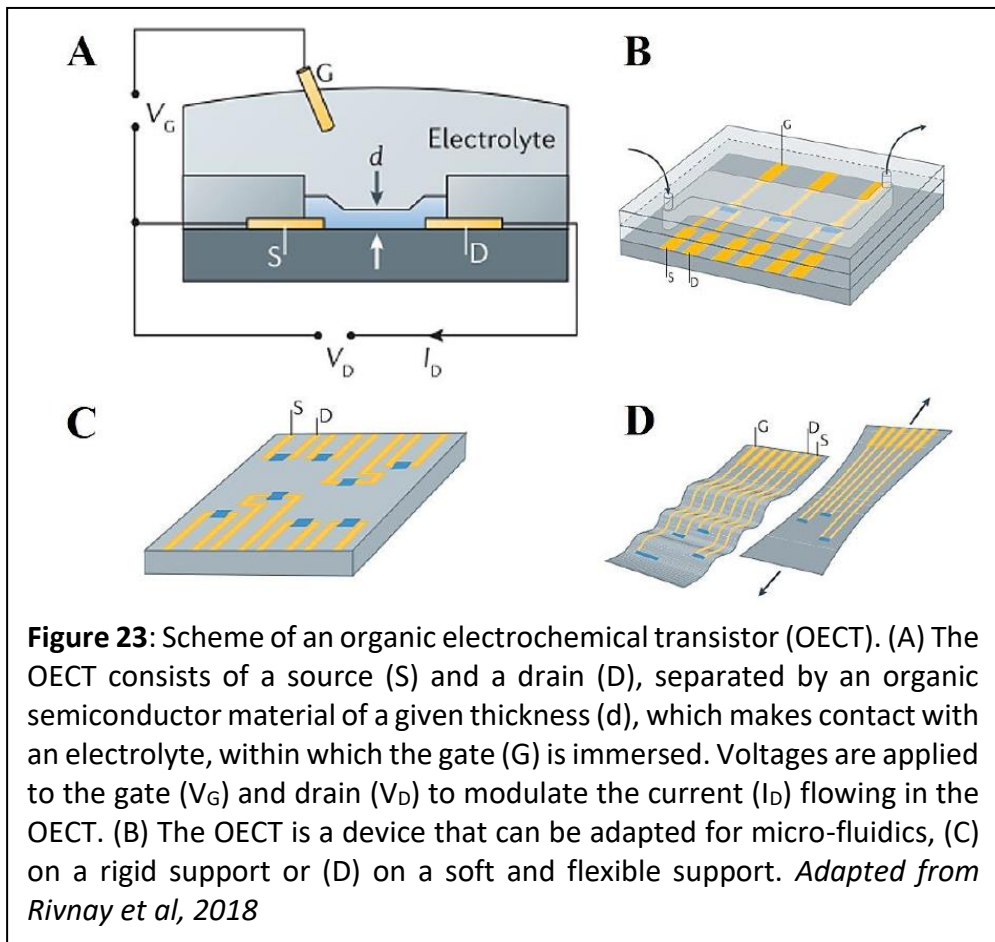
Unfortunately, it remains open, how many cells (10 μ m of diameter) touch an electrode (30 μ m of diameter). While in theory, reducing the size of the electrodes decreases the signal-to-noise ratio, appropriate electrode coverage can remove this problem (Viswam et al. 2019). Therefore, the right combination of electrodes, electrode sizes and electrode material must be found to best answer the question addressed to the system. Another limitation that can be cited for this technique include the fact that we cannot specifically determine which ionic currents are involved.

However, these classical metal electrodes are rigid and cannot be produced by printing on soft, flexible substrates to adapt their geometry for different biological surfaces and tissues while keeping a good signal to noise ratio. The fact that these electrodes are not accessible to chemical modifications also limits the detailed investigation of the contribution of the different ions in the bioelectric signals (Rivnay et al. 2017). Following these observations, the team, through another project, became interested in organic bioelectronics and more particularly in the development of electrochemical transistors, which we will now discuss.

OECTs

Organic bioelectronics and more specifically organic electro-chemical transistors (OECTs) are based on the principle of measuring changes in current through a conducting polymer. These changes are directly related to the electrical activity of the electrogenic cells seeded on this polymer and can also be transformed into potential variations by electronic circuits (Yao et al. 2013). The aim of this method is to provide solutions to the various weaknesses highlighted previously for the MEA technique. Compared to conventional metal electrodes, the amplication is performed directly at the source, thus for less additional noise added. In addition, our team has developed with chemists' biocompatible polymers specific for certain ions (Salinas et al. 2020; Villarroel Marquez et al. 2020), which can be deposited on the surface of OECTs. These ion-specific polymers may be able to provide an extracellular analysis of the contributions of different ionic species to islet cell activity. A first detailed characterisation of the optimal conditions of use for OECTs with low-amplitude signals, such as in islets, has been published (Abarkan et al., 2022).

OECTs offer many biological applications depending on the type of biomolecules or biological information one wishes to detect (Strakosas, Bongo, et Owens 2015). Furthermore OECT can be used to detect



and recognise the presence of biomolecules of interest by being an enzymatic biosensor (Pappa et al. 2018), an immunosensor (He et al., 2012), coupled to artificial receptors (Zhang et al. 2018) or ionic sensors (Han et al. 2020). In addition to these single molecule detections, OECTs are devices that, thanks to their favourable Young's modulus, interface very well with living, tissues or cells. OECT biosensors are therefore emerging as a new strategy for the study of biological systems but also as a new alternative for low-cost toxicological analysis and diagnostics. The portability of OECTs dedicated to the detection of molecules such as cortisol or lactate is increasingly being developed (Khodagholy et al. 2012; Parlak et al. 2018; K. Yang et al. 2018), opening the way for the use of OECTs in the field of health technologies and rapid diagnosis.

However, despite all the progress achieved and published, OECTs are not yet well standardised and therefore not yet at the stage of industrialisation. Thus stability (against air, light, aqueous environments or biological substrates) and performance can vary between channels and sometimes be limiting (Sirringhaus 2009; Klauk 2010). In addition, electronic circuits for signal capture remain poorly developed and are often not adapted to the variable performance of

OECTs produced on demand. This inherent variability and the lack of knowledge about their behaviour during biological recordings precluded long-term quantitative studies in biology. this has been considerably improved by dedicated electrochemists and precise exploration of electrical device parameters (Abarkan et al. 2022).

Conclusion

Different approaches used to study the electrogenic activity of Langerhans islets and slow potentials are a signal of interest for the development of a biosensor based on this specific electrical signature. Currently, commercial MEAs, manufactured by several companies with expertise in the field, offer the possibility of conducting a long term minimally invasive study on the islets and thus obtain standardized recordings of the multi-cellular activity within the micro-organ. These MEAs can also be used under static or dynamic flow conditions. In the context of the development of our new biosensor, in order for the interstitial fluid to be delivered to the islets seeded on the MEA, I had to develop different microfluidic approaches in order to best meet the specifications of this new islet on chip.

5 From CGM to a new islet-based biosensor.

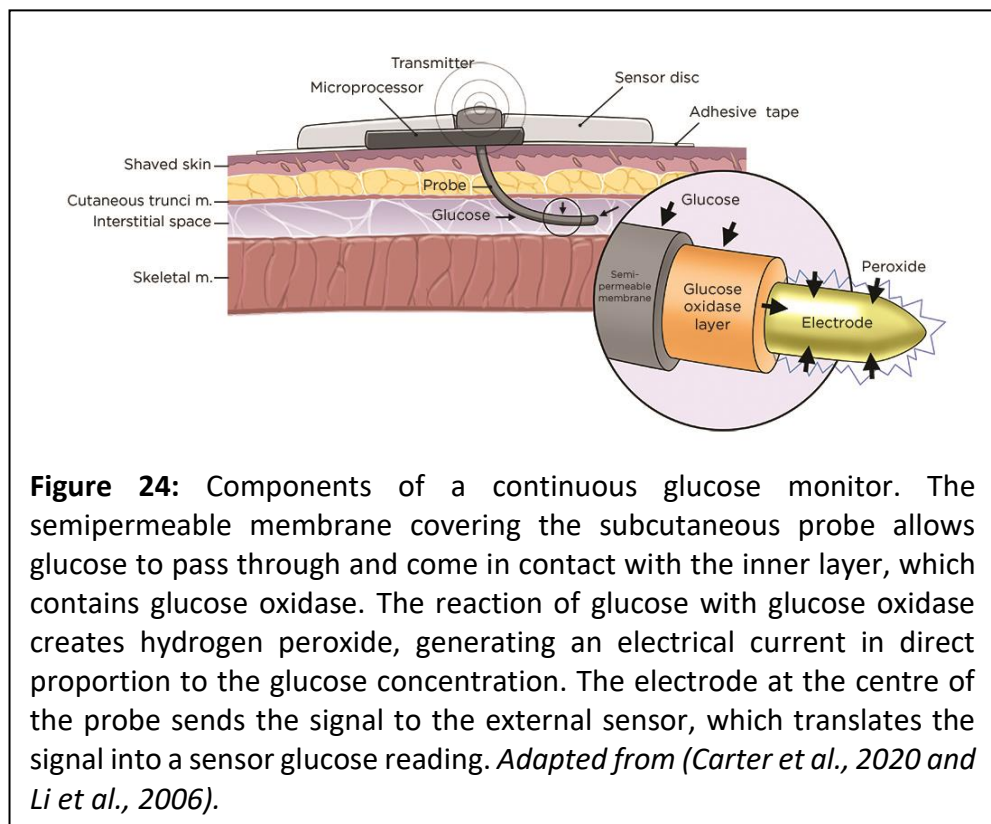
5.1 Analysis of the CGM concept: Strengths and weaknesses.

Blood glucose monitoring is essential in the management of T1DM. In this respect, the emergence of CGM devices has been a true breakthrough. In this new section we will look in detail at how CGMs work, their strengths, but also highlight the weaknesses of these devices.

General principle of CGM:

Of the many glucose sensing mechanisms tested in the laboratory, one method stood out as meeting many of the requirements of medical devices. The most popular technique used for continuous glucose monitoring systems is based on the glucose oxidation (J. Wang 2008). Specifically, CGM devices are based on this principle, which involves a platinum electrode doped with

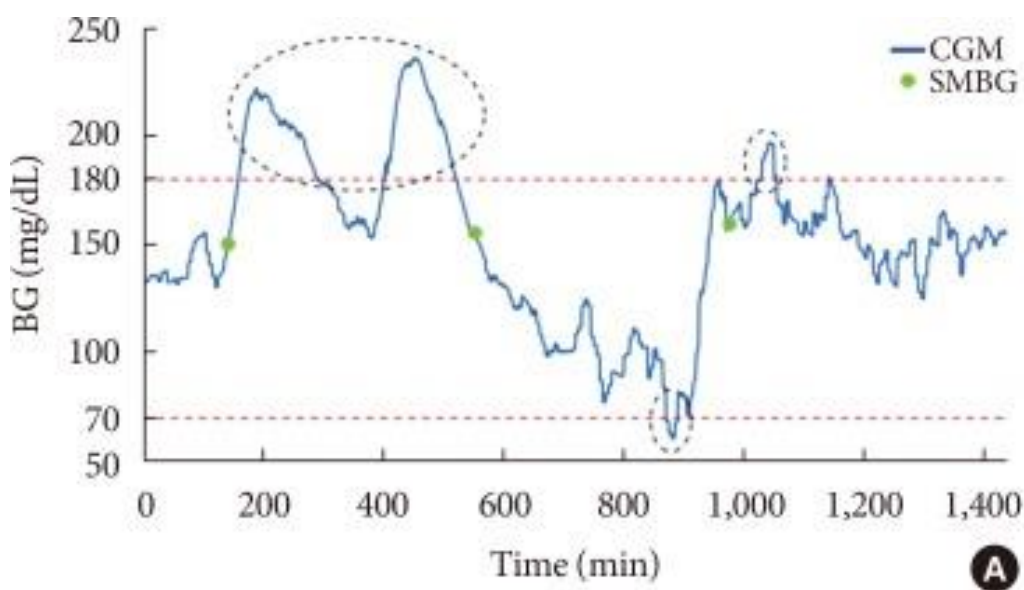
glucose oxidase deposited on a needle inserted into the subcutaneous tissue to trigger and catalyse glucose oxidation. This results in the production of



gluconolactone, hydrogen peroxide and an electric current signal that is ultimately

transformed into a glucose concentration by a calibration process using some self-monitoring of blood glucose (SMBG) samples collected by the patient (Acciaroli et al. 2018).

Continuous glucose monitoring (CGMS) has made a considerable way since its initial introduction in a clinical setting in the 1970's (Kropff et DeVries 2016) and revolutionised blood glucose monitoring in diabetes and opened up new scenarios for daily diabetes management (Acciaroli et al. 2018). CGM sensors provide an almost continuous glucose recording, with blood glucose readings every 1-5 minutes, reducing the need for self-monitoring of blood glucose and greatly increasing information on blood glucose fluctuations and trend (showing that CGM reveals hypoglycaemic and hyperglycaemic events not visible by self-monitoring of blood glucose). Since the first prototypes, the CGM software have evolved significantly. Today, they are able to provide patients with a number of features, such as trends in blood glucose variation and intelligent alarms for hypo-/hyperglycaemic events, thus improving patient self-management. Although CGM users represent only a small proportion of the total diabetic population, mainly due to the economic cost and patient acceptability of the sensors, CGM sensors have been shown to be effective in improving patients' blood glucose control (Battelino et al. 2011; 2017) and enabling the development of new advanced technologies for diabetes management (Facchinetti 2016; Vettoretti et al. 2018).



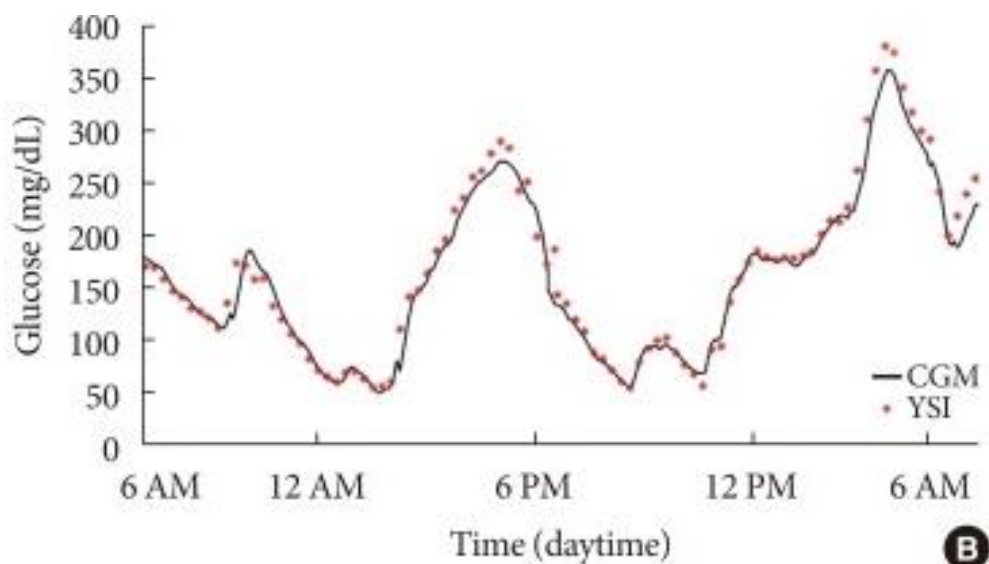


Figure 25: (A) Representative blood glucose (BG) monitoring data obtained with self-monitoring of blood glucose (SMBG; in green) and with continuous glucose monitoring (CGM; in blue). Dotted circles denote hyperglycemic and hypoglycemic episodes that, using only SMBG measurements, are not detectable. (B) Assessment of the accuracy of a CGM sensor can be performed by comparing Yellow Spring Instruments Inc. (YSI) measurements (red stars) versus Dexcom G4 Platinum CGM (black solid line) measurements. For example, mean absolute relative difference can be calculated as the average ratio between the absolute difference between the CGM measurements and the YSI over the YSI. *From Cappon et al 2019.*

The development of CGMs

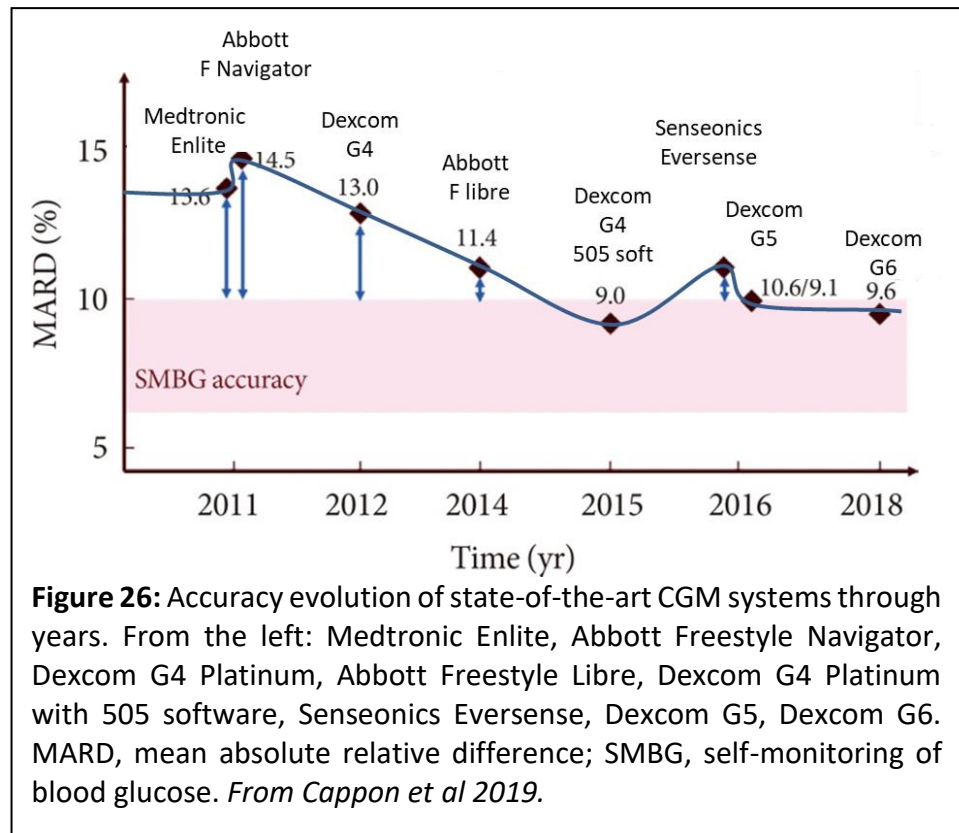
Glucose-based CGM devices moved more widely from the laboratory to the hospital in the 1990s, when the US Food and Drug Administration (FDA) approved the first CGM system for use by healthcare professionals, allowing retrospective patient data to be analysed for review (Wang 2008). However, these early commercial systems suffered from several limitations, the main one being the low accuracy of some measurements. These data were assessed by comparing the CGM trace to very precise and accurate BG concentration values, usually collected in a hospital setting during sampling by healthcare professionals and using laboratory grade medical instruments. In 2004, Medtronic successfully introduced and marketed the first personal real-time CGM system: the Medtronic Real-Time Guardian. This system provided patients with a glucose concentration value every 5 minutes, lasted for 3 days and was able to trigger an alarm when the glucose concentration level became too high or too low, helping users to improve glucose control. Dexcom Inc. introduced the Dexcom SEVEN Plus, which had a longer life span of up to 7 consecutive days. To assess the accuracy of CGMs

there is one metric that is important and that is the mean absolute relative difference (MARD). MARD is computed using the difference between the CGM readings and the values measured at the same time by the reference measurement system (Bailey et al. 2014). Among these quantities, MARD is the most common metric currently used in the literature to assess CGM accuracy (Bailey 2017). In the same year, the Abbott Freestyle Navigator was released, which is equipped with a glucose sensor that can be worn for up to 5 days but with a higher accuracy than the Dexcom seven plus. All of the above systems have a high MARD, above 12.5%. Compared to self-monitoring of blood glucose, which has a MARD of 5-10%, the low accuracy (i.e. high MARD) of these "first generation" CGM systems was one of the major barriers to early adoption of these devices, both by users, who did not feel safe adopting CGM, and by the medical community, whose reluctance to integrate CGM sensors into the daily management of diabetes greatly limited the diffusion of this technology.

Over the past decade, CGM manufacturers have made many efforts to overcome the problems of inaccuracy of their first-generation devices. The first new generation product was the Medtronic Enlite CGM system. This device not only achieved a MARD of 13.6% (Bailey 2017), but also extended the wearing time to 6 days. In addition, it improved the comfort of the sensor by reducing its size and weight, was designed to be waterproof, and allowed blood glucose storage for up to 10 hours if the receiver-transmitter connection is interrupted for any reason. In the same year, Abbott launched the Freestyle Navigator II, a newly designed CGM system that provided blood glucose measurements every minute with a MARD of 12.3% (Geoffrey, Brazg, et Richard 2011). In 2012, Dexcom launched the G4 Platinum, with a smaller sensor, 7-day life span, and reduced MARD to 13% (Christiansen et al. 2013), later improved to 9% in 2014 with new algorithms built directly into the sensor (Bailey et al. 2015). In 2015, Dexcom launched the G5 Mobile (Bailey, Chang, et Christiansen 2014) which achieved a 9% MARD, 7-day wear time, now allowing BG data to be transmitted directly to the user's mobile phone without the need for a dedicated receiver.

In 2016, Abbott released the Freestyle Libre, which has a MARD of 11.4% (Bailey et al. 2015). This CGM system was the first that did not require finger testing during wear. In addition, it extended wear time to 14 days. Unlike Dexcom or Medtronic CGM devices, the Freestyle Libre does not trigger an alarm if blood glucose levels fall outside the safe range and requires the patient to pass the receiver over the transmitter to obtain blood glucose information, and to

do so at least once every 8 hours to avoid losing data. For this reason, the Freestyle Libre is labelled as a flash glucose monitor (FGM), i.e. a device that measures blood glucose continuously but only displays the measured values when scanning the sensor with the receiver. The Freestyle Libre was the first glucose monitoring device that did not require calibration, with the added advantage of



similar performance in terms of accuracy and blood glucose control compared to CGM devices that require two or more calibrations per day, e.g. the G4 Platinum and Freestyle Navigator II (Cappon et al. 2019). Following this technology trend, in 2017 Dexcom launched the G6 (Cappon et al. 2019), a CGM system that can be used without in vivo calibration, for 10 consecutive days, providing the same accuracy as the G5 Mobile. In the same year, Medtronic launched the Guardian Sensor 3, which has been quantified to be 10.6% and 9.1% MARD (Christiansen et al. 2017), when inserted in the abdomen and arm, respectively. This sensor is 80% smaller than the Enlite, and provides up to 7 days of sensor life as well as a shorter start-up time.

To sum up, over the past decade, in addition to achieving accuracy close to or within the range of self-monitoring of blood glucose, CGM systems have also improved in terms of functionality, lifetime and patient convenience. CGM systems are now accepted as standard tools for intensive glucose control in patients with T1DM. However, several important limitations are still present. Annexe 2, table 2.

Weaknesses of CGM systems

Glucose-oxidase based electrochemical sensors suffer from several limits such as their non-linear response within the biological relevant range and most importantly, their dependence of both sensitivity and specificity on the enzyme availability on the electrode surface (Cappon et al. 2019). Moreover, BG readings provided by glucose-oxidase based CGM sensors are affected by delay artefacts, which range from 5 to 10 minutes, due to the time lag between glucose concentration in the interstitial fluid and BG. On one hand, delay is not important when analysing retrospective glucose data, on the other, it can be critical when CGM is used for real-time decision making.

For this reason, further research is currently undergoing to address these issues and designing new CGM sensors able to better meet technological requirements such as sensor size, lifetime, and accuracy. New generation CGM system development also involves the exploration of new glucose sensing technologies beyond glucose-oxidase. In this regard, glucose sensors based on optical sensing have been recently proposed. These sensors provide an alternative to traditional glucose oxidase electrochemical sensors since they have the benefit of being free from electromagnetic interference, simple to design and handling, and characterized by low manufacturing cost (Cappon et al. 2019). These principles have been used to design non-invasive sensors based on near infrared detection and spectroscopy (Vaddiraju et al. 2010), and fully implanted CGM systems based on fluorescence (Chen et al. 2017). In 2016, Senseonics launched the Eversense, the first implantable CGM system to receive the CE mark. As already mentioned, it is based on fluorescence sensing, featuring a lifetime of 90 days, and an accuracy of 11.4% MARD (Dehennis, Mortellaro, et Ioacara 2015). This approach is quite demanding for the patient, who is required to undergo a, even if simple, surgical procedure, but the sensor lifetime makes this system an appealing alternative (Cappon et al. 2019).

CGMs are based on the electrochemical principle of glucose catalysis by glucose oxidase and this is a major limitation.

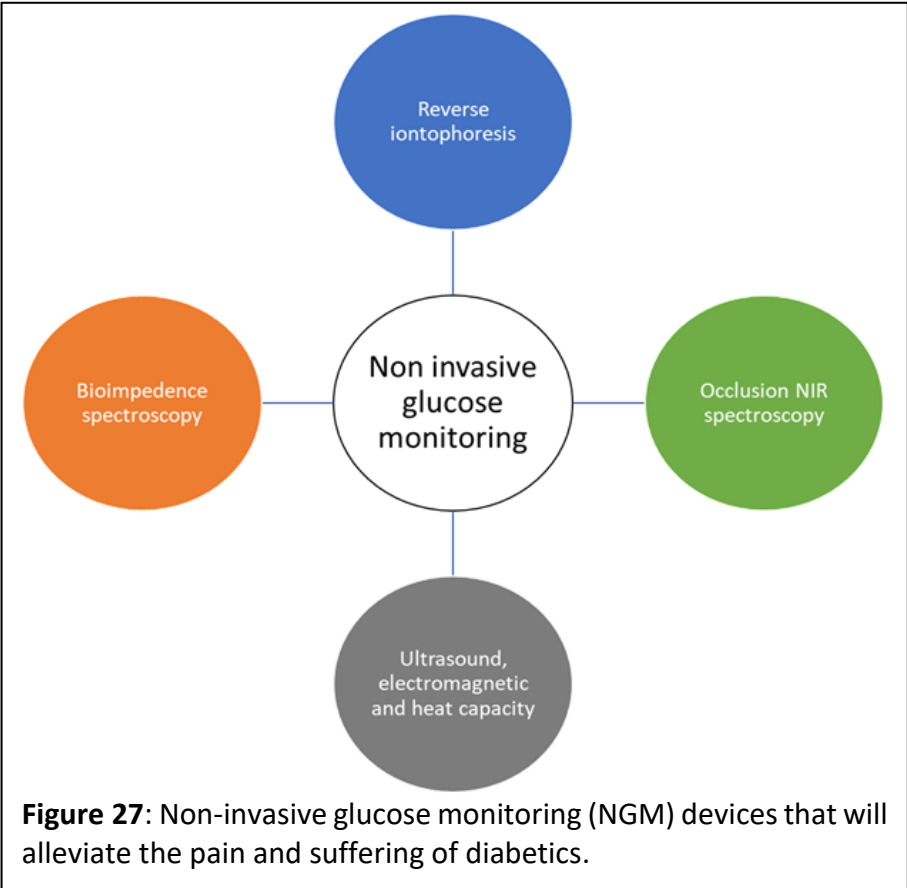
Indeed, as developed at length in the section dealing with carbohydrate homeostasis, glycaemic variations are not only dependent on glucose metabolism (Vetrani et al. 2022). Amino acid and lipid metabolism also play a major role in modulating glycaemic variability.

Therefore, relying solely on a glucose catalysis reaction only gives a partial picture of the patient's insulin requirements.

5.2 Non-invasive glucomonitoring

There is a serious need to develop non-invasive glucose monitoring (NGM) devices that will alleviate the pain and suffering of diabetics. In this section, we will present some of the approaches that

have been developed to design non-invasive devices as an alternative to commercially available CGM systems (Badugu, Lakowicz, et Geddes 2003). For these alternative systems, other body fluids besides blood have therefore been used that have potential for non-invasive glucose monitoring;



among them, saliva, urine and tear fluid are potential candidates (Villiger et al. 2018; Choy et al. 2001; Chen et al. 2017)

Non-invasive devices include: transdermal sensors that pass near-infrared (NIR) light through the stratum corneum to detect glucose concentrations, and external analyses of body fluids

(i.e. saliva, tears, breath) using a variety of optical and electrochemical detection methods (Tang et al. 2020). Annexe 3, Table 3

However, as we can see in the table, these devices also have significant disadvantages that do not currently allow them to be used for reliable blood glucose monitoring (Vashist 2012).

Continuous glucose monitoring (CGMS) has made a considerable way since its initial introduction in a clinical setting in the 1970s (Kropff et DeVries 2016) and has been miniaturized to provided autonomy and comfort. Moreover, a number of studies have clearly shown that CGMS reduces hyperglycemia as compared to other therapies and is thus expected to reduce the dire long-term complications of type 1 diabetes (Kropff et DeVries 2016; Danne et al. 2017).

The major drawbacks in currently marketed technology reside in the occurrence of hypoglycemia with its inherent life-threatening risk due to the powerful action of the hormone insulin and suboptimal glycaemia control especially under disturbances (physical activity, unannounced meals, etc). Although current CGMS have improved the situation compared to non-sensor driven approaches, this problem has to be mastered to provide a generally accepted device and real autonomy in terms of closed-loop.

Control algorithms have an important role in CGMS coupled pump treatment. The concomitant existence of currently some seven different classes or combinations of algorithm types in clinical devices strongly suggests that a sufficient solution has not been found yet. The PID approach is probably the best mastered technique (Hariri 2011; Abbes et al. 2013), it is easier to implement but exhibits insufficient robustness to multiple challenges. Another well-known class of closed loop of control algorithms is the so-called “model predictive approach” (MPC), which makes explicit use of a system model to optimize the future predicted behaviour of a system (human insulin/BGC system in our case). At each sampling time, a finite time optimal control problem is solved over a prediction horizon, using the current state of the system as the initial state. Although this represents a considerable improvement (Pinsker et al. 2016; Del Favero et al. 2014), it still depends on the model for correct prediction. An improvement to this problem results in the optimal control techniques and the H^∞ control approach (Kovács et al. 2009; Ruiz et al. 2012). The obtained performance in terms of glycaemia regulation demonstrates that an improvement of existing CGMS is possible. Finally,

it is interesting to note that a bi-hormonal system (insulin and glucagon) has been investigated (Castle et al. 2010). In outpatients a glucagon channel has been added to the device and compared to mono-hormonal devices or manually regulated insulin pumps (El-Khatib et al. 2017). Benefits from this novel technology do not seem to be unequivocal and some stratification may be required which obviously requires larger cohorts.

A second major drawback is that whole body physiology is not “seen” by the classical sensor. Recently physical activity has been addressed, an important variable in glucose homeostasis, to avoid hypoglycaemia. Though heartbeat could be measured easily, this biological approach is not feasible as hypoglycaemia may well slow heart rate (Novodvorsky et al. 2017), thus disturbing the information sought in the absence of external control. One approach is to reinforce a Closed-Loop (CL) system using MPC algorithm, such as in the Diabeloop project (Quemerais et al. 2014), by a decisional matrix on physical activity, uploaded on an Android OS smartphone linked to Dexcom CGMS and a Cellnovo insulin patch-pump. Similar approaches have been tested in the commercial DexCom system (DeBoer et al. 2017). This underlines the benefit to consider additional informations for an enhanced artificial pancreas although the occurrence of physical activity has still to be anticipated in Diabeloop: this adaptive homeostatic correction is clearly just one of many situations encountered in daily life.

To conclude, none of the current approaches imitates the endogenous regulation of glucose homeostasis in a physiological manner such as biphasic and oscillatory release. This pattern ensures on the one hand rapid decrease in initial glucose levels followed by constant delivery during digestion, and on the other hand avoids rapid desensitization of insulin receptors. Obviously subcutaneous insulin delivery (in contrast to physiological portal release) will partially abnegate oscillatory delivery but recent progress in ultra-fast insulin may allow obtaining some variations in blood levels (Heinemann et Muchmore 2012).

5.3 A new islets-based biosensor:

Pancreatic islets are the “in-born” sensors and actuators, optimally shaped to ensure regulation of glucose homeostasis. The islets’ endogenous algorithms are still largely unknown and encode physiologically important events. Thus, current models do not contain an explicit description of the complex behaviour required for homeostasis. The development of a blood

glucose monitoring system based on the use of Langerhans islets as sensors involves many technological challenges and requires the use of different techniques.

Where to measure glucose?

The presence of biological material in the biosensor makes it necessary to position it extracorporeally. This raises the question of where the most appropriate place to monitor glycemia is. In terms of the body fluids of interest, two candidates naturally present themselves. A measurement in the blood or in the interstitial fluid. This issue has been widely discussed in the CGMs literature. In most cases these devices were subcutaneous, minimally invasive, amperometric/enzymatic biosensor-based systems (Vaddiraju et al. 2010) and consequently provided an indirect evaluation of the plasma blood glucose level by means of a glucose concentration measurement in the extracellular interstitial fluid. When using these devices, the sensor or the sampling probe needs to be inserted through the skin inside the subcutaneous fatty tissue in order to come into contact with the interstitial fluid (Danne et al. 2017). Despite being in the early stages of the CGM development, a number of interstitial fluid sampling and measurement methods have been considered (optical methods (Heinemann 2003), capillary ultrafiltration (Linhares et Kissinger 1992), hypodermic needles (Bantle et Thomas 1997), open-flow microperfusion and impedance/ electromagnetic spectroscopies (Pfützner et al. 2004). CGMs that showed the highest accuracy and reliability performances are those based on one of two types of technology: transcutaneous (or needle-type) systems (Rice, Coursin, et Riou 2012), where the amperometric biosensor is situated on the tip of a thin needle directly implanted in the subcutaneous tissue (Wentholt et al. 2005) or microdialysis-based systems. In the latter, commercialized by Menarini the glucose is harvested from the interstitial fluid, by means of a constant flow of saline buffer, which passes through a subcutaneously implanted microdialysis probe, and leads to a biosensor flowcell placed downstream (Ricci et al. 2007). All of these systems have been designed to operate in the subcutis, rather than in the blood, due to its easy and safe accessibility, and for the possibility of frequent sensor replacement (Gerritsen 2000). The glucose concentration in the interstitial fluid (IFG) demonstrated to have a high correlation with the corresponding plasma glucose value, it is nevertheless known that the IFG differs from BG both in time, generally

presenting changes in delay in regard to the BG (physiological lag time), and in their absolute value of glucose concentration.

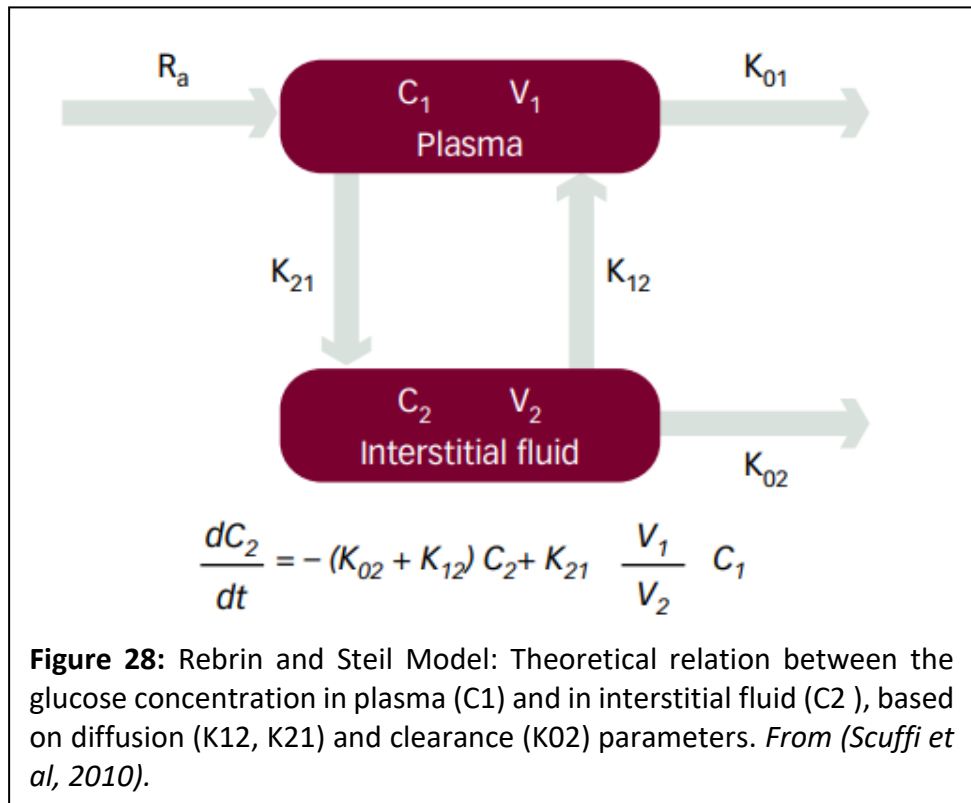
Dealing with interstitial fluid means take into consideration three parameter : time gradient between BG and IFG, magnitude gradient between BG and IFG, and physiological outcomes that can affect these two parameters (Scuffi et al., 2010).

The time gradient defines the delay, or lag time, observed between the variation of the BG value (usually referring to the venous plasma) and the corresponding change in IFG. The term 'lag time' usually refers only to the physiological lag, and thus only to those physiological processes regulating the glucose exchange between blood and interstitium. In several studies, this also included the instrumental lag, specific to the device used for the IFG sampling and measurement. The instrumental lag time also comprises a sampling lag, corresponding to the time needed for glucose transport from the interstitial fluid to the biosensor and a computational lag, related to all the calculation algorithms applied (Scuffi et al., 2010). The main and ongoing concerns related to the lag time are if it is either positive or negative, and thus if the IFG follows or precedes the BG, and if its value is constant or variable (Keenan et al. 2009). In the majority of studies it was observed that the IFG delayed with respect to the BG, independently of whether the BG is rising, falling or reaching nadirs/peaks, with a lag time value that ranged between 5 and 25 minutes (Bm et al. 1995), This confirms a kinetic equilibrium based on a 'two-compartment' model of glucose diffusion from blood to interstitium (Rebrin et al. 1999). In other studies, the IFG was found to anticipate the BG decrease during insulin-induced hypoglycaemia. This was explained by increased glucose uptake from the IF by the surrounding cells, which lead IFG to drop prior to BG, as described by the 'push-pull' model (Aussedat et al. 2000).

Magnitude gradient is the difference in absolute glucose concentration between plasma and IF. This is related both to the glucose concentration value in the two compartments during the steady-states, and to the magnitude of the respective glucose concentration excursions (Kulcu et al. 2003). In some studies (Petersen 1999), involving mainly healthy subjects, the magnitude of the IFG and BG excursions and their values in their respective steady-states were found to be similar. However, a large group of studies agrees that both the glycaemic excursions and steady-state values of IFG and BG can show significant differences (Rebrin et al. 1999), but always maintaining a high correlation factor.

Physiological reactions after implantation of a needle or a probe of a device can also have an impact on IFG measurement. The main effect of these local reactions is transitory and limited to the few hours after the probe implantation, until a new physiological equilibrium at the tissue/probe interface is reached (Ratner 2007). However, some events of daily life can bias this equilibrium. The occurrence of pressures or mechanical shocks on the implantation area can reactivate the local reactions and thus alter the equilibrium at the sensor–tissue interface, leading to another transitory period of lowered IFG versus BG correlation (Gilligan et al. 2004). Although even if a total consensus was not yet achieved on the BG/IFG relationship, a number of mathematical models for the BG versus IFG equilibrium description have been proposed. These models assume of a free diffusion of glucose molecule between blood and interstitium,

and in its uptake from the IF by the surrounding cells (Steil et al. 1996; Freeland et al. 2004). Rebrin and Steil proposed a ‘two-compartments’ model, which described IF and blood as two independent



compartments, separated by a diffusional barrier through which the glucose is free to diffuse based on its concentration gradient (Steil et al. 1996; Rebrin et Steil 2000) .

Moreover, the glucose is cleared from the IF by the surrounding cells, depending from IFG. This Rebrin and Steil model provides an effective mathematical description of two important phenomena experimentally observed in several studies: the IFG follows the BG with a certain lag time; during the steady-states the glucose concentration in the two compartments can be significantly different. The only concern about this model is the assumption that both the

diffusion across the IF/blood barrier and the clearance from the IF are related to BG and IFG values by constants (K_{12} , K_{21} and K_{02} in the equation of Rebrin and Steil), while several evidences suggest that the dependence of these diffusion processes by BG and IFG is variable over the time. Another widely recognised model, based on the 'push-pull' effect, was proposed. This approach hypothesised that during the rising of BG the lag time between BG and IF is caused by the glucose diffusion (push) from blood to IF, while during the falling period of BG the IFG decreases in advance with respect of BG, due to the insulin-induced uptake (pull) of glucose by the surrounding cells (Aussedat et al. 2000). This model allows explanation how in some particular conditions (e.g. insulin-induced hypoglycaemia) the drop of IFG can anticipate that of BG (Schmidtke et al. 1998; Thomé-Duret et al. 1996). The previous approaches were further refined by Groenendaal et al., reporting a model where a specific equilibrium between IFG and BG was described for each skin layer (epidermis, dermis, adipose tissue) (Groenendaal et al. 2010).

In conclusion, the experimental evidence in the literature suggests that BG and IFG are correlated by a kinetic equilibrium, which has as consequences a time and magnitude gradient in glucose concentration between blood and interstitium (Kulcu et al. 2003). For the development of a new extracorporeal islet-based biosensor interstitial fluid is the right localisation to do the glycaemia measurement. It's a good compromise between easily access and precision of the measurement.

How to measure glucose?

The use of living cells in the sensor calls for caution and stringent procedures. For that reason, the use of microdialysis and safety valves to provide the analyte instead of membranes separating cells from patient's body upon implantation, although major progress has been made in the latter field (Schweicher, Nyitray, et Desai 2014). The microdialysis approach has been used previously in diabetes therapy and allows reliable separation between patient and biosensor (Heinemann 2003).

Microdialysis was introduced by Ungerstedt and Pycock and has been used mainly in neuroscience research to quantify the metabolites present in cerebral spinal fluid (Ungerstedt 1991). However, over the last decade it has been increasingly applied to various tissue studies

for in situ monitoring of different biomarkers in basic and clinical studies (Ungerstedt 1997; 1991; MacLean, Sinoway, et Leuenberger 1998) . The basic principle of microdialysis is to reproduce the characteristics of a blood capillary. Indeed, the capillaries and the semi-permeable membrane are surrounded by substrates and metabolites in the extracellular fluid of the tissue (Müller 2002).

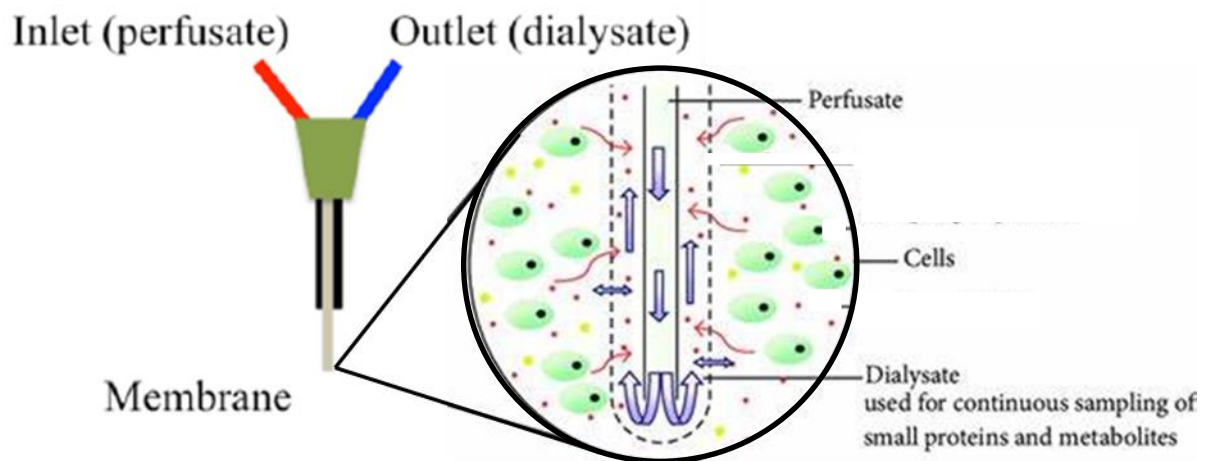


Figure 29: Microdialysis principle, scheme of a microdialysis probe and details of the exchanges at the level of the semi permeable membrane. Microdialysis membrane is depicted as a tip, which is connected via a shaft to the inlet and outlet tubings; The semipermeable membrane limits the diffusion of large molecules *Adapted from Kalkhof et al., 2014.*

These molecules diffuse through the membrane portion of the catheter and equilibrate with the perfusion fluid, which is pumped through the catheter at very low flow rates. Changes in the concentration of a substrate in the surrounding medium are reflected by subsequent changes in the dialysate (Lönroth et Smith 1990). Rather than inserting an instrument into the tissue, the microdialysate is extracted and subsequently analysed in the laboratory or clinic at the patient's bedside.

A typical setup for a microdialysis system requires a syringe pump, a microdialysis probe (also known as catheter), and connecting tubes (Kho et al. 2017). Among all the components required for microdialysis sampling, the microdialysis probe is the most important component (de Lange, de Boer, et Breimer 2000; Min et al. 2016) and will be in contact with the target site. Recovery of microdialysis sampling depends on the probe. Basic designs for microdialysis probes, linear, u-shaped or looped, OR concentric (Plock et Kloft 2005; Kit Lee 2013). Other popular designs for microdialysis probes include the shunt probe and the side-by-side probe,

as portrayed in (Plock et Kloft 2005; Kho et al. 2017). Microdialysis probe configuration mainly depends on the target site. For our utilization in subcutaneous compartment, a linear design of the probe is recommended (Baumann et al. 2019), indeed this kind of design is commonly used for sampling in soft peripheral tissues such as skin, lung, kidney, and muscle because it's easy to implant, and can follow the movement of the tissue (Min et al. 2016).

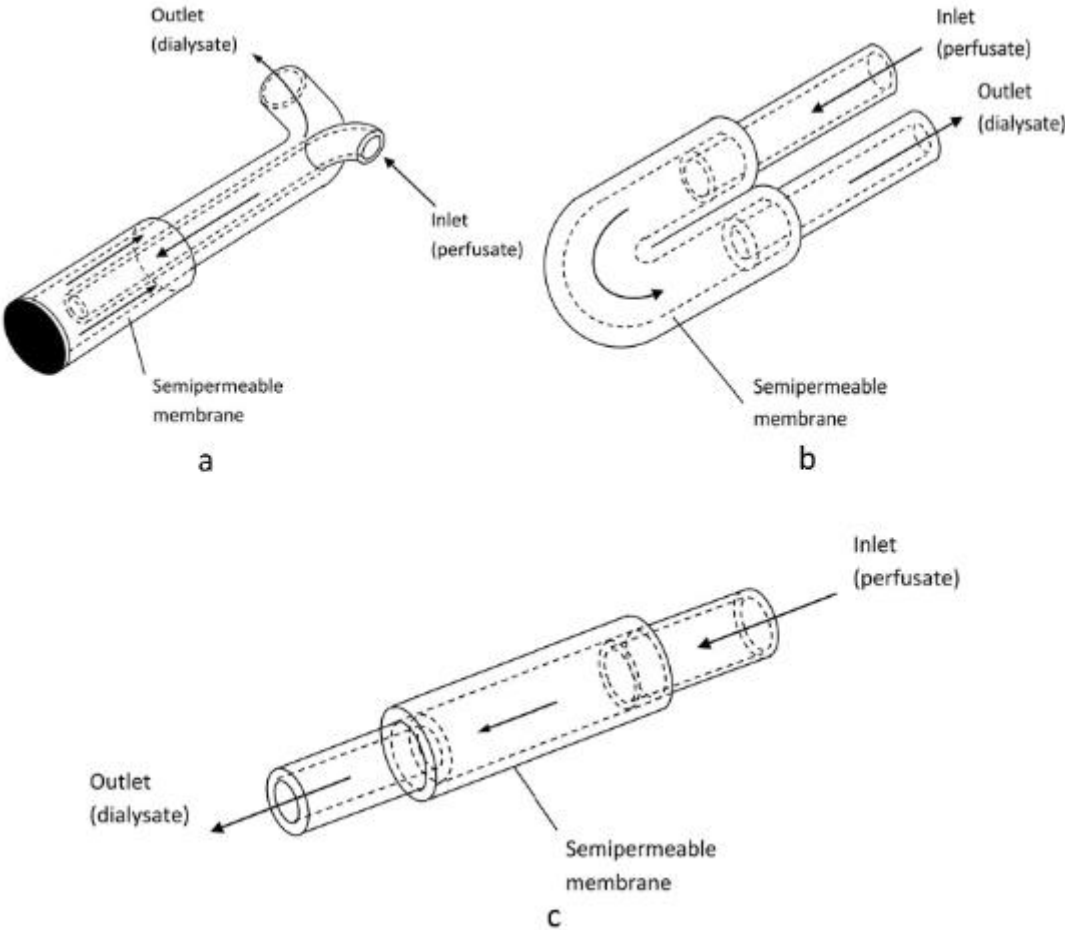


Figure 30: Schematic illustration of the more common microdialysis probe designs: a concentric, b loop, and c linear microdialysis probes. *From (Kho et al. 2017)*

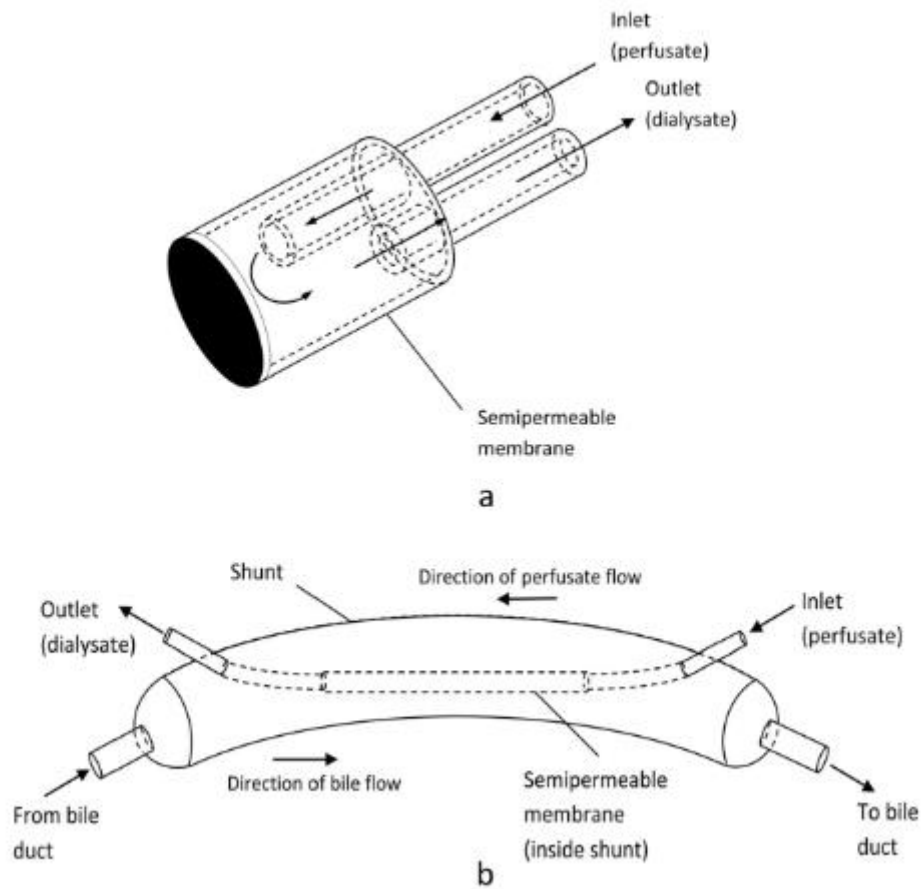


Figure 31: Schematic illustrations of microdialysis probe designs: a side-by-side and b shunt. From (Kho et al. 2017).

Recovery percentage depends on several factors, such as diffusion rate, flow rate, flux, membrane length, membrane type/pore size, and perfusion liquid. The best results require optimization of each factor (Kho et al. 2017). For example, the lowest flow rate, longest practical membrane, and maximum sampling time will yield samples with the highest concentration of the analyte. This is because the membrane is maximizing surface area for diffusion, while the slow flow rate is giving diffusion plenty of time to equilibrate; the sampling time determines the absolute content each sample will contain (Hammarlund-Udenaes 2017). This example is a simplified understanding of the factors that must be considered.

Diffusion: The diffusion rate is inversely proportional to the molecular size. This means that as the molecular weight of the analyte increases, the diffusion rate will decrease. If the diffusion rate decreases, then the recovery percent decreases. This essentially forces a lower flow rate for large molecules (Snyder et al. 2001). Next, hydrophobicity also plays a role in the diffusion rate and must be considered when analysing large molecules, such as neuropeptides. Hydrophobic

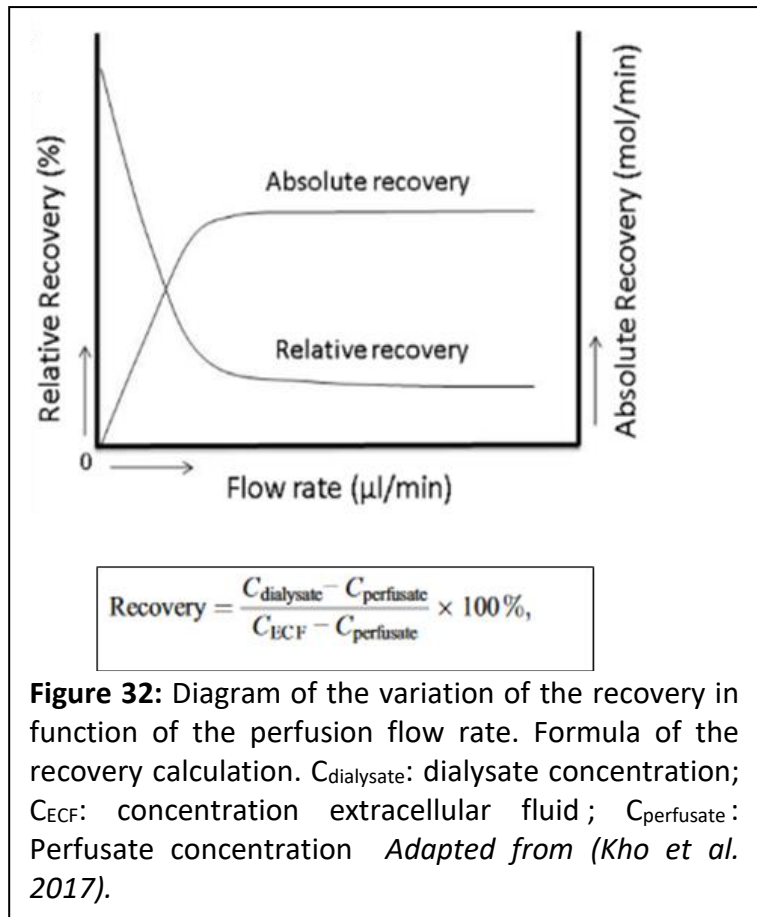


Figure 32: Diagram of the variation of the recovery in function of the perfusion flow rate. Formula of the recovery calculation. $C_{\text{dialysate}}$: dialysate concentration; C_{ECF} : concentration extracellular fluid; $C_{\text{perfusate}}$: Perfusate concentration *Adapted from (Kho et al. 2017)*.

molecules also exhibit characteristics which make monitoring of concentration changes (primarily decreases) difficult since these changes take significantly longer to equilibrate (Chefer et al. 2009). The concentration of the target analyte can be depleted from the area around the probe faster than it can be supplied by the cells or diffused from surrounding extracellular fluid; This is partly because of diffusion in tissue taking longer than in aqueous solutions due to limited extracellular fluid and indirect diffusion pathways between cells. Analytes may attach to cells along the way and slow down their diffusion.

Flow Rate and Flux: Low flow rate creates low pressure in the probe; when using a perfusion liquid that mimics extracellular fluid besides the low pressure, there is a minimal ionic flux. The principle of flux can estimate extracellular concentrations of the target analyte (E. C. M. de Lange 2013). To do this, the perfusate is spiked with a known concentration of the target analyte and then pumped through the probe. The dialysate is analysed for differences in concentration; decreased analyte concentration in the dialysate shows that extracellular fluid has a lower concentration of the analyte, therefore, the analyte diffused from the perfusate to the extracellular fluid (Kit Lee 2013). If the concentration of the analyte in the dialysate was

found to be higher than its initial concentration, then it can be inferred that extracellular fluid is higher in analyte concentration, therefore, the analyte diffused from the extracellular fluid into the perfusate.

Perfusion liquid: The perfusion liquid should be as close as possible in nature to the extracellular fluid but with a lower osmolarity in order to induce a diffusion gradient. Usually Ringer's solution (148 mM NaCl, 4 mM KCl, 3 mM CaCl₂) (Khan et al. 2015) which has higher calcium and potassium levels than interstitial fluid (148 mM NaCl, 4 mM KCl, 1.2 mM CaCl₂, 0.85 mM MgCl₂). Osmolarity is then adjusted with molecules like clinical grade Dextran 60 (μ dialysis).

In conclusion, the use of microdialysis allows the use of live cells in the sensor in a safe manner, as the islets in the biosensor are separated from the patient's body, while allowing access to the interstitial fluid.

However, the use of this technology requires working at very low perfusion rates in order to have an optimal recovery percentage. This can lead to long delays before the dialysate arrives in the biosensor, as well as the possible drying of the islets. To manage these constraints, the use of microfluidics allows to work with very low volumes of dialysate and micrometric workflows.

5.4 Microfluidics: the flow management solution for the islets on chip biosensor

The constant need for miniaturization and multiplexing of systems in different scientific fields requires microfluidics to control small volumes of fluid.

Microfluidics is defined as the science and technology of systems that handle small volumes of fluids of less than a microlitre, using channels of the size of a few hundred or tens of micrometres (Whitesides 2006). Microfluidics can also be defined as a discipline dealing with the flow of simple or complex, single or multiphase fluids in artificial microsystems, i.e. manufactured using the new microfabrication techniques inherited from microelectronics

(Tabeling 2003). These definitions show that microfluidics is conceived as a science that encompasses the study of phenomena and fluid mechanics on a micrometric scale, but also as a technique that contains an applicative dimension. Microfluidics, although recent, derives from mechanisms that have been present in nature for millions of years. In the plant world, the tree, for example, is a complex microfluidic system. It drains sap to thousands of leaves in a homogeneous way, relying on a network of millions of small capillaries, whose diameters vary from hundreds of microns to about thirty nanometres. The tree manages this microfluidic network. It even manages to work under negative pressure, which, from a hydraulic engineering point of view, is an exceptional performance. Of course, bubbles nucleate permanently in the capillaries draining the sap. But there are thousands of built-in valves in the tree that prevent the formation of a general embolism (Tabeling 2003).

In the animal kingdom, we can also mention the spider, which is a real expert in microfluidics. To weave its web, it manages micrometric flows of proteins, solidifies them, and produces a continuous flowing, hair-thin fibre whose adhesive properties are optimised for insect capture (Konwarh, Gupta, et Mandal 2016). In humans, our bodies manage hundreds of micrometric flows in a highly controlled manner. Over a wide range of scales, from a few nanometers (size of a protein such as aquaporin) (B.-J. Jin et Verkman 2017) to hundreds of microns (diameters of large blood capillaries) (Vedula et al. 2017).

The field of microfluidics lies at the crossroads of four major fields: molecular analysis, biodefense, molecular biology and microelectronics (Lei et al., 2018; Daw et Finkelstein, 2006). Molecular analysis was the first to contribute to microfluidics, indeed the distant origins of microfluidics lie in microanalysis methods - gas chromatography (GC), high pressure liquid chromatography (HPLC) and capillary electrophoresis (CE) - which, in capillary format, revolutionised chemical analysis (Whitesides 2006). These methods have made it possible to achieve high sensitivity and high resolution simultaneously using very small amounts of sample. With the success of these micro-analytical methods, it seemed obvious to develop new, more compact and versatile formats and to look for further applications of microscale methods in chemistry and biochemistry.

A second and very different factor that drove the development of microfluidic systems was the realisation after the end of the Cold War that chemical and biological weapons posed a major military and terrorist threat (Whitesides 2006). To counter these threats, the Defense Advanced Research Projects Agency (DARPA) of the US Department of Defense supported a

series of programmes in the 1990s to develop field-deployable microfluidic systems designed to serve as detectors of chemical and biological threats. These programmes were the main stimulus for the rapid growth of academic microfluidic technology.

The third impetus for the development of microfluidics came from the field of molecular biology. The explosion of genomics in the 1980s, followed by the advent of other areas of microanalysis related to molecular biology, such as high-throughput DNA sequencing, necessitated analytical methods with much higher throughput, sensitivity and resolution than previously envisaged in biology. Microfluidics has offered approaches to overcome these problems. The fourth contribution has come from the development of photography and microelectronics (Whitesides 2006). The initial hope of microfluidics was that photolithography and associated technologies, which had been so successful in silicon microelectronics and microelectromechanical systems (MEMS), would be directly applicable to microfluidics (Tabeling 2003).

More generally, everyday objects based on microfluidic techniques are now commonplace, from inkjet print heads to pregnancy tests. These technologies have thus become unavoidable and have undergone exponential development over the last 10 years.

In the medical field, the use of microfluidics opens new doors, both in the clinical and research fields. It can push back the limits of the tools currently used in the drug development process, cell cultures and animal models, which have highlighted the need for a powerful new tool capable of reproducing human physiology *in vitro* to the maximum extent (Maschmeyer et Kakava 2020). Advances in microfluidics have brought the realisation of this tool closer than ever. It is on this last point that we will discuss in the following chapter and think specifically about the microfluidic field of Organ-on-chip.

Organ-On-Chip (OOC):

For centuries, animal experiments have contributed greatly to our understanding of disease mechanisms, but their value in understanding the full pathophysiological mechanisms and in predicting the efficacy of drug treatments in the clinic has limitations (Kola et Landis 2004). Animal models, and even genetically modified models or models with experimentally induced pathologies, often do not accurately reflect human pathology (Bracken 2009) and therefore cannot predict with certainty what will happen in humans (Pun, Haney, et Barrile 2021). In

addition, the growing awareness of animal rights in our societies has led to measures to avoid the use of animals in research (Doke et Dhawale 2015). In 2018, for example, nearly two million animals were used in French laboratories according to a survey by the Ministry of Research (« Enquête statistique sur l'utilisation des animaux à des fins scientifiques » s. d.). Of these, 75% were involved in so-called "light" or "moderate" procedures. Only 18.7% were involved in 'severe' procedures, and 6.3% in 'no awakening' procedures. These figures, in the eyes of a growing proportion of the population, have become unacceptable and have led to a near unanimous vote in the European Parliament on 16 September 2021 to almost completely stop the use of animal models by 2030, except in a few studies on specific diseases such as cancer (« Texts Adopted - Plans and Actions to Accelerate a Transition to Innovation without the Use of Animals in Research, Regulatory Testing and Education - Thursday, 16 September 2021 » s. d.) .

It is on the basis of these findings, both scientific and ethical, that organ-on-a-chip (OOC) technology and bioengineered tissues have emerged as promising alternatives for a wide range of applications in biodefence, drug discovery (Pammolli et al. 2020) and development and precision medicine. Recent technological breakthroughs in stem cell and organoid biology, OOC technology and 3D bioprinting have all contributed to a significant advance in our ability to design, assemble and fabricate biomimetic living organ systems that more accurately reflect the structural and functional characteristics of human tissues in vitro (Bhatia et Ingber 2014), and allow for improved predictions of human responses to drugs and environmental stimuli.

Islets-on-chip:

A variety of microfluidic devices have been introduced to recreate native islet microenvironments and to understand pancreatic β -cell kinetics in vitro. This kind of platforms has been shown fundamental for the study of the islet function and to assess the quality of these islets for subsequent in vivo transplantation. However, islet physiological systems are still limited compared to other organs and tissues, evidencing the difficulty to study this "organ" and the need for further technological advances (Rodríguez-Comas et Ramón-Azcón 2021).

The study of insulin secretion aimed at addressing islet functionality requires monitoring insulin release over time. However, the existing standard assays for islet functionality and viability present limited physiological relevance: usually, it involves numerous animals to assess the capacity of the pancreas to secrete insulin after a glucose challenge and/or static assay incubations of isolated islets subjected to low and high glucose concentrations in order to evaluate the insulin stimulation index (Rodríguez-Comas et Ramón-Azcón 2021). These experiments are laborious, require long processing time, and are usually followed by off-line quantification of insulin by an enzyme-linked immunosorbent assays (ELISA) or a radioimmunoassay (Shen, Prinyawiwatkul, et Xu 2019). Hence, its readout is not obtained in real-time, making it impossible to measure rapid spatiotemporal responses. Additionally, these measurements do not have the sufficient sensitivity to measure insulin released by a single islet, and consequently these measurements are usually performed using batches of islets. Culturing pancreatic islets from rodents or human donors is difficult. For this reason, minimizing the number of islets required for experiments is fundamental. Moreover, the release of hormones from pancreatic islets occurs within minutes in a pulsatile fashion in response to an appropriate stimulus. Thus, to resolve the secretion dynamics, methods able to quantify insulin secretion with high temporal resolution are required. New high-technological advances have allowed the development of microfluidic organ-on-a-chip systems to recapitulate in vivo cellular models with a high level of control. Recently, they have been defined as “microfabricated cell culture devices designed to model the functional units of human organs in vitro” (Park, Georgescu, et Huh 2019). These new technological devices are emerging as a powerful tool for the study of multifactorial pathologies such as diabetes. Organ-on-chips are usually based on polymeric platforms where living microtissues can be cultured and, in combination with microfluidics, mimic specific functions of one or multiple organs.

The development of a biosensor using an islet on chip platform requires a precise specification of the characteristics and constraints of the device. Indeed, the use of microfluidics, although offering many advantages, also obliges us to face various difficulties inherent to the management of such small volumes of fluid.

The design of any new microfluidic device involves a methodology common to all OOC development. The principles to manufacture all OOC based platforms are almost similar.

Basically, after considering various parameters to emulate the specifications of a specific organ, the desired design would be drawn with a design and drafting software (e.g., AutoCAD, CATIA) (Schmidt 1998; Kovacs, Maluf, et Petersen 1998). Later, an appropriate microfabrication technique (e.g., photolithography, stereolithography, soft lithography etc.) according to the aims of the device will be used to fabricate the device (Azizipour et al. 2020). Cell culture or tissue culture will be performed on the biochip in order to mimic the functionality of a specific organ and to perform biochemical or biophysical assays or drug testing (Voldman 2003).



Figure 33: General process of development of an OOC. *Adapted from (Azizipour et al. 2020).*

The first point to consider is the evaluation of the specificities of the islet on chip. What are the specificities of the Langerhans islet culture for their use as a biosensor? The chip should contain a few islets (10 to 20), in a volume small enough to be compatible with the supply of dialysate through microdialysis but large enough to allow a good supply of nutrients and oxygen to the cell (Jaffredo et al. 2021). In addition, the design of the microfluidic chip must be compatible with an alignment on a commercial Multi-Channel System multielectrode array (Raoux et al. 2012a) and allow for long term use in order to limit the change of biosensor by the patient and thus promote patient acceptability.

Long-term culture in microfluidics exposes two major difficulties common to the microfluidic field. Indeed, the first risk of working at low flow rates over a long period is the formation of bubbles (He et al. 2021).

Gas bubbles present a frequent challenge to the on-chip investigation and culture of biological cells and, small organs. The presence of a single bubble can adversely impair biological function and often viability as it increases the wall shear stress in a liquid-perfused microchannel by at least one order of magnitude (Lochovsky, Yasotharan, et Günther 2012).

Unwanted bubbles can also lead to severe cell damage by rupturing the cell membrane (Zheng et al. 2010; Lochovsky, Yasotharan, et Günther 2012) and device malfunction by disrupting the local electric field (Berthod et al. 2002).

Different parameters must be considered in order to avoid the formation of bubbles:

Chip design: At the design stage, certain parameters must be considered that can lead to bubble formation. Changes in geometry leading to sudden changes in shear stress and the implementation of angular structures are the main nucleating features within a design (Pereiro et al. 2019).

Fluid switch: When changing the injected liquid during an experiment, the same phenomenon can appear. If you change the liquid inside the reservoir, you might need some time to eliminate the amount of air introduced into the microfluidic setup (Sung et Shuler 2009).

Porous material: Porous and gas-permeable material, such as PDMS, can induce air bubbles inside microfluidic chips, especially in long term experiments (Duffy et al. 1998).

Dissolved gas: Gas contained in gaseous form in the liquids used during the experiment can cause air bubbles to form. It is especially the case when the liquids are heated during the experiments (Cheng et Lu 2014).

Working with live cells within a device also requires care to avoid clogging the chip or tubing with cell debris or cell dislodgement during perfusion (Lochovsky, Yasotharan, et Günther 2012).

The development of a microfluidic chip in the laboratory also imposed constraints on the implementation of microfabrication. We will now outline the techniques used to build the chip, once the design has been thought out.

Production of the chip:

The ability to fabricate biocompatible constructs to model biomechanical forces was long limited to a small number of specialised research teams, the invention of an optically transparent and cost-effective silicon material, poly dimethyl siloxane (PDMS) in the late 1990s, combined with the use of soft lithography and precise mechanoactuators (Duffy et al. 1998),

was a revolution and thus enabled the implementation of dynamic culture to many fields of study.

PDMS or dimethicone, is a polymer widely used in the manufacture and prototyping of microfluidic chips. It is an organo-mineral polymer (a structure containing carbon and silicon) of the siloxane family (a word derived from silicon, oxygen and alkane) (Walker et Naisbitt 2019). Outside of microfluidics it is used as a food additive (E900), in shampoos, as an anti-foaming agent in drinks or in lubricating oils (Becker et al. 2014).

For the manufacture of microfluidic devices, PDMS (liquid) mixed with a cross-linking agent is poured onto a microstructured mould and heated to obtain a replica of the elastomer mould (cross-linked PDMS).

Formula of PDMS is : $(C_2H_6OSi)_n$ and $CH_3[Si(CH_3)_2O]_nSi(CH_3)_3$, where n is the number of repeats of the monomer . Depending on the size of the monomer chain, the non-crosslinked PDMS can be almost liquid or semi-solid. The siloxane linkages provide a flexible polymer chain with a high level of viscoelasticity (Mata, Fleischman, et Roy 2005).

After cross-linking, PDMS becomes a hydrophobic elastomer. Thus polar solvents such as water have difficulty wetting PDMS (water forms drops and does not spread) and leads to the adsorption of hydrophobic contaminants present in water on the PDMS surface (Lin et Chung 2021). Oxidation of PDMS using a plasma, changes the surface chemistry of PDMS and produces silanol (SiOH) endings on its surface. This process also makes the surface resistant to adsorption of hydrophobic and negatively charged molecules. In addition, plasma oxidation of PDMS allows the PDMS surface to be functionalized with trichlorosilane or to be covalently bonded (on an atomic scale) to a glass surface that has also been oxidized through the creation of Si-O-Si bonds (Auner et al. 2019).

The manufacture of a PDMS microfluidic chip basically consists of 6 steps (Velve-Casquillas et al. 2010):

- (1) The moulding step allows the microfluidic chips to be mass-produced from a mould.
- (2): A mixture of PDMS (liquid) and cross-linking agent (to harden the PDMS) is poured onto the mould and placed in an oven.

(3): Once the PDMS is cured, it can be peeled off the mould. A replica of the PDMS microchannels.

(4): To allow for fluid injection during future experiments, the inlets and outlets of the microfluidic device are pierced with a needle or punch the size of the future outer tubes.

(5): Finally the face of the PDMS block with the microchannels and the glass substrate are treated with O₂

(6): The plasma treatment of the surface allows the PDMS and the glass substrate to be bonded to close the microfluidic chip.

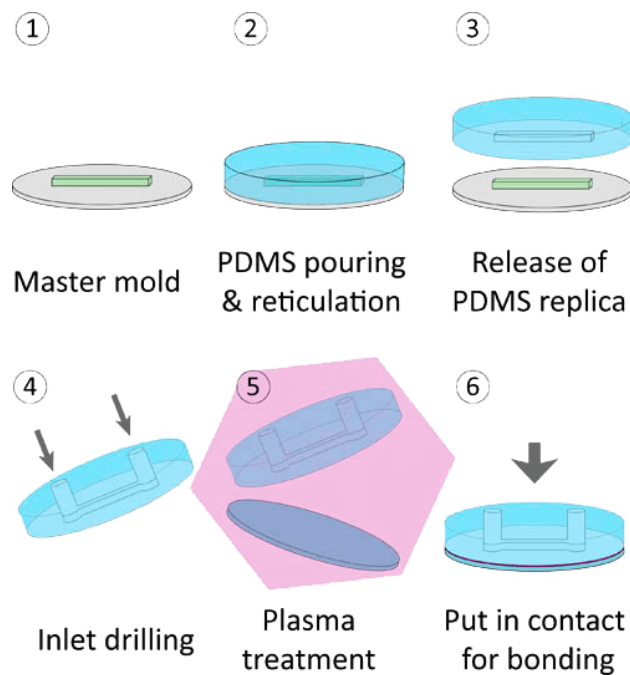


Figure 34: Protocols of the fabrication of a PDMS microfluidic chip. (1) Design and microfabrication of a wafer, (2) realization of PDMS step of reticulation and pouring, (3) demolding of the PDMS chip, (4) punching of the inlet and outlet for tubings connexion, (5) plasma treatment for activation of the surfaces, (6) alignment of the PDMS chip. *From (Velve-Casquillas et al. 2010)*

In conclusion, PDMS has many advantages for the manufacture of microfluidic chips in the laboratory. Its biocompatibility, ease of use and plasma activation capability, which allows alignment on glass surfaces such as MEAs, make it suitable for routine chip prototyping and production. In addition, it allows the construction of chips compatible with the islet on chip specifications outlined above in the previous paragraph and the gas permeability of this material is very important for cell culture.

In this chapter we have discussed the various technical issues involved in the development of a new biosensor based on the use of islets of Langerhans as a blood glucose sensor. However, there is one last point of interest that needs to be addressed before moving on to the presentation of the thesis objectives. Are islets, although ideal glucostats, the only possible candidates as sensors?

5.5 Sensor, which biological substrate to use?

The use of primary cultured Langerhans islets has many advantages in terms of sensing. Indeed, in addition to being the body's natural glucostats (Rorsman et Ashcroft 2018), they are natural organoids, with a cohesive structure allowing for manipulation compatible with the loading of a microfluidic chip (Y. Wang et al. 2010). However, the use of native islets also raises logistical issues related to the difficulty of supply.

The use of murine islets within an islet-based biosensor is complicated beyond the laboratory doors. This point raises many questions for the development of this device. Indeed, as we discussed in the section on therapeutics for the treatment of type 1 diabetes, the supply of human cadaveric islets involves many difficulties (Kulkarni et Stewart 2014). Only 70 centres worldwide practice the isolation of human islets from cadaveric donors, and there is a real lack of organ donations (Ng et al. 2019). Finally, it should be noted that there is great variability between the resulting preparations of the isolations (J.-C. Henquin 2019).

In view of this, it is therefore useful to consider possible alternatives to the use of native islets and to explore possibilities such as the formation of artificial spheroids from clonal cell lines or stem cells.

Rodent cell lines

Research in the beta-cell field profited from the establishment of insulin-secreting cell lines. The first lines were generated from adult rats and hamsters. RIN lines (Gazdar et al. 1980)

have been derived from a rat insulinoma induced following sublethal irradiation (Chick et al. 1977). Insulin gene expression decreased with passages and glucose-stimulated insulin secretion is limited. Following specific culture conditions, other cell lines were next derived from the same rat insulinoma, such as the widely used INS-1 cell line (Asfari et al. 1992). This line was found to be stable with time, insulin contents are high, and glucose induced insulin secretion. More than 20 years after its first publication, this line remains widely used by the scientific community.

More recently, a number of independent mouse pancreatic beta-cell lines were established by targeted oncogenesis from transgenic mice expressing large-T antigen of simian virus 40 (SV40T antigen) under the control of the insulin promoter. The basis of this approach was the demonstration that insulinomas develop in transgenic mice expressing SV40T under the control of the rat insulin promoter (Hanahan 1985). With this approach, S. Efrat and colleagues developed a number of lines named β -TCs (Knaack et al. 1994). A few years later, other lines such as MIN6 cells have been produced using the same approach (Miyazaki et al. 1990). Min6 cells and its subclones, such as MIN6B1 (Lilla et al. 2003), have been shown to represent useful experimental tools to dissect the function of cell-cell contact in insulin secretion (Jaques et al. 2008).

Taken together, we have learned a lot during the past years on rodent beta cells. It is also clear that human beta cells are not identical to rodent beta cells. If the objective is to attempt to translate fundamental data to patients with diabetes or to develop a medical device based on islets, it is crucial to find ways to further study human beta cells.

Human cell lines

During the past 30 years, a number of β cell lines have been established from x-ray-induced insulinomas in adult rats (Asfari et al. 1992; Gazdar et al. 1980) or derived by simian virus 40 transformation of adult hamster islet cells (Santerre et al. 1981). These lines have been extremely useful for detailed study of rodent β cells. Since many differences exist between rodent and human β cells, attempts have been made to generate human β cell lines from many human pancreatic sources, such as adult islets, fetal pancreases, or insulinomas. However, insulin production by these cells was extremely low or these cells were capable of

producing insulin only over a few passages (de la Tour et al. 2001). In 2005, Narushima et al. (Narushima et al. 2005) reported that they successfully established a functional human β cell line, NAKT-15. Although this particular human β cell line looked promising for cell therapy of diabetes mellitus and drug screening (Hohmeier and Newgard 2005), no new reports on the utility of this line have been published since 2005. Thus, developing a functional human β cell line still remains crucial. One way to create human cell line is to start from human fetal buds. Human fetal pancreatic buds are transduced with a lentiviral vector that expressed SV40LT under the control of the insulin promoter. The transduced buds are then grafted into SCID mice so that they could develop into mature pancreatic tissue (Ravassard et al. 2011). Upon differentiation, the newly formed SV40LT-expressing β cells proliferate and form insulinomas. The resulting β cells are then transduced with human telomerase reverse transcriptase (hTERT), graft into other SCID mice, and finally expand in vitro to generate cell lines (Ravassard et al. 2011). One of these cell line is EndoC- β H1. EndoC- β H1 cells contained 0.48 μ g of insulin per million cells, were stable at least for 80 passages, and expressed many specific β cell markers, without any substantial expression of markers of other pancreatic cell types. EndoC- β H1 cells secrete insulin in response to glucose stimulation, and insulin secretion is enhanced by known secretagogues, such as exendin-4, glibenclamide, and leucine. Finally, transplantation of EndoC- β H1 cells into mice reversed chemically induced diabetes (Ravassard et al. 2011).

Limitations of stem cells and cell lines

Even if stem cells and cell line present advantages, native human islets also consist of non- β endocrine cells such as α , δ , γ , and ϵ cells. These cells interact with each other and with β cells in feedback loops that determine islet function. Cell lines of these non- β endocrine cells could help us reconstruct and dissect the interactions between the different endocrine cells within human pancreatic islets (Caicedo 2013; van der Meulen et al. 2017). Such cell lines are not available for human and are very limited for rodent. In rodents, few α cell lines have been described and used. An early one, In-R1-G9, was derived from a transplantable hamster insulinoma (Takaki et al. 1986; Drucker, Philippe, et Mojsov 1988). A second example is represented by the α TC cell line that was derived from a glucagonoma generated in transgenic

mice expressing SV40 early region under the control of the glucagon promoter (Efrat et al. 1988; Powers et al. 1990). It is thus evident that more lines are needed from both rodents and humans.

In the development of an islet-based biosensor, the diversity of cell types in native islets is a key element to provide optimal information on insulin requirements by considering all the information derived from the composition of glucose, nutrients, hormones and amino acids in the patient's interstitial fluid.

Studies and Manuscripts

Biological substrate characterisation: Manuscript n°1

In our quest for a suitable biological substrate for the sensor, available at a large scale, we explored whether 3D spheroids may enhance clonal β -cell function using human EndoC- β H1 and rodent INS-1 cells. Recording with micro-electrode arrays (MEA) allows dynamic monitoring of electrical activity and the multicellular slow potentials (SP) provide insight in the degree of physiological important cell-cell coupling.

Our results indicate that spheroids of human EndoC- β H1 cells show a higher degree of cell-cell coupling in terms of frequency and amplitude, the latter reflecting the number of cells coupled. This is accompanied by a considerable improvement in the glucose-stimulated secretion index. In term of electrical activity, we observed an increase in frequencies and amplitudes in 3D versus 2D cultures correlated well with an increase in insulin secretion. The improvement in insulin secretion observed here was comparable to published data and is likely to be a consequence of improved coupling though other factors may be involved. In our hands 2D cultures of primary islet cells resulted in higher frequency and amplitudes as compared to reaggregated 3D islets. As islets contain different cells types and especially α -cells are important for β -cell activity, this may indicate that islet structure in terms of cell type topology was not restored during aggregation.

We also tried whether another frequently used cell line, ie. rat insulinoma derived INS-1 cells, may be capable of spheroid formation. However, those spheroids proved to be unstable to repetitive pipetting and even when handled with considerable care, spheroids rapidly disaggregated when cultured on MEAs precluding their use in 3D conformation (data not shown). Moreover, in 2D cultures a considerable number of cells or cell clusters did not respond in terms of measurable electrical activity upon increases of glucose. We therefore tested whether an increase in the expression of CX36, required for intercellular coupling, may improve their electrical responses.

To this end INS-1 cells were transduced with viral particles encoding either GFP as a control or human connexin 36 (CX36). We compared the electrical responses in terms of SP frequency and amplitude of GFP- and of CX36-transduced cells in response to 3 or 11 mM glucose and a mix of stimulatory drugs in the presence of 11 mM glucose. We observed a

considerable difference in their reactivity in terms of electrodes covered with cells which recorded changes in electrical activity. Whereas in GFP-transduced cells only a minority of cells responded to an increase in glucose, more than a half were active in the case of connexin-36 transduced cells. In fact, most of the GFP-transduced cells did not respond to glucose or glucose and stimulatory drugs.

Instability of spheroid formation may be a property inherent to INS-1 cells. It is also of note that these previously reported INS-1 spheroids showed either a considerable right shift of glucose dependency or a stark reduction in glucose induced insulin secretion and looked in general fragile. CX36 overexpression induced a coherent pattern in electrical activity and insulin secretion: an increase in glucose-sensitive cells, reduced basal electrical and secretory activity and consequently almost doubling in GSIS. These observations are in line with the general function of CX36 in islets and more specifically with previous observations in INS-1 cells upon decreased CX36 expression.

In conclusion, EndoC- β H1 spheroids provide a model to test the effect of different variables on physiological cell-cell coupling by MEA analysis in line with the advocated utility in drug testing. In the same vein CX-36 transduced cells may be suitable, but obviously restricted to rodents. These models may also be of interest as biological substrate for organs on chips and micro-organ-based sensors for continuous nutrient sensing.

Spheroid formation or connexin overexpression enhances electrical coupling and insulin secretion in clonal islet β -cells

Emilie Puginier *, Karen Leal-Fischer *, Julien Gaitan, Matthieu Raoux, Jochen Lang

Laboratory of Membrane Chemistry and Biology (CBMN), CNRS UMR 5248, Université de Bordeaux, Allée de Geoffrey St Hilaire, 33600 Pessac, France

* Equal contribution

Correspondence to: jochen.lang@u-bordeaux.fr

KEYWORDS: 3D, spheroids, microelectrode array, insulin, islets, EndoC- β H1, INS-1 cells

ABSTRACT

Pancreatic islets are important in nutrient homeostasis and improved cellular models of clonal origin may provide useful approaches especially in view of relatively scarce primary material. Close contact and coupling between β -cells are a hallmark of physiological function providing reduced signal/noise ratios. Recording with micro-electrode arrays (MEA) allow dynamic monitoring of electrical activity and the multicellular slow potentials (SP) provide insight in the degree of cell-cell coupling. We have therefore explored whether 3D spheroids may enhance clonal β -cell function using human EndoC- β H1 and rodent INS-1 cells. 3D EndoC- β H1 exhibited increased signals in terms of SP frequency or amplitude as to compared to monolayers and even single cell action potentials were quantifiable. The enhanced electrical signature was accompanied by an increase in the glucose stimulated insulin secretion (GSIS) index. In contrast, INS-1 cells did not form stable spheroids, but overexpression of connexin 36, required for cell-cell coupling, increased glucose responsiveness, dampened basal activity and consequently augmented GSIS. In conclusion, these models may provide surrogates for primary islets in extracellular electrophysiology.

INTRODUCTION

Pancreatic islets are important in nutrient homeostasis and their dysfunction leads to a major metabolic disease, diabetes [1, 2]. Studies on primary islet cells are hampered by the relative scarceness of native material, especially in the case of human origin which moreover differ in several important aspects from rodent islet cells [3]. In Europe human islets are obtained from organ donors and provided to researchers only when of insufficient quality or lack of possibility to transplant. Consequently, clonal β -cell lines still provide useful models. This approach has been considerably improved by the establishment of a human β -cell line, EndoC- β H1 cells and their derivatives [4-6].

In contrast to 2D monolayer cells in culture, islets are native organoids and considerable effort has been spent to assemble clonal β -cells in 3D aggregates or spheroids. Such an assembly should increase contacts between β -cells and physical coupling between β -cells are known to be of importance for physiological response and are mediated by connexin 36 (CX36)[7, 8]. Connexins form hexameric arrays or hemichannels, termed connexons, in the plasma membrane and dock end-to-end with a connexon in the membrane of closely opposed cells [9]. These gap junctional channels provide electrical coupling between β -cells [10-12] with subsequent synchronisation. In contrast to primary β -cells, connexin 36 expression is generally low in β -cell lines [13]. Connexin mediated coupling not only entrains cells upon arrival of a stimulus, but also dampens hyperactive cells and thus reduce spontaneous activity [14-16]. This results in an improved signal/noise ratio, which is also a prominent feature of native islets as compared to 2D primary or clonal β -cell cultures.

A number of approaches have been used to generate spheroids from clonal β -cells [17, 18] such as specific media and plating in proprietary wells or microgravity (hanging drop) for human EndoC- β cells [19-22] or rodent β -cell lines [23-26]. Although a number of parameters such as ultrastructure, electrophysiology, survival and secretion has been tested, the question of β -cell coupling had not been addressed and the functional equivalent for enhanced function in spheroids thus remains unknown.

Coupling between cells can be determined by biophysical methods such as dye exchange and patch clamp or indirectly been deduced from measuring of calcium dynamics and their synchronisation [27-29]. Extracellular electrophysiology such as micro-electrode arrays (MEA) offers a more direct and unbiased approach as the so-called slow potentials (SP) [30, 31] are

multicellular events strictly depending on gap junction coupling by CX36 in islet cells and their amplitude reflects to a certain degree the number of coupled cells [30, 32]. Moreover, electrical activity as determined by MEAs is coupled to secretion and its glucose concentration dependency allows to distinguish small increases in glucose in human or mouse islets [30, 32]. Obviously coupling spheroids to MEAs requires electrical contact and precludes certain methods of spheroid formation such as coculture with endothelial cells [33] or encapsulation [34]. Using electrical activity as output offers certain advantages as compared to optical or immunological approaches such as absence of bleaching or destructive analytical methods. It is also easier to miniaturize and to multiplex, and signals can even be analysed online [35].

Using 3D spheroids and MEAs we have now determined coupling in EndoC- β H1 cells. Our data indicate that stimulus-dependent coupling is considerably enhanced in 3D spheroids thus providing a base for their improved activity. In contrast, a widely used rat clonal β -cell line, INS-1, did not form stable spheroids but expression of CX36 were able to considerably improve their responsiveness and activity. Both cell models may provide paradigms to test effects that depend on physiological β -cell coupling.

MATERIALS AND METHODS

1. Materials

EndoC- β H1 cells [4] were kindly provided by Human Cell Design (Toulouse, France). IBMX, forskolin and glibenclamide were purchased from Sigma, GIP-1 from Bachem (Bubendorf, Switzerland). The following primary antibodies were used (Invitrogen): CX36 mouse anti-Human (clone 1E5H5), rabbit recombinant ANTI-FLAG M2 antibody (Invitrogen 710662), guinea pig anti bovine insulin (Linco, St. Charles, MO, USA) and monoclonal anti-GFP. The following secondary antibodies were used: anti-mouse or anti-rabbit HRP (dilution 1/2000; GE Healthcare); anti-mouse or anti-rabbit alexa568 (dilution 1/300; Invitrogen A11012 and A11031), donkey anti-guinea pig (Jackson Laboratories, Bar Harbour, ME, USA). Note that two other primary polyclonal antibodies did not provide any reliable signal in islets or brain for CX36 (Invitrogen 701194 and 516300). pLenti-C-Myc-DDK (RC210158L1; carrying the ORF of human CX36; GJD2; NM_020660) was obtained from Origene (Rockville, Md, USA).

2. Methods

2.1. Cell Culture, spheroid formation and viral transduction

EndoC- β H1 cells [4] were cultured according to the manufacturers protocol in OPTI β 1 (Human Cell Design, Toulouse, France). INS-1E and INS-813 cells were cultured as described previously [36, 37] and primary mouse islets were prepared and cultured as published [31, 32, 38]. Spheroids were formed complete medium either by hanging drop for 5 days in 30 μ l containing 500 islet cells or using a commercial plate (Sphericalplate 5D, Kugelmeiers; Erlenbach, Switzerland) with indicated cell concentrations. Physical stability was tested by 10 times pipetting trough 100 μ l cones and visual inspection with a microscope. Spheroid dimensions were determined on microscopic images using ImageJ v1.53. Lentiviral vector production was done by Vect'UB of the Bordeaux University. Lentiviral vector was produced by transient transfection of 293T cells according to standard protocols. In brief, subconfluent 293T cells were cotransfected with lentiviral genome (psPAX2) [39], with an envelope coding plasmid (pMD2G-VSVG) and with vector constructs. Viral titers of pLV lentivectors were determined by transducing 293T cells with serial dilutions of viral supernatant and EGFP expression was quantified 5 days later by flow cytometry analysis. For transduction of INS-1 cells, 750.000 cells were incubated in 500 μ l of RPMI and 5 MOI of corresponding viral particles overnight, washed and placed in complete RPMI medium for 5 days prior to plating.

2.2. Secretion assays and immunocytochemistry

Static secretion assays were performed as described [40] using Krebs-Ringer bicarbonate HEPES buffer (KRBH, concentrations in mM, 135 NaCl, 3.6 KCl, 5 NaHCO₃, 0.5 NaH₂PO₄, 0.5 MgCl₂, 1.5 CaCl₂, 10 HEPES, 0.1% w/v BSA, pH 7.4) and commercial ELISAs (Merckodia, Uppsala, Sweden). Immunocytochemistry was performed as described [41] and images acquired with a CAMSCOP CMOS camera (SCOP-Pro, Ballancourt, France) linked to an inverted fluorescent microscope (TS100, Nikon; Champigny, France).

2.3. Electrophysiology

MEA recordings (60Pedot-MEA200/30iR-Au-gr, \varnothing 30 μ m, 200 μ m inter-electrode distance; MCS, Tübingen, Germany) were performed at 37°C in solutions containing (in mM) NaCl 135, KCl 4.8, MgCl₂ 1.2, CaCl₂ 1.2 or 2.5 in the case of INS cells HEPES 10 mmol/l and glucose as indicated (pH 7.4 adjusted with NaOH) [32, 42, 43]. MEAs were coated with Matrigel (2% v/v) (BD Biosciences, San Diego, CA) prior to seeding of cells, spheroids or islets. Electrodes with noise levels >30 μ V peak-to-peak were regarded as artefacts, connected to the ground and not

analysed. Extracellular field potentials were acquired at 10 kHz, amplified and band-pass filtered at 0.1-3000 Hz with a USB-MEA60-Inv-System-E amplifier (MCS; gain: 1200) or a MEA1060-Inv-BC-Standard amplifier (MCS; gain: 1100) both controlled by MC_Rack software (v4.6.2, MCS) [31, 32].

2.4. Statistics

Graphics, quantifications, and statistics were performed with Prism software (v7; GraphPad, La Jolla, CA). Data are presented as means and SEM. The minimal value of mean SP frequency after the first peak (corresponding to the nadir) was taken as the limit between phases [32]. Gaussian distributions were tested by Shapiro-Wilk test and comparison of two groups with paired data by two-tailed unpaired t-tests or nonparametric Mann-Whitney tests. For more than two, groups, one-way ANOVA with Tukey post hoc or nonparametric Dunn tests were used.

RESULTS

Spheroids of human EndoC- β H1 cells were generated using micro-structured plastic wells for culture and we tested first the assembly and growth properties. As given in Fig. 1A.i, EndoC- β H1 cells formed round and regular spheroids with a rather homogenous staining for insulin. Based on our experience with the culture of islets, which are native spheroids, we opted for an intermediate diameter of 100 μ m (Fig. 1 A.ii) and used the corresponding protocol for all further experiments. These spheroids were mechanical stable after repetitive pipetting and conserved their spheroid form during culture on microelectrode arrays (Fig. 1 A.iii).

We next examined their electrical activity by comparing 2D monolayer culture of EndoC- β H1 versus spheroids on microelectrode arrays. The observed slow potentials (SP) reflect activity of electrically coupled cells [30], a hallmark of physiological β -cell behaviour [7, 44]. Their amplitude is related to the numbers of cells coupled [30, 32]. Raising glucose from 3 to 11 mM significantly increased SP frequency and amplitude in 2D culture and in spheroids and the effect was considerably more pronounced in the latter (Fig. 2A, B). The further addition of the incretin GLP-1 at the physiological concentration of 50 pM provoked a slight further increase in both cases which did not reach significance. Increasing cellular cAMP levels by the direct adenylate cyclase activator forskolin and the phosphodiesterase inhibitor IBMX, in the presence of 11 mM glucose, significantly increased frequencies as compared to 11 mM glucose alone in 2D culture and spheroids. Similar results were observed for amplitudes, and again the effects were considerably more pronounced in spheroids as compared to 2D cultures (Fig. 2A, B).

In contrast to the very robust SP signals, single cell action potentials are considerably more difficult to detect in conventional MEAs and their amplitudes cannot be reliably determined. [42]. Moreover, as only the frequency but not the amplitude of APs varies with glucose stimulation [31], we only analysed their frequency. In 2D cultures we were not able to identify APs with certainty, probably due to their extremely low amplitude. In contrast, recordings of spheroids clearly showed APs which varied with an increase in glucose concentration and significant effects of GLP-1 as well as effects of IBMX/forskolin were observed as compared to elevated glucose alone. As a comparison to EndoC- β H1 cells we examined also mouse islets, either as dispersed single cell 2D culture or after reaggregation in spheroids (Fig. 2 C, D). In both cases, large effects were present in terms of frequency and amplitude when increasing glucose from 3 to 11 mM and a small but significant effect was observed for GLP-1 (50 pM) in the presence of 11 mM glucose.

Finally, we measured insulin secretion from 2D cultures and 3D EndoC- β H1 spheroids (Fig. 2 E). Glucose-induced stimulation was clearly apparent as well as further potentiation by IBMX/forskolin. Similar to electrical activity, basal release and stimulated insulin secretion was more pronounced in spheroids as compared to 2D cultures and glucose-induced insulin secretion (GSIS) increased from 2.6 in monolayers to 4.5 in spheroids.

We also tried whether another frequently used cell line, ie. rat insulinoma derived INS-1 cells [45], may be capable of spheroid formation. However, those spheroids proved to be unstable to repetitive pipetting and even when handled with considerable care, spheroids rapidly disaggregated when cultured on MEAs precluding their use in 3D conformation (data not shown). Moreover, in 2D cultures a considerable number of cells or cell clusters did not respond in terms of measurable electrical activity upon increases of glucose. We therefore tested whether an increase in the expression of CX36, required for intercellular coupling, may improve their electrical responses.

To this end INS-1 cells were transduced with viral particles encoding either GFP as a control or human connexin 36 (CX36). Human connexin was expressed, intracellularly and also fine rims could be observed compatible with location at the plasma membrane (Fig. 3 A). In contrast, incubation with the anti-connexin antibody did not reveal any staining in GFP-transduced cells (Fig. 2 A). Immunoblot analysis of non-transduced cells and cells transduced with GFP or CX36 revealed expression of GFP or of CX36 only in the correspondingly transduced cells as bands appearing at approximately 25 kDa (GFP) or around 36 kDa (CX36) upon co-staining with GFP- and CX36 antibodies (Fig. 3B).

We subsequently compared the electrical responses in terms of SP frequency and amplitude of GFP- and of CX36-transduced cells in response to 3 or 11 mM glucose and a mix of stimulatory drugs in the presence of 11 mM glucose (Fig. 4). We first observed a considerable difference in their reactivity in terms of electrodes covered with cells which recorded changes in electrical activity (Fig. 4B). Whereas in GFP-transduced cells only a minority of cells responded to an increase in glucose, more than a half were active in the case of connexin-36 transduced cells. In fact, most of the GFP-transduced cells did not respond to glucose or glucose and stimulatory drugs (glibenclamide, Bay K8644, forskolin) in line with observations from cultures of native INS-1 cells (data not shown). We subsequently analysed in detail the recordings from those electrodes covered with cells that responded at least to an increase in glucose from 3 to 11 mM (Fig. 4, C-F). In both, GFP- or CX36-transduced cells, the change from complete culture medium to 3 mM glucose reduced activity in terms of frequency and

amplitudes. Note that complete culture medium contains 11 mM glucose and amino acids, the latter are known to enhance glucose effects [46]. Subsequent change from 3 to 11 mM glucose increased slightly but not significantly frequency and amplitude in GFP-transduced cells whereas a significant effect was observed in CX36-transduced cells. Further exposure to stimulatory drugs significantly increased responses in CX36-transduced cells, whereas only amplitude but not frequency was enhanced in GFP-transduced cells. Finally, we determined insulin secretion in non-transduced and GFP- or CX36-transduced cells. Under all three conditions (non-transduced, GFP-transduced or CX-36 transduced cells) insulin content did not vary. Clearly, CX-36 expression reduced basal secretion (at 3 mM glucose) in CX-36 transduced cells as compared to the two other conditions.

In all three cell types, an increase in glucose stimulated secretion was observed. GSIS amounted to 1,9 in non-transduced and GFP transduced cells, but increased to 5,7 in CX36 transduced cells. Although CX36-transduced cells secreted 20% more insulin than GFP-transduced cells at 15 mM glucose, the increase in GSIS was mainly due to an approximately 60% reduction in basal secretion at 3 mM glucose in CX36-transduced cells. Forskolin in the presence of 15 mM glucose further enhanced insulin secretion and again to a greater degree extent (20%) in CX-36 transduced cells as compared to GFP-transduced or non-transduced cells.

DISCUSSION

Our results indicate that spheroids of human EndoC- β H1 cells show a higher degree of cell-cell coupling in terms of frequency and amplitude, the latter reflecting the number of cells coupled. This is accompanied by a considerable improvement in the glucose-stimulated secretion index. The lack of stable spheroid formation in rat clonal INS-1 β -cells may be overcome by the enhanced expression of connexin 36, which also improves GSIS index mainly by lowering basal secretion.

3D spheroids of human EndoC- β H1 or - β H3 were generated previously using microgravity (“hanging drop”) or co-culture on human umbilical vein or islet-derived endothelial cells [19-21]. These spheroids exhibited a GSIS index similar to that observed in our study whereas spheroid formation by culture on non-adherent plastic did not improve GSIS to the same extent [22]. The method employed here by us has the advantage of simplicity as well as controlled and

reproducible spheroid size. Reproducible size is an important factor in standardisation as large spheroids may undergo core necrosis [47], whereas variation in size may lead to differences in cell-cell coupling [48, 49] and insulin secretion [50]. We have not tested systematically another approach, ie. agarose moulds? but clearly these moulds or the proprietary Sphericalplates provide the most reproducible morphology with the least hand-on time [51]. Microgravity, as used here for reaggregation of islets, is an option when cells are scarce but was in our hands plagued by bacterial contamination. An attractive alternative, especially when using extracellular electrophysiology, may be given by cell electrophoresis [43].

Clearly spheroid formation provided far more robust electrophysiological data and even permitted to reliably detect action potentials which are difficult to monitor in monolayers even when using electrodes coated with a conducting polymer [43]. The increase in frequencies and amplitudes in 3D versus 2D cultures correlated well with an increase in insulin secretion. The improvement in insulin secretion observed here was comparable to published data [5, 20] and is likely to be a consequence of improved coupling though other factors may be involved. In contrast to other studies, we did not observe any significant effect by activating the GLP-1 receptor. However, we used here physiological concentrations of GLP-1, which were active according to the electrophysiological data of mouse islets in line with our previous data [32], in contrast to the use of the incretin mimetic peptide exendin-4 in other studies, which is always more potent [5, 20]. In our hands 2D cultures of primary islet cells resulted in higher frequency and amplitudes as compared to reaggregated 3D islets. As islets contain different cells types and especially α -cells are important for β -cell activity [52], this may indicate that islet structure in terms of cell type topology was not restored during aggregation.

We were not able to form stable spheroids using rat insulinoma INS-1 cells [45], a widely used and relevant clonal β -cell model. Spheroids of these cells have been published but were overall of variable sizes and poorly defined borders although the methods used for spheroid formation provided useful spheroids in another β -cell lines such as MIN6 [23, 53-55]. Thus, non-satisfactory spheroid formation may be a property inherent to INS-1 cells. It is also of note that these previously reported INS-1 spheroids showed either a considerable right shift of glucose dependency or a stark reduction in glucose induced insulin secretion [53, 54]. CX36 overexpression induced a coherent pattern in electrical activity and insulin secretion: an increase in glucose-sensitive cells, reduced basal electrical and secretory activity and consequently almost doubling in GSIS. These observations are in line with the general function

of CX36 in islets [9] and more specifically with previous observations in INS-1 cells upon decreased CX36 expression [56].

In conclusion, EndoC- β H1 spheroids provide a model to test the effect of different variables on physiological cell-cell coupling by MEA analysis in line with the advocated utility in drug testing [5]. In the same vein CX-36 transduced cells may be suitable, but obviously restricted to rodents. These models may also be of interest as biological substrate for organs on chips and micro-organ based sensors for continuous nutrient sensing [35, 57, 58].

ACKNOWLEDGEMENTS

This work was funded by ANR-18-CE17-0005 DIABLO (to JL), and the French Ministry of Research (to JL). We thank the vectorology platform Vect'UB (CNRS UMS3427, INSERM US005, Univ. Bordeaux) for providing lentiviral particles and technical support. We are grateful to Human Cell Design (Toulouse, France) for providing us with EndoC- β H1 cells and OPTI β 1 medium.

REFERENCES

1. Zaharia, O.P., et al., *Risk of diabetes-associated diseases in subgroups of patients with recent-onset diabetes: a 5-year follow-up study*. *Lancet Diabetes Endocrinol*, 2019. **7**(9): p. 684-694.
2. Ashcroft, F.M. and P. Rorsman, *Diabetes mellitus and the β cell: the last ten years*. *Cell*, 2012. **148**(6): p. 1160-71.
3. Rorsman, P. and M. Braun, *Regulation of insulin secretion in human pancreatic islets*. *Annu Rev Physiol*, 2013. **75**: p. 155-79.
4. Ravassard, P., et al., *A genetically engineered human pancreatic β cell line exhibiting glucose-inducible insulin secretion*. *The Journal of Clinical Investigation*, 2011. **121**(9): p. 3589-3597.
5. Tsonkova, V.G., et al., *The EndoC- β H1 cell line is a valid model of human beta cells and applicable for screenings to identify novel drug target candidates*. *Mol Metab*, 2018. **8**: p. 144-157.
6. Scharfmann, R., W. Staels, and O. Albagli, *The supply chain of human pancreatic β cell lines*. *J Clin Invest*, 2019. **129**(9): p. 3511-3520.
7. Farnsworth, N.L. and R.K. Benninger, *New insights into the role of connexins in pancreatic islet function and diabetes*. *FEBS Lett*, 2014. **588**(8): p. 1278-87.
8. Vozzi, C., et al., *Adequate connexin-mediated coupling is required for proper insulin production*. *J Cell Biol*, 1995. **131**: p. 1561-72.
9. Bosco, D., J.A. Haefliger, and P. Meda, *Connexins: key mediators of endocrine function*. *Physiol Rev*, 2011. **91**(4): p. 1393-445.
10. Benninger, R.K., et al., *Gap junction coupling and calcium waves in the pancreatic islet*. *Biophys J*, 2008. **95**(11): p. 5048-61.
11. Moreno, A.P., et al., *Biophysical evidence that connexin-36 forms functional gap junction channels between pancreatic mouse beta-cells*. *Am J Physiol Endocrinol Metab*, 2005. **288**(5): p. E948-56.
12. Speier, S., et al., *Cx36-mediated coupling reduces beta-cell heterogeneity, confines the stimulating glucose concentration range, and affects insulin release kinetics*. *Diabetes*, 2007. **56**(4): p. 1078-86.

13. Calabrese, A., et al., *Connexin 36 controls synchronization of Ca²⁺ oscillations and insulin secretion in MIN6 cells*. *Diabetes*, 2003. **52**(2): p. 417-24.
14. Wellershaus, K., et al., *A new conditional mouse mutant reveals specific expression and functions of connexin36 in neurons and pancreatic beta-cells*. *Exp Cell Res*, 2008. **314**(5): p. 997-1012.
15. Ravier, M.A., et al., *Loss of connexin36 channels alters β -cell coupling, islet synchronization of glucose-induced ca²⁺ and insulin oscillations, and basal insulin release*. *Diabetes*, 2005. **54**(6): p. 1798-1807.
16. Rocheleau, J.V., et al., *Critical role of gap junction coupled K_{ATP} channel activity for regulated insulin secretion*. *PLoS Biol*, 2006. **4**(2): p. e26.
17. Akolpoglu, M.B., et al., *Recent advances in the design of implantable insulin secreting heterocellular islet organoids*. *Biomaterials*, 2021. **269**: p. 120627.
18. Cui, X., Y. Hartanto, and H. Zhang, *Advances in multicellular spheroids formation*. *J R Soc Interface*, 2017. **14**(127).
19. Lecomte, M.J., et al., *Aggregation of Engineered Human β -Cells Into Pseudoislets: Insulin Secretion and Gene Expression Profile in Normoxic and Hypoxic Milieu*. *Cell Med*, 2016. **8**(3): p. 99-112.
20. Spelios, M.G., et al., *Human EndoC- β H1 β -cells form pseudoislets with improved glucose sensitivity and enhanced GLP-1 signaling in the presence of islet-derived endothelial cells*. *Am J Physiol Endocrinol Metab*, 2018. **314**(5): p. E512-e521.
21. Urbanczyk, M., et al., *Controlled heterotypic pseudo-islet assembly of human β -cells and human umbilical vein endothelial cells using magnetic levitation*. *Tissue Eng Part A*, 2020. **26**(7-8): p. 387-399.
22. Zbinden, A., et al., *Non-invasive marker-independent high content analysis of a microphysiological human pancreas-on-a-chip model*. *Matrix Biol*, 2020. **85-86**: p. 205-220.
23. Hashim, M., et al., *Inhibition of *snat5* induces incretin-responsive state from incretin-unresponsive state in pancreatic β -cells: study of β -cell spheroid clusters as a model*. *Diabetes*, 2018. **67**(9): p. 1795-1806.

24. Kusamori, K., et al., *Increased insulin secretion from insulin-secreting cells by construction of mixed multicellular spheroids*. Pharm Res, 2016. **33**(1): p. 247-56.
25. Zhang, M., et al., *Three-dimensional cell-culture platform based on hydrogel with tunable microenvironmental properties to improve insulin-secreting function of MIN6 cells*. Biomaterials, 2021. **270**: p. 120687.
26. Jo, Y.H., et al., *Pseudoislet of hybrid cellular spheroids from commercial cell lines*. Transplant Proc, 2013. **45**(8): p. 3113-7.
27. Calabrese, A., et al., *Connexin 36 controls synchronization of ca^{2+} oscillations and insulin secretion in MIN6 Cells*. Diabetes, 2003. **52**(2): p. 417-424.
28. Stephan, J., S. Eitelmann, and M. Zhou, *Approaches to study gap junctional coupling*. Frontiers in Cellular Neuroscience, 2021. **15**.
29. Westacott, M.J., et al., *Age-dependent decline in the coordinated ca^{2+} and insulin secretory dynamics in human pancreatic islets*. Diabetes, 2017. **66**(9): p. 2436-2445.
30. Lebreton, F., et al., *Slow potentials encode intercellular coupling and insulin demand in pancreatic beta cells*. Diabetologia, 2015. **58**(6): p. 1291-9.
31. Abarkan, M., et al., *Vertical organic electrochemical transistors and electronics for low amplitude micro-organ signals*. Adv Sci (Weinh), 2022: p. e2105211.
32. Jaffredo, M., et al., *Dynamic uni- and multicellular patterns encode biphasic activity in pancreatic islets*. Diabetes, 2021. **70**(4): p. 878-888.
33. Seo, H., J. Son, and J.K. Park, *Controlled 3D co-culture of beta cells and endothelial cells in a micropatterned collagen sheet for reproducible construction of an improved pancreatic pseudo-tissue*. APL Bioeng, 2020. **4**(4): p. 046103.
34. Bal, T., et al., *Sensitivity study for the key parameters in heterospheroid preparation with insulin-secreting β -cells and mesenchymal stem cells*. ACS Biomater Sci Eng, 2019. **5**(10): p. 5229-5239.
35. Perrier, R., et al., *Bioelectronic organ-based sensor for microfluidic real-time analysis of the demand in insulin*. Biosens Bioelectron, 2018. **117**: p. 253-259.
36. Hastoy, B., et al., *A central small amino acid in the vamp2 transmembrane domain regulates the fusion pore in exocytosis*. Sci Rep, 2017. **7**(1): p. 2835.

37. Roger, B., et al., *Adenylyl cyclase 8 is central to glucagon-like peptide 1 signalling and effects of chronically elevated glucose in rat and human pancreatic beta cells.* Diabetologia, 2011. **54**(2): p. 390-402.
38. Abarkan, M., et al., *The glutamate receptor GluK2 contributes to the regulation of glucose homeostasis and its deterioration during aging.* Mol Metab, 2019. **30**: p. 152-160.
39. Dull, T., et al., *A third-generation lentivirus vector with a conditional packaging system.* J Virol, 1998. **72**(11): p. 8463-71.
40. Dubois, M., et al., *Glucotoxicity inhibits late steps of insulin exocytosis.* Endocrinology, 2007. **148**(4): p. 1605-14.
41. Saeed, S., et al., *Loss-of-function mutations in ADCY3 cause monogenic severe obesity.* Nat Genet, 2018. **50**(2): p. 175-179.
42. Koutsouras, D.A., et al., *Simultaneous monitoring of single cell and of micro-organ activity by PEDOT:PSS covered multi-electrode arrays.* Mat Sci Eng: C, 2017. **81**: p. 84-89.
43. Pedraza, E., et al., *Guiding pancreatic beta cells to target electrodes in a whole-cell biosensor for diabetes.* Lab Chip, 2015. **15**(19): p. 3880-90.
44. Nlend, R.N., et al., *Connexin36 and pancreatic beta-cell functions.* Arch Physiol Biochem, 2006. **112**(2): p. 74-81.
45. Janjic, D. and M. Asfari, *Effects of cytokines on rat insulinoma INS-1 cells.* J Endocrinol, 1992. **132**(1): p. 67-76.
46. Merglen, A., et al., *Glucose sensitivity and metabolism-secretion coupling studied during two-year continuous culture in INS-1E insulinoma cells.* Endocrinology, 2004. **145**(2): p. 667-78.
47. Ichihara, Y., et al., *Size effect of engineered islets prepared using microfabricated wells on islet cell function and arrangement.* Heliyon, 2016. **2**(6): p. e00129.
48. Jo, J., M.Y. Choi, and D.S. Koh, *Size distribution of mouse Langerhans islets.* Biophys J, 2007. **93**(8): p. 2655-66.

49. Nittala, A. and X. Wang, *The hyperbolic effect of density and strength of inter beta-cell coupling on islet bursting: a theoretical investigation*. Theor Biol Med Model, 2008. **5**: p. 17.
50. Reaven, E.P., et al., *Effect of variations in islet size and shape on glucose-stimulated insulin secretion*. Horm Metab Res, 1981. **13**(12): p. 673-4.
51. Wassmer, C.H., et al., *Engineering of primary pancreatic islet cell spheroids for three-dimensional culture or transplantation: a methodological comparative study*. Cell Transplant, 2021. **29**: p. 963689720937292.
52. Moede, T., I.B. Leibiger, and P.O. Berggren, *Alpha cell regulation of beta cell function*. Diabetologia, 2020. **63**(10): p. 2064-2075.
53. Amin, J., et al., *A simple, reliable method for high-throughput screening for diabetes drugs using 3D β -cell spheroids*. J Pharmacol Toxicol Methods, 2016. **82**: p. 83-89.
54. Ntamo, Y., et al., *In vitro characterization of insulin-producing β -cell spheroids*. Front Cell Dev Biol, 2020. **8**: p. 623889.
55. Sabra, G. and P. Vermette, *A 3D cell culture system: separation distance between INS-1 cell and endothelial cell monolayers co-cultured in fibrin influences INS-1 cells insulin secretion*. Biotechnol Bioeng, 2013. **110**(2): p. 619-27.
56. Le Gurun, S., et al., *Connexin-36 contributes to control function of insulin-producing cells*. J Biol Chem, 2003. **278**(39): p. 37690-7.
57. Olcomendy, L., et al., *Integrating an islet-based biosensor in the artificial pancreas: in silico proof-of-concept*. IEEE Trans Biomed Eng, 2021.
58. Renaud, S., B. Catargi, and J. Lang, *Biosensors in diabetes : how to get the most out of evolution and transpose it into a signal*. IEEE Pulse, 2014. **5**(3): p. 30-4.

FIGURE LEGENDS

Figure 1: Generation of Spheroids. **A:** Generation of EndoC- β H1 3D spheroids. i, image of spheroid formed and staining for insulin (red) and with DAPI (blue); ii, time course of spheroid formation and size at different cell numbers; iii, EndoC- β H1 3D spheroids on a micro-electrode array. **B,** formation of islet spheroids. i petri with hanging drops; ii, 3D islets formed; iii, staining for insulin, glucagon and with DAPI.

Figure 2: Functional characterisation of spheroids from EndoC- β H1 cells or primary mouse islets. **A:** Recording of monolayer (2D) or spheroids (3D) of EndoC- β H1 cells seeded on micro-electrode arrays and exposed to Glucose (3 mM, G3; 11 mM, G11), GLP-1 (50 pM) in the presence of 11 mM glucose (GLP1) or IBMX (100 μ M) and Forskolin (1 μ M) in the presence of 11 mM glucose (I/F). Mean traces of slow potential (SP) frequency and amplitudes as well as action potential (AP) frequency bare given; mean, black, SEM grey. Time bars equal 20 min (in all traces). **B:** Statistical evaluations of area under the curves of A (AUC; for 30 min, given as value/min). **C:** Recording of monolayer (2D) or reassembled spheroids (3D) of primary mouse seeded on micro-electrode arrays. Abbreviations for conditions and statistical tests as in A. **D:** Statistical evaluations of area under the curves of C (AUC; for 30 min, given as value/min). **E:** Insulin secretion (static incubations) of monolayer (2D) or spheroids (3D) of EndoC- β H1 cells during 1h incubation, abbreviations as in A. insulin contents were comparable between monolayers and spheroids (479,8 \pm 42 ng/100.000 cells monolayers vs. 444,5 \pm 69,2 ng/100.000 cells spheroid). *, 2p<0.05; **, 2p <0.01; ***, 2p <0.001; ANOVA and Tukey posthoc test. ++, 2p<0.01; +++, 2p<0.001 in paired Tukey posthoc test; n, given in corresponding figures.

Figure 3: CX36 expression in transduced INS-1 cells. **A,** immunofluorescence images of INS-1 cells transduced either with eGFP or with CX36 encoding viral particles which were stained either for insulin or for CX36 as indicated. Bars, 10 μ m. **B,** immunoblot of control (non-transduced) or transduced cells with either eGFP or connexin-36 tagged with a myc-epitope. Left panel, protein transfer; right panel, corresponding blot co-incubated with anti-eGFP and anti-myc. Molecular weight markers are given in kDa.

Figure 4: Electrophysiological analysis and insulin secretion of GFP or CX36 expressing transduced INS-1 cells. **A,** Scheme of static incubation of INS-1 cells with culture medium (CM), 3 or 11 mM glucose (G3, G11) or 11 mM glucose in the presence of diazoxide (G11D). **B,** relative responsivity of GFP- or CX36 (CX36) transduced cells expressed as absence of

effect, stimulation by 11 mM glucose (versus 3 mM) or only stimulated by drugs (no effect of G11 alone; increase versus G3 by glibenclamide 200 nM, Bay K8644, forskolin 1 μ M). Note that glucose-sensitive cells were always also drug sensitive. For further analysis (C-F) only those electrodes covered by cells were analysed where an increase in glucose increased electrical activity. **C**, Mean SP frequencies (\pm SEM) in GFP- or CX36 transduced cells. **D**, statistics of C. **E**, Mean SP amplitudes (\pm SEM) in GFP- or CX36 transduced cells. **F**, statistics of E. **G**, Insulin content and insulin secretion from non-transduced cells (CON) or GFP- (GFP) or CX36 (CX36) transduced cells incubated at 3 mM glucose (G3), 15 mM glucose (G15) or 15 mM glucose and 1 μ M forskolin (G15 F), n=6. Statistics: Tukey or Dunn post-hoc tests; *, 2p<0.05; **, 2p<0.01; ***, 2p<0.001; n as indicated.

FIGURES

Fig. 1

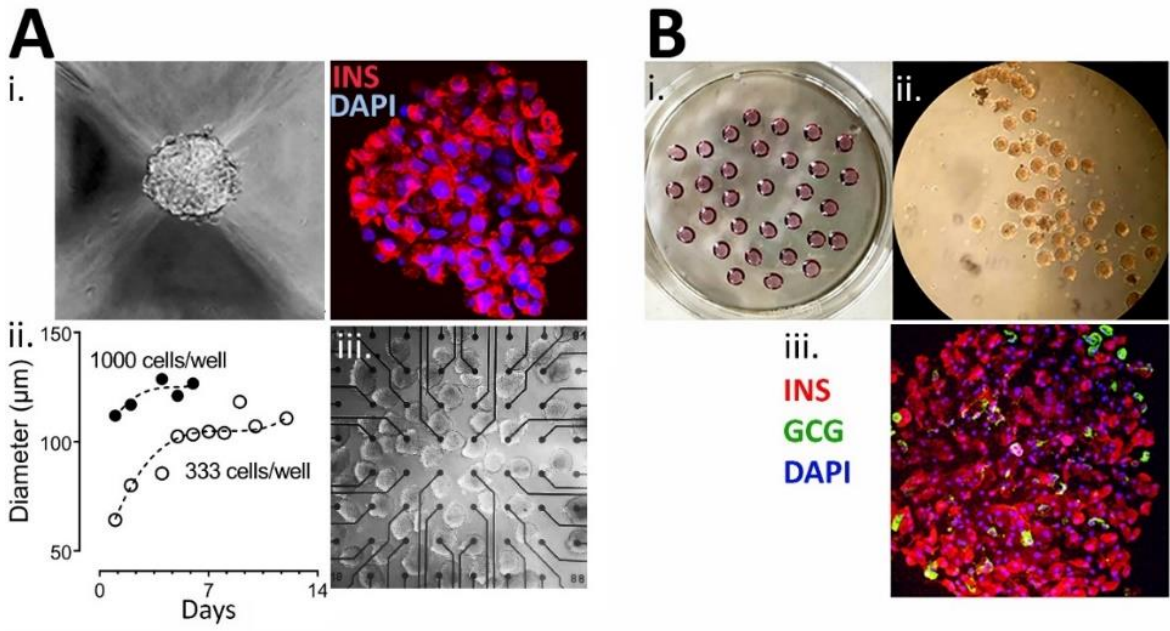


Fig. 2

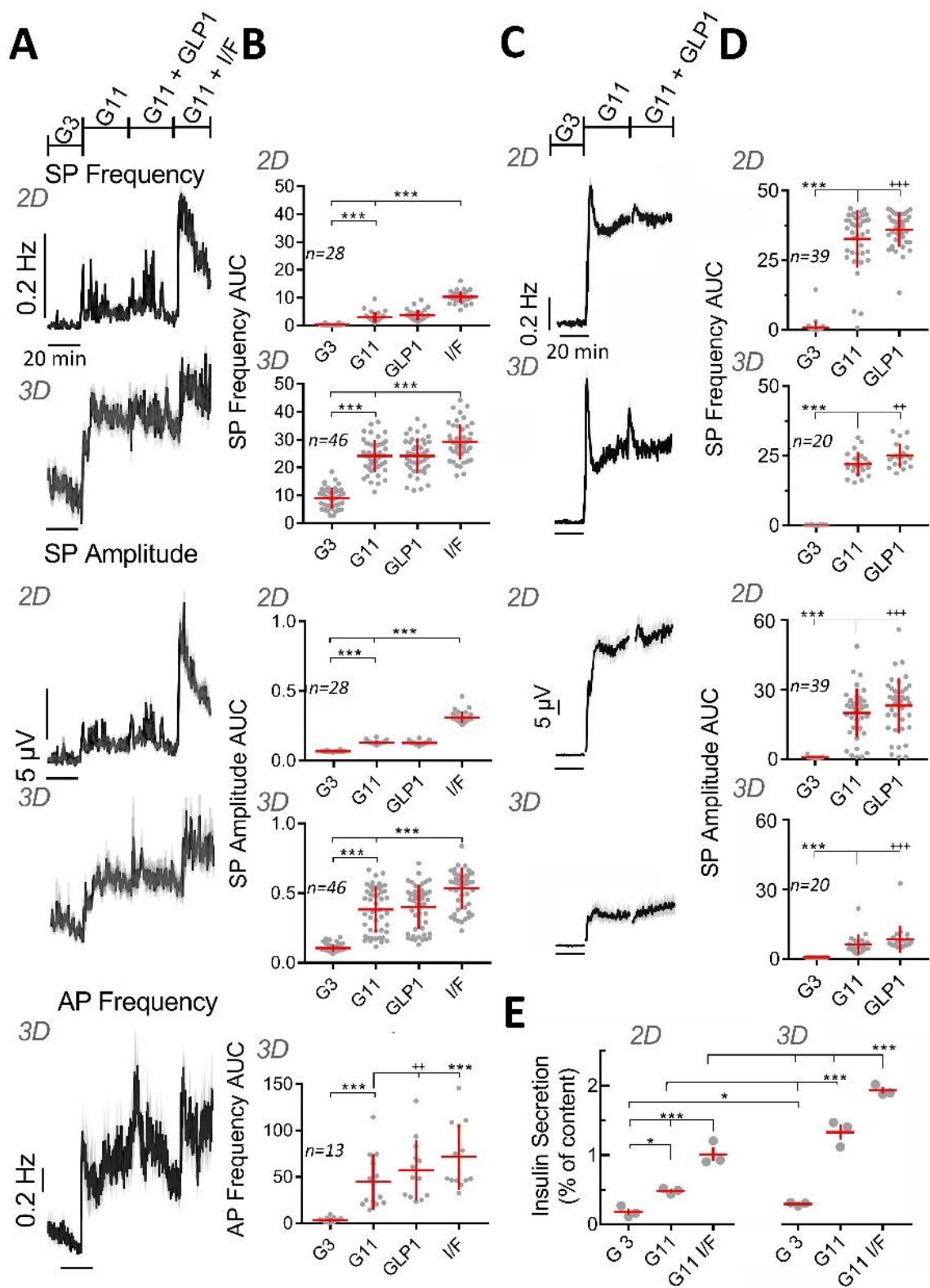


Fig. 3

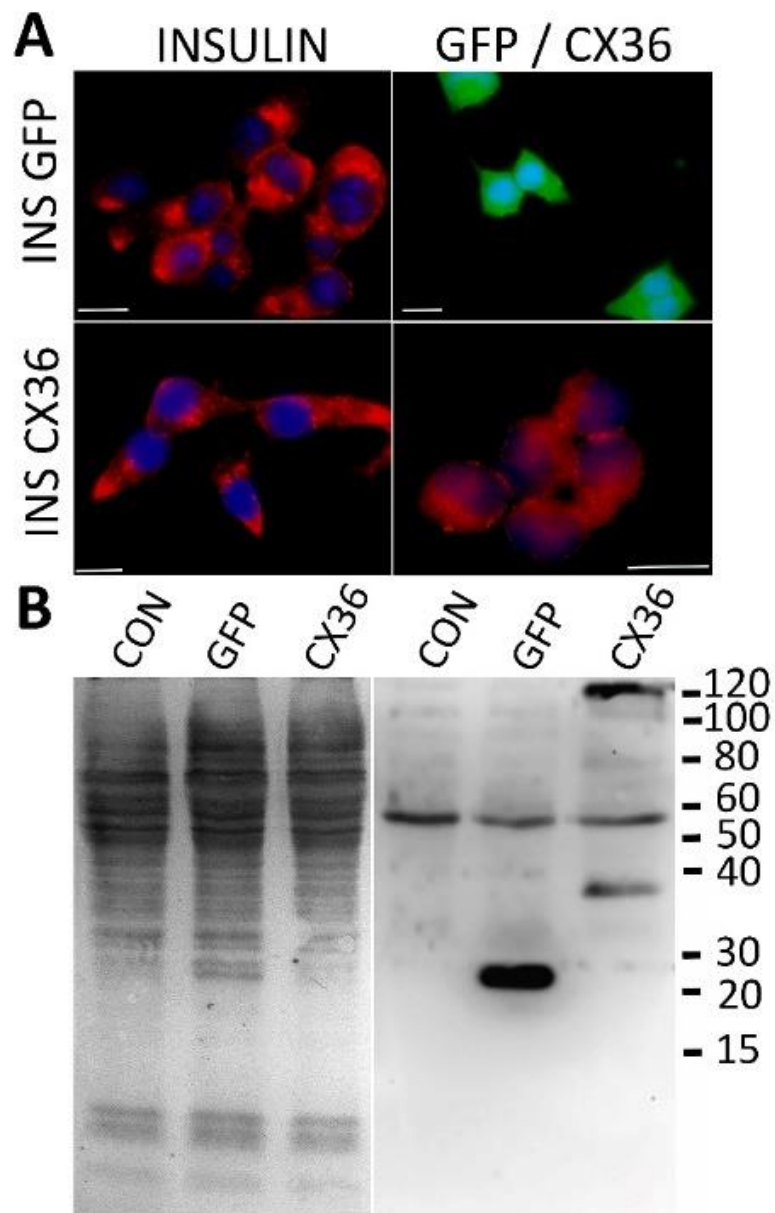
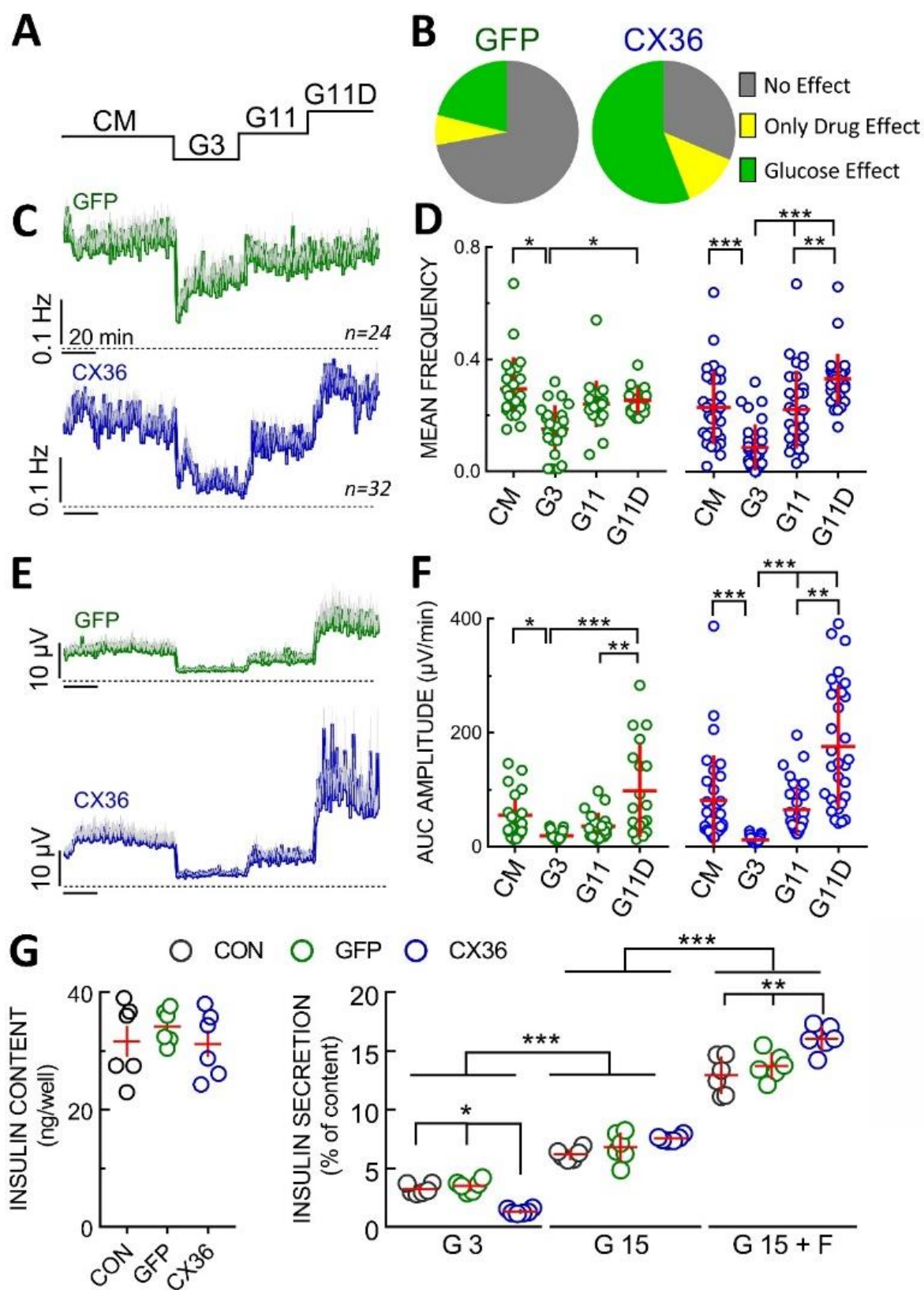


Fig. 4



Development of an islets on chip microfluidic device : Manuscript n°2

Biphasic secretion is a characteristic found in many endocrine microorganisms. This particular kinetics is adapted to physiological needs and does not require a feedback loop. Although this phenomenon is common in neuroendocrine cells and has been widely described, the origin of these biphasic kinetics as well as the transition between the first and second phase have not yet been fully identified. The aim of this study is to elucidate the role of cellular and multicellular β -cell signalling in this biphasic kinetics in both a physiological and pathophysiological context. Alterations in this kinetics are observed under the pathological conditions of type 2 diabetes but also in a physiological setting during ageing. As already developed in part four of the introduction, electrophysiological recordings by MEAs constitute a non-invasive approach allowing investigations over several hours, such as the digestive process, with a high temporal resolution (kHz).

Protocols mimicking physiology and pathophysiology, using several types of MEAs (Titanium, PEDOT, high density), and combining MEAs with microfluidics to follow in parallel electrical signals and insulin secretion, have allowed to determine the major role of multicellular signals (SPs) in both secretory phases and their alteration under pathophysiological conditions in mice and humans.

The data in this article allow us to draw a new multicellular model of biphasic islet activation. The biphasic secretion is encoded, upstream of the vesicle pools, at the level of the microorganism by a dynamic change of single-cell (APs) and multicellular (SPs) electrical signals. In the first phase, small groups of highly active but desynchronised cells dominate (high-frequency, low-amplitude SPs, desynchronised between different regions of the same islet) to respond rapidly and extensively to increased blood glucose. In the second phase, the overall activity slows down and these functional units expand due to increased electrical couplings between β -cells (lower frequency, high amplitude SPs synchronised between different regions of the islet). The couplings allow to decrease the electrical and secretory activity in the second phase, as shown by the correlations between the amplitude and frequency of SPs and insulin secretion obtained with microfluidic MEAs. These couplings certainly allow the installation of an "economic" mode of islet activity to cope with the relatively long duration of digestion. This dynamic organisation is modulated by the incretin

hormone GLP-1 which, at picomolar postprandial concentrations, acts only on the second phase by increasing the couplings (SPs) without effect on the individual cell activity (APs). Finally, ageing or diabetogenic conditions (glucotoxicity) alter the multicellular activity in both phases. These results show that, although the organisation into vesicle pools plays a role, it is rather an adaptation following the electrical changes and modulations of the couplings in the islets.

It was essential to develop a technique to correlate the electrical activity of the islets with insulin secretion.

For this manuscript, I was responsible for the development of the microfluidic system. I established the specifications for the development of microfluidic MEAs that allow the recording of islet electrical activity while being able to collect insulin secretion in order to establish the correlation between these two parameters. I modelled, developed the protocols for the fabrication of the devices, developed protocols for seeding and culturing the islets within the microfluidic MEAs. I also carried out the experiments that gave rise to the results presented in figure 2 of this article. Thanks to this device, we were able to establish, together with the microelectronics experts, the relationship allowing us to predict insulin secretion from the electrical activity of the islets.

This article was an essential step in my project, as it allowed me to develop and validate the microfluidic MEAs device that I was able to use for the proof of concept of the islet-based biosensor. In addition, we determined the predictive power of the electrical activity of the islets for the determination of insulin requirements. This element is fundamental to use the algorithms of the islets as control of an insulin pump in the framework of the development of a new medical device.



Dynamic Uni- and Multicellular Patterns Encode Biphasic Activity in Pancreatic Islets

Manon Jaffredo,¹ Eléonore Bertin,¹ Antoine Pirog,² Emilie Puginier,¹ Julien Gaitan,¹ Sandra Oucherif,¹ Fanny Lebreton,³ Domenico Bosco,³ Bogdan Catargi,^{1,4} Daniel Cattaert,⁵ Sylvie Renaud,² Jochen Lang,¹ and Matthieu Raoux¹

Diabetes 2021;70:878–888 | <https://doi.org/10.2337/db20-0214>

Biphasic secretion is an autonomous feature of many endocrine micro-organs to fulfill physiological demands. The biphasic activity of islet β -cells maintains glucose homeostasis and is altered in type 2 diabetes. Nevertheless, underlying cellular or multicellular functional organizations are only partially understood. High-resolution noninvasive multielectrode array recordings permit simultaneous analysis of recruitment, of single-cell, and of coupling activity within entire islets in long-time experiments. Using this unbiased approach, we addressed the organizational modes of both first and second phase in mouse and human islets under physiological and pathophysiological conditions. Our data provide a new uni- and multicellular model of islet β -cell activation: during the first phase, small but highly active β -cell clusters are dominant, whereas during the second phase, electrical coupling generates large functional clusters via multicellular slow potentials to favor an economic sustained activity. Postprandial levels of glucagon-like peptide 1 favor coupling only in the second phase, whereas aging and glucotoxicity alter coupled activity in both phases. In summary, biphasic activity is encoded upstream of vesicle pools at the micro-organ level by multicellular electrical signals and their dynamic synchronization between β -cells. The profound alteration of the electrical organization of islets in pathophysiological conditions may contribute to functional deficits in type 2 diabetes.

Biphasic secretion is a common physiological feature in a number of hormone and neuro-hormone-secreting

micro-organs (1–4). Pancreatic islets represent a well-described model of biphasic secretion (4,5): a first peak phase (5–15 min) is followed by a decrease in the secretion rate, called nadir, and a subsequent second long-lasting plateau phase (6,7) and installation of pulsatility (8). Insulin secreted during the first phase immediately reaches the liver to rapidly regulate blood glucose levels. The second phase targets more distant organs as long as glycemia remains elevated (9). This optimized kinetic is strongly altered during aging and in type 2 diabetes (10–14). As biphasic insulin profiles persist *ex vivo* (6), multiorgan feedback loops are not required, and patterns are encoded at the micro-organ level.

Although the phenomenon *per se* has been extensively described, it is still not understood how this phasic organization is achieved and what drives the progression from first to second phase. β -Cell metabolism has been monitored via mitochondrial membrane potential, oxygen consumption, or metabolic coupling factors. Metabolism increases upon glucose stimulation, with, often (15,16) but not always (17,18), a discrete and brief peak of 1–2 min during the first phase before raising again during the nadir while secretion decreases; thus, these metabolic profiles do not explain secretion patterns. The organization of insulin-secreting vesicles in distinct functional pools in β -cells has been widely invoked to explain biphasic secretion (19–21). Interestingly, biphasic activation is a multicellular process since it is profoundly altered in dissociated islets and connexin-36 knockout mice (22,23). Hence, vesicle pool

¹University of Bordeaux, CNRS, Institute of Chemistry and Biology of Membranes and Nano-objects, UMR 5248, Pessac, France

²University of Bordeaux, CNRS, Institut National Polytechnique de Bordeaux, Laboratoire de l'Intégration du Matériau au Système, UMR 5218, Talence, France

³Cell Isolation and Transplantation Center, Department of Surgery, Geneva University Hospitals, University of Geneva, Geneva, Switzerland

⁴University of Bordeaux, Hôpital Saint-André, Endocrinology and Metabolic Diseases, Bordeaux, France

⁵University of Bordeaux, CNRS, Aquitaine Institute for Cognitive and Integrative Neuroscience, UMR 5287, Bordeaux, France

Corresponding author: Matthieu Raoux, matthieu.raoux@u-bordeaux.fr

Received 2 March 2020 and accepted 11 January 2021

This article contains supplementary material online at <https://doi.org/10.2337/figshare.13562354>.

© 2021 by the American Diabetes Association. Readers may use this article as long as the work is properly cited, the use is educational and not for profit, and the work is not altered. More information is available at <https://www.diabetesjournals.org/content/license>.

organization may not represent the main determinant of biphasic activation in islets.

Different approaches have been used to investigate multicellular processes in islets. Analysis of intraislet connectivity by dynamic imaging has provided an elegant model of highly active leader cells (24,25), in line with β -cell heterogeneity (26), but requires complex mathematical offline reconstruction and may potentially introduce bias (24,27). In addition, the existence of such hub cells is still debated (28), and inherent restrictions have limited such experiments to short periods. Consequently, they do not inform about the dynamic evolution of the entire micro-organ.

We have therefore sought for a more direct approach endowed with high temporal resolution (kHz) and useable throughout the hours of postprandial islet activation, a situation in which rundown in optical and classical electrophysiological approaches may occur. Analysis of extracellular electrical field potentials with multielectrode arrays (MEAs) of intact islets avoids such drawbacks (29,30). Both unicellular and multicellular signals can be observed in the form of single-cell action potentials (APs) (29,31) and multicellular slow potentials (SPs) for hours or even days (30,32). SPs represent robust and specific signals propagated among β -cells via connexin-36 in both rodent and human islets (32). Hence, this approach provides a dynamic, direct, and unbiased measurement of unicellular and of micro-organ behavior via APs and SPs.

We have therefore addressed the question how biphasic activity of pancreatic islet micro-organs is encoded in terms of single-cell and coupled electrical activity throughout a physiological time span and how this is disrupted in pathophysiological states.

RESEARCH DESIGN AND METHODS

Mouse Islets

Adult male C57BL/6J mice (10–20 weeks of age, except for Fig. 7A and B: 12–45 weeks) were sacrificed by cervical dislocation according to University of Bordeaux ethics committee guidelines. Islets were obtained by enzymatic digestion and handpicking (29,30,32). MEAs were coated with Matrigel (2% v/v) (BD Biosciences, San Diego, CA), and intact islets were seeded (one pancreas per MEA) and cultured at 37°C (5% CO₂, >90% relative humidity) in RPMI medium (11 mmol/L glucose, except for glucotoxic conditions: 20 mmol/L in Fig. 7C and D) (Thermo Fisher Scientific, Waltham, MA) as described (29,30,32).

Human Islets

Human islets (healthy donors; for details, see Supplementary Material) were isolated at the Geneva Cell Isolation and Transplantation Center (29,32), distributed through the European Consortium for Islet Transplantation, and authorized by the ethical committee (Comités de Protection des Personnes; 16-RNI-10). Human islets were

cultured on MEAs under the same conditions as mouse islets but using CMRL-1066 medium (5.6 mmol/L glucose, except for glucotoxic conditions) (Thermo Fisher Scientific) (29,32).

MEAs

Different MEAs (Multi Channel Systems GmbH [MCS], Reutlingen, Germany) were used to address specific questions. Standard MEAs (60MEA200/30iR-Ti-gr, 59 titanium nitride electrodes [TiN], \varnothing 30 μ m, 200 μ m interelectrode distance) permitted the recording of SPs of \sim 1 islet/electrode (1.0 ± 0.1 islets/electrode, $n = 49$ islets, $N = 3$ independent preparations). Recordings of different intraislet regions were performed using high-density MEAs (HD-MEAs) (60HexAMEA40/10iR-ITO-gr, 59 TiN electrodes, \varnothing 10 μ m, 40 μ m interelectrode due to the flow). Both MEAs were continuously perfused at 0.5 mL/min (Reglo ICC; Ismatec, Glattbrugg, Switzerland).

To measure simultaneously electrical parameters and insulin secretion (ELISA 80-INSMSU-E01; ALPCO, Salem, NH), microfluidic MEAs (μ MEAs) were developed using MEA200/30iR-Ti-gr with a microfluidic channel (\varnothing 0.8 mm) in polydimethylsiloxane and perfused at 8 μ L/min (MFCS-EZ; Fluigent, Villejuif, France). Kinetics of medium changes were determined as published (30).

Finally, poly(3,4-ethylenedioxythiophene) (PEDOT) and carbon nanotube-covered MEAs (PEDOT-MEAs) (60Pedot-MEA200/30iR-Au-gr, electrode arrangement as in standard MEAs) were used to detect APs, which are hardly discernable otherwise (29), and solutions were replaced by pipetting to avoid mechanical artifacts.

Extracellular Electrophysiological Recordings

MEA recordings were performed at 37°C, pH 7.4 (29,32), in solutions containing 1.2 mmol/L CaCl₂ for mouse islets (2.5 mmol/L in Supplementary Fig. 5B–D) or 1.8 mmol/L for human islets as published previously (29,32), which is close to physiological levels and provides sufficient driving force for SP quantification. When specified, a solution without CaCl₂ was applied to evaluate basal activity. Glucagon-like peptide 1 (GLP-1) solutions (Bachem Bio-Science Inc, King of Prussia, PA) were prepared ex tempore. Electrodes with noise levels >30 μ V peak-to-peak were regarded as artifacts, connected to the ground, and not analyzed ($3.6 \pm 1.7\%$ of electrodes; $N = 5$). Extracellular field potentials were acquired at 10 kHz, amplified, and band-pass filtered at 0.1–3,000 Hz with a USB-MEA60-Inv-System-E amplifier (MCS; gain: 1,200) or an MEA1060-Inv-BC-Standard amplifier (MCS; gain: 1,100), both controlled by MC_Rack software (v4.6.2, MCS).

Intracellular Recordings

Intracellular recordings were performed simultaneously with extracellular recordings on standard MEAs. Intracellular potentials of islet cells were measured by current-clamp (10 kHz sampling rate, 10 kHz low-pass filter) with sharp glass Clark micropipette microelectrodes (Harvard

Apparatus, Les Ulis, France) filled with 3 mmol/L KCl (96 ± 18 Mega Ω ; $n = 17$) and coupled to an Axoclamp-2B amplifier (Molecular Devices, San Jose, CA) controlled by Spike2 software (v7.01; Cambridge Electronic Design Ltd, Cambridge, U.K.). A common reference electrode was used for both recordings. An electrical artifact observable on both recordings was used to synchronize intra- and extracellular traces.

Quantifications

Images of islets on MEAs were taken before and after each experiment to localize electrodes covered with islets ($44.1 \pm 7.4\%$ of electrodes; $N = 5$ independent preparations). Islet cell monolayer surfaces were quantified with ImageJ software (v1.52d; National Institutes of Health, Bethesda, MD). Electrophysiological data were analyzed with MC_Rack software. SPs and APs were isolated using a 2-Hz low-pass filter or a 3–700-Hz band-pass filter, respectively, and frequencies were determined using the threshold module of MC_Rack with a dead time (minimal period between two events) of 300 ms (SPs) and 10 ms (APs). The peak-to-peak amplitude module of MC_Rack was used to determine SP amplitudes. Simultaneous extra- and intracellular recordings were analyzed with Spike2 software.

Analysis of Intraislet Synchrony

After filtering at 2 Hz, SPs were detected using the peak detection module of Spike2 with a threshold of $-15 \mu\text{V}$. The degree of synchrony between SPs on electrodes was computed with MATLAB (vR2012B; MathWorks, Natick, MA) following a method based on Schreiber et al. (33), originally used to compute synchronization between trains of neuronal spikes (Supplementary Methods and Supplementary Fig. 1).

Data Presentation and Statistical Analysis

Experiments were replicated on at least three independent biological preparations, except when indicated. If not stated otherwise, N represents the number of independent preparations and n the number of electrodes analyzed. Graphics, quantifications, and statistics were performed with Prism software (v7; GraphPad, La Jolla, CA). Data are presented as means and SEM or whiskers boxes (box, 25th to 75th percentiles; line in the middle of the box, median; + or ■, mean; and whiskers, 10–90th percentiles). The minimal value of mean SP frequency after the first peak (corresponding to the nadir) was taken as the limit between phases.

Gaussian distributions were tested by D'Agostino-Pearson test and comparison of two groups with paired data by two-tailed paired t tests or nonparametric t tests with Wilcoxon matched-pairs signed-rank test. Two groups with unpaired data were compared using two-tailed unpaired t tests or nonparametric Mann-Whitney tests. For more than two groups, one-way ANOVA with Tukey post hoc or nonparametric Dunn tests were used.

Data and Resource Availability

Data sets generated and/or analyzed during the current study are available from the corresponding author upon reasonable request.

RESULTS

Biphasic Glucose-Induced Insulin Secretion Is Encoded by Multicellular SPs

Intact mouse islets were cultured on MEAs (Fig. 1A) to record noninvasively extracellular field potentials. As previously described, two types of signals were observed (Fig. 1B): the well-known unicellular APs and the more recently described SPs (29,30), which are of multicellular origin and require β -cell coupling via connexin-36 (32). We first monitored the frequency and amplitude of SPs in islets to determine whether they correlate to well-known biphasic secretion patterns. When islets were stimulated by an increase in glucose from 3 mmol/L to the moderate concentration of 8.2 mmol/L (Fig. 1C), a clear biphasic electrical profile of SPs was triggered, in terms of both frequencies and amplitudes (Fig. 1C). Each phase owned a specific electrical "signature": SPs of high frequencies but small amplitudes in the first phase and lower frequencies but increasing amplitudes during the second phase (Fig. 1D). Hence, electrical coupling modes of islet β -cells are biphasic and develop in a dynamic fashion.

Another known insulin secretagogue, L-leucine, bypasses glycolysis. Stimulating the same islets with either glucose or leucine (Fig. 1E), the first electrical phase was comparable between the two molecules in terms of peak of SP frequencies. However, in the case of leucine, SPs were largely reduced in the second phase (Fig. 1E and F). Thus, the metabolism of the main stimulator (i.e., glucose) triggers a full second electrical phase, while leucine may require coactivation of additional metabolic pathways, such as by glutamine (34).

By introducing microfluidics in μMEAs (Fig. 2A and B), we simultaneously recorded SPs and insulin secretion (Fig. 2C). Biphasic kinetics of SP frequencies were highly correlated with biphasic insulin secretion (Fig. 2C). Moreover, maximal correlation was obtained when both SP frequencies and amplitudes were taken into account (Fig. 2C and D), supporting the view that multicellular SPs, upstream of secretory pools, constitute the main regulator of biphasic insulin secretion.

Intraislet Electrical Coupling Enlarges Considerably in the Second Phase

The magnitude of extracellular electrical signals often mirrors the degree of cell synchrony, at least in the brain (35). We hypothesized that the increase of SP amplitude during the second phase was due to an increase in β -cell synchrony within an islet. Since standard MEAs do not offer spatial resolution below the dimensions of a single islet (Supplementary Fig. 2A), we used HD-MEAs providing ~ 10 times more electrodes per islet, which permitted multisite analysis of single islets without affecting the

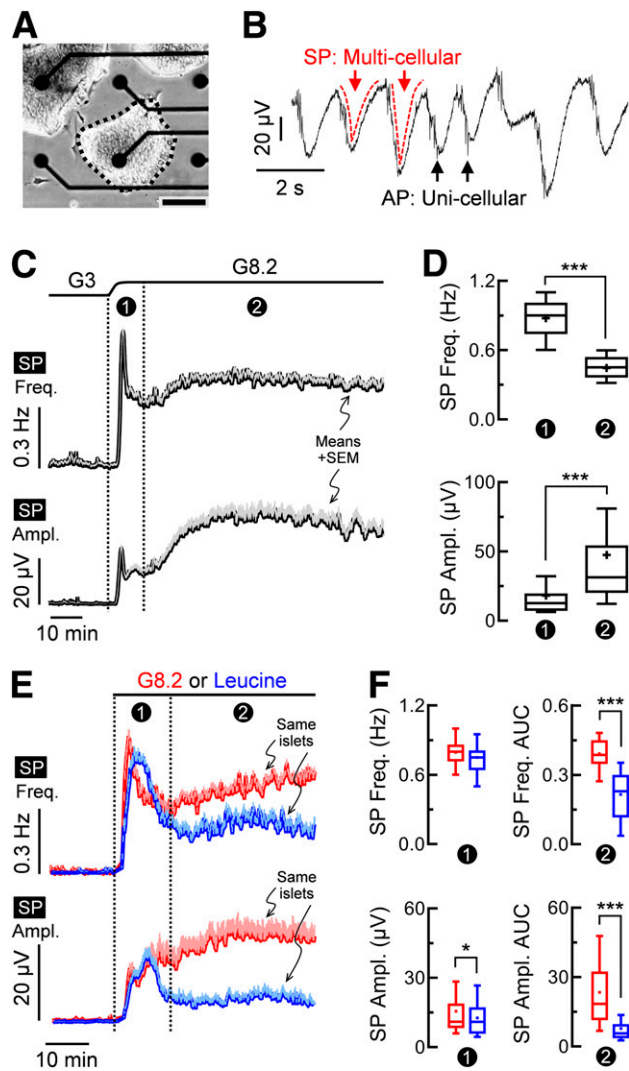


Figure 1—A physiological increase in glucose induces a biphasic electrical profile of SPs. **A:** Mouse islet (dotted line) on an extracellular electrode of a MEA. Scale bar: 100 μm . **B:** Recording from one MEA-electrode when islets are maintained at 8.2 mmol/L glucose shows two types of electrical signals: multicellular SPs and unicellular APs. **C:** Mouse islets were stimulated by an increase in glucose from 3 to 8.2 mmol/L. As in all figures, ① and ② indicate the first and the second phase, respectively, and glucose concentrations are indicated as G followed by the concentration in millimoles per liter (e.g., G8.2 for 8.2 mmol/L glucose in this figure). Means + SEM of SP frequencies (Freq.) and amplitudes (Ampl.) were reported ($N = 7$, $n = 104$). See RESEARCH DESIGN AND METHODS for the optical determination of the kinetics of changes in glucose concentrations (black line at the top). **D:** Statistics on data in **C**. Top panel: peak frequency of SPs during the first phase and mean frequency during the second phase (>25 min after glucose change) were determined for each electrode. Bottom panel: mean amplitude during the two phases. **E:** Islets were first stimulated with glucose (red, 3–8.2 mmol/L). Then, >100 min later, the same islets were stimulated with L-leucine (blue, 20 mmol/L in the presence of G3) and kinetics of SP frequencies and amplitudes were compared. Note that, under these conditions, two consecutive electrical responses to G8.2 were similar ($N = 5$). **F:** Statistics on data in **E** ($N = 2$, $n = 29$). Left: peak frequencies and mean amplitudes during the first phase. Right: AUCs of SP frequencies and amplitudes during the second phase normalized over time. * $2P < 0.05$; *** $2P < 0.001$.

signal-to-noise ratio (Supplementary Fig. 2B). The two electrical phases of SPs were again clearly observable regarding frequencies and amplitudes (Supplementary Fig. 2C and D) and pulsatility appeared after 40–60 min with a mean pulse period of ~ 4 min (Supplementary Fig. 2D–F), similar to insulin secretion data (8,36). Note that islet inactivation following glucose decrease was rapid (<5 min) and not phasic (Supplementary Fig. 2C and D). In the representative HD-MEA illustrated in Fig. 3, two electrodes covered by the same islet were compared with each other (intraislet) and to a third electrode contacting another islet (interislets) (Fig. 3A). All three electrodes revealed SPs of high frequencies and small amplitudes during the first phase and the inverse during the second phase (Fig. 3B). The increase in SP amplitudes in the second phase was concomitant with a clear synchronization of SPs within a given islet, but not between different islets (Fig. 3B). Such absence of interislets synchrony suggests that extraislet mechanisms are involved in the whole pancreas synchrony during pulsatile secretion (8,36). A dynamic MATLAB code was then developed to quantify the degree of interelectrode synchrony during the biphasic activation (Supplementary Methods and Supplementary Fig. 1). At 3 mmol/L glucose, islets rarely generated SPs, and consequently, intraislet synchronies were absent (Fig. 3C, left). When islets were stimulated by 8.2 mmol/L glucose, the different regions within the same islet partially synchronized in the first phase (Fig. 3C, middle), and this intraislet synchrony considerably increased during the second phase (Fig. 3C, right). Statistical comparisons confirmed specific electrical coupling modes for each phase, and SP synchrony was positively correlated with amplitude and negatively correlated with frequency (Fig. 3D). Thus, SP amplitude represents a direct, nonbiased, and continuous measurement of intraislet connectivity, and synchrony is accompanied by the generation of larger functional clusters of lesser activity.

We further addressed the nature of the SPs and islet β -cell coupling by simultaneous extracellular and intracellular recordings. To that end, standard MEAs were used: SPs were measured on a microelectrode at steady state during the second phase, while membrane potentials were recorded with sharp microelectrodes introduced into cells located at different positions within the same islet (Fig. 3E). Single-cell recordings showed slow and regular plateau depolarizations (Fig. 3E), also known as slow Ca^{2+} waves (18,37). Up to four cells within the same islet were investigated: regardless of their position, intracellular plateau depolarizations were always synchronized with SPs captured via the MEA-electrode located at the bottom of the islet (Fig. 3E). Glucose responses were observed in the majority of cells (63.6%), and 85.7% of them were synchronized with extracellular SPs (Fig. 3F). Hence, multicellular SPs represent summations of synchronized intracellular slow plateau depolarizations of β -cells. These data also indicate that electrical coupling concerns almost the entire islet during the second phase.

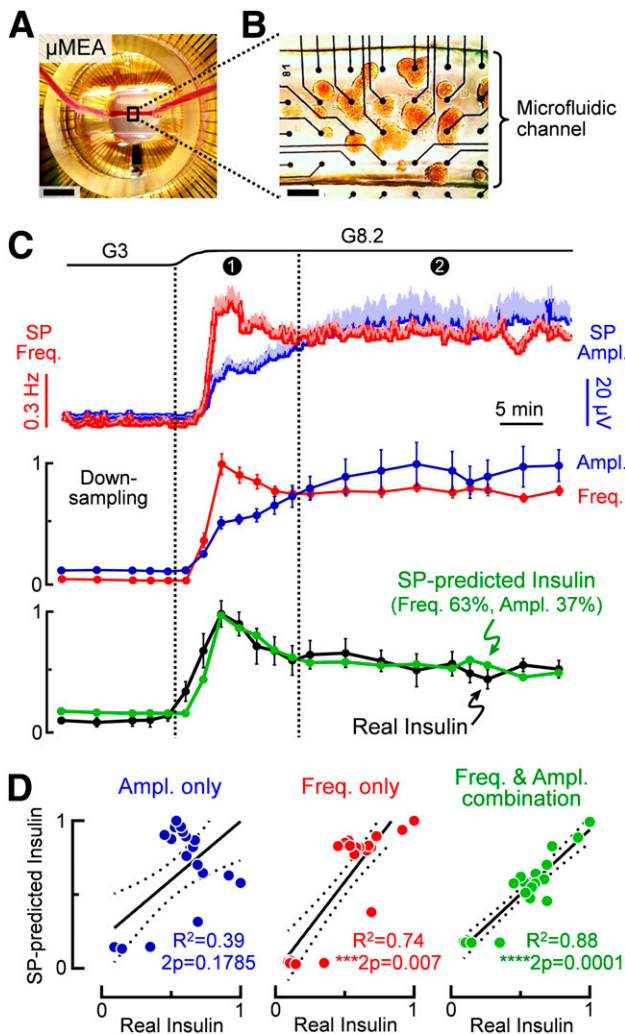


Figure 2—Combination of SP frequencies and amplitudes is highly correlated with biphasic insulin secretion, as shown with μ MEAs. **A**: Image of a μ MEA loaded with a phenol red solution showing the microfluidic channel at the center. Scale bar: 0.5 cm. **B**: Mouse islets cultured in the microfluidic chamber. Scale bar: 200 μ m. **C**: Simultaneous measurements of SP frequency (Freq.), SP amplitude (Ampl.), and insulin secretion in μ MEAs provide correlations between SP and insulin biphasic kinetics. **C**, top: islets were stimulated by an increase in glucose from G3 to G8.2, and kinetics of SP Freq. and Ampl. (means \pm SEM) were monitored during the first (1) and second (2) phase ($n = 18$ islets from $N = 4$ independent experiments). **C**, middle: SP Freq. and Ampl. (means \pm SEM) were normalized and resampled to match insulin sampling periods. **C**, bottom: “Real Insulin” in black is the normalized insulin secretion (means \pm SEM; $N = 4$ independent experiments). In green, “SP-predicted Insulin” represents the optimal combination of SP Freq. and Ampl. with the formula: SP-predicted Insulin = $a \times \text{Freq.} + b \times \text{Ampl.} + c$, where $a = 1.15 \pm 0.14$, $b = -0.67 \pm 0.14$, and $c = 0.23 \pm 0.05$ (SD; $R^2 = 0.88$). **D**: Spearman correlation coefficients (R^2) show that insulin secretion data are poorly correlated with SP Ampl. (left), significantly correlated with SP Freq. (middle), and that the combination of both Freq. and Ampl. (see the formula detailed above) fully predicts insulin secretion ($N = 4$ independent experiments).

Multicellular SPs Drive the Biphasic Electrical Encoding

We next addressed the relationship between single-cell APs and multicellular SPs and their respective contribution to

the biphasic encoding. Low signal-to-noise ratio of metal electrodes at high frequencies prevents the analysis of APs (29). Therefore, we switched to PEDOT-MEAs with electroactive polymer-covered electrodes (Fig. 4A), which optimizes AP detection (29) (Fig. 4B). The duration of extracellular APs was ~ 100 ms (Fig. 4C), as expected (38). Islets were stimulated by glucose within the narrow physiological range (5.5–8.2 mmol/L), different from supraphysiological levels used in our previous studies (29–32). A measurement of 5.5 mmol/L glucose appeared to be the threshold concentration since a small biphasic response was observed for SPs but not for APs, whereas 6 and 8.2 mmol/L glucose triggered strong biphasic activities for both SPs and APs (Fig. 4D) in $\sim 90\%$ of islets (Supplementary Fig. 3A) after a short delay (Supplementary Fig. 3B). At 5.5 mmol/L glucose, 45% of islets responded (Supplementary Fig. 3A) with a longer delay (Supplementary Fig. 3B). At this threshold concentration, the presence of SPs, but of small amplitudes and with few APs (Fig. 4D and E), is in line with intracellular recordings in intact islets (39) and may be explained by some β -cells with some K_{ATP} channel activity at 5.5 mmol/L glucose sufficient to restrain signal propagation.

We also observed further differences in glucose concentration dependency (Fig. 4E). SP amplitudes increased during the first and second phase between 5.5 and 6 mmol/L glucose but remained stable upon a further increase in glucose. In contrast, frequencies of SPs and APs continued to augment until 8.2 mmol/L glucose mainly in the second phase. As maximal SP amplitude represents the size of the functional cell clusters, clusters increase significantly between the two phases for all tested concentrations (Supplementary Fig. 3C). Collectively, these data suggest that increasing glucose from 3 to 8.2 mmol/L recruits more islets and generate more active cell clusters (SP frequency), whereas maximal cluster size is reached already at 6 mmol/L glucose (SP amplitude).

To understand the relative contribution of multicellular and unicellular signals during the transition between first and second phase, SP and AP kinetics were normalized. SP and AP kinetics were similar for the first phase at 5.5 and 6 mmol/L glucose (Fig. 4F, left and middle). Major differences were evident in the second phase at these two concentrations: the small second phase at 5.5 mmol/L glucose involved mainly SPs. Although biphasic patterns of APs started to appear at 6 mmol/L, SPs were still more pronounced especially at the beginning of the second phase as evidenced by differences in the area under the curve (Δ AUC) of the respective signals. Moreover, even at 8.2 mmol/L, SPs were far more prominent than APs during the nadir and beginning of the second phase (Fig. 4F, right), a period when insulin secretion persists, albeit at a lower level (Fig. 2). The subsequent development of SPs during the second phase indicates that β -cells synchronize, probably once they are in a metabolic steady state with K_{ATP} channels blocked to a similar extent. Hence, SP dynamics accurately mirror insulin secretion patterns as

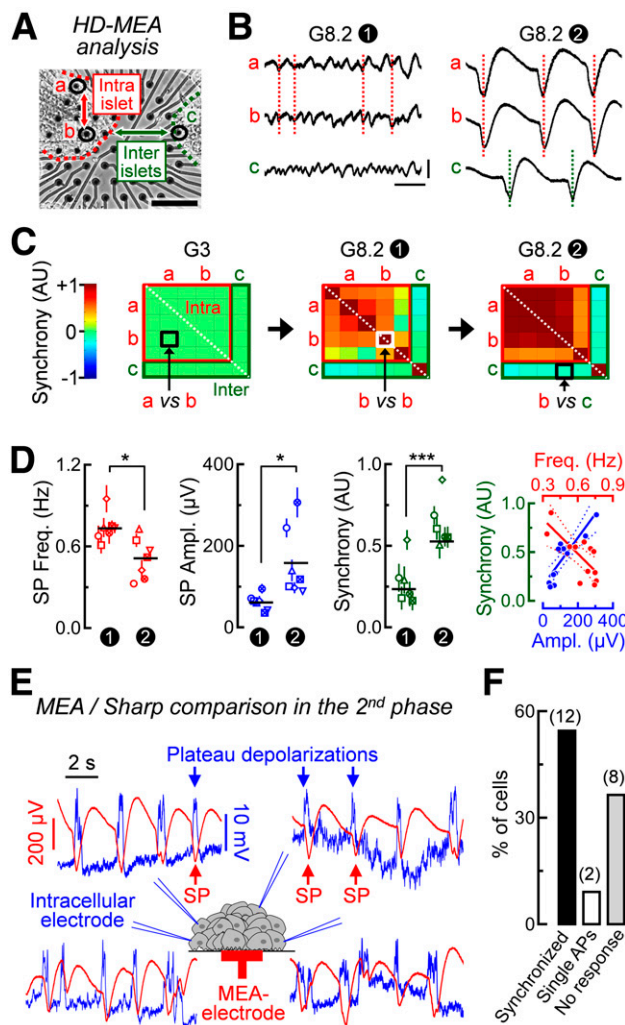


Figure 3—Intra-islet coupling increases in the second phase as revealed by HD-MEAs and by simultaneous extracellular and intracellular recordings. **A:** Two mouse islets on an HD-MEA. Circled electrodes contacting the same islet (intra-islet) or different islets (interislets) are presented in **B** and **C**. Scale bar: 100 μ m. **B:** SPs on the three electrodes presented in **A** during the two phases (1 and 2) at G8.2. Red dotted lines indicate synchrony between intra-islet electrodes. This intra-islet synchrony increases from the first to the second phase. No synchrony was observed between interislet electrodes (green dotted lines). Scale bars: 2 s (horizontal) and 100 μ V (vertical). **C:** Representative correlation matrices obtained at different time points (G3; G8.2 first and second phase) comparing the SP synchrony between intra- and interislet electrodes (see Supplementary Methods and Supplementary Fig. 1 for the generation of correlation matrices). The color code is given on the left with arbitrary units (AU): +1, complete synchrony (e.g., when one electrode is compared with itself such as b vs. b); 0, no synchrony or no SPs; and -1, opposition of phases). Correlations between electrodes depicted in **A** and **B** are given as examples. **D:** Seven islets ($N = 7$, $n = 2$ –13 electrodes each) were analyzed on HD-MEAs. Left three panels: means (\pm SEM) of frequency (Freq.), amplitude (Ampl.), and intra-islet synchrony of SPs for the two phases at G8.2. Each symbol corresponds to one islet. Black horizontal lines indicate means of all islets. $*2P < 0.05$; $***2P < 0.001$. Right panel: synchrony of SPs is correlated with SP amplitude (Spearman correlation test: $R^2 = 0.77$; $***2P = 0.0003$; $n = 12$) and inversely correlated with SP frequency ($R^2 = 0.56$; $**2P = 0.0062$; $N = 6$ islets, $n = 12$). **E:** Simultaneous extracellular and intracellular recordings of a mouse islet. Glucose-evoked SPs generated by an islet were recorded extracellularly with an MEA-electrode (red). At the same time, an intracellular sharp

microelectrode was introduced into different cells of the same islet. Intracellular plateau depolarizations (blue) were systematically synchronized with SPs. **F:** Proportions of: 1) cells with plateau depolarizations in synchrony with SPs as in **E**, 2) cells with continuous single AP patterns instead of plateau depolarizations, and 3) cells without glucose response. In parentheses are the numbers of cells (recorded on five different MEAs).

The Three-Dimensional Structure of Islets and Physiological Levels of Ca^{2+} Are Required for Optimal Connectivity and Biphasic Responses

To ascertain that not only signals from the outer layer of islet cells contribute, we also performed experiments in two-dimensional (2D) monolayers of islet cells (Supplementary Fig. 4). Biphasic behavior was observed in this configuration, but SPs were reduced in the second phase, in line with a 2D coupling in monolayers versus a three-dimensional connectivity in islets (Supplementary Fig. 4A and B). Furthermore, SPs were of higher amplitudes in large monolayers than in medium and small ones, which confirms that SP amplitudes reflect the size of functional β -cell clusters (Supplementary Fig. 4C and D). We would also like to stress that our recordings were performed with physiological glucose and extracellular Ca^{2+} concentrations. Indeed, supraphysiological Ca^{2+} levels exceeding twice the normal concentrations are often used (5,18,37), but create artifactual coupling patterns altering SP and AP dynamics (Supplementary Fig. 5).

Physiological Postprandial Levels of GLP-1 Act Only on the Second Phase by Enhancing Multicellular Coupling Signals (SPs) in Mouse and Human Islets

Intestinal incretin hormones such as GLP-1 are major modulators of insulin secretion. Effects of postprandial levels of GLP-1 on the two phases of islets activation have never been assessed. Moreover, GLP-1 has rarely been used at physiological picomolar concentrations (32,40), and different pathways may be activated at pharmacological nanomolar concentrations (40). We therefore stimulated the same mouse islets with different glucose concentrations in the absence or presence of 50 pmol/L GLP-1 during both phases. At 5.5 mmol/L glucose, only very weak responses were observed (Fig. 5A) in few islets (Fig. 5C, top), but in the presence of GLP-1, a far greater number of islets became glucose responsive (Fig. 5C, top), and the hormone considerably amplified the second phase (Fig. 5A and D). To confirm that the effect is restricted to the second phase, we examined the effect of picomolar GLP-1 at 8.2 mmol/L glucose. Islets generated two electrical phases for SPs and APs (Fig. 5B), and GLP-1 did not recruit more active islets at this glucose concentration (Fig. 5C, bottom). Again, GLP-1 specifically increased only the second phase and concerned only multicellular coupling

microelectrode was introduced into different cells of the same islet. Intracellular plateau depolarizations (blue) were systematically synchronized with SPs. **F:** Proportions of: 1) cells with plateau depolarizations in synchrony with SPs as in **E**, 2) cells with continuous single AP patterns instead of plateau depolarizations, and 3) cells without glucose response. In parentheses are the numbers of cells (recorded on five different MEAs).

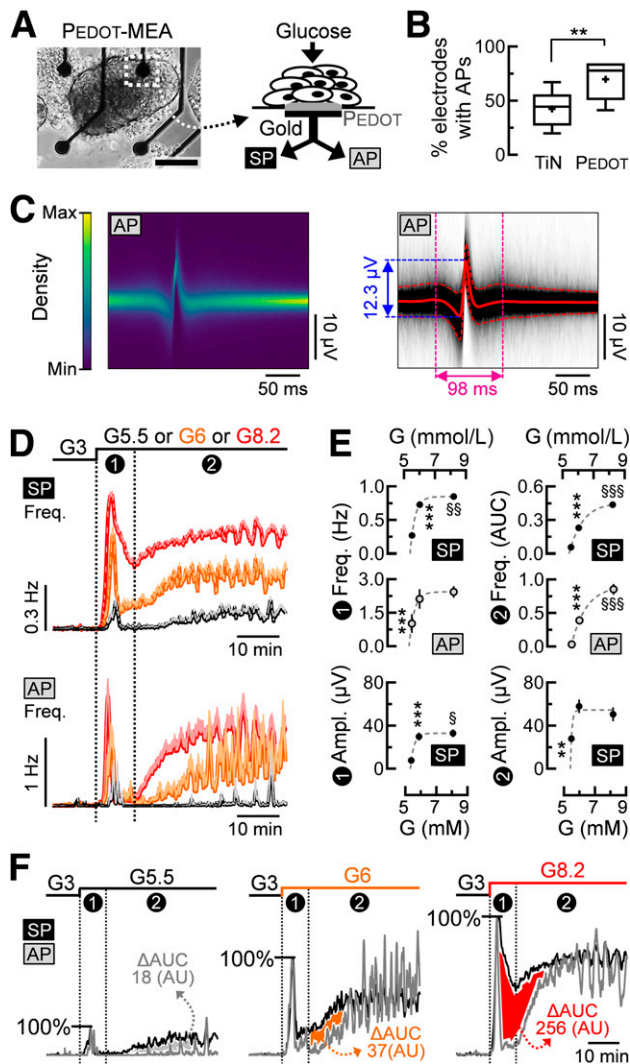


Figure 4—Glucose dependency of multicellular (SP) and unicellular (AP) signal kinetics analyzed with polymer-covered MEA electrodes (PEDOT). **A**: Image (scale bar: 100 μm) and scheme of an islet on a PEDOT-electrode. Metal electrodes are covered with a conductive polymer composed of PEDOT and carbon nanotubes to optimally detect both SPs and APs. **B**: Comparison of metal (TiN) and PEDOT-electrodes regarding the proportion of electrodes with detectable APs (TiN: $N = 21$ MEAs; PEDOT: $N = 7$ MEAs). $**2P < 0.01$. **C**, left: 2D density histogram generated from 21,824 APs ($N = 18$ islets). Sample densities are represented according to the color code in the 2D matrix (time, amplitude). **C**, right: overlay of 21,824 APs (black) and mean \pm SD (red) showing extracellular AP duration and amplitude. **D**: Kinetics of SP and AP frequencies (Freq.) (means \pm SEM) during the two phases evoked by an increase in glucose from G3 to G5.5 (black), G6 (orange), and G8.2 mmol/L (red) ($N = 3-6$, $n = 38-114$). **E**: Statistics. Gray dotted lines: best fitting curves. Top and middle left: peak frequencies of SPs and APs during the first phase (1) were determined for each electrode. SPs: $***P < 0.001$ for G5.5 vs. G6; $§§P < 0.01$ for G6 vs. G8.2. APs: $***P < 0.001$ for G5.5 vs. G6 and G8.2. Top and middle right: AUCs of SP and AP frequencies during the second phase (2) normalized over time. $***P < 0.001$ for G5.5 vs. G6; $§§§P < 0.001$ for G6 vs. G8.2. Bottom: maximal amplitudes of SPs (means of the 10th biggest SPs for each electrode) during the two phases. $***P < 0.001$ for G5.5 vs. G6; $§P < 0.05$ for G5.5 vs. G8.2; $**P < 0.01$ for G5.5 vs. G6 and G8.2. See also Supplementary Fig. 3 for complementary analysis. **F**: Comparisons of normalized SP and AP frequency kinetics show that SPs are necessary for the transition between phases. For each glucose

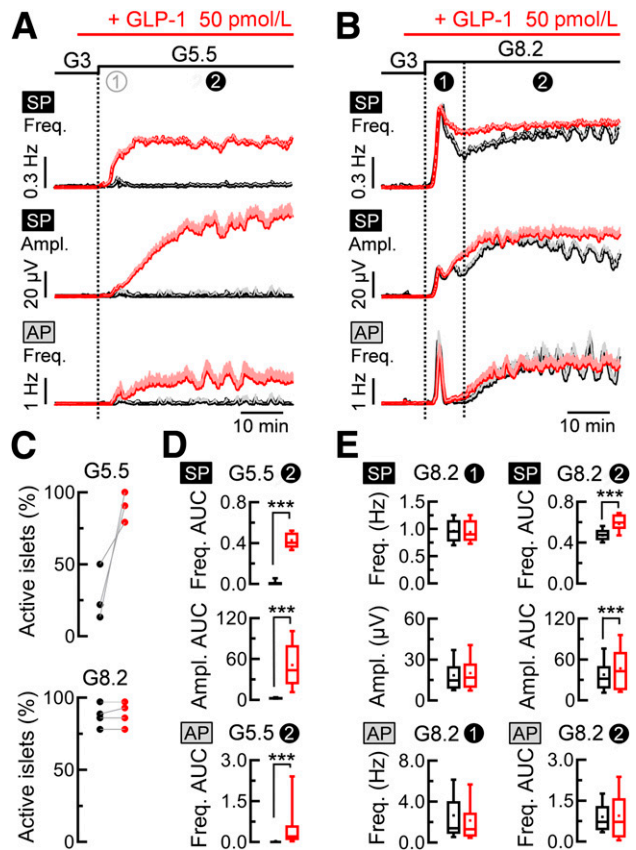


Figure 5—Postprandial levels of GLP-1 act only on the second phase by enhancing multicellular coupling (SP) in mouse islets. **A** and **B**: Mouse islets on PEDOT-MEAs were stimulated by an increase in glucose from G3 to G5.5 (**A**) or to G8.2 (**B**) (black curves). At >100 min later, the same islets were glucose stimulated in the same way but in the presence of 50 pmol/L of GLP-1 applied 5 min before glucose increase (red curves). Kinetics of SP and AP frequency (Freq.) and SP amplitude (Ampl.) (means \pm SEM) are given. **C**: Proportion of islets responding electrically to G5.5 or G8.2 with or without GLP-1. **D** and **E**: Statistics on data given in **A** ($N = 3$; $n = 49$ for SPs and $n = 38$ for APs) and **B** ($N = 4$; $n = 64$ for SPs and $n = 41$ for APs). Peak frequency and mean amplitude of SPs and peak frequency of APs during the first phase were determined for each electrode. AUCs of SP frequency, SP amplitude, and AP frequency during the second phase were normalized over time. $***2P < 0.001$.

signal (SPs) without affecting single-cell activities (APs) (Fig. 4B and E). Note that the activity of islets exhibited oscillations after ~ 40 min in G8.2 that disappeared upon GLP-1 (Fig. 5B and Supplementary Fig. 6), confirming a previous observation that the incretin triggers continuous electrical activity in β -cells (40). Moreover, fitting of SP frequencies showed that picomolar GLP-1 accelerated the appearance of the second phase (Supplementary Fig. 6). Thus, postprandial levels of GLP-1 act only on the second phase by enhancing β -cell cluster activity and coupling.

concentrations, ΔAUC is given as the difference between normalized AUCs of SP and AP frequencies. AU, arbitrary units.

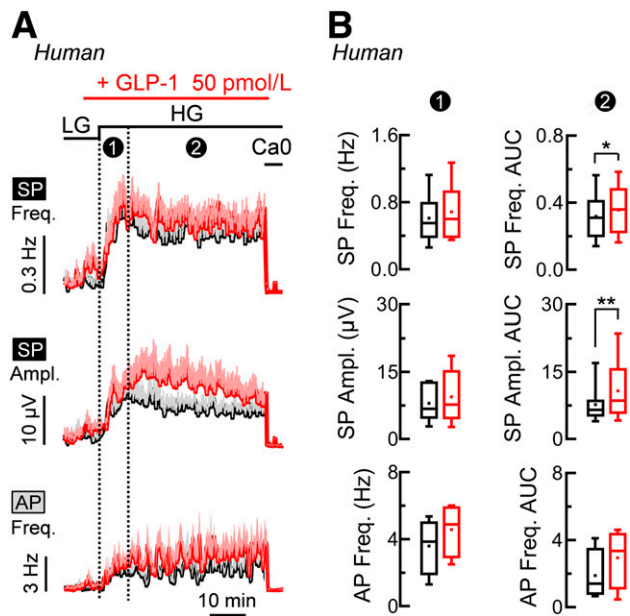


Figure 6—Postprandial levels of GLP-1 act only on the second phase by enhancing multicellular coupling (SP) but not single-cell activities (AP) in human islets. **A:** Human islets on a PEDOT-MEA were stimulated by an increase in glucose from 1 mmol/L (low glucose [LG]) to 11 mmol/L (high glucose [HG]) (black). Then, >100 min later, the same islets were stimulated in the same way by glucose but in the presence of 50 pmol/L of GLP-1 applied 5 min before HG (red). Note that, under these conditions, two consecutive electrical responses to G11 only were similar. Kinetics of SP frequencies (Freq.) and amplitudes (Ampl.) and of AP frequencies before and during the two phases are given (means + SEM). Note that first phases were less marked for APs than for SPs. At the end of the protocol, a solution depleted in Ca^{2+} (Ca0) was applied to determine the basal activity. **B:** Statistics ($n = 4-10$). ①: peak frequency of SPs and APs and mean amplitude of SPs during the first phase were determined for each electrode. ②: AUCs of SP frequency, SP amplitude, and AP frequency during the second phase normalized over time. * $2P < 0.05$; ** $2P < 0.01$.

GLP-1 action was also examined in human islets. An increase in glucose provoked SPs with a biphasic profile as in mice, which was less pronounced for APs (Fig. 6A). The data confirmed the specific action of GLP-1 in human islets on the second phase of SPs, but not on APs (Fig. 6B).

Aging and Glucotoxicity Impair Biphasic Activity

Aging and type 2 diabetes impair not only the overall quantity of insulin secreted, but also the kinetics (10,13,14). The comparison of SP kinetics between young adult and middle-aged mice revealed that both electrical phases were altered by aging (Fig. 7A): the reactivity of clusters (SP frequencies) was affected without changes in the extent of coupling (SP amplitudes) (Fig. 7B).

Glucotoxicity recapitulates parts of the diabetic state (41). Mouse islets were exposed to a glucotoxic medium (20 mmol/L glucose for 64 h). In these conditions, islets exhibited increased basal SP activities at low glucose (Fig. 7C and D) in line with the increase in basal secretion in glucotoxicity (41). Upon glucose stimulation, the first phase (i.e., high SP frequencies and low SP amplitudes)

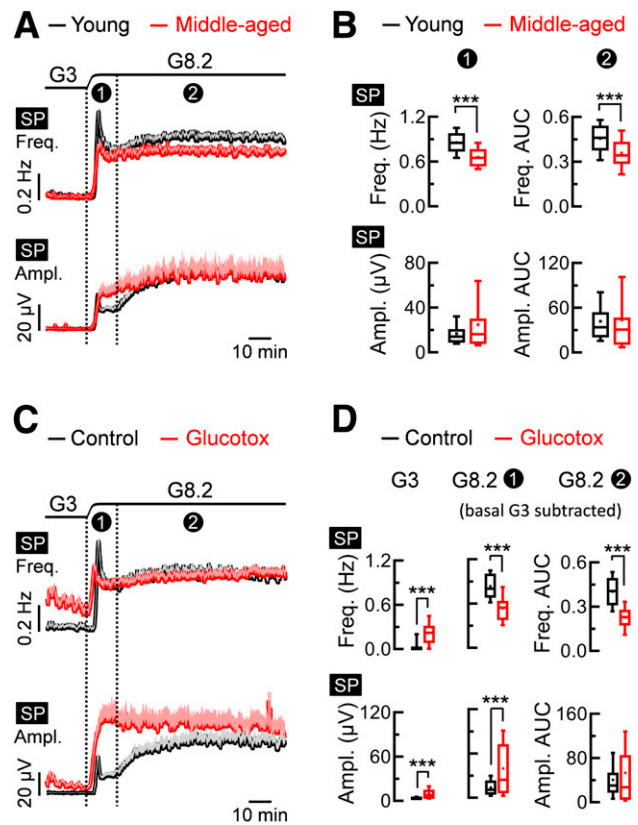


Figure 7—Aging and glucotoxicity alter the biphasic electrical profile of SPs in mouse islets. **A:** Islets from young adult (12–13 weeks, black) or middle-aged mice (39–45 weeks, red) on standard MEAs (metal electrodes) were stimulated by an increase in glucose from G3 to G8.2. Kinetics of SP frequency (Freq.) and amplitude (Ampl.) are given for the two phases (mean + SEM). **B:** Statistics on data in A ($N = 3-5$; $n = 46-58$). **B, left:** peak frequency and mean amplitude of SPs during the first phase were determined for each electrode. **B, right:** AUCs of SP frequencies and amplitudes of the second phase normalized over time. *** $2P < 0.001$. **C:** Islets from young adult mice cultured on standard MEAs were stimulated as in A, and kinetics of SP frequency and amplitude (means + SEM) were determined as in A for the same islets exposed to two conditions: before (culture at 11 mmol/L glucose, Control, black) and 64 h after subsequent culture at 20 mmol/L (Glucotox, red). **D:** Statistics on data in C ($N = 3$, $n = 43$). G3: means of SP frequencies and amplitudes over 10 min preceding G8.2. G8.2①: peak frequencies and mean amplitude of SP during the first phase were determined for each electrode. G8.2②: AUCs of SP and frequencies and amplitudes of the second phase normalized over time. For G8.2① and G8.2②, basal activities at G3 were subtracted for both control and glucotoxic conditions. *** $2P < 0.001$.

was considerably altered (Fig. 7D), with a second phase mode starting very early (Fig. 7C). Alterations of biphasic activity were confirmed in human islets exposed to glucotoxicity, and these effects were partially reversible, mainly in terms of coupling signals, as indicated by SPs, but not in regard to single-cell activity (APs) (Fig. 8A and B).

DISCUSSION

Our data provide a new model for the origin of biphasic islet activation based on analysis of single-cell and of micro-organ electrical activity with high spatiotemporal

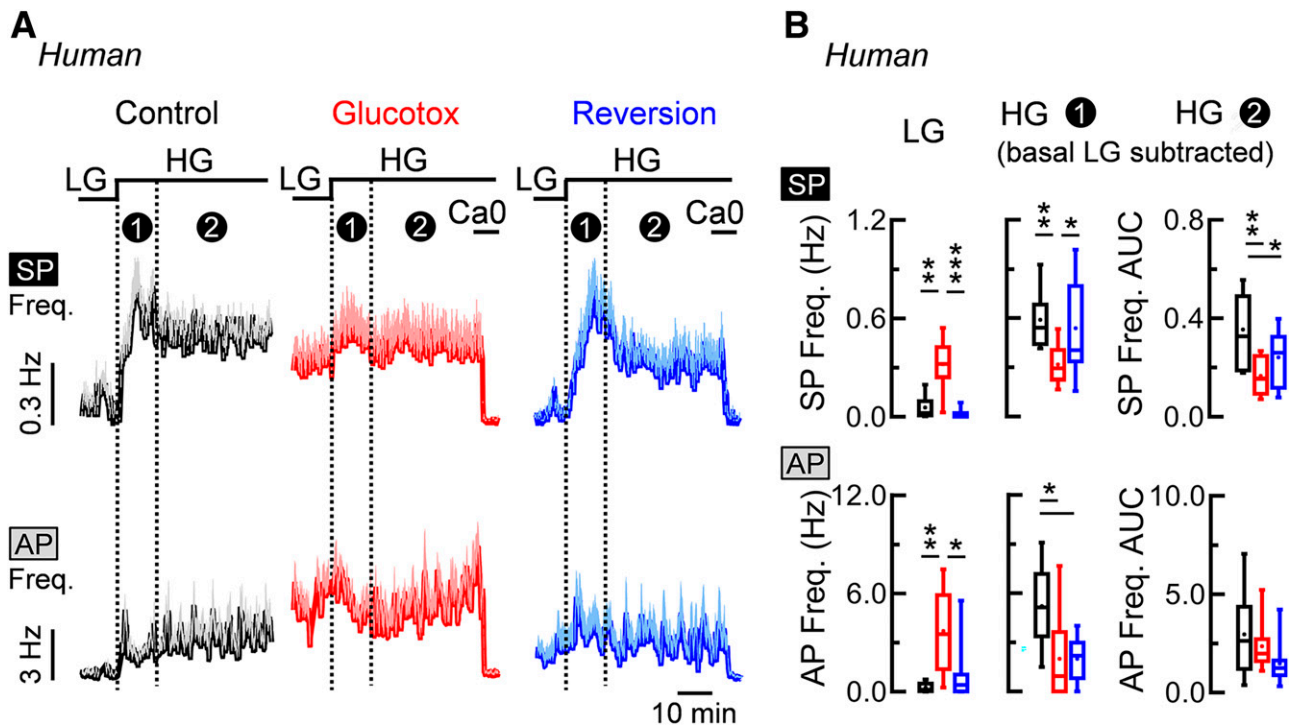


Figure 8—Glucotoxicity in human islets alters basal activity and biphasic electrical profiles. Human islets cultured on PEDOT-MEAs were stimulated by an increase in glucose from 1 mmol/L (low glucose [LG]) to a high concentration triggering a biphasic electrical response (high glucose [HG], 7 or 11 mmol/L, depending on the donor). **A**: Kinetics of SP and AP frequencies (Freq.) (means + SEM) before and during the two phases were determined for the same islets of the same donors in three consecutive conditions: before (culture at 5.6 mmol/L glucose, Control, black), 64 h after subsequent culture at 20 mmol/L (Glucotox, red), and 69 h after further subsequent culture at 5.6 mmol/L (Reversion, blue). **B**: Statistics ($N = 2, n = 10\text{--}15$). LG: means of SP and AP frequency before HG. HG①: peak frequencies of SP and AP during the first phase were determined for each electrode. HG②: AUCs of SP and AP frequencies of the second phase normalized over time. For HG① and HG②, the basal activity at LG was subtracted in the three conditions. * $P < 0.05$; ** $P < 0.01$; *** $P < 0.001$.

resolution. Our protocols mimicked relevant physiological characteristics in terms of time spans, concentrations of glucose, GLP-1 (42), as well as Ca^{2+} levels, as the supra-physiological concentrations often used of this cation (5,18,37) considerably distort islet activity.

Our data indicate that progressive multicellular organization establishes the physiological biphasic pattern in both mouse and human islets. Upon glucose stimulation, the first phase originates from a multitude of small β -cell clusters, highly active but poorly coordinated, whereas during the subsequent second phase, clusters enlarge and contain less active but highly synchronized β -cells (Supplementary Fig. 7A and B), in accordance with previous observations using Ca^{2+} imaging in pancreas slices (27). Parallel monitoring of SPs and insulin secretion shows that the overall activity of β -cell clusters in terms of frequency contributes far more than the extent of coupling (given by the amplitude) to biphasic secretion, while the combination of both frequency and coupling is most closely correlated with the biphasic insulin pattern.

The effects of postprandial levels of GLP-1 on both phases were also investigated in this study for the first time. Physiological levels of incretin promote only the second phase by enhancing multicellular signals but not single-cell activities (Supplementary Fig. 7A and B). GLP-1

increases the size of clusters (SP amplitude), their level of activity (SP frequency), and the time spent in active periods. Moreover, GLP-1 also accelerates the installation of the second phase. As the second phase coupling mode constitutes an economic mode, it is certainly more favorable for prolonged activity during the digestion. Its further prominence in the presence of GLP-1 may contribute to protective effects of the incretin on β -cells (43) and certainly underlies its specific secretory effects in vivo on the second phase in humans (44,45). In contrast, aging reduces the reactivity, but not the size, of β -cell clusters, similar to glucotoxicity, for which, in addition, an increased basal activity is observed (Supplementary Fig. 7A and C).

Biphasic hormone secretion has generally been explained by distinct granule pools (19–21). Differential Ca^{2+} sensitivities and kinetics have been observed by intracellular electrophysiology (46), which records, however, only a fraction of the phases. Interestingly, imaging vesicle movements does not unambiguously provide support for distinct vesicle pools as a base for biphasic hormone release (19,47). In addition, biphasic β -cell activity requires multicellular processes (22,23). Multicellular SPs drive the transition between phases, and their profiles clearly mirror the biphasic and monophasic insulin

secretions evoked by glucose and leucine, respectively (34). Since electrical SPs occur upstream of exocytosis, our data support the view that SPs propagating across islet β -cells constitute the master regulator of biphasic organization. The other biphasic mechanisms observed downstream at the cytoskeleton and insulin granule levels (5,19–21) may represent a precise adaptation contributing to the amplification of biphasic secretion kinetics.

This dynamic organization appears well adapted to physiological and metabolic requirements. Indeed, the high but poorly synchronized activity of the first phase (Supplementary Fig. 7A and B) provides a rapid and prominent homeostatic response but is rather energy consuming and potentially toxic due to the cytosolic accumulation of Ca^{2+} . In the second phase, an increase in coupling concomitant with a reduction of the overall activity prevents such excesses (Supplementary Fig. 7A and B) and may constitute a more economical long-term activity.

The considerable reduction of the first electrical phase upon aging and glucotoxicity (Supplementary Fig. 7A and B) is in line with the clinical data (10–14). Westacott et al. (48) reported that aging alters coupling in mouse and human islets, but the impact on each phase has not been addressed. In the present study, the reduction in SP frequency in the first phase suggests that the basic organizational mode in clusters is not changed per se during this period, but the overall activity of clusters is decreased. Moreover, increase in basal activity blunted the net increment in second-phase activity contributing to the well-known phenomenon of glucose insensitivity (49).

The unbiased long-term approach used in this study provides a new model of islet activation and its derangements. The methodology may be of considerable value to evaluate disease models and maturation; for example, in the setting of normal or patient-obtained stem cell-derived surrogate islets. Finally, better understanding of islet endogenous algorithms as presented in this study may also improve development of new commands driving insulin pumps for the therapy of diabetes (50).

Acknowledgments. The authors thank the colleagues at the University of Bordeaux Animal Facility for help.

Funding. This study was supported by the following grants: European Regional Development Fund Diaglyc (to J.L. and S.R.), Agency Nationale de la Recherche ANR-18-CE17-0005 DIABLO (to J.L. and S.R.), Ministère de l'Éducation Nationale, de l'Enseignement Supérieur et de la Recherche Excellence PhD Scholarship (to M.R. and M.J.), and Université de Bordeaux PEPS Idex/CNRS (to M.R.).

Duality of Interest. No potential conflicts of interest relevant to this article were reported.

Author Contributions. M.J., J.L., and M.R. conceived the study. M.J., E.B., A.P., E.P., J.G., S.O., D.C., and M.R. performed experiments. M.J., E.B., A.P., J.L., and M.R. analyzed data. M.J., J.L., and M.R. wrote the manuscript. F.L. and D.B. provided human islets. B.C., S.R., J.L., and M.R. procured funding. M.R. is the guarantor of this work and, as such, had full access to all of the data in the study and takes responsibility for the integrity of the data and the accuracy of the data analysis.

Prior Presentation. Parts of this study were presented as abstracts and oral communications at the annual meeting of the European Association for the Study of Diabetes, Berlin, Germany, 1–5 October, 2018, Congress of the Société Francophone du Diabète, Nantes, France, 20–23 March 2018, and the Keystone Symposia, Islet Biology: From Gene to Cell to Micro-Organ, Santa Fe, NM, 27–31 January 2020.

References

- Freeman ME, Kanyicska B, Lerant A, Nagy G. Prolactin: structure, function, and regulation of secretion. *Physiol Rev* 2000;80:1523–1631
- Kadota C, Ohta M, Takahashi M. Dynamic response to follicle-stimulating hormone of secretion of progesterone by superfused rat ovarian granulosa cells. *Mol Cell Endocrinol* 1988;59:213–220
- Voets T, Neher E, Moser T. Mechanisms underlying phasic and sustained secretion in chromaffin cells from mouse adrenal slices. *Neuron* 1999;23:607–615
- Grodsky GM. A threshold distribution hypothesis for packet storage of insulin and its mathematical modeling. *J Clin Invest* 1972;51:2047–2059
- Rorsman P, Ashcroft FM. Pancreatic β -cell electrical activity and insulin secretion: of mice and men. *Physiol Rev* 2018;98:117–214
- Henquin JC, Nenquin M, Stiernet P, Ahren B. In vivo and in vitro glucose-induced biphasic insulin secretion in the mouse: pattern and role of cytoplasmic Ca^{2+} and amplification signals in beta-cells. *Diabetes* 2006;55:441–451
- Robbins DC, Jaspan J, Vasquez B, Van Cauter E. Biphasic patterns of peripheral insulin and glucose levels after lunch in normal subjects. *Diabetes Care* 1987;10:293–299
- Nunemaker CS, Wasserman DH, McGuinness OP, Sweet IR, Teague JC, Satin LS. Insulin secretion in the conscious mouse is biphasic and pulsatile. *Am J Physiol Endocrinol Metab* 2006;290:E523–E529
- Tokarz VL, MacDonald PE, Klip A. The cell biology of systemic insulin function. *J Cell Biol* 2018;217:2273–2289
- Del Prato S. Loss of early insulin secretion leads to postprandial hyperglycaemia. *Diabetologia* 2003;46(Suppl. 1):M2–M8
- Stumvoll M, Fritsche A, Häring HU. Clinical characterization of insulin secretion as the basis for genetic analyses. *Diabetes* 2002;51(Suppl. 1):S122–S129
- Weiss R, Caprio S, Trombetta M, Taksali SE, Tamborlane WV, Bonadonna R. Beta-cell function across the spectrum of glucose tolerance in obese youth. *Diabetes* 2005;54:1735–1743
- Szoke E, Shrayyef MZ, Messing S, et al. Effect of aging on glucose homeostasis: accelerated deterioration of beta-cell function in individuals with impaired glucose tolerance. *Diabetes Care* 2008;31:539–543
- Chang AM, Halter JB. Aging and insulin secretion. *Am J Physiol Endocrinol Metab* 2003;284:E7–E12
- Luciani DS, Misler S, Polonsky KS. Ca^{2+} controls slow NAD(P)H oscillations in glucose-stimulated mouse pancreatic islets. *J Physiol* 2006;572:379–392
- Li J, Shuai HY, Gylfe E, Tengholm A. Oscillations of sub-membrane ATP in glucose-stimulated beta cells depend on negative feedback from Ca^{2+} . *Diabetologia* 2013;56:1577–1586
- Taddeo EP, Stiles L, Sereda S, et al. Individual islet respirometry reveals functional diversity within the islet population of mice and human donors. *Mol Metab* 2018;16:150–159
- Gilon P, Henquin JC. Influence of membrane potential changes on cytoplasmic Ca^{2+} concentration in an electrically excitable cell, the insulin-secreting pancreatic B-cell. *J Biol Chem* 1992;267:20713–20720
- Seino S, Shibasaki T, Minami K. Dynamics of insulin secretion and the clinical implications for obesity and diabetes. *J Clin Invest* 2011;121:2118–2125
- Henquin JC, Ishiyama N, Nenquin M, Ravier MA, Jonas JC. Signals and pools underlying biphasic insulin secretion. *Diabetes* 2002;51(Suppl. 1):S60–S67
- Rorsman P, Eliasson L, Renström E, Gromada J, Barg S, Göpel S. The cell physiology of biphasic insulin secretion. *News Physiol Sci* 2000;15:72–77

22. Chertow BS, Baranetsky NG, Sivitz WI, Meda P, Webb MD, Shih JC. Cellular mechanisms of insulin release. Effects of retinoids on rat islet cell-to-cell adhesion, reaggregation, and insulin release. *Diabetes* 1983;32:568–574
23. Head WS, Orseth ML, Nunemaker CS, Satin LS, Piston DW, Benninger RK. Connexin-36 gap junctions regulate in vivo first- and second-phase insulin secretion dynamics and glucose tolerance in the conscious mouse. *Diabetes* 2012;61:1700–1707
24. Johnston NR, Mitchell RK, Haythorne E, et al. Beta cell hubs dictate pancreatic islet responses to glucose. *Cell Metab* 2016;24:389–401
25. Salem V, Silva LD, Suba K, et al. Leader β -cells coordinate Ca^{2+} dynamics across pancreatic islets in vivo. *Nat Metab* 2019;1:615–629
26. Dorrell C, Schug J, Canaday PS, et al. Human islets contain four distinct subtypes of β cells. *Nat Commun* 2016;7:11756
27. Markovič R, Stožer A, Gosak M, Dolensšek J, Marhl M, Rupnik MS. Progressive glucose stimulation of islet beta cells reveals a transition from segregated to integrated modular functional connectivity patterns. *Sci Rep* 2015;5:7845
28. Satin LS, Zhang Q, Rorsman P. “Take me to your leader”: an electrophysiological appraisal of the role of hub cells in pancreatic islets. *Diabetes* 2020;69:830–836
29. Koutsouras DA, Perrier R, Villarroel Marquez A, et al. Simultaneous monitoring of single cell and of micro-organ activity by PEDOT:PSS covered multi-electrode arrays. *Mater Sci Eng C* 2017;81:84–89
30. Perrier R, Pirog A, Jaffredo M, et al. Bioelectronic organ-based sensor for microfluidic real-time analysis of the demand in insulin. *Biosens Bioelectron* 2018;117:253–259
31. Raoux M, Bornat Y, Quotb A, Catargi B, Renaud S, Lang J. Non-invasive long-term and real-time analysis of endocrine cells on micro-electrode arrays. *J Physiol* 2012;590:1085–1091
32. Lebreton F, Pirog A, Belouah I, et al. Slow potentials encode intercellular coupling and insulin demand in pancreatic beta cells. *Diabetologia* 2015;58:1291–1299
33. Schreiber S, Fellous JM, Whitmer D, Tiesinga P, Sejnowski TJ. A new correlation-based measure of spike timing reliability. *Neurocomputing* 2003;52-54:925–931
34. Liu YJ, Cheng H, Drought H, MacDonald MJ, Sharp GW, Straub SG. Activation of the K_{ATP} channel-independent signaling pathway by the nonhydrolyzable analog of leucine, BCH. *Am J Physiol Endocrinol Metab* 2003;285:E380–E389
35. Buzsáki G, Anastassiou CA, Koch C. The origin of extracellular fields and currents—EEG, ECoG, LFP and spikes. *Nat Rev Neurosci* 2012;13:407–420
36. Pøksen N, Hollingdal M, Juhl C, Butler P, Veldhuis JD, Schmitz O. Pulsatile insulin secretion: detection, regulation, and role in diabetes. *Diabetes* 2002;51(Suppl. 1):S245–S254
37. Zhang M, Goforth P, Bertram R, Sherman A, Satin L. The Ca^{2+} dynamics of isolated mouse beta-cells and islets: implications for mathematical models. *Biophys J* 2003;84:2852–2870
38. Jacobson DA, Kuznetsov A, Lopez JP, Kash S, Ammälä CE, Philipson LH. Kv2.1 ablation alters glucose-induced islet electrical activity, enhancing insulin secretion. *Cell Metab* 2007;6:229–235
39. Drews G, Krippeit-Drews P, Düfer M. Electrophysiology of islet cells. *Adv Exp Med Biol* 2010;654:115–163
40. Shigeto M, Ramracheya R, Tarasov AI, et al. GLP-1 stimulates insulin secretion by PKC-dependent TRPM4 and TRPM5 activation. *J Clin Invest* 2015;125:4714–4728
41. Jonas JC, Bensellam M, Duprez J, Elouil H, Guiot Y, Pascal SM. Glucose regulation of islet stress responses and beta-cell failure in type 2 diabetes. *Diabetes Obes Metab* 2009;11(Suppl. 4):65–81
42. Elliott RM, Morgan LM, Tredger JA, Deacon S, Wright J, Marks V. Glucagon-like peptide-1 (7-36)amide and glucose-dependent insulinotropic polypeptide secretion in response to nutrient ingestion in man: acute post-prandial and 24-h secretion patterns. *J Endocrinol* 1993;138:159–166
43. Aaboe K, Krarup T, Madsbad S, Holst JJ. GLP-1: physiological effects and potential therapeutic applications. *Diabetes Obes Metab* 2008;10:994–1003
44. Quddusi S, Vahl TP, Hanson K, Prigeon RL, D’Alessio DA. Differential effects of acute and extended infusions of glucagon-like peptide-1 on first- and second-phase insulin secretion in diabetic and nondiabetic humans. *Diabetes Care* 2003;26:791–798
45. Woerle HJ, Carneiro L, Derani A, Göke B, Schirra J. The role of endogenous incretin secretion as amplifier of glucose-stimulated insulin secretion in healthy subjects and patients with type 2 diabetes. *Diabetes* 2012;61:2349–2358
46. Mislser S, Zhou Z, Dickey AS, Silva AM, Pressel DM, Barnett DW. Electrical activity and exocytotic correlates of biphasic insulin secretion from beta-cells of canine islets of Langerhans: contribution of tuning two modes of Ca^{2+} entry-dependent exocytosis to two modes of glucose-induced electrical activity. *Channels (Austin)* 2009;3:181–193
47. Gandasi NR, Yin P, Omar-Hmeadi M, Ottosson Laakso E, Vikman P, Barg S. Glucose-dependent granule docking limits insulin secretion and is decreased in human type 2 diabetes. *Cell Metab* 2018;27:470–478.e4
48. Westacott MJ, Farnsworth NL, St Clair JR, et al. Age-dependent decline in the coordinated $[\text{Ca}^{2+}]$ and insulin secretory dynamics in human pancreatic islets. *Diabetes* 2017;66:2436–2445
49. Ferrannini E. The stunned beta cell: a brief history. *Cell Metab* 2010;11:349–352
50. Steil GM, Grodsky GM. The artificial pancreas: is it important to understand how the β cell controls blood glucose? *J Diabetes Sci Technol* 2013;7:1359–1369

SUPPLEMENTARY MATERIAL

The MATLAB script used for intra-islet synchrony analysis (related to **Fig. 3A-D** and **Supplementary Fig. 1**) is detailed bellow.

```
- evt_correlation.m -----  
---  
  
function [correlation_matrix,gauss_sig] =  
evt_correlation(timestamps_in,Fs,sigma_s,varargin)  
% evt_correlation.m  
% - Computes time correlation between events across N channels. Yields an NxN  
% correlation matrix and a representation of all events and their region of influence.  
%  
% Outputs  
% - correlation_matrix : Correlation matrix (shows correlation index for channels  
% (i,j))  
% - gauss_sig : Smooth event signal for every channel  
%  
% Inputs  
% - timestamps_in : Input timestamps. Cell of vectors (one vector of timestamps  
% per channel). No unit (Nbr of samples).  
% - Fs : Sampling frequency (Hz)  
% - sigma_s : width of the gaussian (temporal tolerance for event  
% correlation)  
% - varargin : additional arguments ('nv' makes the function non-verbose)  
  
% Parse additional arguments  
if ~isempty(varargin)  
    for i=1:length(varargin)  
        if isequal(varargin{i},'nv')  
            % Non-verbose flag  
            VERBOSE = 0;  
        end  
    end  
end  
end  
  
% Verbose flag check  
if ~exist('VERBOSE')  
    VERBOSE = 1;  
end  
  
% Check all signals for largest timestamp and preallocate memory for event signals  
Nsignals = length(timestamps_in);  
Lmax = 0;  
for i=1:Nsignals  
    sp_timestamps = timestamps_in{i};  
    sp_timestamps = sort(sp_timestamps(:));  
    tmpmax = max(sp_timestamps);  
    if ~isempty(tmpmax)  
        Lmax = max(Lmax,tmpmax);  
    end  
end
```



```

    end
end

events = zeros(Nsignals,Lmax);

% Generate gaussian waveform
gauss_width_s = 5*sigma_s;
x = -gauss_width_s:1/Fs:gauss_width_s;
sigma = sigma_s;
H = gaussmf(x,[sigma 0]);

% Generate smooth events (convolve event signal with gaussian)
gauss_sig = zeros(Nsignals,Lmax-1); % Preallocate
for i=1:Nsignals
    % Generate event signal
    sp_timestamps = timestamps_in{i};
    sp_timestamps = sort(sp_timestamps(:));
    events(i,sp_timestamps) = 1;
    % Smooth it out
    gauss_sig(i,:) = fastconv(events(i,:),H,0); % Fast convolution (fft, product,
ifft)
end

% Generate correlation matrix
correlation_matrix = zeros(Nsignals,Nsignals);
if ~isempty(gauss_sig)
    k = 0; % Counter to keep track of how many correlations have been computed
    for i=1:Nsignals
        for j=1:Nsignals
            correlation_matrix(i,j) = corr(gauss_sig(i,:)','gauss_sig(j,:)'); % Compute
correlation index for channel couple (i,j)
            k = k+1;
            if VERBOSE % Print progress every 100 correlations computed
                if mod(k,100) == 0
                    disp(['Event correlation: ' num2str(k) ' out of '
num2str(Nsignals*Nsignals) ' done.'])
                end
            end
        end
    end
    if VERBOSE % Success message
        disp(['Event correlation: all done.'])
    end
    correlation_matrix(isnan(correlation_matrix))=0; % Nullify NaN (Not A Number)
values
end

end

- fastconv.m -----
---
function [y]=fastconv(x, h, dim)

Ly=length(x)+length(h)-1;
Ly2=pow2(nextpow2(Ly));

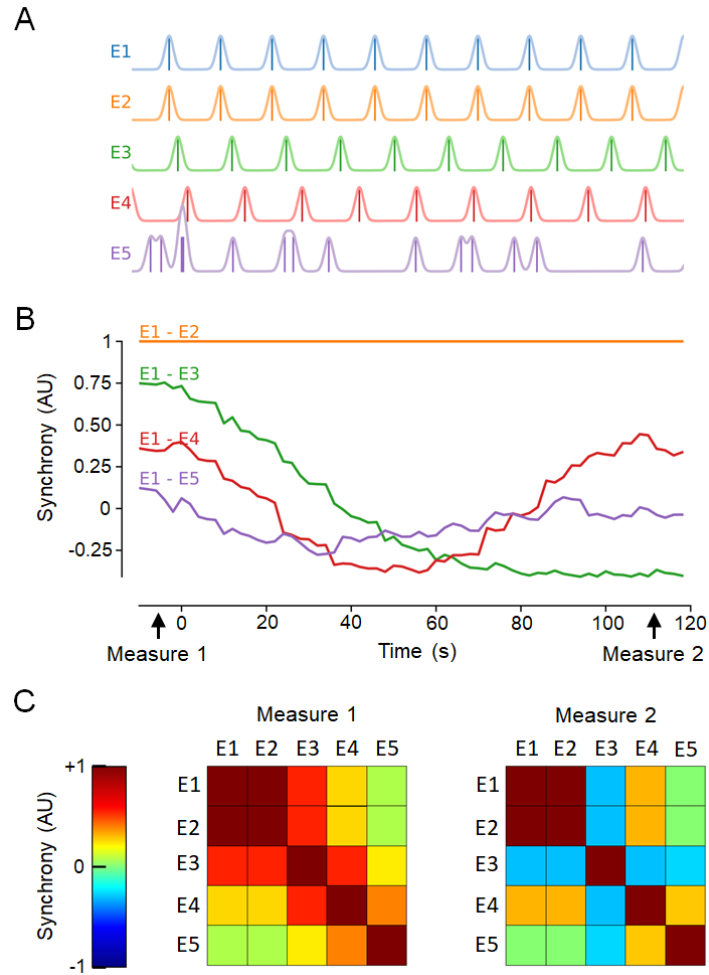
X=fft(x, Ly2); % Fast Fourier transform
H=fft(h, Ly2); % Fast Fourier transform

```

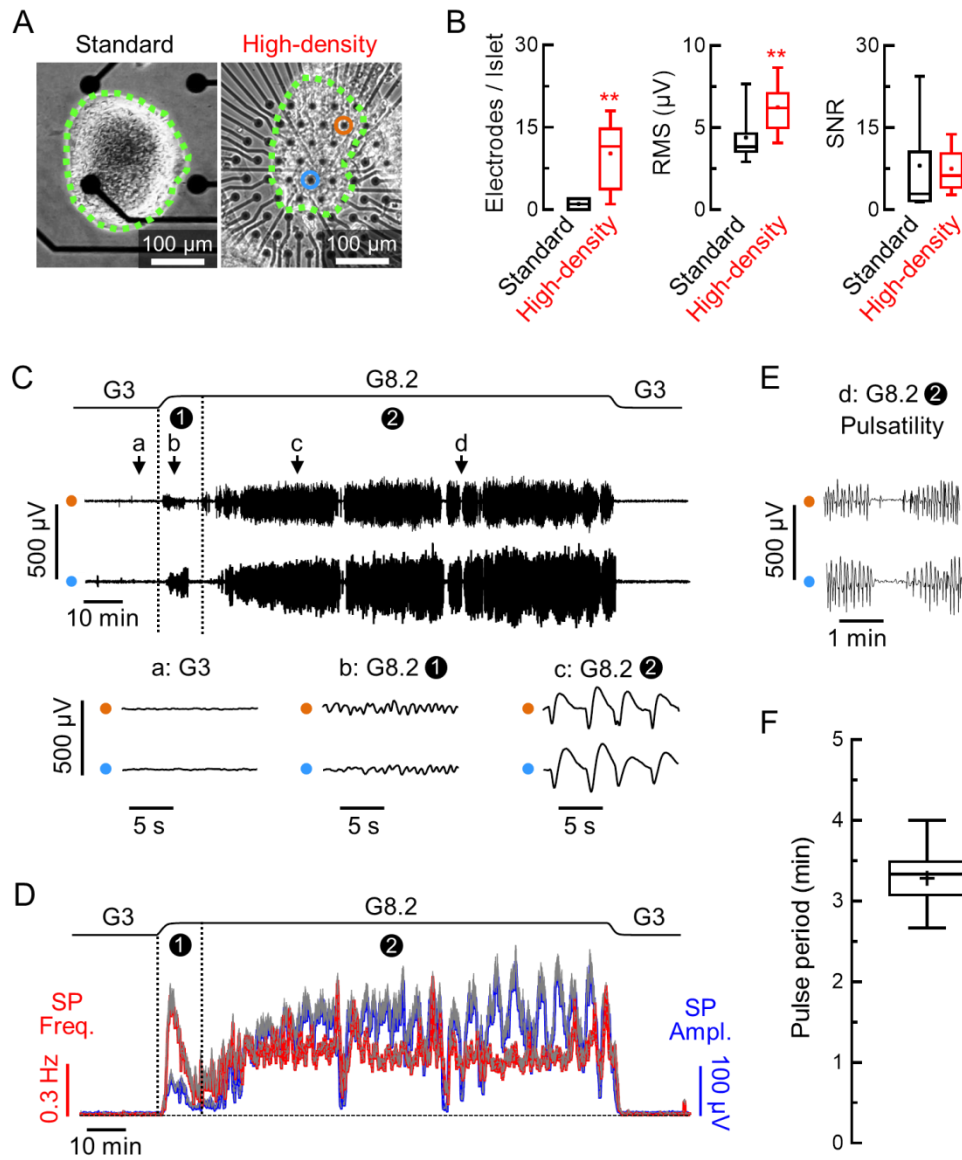
```
if size(X) ~= size(H)
    H=H';
end
Y=X.*H; % Multiply ffts
y=real(iff(Y, Ly2)); % Inverse fast Fourier transform

if dim==0 % Yield only center part (preserve signal length, time-aligned)
    y=y(round(length(h)/2):1:Ly-round(length(h)/2));
elseif dim==1 % Real time (preserve signal length, delayed)
    y=y(1:1:length(x));
elseif dim==2 % Full size
    y=y(1:1:Ly);
end
```

SUPPLEMENTARY FIGURES & LEGENDS

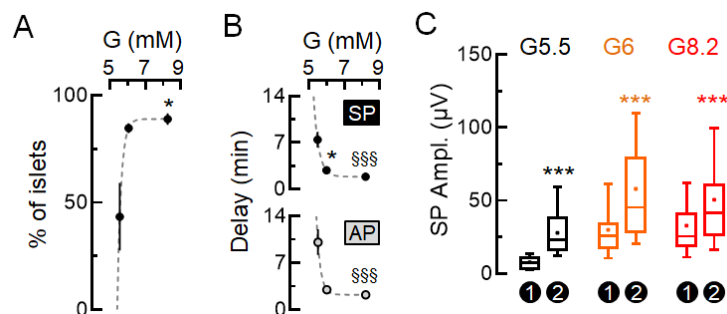


Supplementary Fig. 1. Simulations in MATLAB illustrating the method used to compute temporal event correlations and their matrix representation. To quantify the degree of SP synchrony between electrodes during the biphasic activation, a dynamic code was developed, inspired from works in neurons by Schreiber and colleagues (33). **(A)** Temporal detection of events (vertical lines) and continuous signals constructed by correlating events with Gaussian curves on 5 electrodes (E1 to E5). The time axis is as in **(B)**. E1 and E2 are identical trains of regular events. E3 is a regular train of events, at 95% of the speed of E1. E4 is a regular train of events, at 90% of the speed of E1. E5 is a random train of events. **(B)** Time-dependent correlation measurements (synchrony; AU, arbitrary units) between E1 and E2-E5. Colors indicate with which electrode E1 is compared, following the color indicated in **(A)**. **(C)** Matrix representations of correlation at the two time points indicated in **(B)**. Each square represents the degree of synchrony (color code on the left), between -1 and 1, of the couple of electrodes given by its coordinates (hence the unitary diagonal). The degree of synchrony varies between -1 and +1: +1 representing SPs perfectly synchronized, 0 representing the absence of SP or SPs without any synchrony, and -1 representing SPs in opposition of phases.

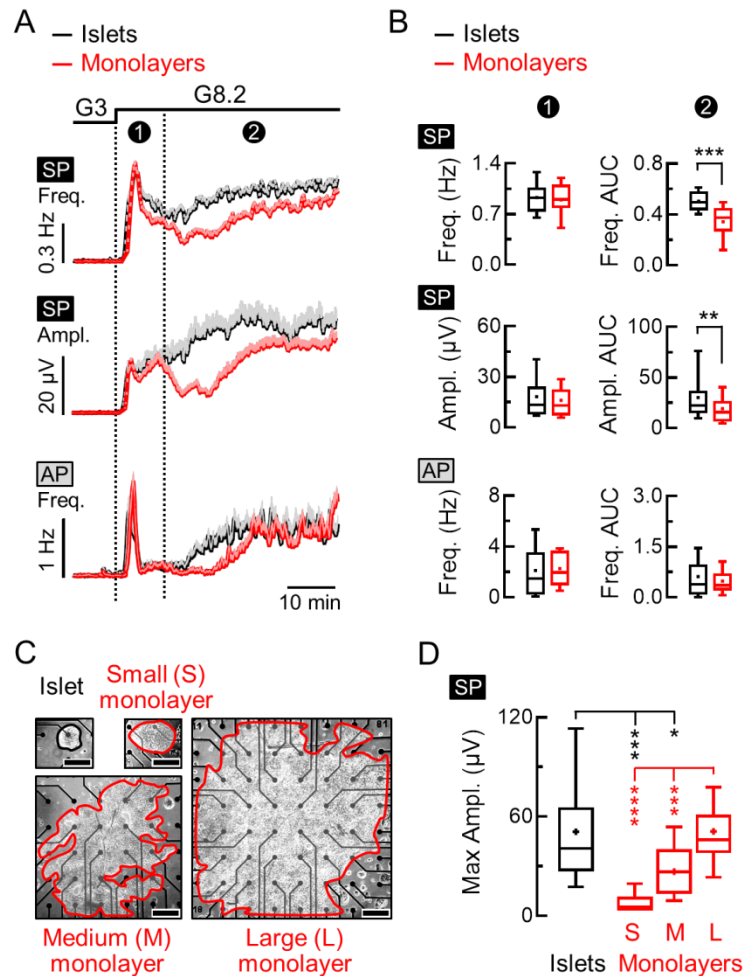


Supplementary Fig. 2. Monitoring of SPs in different regions of an islet with high-density (HD) MEAs. (A) Comparison of a standard MEA (4/59 electrodes shown) and a HD-MEA (59/59 electrodes shown). An islet is delimited by green dots. Note the difference between the size of the electrodes (images at identical scales): ϕ 30 μm for standard MEAs and 10 μm for HD-MEAs. Data from encircled electrodes (orange and light blue) are shown as examples in (C) and (E) (B) HD-MEAs increased the number of electrodes per islets (left panel; N=3-4 MEAs, n=8-49 islets). The smaller electrode diameter increased the noise level (middle panel; root mean square - RMS - noise level, N=3 MEAs, n=12 uncovered electrodes) without affecting the signal-to-noise ratio (SNR) of the very robust SPs (right panel, N=3 MEAs, n=26-30). The RMS noise level was measured with Spike2 on unfiltered traces with a time constant of 5 s and the SNR was taken as the ratio of RMS noise levels between covered and uncovered electrodes when islets were stimulated by glucose ≥ 8.2 mM for >20 min. ** $2p < 0.01$, *** $2p < 0.001$. (C) Top traces:

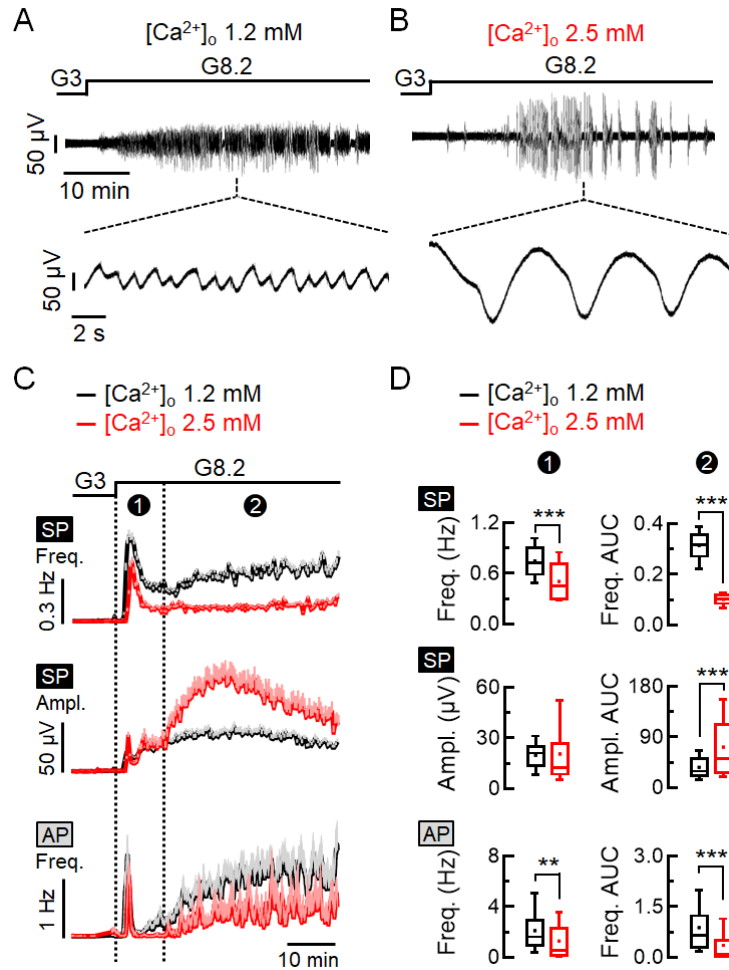
representative recordings of SPs from the 2 electrodes indicated in orange and light blue in (A) during the 1st (①) and the 2nd (②) phases induced by G8.2 and during the decrease of glucose level to G3. See methods for the optical determination of the kinetics of changes in glucose concentrations (black line at the top). Bottom traces: portions of top traces with higher temporal resolution at the timestamps indicated by a, b and c. (D) Kinetics of SP frequency (red) and amplitude (blue) measured in a mouse islet on a HD-MEA (means +SEM, n=13 electrodes) during the 1st (①) and the 2nd (②) phases induced by G8.2 and during the decrease of glucose level to G3. (E) Portions of top traces shown in (C) with higher temporal resolution at the timestamp d showing the appearance of SP pulsatility during the 2nd phase. (D) Period of the pulsatility (number of pulses per min) measured after 40 min at G8.2 and during 40 min (N=7 islets).



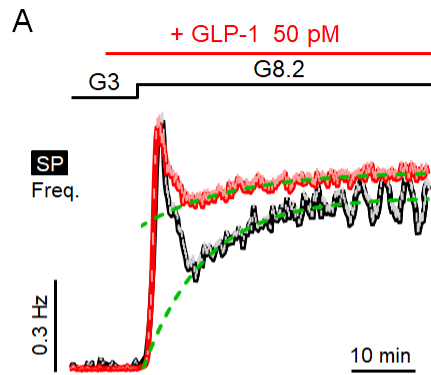
Supplementary Fig. 3. SP and AP analysis in response to glucose. Concentration-dependencies to glucose (G) of the electrical responses generated by mouse islets were analyzed with polymer-coated MEA-electrodes. **(A)** Proportion of islets (means \pm SEM) responding electrically to G5.5, G6 and G8.2. * $p < 0.01$ for G8.2 vs. G5.5. **(B)** Delays (means \pm SEM) between the change in concentration and the first SPs (top) and APs (bottom). * $p < 0.05$ for G5.5 vs. G6 and §§§ $p < 0.001$ for G8.2 vs. G5.5 and G6. Gray dotted lines are the best fitting curves. **(C)** Statistics comparing maximal amplitude of SPs (means of the 10th biggest SPs for each electrode) during the 1st (1) vs. the 2nd (2) phase for each glucose concentration. *** $2p < 0.001$. (N=3-6, n=29-114).



Supplementary Fig. 4. SP and AP analysis of islets versus islet cell monolayers on polymer-coated MEA-electrodes. (A and B) Comparison of glucose-induced electrical responses of native islets and islet cell monolayers. (A) Mouse entire islets (black) or mouse islet cells in monolayers (red) cultured on PEDOT-MEAs were stimulated by an increase in glucose from G3 to G8.2. Kinetics of SP frequency and amplitude as well as AP frequency during the two phases were evaluated (means +SEM). (B) Statistics on data in (A) (N=3, n=40-80). Left: peak frequency and mean amplitude of SPs and peak frequency of APs during the 1st phase were determined for each electrode. Right: AUCs of SP frequency, SP amplitude and AP frequency during the 2nd phase normalized over time. (C) Influence of the size of islet cell monolayers on the maximal amplitude of SPs. Left: representative images (scale bars 200 μ m) of an islet (surrounded in black) and a small (<0.1 mm²), a medium (0.1-0.5 mm²) and a large (>0.5 mm²) islet-cell monolayer (surrounded in red). Right: maximal amplitudes of SPs (means of the 10th biggest SPs during the 2nd phase) of islets, small (S), medium (M) and large (L) islet-cell monolayers (n=6-46). * 2p<0.05, ** 2p<0.01, *** 2p<0.001, **** 2p<0.0001.



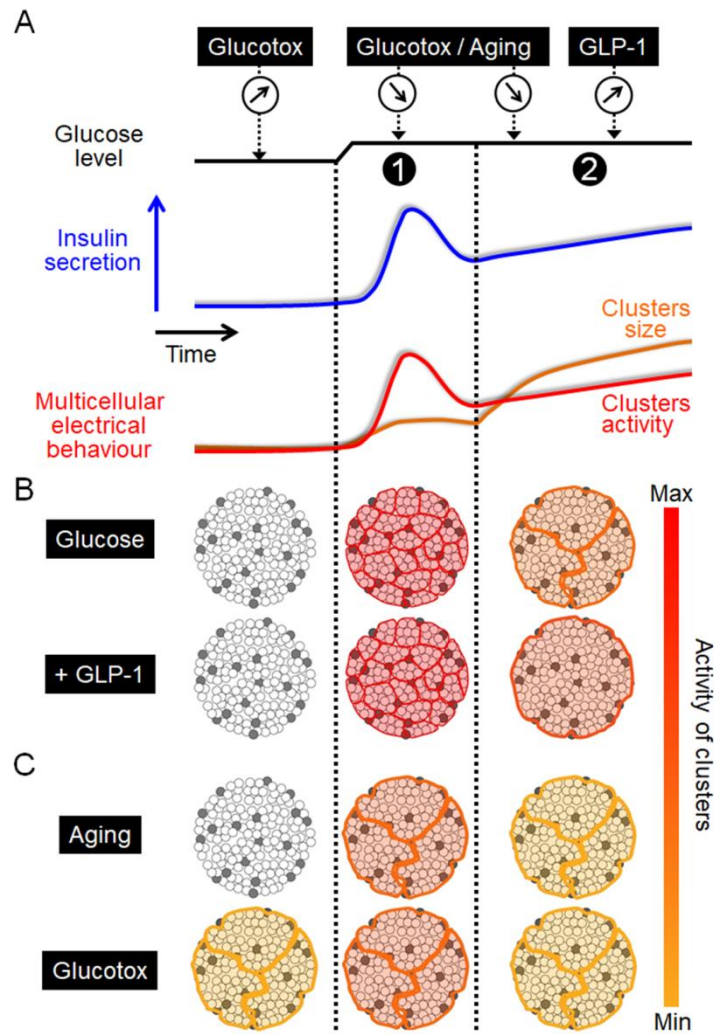
Supplementary Fig. 5. Supraphysiological extracellular Ca^{2+} levels considerably alter SP and AP dynamics. (A and B) Top traces: representative recordings of the electrical activity of the same mouse islet stimulated by an increase in glucose from G3 to G8.2 in the presence of two different concentrations of extracellular Ca^{2+} ($[Ca^{2+}]_o$) as indicated (PEDOT-MEA; Bandpass: 0.1-700 Hz). Bottom traces: portions of top traces at higher temporal resolution (representative of $n=26$ recordings from $N=3$ independent biological preparations). (C) Kinetics of SP frequency and amplitude as well as AP frequency during the two phases in the two Ca^{2+} conditions (means \pm SEM). Similar results were obtained regardless of the concentration of Ca^{2+} tested first ($N=3$). (D) Statistics ($N=3$; $n=26$ for SPs and $n=20$ for APs). Left: peak frequency and mean amplitude of SPs and peak frequency of APs during the 1st phase were determined for each electrode. Right: AUCs of SP frequency, SP amplitude and AP frequency during the 2nd phase normalized over time. ** $2p < 0.01$, *** $2p < 0.001$.



B

One-phase decay	Ctr	GLP-1
Y0 (s)	-544.52	-6
Plateau (Hz)	0.468	0.6202
K	0.002291	0.001191
Half Life (s)	302.5	582.1
Tau (s)	436.4	839.8

Supplementary Fig. 6. Physiological (picomolar) levels of GLP-1 increase and promote the passage from the 1st to the 2nd phase. (A) SP frequency kinetics and best fits (green) of the 2nd phase obtained on mouse islets stimulated by increasing glucose from G3 to G8.2 in the absence (black) and in the presence of GLP-1. GLP-1 was applied 5 min before changing glucose concentrations and was present during the stimulation by G8.2 (means +SEM; N=4-6, n=64). (B) Details of the fitting curve parameters for the stimulation with G8.2 alone (Ctr) and with G8.2 and GLP-1.



Supplementary Fig. 7. Proposed functional model. (A) Biphasic insulin secretion induced by glucose and corresponding multicellular electrical behavior of islets in terms of activity (i.e. SP frequency) and of cluster sizes (i.e. SP amplitude). Modulations of phases in physiological and pathophysiological conditions are indicated on top. (B and C) Representation of the multicellular behavior of an islet during glucose-induced phases in different physiological and pathophysiological conditions. Unfilled and filled circles represent β and non- β -cells, respectively. Intra-islet clusters are represented by colored areas. Relative sizes of clusters are represented, as well as their level of activity with the color code on the right. (B) Model in physiological conditions: upon glucose stimulation, the 1st phase originates from a multitude of highly active small β -cell clusters, but poorly coordinated together, whereas during the subsequent 2nd phase, clusters enlarge and contain less active but highly synchronized β -cell clusters. Physiological levels of GLP-1 promote only the 2nd phase by enhancing multicellular signals (size and activity of clusters). (C) Model in aging and glucotoxicity (glucotox). Aging reduces the reactivity, but not the size, of β -cell clusters, similarly to glucotoxicity for which in addition an increased basal activity is observed.

Proof of concept of the islet-based biosensor in rodents: Manuscript n°3

Continuous glucose monitoring has considerably improved insulin delivery. However, currently used electrochemical sensors react to glucose only. The ideal sensor, ie islets, captures various nutrients and hormonal regulators, reacts in a biphasic manner and is differentially modulated by non β -islet cells. We have previously demonstrated in-vitro that islet electrical activity, measured extracellularly as slow potentials (SP) by micro-electrode arrays (MEA), faithfully reflects biphasic activation and hormone secretion. As a subsequent step towards a bio-inspired artificial pancreas we have now set out to test this approach as open loop in rodent in-vivo.

In order to successfully establish the proof of concept of this new device, we worked step by step in order to successfully assemble in the animal the different elements essential for the implementation of the sensor together. The first step was to collect serum from the rat and apply it to the islets seeded on a PDMS microwell static MEA in order to work on a small volume. Following this step, and the observation that the electrical response of the islets was consistent in terms of frequency and amplitude variation with the different glucose variations, we implanted the animals with a microdialysis device in order to recover the dialysate during the glucose tolerance test IPGTT. During the IPGTT, the blood glucose level of the animal is monitored by caudal blood measurement and the glucose concentration of the dialysate is determined after the experiment by glucose determination in the samples with glucose oxidase. The microdialysis recovery had been characterised in vitro and led to a choice of work flow rate of 1 μ l/min, which offered the best compromise between glucose recovery and flow rate compatible with the subsequent implementation of microfluidics. The dialysate collected during the IPGTT was then applied to the islets seeded in microwells on MEA. Again, we were able to observe electrical activity consistent in frequency and amplitude with the dialysate concentrations. In a final step, we were able to link the microdialysis implanted on the anaesthetised animal to a microfluidic circuit allowing the dialysate to be delivered in real time to the seeded islets in a microfluidic chip that we developed compatible with a commercial MEA. During the experiment, the animal is anaesthetised, the catheter is implanted, and after the pump is switched on, the catheter is connected to the microfluidic

circuit, the electrical activity of the islets is then recorded in real time. A blood glucose measurement is performed in the animal at the caudal level every 15 minutes and the dialysate is collected for 15 minutes every 15 minutes at the exit of the microfluidic circuit after the passage on the islets in order to determine after the experiment to which average concentration of glucose the islets were exposed over this period of time. At the end of these experiments we were able to establish a correlation between the blood glucose variation profile, the variation of glucose within the dialysate and the variation of the electrical activity of the islets in terms of frequency and amplitude.

In conclusion, we were able to establish the feasibility of a device in-vivo based on the electrical activity of the islets of Langerhans, by establishing a high correlation between electrical activity of the islets and glycaemic variations in the animal. The biosensor was able to follow the dynamics of blood glucose variations. The next step in the development of the sensor would be to optimise the microfluidic circuit to reduce the different delays between the animal and the islets on the MEA.

Continuous monitoring in-vivo with a micro-organ based microfluidic biosensor

Emilie Puginier *, Antoine Pirog*, Florence Poulletier de Gannes², Julien Gaitan¹, Annabelle Hurtier², Marie Monchablon^{1,2}, Matthieu Raoux¹, Sylvie Renaud², Jochen Lang¹

¹ CNRS UMR 5248, Institute of Chemistry and Biology of Membranes and Nano-objects (CBMN), Univ. Bordeaux, Allée de Geoffrey St Hilaire, 33600 Pessac, France

² CNRS UMR 5218, Intégration du Matériau au Système (IMS), Bordeaux INP, Univ. Bordeaux, Talence, France

* Equal contribution

Correspondence to: jochen.lang@u-bordeaux.fr

KEYWORDS:

microelectrode array, islets, biosensor, diabetes, continuous glucose monitoring

ABSTRACT

Continuous monitoring of physiological parameters has numerous applications and is used in diabetes therapy. Current approaches to detect glucose rely on enzyme-linked electrochemical probes. In contrast, monitoring of a few electrogenic pancreatic islets in a biosensor may harness the computational power of the micro-organ made for nutrient detection and provide a more appropriate read-out. Moreover, this sensor also integrates information from the whole organism. Extracellular electrophysiology captures slow potentials (SPs), which reflect coupled islet β -cell activity and is a method of choice for non-destructive long-term monitoring of islet activity in-vitro. We have now developed a microfluidic microelectrode chip containing a few islets and linked to interstitial fluids in live rats by subcutaneous microdialysis. Blood and dialysate glucose were determined concomitantly with islet electrical activity either off-line or on-line during an intraperitoneal glucose or insulin challenge. The electrical activity in terms of slow potentials monitored by this biosensor reacts proportionally to glucose levels off-line in serum or dialysed interstitial fluid. On-line monitoring reveals an excellent correlation between islet slow potential frequency and to a slightly lesser degree to slow potential amplitudes. Statistical analysis reveals a robust signal highly correlated to glucose concentrations with little variation between animals. Micro-organ based biosensors in general harness multiple parameters. They provide a read-out closer to physiology and may be of use also in the therapy of diabetes.

INTRODUCTION

Pancreatic islets are at the centre of nutritional homeostasis and their demise cause the most common metabolic disease, that is type 1 or type 2 diabetes which both are characterized by increased blood glucose (Ashcroft and Rorsman, 2012; Charles and Leslie, 2021; Pigeyre et al., 2022). Within the islet micro-organ, the insulin-containing β -cells function as actuator, which secrete insulin, the only glucose lowering hormone, as well as sensors, that measure the amount of nutrients available in the blood and thus turn food into a command for insulin release. An increase in ambient nutrient levels leads to an increase in β -cell metabolism and subsequently a change in ion channel activity and thus transmembrane ion fluxes (Rorsman and Braun, 2012). The ensuing depolarisation and calcium influx via voltage dependent ion channels induces highly regulated insulin release. The changes in ion channel activities are further regulated by hormones, eg the stress hormone adrenalin or enteric peptide hormones (De Marinis et al., 2010). Thus, transmembrane ion fluxes provide an integrative read-out according to nutritional status and to the state of the organism.

Type 1 diabetes is an autoimmune disease characterized by a large or complete loss of islet β -cells and this requires hormone replacement therapy (Atkinson et al., 2014). As insulin, like most peptide hormones, exerts a powerful action in the picomolar range, its concentration has to be carefully titrated to achieve therapeutic levels and avoid life-threatening hypoglycaemia. Previously this was achieved via repetitive daily determinations of blood glucose levels by finger pricks. Recent technological advancements permit continuous blood glucose monitoring (CGM) via a subcutaneous electrochemical electrode (Lee et al., 2021; Teo et al., 2022). The use of CGMs has considerably reduced the pain for the patients and increased therapeutic precision as compared with previous discontinuous surveillance of glucose levels. This has led to the concept of an artificial pancreas as a closed loop system where a subcutaneous sensor measures glucose in the interstitial fluid and commands a small insulin injecting pump as actuator via appropriate algorithms (Cobelli et al., 2011). Despite the progress achieved during the last 50 years, the system still requires announcements of meals or physical activity and can provoke hypoglycaemia (Lee et al., 2021; Teo et al., 2022). Other therapeutical approaches such as transplantation of donor islets or of β -like cells are either reserved for severe unstable diabetes or still not sufficiently advanced for therapy

As pancreatic islets have been developed by half a billion years of evolution (Falkmer, 1979; Youson and Al-Mahrouki, 1999), they provide a fairly optimal sensor. In contrast to CGM they do not measure glucose but rather a demand in insulin. In addition, they contain internal inhibitory and stimulatory circuits given by the presence of the different cell types present in addition to β -cells (Campbell and Newgard, 2021). Moreover, in terms of activity they react stronger to a decrease in glucose than to an increase and this endogenous algorithm provides a clinical safety mechanism against hypoglycaemia (Keenan et al., 2012 ; Lebreton et al., 2015). Using these micro-organs as biosensor could offer considerable advantages in monitoring the nutritional state including glucose.

The capture of electrical cellular signals as signatures of activity offers a number of advantages as compared to other approaches, such as on-line signal analysis (Perrier et al., 2018; Pirog et al., 2018), no gene transfer or chemical probes are required for signal generation and electronics are well suited for miniaturization. We have previously studied and analysed in detail the electrical responses of human and rodent islets in-vitro using extracellular electrophysiology with multielectrode arrays, a non-invasive method that allows recording over long time periods (Abarkan et al., 2019; Abarkan et al., 2022; Jaffredo et al., 2021; Lebreton et al., 2015). These electrical signatures of islet activity, as recorded in-vitro by MEAs, can be introduced in a simulator of human metabolism in T1D patients, called UVA/Padova (Cobelli and Dalla Man, 2021). This computer model simulates the glucose-insulin dynamics in T1D patients, and is approved by the US Food and Drug Administration (FDA) as an alternative for pre-clinical testing of insulin therapies, including closed-loop algorithms. Within this in-silico model, an islet biosensor-based artificial pancreas was as efficient as standard CGMs and even outperformed them under challenging conditions (Olçomendy et al., submitted; Olcomendy et al., 2021).

We therefore asked now whether monitoring the electrical activity of a few islets may provide a sensor for continuous glucose measurements in live animals. To this end we developed stepwise microfluidic micro-electrode arrays containing a few islets and interfaced with the interstitial fluid via microdialysis. Our data and their analysis indicate faithful monitoring of glucose levels in rats during glucose tolerance tests and subsequent to insulin injections.

MATERIALS AND METHODS

Animals, surgery and islet preparation. Animal experiences were conducted along ethical guidelines and authorized (APAFIS#25037-2020040917179466). Male Wistar rats (Charles River, Lyon, France), mean age 10.4 weeks and with a mean weight of 384 g were placed on a heated pad and anaesthetized with isoflurane (starting with 3.5%, 2l/min; maintenance by 1.5%) and for analgesia meloxicam was given subcutaneously (1mg/kg) 30 min before implantation of the catheter as well as a local anesthetic was applied (lidocaine 2,5 % and prilocaine 2,5 % cream). To insert the microdialysis catheter a small incision was placed on the right interscapular area after shaving and disinfection. The incision site was subsequently closed by small sutures. For the preparation of islets, adult male C57BL/6J mice (10–20 weeks of age) were sacrificed by cervical dislocation according to University of Bordeaux ethics committee guidelines. Islets were obtained by enzymatic digestion and handpicking. MEAs were coated with Matrigel (2% v/v) (BD Biosciences, San Diego, CA) as described (Abarkan et al., 2022; Jaffredo et al., 2021; Lebreton et al., 2015). Islets were seeded on MEAs and cultured for 3 days at 37°C.

Microfluidic MEA chips. For dynamic experiments, a microchannel was fabricated with PDMS-based elastomer Sylgard 184 (Dow Corning, St Denis, France) and the channel mould was fabricated by using a Siu-8 wafer with a channel of 0.8 mm in diameter. PDMS on the wafer was cured by 2 h of heating at 70 °C. The microchannels were subsequently then aligned on the MEA by O₂-plasma activated MEAs under a microscope in a cleanroom. For static incubations, the chip consisted of a PDMS microwell of 3 mm in diameter and in height. Fluid shear stress was simulated using Autodesk Fusion 360® (Autodesk, Inc., San Raphael, CA), for multiphysical simulations and COMSOL 5.3 (COMSOL, Inc., Burlington, MA) for fluid dynamics computation. First a 3D simulation was carried out where the flow in the microfluidics channel is simulated following Navier Stokes equations, with a laminar flow boundary condition at the inlet. The inlet is defined in a flow rate manner, with several values: 0.2 µl/min, 1 µl/min, 5 µl/min. Subsequently a stationary study was carried out. The shear stress is deduced from the results of the study using the following definition: $\tau = \mu \Delta \vec{u}$ where μ is the dynamic viscosity of water at 37°C and \vec{u} is the velocity field.

Analysis of delays in fluid transport. The delay between recording sites introduced by the transit of dialysate through the microfluidic chip and tubes was determined through analysis of videos taken with a binocular camera Moticam 5+ (Motic, Hong Kong, HK) during phenol red

perfusions (stepwise gradient) under conditions identical to experimental conditions, i.e. from microdialysis to dialysate collection (see Fig. 1). Phenol red solution was passed through microdialysis and the microfluidic MEA of 1 $\mu\text{l}/\text{min}$ and images were taken (at 25 Hz) of the microfluidic channel and the outlet of the microfluidic MEA where later in experiments the dialysate was collected. Video files were analysed with an ad hoc program written in Python (Python 3.7, imageio 2.6.1, numpy 1.18.1, pandas 1.0.4) that measured a differential rate of change in colour for each zone of interest. The program functions as follows: the video is first down-sampled to 10 Hz (no interpolation) and cropped to a 51x51pixels region of interest (ROI). The pixels in the ROI are spatially averaged which yields a single vector of red, green, and blue components indicating the average colour in the ROI for every frame and the red component is filtered out. The same operations are performed in a 51 \times 51 pixels region of reference (ROR) where the variations in red, green and blue components are deduced from those of the ROI to produce a differential measurement that compensates for changes in ambient light. The red, green, and blue components of the differential measurement are then merged (unweighted sum) and differentiated. Finally, a moving average is applied (10 samples) for denoising and the data are normalized (fold of maximum value). The delay from the microdialysis pump to the zone of interest was measured as the peak of the calculated rate of colour change.

Data from different recording sites were synchronized to compensate for the lag introduced by the transit of dialysate through the microfluidic chip and tubes. All data were synchronized assuming $t = 0$ corresponds to the IP injection of glucose. The delay between blood glucose measurements and dialysate measurements due to the diffusion of glucose in the animal's subcutaneous space (Δt_{SQ}) was estimated with cross-correlation analyses on experimental data.

The corrected time vector t_{metric}^c for each recorded metric is therefore, in relation to its original t_{metric} : $t_{BG}^c = t_{BG} - \Delta t_{SQ}$; $t_{DG}^c = t_{DG} - (\Delta t_{\text{rat-outlet}} + \Delta t_{SQ})$; $t_{\text{frequency SP}}^c = t_{\text{frequency SP}} - (\Delta t_{\text{rat-electrodes}} + t_{\text{ephy}}^0)$; $t_{\text{amplitude SP}}^c = t_{\text{amplitude SP}} - (\Delta t_{\text{rat-electrodes}} + t_{\text{ephy}}^0)$. Datasets with corrected time vectors were generated with a Python script (Python 3.7, pandas 1.0.4).

Electrophysiology: MEAs (60 PedotMEA200/30i R-Au-gr, \varnothing 30 mm, 200 mm interelectrode distance) were purchased from Multi Channel Systems GmbH (MCS, Reutlingen, Germany). As described previously (Abarkan et al., 2022; Jaffredo et al., 2021; Perrier et al., 2018), extracellular field potentials were acquired at 10 kHz, amplified, and band-pass filtered at 0.1–

3,000 Hz with a USB-MEA60-Inv-System-E amplifier (MCS; gain: 1,200) or an MEA1060-Inv-BC-Standard amplifier (MCS; gain: 1,100), both controlled by MC_Rack software (v4.6.2, MCS). Electrophysiological data were analysed with MC_Rack software. SPs were isolated using a 2-Hz low-pass filter and frequencies were determined using the threshold module of MC_Rack with a dead time (minimal period between two events) of 300 ms (SPs). The peak-to-peak amplitude module of MC_Rack was used to determine SP amplitudes.

Microdialysis, glucose injections and measurements. Linear interscapular subcutaneous catheter (30 mm membrane, 20 kDa cut off; Microdialysis AB) were inserted under anaesthesia (1.5% isoflurane, 1 mg/kg meloxicam). For dialysis, Ringer dextran-60 was used (pump 107, Microdialysis AB, Kista, Sweden). For glucose or insulin tests, 2 g/kg of glucose or 2.5 U/kg of insulin were injected intraperitoneally. Blood glucose was measured after droplet collected at the caudal vein with a freestyle papillon glucometer (Abbott, Rungis, France). Glucose in the dialysate was determined using a glucose oxidase-based kit (Biolabo, Maizy, France). Human male plasma was obtained from Sigma (H4522; Sigma-Aldrich, Saint Louis, MO, USA) and contained 6 mM glucose.

Respiration rate. The respiration rate of anaesthetised rats was measured through analysis of video files, using an ad hoc program written in Python (Python 3.7, imageio 2.6.1, numpy 1.18.1, scipy 1.6.2, pandas 1.0.4) that detects oscillating movement on the rat's fur. The program functions as follows: the video is cropped to a region of interest where movement caused by breathing is clearly visible. The video is converted to greyscale and differentiated to highlight movement. A quantity of movement is estimated for each frame by measuring the standard deviation of the differentiated pixels in the region of interest. A 0.1-2.0 Hz filter is applied to this signal and its frequency components are analysed in a spectrogram (Fast Fourier Transform, 10 s rectangular window, 0.1 s overlap). The breathing rate is retrieved by measuring the frequency of the main peak at each instant in the spectrogram through peak detection.

Statistics: Correlations between electrophysiological data (SP frequencies and SP amplitudes) and glucose measurements (capillary and dialysate) were calculated using Spearman correlation in Python (Python 3.7, scipy 1.3.0). Electrophysiological data were resampled using windowed AUCs (see below) prior to correlation, in order to match glucose measurements. For correlation the AUC of electrophysiological data (SP frequencies and SP amplitudes) were calculated using the trapezoidal rule in time windows surrounding each glucose measurement (capillary or

dialysate) : AUCs used for correlation with BG measurements were calculated in a $[-90\text{ s}; +90\text{ s}]$ time window around each BG data point ; AUCs used for correlation with DG measurements were calculated in a $[+0\text{ s}; +900\text{ s}]$ time window following each DG data point, identical to the window of dialysate collection for the corresponding DG measurement. The distinction between time windows was made because capillary blood glucose measurements were punctual (representative of a short time window), whereas the collection of dialysate samples spanned over 15 min each (representative of a 15 min time window). The diffusion delay Δt_{SQ} was estimated using cross-correlation between electrophysiological data and windowed AUCs of DG measurements. Δt_{SQ} was measured at peak correlation for each experiment individually, as it was assumed to be animal-dependent. Other statistical analyses of electrophysiological data were performed using GraphPad PRISM v7.00 (San Diego, CA, USA) with ANOVA and posthoc tests (Dunn or Tukey) as given in the Figure legends. In the case of repetitive measurements, Geisser-Greenhouse correction was applied in the case of normal distribution.

RESULTS

A biosensor using heterologous live cells, such as pancreatic islets, has to be conceived as an extracorporeal device and microdialysis can provide continuous access to bodily fluids such as interstitial liquids. As the amount of interstitial fluid that can continuously be retrieved is limited, miniaturisation is required. To test an islet-based biosensor for continuous nutrient monitoring, interfacing of the animal with the sensor has to be developed as given in Figure 1. Interstitial fluid is obtained via a microfluidic pump and a subcutaneous microdialysis catheter which is linked to a chip consisting of the sensor, a microelectrode array with islets attached to its electrodes and the microfluidic system to pass the dialysate to these islets (Fig 1A). To assess the biosensors' characteristics, recordings have to be compared with blood glucose, which can be measured after repetitive small incisions at the rat's tail vein and dialysate was also sampled after passage through the chip to determine its glucose concentration. This configuration has to deal with a number of delays between blood glucose and the sensor. First, diffusion of glucose in the interstitial space requires some 10 minutes in man (Basu et al., 2013) and rat (Aussedat

et al., 2000). Second, in this laboratory set-up a certain length of tubing is required to link the component introducing additional delays between the point of dialysis and the microfluidic MEA (μ MEA) as well from the μ MEA to the point of glucose measuring in the dialysate at the outlet (Fig. 1B). We have tested these delays using phenol red as dye in the fluids (Fig. 1B, see also Methods) and the resulting delay time was used throughout when comparing different parameters on a time scale. Fig. 1 C to E shows the actual set-up on the bench with a video-microscope to potential formation of bubbles in the microfluidic channels (Fig. 1C) and the configuration while monitoring the rats with implanted interscapular catheter (Fig. 1D) and the recording unit protected from surrounding noise in Fig. 1E.

The final device was interfaced gradually. Previous work had used defined electrophysiological buffers and revealed the presence of two different electrical islet cell signals that can be recorded by extracellular physiology; single cell action potentials that are difficult to capture due to their minute amplitude, and robust slow potentials (SP) that are generated by cell to cell coupling. Their amplitude depends on the degree of coupling between β -cells, which is hallmark of physiological islet function (Bosco et al., 2011; Lebreton et al., 2015). We first tested the response to human or rat serum containing different glucose concentrations in static incubation in MEAs with home-made PDMS microwells to allow assaying of a few microliters of analyte. As shown in Figure 2A and B, islets exhibit strong responses in the presence of culture medium containing 11 mM glucose and rich in amino-acids. Replacing medium by human serum (6 mM glucose) induces a rapid decrease in electrical responses. Subsequently islets were exposed sequentially to human serum which glucose levels were adapted to 9, 12 or 15 mM glucose. Statistical evaluation of the corresponding areas under the curve (AUCs) revealed significant differences in activity between all the glucose ramps from 6 to 15 mM and a high correlation between glucose concentrations in human serum and recorded responses suggesting a good discrimination power of the biosensor. In a next step, we performed an intraperitoneal glucose tolerance test in a rat with a basal glucose level of 9.4 mM. Injection of 2mg/kg of glucose lead to a transient increase in blood glucose (Fig. 2F) to 22.9 mM followed by a slow decrease to 11.9 and 8.6 Mm. At each determination of blood glucose, sera were prepare and added ex tempore to MEAs equipped with PDMS microwells. The change from 9.4 to 22.9 mM glucose induced a strong response in the biosensor in terms of SP frequency and amplitude. Means were clearly distinct among the conditions but they became significantly different among all conditions for SP frequencies.

Having thus validated that the islet-based biosensor can be used with serum and provides discrimination between glucose levels differing by a few millimoles/liter, we tested rat microdialysis off-line with the MEA biosensor (Fig. 3). A small range of flow rates provided sufficient glucose recovery from a test sample and the rate of 1 μ l/min was chosen for all subsequent experiments (Fig. 3A) and provided 78% recovery of glucose levels by microdialysis during a glucose tolerance test in rat (Fig. 2 B). Testing the two dialysates in the biosensor resulted in a strong increase in activity when changing from 5.8 to 15 mM glucose in terms of frequencies (Fig. 2C, D) and of amplitudes (Fig. 2 E, F). Notably a first and second phase was visible especially in terms of frequencies and amplitudes (Fig. 2C, E), which is due to differences in the organisation of islet β -cell responses (Jaffredo et al., 2021).

To accommodate the small flow rates of microdialysis we developed initially explored more complex configurations allowing single islet trapping and incorporation of metal electrodes. Although such a set-up worked satisfactorily in-vitro, this was not the case when interfacing this with microdialysis and a live animal despite all diligence and bubble traps. We therefore opted for a simpler and more robust approach (Fig. 4) consisting of a PDMS block with a single channel, inlet and outlet (Fig. 4A) that we can align on half of the 60 electrodes of a commercial MEAs in a cleanroom under a binocular microscope as shown in Fig. 4B. The microfluidic channel is charged with islets that cover a reasonable number of electrodes and stay in good shape (Fig. 4C). Simulations of flow dynamics revealed shear stress mainly at the bottom of the channel where islets are adhering but the maximal value of 250 μ Pa predicted at a flow of 1 μ l/min remains still below values that have been reported as critical (Glieberman et al., 2019; Silva et al., 2013).

We coupled this optimized μ MEA to microdialysis to compare electrical activity profiles of the biosensor with blood and dialysate glucose values as an indicator for its potential usefulness in continuous nutrient monitoring. As an independent control of the condition of the animal we controlled respiration rates as breathing may influence the performance of the interscapular microdialysis catheter and also introduce mechanical artefacts on the bio sensor device. As given in Fig. 5A, respiration rate was stable and in a normal range of 1 Hz throughout the entire procedure. After a first glucose injection, we observed a rapid increase in blood glucose which reached its maximum after 40 to 60 min, whereas dialysate glucose was retarded by around 10 min. Both measures were discontinuous and their frequency could not be increased in the absence of an intravascular catheter and the low microdialysis flow rate requires a minimal

collection time for subsequent glucose determination. We can therefore not precisely determine the delay time due to interstitial glucose diffusion. The increase in glucose was mirrored by an increase in electrical activity in terms of slow potential frequency and amplitude and a peak was attained at 60 to 70 min followed by a decrease in line with glucose concentrations. Note that the slow physiological increase in glucose here did not induce a biphasic electrical response in contrast to the clear presence of biphasic pattern after stepwise increases in glucose (Fig. 2B and 3C). To test the reactivity of the system, insulin was injected and as expected blood as well as dialysate blood glucose levels decreased correspondingly. Subsequently to both injections of insulin a marked decrease in electrical activity was apparent (Fig. 5C, D).

In contrast to in-vitro systems, where precise concentrations can be imposed, the absolute changes and kinetics in glycemia vary among animals. Moreover, the electrical activity of the biosensor islets is monitored at a microsecond scale, whereas blood or interstitial glucose is measured at far greater intervals. To obtain insight about the correlation between blood glucose or interstitial glucose and biosensor responses we calculated the AUCs of electrical responses over the same time span as the fluid collection span for four (dialysate glucose) or five (blood glucose) independent experiments to compare equal time spans. Linear regression analysis for each independent experiment provided a set of graphs that were highly parallel in the case of SP frequencies whereas more different slopes were observed for amplitudes (Fig. 6A, B). Each of these regressions for a given experiment were highly significant. Analyses for dialysate glucose are given in Suppl. Fig. 1. A comprehensive view of R^2 values is provided in Fig. 6C. The biosensor response in terms of frequencies versus amplitudes was highly correlated as were electrical activities versus blood glucose levels with means around 0.9. The correlation between electrical responses and dialysate were more scattered which may be due to its measurement after passage through the microfluidic MEA and potential diffusion phenomena especially at low flow rates was highly significant for association with R^2 mean values between 0.8 and 0.9 (Fig. 6C). The scatter plot in Fig. 6D shows the coefficient of determination of linear regressions and the identified slopes, which measure the linearly dependent nature of the studied metrics regardless of basal values. The spread of values on either axis helps visualize the homogeneity of the results across experiments. As such, the clustering of our experimental values in the scatter plot reflects the repeatability of the fold increases in the studied metric relative to basal conditions.

DISCUSSION

Continuous monitoring of nutrient levels remains a major challenge in diabetes therapy and despite a remarkable progress over the last 50 years, an autonomous closed loop system is not available (Cobelli et al., 2011; Lee et al., 2021; Teo et al., 2022). Our work here demonstrates the feasibility of a label free microorgan-based biosensor and its precise recording of vital parameters.

Regression analysis over a number of in-vivo experiments indicates a remarkable homogeneity in terms of sensor responses to different glucose levels despite the variability in biological systems. In each experiment different animals as well as different preparation of islets for the biosensor were used and intrastrain variation in metabolic responses is well known (Rose et al., 2013; Rothwell and Stock, 1980). As frequency and amplitudes of slow potentials were analysed, the question arises whether one or the other quality is closer related to glucose levels. Previous in-vitro experiments suggested that slow potential frequencies reflect more closely insulin secretion and is further refined when taking also amplitudes into account (Jaffredo et al., 2021). However, in-vitro experiments use strong square shaped stimulation by sudden increase in glucose and provoke a biphasic response. Such a biphasic response was also apparent here upon sudden increase by externally applied 2 mM glucose but not during slow increases when coupled to microdialysis. The existence of biphasic activity and secretion in-vivo in man is debated and may be absent during absorption of a meal (Rorsman and Ashcroft, 2018). Our data suggest that a frequency-based analysis may be more robust during in-vivo applications. Interestingly, the biosensor reacted strongly to insulin injection despite minor concomitant decreases in blood and dialysate glucose. It is known that glucose dependency of insulin secretion displays a hysteresis when comparing increases versus decreases in glucose levels (Keenan et al., 2012). This serves as a kind of safety break to avoid hypoglycaemia and is also found in isolated islets in-vivo (Lebreton et al., 2015). Although we have not investigated the existence of a hysteresis here, one may speculate that the considerable decrease upon insulin injection observed here may be due to such an islet mechanism.

We have also projected a possible packaging of an islet-based biosensor (see Supplemental Figure 2) including microdialysis and an insulin reservoir. Although the qualities of a micro-organ biosensor are evident, there are also limitations and obstacles. In contrast to enzyme-based electrochemical sensors, microdialysis is necessary with concomitant space requirements and device duration. Note, however, that an electrochemical sensor linked to

microdialysis had been commercialized and successfully used in humans (Ricci et al., 2007; Ricci et al., 2005). As islet encapsulation techniques are constantly evolving, direct implantation of such a device may eventually be possible in the future (Yang et al., 2021). A clear limitation is given by the type of islets to be used in the sensor. Reaggregated human donor islets exhibit excellent function (Sachs et al., 2020) but may raise ethical issues by diverting islets from use in transplantation. Alternatively, a new human β -cell line has shown promising functional characteristics and can be arranged in spheroids although such an approach would lose inherent islet characteristics conferred by other cell types in the micro-organ (Szczerbinska et al., 2022).

A large number of biosensors have been developed in the past relying on electrodes, enzymes, genetically encoded fluorescent probes or genetically modified micro-organisms (Faheem and Cinti, 2022; Reddy et al., 2016). To the best of our knowledge our work presents the first attempt to use a micro-organ as biosensor. Cells receive enormous amounts of information from their environment, compute the appropriate output almost instantaneously on a millisecond scale and the complexity of the regulatory is further enhanced by the presence of distinct cell types. Astonishingly in the wide array of applications envisaged for the rapidly expanding field of organoid biology, harnessing the resulting sensory and computational power of these assemblies has not been envisaged.

ACKNOWLEDGEMENTS

This work was funded by ANR-18-CE17-0005 DIABLO (to JL and SR) and a grant of the Société Francophone du Diabète (to JL). We are grateful to Céline Cruciani-Guglielmacci and Christophe Magnan for helpful advices on surgery.

AUTHOR CONTRIBUTIONS

JL, SR and MR conceived the project; JL and SR procured funding; EP, JL, AP and SR co-wrote the manuscript; EP, AP, FPG, AH, MM and JG researched; EP, AP, MM, MR and JL analyzed the data. All authors have consented to the submitted manuscript.

REFERENCES

- Abarkan, M., Gaitan, J., Lebreton, F., Perrier, R., Jaffredo, M., Mulle, C., Magnan, C., Raoux, M., and Lang, J. (2019). The glutamate receptor GluK2 contributes to the regulation of glucose homeostasis and its deterioration during aging. *Mol Metab* 30, 152-160.
- Abarkan, M., Pirog, A., Mafilaza, D., Pathak, G., N'Kaoua, G., Puginier, E., O'Connor, R., Raoux, M., Donahue, M. J., Renaud, S., and Lang, J. (2022). Vertical Organic Electrochemical Transistors and Electronics for Low Amplitude Micro-Organ Signals. *Adv Sci (Weinh)*, e2105211.
- Ashcroft, F. M., and Rorsman, P. (2012). Diabetes mellitus and the β cell: the last ten years. *Cell* 148, 1160-1171.
- Atkinson, M. A., Eisenbarth, G. S., and Michels, A. W. (2014). Type 1 diabetes. *Lancet* 383, 69-82.
- Aussedat, B., Dupire-Angel, M., Gifford, R., Klein, J. C., Wilson, G. S., and Reach, G. (2000). Interstitial glucose concentration and glycemia: implications for continuous subcutaneous glucose monitoring. *Am J Physiol* 278, E716-E728.
- Basu, A., Dube, S., Slama, M., Errazuriz, I., Amezcua, J. C., Kudva, Y. C., Peyser, T., Carter, R. E., Cobelli, C., and Basu, R. (2013). Time Lag of Glucose From Intravascular to Interstitial Compartment in Humans. *Diabetes* 62, 4083-4087.
- Bosco, D., Haefliger, J. A., and Meda, P. (2011). Connexins: key mediators of endocrine function. *Physiol Rev* 91, 1393-1445.
- Campbell, J. E., and Newgard, C. B. (2021). Mechanisms controlling pancreatic islet cell function in insulin secretion. *Nat Rev Mol Cell Biol* 22, 142-158.
- Charles, M. A., and Leslie, R. D. (2021). Diabetes: Concepts of β -Cell Organ Dysfunction and Failure Would Lead to Earlier Diagnoses and Prevention. *Diabetes* 70, 2444-2456.
- Cobelli, C., and Dalla Man, C. (2021). Minimal and Maximal Models to Quantitate Glucose Metabolism: Tools to Measure, to Simulate and to Run in Silico Clinical Trials. *J Diabetes Sci Technol*, 19322968211015268.
- Cobelli, C., Renard, E., and Kovatchev, B. (2011). Artificial pancreas: past, present, future. *Diabetes* 60, 2672-2682.
- De Marinis, Y. Z., Salehi, A., Ward, C. E., Zhang, Q., Abdulkader, F., Bengtsson, M., Braha, O., Braun, M., Ramracheya, R., Amisten, S., *et al.* (2010). GLP-1 inhibits and adrenaline stimulates glucagon release by differential modulation of N- and L-type Ca^{2+} channel-dependent exocytosis. *Cell Metab* 11, 543-553.
- Faheem, A., and Cinti, S. (2022). Non-invasive electrochemistry-driven metals tracing in human biofluids. *Biosens Bioelectron* 200, 113904.
- Falkmer, S. (1979). Immunocytochemical studies of the evolution of islet hormones. *J Histochem Cytochem* 27, 1281-1282.
- Glieberman, A. L., Pope, B. D., Zimmerman, J. F., Liu, Q., Ferrier, J. P., Kenty, J. H. R., Schrell, A. M., Mukhitov, N., Shores, K. L., Tepole, A. B., *et al.* (2019). Synchronized stimulation and continuous insulin sensing in a microfluidic human Islet on a Chip designed for scalable manufacturing. *Lab Chip* 19, 2993-3010.

- Jaffredo, M., Bertin, E., Pirog, A., Puginier, E., Gaitan, J., Oucherif, S., Lebreton, F., Bosco, D., Catargi, B., Cattaert, D., *et al.* (2021). Dynamic uni- and multicellular patterns encode biphasic activity in pancreatic islets. *Diabetes* 70, 878-888.
- Keenan, D. M., Basu, R., Liu, Y., Basu, A., Bock, G., and Veldhuis, J. D. (2012). Logistic model of glucose-regulated C-peptide secretion: hysteresis pathway disruption in impaired fasting glycemia. *Am J Physiol Endocrinol Metab* 303, E397-409.
- Lebreton, F., Pirog, A., Belouah, I., Bosco, D., Berney, T., Meda, P., Bornat, Y., Catargi, B., Renaud, S., Raoux, M., and Lang, J. (2015). Slow potentials encode intercellular coupling and insulin demand in pancreatic beta cells. *Diabetologia* 58, 1291-1299.
- Lee, I., Probst, D., Klonoff, D., and Sode, K. (2021). Continuous glucose monitoring systems - Current status and future perspectives of the flagship technologies in biosensor research. *Biosens Bioelectron* 181, 113054.
- Olçomendy, L., Cassany, L., Pirog, A., Franco, R., Puginier, E., Jaffredo, M., Gucik-Derigny, D., Ríos, H., Ferreira de Loza, A., Gaitan, J., *et al.* (submitted). Towards the integration of an islet-based biosensor in closed-loop therapies for patients with Type 1 Diabetes. *Front Physiol*.
- Olcomendy, L., Pirog, A., Lebreton, F., Jaffredo, M., Cassany, L., Gucik Derigny, D., Cieslak, J., Henry, D., Lang, J., Catargi, B., *et al.* (2021). Integrating an islet-based biosensor in the artificial pancreas: in silico proof-of-concept. *IEEE Trans Biomed Eng PP*.
- Perrier, R., Pirog, A., Jaffredo, M., Gaitan, J., Catargi, B., Renaud, S., Raoux, M., and Lang, J. (2018). Bioelectronic organ-based sensor for microfluidic real-time analysis of the demand in insulin. *Biosens Bioelectron* 117, 253-259.
- Pigeyre, M., Hess, S., Gomez, M. F., Asplund, O., Groop, L., Pare, G., and Gerstein, H. (2022). Validation of the classification for type 2 diabetes into five subgroups: a report from the ORIGIN trial. *Diabetologia* 65, 206-215.
- Pirog, A., Bornat, Y., Perrier, R., Raoux, M., Jaffredo, M., Quotb, A., Lang, J., Lewis, N., and Renaud, S. (2018). Multimed: an integrated, multi-application platform for the real-time recording and sub-millisecond processing of biosignals. *Sensors (Basel)* 18.
- Reddy, B., Salm, E., and Bashir, R. (2016). Electrical chips for biological point-of-care detection. *Ann Rev Biomed Eng* 18, 329-355.
- Ricci, F., Caprio, F., Poscia, A., Valgimigli, F., Messeri, D., Lepori, E., Dall'Oglio, G., Palleschi, G., and Moscone, D. (2007). Toward continuous glucose monitoring with planar modified biosensors and microdialysis. Study of temperature, oxygen dependence and in vivo experiment. *Biosens Bioelectron* 22, 2032-2039.
- Ricci, F., Moscone, D., Tuta, C. S., Palleschi, G., Amine, A., Poscia, A., Valgimigli, F., and Messeri, D. (2005). Novel planar glucose biosensors for continuous monitoring use. *Biosens Bioelectron* 20, 1993-2000.
- Rorsman, P., and Ashcroft, F. M. (2018). Pancreatic beta-cell electrical activity and insulin secretion: of mice and men. *Physiol Rev* 98, 117-214.
- Rorsman, P., and Braun, M. (2012). Regulation of insulin secretion in human pancreatic islets. *Annu Rev Physiol* 75, 155-179.

- Rose, R., Kheirabadi, B. S., and Klemcke, H. G. (2013). Arterial blood gases, electrolytes, and metabolic indices associated with hemorrhagic shock: inter- and intrainbred rat strain variation. *J Appl Physiol* (1985) *114*, 1165-1173.
- Rothwell, N. J., and Stock, M. J. (1980). Intra-strain differences in the response to overfeeding in the rat. *Proc Nutr Soc* *39*, 20a.
- Sachs, S., Bastidas-Ponce, A., Tritschler, S., Bakhti, M., Böttcher, A., Sánchez-Garrido, M. A., Tarquis-Medina, M., Kleinert, M., Fischer, K., Jall, S., *et al.* (2020). Targeted pharmacological therapy restores β -cell function for diabetes remission. *Nat Metab* *2*, 192-209.
- Silva, P. N., Green, B. J., Altamentova, S. M., and Rocheleau, J. V. (2013). A microfluidic device designed to induce media flow throughout pancreatic islets while limiting shear-induced damage. *Lab Chip* *13*, 4374-4384.
- Szczerbinska, I., Tessitore, A., Hansson, L. K., Agrawal, A., Ragel Lopez, A., Helenius, M., Malinowski, A. R., Gilboa, B., Ruby, M. A., Gupta, R., and Ämmälä, C. (2022). Large-scale functional genomics screen to identify modulators of human β -cell insulin secretion. *Biomedicines* *10*.
- Teo, E., Hassan, N., Tam, W., and Koh, S. (2022). Effectiveness of continuous glucose monitoring in maintaining glycaemic control among people with type 1 diabetes mellitus: a systematic review of randomised controlled trials and meta-analysis. *Diabetologia*. doi: 10.1007/s00125-021-05648-4. Online ahead of print
- Yang, K., O'Cearbhaill, E. D., Liu, S. S., Zhou, A., Chitnis, G. D., Hamilos, A. E., Xu, J., Verma, M. K. S., Giraldo, J. A., Kudo, Y., *et al.* (2021). A therapeutic convection-enhanced macroencapsulation device for enhancing β cell viability and insulin secretion. *Proc Natl Acad Sci U S A* *118*.
- Youson, J. H., and Al-Mahrouki, A. A. (1999). Ontogenetic and phylogenetic development of the endocrine pancreas (islet organ) in fish. *Gen Comp Endocrinol* *116*, 303-335.

FIGURES AND LEGENDS

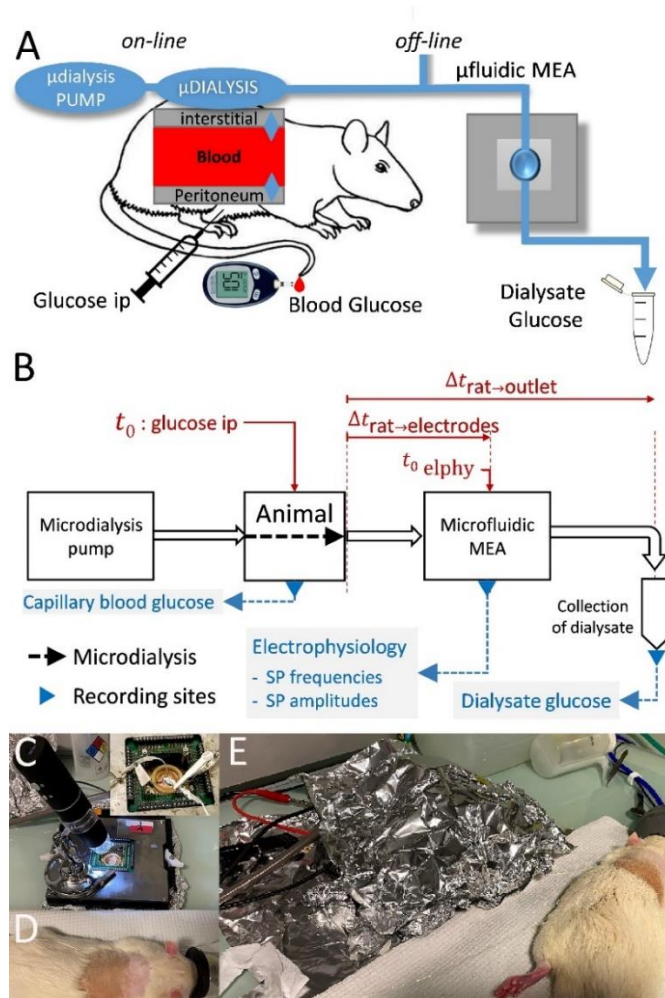


Figure 1: Experiment design. **A:** Anaesthetized rats were subjected to an intraperitoneal glucose tolerance test and blood glucose determined. In off-line experiments, serum samples were added directly to the microfluidic MEA; in on-line experiments, interstitial fluids were dialyzed at $1\mu\text{l}/\text{min}$ and fed to the microfluidic MEA. Glucose concentrations in the dialysate were determined off-line from an outflow channel of the microfluidic MEA. **B:** Full set-up and work flow for on-line experiments. Time points in the experiment and delays introduced by tubings between microdialysis and the different recording sites are given. $\Delta t_{\text{rat} \rightarrow \text{electrodes}}$ was equal 750 s , $\Delta t_{\text{rat} \rightarrow \text{outlet}}$ (collection of dialysate) was 2460 s as determined by video films using a dye (see Methods). **C,** MEA setup with microscope video camera to inspect flow; insert, enlarged view of the MEA itself and microfluidic inlet/outlet. **D:** anesthetized rat with dorsal subcutaneous catheter inserted. **E,** set-up during the experiment, the MEA is covered with aluminium to shield external noise.

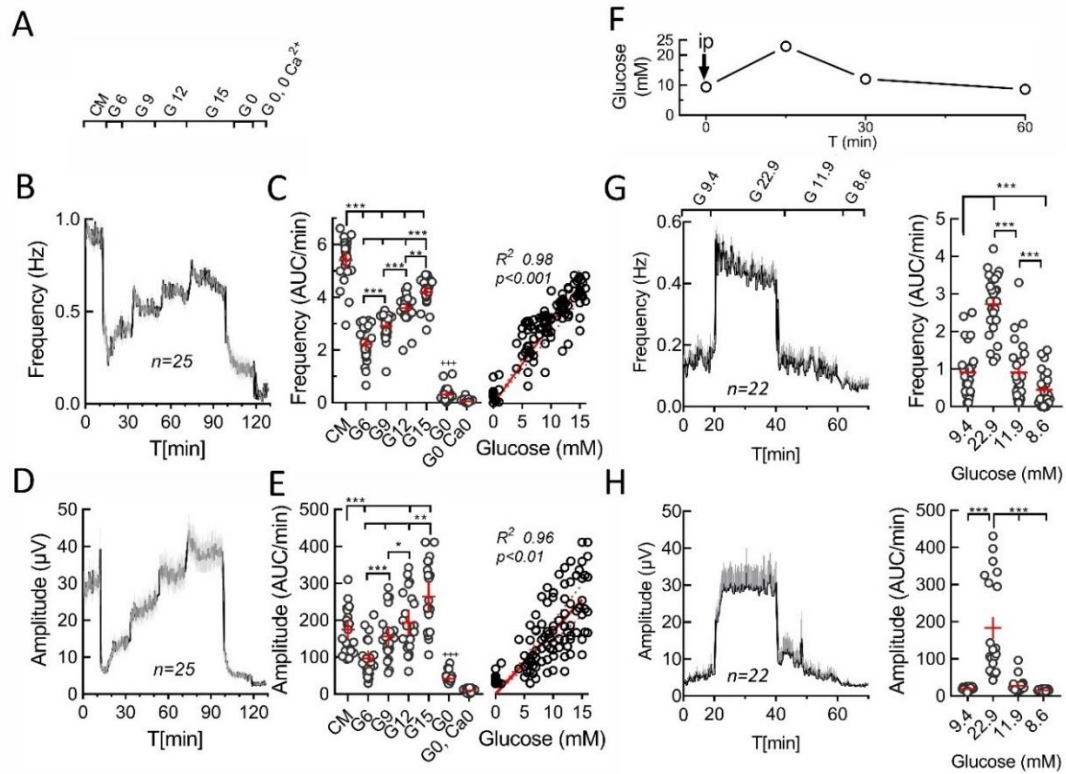


Figure 2: Ex-vivo monitoring of human or rat serum glucose. **A:** Different stimuli used; CM, culture medium containing amino acids and 11 mM glucose; G6, human serum containing 6 mM glucose; G9 to G15, human serum adjusted to 9, 12 or 15 mM glucose; G 0, buffer containing no glucose; G0, 0 Ca²⁺, buffer containing no glucose or calcium. **B:** Frequencies of slow potentials as recorded by MEAs under the different conditions given in A. **C:** left panel, Areas under the curve from B determined during the first 10 min of each stimulus and expressed as AUC/minute. Right panel, correlation analysis. **D:** Amplitudes of slow potentials recorded by MEAs under the different conditions given in A. **E:** left panel, Areas under the curve from B determined during the first 10 min of each stimulus and expressed as AUC/minute. Right panel, correlation analysis. **F:** Intraperitoneal glucose tolerance test in an anaesthetized rat and blood samples were collected at indicated time points, sera prepared and glucose concentrations determined. **G:** Left panel, effect of rat sera in microfluidic MEAs on slow potential frequencies. Glucose concentrations in the sera are given. Right panel, statistical analysis of AUCs determined as in C. **H:** Left panel, effect of rat sera on microfluidic MEAs on slow potential amplitudes during same recordings as in G. Right panel, statistical analysis of AUCs determined as in C. *, 2p<0.05; **, 2p<0.01; ***, 2p<0.001; +++, 2p<0.001 as compared to the presence of different glucose concentration. ANOVA and paired Tukey post-hoc tests, n as given in the corresponding panels.

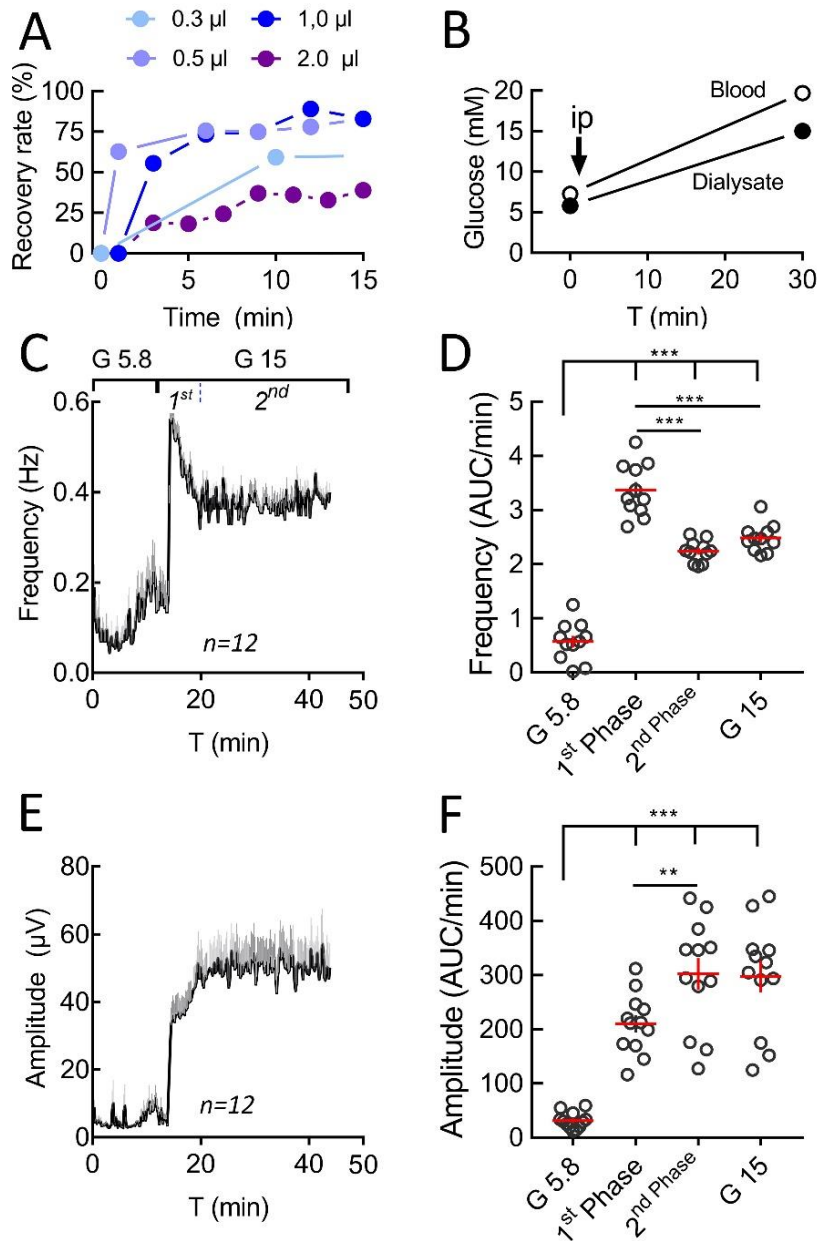


Fig. 3 Characterization of subcutaneous microdialysis and dialysate effect on islet electrical activity. **A:** Recovery rates for glucose in saline buffer at different flow rates per minute. **B:** Glucose concentrations in rat capillary blood and in dialysate (flow rate 1 μ l/min) after intraperitoneal injection of glucose (ip). **C:** Effect of corresponding dialysates (at 5.8 or 15 mM glucose) on islet slow potential frequencies. **D:** Statistics of areas under the curve (G 5.8, 0-14 min; 1st phase 14-18 min; 2nd phase 20-43 min; G15 14-43 min; expressed as AUC/min). **E:** Effect of corresponding dialysates (at 5.8 or 15 mM glucose) on islet slow potential amplitudes. **D:** Statistics of areas under the curve (details see D). **, 2p <0.01; ***, 2p <0.001; Tukey post-hoc test).

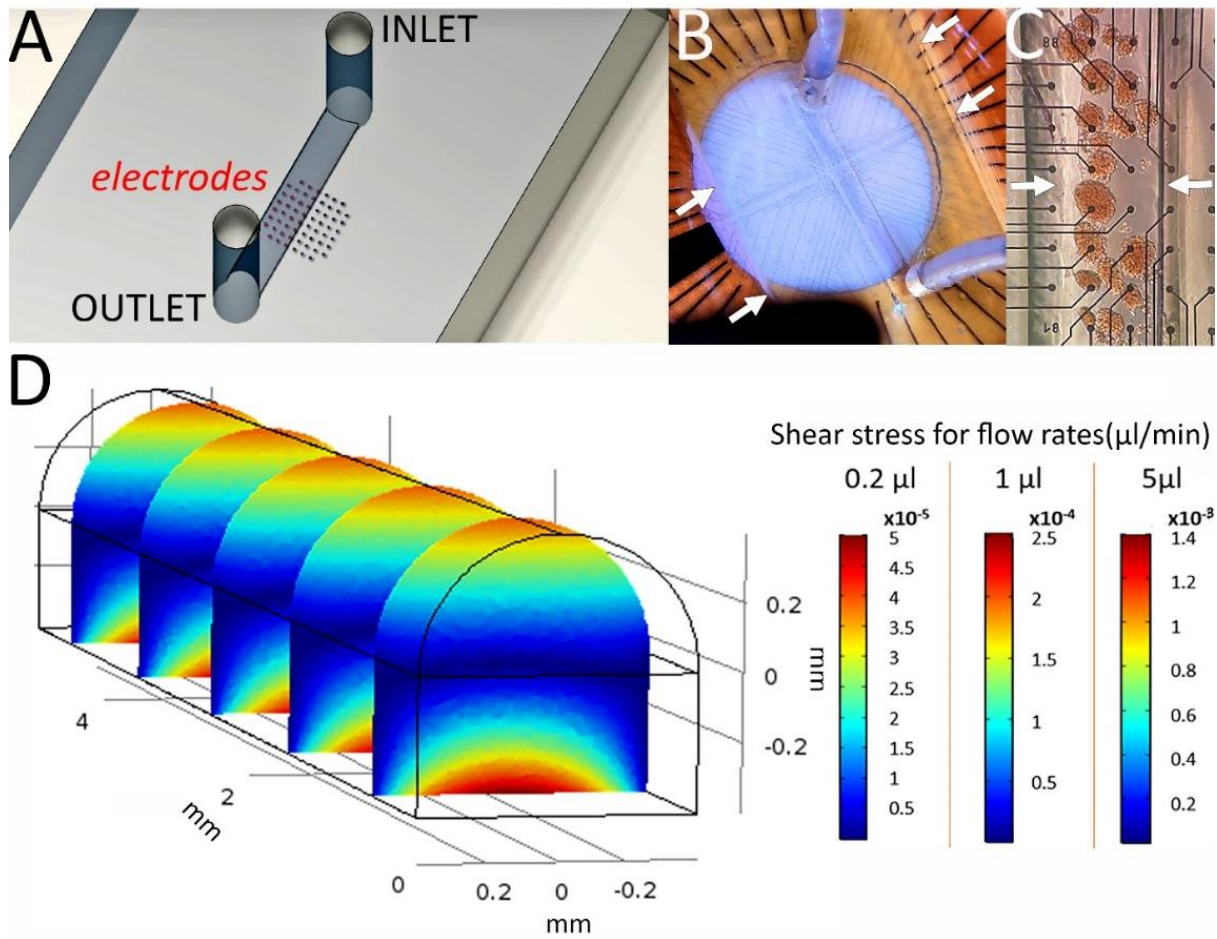


Figure 4: Characterization of microfluidic micro-electrode arrays. **A:** Layout of microfluidic MEA. **B:** View of a microfluidic PDMS device on a MEA, inlet and outlet are visible. Arrows, border of the PDMS device. Zoom on the electrodes aligned in the microfluidic channel of the chip. **C:** View of the microfluidic channel with electrodes and islets attached. CAD view of the channel on the electrode layout of the MEA. Arrows, lateral borders of the channel. **D.** Multiphysics simulations provide a rainbow view of the shear stress as z axis repartition over the channel at a flow-rate of 0.2, 1 or 5 $\mu\text{l}/\text{min}$. Scales on the right show the color codes of the values reached for the different flow rates simulated (color codes were adapted scaled here for different flow rates to apply all for the simulation shown on the left).

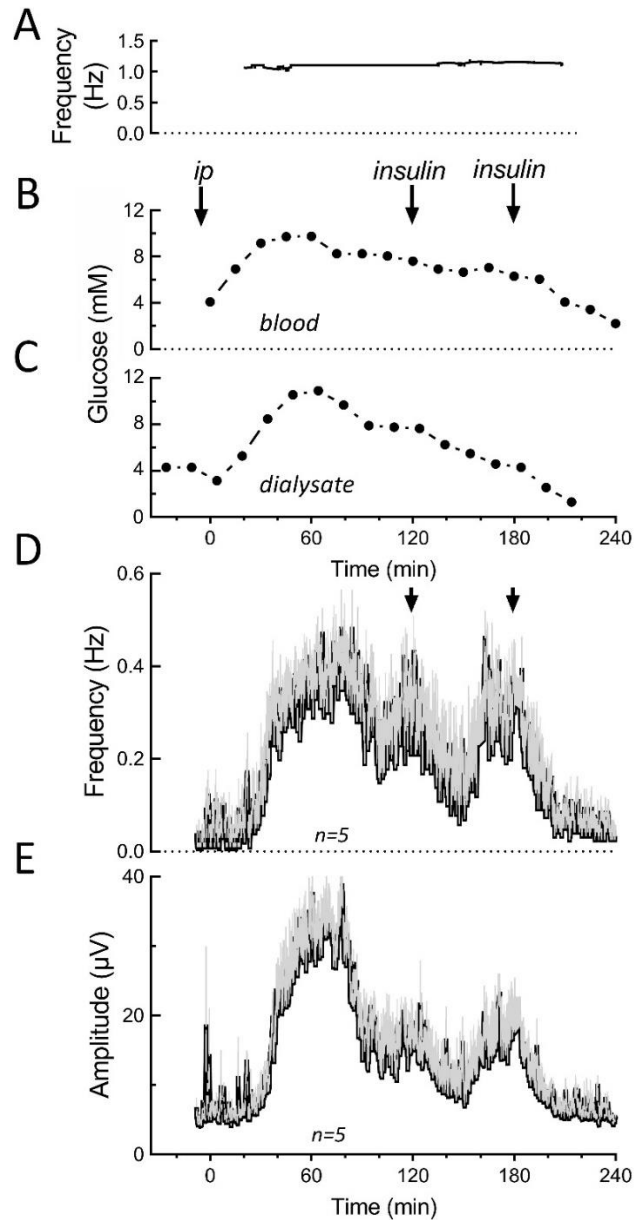


Figure 5: In-vivo monitoring of blood or interstitial glucose concentrations and dialysate evoked islet cell activity in the microfluidic MEA device. The time scales given here take into account the determined delays between microdialysis and microfluidic MEA (electrical recordings) as well as MEA outlets where glucose was determined in the dialysate (see Fig. 1). **A:** Respiration rate of anaesthetized rat. **B:** Blood glucose levels, arrows indicate intraperitoneal glucose injection or subcutaneous insulin injections. **C:** Dialysate glucose levels as measured after its passage through the microfluidic MEA. **D:** Islet electrical activity in terms of slow potential frequencies. Arrows indicate time of insulin injection. **E:** Islet electrical activity in terms of slow potential amplitudes.

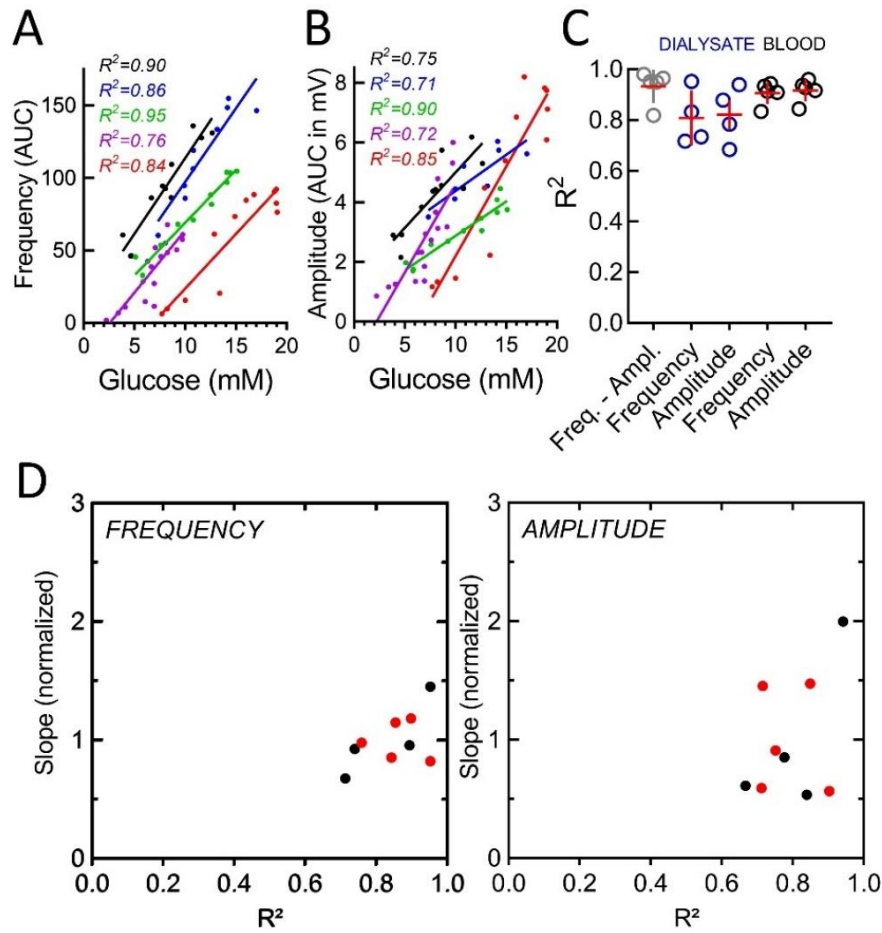
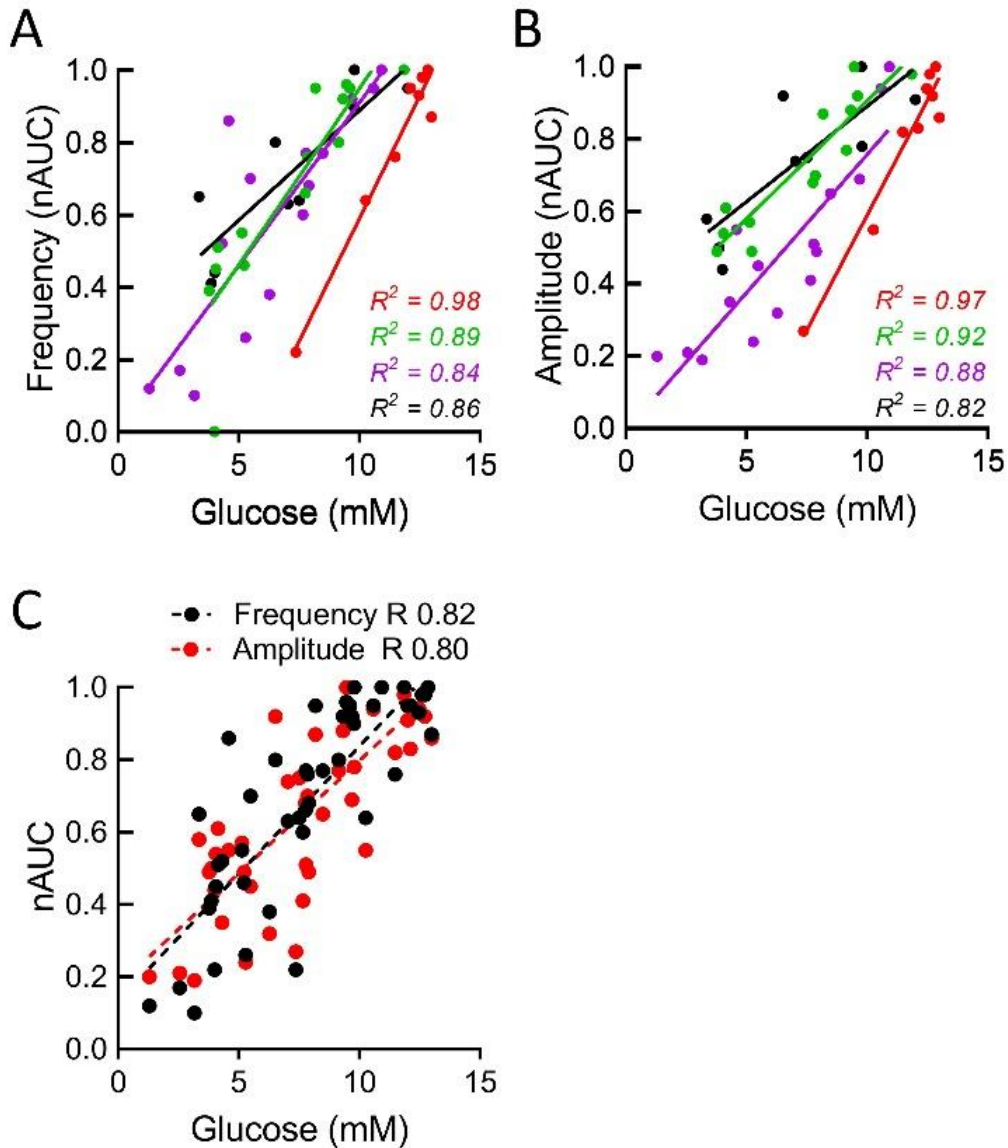
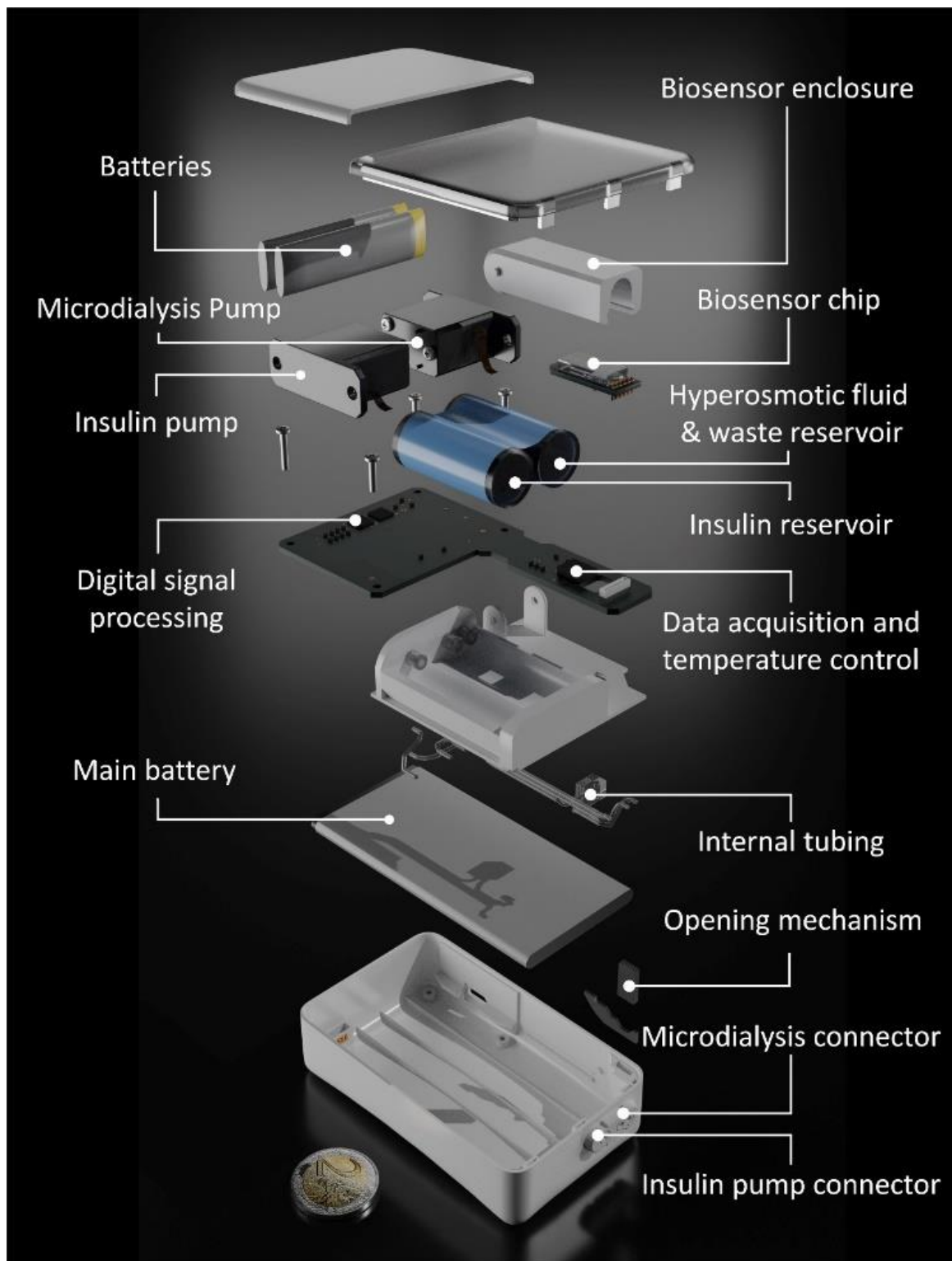


Figure 6: Correlation between electrical signal and blood glucose levels. A: Linear regressions between glucose levels and slow potential frequencies. Each color represents one experiment (animal) and corresponding Spearman R^2 values are indicated. Data points represents AUCs for a given blood glucose value and regression curves are given. **B:** Linear regressions between blood glucose levels slow potential amplitudes. Color codes as in A, corresponding R^2 values are indicated. **C:** Coefficient of determination R^2 for slow potential frequencies vs amplitudes over the blood glucose range during experiments (grey) as well as “for frequency or amplitudes versus glucose values either in dialysate (blue) or blood (black). Each data point represents one experiment (animal), mean and SEMs are given. **C and D:** Distribution of slopes vs R^2 values for slow potential frequencies or amplitudes. R^2 and slope values are from regression analyses between electrical signals and blood glucose levels, each point represents one experiment (animal).

SUPPLEMENTARY MATERIAL



Supplementary Figure 1: Correlation analysis of electrical activity of islets versus dialysate glucose. **A:** Correlation analysis blood glucose levels slow potential frequencies. Each color represents one experiment (animal) and corresponding Spearman R^2 values are indicated. Data points represents AUCs for a given blood glucose value and regression curves are given. **B:** Correlation analysis blood glucose levels slow potential amplitudes. Color codes as in A, corresponding R^2 values are indicated. **C:** Correlation factor of slow potential frequencies versus amplitudes at a given dialysate glucose concentration.



Supplemental Figure 2: Packaging of an extracorporeal islet-based glucose monitor. Blow-up presentation of a possible packaging of the microfluidic microelectrode device for extracorporeal use as a islet-based sensor of the demand in insulin in humans.

Evolution and development of microfluidics during the thesis

In the context of the development of a microfluidic chip adapted to the islet-based biosensor, a series of microfluidic systems have been designed and tested in collaboration with several partners. In this part of the manuscript I will discuss the different approaches that led to the validation and use of a simple and linear microfluidic system.

Microfluidic chip for trapping of individual islets on a custom MEA:

I started in a collaboration with the IES (Institut d'électronique, Montpellier) which has experience in microfluidics and in collaboration with IMS (Intégration du Matériau au Système; Talence; Renaud group). First a PDMS chip was designed with a complex design. In parallel, we designed a custom multi-electrode array with electrodes matching the microfluidic pattern. The purpose of the chip was to trap an individual islet on a specific electrode surrounded by a basket of PDMS pillars (Figure 1C). A corresponding PDMS block comprising several patterns was aligned on the MEA (Fig 1A). During the initial tests, we noted various problems. First, only one pattern was perfused, the other electrodes were not immersed and generated considerable noise. Based on this observation, I cut out and aligned a single pattern on the MEAs. Thus, we could immerse the other electrodes in a working solution bath during the experiment. Note that the electrode array in this case was homemade and not from a commercial source. and presented problems of signal stability. Indeed, starting the microfluidic perfusion we observed a slow noise which obscured the specific signals and thus did not permit of SP frequencies and amplitudes.

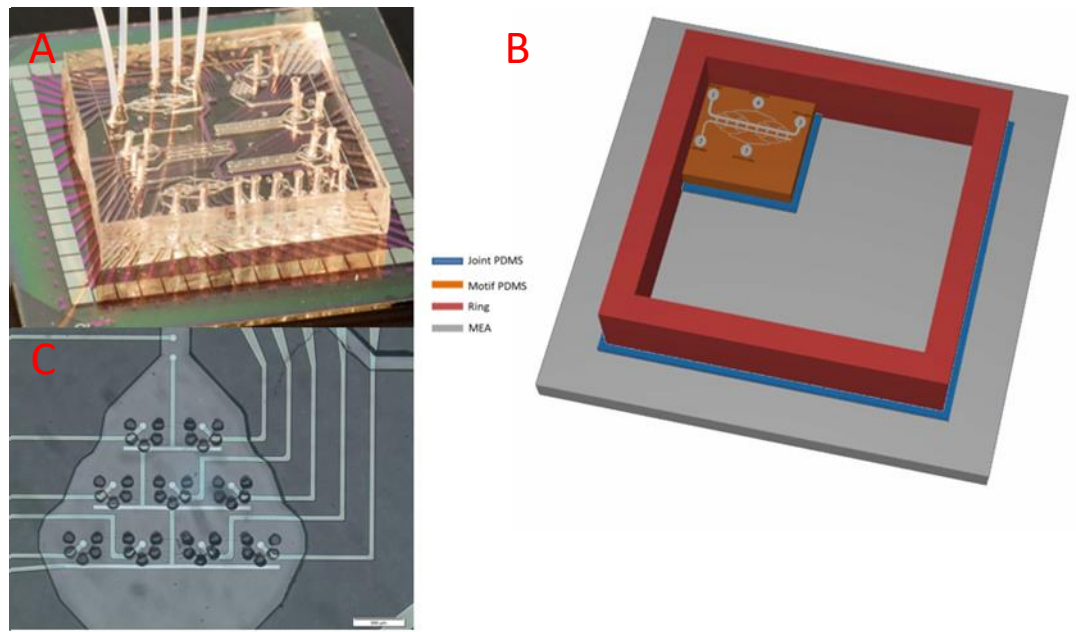


Figure 1: IES device for trapping single islets. A) a photograph of the multi-patterned PDMS chip, aligned to a homemade IES MEA. B) 3D model of the device tested on a commercial MEA, only one pattern is aligned to the electrodes so that the other electrodes not used during the electrophysiological recording can be immersed in the working solution. C) a photograph of the basket design used on a commercial MEA.

I therefore chose to continue the characterisation of the microfluidic chip by aligning the basket design with a commercial MEA (60MEA200/30iR-Ti-gr, MultiChannel System, Reutlingen, Germany). Despite the fact that the chip design did not perfectly coincide with the design of the MEA electrodes, we were able to achieve an alignment that allowed us to load the islets and obtain a first electrophysiological recording.

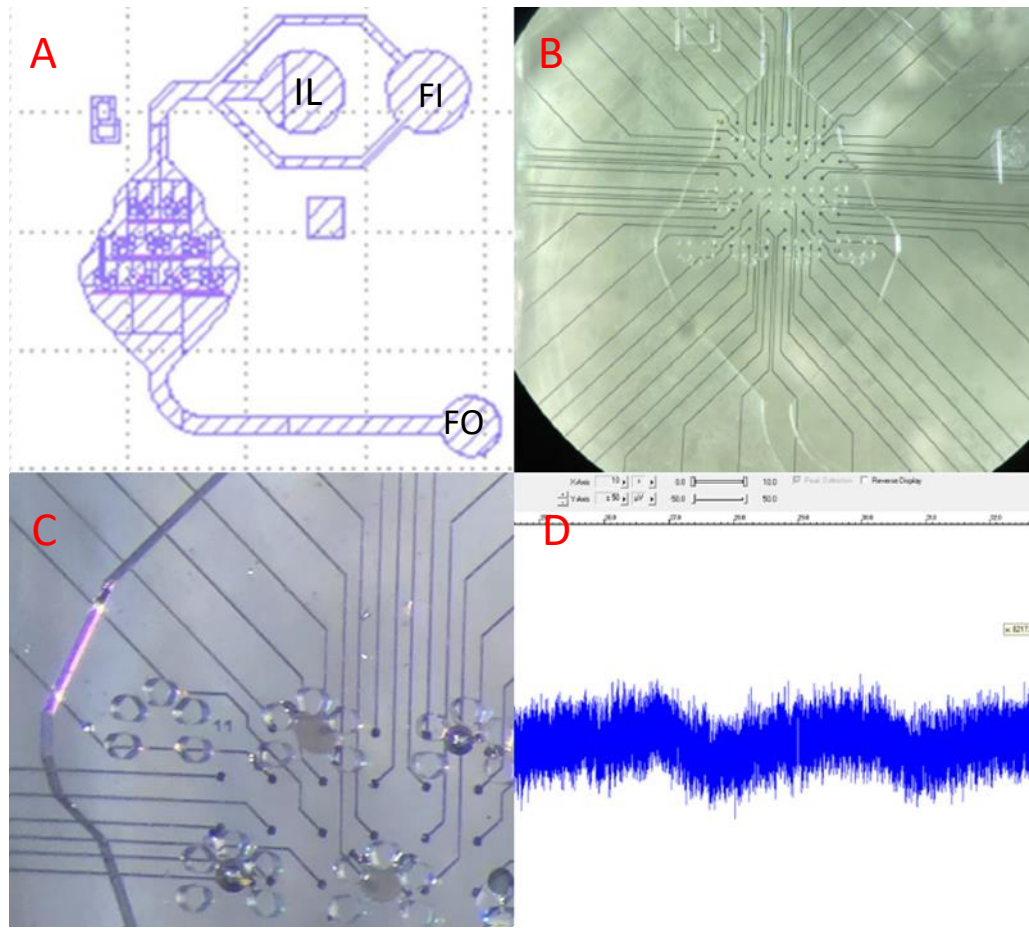


Figure 2: Alignment of a microfluidic IES pattern on a commercial MCS MEA: A) 2D modelling of the basket pattern FI: Flow inlet, IL: Islet loading, FO: Flow outlet. B) binocular photograph of the chip aligned on the MCS MEA. C) photograph of islet trapping on the electrodes during the experiment. D) screen capture of the electrophysiological trace observed in the MCRack software, appearance of the first SPs after 3h of adhesion within the device.

The use of the improved device allowed the recording of SPs, but still had a number of constraints that were incompatible with its further use in the development of our islet-based biosensor. This system required a very complex scheme for loading the islets into the device as long-term culture could not be performed. Indeed, we had to load the islets on the day of the experiment by titrating the flow rate in order to trap the islets in the baskets, then wait 3 hours at low flow ($<5\mu\text{l}/\text{min}$) to obtain adhesion of the islets. Although we had reckoned that that baskets would trap them, sufficient physical contact with the electrodes was required to observe electrical signals, which were in fact of weak amplitudes. This additional 3 hours delay for loading and adhesion under constant flow increased considerably the appearance of bubble formation.

Pressure gradient simulation

Identifying the source of bubble formation in the original motifB

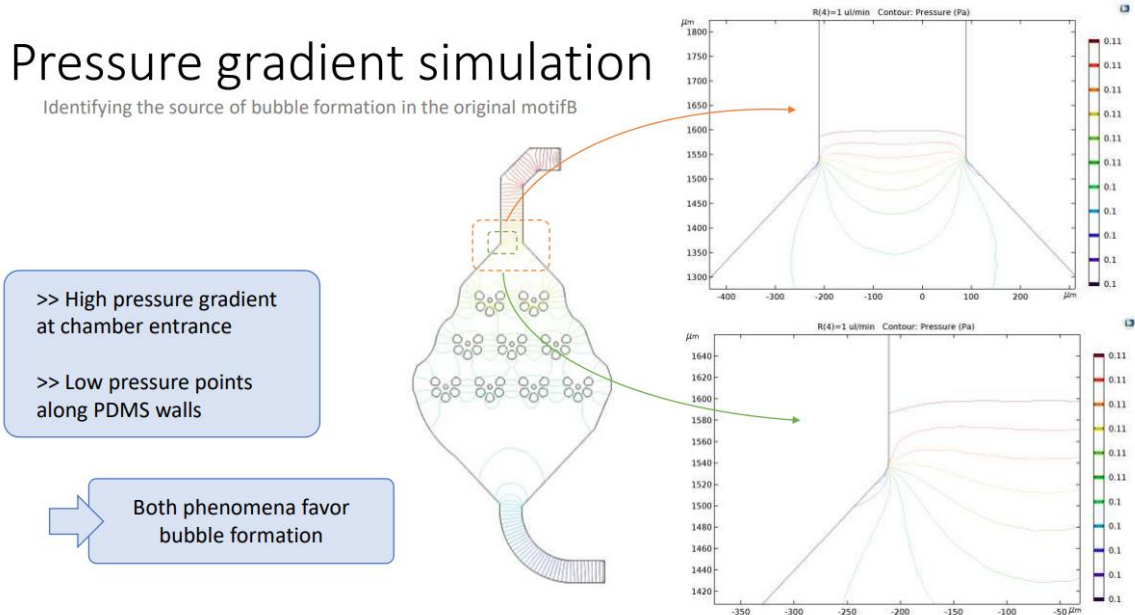


Figure 3: Simulation of the pressure gradient in the chip. Pressure gradient is given by a color code, from high pressure in red to low pressure in dark blue.

Clearly such a risk would not have been compatible with experiments in living animals and the duration of anaesthesia tolerated by the animals. This design, moreover, was particularly susceptible to bubble formation, so-called nucleation problems. The passage from a narrow channel to a large cavity containing the trapping baskets leads to reduction in pressure and flow, which in turn favours the formation of small bubbles at the exit of the channel. These bubbles subsequently expanded within the cavity, and completely blocked the baskets.

In view of these observations, we decided to design less complex devices.

Development of a simple microfluidic chip:

Following the experiences with the previous microfluidic chip, I was able to draw up a specification of the essential criteria for the development of a suitable chip for the further development of the islet-based biosensor.

These criteria are:

- A design compatible with the outlay of commercially available MEAs

- In-chip loading of the islets (easy to load with a pipet) and off-chip microfluidic culture
- Simple, constant size design, not subject to bubble formation
- Low dead volume
- Compatible with a flow rate between $1\mu\text{l}/\text{min}$ and $10\mu\text{l}/\text{min}$

To develop this chip, I chose to opt for a linear configuration— and a design that can be used by means of my lab, the Lang group to this end, I started by moulding 0.8 cm long pieces of tubing in PDMS. By demoulding these pieces of tubing, I obtained a channel in the PDMS, and I subsequently punched a inlet and a outlet with a 1 mm diameter puncher. To align on the MEA I then did an oxygen plasma activation.

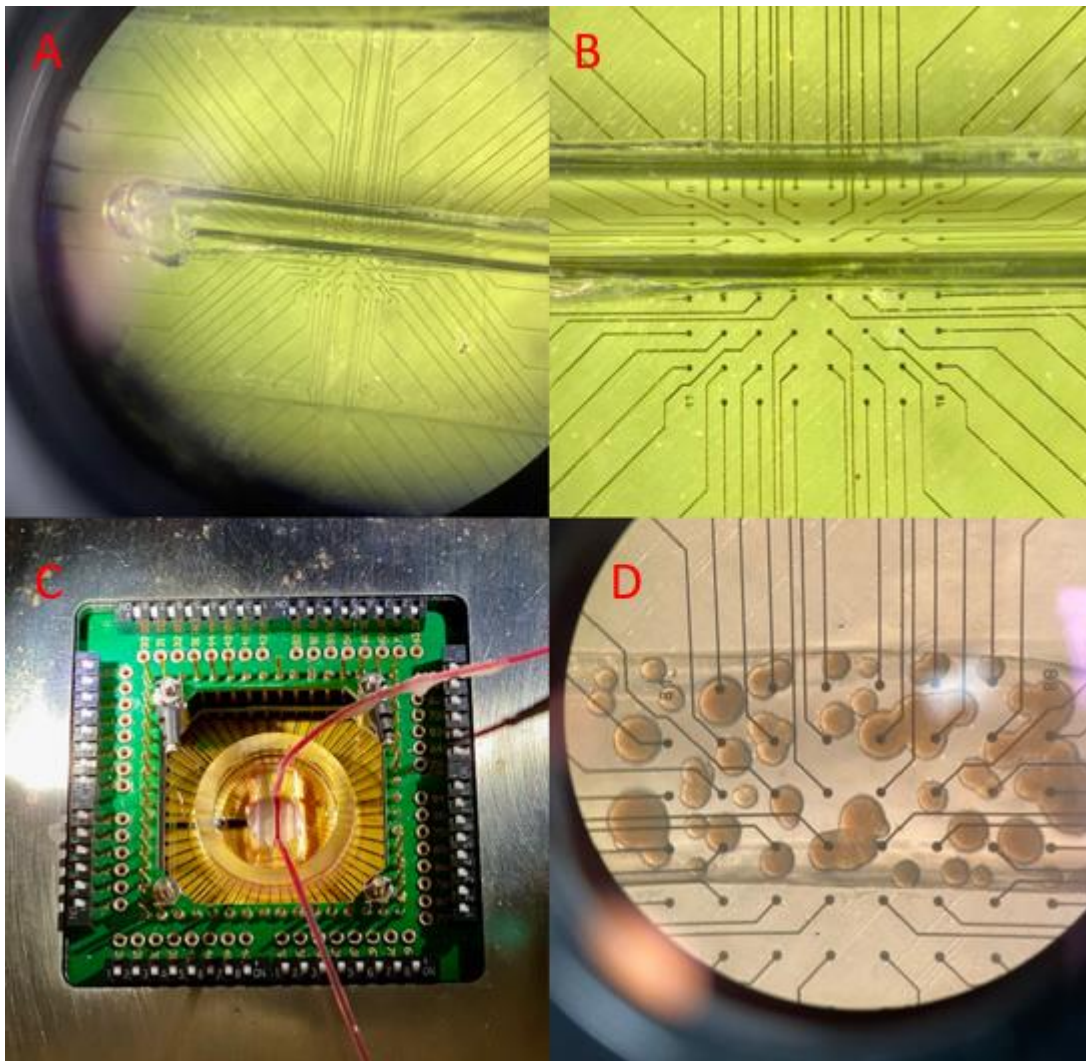


Figure 4: Single linear microfluidic chip. A) Binocular photograph of the aligned pattern on a commercial MEA (MCS, Reutigen, Germany). B) Binocular photograph of electrodes within the microfluidic channel (0.8 mm diameter). C) Photograph of the microfluidic MEA placed into the commercial amplifier (MCS, Reutigen, Germany), Med in and out connected, during characterisation of kinetics and dead volumes using the dye phenol red. D) microscopic photograph of islets loaded into the microfluidic chip and adhering to the electrodes.

I first used this design for the experiments in the publication by my colleague, Manon Jaffredo (Jaffredo et al. 2021), as well as for the development of the microdialysis biosensor in in vivo experiments. This design, although simple, is compatible with long-term experiments that per se increase the risk of bubble formation. In this design, bubbles may form, but they can pass through the channel without blocking the flow. Since the first microfabrication of this chip, I have optimised the system by developing a silicium wafer, which facilitates the casting and demoulding of the PDMS and allows for standardised channels.

In parallel with these microfluidic developments, I also worked on another device that combines the advantages of both devices.

Modelling and design of a linear microfluidic chip allowing individual islet trapping on an electrode:

Successfully combining a linear pattern with the possibility of individually recording the electrical activity of an islet on an electrode would open up numerous possibilities both in terms of fundamental research for the study of islets and for the industrial development of a medical device. Indeed, this would allow the number of islets on a chip to be reduced.

With this idea in mind, and by reviewing the literature, we looked at a design developed by a team from Berkeley.

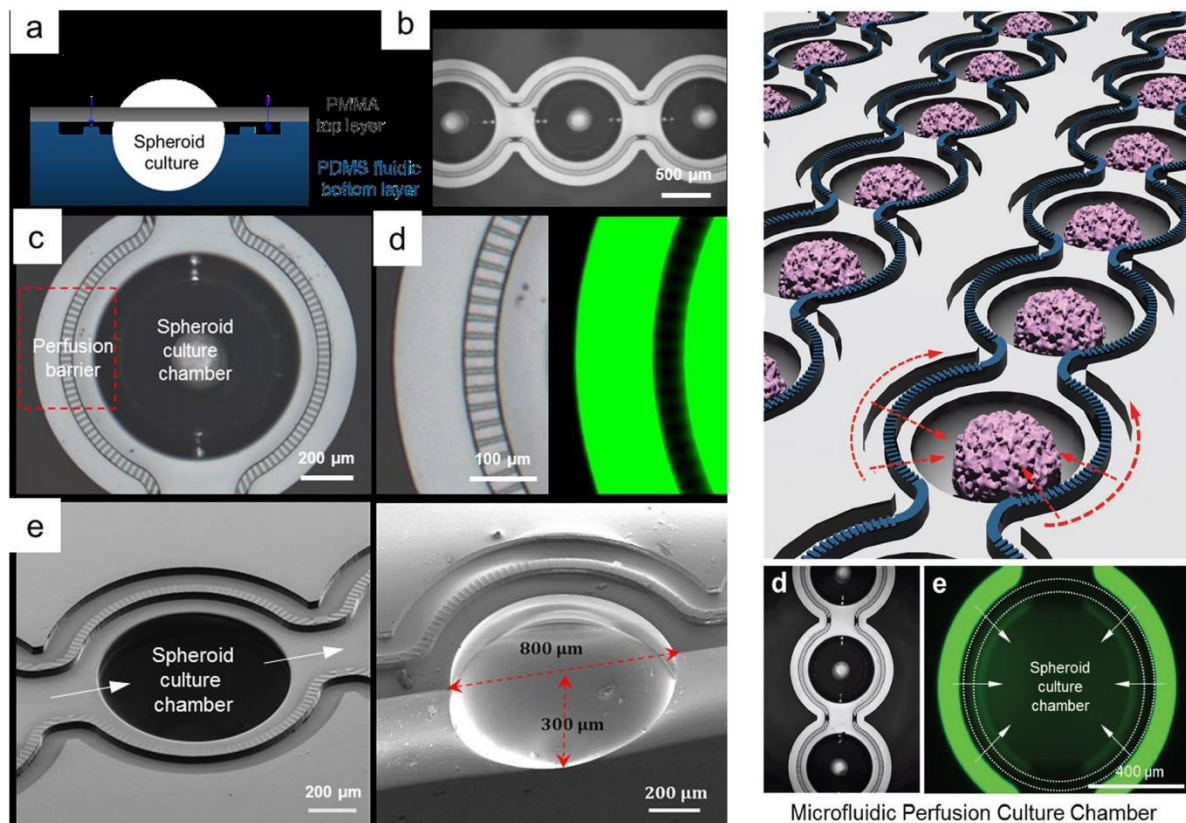


Figure 5: Original device developed by Lee and colleagues at UC Berkeley. a) Cross sectional view of the MAP. b) Micrograph of the microfluidic spheroid culture device. c) Enlarged bright field image of the culture area. d) Enlarged brightfield and fluorescent images of the perfusion barrier. e) Scanning electron microscope images of the islet on a chip showing the endothelial like perfusion. Adapted from (Lee et al. 2018)

In the design developed by Lee and colleagues (Lee et al. 2018), a PMMA chip has a series of half domes with a central channel through which the chip can be loaded and a secondary perfusion network on either side of the dome, allowing a gentle flow, thus avoiding significant shear stress to the spheroids. PMMA is for polymethyl methacrylate which is a transparent thermoplastic polymer obtained by polyaddition whose monomer is methyl methacrylate. This polymer is better known by its first commercial name of Plexiglas. The use of such a polymer allows for solid, long-lasting chips, and it is often used in the development of medical devices due to its high biocompatibility. Using single cells instead of organoids considerably eases loading and may be of considerable interest also when using stem-cell derived pseudo-beta cells. Indeed, such a design could be coupled to continuous flow and cell culture and thereby permit to monitor differentiation of such stem-cell derived pseudo-islets. Indeed, Lee's group completely dissociated the islets after their purification and loaded the chip with a solution of dissociated islet cells and endothelial cells. After loading, the cells will sediment

to the bottom of the domes and the gentle flow around the top of the domes will contribute to the formation of spheroids.

Based on this design, I was interested in how we could adapt this system with our use of MEAs for electrophysiological studies.

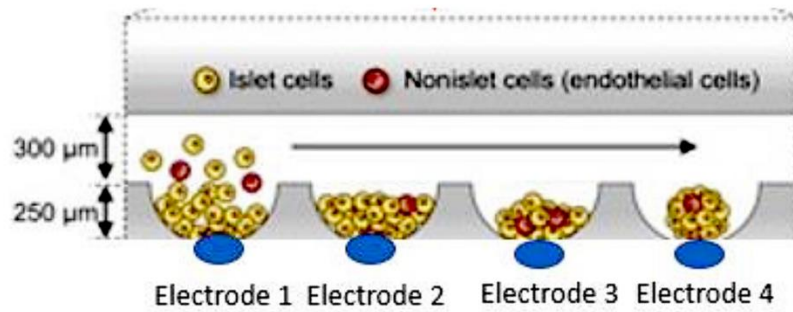


Figure 6: Schematic of dome design adaptation to electrodes.

To adapt this device to MEAs, we would have to propose a design where the domes would be open at the bottom in order to accommodate the electrodes at the bottom of the cupola. Such a chip adapted to our MEAs is complex to machine and required us to call on specialist microfabrication providers. It is with this in mind that we have put together a 2D and 3D modelling file in collaboration with Thomas Bennetton (Centre de recherche Paul Pascal, Pessac) in order to contact one of the leading companies in the industrial microfluidic chip manufacturing market, Micronite (Enschede, Netherland).

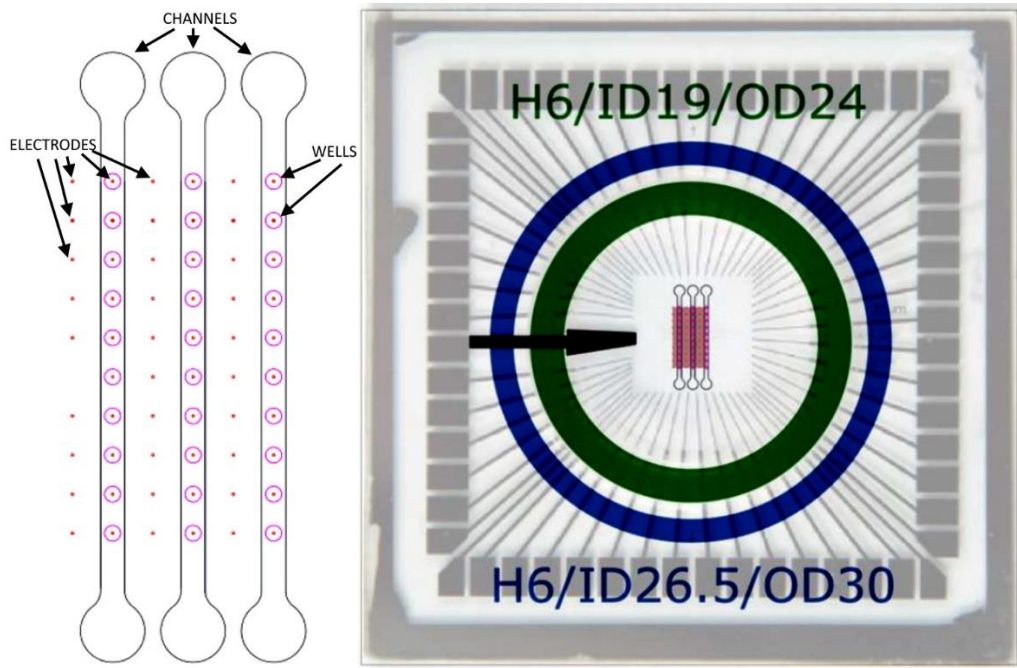


Figure 7: 2D representation and scaling of the device on an MEA. Left panel 2D representation of the chip aligned on a 10x6 MCS electrode array. Right panel showing the chip scaled to the MEA and showing 2 possible ring sizes. In green ring height 6 mm, inner diameter 19 mm and outer diameter 24 mm. In blue ring height 6 mm, inner diameter 26.5 mm, outer diameter 30 mm.

We first represented the desired design in 2D and made a scale representation of the MEA design. Then, once this scaling was validated, we would be able to move on to a 3D wireframe representation.

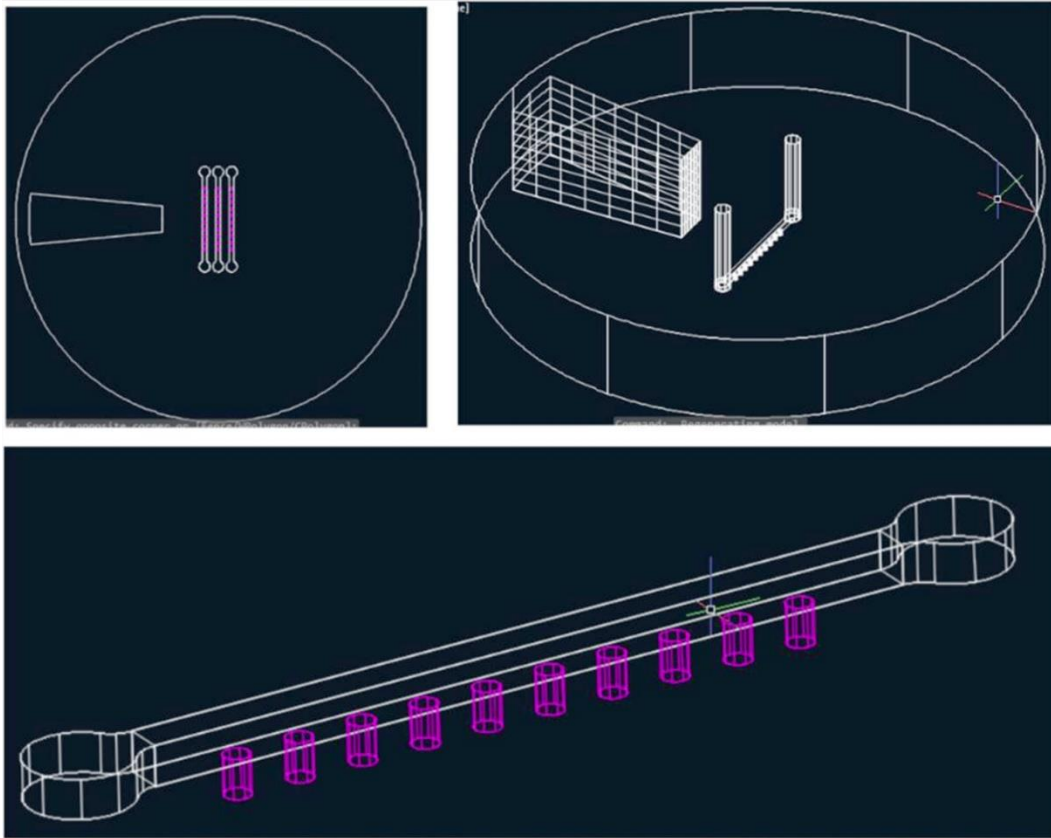


Figure 8: Wireframe representation of the microfluidic chip optimised to be compatible with a 10x6 MEA MCS electrodes. A first layer comprises the inlets and outlets of fluids and the channels. In this example, its thickness is 6 mm. The height of the channels is 300 microns. A second layer which includes the traps. Its thickness here is 0.8 mm. It is necessary at this level to see with the manufacturer what thickness is achievable, knowing that it defines the depth of the traps.

To finalise the representation of the chip, we made an extruded representation of the device and modelled how to assemble the different parts of the device.

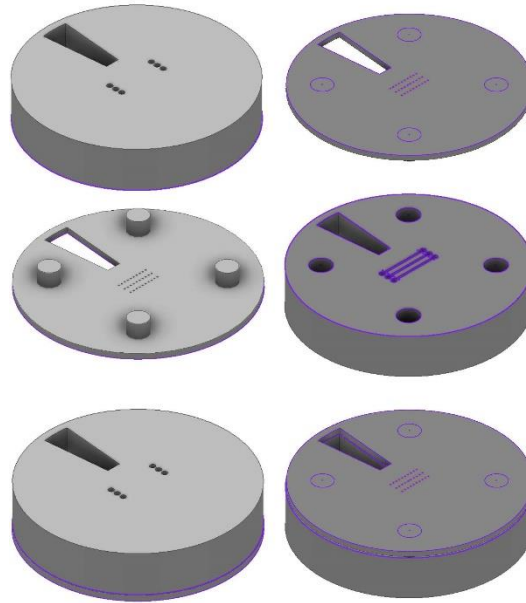


Figure 9: 3D view of the chip. The two layers are sandwiched together. We have placed markers so that the layers line up as they fit together.

After the completion of this design work, we discussed with a commercial service (Micronit, Netherland). The project is feasible; however, costs would surpass 50 kEuros because of the small quantity of chips to be machined.

Currently in the laboratory, one of my colleagues, Marie Monchablon, is working on the possibility of making MEAs with a layer of silicium cast on top of the MEA to obtain domes that can trap islets. This project is being developed in collaboration with the IES.

Conclusion:

During these three years of development of a microfluidic chip adapted to the islet-based biosensor, we have explored different approaches. The use of a complex design, such as the one developed by IES, is not compatible with the constraints imposed by the experimental time required to carry out the proof of concept in vivo in rats. Following these observations, we have developed a simple microfluidic system, allowing the loading of a group of islets, and a culture outside any microfluidic perfusion. Although this design is suitable for the proof of concept of the biosensor, we can however imagine for the future a chip model that would take the strong points of the IES and simple linear devices, inspired by the design developed by Lee's team in Berkeley. This linear design, with open domes on the MEA electrodes, would

allow for simple loading, isolated islet trapping in the open domes on the electrodes, while presenting low shear stress and low risk of bubble blockage

Validation of a homemade acquisition system SYAM: Manuscript n°4

Islet biosignals are recorded on 60-channel MEAs. With amplitudes as low as only a few hundreds of microvolts, multichannel low-noise amplifiers are necessary to record relevant electrical signatures. Meanwhile, to ensure true-to-life response of islets, the MEA must be kept at body temperature and fluids must be channelled continuously with microfluidic systems.

During the development of the biosensor in DIABLO project, these functions were performed by proprietary systems from Multichannel Systems (MCS, Reutlingen, Germany): the MCS MEA1060-Inv preamplifier, the MCS USB-ME64 acquisition system, and the MCS TC01 temperature controller. With the objective of incorporating the biosensor in a closed-loop, The microelectronic team from the IMS developed a custom electronic system, SYAM (System for Acquisition with Microfluidics), which integrates the three functions of the MCS equipment. The system was validated during static and microfluidic experiment where murine islets were recorded in a 60-electrode MEA with PEDOT electrodes for static recording and Titan electrodes for microfluidic recording. In these different experiments we observed a clear islet activity, consistent with is observed with the MCS system. For these experiments, I realised the culture and the recordings for the biological validation of the device.

With this system, the DIABLO consortium eliminates the dependence on proprietary material in the acquisition chain, and provide grounds for further integration.

Introduction

The biosensor developed in DIABLO measures the extracellular electrical activity of live pancreatic islets with planar Micro-Electrode Arrays (MEAs). Recording of such biosignals is delicate, as they range only a few hundreds of microvolts, with some electrical signatures rarely exceeding tens of microvolts. Because of this, proper acquisition is strongly dependent on appropriate electronics that will amplify signals with minimal added noise, while maintaining cells in a noise-free, temperature-controlled environment. Then, electrical signatures such as action potentials and slow potentials are extracted with dedicated processing electronics with multichannel capabilities and minimal latency.

This deliverable describes the development of custom electronics for the acquisition and real-time processing of biosignals of pancreatic islets, as recorded on planar MEAs.

I Signal acquisition

I.1 Context

Islet biosignals are recorded on 60-channel MEAs. With amplitudes as low as only a few hundreds of microvolts, multichannel low-noise amplifiers are necessary to record relevant electrical signatures. Meanwhile, to ensure true-to-life response of islets, the MEA must be kept at body temperature and fluids must be channelled continuously with microfluidic systems.

During the development of the biosensor in DIABLO, these functions were performed by proprietary systems from Multichannel Systems (MCS, Reutlingen, Germany): the MCS MEA1060-Inv preamplifier, the MCS USB-ME64 acquisition system, and the MCS TC01 temperature controller. With the objective of incorporating the biosensor in a closed-loop, we developed a custom electronic system, SYAM (System for Acquisition with Microfluidics), which integrates the three functions of this MCS equipment. With this system, we eliminate the dependence on proprietary material in the acquisition chain, and provide grounds for further integration.

I.2 Specifications

SYAM is designed according to the following specifications and constraints:

- 60-channel, 16-bit, 10 kHz data acquisition¹
- Temperature control at 37°C
- Easy access to the MEA for insertion and manipulation of microfluidic tubing
- Must include a Faraday cage

The system is powered by a 12 V, 5.42 A power supply.

I.3 Construction

SYAM was designed to fit acquisition and thermal control in a single device, in contrast with MCS equipment that achieves the same function with three separate pieces of equipment. An exploded view of the system is shown in Fig. 1, with a list of all its components. It is composed of two main sub-systems: the main body (elements 7-25 in Fig. 1), which includes electronics

¹ Legacy from the MCS equipment, which has identical specifications

for thermal control, backlighting, user controls, and shielding, and an acquisition stage (elements 1-6 in Fig. 1). Relevant system dimensions are shown in Table 1. In the following descriptions, numbers between parentheses refer to the numbered elements in Fig. 1.

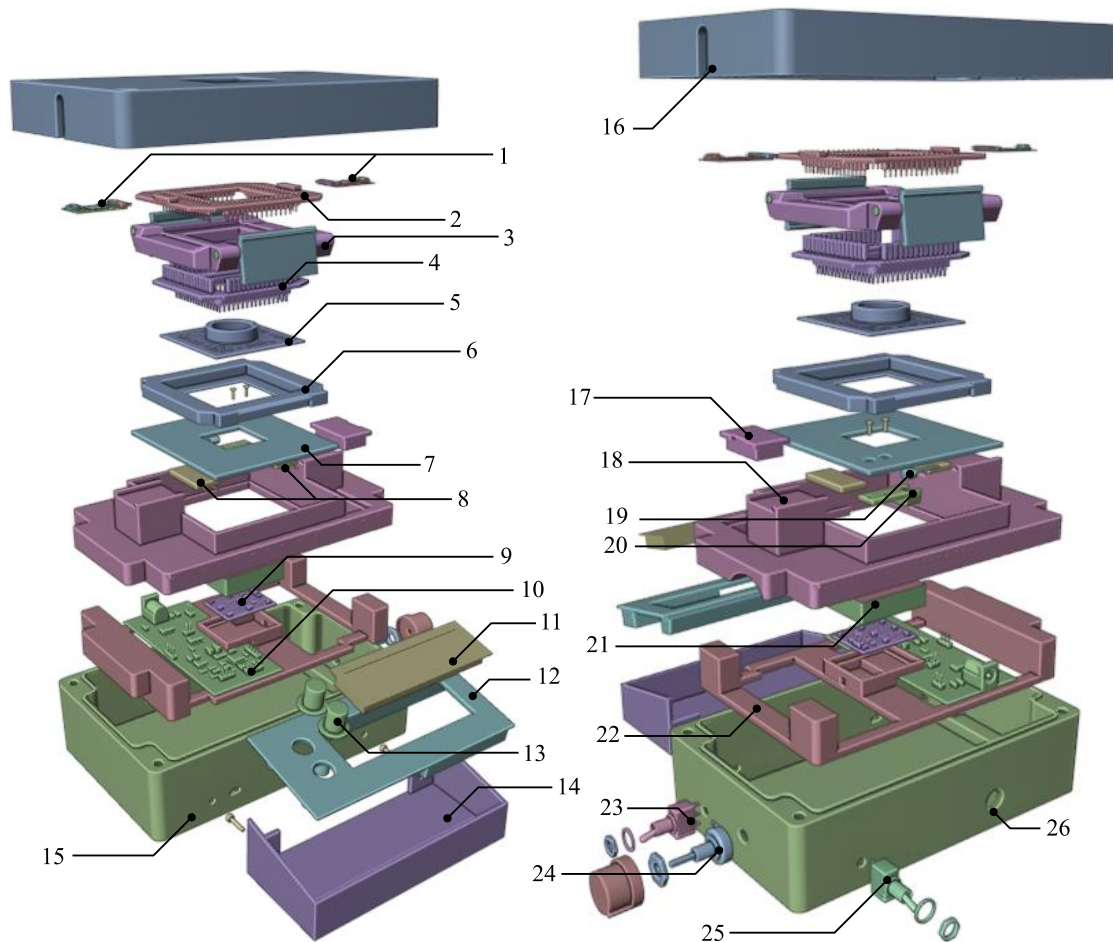


Fig. 1. Exploded view of the system. Screws, nuts and washers are left unnumbered. **1.** 2x Intan RHD2132 amplifiers. **2.** Electronic board for routing signals from standard 2.54 mm connectors to Omnetics nano-strip. **3.** MEA clamp. **4.** Electronic board for routing signals from pogo-pins to standard 2.54 mm connectors. **5.** MEA. **6.** MEA socket. **7.** Heat plate. **8.** Power resistors (heating element). **9.** Backlighting board. **10.** Thermal controller board. **11.** LCD display. **12.** Front panel. **13.** Control buttons. **14.** Front panel casing. **15.** Metal casing (bottom). **16.** Metal casing (top). **17.** Plug for microcontroller access. **18.** Internal structure (top). **19.** Temperature sensor. **20.** Temperature sensor casing. **21.** Backlighting diffuser. **22.** Internal structure (bottom) **23.** Backlighting ON/OFF switch. **24.** Backlighting dimmer knob. **25.** Temperature controller ON/OFF switch. **26.** Power input (12 V DC)

Table 1: SYAM dimensions

Whole system	$178 \times 160 \times 60 \text{ mm}^3$
Top opening (MEA access area)	$32 \times 32 \text{ mm}^2$
Distance from top of the lid to the MEA	29 mm
Supported MEA dimensions	$49 \times 49 \text{ mm}^2$ (1 mm thick)
Heat plate opening (backlighting area)	$24 \times 24 \text{ mm}^2$

1.3.a Main body

The main body of the systems consists of a 161×100×61 mm³ Hammond (ref. 1550Z117BK) aluminium casing (15-16) that houses all sensitive electronics, and a custom-made plastic casing (12, 14) with user controls and LCD display. The aluminium casing (15) was machined to accommodate knobs, switches, and power supply for temperature control and backlighting (23-26). The casing lid (16) was also machined to leave openings on the sides for cables, and a 32×32 mm² opening on the top for MEA access. Except for the metallic parts (i.e. the metal casing, the aluminium heating plate, and all screws, nuts and washers), all parts of the main body's structure were 3D-printed from PLA.

Acting as a Faraday case, the painted aluminium casing was sanded off to the bare metal on select surfaces in order to guarantee electrical contact between elements of the electromagnetic shielding (e.g. Between the casing and its lid), and to allow external ground connections in the existing screw holes. Concerning the 3D-printed parts, surfaces where electromagnetic shielding was required were covered with conductive copper tape.

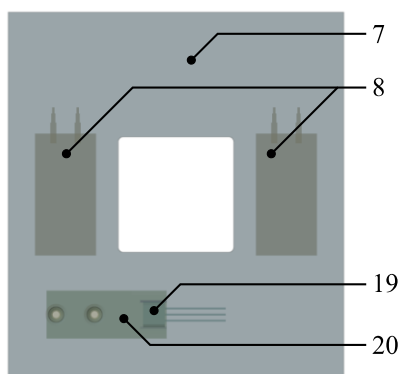


Fig. 2. Heat plate. Top view, with transparency. Notations consistent with Fig. 1. **7.** Heat plate. **8.** Power resistors (heating element). **19.** Temperature

inside the casing, the temperature control board (10) and backlighting board and diffuser (9, 21) are housed in the internal structure (18, 22). The upper part of this complex structure (18) has a pluggable (17) opening to access the thermal controller's configuration port, and a large central opening that accommodates the heat plate (7) and the acquisition stage, with resting surfaces for both the MEA socket (6) and the preamplifiers (1) (see 1.3.b).

The heat plate, shown in Fig. 2, is a 70×76×2 mm³ piece of aluminium (7). Underneath it, the heating element (8) is glued with thermal paste, and the temperature sensor (19) is pressed with a screwed casing (20). A ground wire is run from one of the screws to reduce noise from the heating circuit. A 24 × 24 mm² opening is machined out from the centre of the plate, for backlighting of a large surface area. Even though the active area of most MEAs is considerably smaller, such a large opening accommodates a wide variety of possible MEA layouts, and helps with microscopy and MEA manipulation while the system is closed.

1.3.b Acquisition stage

The main purpose of the acquisition stage's mechanical assembly is to secure the contact between spring-loaded connectors (pogo pins) and the MEA. To that end, a clamping system was fabricated, in which the MEA (5) is secured in place between two pieces (3,6) dimensioned to accommodate 60-electrode MEAs from MCS. The lower piece, a simple socket with grooves on the sides for clamping, was 3D-printed from PLA. The upper piece (3), more complex and with more mechanical constraints, was 3D-printed out of resin and clamps to the lower piece with a couple of articulated mechanical hooks. Glued to its bottom, an electronic board (4) with 60 pogo-pins ensures electrical contact with the MEA. A secondary electronic board (2), plugged on top, re-routes signals from the pogo-pins to the preamplifiers (1).

The whole assembly is dimensioned to sit on top of the heating plate, with supports underneath the preamplifiers, and ample room to close the casing's lid to shield the acquisition's delicate electronics from external noise.

1.4 Signal acquisition

To maintain compatibility with ongoing projects, the acquisition stage was designed for compatibility with MCS's 60-electrode MEAs. Both signal preamplification and analogue-to-digital conversion are handled by two commercially available 32-channel Intan RHD2132 headstage amplifier boards (Intan Technologies, Los Angeles, California). Their specifications, fitting our constraints (i.e. same as or exceeding MCS equipment detailed in 1.1), are detailed in Table 2. While it is still a commercial solution, Intan provides the sources for all its equipment and sells its acquisition chips in QFN packages; This makes it a cost-efficient and sustainable choice for us, with prospects for future custom development.

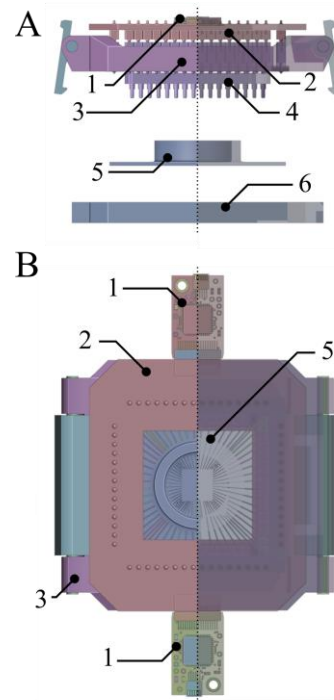


Fig. 3. Acquisition stage.

Transparency highlights the cut-outs for access to the MEA and backlighting.

A. Side view. **B.** Top view. Notations consistent with Fig. 1. **1.** 2x Intan RHD2132 amplifiers. **2.** Electronic board for routing signals from standard 2.54 mm connectors to Omnetics nano-strip. **3.** MEA clamp. **4.** Electronic board for routing signals from pogo-

Table 2: Specifications for one Intan RHD2132 headstage amplifier

Number of channels	32
Max. sampling frequency for 32 channels	30 kHz
Resolution	16 b
Gain	192
Input-referred noise	$2.4 \mu V_{\text{rms}}$
Interface	SPI

Two electronic boards for signal routing were fabricated. The first board (4 in Fig. 1) makes use of pogo-pins to contact the sixty MEA pads and re-routes them to standard 2.54 mm connectors. The second board (3 in Fig. 1) re-routes the signals from the latter 2.54 mm connectors to two male Omnetics nano-strip connectors (termed Ports A and B) compatible with the Intan preamplifiers. Additionally, an easily accessed switch allows to connect pin #15 to the ground, as it is used as a reference electrode in MCS's MEAs. Note that, due to MEAs having only 60 electrodes and two preamplifiers having 64 channels, four pins of the preamplifier connectors are permanently grounded (Port B, inputs 0, 1, 30, 31).

To assess electrical performance of the acquisition stage, the mean RMS noise and mean DC offset were measured. All channels were grounded using a ground plate in place of an MEA, and measurements were conducted in three different running conditions: 1) with temperature control disabled (but LCD screen and user controls active), 2) with temperature control enabled, and 3) with power cut-off from the thermal controller (i.e. only the preamplifiers are powered via SPI). Results are shown in Fig. 5 below, showing very low, invariant DC offset as well as very little variation in input-referred noise, marginally affected by temperature control and very close to that advertised by Intan ($2.4 \mu\text{V}_{\text{rms}}$). Power Spectral Density (PSD) analyses of recordings reveal spectral lines indicative of periodic noise. As shown in Fig. 5, this noise can be attributed to both the Intan preamplifiers and the thermal controller, as some lines are already present without temperature control. It is however easily filtered and, as shown later in I.6, does not hinder recording and processing.

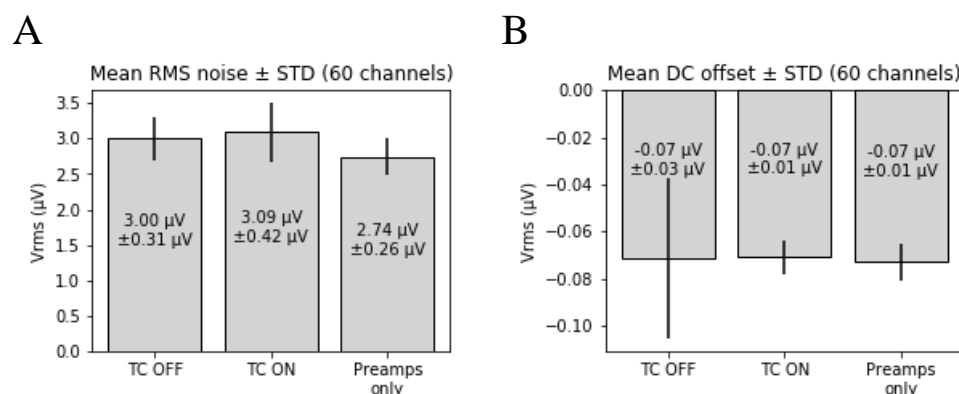


Fig. 4. Noise and offset metrics on all electrodes with temperature control disabled (TC OFF), temperature control enabled (TC ON), and with no electronics active except Intan preamplifiers (Preamps only). **A.** Mean RMS noise. **B.** Mean DC offset.

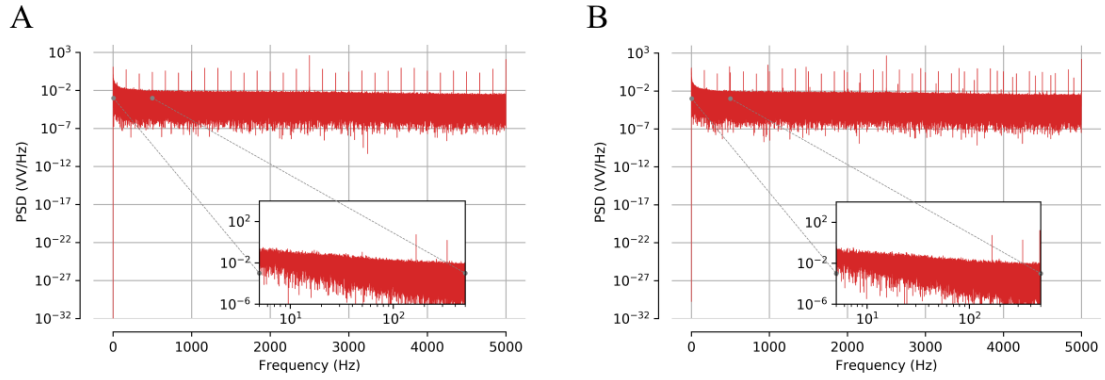


Fig. 5. Power spectral density (PSD) of one grounded channel with A. no electronics active except Intan preamplifiers, and B. with temperature control enabled. Experimental data were recorded at as sampling rate of 10 kHz.

I.5 Thermal controller

I.5.a Implementation

The heating element for temperature control consists of two 20 Ω high power resistors (CGS MPC5 200J) in parallel, glued to the bottom of an aluminium plate. Located underneath the MEA, it acts as a thermal diffusor. Temperature is measured with an LM35 temperature sensor located underneath the aluminium plate, at a distance from the heating elements (see Fig. 2). As shown on the principle scheme in Fig. 6, the controller is digitally implemented in an ATMEGA 328P microcontroller, which interfaces the sensor and heating element with their respective conversion and PWM (Pulse Width Modulation) driver analogue stages.

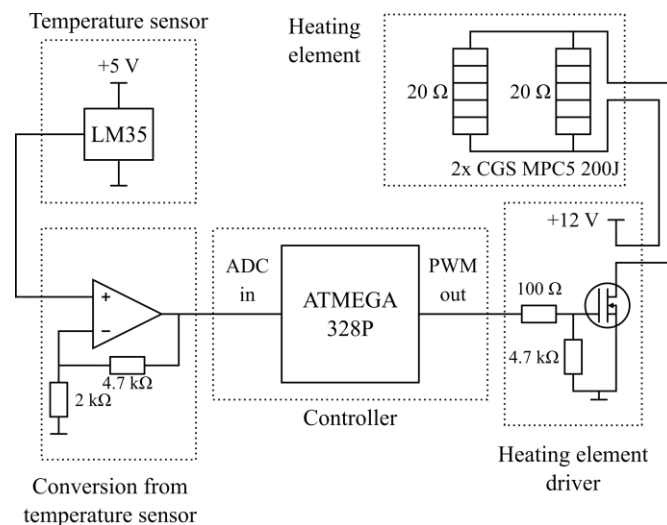


Fig. 6. Principle scheme for the temperature control loop. Schematics for the power stage, decoupling, user interface, and the ATMEGA microcontroller's electrical environment are not represented.

Table 3 : Temperature control properties

Hardware properties		
Measuring range	temperature	0 - 149.25°C
Measurement bit depth		10 bits
Resolution		0.14576°C
Sensor type		LM35
Heating element		(2x 20 Ω in parallel)
Controller properties		
Controller proportional gain		12.468
Controller integral constant	time	2808.2 s
Sampling frequency		2 Hz
Target range		30 - 40°C

With very few sources for disturbances, the controller was implemented as Proportional-Integral (PI). Its parameters were identified for maximum stability and absence of overshoot to reduce risks of overheating the islets. Its parameters are shown in table 3 and its digital implementation in eq. (1) below, where $U[k]$ is the PWM command at state k , and E is the error.

$$U[k] = U[k - 1] + 12.46888705 \times E[k] - 12.466667E[k - 1] \quad (1)$$

1.5.b Configuration

The controller's target may be configured between 30 to 40°C using two push buttons that increase or decrease it by steps of 0.5°C. Additionally, pushing both buttons simultaneously will toggle temperature control ON or OFF. User instructions and measured temperature are displayed in real-time on the LCD screen.

1.5.c Measurements

The step response of temperature control was measured using SYAM's internal temperature sensor and a type K temperature probe at the centre of the MEA's culture well. The plate's temperature equilibrates at 37°C after roughly 900 s, but the well's temperature only reaches 32.8°C. This temperature is however sufficient for experiments (in the same experimental conditions MCS's temperature controller only reaches 34.4°C). Moreover, temperature in the culture well is highly dependent on the MEA's geometry: we utilize coverslips in the well that help reduce evaporation and are expected to also help retain heat. Still, we are designing an alternative heating plate with increased contact surface with the MEA in hope of gaining an extra few degrees.

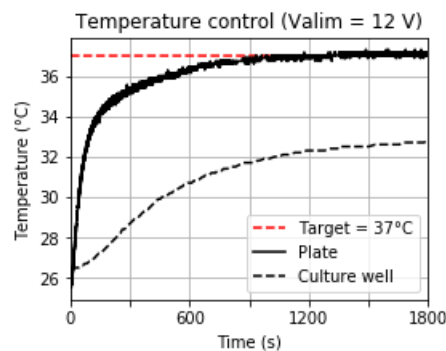


Fig. 7. Step response of temperature control during system startup at room temperature.

1.6 Experimental validation

The system was validated during an experiment where murine islets were recorded in a 60-electrode MEA with PEDOT electrodes. Of all the electrodes, 16 exhibited clear islet activity, consistent with is observed with the MCS system. Despite a lower signal-to-noise ratio recorded signals showed clear action potentials and slow potentials (showed in Fig. 8 below) perfectly exploitable by our detection algorithms, indicating that SYAM is indeed a viable replacement for MCS systems in our project.

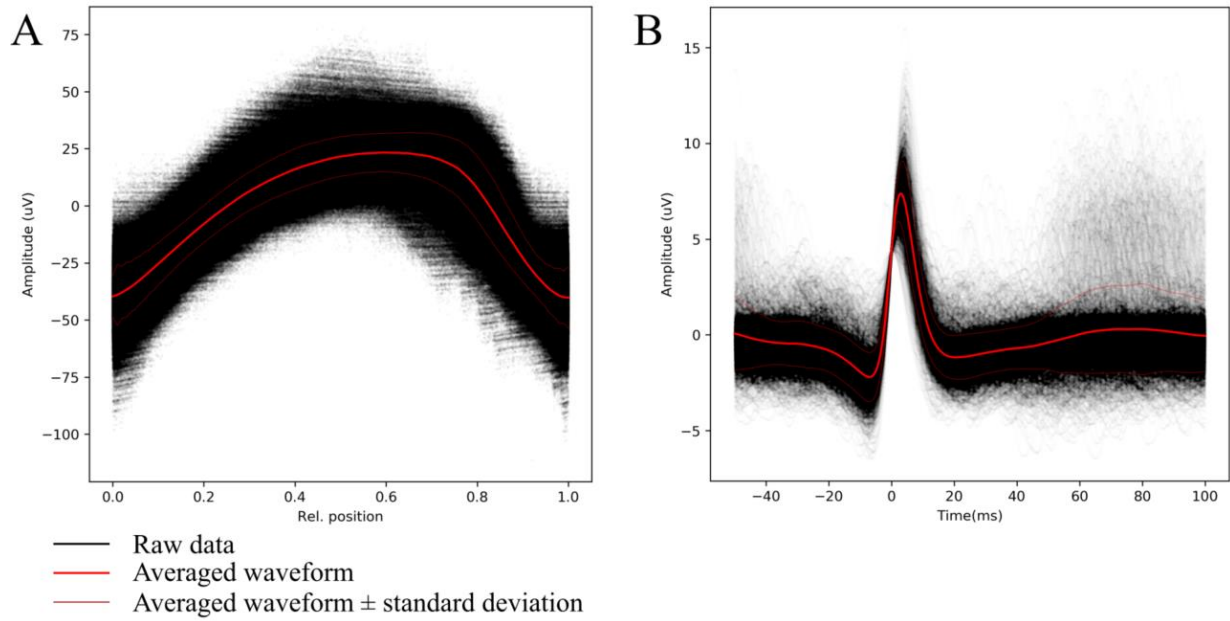


Fig. 8. Representative waveforms recorded with SYAM. Events were detected offline. **A.** Slow potential waveforms, normalized in time, superimposed, and averaged over 430 slow potentials from one electrode, at culture medium. Mean slow potential period was 1.40 ± 0.12 s. **B.** Action potential waveforms, superimposed and averaged over 2226 action potentials from one electrode, at culture medium.

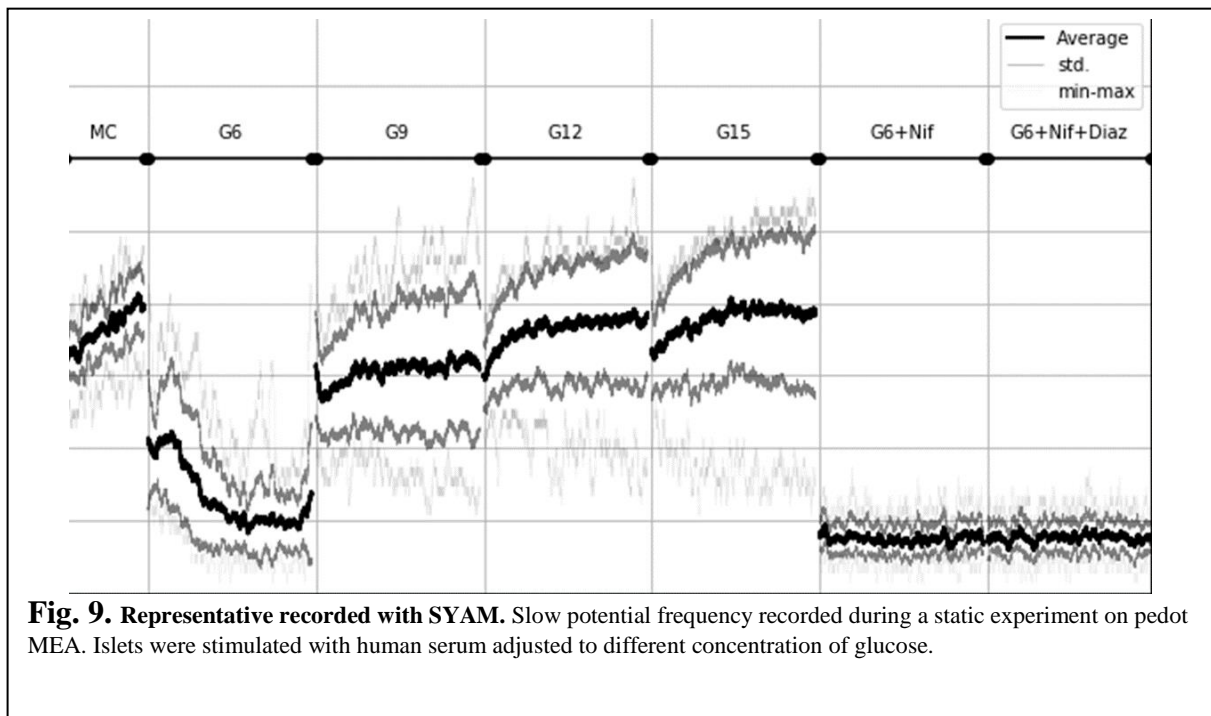


Fig. 9. Representative recorded with SYAM. Slow potential frequency recorded during a static experiment on pedot MEA. Islets were stimulated with human serum adjusted to different concentration of glucose.

II Signal processing

The hardware acquisition and processing system has been upgraded from the Multimed system [1] that was used for the preliminary results. Multimed is a system that is capable of acquiring and processing signals from various source materials, with a reconfigurable processing architecture taking advantage of an FPGA (Field Programmable Gate Array) chip. Recorded signals can then be displayed in real-time, stored, or utilized to generate feedback stimulation triggers. Overall, it may be used as a standalone analysis station for fundamental research or as a prototyping architecture for implantable prosthetics.

Multimed's architecture design is primarily motivated by the real-time constraint (processing multichannel data with low and reliable latency). This resulted in the implementation of two separate functional groups, as highlighted in Fig. **Erreur ! Source du renvoi introuvable.**, with different aims and different levels of constraint. One group is the processing chain, a sub-architecture responsible for critical real-time signal processing. It performs operations on input signals with fully pipelined or parallelized algorithms with predictable and reliable latency. The other is the interface group, which is responsible for managing configuration, recording, and display. It constitutes an environment that controls processing and distributes data between peripherals. It does not take part in signal processing, and consequently, it has a weaker time constraint. This flexibility in latency and refresh rate justifies the use of a softcore processor, which in turn, facilitates development.

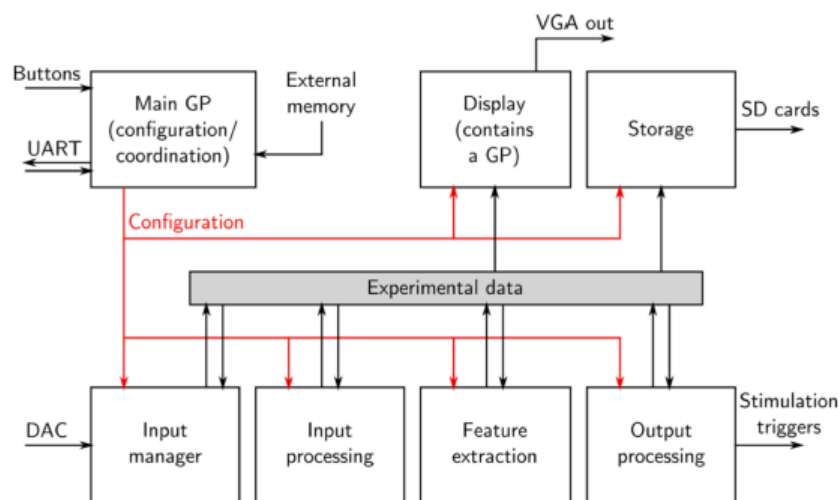


Fig. 10. High-level data flow of Multimed, as implemented in the FPGA. The generic processor (GP) is separate from the data processing chain and only helps as a means of communicating and configuring. All of the digital processing modules feed off the same data bus (Experimental data), minimizing dependencies and facilitating complex connections.

For the new version, we re-used the real-time processing architecture that proved to be relevant, but we updated the acquisition part. The upgrade decision is dictated for both technical and scientific reasons. First, a custom acquisition platform makes no more sense when the state of the art provides commercial analogue front-ends that fit our need. Secondly, using a maximum of commercially available boards in the system makes it both easier and cheaper to reproduce the experimental setup.

We chose to use the hardware front-ends from INTAN, both for their flexibility and the extensive documentation this company provides for its devices. Its RHD2xxx series contains acquisition devices capable of unipolar or bipolar amplification/measurements, and up to 128 input channels for unipolar inputs. The system currently uses the RHD2132 modules for amplification and digital acquisition which features 32 unipolar inputs and converts up to 1 Msamples/s with a 4 μ V quantum.

The system is still designed around a FPGA (Field Programmable Gate Array) which holds side devices control and hardware real-time computing (see Fig. **Erreur ! Source du renvoi introuvable.**). We choose a commercial board from Digilent for its large choice of extension modules (Pmods) which include SDcard sockets for data storage. Although the current design is based on a NEXYS-4-DDR board which features an Artix-100 FPGA (a student prototyping system), switching to much larger devices is possible as soon as needed thanks to the modularity of the system.

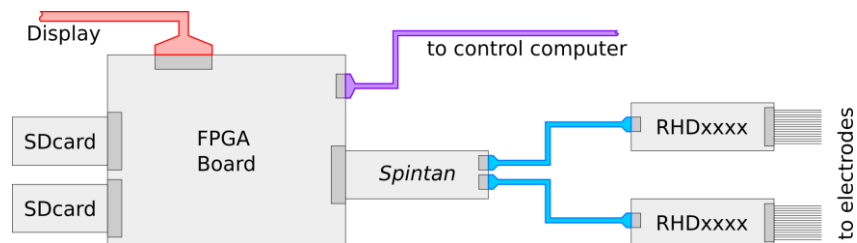


Fig. 11. Description of the electronic setup for the real-time acquisition and processing platform.

RHD2xxx series modules require specific LVDS (Low Voltage Differential Signals) wires for control and data retrieval. Although modern FPGAs can handle such standards, the way Pmod connectors are implemented on the board is not compatible. Therefore, we designed the *SPINTAN* board, a conversion board that switches connection standards from CMOS 3.3 V (the standard and robust way FPGA handle their inputs/outputs) to LVDS. This board requires one Pmod connector for FPGA connection and features two connectors for RHD2xxx control. It is therefore possible to acquire up to 256 unipolar inputs with a single *SPINTAN* board controlling two 128-channel RHD2xxx devices.

The only custom board is the *SPINTAN* board, shown in Fig. **Erreur ! Source du renvoi introuvable.** which is relatively simple and cheap, other board being commercially available. The full setup is simple to maintain and replicate. Most of the design time is focused on the FPGA configuration, the control software and the mechanical system.

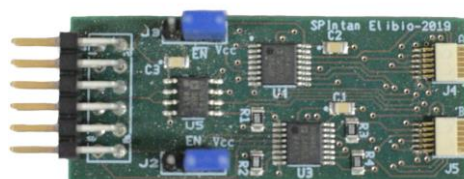


Fig. 2. Photograph of the SPINTAN board

- [1] A. Pirog *et al.*, "Multimed: An integrated, multi-application platform for the real-time recording and sub-millisecond processing of biosignals," *Sensors (Switzerland)*, vol. 18, no. 7, 2018.

Design of a simple microfluidic chip adapted to OECTs: Manuscript n°5

Recordings of electrical activity can be made with classical electrophysiology techniques using intracellular electrodes, such as the patch-clamp, which is a very powerful method for studying the unitary currents of particular channels. But it has several limitations that make it difficult to use and incompatible with the study of islets over long periods of time. These limitations can be overcome by using extracellular recordings, such as microelectrode arrays (MEAs). This type of recording does not damage the cells and allows them to be studied over long periods of time.

Flexible organic electronics are opening up new possibilities by improving extracellular recordings such as the organic electrochemical transistor (OECT). Their electronic/ionic conductivity allows richer electrical recordings and amplification of local signals with an excellent signal to noise ratio. They have already been used with neuronal and cardiac cells. Based on this observation, OECTs should therefore allow their use with other electrogenic cells with low amplitude signals, such as pancreatic β cells. Furthermore, these polymers can be printed on rigid or flexible substrates, which opens the way for their implementation in devices such as organ-on-chips. Another possibility is to make the OECTs specific to ion types, which would further improve the quality of the information collected by identifying the specific involvement in the signals of different channels. This line of research and development is being carried out in the laboratory within the framework of ANR Multispot funding to develop ion-sensitive polymer OECTs.

This OECTs approach has never been used for islets. OECTs are not industrialised and are "home-made". They are vertical OECTs that have never been tested with excitable cells. These OECTs have very good performance and show good amplification and quality of the recorded signals. However, the in-house production of these devices leads to heterogeneity between devices. The stability of the performance of OECTs over the long term and in contact with biological substrates is crucial to perform quantitative biological studies over several days. Indeed, in the literature, only short-term studies, of the order of a few milliseconds, showing

biological validity are present. The behaviour of excitable cells and their signals according to different electrical parameters (V_{DS} , V_{GS}) has never been fully studied to date. Finally, no commercial circuit for processing biological signals via OECTs is yet available.

In this manuscript, OECTs were first characterised in detail by studying their performance in several ranges of V_{DS} , V_{GS} , without cells, for several days and under different electrolyte conditions. Electronics specialists from the Material to System Integration (IMS) in Bordeaux developed a microelectronic board, intended for electrophysiological recordings, which converts and amplifies the IDS current of the OECT into an analysable potential.

The circuit was first validated with cardiac clonal cells (HL-1) having spontaneous electrical activity, with large amplitude action potentials and a very good signal-to-noise ratio. These studies on cardiac cells made it possible to test the stability of the biological preparation according to the electrical polarisation conditions of the vertical OECTs. In a second step, the electrical activity of the islets of Langerhans was recorded on the OECTs. These recordings showed slow potentials (SPs), and action potentials (APs). The frequency of APs and SPs is significantly increased at 11 mM high glucose compared to 3 mM low glucose.

Within this manuscript, my contribution has been the development of a PDMS microfluidic well adapted to the structure of OECTs, Figure 7, as well as the development of a protocol for aligning the microfluidic device to the OECTs, which do not allow alignment of the PDMS chip via oxygen plasma activation. I also developed an islet seeding protocol suitable for the use of microwells on transistors.

In conclusion, the laboratory developed microelectronic circuitry for monitoring electrical signals of excitable cells recorded by OECTs and carefully standardized electrical parameters. The heart cells allowed to validate the conversion circuit and to determine the parameters of detection of the signals with optimal signal/noise ratio.

In the perspective of my thesis project, this new approach by OECTs allows to consider alternatives to the costly use of MEAs while allowing a recording of the electrical activity of the islets with an optimal signal-to-noise ratio. The possibility of printing transistors on flexible materials also has multiple advantages in the development of a medical device such as the islet-based biosensor. Finally, this work opens the use of OECT for biomedical use beyond its original applications to biological systems of high amplitudes.

Vertical Organic Electrochemical Transistors and Electronics for Low Amplitude Micro-Organ Signals

Myriam Abarkan, Antoine Pirog, Donnie Mafilaza, Gaurav Pathak, Gilles N'Kaoua, Emilie Puginier, Rodney O'Connor, Matthieu Raoux, Mary J. Donahue, Sylvie Renaud, and Jochen Lang*


Electrical signals are fundamental to key biological events such as brain activity, heartbeat, or vital hormone secretion. Their capture and analysis provide insight into cell or organ physiology and a number of bioelectronic medical devices aim to improve signal acquisition. Organic electrochemical transistors (OECT) have proven their capacity to capture neuronal and cardiac signals with high fidelity and amplification. Vertical PEDOT:PSS-based OECTs (vOECTs) further enhance signal amplification and device density but have not been characterized in biological applications. An electronic board with individually tuneable transistor biases overcomes fabrication induced heterogeneity in device metrics and allows quantitative biological experiments. Careful exploration of vOECT electric parameters defines voltage biases compatible with reliable transistor function in biological experiments and provides useful maximal transconductance values without influencing cellular signal generation or propagation. This permits successful application in monitoring micro-organs of prime importance in diabetes, the endocrine pancreatic islets, which are known for their far smaller signal amplitudes as compared to neurons or heart cells. Moreover, vOECTs capture their single-cell action potentials and multicellular slow potentials reflecting micro-organ organizations as well as their modulation by the physiological stimulator glucose. This opens the possibility to use OECTs in new biomedical fields well beyond their classical applications.

1. Introduction

Electrical signals in cells and micro-organs provide the base for key biological events such as brain activity, heartbeat, or vital hormone secretion. Their capture allows not only crucial insight into physiological phenomena but also opens the possibility to develop diverse biosensors for continuous monitoring and consecutive therapy.^[1,2] Electrical signals are generated by single cells as action potentials and also by cell groups, regions, or micro-organs as field potentials in defined regions or micro-organs that can be recorded extracellularly.^[3] Concomitant multi-parametric analysis of these electrical signals not only provides insight into the activity of a given cell but also informs about higher organizational modes.^[4,5] Although extracellular recording configurations do not provide the same richness in information as intracellular recordings, this approach keeps the biological substrate intact, does not disturb metabolic events underlying or shaping electrical activity and permits long-term recordings necessary to understand physiological function and for the development of biosensors.

M. Abarkan, E. Puginier, M. Raoux, J. Lang
UMR CNRS 5248 (CBMN, Chemistry and Biology of Membranes)
Univ. Bordeaux
Av Geoffroy St Hilaire, Pessac F-33600, France
E-mail: jochen.lang@u-bordeaux.fr

A. Pirog, D. Mafilaza, G. N'Kaoua, S. Renaud
UMR CNRS 5218 (IMS, Integration of Materials into Systems)
Univ. Bordeaux
Bordeaux Institut National Polytechnique
351 Cours de la Libération, Talence F-33405, France
G. Pathak, R. O'Connor, M. J. Donahue
Department of Bioelectronics
Mines Saint Etienne
CMP-EMSE
MOC
Gardanne 13541, France
G. Pathak, M. J. Donahue
Linköping University
Department of Science and Technology (ITN)
Laboratory of Organic Electronics
Linköping SE-581 83, Sweden

 The ORCID identification number(s) for the author(s) of this article can be found under <https://doi.org/10.1002/advs.202105211>

© 2022 The Authors. Advanced Science published by Wiley-VCH GmbH. This is an open access article under the terms of the Creative Commons Attribution License, which permits use, distribution and reproduction in any medium, provided the original work is properly cited.

DOI: 10.1002/advs.202105211

Electrical signals offer several advantages as compared to other activity read-outs. Indeed, electrical signals are easier to analyze and quantify and moreover, in contrast to imaging, far higher sampling rates are feasible and optical probes are not required. This avoids problems such as the use of transgenics or organic molecules with inherent difficulties in their tissue or micro-organ penetrance and potential genetic bias as well as ensuring general applicability in human tissue. Fluorescence bleaching or heat generation is not an issue in recording electrical signals and all components are well suited for miniaturization.^[6] The signal to noise ratio (SNR), however, poses a major issue in electrical recordings. Although this may be less prominent in neurons or cardiomyocytes which are endowed with depolarizations of considerable amplitude, other vital cells of the body, such as endocrine cells, depolarize only to far smaller amplitudes.^[7] Coating metal electrodes with the conducting polymer poly(3,4-ethylenedioxythiophene) polystyrene sulfonate (PEDOT:PSS) offers some improvement in extracellular recordings, however the recording of biologically important small action potentials by MEAs remains difficult.^[5,8] Some transistor technologies offer an attractive means to address this problem as signals are amplified directly at the source by their intrinsic voltage-to-current conversion, thus reducing noise in contrast to classical metal electrodes.^[9] The recent developments in organic electrochemical transistors (OECTs) offer unprecedented versatility in terms of fabrication methods, sensor geometry, miniaturization, stability in aqueous environments, cell or tissue interaction, and low-cost printing.^[10] The geometry of the OECT itself also profoundly influences the behavior of the transistor and notably vertical OECTs (vOECT) exhibit very high transconductance as well as good cut-off frequencies.^[11,12] Moreover, the vOECT geometry favors device density, an important advantage in future miniaturization and development of high-density arrays for improved spatial resolution.

OECTs are promising tools for fundamental research and as components of biosensors or biomedical devices. Their remarkable characteristics have been used in the field of classical bioelectronics, that is, brain or heart recordings, to gain insight using EEG- or ECG-like configurations, and taking advantage of their favorable biocompatibility and form factor.^[13] Moreover, successful uses of OECTs have been reported for neural probes as well as in cellular recordings of cardiomyocytes, yet some important issues remain to be addressed.^[14–22] Long-term quantitative observations of living material rely on the assumption of operational stability of OECTs over a prolonged period of time. While physical stability has been reported previously this issue has often not been addressed quantitatively for prolonged polarized states with few exceptions.^[16,23–25] Moreover, the fabrication of OECT multichannel devices entails some variation between the probes, which have to be controlled or equalized. For example, this may be achieved via corresponding calibration of the electrical circuits to provide meaningful quantitative read-outs in long-term experiments. To account for transistor properties, a parameter extraction methodology is required. Finally, electrogenic cells generate signals of different amplitudes. Neurons or cardiomyocytes depolarize to considerably larger values (+40 mV) than endocrine cells, such as the islets (0 mV), required for nutrient homeostasis and a major player in diabetes.^[7,26,27] Here we demonstrate the possibility to fully exploit the potential of OECTs in fundamen-

tal research and potential biomedical applications through their use with micro-organs such as the islets, which are inherently far more difficult to monitor.

2. Results

2.1. Chip Geometry and Vertical OECT Electrical Performance

The vOECTs used here have source and drain gold contacts in different planes (**Figure 1**). This vertical configuration allows arranging a higher number of transistors in a given geometrical area, thus increasing the spatial resolution (**Figure 1A,B**). The maximal transconductance, g_{\max} , which defines amplification potency, is inversely related to channel length, which can be considerably reduced to sub-micrometer dimensions in the vertical arrangement.^[11,12] As shown in **Figure 1B**, our chip consisted of 12 vOECT channels and 12 electrodes on each side of the midline of the device (for details on electrodes, see **Figure S1**, Supporting Information). Steady-state characterization of the transistors was performed by measuring vOECT output and transfer characteristics (**Figure 1C,D**), demonstrating p-type characteristics with the expected excellent maximal transconductance g_{\max} of ≈ 20 mS as reported previously.^[12]

2.2. Electronic Board for Data Acquisition

Multichannel hardware is currently not commercially available to connect sensor devices, provide transistor voltage bias, and convert OECT drain currents into readable voltage signals. We therefore developed a custom board which also addresses variability among channel transconductances that may interfere with interpretation of analyzed biological signals. For this reason we included individually tunable drain–source voltage biases to gain homogeneity (**Figure 2A**). Adding a device specific connection board, which we termed ROKKAKU, allows adaptation to different OECT chip layouts, and fabrications schemes. The connection board matches the positions of all OECTs and electrodes present on a sensor device to record all signals simultaneously (**Figure 2B**).

Subsequently, a polarization and conversion board, named CHOSEI, allows the conversion of currents measured by the OECTs to voltages for further acquisition by conventional acquisition hardware (here INTAN) through means of a 560 Ω load resistor, as well as the adjustment of the drain–source polarization voltage for each OECT channel (**Figure 2B**, **Figure S2**, and **Table S1**, Supporting Information). An output connector with 24 pins on the board plugs connects the OECTs and electrodes to an INTAN recording system. Importantly, ROKKAKU/CHOSEI can be used for vOECT characterizations, stimulations, and electrophysiological recordings. Details of the setup and use in various experiments are given in **Figure S2** and **Table S1**, Supporting Information.

The output characteristics of the transistor were determined as shown in **Figure 2C**. The boards did not distort by saturation or non-linearity the observed drain current I_{DS} as a function of voltage V_{DS} for the tested gate voltages V_{GS} . To address channel-to-channel variations in performance and to permit a uniform V_{DS}

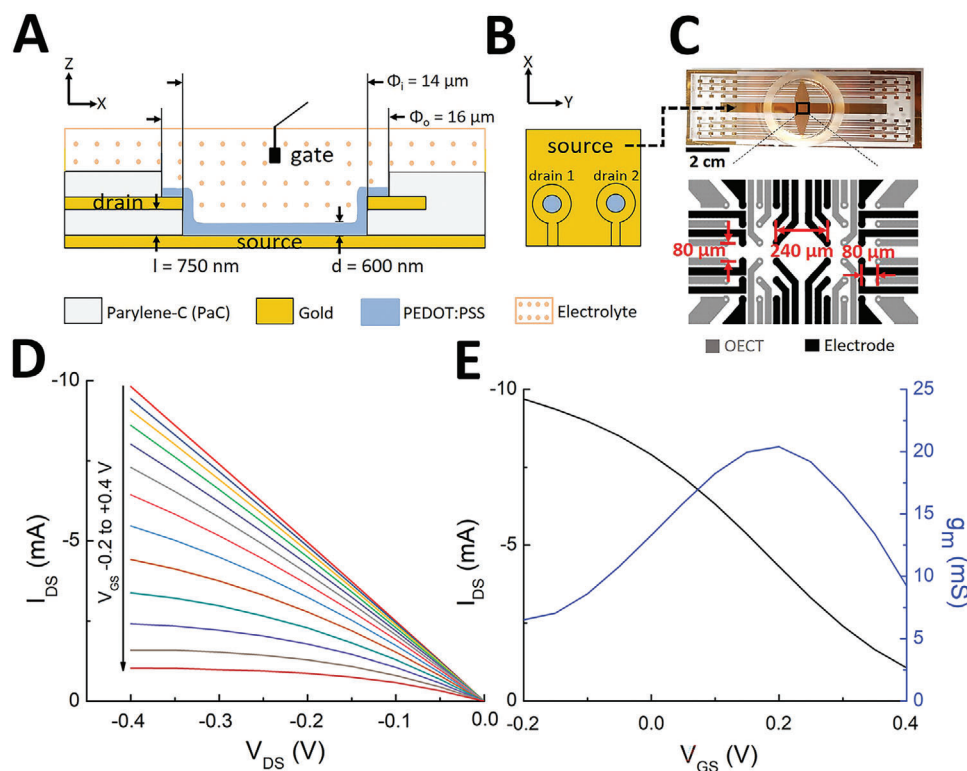


Figure 1. Structure and physical performance of vertical PEDOT:PSS OECT devices. A,B) Cross-sectional view (A) and top view (B) demonstrating the layout of the transistor with a common source but individual drains and the layers dimensions: l , the parylene-C layer thickness between drain and source contacts (750 nm); d , the PEDOT:PSS layer thickness (600 nm). Φ_i and Φ_o , inner well and outer well dimensions, respectively. An Ag/AgCl gate electrode inside the electrolyte solution is used for each experiment. C) Photograph of the device (scale bar: 2 cm) with the common source visible (see arrow) and layout showing 12 OECTs and 12 electrodes in each side of an OECT array as well as dimensions. D) Output characteristics of a vertical PEDOT:PSS transistor in physiological solution showing the drain current I_{DS} as a function of drain voltage V_{DS} ($= -0.4$ V) for gate voltages V_{GS} varying from -0.2 to 0.4 by 0.05 V steps. E) Transfer curve and resulting transconductance at $V_{DS} = -0.4$ V.

for all OECT channels on a given array, we adjusted the drain–source voltage bias of each OECT channel to the same V_{DS} via the CHOSEI potentiometers.

As shown in Figure 2D the application of a supply voltage common to all load resistors results in a considerable scattering of V_{DS} by $\approx 30\%$ between the extrema. In contrast, individualization of supply voltages by fine tuning with CHOSEI’s potentiometers biased every OECT at V_{DS} values that varied only by 5% (Figure 2D). A variation of 30% can substantially alter quantitative read-outs in terms of recorded cellular signals (for example see variation of $V_{DS} -0.1$ versus -0.2 V in Figure 5B). We also compared the noise of resistors of values equivalent to the drain–source junction of the vOECTs in the dry vOECTs or in the wet setup of vOECTs or electrodes seeded with HL-1 cells (Figure S3, Supporting Information). Thus, the board will provide truly comparable read-outs in terms of amplitude without adding additional noise and maximum sensitivity is not limited by transistor noise. Subsequently we tested our electronic setup by using simulated biological signals by imposing electric pulses via an electrode present on the chip and recording either via electrodes or via vOECT channels (Figure S4, Supporting Information). The output signals recorded with OECTs clearly have signal-to-noise ratios superior to those captured by electrodes.

2.3. Electrical Performances and Stability of the Vertical OECTs

In order to evaluate whether vOECTs can be used for cell or micro-organ recording and we measured the electrical performances in KCl solution, physiological buffered salt solution as well as culture medium containing serum, without or with coating of devices with extracellular matrix that improves cell adhesion. The vOECTs were stable for up to 10 days during these short-term measurements at V_{GS} from -0.2 to 0.4 V (Figure S5, Supporting Information).

Meaningful biological experiments require recordings over hours at least, so we consequently evaluated the stability of the vOECTs for consecutive measurements comparing ranges of bias voltages and maintain drain–source polarization in between measurements (Figure 3 and Figure S5, Supporting Information). The transfer curve and the transconductance at $V_{DS} -0.4$ V, for V_{GS} varying from -0.2 to 0.6 V are considerably decreased during a second measurement after 10 min constant bias at $V_{DS} = 0.4$ V (Figure 3A), as compared to a narrower range of V_{GS} varying only from -0.2 to 0.4 V (Figure 3B). However, using a longer active time range of 4 h, electrical performances for V_{GS} varying from -0.2 to 0.4 V were also decreased and full stability was attained only when V_{GS} variation were reduced to 0 to 0.2 V (Figure 3C,D).

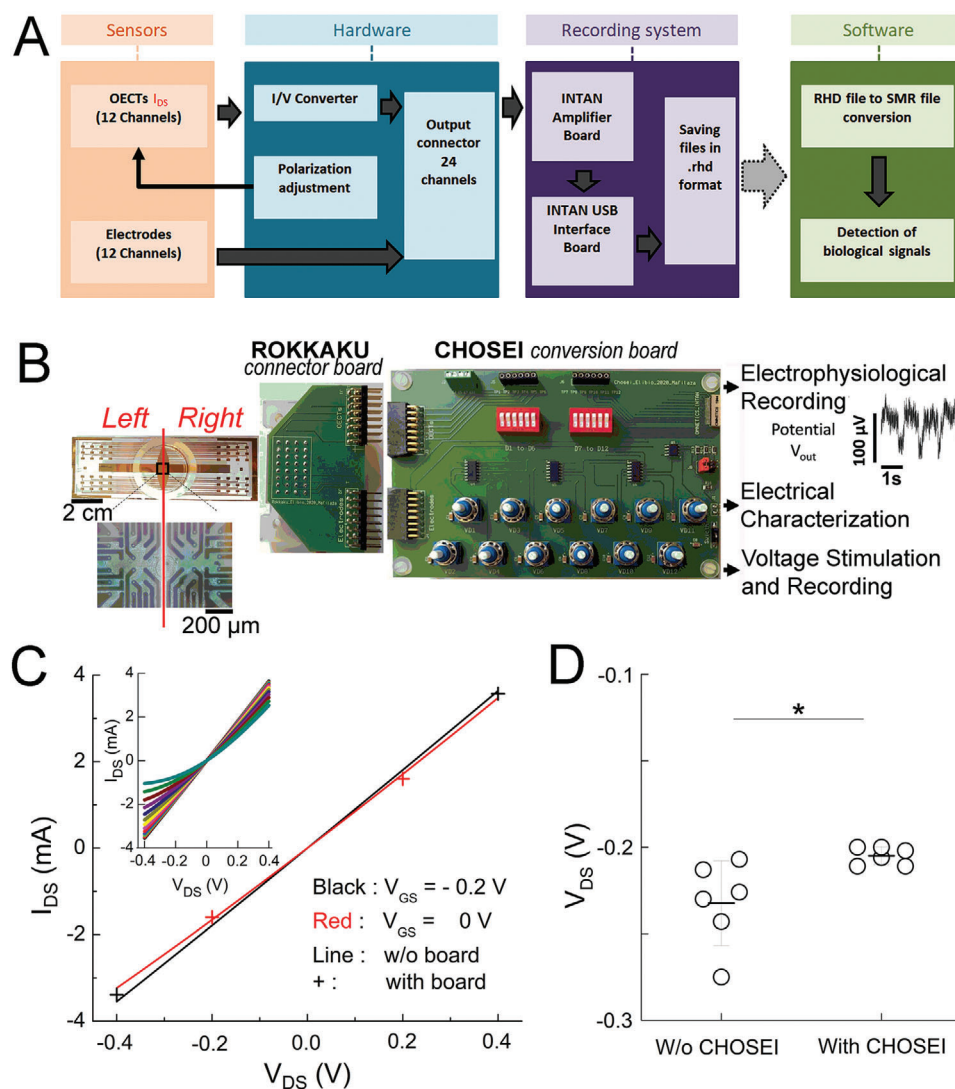


Figure 2. Electronic board for data acquisition. A) Block diagram of the acquisition process and data flow. The designed hardware connects the sensor device, allows voltage bias application to the transistors, adjusts the drain-source voltage bias, and performs the conversion of drain currents from the OECTs into voltage signals. Recording files, saved in INTAN format (.rhd) are converted to Spike2 format (.smr) for analysis. B) Working setup for recording: system hardware components and their connections to record 24 OECT channels simultaneously. The device-specific connector board ROKKAKU connects all OECTs and electrodes to the CHOSEI board which permits coarse and fine tuning of the drain-source voltage bias for each channel and converts I_{DS} to an analyzable voltage signal. C) Output characteristics of the board with the transistor drain current, I_{DS} as a function of negative and positive drain voltage, V_{DS} ($= -0.4$ and 0.4 V) for a gate voltage, V_{GS} ($= -0.2$ and 0 V). Inset: output characteristics of the transistor with the drain current, I_{DS} as a function of negative and positive drain voltage, V_{DS} , for a gate voltage, V_{GS} from -0.2 to 0.4 V. V_{DS} corresponds to the value indicated by the Agilent voltmeter (Figure S2E, Supporting Information) and was obtained by common coarse tuning (via the J8 jumper), then individualized fine tuning via the corresponding potentiometers connected individually to each of the load resistors until the desired V_{DS} was obtained. D) Drain-source voltage bias (here set to $V_{DS} = -0.2$ V) of OECT channels with or without adjustment by CHOSEI. Means \pm SEM; Mann-Whitney test; $*2p < 0.05$; $N = 6$.

Subsequently we used this gate range to evaluate vOECTs with cells for stability. For these experiments we employed first the established cardiomyocyte-like cell line HL-1 as a model since OECT recordings with such cell types have been published previously.^[16–18,28,29] Moreover, these atrial cardiac muscle-derived HL-1 cells are well known to maintain the cardiac-specific phenotype and action potentials during the culture period.^[30] The vOECTs used in this series of experiments were characterized before cell seeding, during culture of HL-1 cells on the chip,

and after removal of cells. To evaluate the uniformity of maximal transconductance g_m , all channels of an array were measured (Figure 4). The g_m for all vOECT channels was stable and amounted to ≈ 20 mS before cell culture, that is, in the presence of physiological buffered salt solution. Culturing the HL-1 cells for 6 days led to a uniform reduction of g_m to ≈ 10 mS. We attribute these changes to the adherent confluent layer of cardiomyocytes, which introduce an additional resistance in the electrical circuit and impede the diffusion of ions.^[31–34] The observed reduction persisted

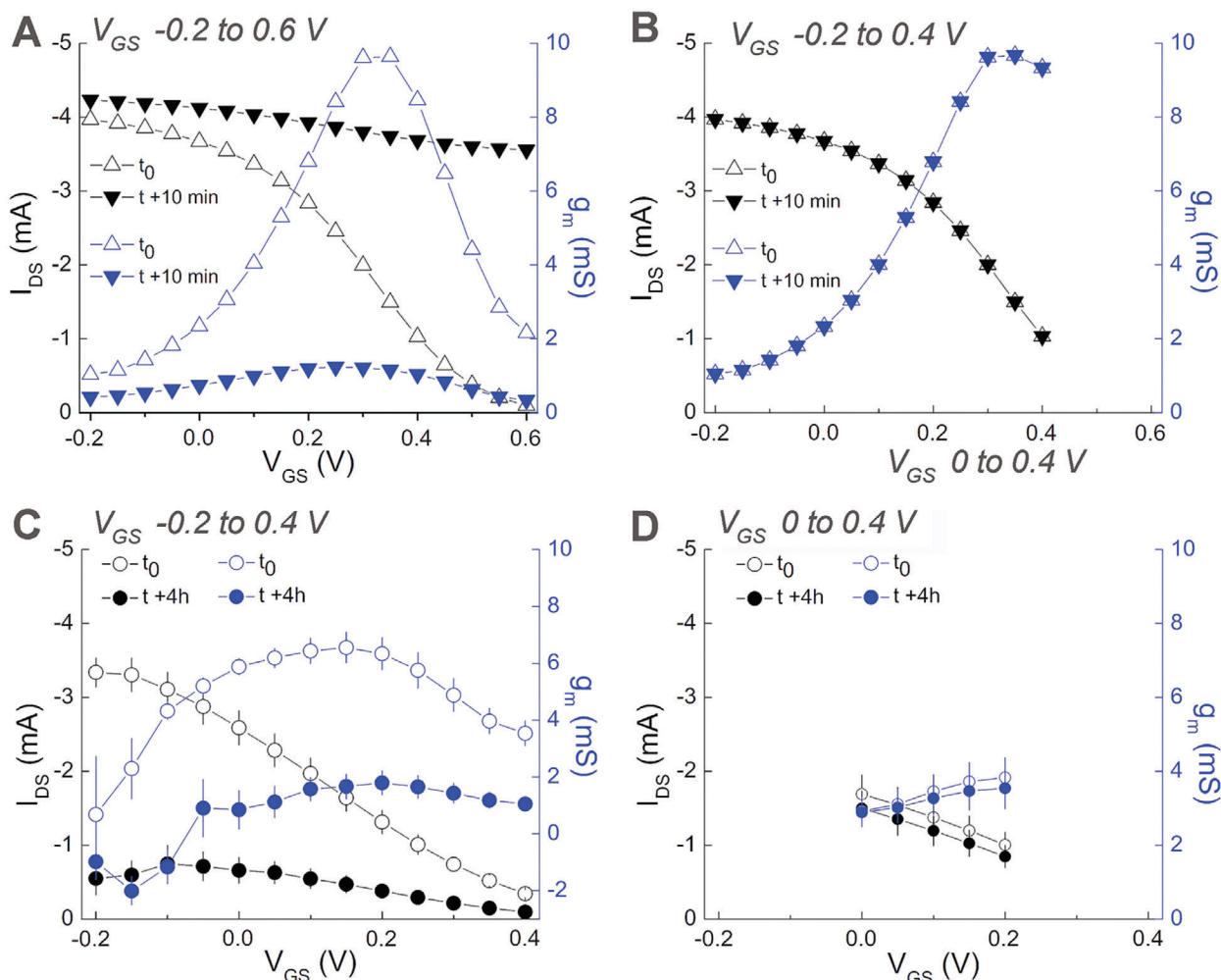


Figure 3. Influence of voltage bias on the stability of vertical OECTs performances in physiological buffered salt solution. A) Transfer curves and resulting transconductances for two consecutive measurements at $V_{DS} = -0.4$ V, for V_{GS} varying from -0.2 to 0.6 at 0.05 V steps. Measurements were separated by 10 min pause under constant $V_{DS} = -0.4$ V. B) Analogous conditions same as (A) but V_{GS} varying from -0.2 to 0.4 V. C) Analogous conditions as in (A) but varying V_{GS} from -0.2 to 0.4 V and measurements after 4 h of constant polarization. D) Same as in (A) but varying V_{GS} only from 0 to 0.2 V at t_0 (initial measurement) or after 4 h of constant polarization. $N = 6$, means + SEM. Experimental details see also Figure S5, Supporting Information.

after the removal of cells, probably due to the known presence of residual proteins (Figure 4A–D).

As g_m does not change between culturing cells and after removal, vOECTs can be reused if specific electrical conditions are applied, as permitted by the electric board described above. The impedance of each OECT channel before recording (with and without cells) and after recording experiments (Figure 4E) was in line with differences introduced by characterization in the absence of cells, some decrease in performance in the presence of cell layers, and some deterioration due to usage. Note that cell density does not change during the short experiment time.

2.4. Monitoring Electrical Activity of HL-1 Cardiomyocytes

To investigate the stability of the biological preparation on the array along with various voltage biases, cardiac cells were used first. The action potentials were measured after 6 days of cul-

ture on vOECTs to ensure spontaneous electrical activity. Transfer curves and the resulting transconductance values of vOECTs covered with HL-1 cells indicated $g_{m, max}$ at $V_{GS} = 0.2$ V, which increased from $V_{DS} = -0.1$ to -0.3 V (Figure 5A). We gradually tested these different ranges of polarization with increasing/decreasing sweeps of V_{GS} from 0 to 0.2 V and representative traces are given in Figure 5B. At $V_{DS} = -0.3$ V and, $V_{GS} = 0.2$ V signals from HL-1 cells were lost and the confluent cell layer was disrupted. We believe that this occurred subsequent to damage of the vOECT above $V_{DS} = -0.3$ V/ $V_{GS} = 0.1$ V as upon return to $V_{DS} = -0.3$ V/ $V_{GS} = 0.0$ V only large noise was recorded which is not consistent with loss of vOECT-cell contact only. To reliably extract action potentials, filters were chosen by parametric analysis. The detection of action potentials by vOECTs or electrodes was robust over a large range of the adaptive threshold σ with a high-pass filter of 10 Hz and low pass filter of 100 Hz (Figure S7A,B, Supporting Information). As cardiomyocyte action potentials are regularly spaced in time, we could also evaluate their frequency from the inter-

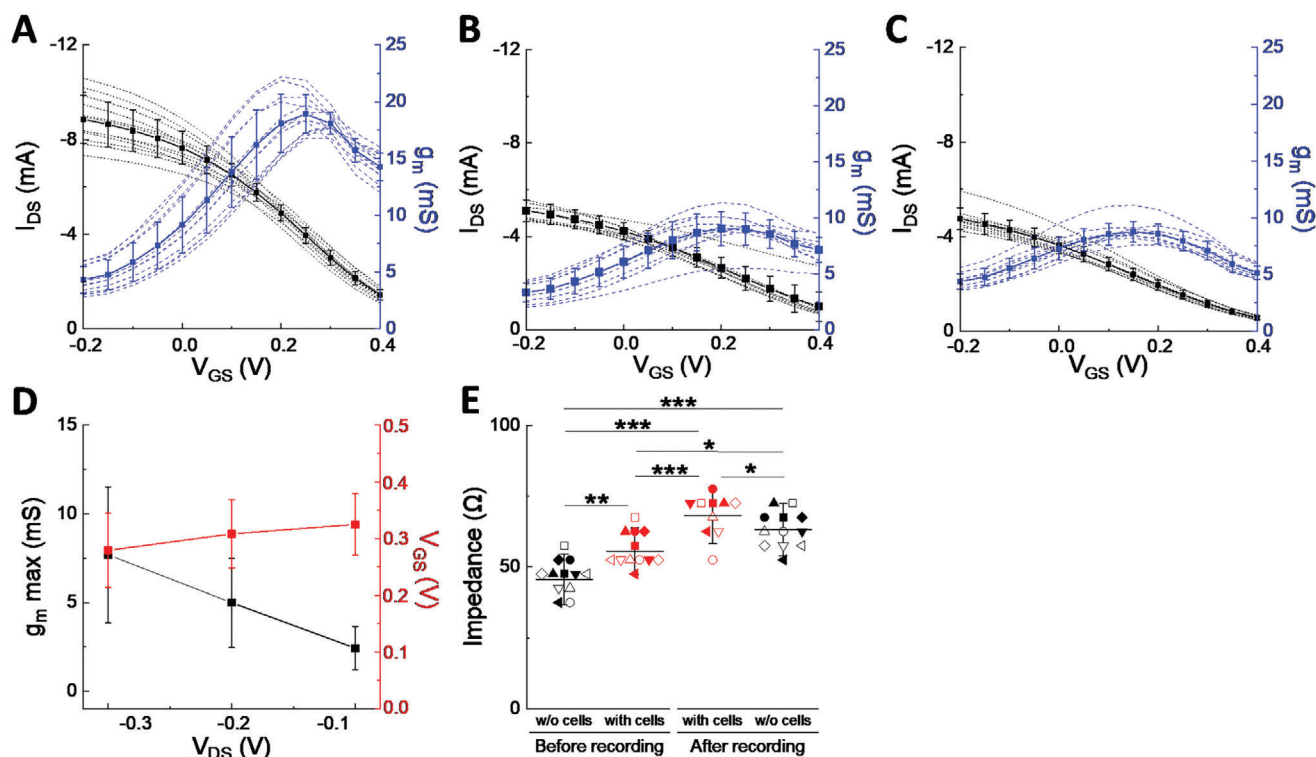


Figure 4. Performance and Stability of vertical OECTs before, during, and after culture of HL-1 cardiomyocytes. A) Transfer curve and resulting transconductance at V_{DS} 0.4 V, for V_{GS} varying from -0.2 to 0.4 V in physiological buffered salt solution before seeding cells on the vOECTs array, $N = 12$. B) In culture medium with HL-1 cardiomyocytes seeded on vOECTs array, $N = 10$. C) In physiological buffered salt solution after removal of HL-1 cardiomyocytes, $N = 10$. D) Summary plot of different imposed drain voltages on g_m max and V_{GS} with HL-1 cells in culture medium on OECTs array, $N = 10$. E) Impedance of vOECTs without cells (in physiological buffered salt solution) and with cells (in culture medium) before electrophysiological recordings and afterwards first with cells attached and then after removal of cells. $N = 10$ – 12 . Given are means \pm SEM; ANOVA and Tukey's post-hoc analysis; * $2p < 0.05$, ** $2p < 0.01$, *** $2p < 0.001$.

spike interval (ISI) by identifying a Gaussian distribution (Figure S7C,D, Supporting Information). The shape and amplitude of action potentials under the different electric conditions is given in Figure 5C and although obviously their amplitude differed, kinetics remained comparable. The mean shape of action potentials at $V_{DS} -0.2$ V and $V_{GS} 0.2$ V (Figure 5D) represents the precise inverse of action potentials captured by electrodes on the same chip.

As cardiomyocyte action potentials are regularly spaced in time, we could also evaluate their frequency from the interspike interval (ISI) by identifying a Gaussian distribution (Figure S7C,D, Supporting Information). The shape and amplitude of action potential under the different electric conditions is given in Figure 5C and although obviously their amplitude differed, kinetics remained comparable. The mean shape of action potentials at $V_{DS} -0.2$ V and $V_{GS} 0.2$ V (Figure 5D) represents the precise inverse of action potentials captured by electrodes on the same chip.

Electrophysiological signals are measured by OECTs as current fluctuations (I_{DS}) which are in turn converted to a potential using our developed electronic boards, whereas electrodes directly sense the potential. In this series of experiments, the SNR of HL-1 APs is between 3 and 6 at optimal conditions (Figure 5E). Importantly, the frequency of action potentials (≈ 1 Hz) did not change during the different electrical conditions (Figure 5E), whereas the amplitude was clearly most prominent at $V_{DS} -0.2$ V and $V_{GS} 0.2$ V and changed according to maximal transduc-

tance (Figure 5B,E). Note that values for $V_{GS} -0.3$ V are only given up to $V_{DS} 0.1$ V due to transistor breakdown (see Figure 5B). Comparison to electrodes on the same devices indicated similar SNR for PEDOT-covered electrodes, whereas mean amplitudes were clearly lower (Figure 5F). The signal shape of action potentials is determined by the different expression levels of several ion channels in the cell membrane and the apparent signal amplitude is mainly influenced through the cell coverage by the sensor and the cell/sensor resistance. Stability in action potential shape and frequency strongly indicate that the electrical parameters used here do not influence the biological behavior of the cells. Finally, we evaluated the propagation of action potentials across the vOECT channels on the chip. The maps show a stable direction of action potential propagation at $V_{DS} -0.2$ (Figure 5G) or -0.1 V and $V_{DS} -0.3$ V (Figure S5E, Supporting Information) before cell and/or vOECT damage occurred in the latter condition. We also observed a well-known rhythmicity of action potentials as well as their sensitivity to nor-epinephrine and the calcium channel blocker nifedipine (Figure S8, Supporting Information).

2.5. Monitoring the Activity of Endocrine Pancreatic Islets

After validating our electronic board and establishing the stable drain-source and gate-source voltage bias region, we addressed

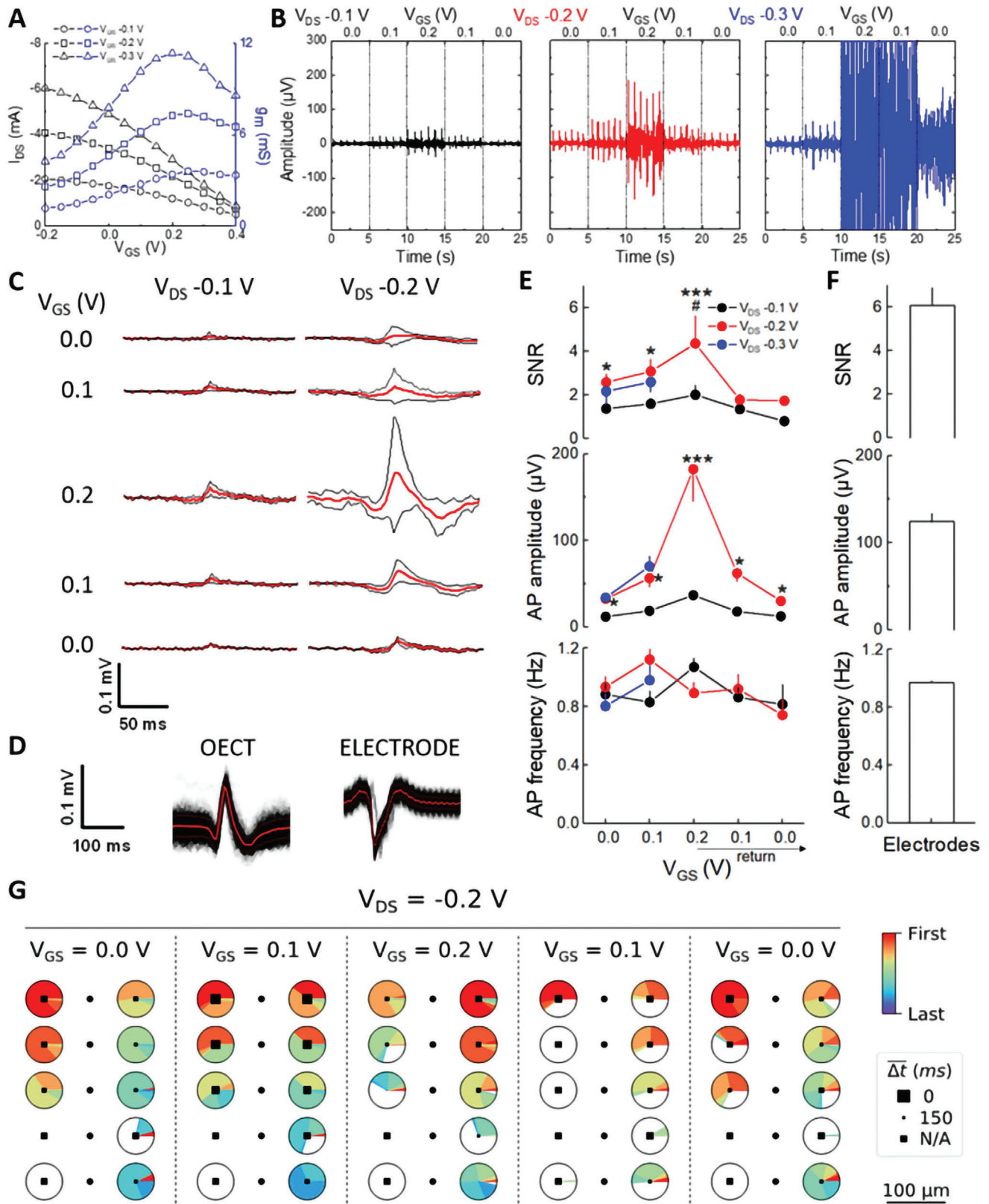


Figure 5. Recording of HL-1 cardiomyocytes with vOECTs. A) Transfer curves and resulting transconductances of OECTs array covered with HL-1 cells at V_{DS} and V_{GS} values used for recording of action potentials. B) Recorded spontaneous action potential at different V_{DS} and a sweep of V_{GS} . 5 s of 15 min recordings per condition are shown. At $V_{DS} = -0.3$ V, $V_{GS} = 0.2$ V damage to HL-1 cell layers was observed. C) Shapes of action potentials observed

the recording of a more difficult biological sample on vOECTs, that is, pancreatic islets. These primary micro-organs are non-proliferating and known for action potentials of far smaller amplitude than cardiomyocytes and as a primary micro-organ they are more demanding in terms of culture in contrast to cell lines. The characteristics of vOECTs before, during, and after culture were comparable to what was observed for clonal HL-1 cells (Figure 6A,B).

To test physiological function, islets on vOECTs were exposed to either 3 mM glucose, at which the main type of islet cells, that is, β -cells, are known to remain rather inactive, or to 11 mM glucose where the intracellular metabolism of the sugar leads to β -cell depolarization and secretion of the hypoglycemic hormone insulin.^[5,35] Interestingly, dispersed islet cell clusters of these micro-organs exhibit two types of electrical signals similar to neurons, action potentials generated by any single islet cells and so-called slow-potentials, a spatial summation of coordinated β -cell activity and coupling.^[36,37] Using a bias of $V_{DS} - 0.1 \text{ V}/V_{GS} 0.2 \text{ V}$ detected APs were well detected, whereas SPs were apparent upon inspection of traces but could not reliably be extracted (Figure S10A, Supporting Information). Action potentials were absent at low glucose (3 mM), but appeared at high glucose stimulation (11 mM) and similar to HL-1 cell recordings, only action potential amplitude but not action potential frequency was altered by applying different biases (Figure S10B, Supporting Information). This suggests again that a change in biases alters the transconductance but does not alter the behavior of the cells. Observed frequencies were in line with previously published frequencies recorded with micro-electrode arrays.^[5,8] Using a bias of $V_{DS} - 0.2 \text{ V}/V_{GS} 0.1 \text{ V}$, we observed both APs and SPs (Figure 6C) and high pass filter of 0.2 Hz and low pass filter of 4 Hz (4th order) can be used under this voltage bias to detect and extract robustly these SPs (Figure S11, Supporting Information).

We have also determined the mean shape of APs and SPs. APs were of ≈ 100 ms duration, similar as described for MEAs, and SPs were as expected of much longer duration. However, the mean AP amplitude on vOECTs was 69 μV , whereas only 12 μV has been published for islet recordings via MEAs.^[5] Both, APs and SPs, were glucose-dependent and faithfully reflect nutrient-induced islet activation (Figure 6E,F). Note that only AP frequency but not amplitude increased at stimulatory glucose levels, as can be expected from a unitary signal. In contrast, in the case of SPs both, frequency and amplitude, increased as the latter reflects electrical coupling between single β -cells, a hallmark in the change of micro-organ organization at stimulatory glucose levels.^[5,36]

In order to investigate intact islet micro-organs as well, we set up a simple microfluidic device on the OECTs to reduce liquid volumes and ensure sufficient channel coverage (Figure 7B,C). A

change from culture medium, containing 11 mM glucose, to electrophysiological buffer with 3 mM glucose, lead to a rapid drop in activity (Figure 7A,D). Subsequent exposure to 8, 11, and 15 mM glucose increased AP and SP frequencies in a dose dependent manner, whereas their amplitude remained stable as expected for unitary signals (Figure 7D–F). The increase in electrical activity was mirrored by increased insulin secretion. In contrast, the non-metabolizable sugar 3-O-methyl-glucose or mannitol did not elicit any electrical response excluding potential osmotic effects and underscoring the specificity of the recordings.

3. Discussion

Extracellular recordings of cells or organs have considerably enriched our knowledge about their function as single units or in networks. They have provided important operational medical devices and have considerable further potential for future applications.^[2] Within this field, organic bioelectronics are especially promising in view of their potential chemical variabilities, tuneable physicochemical characteristics, mixed conducting properties, and plasticity in form factors.^[10] Variations in OECT geometry, such as vertical OECTs, provide significant improvements in general transistor characteristics useful for biological signal acquisition.^[12] Our study demonstrates now for the first time the use of these vertical PEDOT:PSS-based OECTs (vOECT) as biosensors to perform recordings of cells and micro-organs. In our goal to provide physiologically meaningful quantitative recordings our main findings include: i) electronic means and characterization methodology to overcome unavoidable imperfections in the device production process; ii) carefully chosen polarization protocols under biological conditions; iii) the recording and extraction of uni- and multicellular events in a micro-organ, the endocrine pancreatic islets, with far smaller signal amplitudes than those recorded previously.

vOECTs are known for their high transconductance exceeding those of planar devices by about a factor of 5, while simultaneously reducing the spatial footprint.^[12] The sub-micrometric size of the channel may increase the risk of electric breakdown, however, and voltage biases had to be carefully adapted. Note that often reported physical characterization parameters are obtained during short (seconds) biasing. In contrast, physiologically meaningful recordings may span continuously from minutes to hours, such as during nutrient stimulation of pancreatic islets in-vitro, mimicking the effects of a meal and the postprandial period.^[5] To obtain reliable vOECT function we had to carefully titrate the conditions in different settings and to use electrical parameters clearly below the optimal biasing regime for maximum transconductance. Moreover, a culture of cells on vOECT arrays reduced their performance by introducing an addi-

at conditions given in the left and middle panel of (B). Means, red lines; standard deviations, black; $n = 8$ channels. D) Comparison of extracted mean configuration of HL-1 action potentials observed by vOECTs ($V_{DS} - 0.2 \text{ V}$, $V_{GS} 0.2 \text{ V}$; $n = 253$ AP) versus electrodes (MEA; $n = 314$ AP); red, means; black, standard deviations. For filters used, see Figure S7, Supporting Information. E) Top panel: SNRs of conditions used in (B) to (D). Middle panel: Action potential amplitudes of HL-1 cells evolved at different V_{DS}/V_{GS} with a maximum at $V_{DS} - 0.2 \text{ V}$, $V_{GS} 0.2 \text{ V}$. Lower panel: Action potential frequency of HL-1 cells at different V_{DS}/V_{GS} remained stable. Means \pm SEM; ANOVA, Tukey's analysis; $V_{DS} - 0.2 \text{ V}$ versus $V_{DS} - 0.1 \text{ V}$, * $2p < 0.05$, *** $2p < 0.001$; $V_{GS} 0.2 \text{ V}$ versus other V_{GS} at same V_{DS} , # $2p < 0.05$; $N = 8$. F) Analysis of recordings via electrodes on the same devices, $N = 3$. G) Analysis of action potential propagation across the vOECT chip at $V_{DS} - 0.2$ and indicated V_{GS} sweep. The pie charts indicate the relative occurrence of being first or last action potential in a series of events (color code at the right). The size of solid squares in the pie chart indicates the mean time delay of the action potentials.

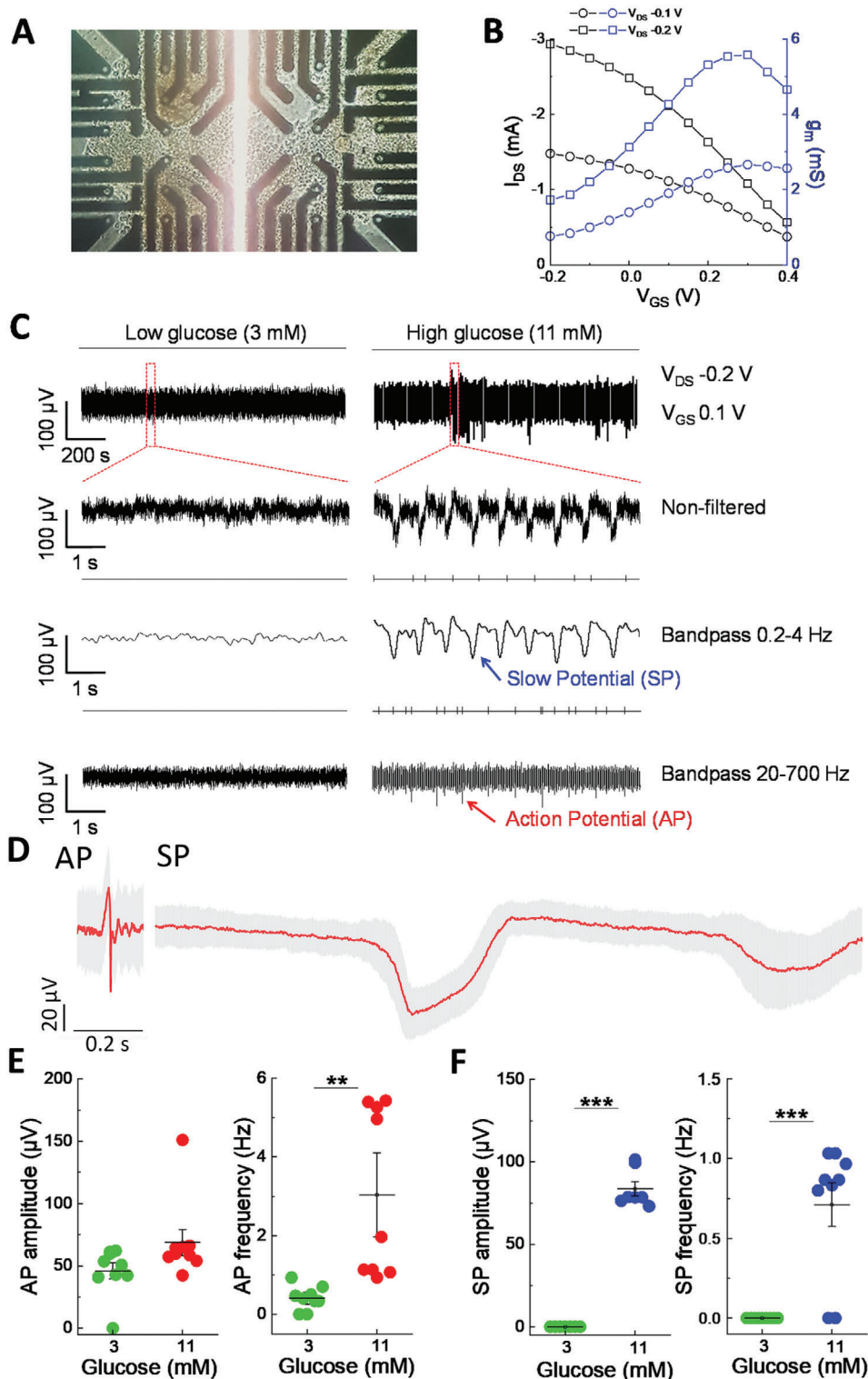


Figure 6. Recording of endocrine islet cells on vOECTs. A) vOECT Array with pancreatic islet cell clusters. B) Transfer and transconductance curves at $V_{DS} -0.1$ and -0.2 V at $V_{GS} -0.2$ to 0.4 V of vOECTs with islets in culture medium. C) Representative raw and filtered recordings of islets at low glucose (non-stimulatory, 3 mM) and high glucose (stimulatory, 11 mM) in physiological buffered ion solution at $V_{DS} -0.2$ V and $V_{GS} 0.1$ V. The different time scales are shown as well as non-filtered and band pass filtered traces (0.2–4 Hz, 20–700 Hz). The presence of slow potentials reflecting islet β -cell coupling are indicated. D) Average AP and SP at 15 mM glucose ($V_{DS} -0.2$ V, $V_{GS} 0.1$ V; mean in red and SEM in gray; AP mean amplitude 69 μ V, $n = 303$; SP mean amplitude 110 μ V, $n = 141$). E,F) Action potential and slow potential amplitudes and frequencies at low glucose and high glucose stimulation ($V_{DS} -0.2$ V, $V_{GS} 0.1$ V). Means \pm SEM; paired t -test; $**2p < 0.01$, $***2p < 0.001$; $N = 9$.

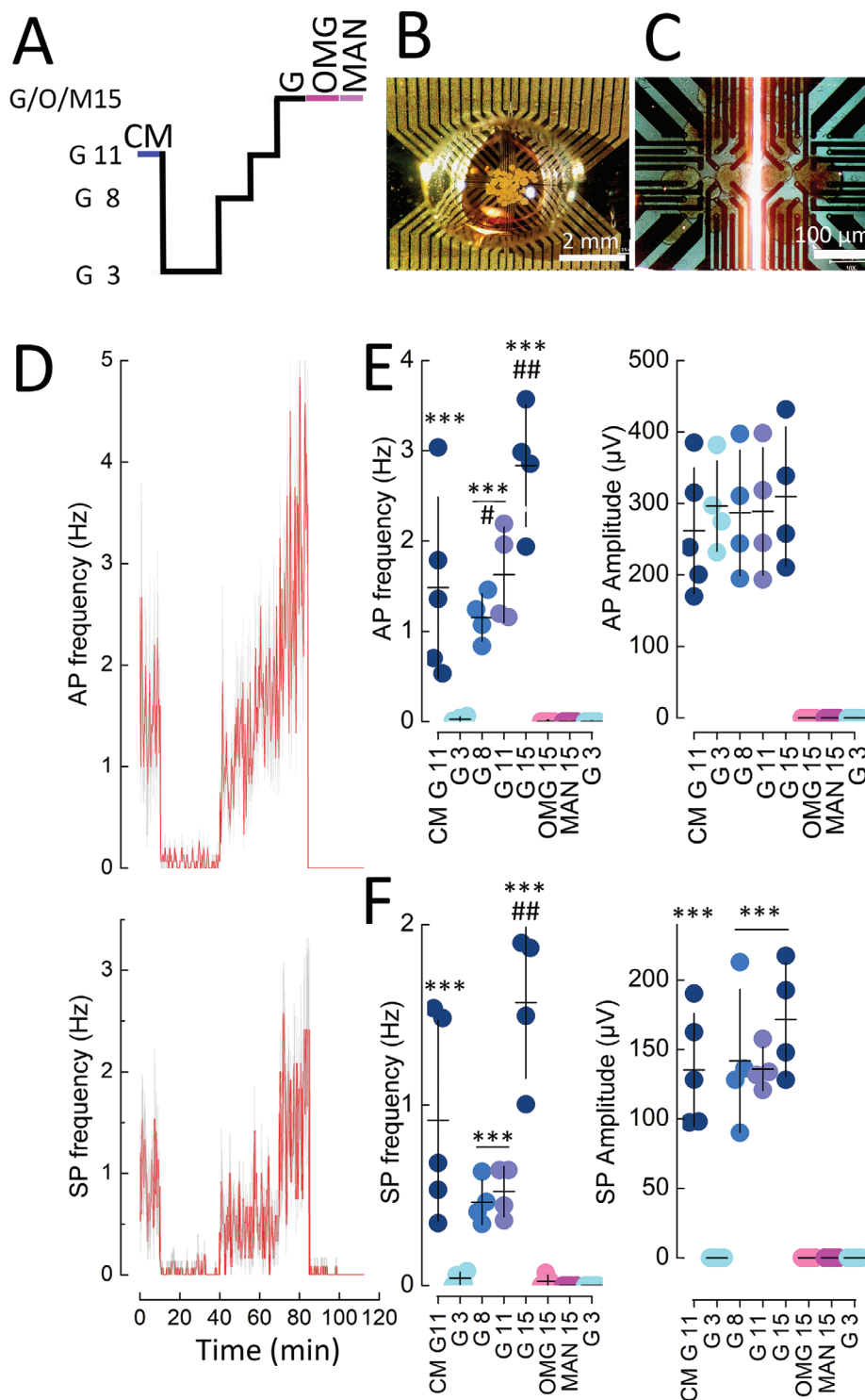


Figure 7. Recording of islet micro-organs on vOECTs at different glucose concentrations and in the presence of non-metabolizable sugars. A) Stimulation protocol with 3, 8, 11, or 15 mm glucose (G), in the presence of culture medium (CM; containing 11 mm glucose and amino acids) or in the presence of non-metabolizable 15 mm 3-ortho-methylglucose (OMG) or 15 mm mannitol (MAN). B) View of islets seeded on vOECTs in a PDMS microfluidic well. C) Enlarged view of islets on vOECTs just prior to recording. D) Time course of action potential (AP) and slow potential (SP) frequencies during the stimulation protocol given in (A). Means in red, SEM in grey. E) Mean action potential frequencies and amplitudes during the indicated conditions. F) Mean slow potential frequencies and amplitudes during the indicated conditions. In (E) and (F) means (horizontal bar) and SEM (vertical bars) are indicated. Tukey post-hoc test; *** $2p < 0.001$ versus G3, ## $2p < 0.01$ versus G11 or G8. #, $2p < 0.05$ versus G8. Glucose concentrations (G3–G15) and electrical activity were highly correlated (frequencies AP, $r^2 = 0.9852$, $p = 0.004$; frequencies SP, $r^2 = 0.8528$, $p = 0.03$). Insulin secretion raised from 0.91 ± 0.19 ng/mL/15 min at G3 to 11.04 ± 0.18 ng/mL/15 min at G8 ($2p < 0.001$).

tional resistive layer. This effect persisted even after cell removal, probably due to the shedding of extracellular matrices. However, even under those considerations, the maximum transconductance was still superior to those reported for planar OECTs in cellular applications.^[14–20] Note also that most reports on transconductances for planar OECTs used in cellular studies have not addressed this issue and it is often not always clear whether reported values correspond to characterizations in the absence or presence of cells, or the extent and duration of previous polarizations. Our exploration of these issues stresses the importance of carefully controlling those parameters in order to obtain quantitatively reliable data over the entire recording period. In the same respect, homogeneity of electrical bias is equally important for biological recordings as small differences in performance between OECT channels may result in different amplification of the signal of interest; this leads to errors in the determination of frequencies due to missing events and errors in the comparison of amplitudes. Detailed and quantitative electrophysiological work on cell signalling and activity using OECTs is still missing despite the multiple demonstrations of their potential usefulness. According to previous studies the maximal transconductance g_{max} may vary within an OECT chip by a factor of 1.2 to 5 and often this source of error in biological recordings has not been reported.^[17–18,22] Clearly the development of tuneable boards here has resolved a bottleneck.

The vOECT geometry makes them especially suitable for the future generation of high-density electrophysiological probes where each probe matches a single cell to obtain crucial spatial information.^[38,39] Note that so-called high-density MEAs consist essentially of a multiplication of electrodes and thus recordable surface but not a substantial improvement of spatial resolution. Obviously, such a setup will only be meaningful if homogeneity of maximal transconductances will either be ensured during production, which most likely presents a major challenge, or if they will be correctly tuned prior to experiments as in our case.

Interfacing biological substrate and organic materials constitutes another important issue in obtaining reliable data. The physicochemical properties of organic polymer transistors are highly favorable for interaction with living cells and organs in terms of tissue reactions and damage.^[13,40] Indeed, PEDOT:PSS has also been proven innocuous in tests on insulin-secreting cells.^[41] In addition, transient influences of the electrically biased polymer on cell activity have to be ruled out. Interestingly, when using different electric biases we did not observe any change in frequency or signal propagation of the biological signals in excitable cells such as cardiomyocytes or islet cells. In contrast, recorded signal amplitudes varied as expected according to the measured transconductance values. Our data are in line with observations made using direct electrical stimulation as well as concomitant recording via OECTs and optical detection of another cell depolarization-induced intracellular signal, that is, increase in free cytosolic calcium signals.^[42] Thus, at least under the conditions we used, it is highly unlikely that electrical activities of the recorded cells were changed by the operational device.

The signal quality obtained from islet cells by recording with vOECTs compare rather favorably to those obtained by another extracellular approach, that is, multielectrode-arrays (MEA) containing PEDOT:PSS covered electrodes. The unicellular action potentials recorded by vOECTs under glucose stimulation show

similar frequency to those published, that is, in the range of 0.5 to ≈ 4 Hz, whereas the amplitudes captured by vOECTs largely exceed the value of 12 μ V reported for PEDOT carbon nanotubes coated electrodes in MEAs which excluded their use of their amplitudes as a robust marker in contrast to amplitudes recorded by vOECTs.^[5,8] Similarly, the frequency of the multicellular slow potentials is in line with previously reported data, where again the amplitude was considerably larger by a factor of two to three as compared to those previously captured by MEAs.^[5,35,36,43] SPs are of major importance as they are tightly related to insulin secretion, they are deregulated in pathophysiological conditions and their signature is capable of ensuring normoglycemia in a human in-silico model of an artificial pancreas as a read-out of glucose levels.^[5,44] Thus, the amplifying power of the vOECT clearly improves detection, and in combination with the appropriate tunable electronics, is now useable for experiments on excitable cells or micro-organs of major medical importance such as islets, known for their small signal amplitude.

4. Conclusion

Our data on endocrine islet β -cells considerably expand the usefulness of vOECTs in biological and biomedical applications. This study demonstrates the excellent capacity of vOECT to simultaneously capture rapid signals, such as action potentials, as well as slow signals such as multicellular slow potentials. Our work also clearly demonstrates that not only cells or tissues with high amplitude signal, such as neurons and cardiomyocytes, are accessible to OECTs, but also other electrogenic cells with low amplitude signals and well known for their pivotal role in human homeostasis and in a major disease, that is, diabetes.^[26,27] The qualities of OECTs in general and of vOECTs in particular, open interesting new possibilities. Non-invasive monitoring is crucial for physiological long-term experiments to understand micro-organ function. Their facile deposition, variability in form factors and biocompatibility may also provide more versatility to microfluidic multi-organ chips.^[45,46] Moreover, bridging bioelectronics and human tissue has already provided proof of concept for a number of fascinating future biomedical applications in various pathologies.^[47–50] OECTs may find an additional role also in a bioinspired artificial pancreas, based on the nutrient-stimulated electrical activity of islet cells, for bioelectronic organ replacement.^[43,44,51,52]

5. Experimental Section

vOECT Fabrication and Characterization: The fabrication process has been reported previously.^[12,14] Prior to cell culture devices were treated with plasma (9.82 W/L) for 2 min to favor cell adhesion as described for microelectrode arrays.^[53] Electrical characterization was carried out in physiological buffered salt solution containing (in millimolar): NaCl 135, KCl 4.8, $MgCl_2$ 1.2, $CaCl_2$ 1.2–1.8, HEPES 10 pH 7.4 adjusted with NaOH) with an Ag/AgCl pellet (Multichannel Systems, Tübingen, Germany) gate electrode. A KEITHLEY 2612B dual channel Source Meter was used along with custom LabVIEW software to carry out polarization measurements. The measurement of drain conductance current (I_{DS}) with changing V_{GS} was used in the calculation of the intrinsic transconductance, $g_m = \Delta I_{DS} / \Delta V_{GS}$ and OECT characteristic curves were plotted using Origin software

HL-1 Cell Culture: HL-1 cells were kindly provided by M. Gramlich (RWTH Aachen, Germany) and cultured according to published protocols

in Claycomb medium (51800C, Sigma-Aldrich, Germany) supplemented with 10% fetal bovine serum (FBS) (v/v) (Eurobio, Courtaboeuf, France), 100 U mL⁻¹ penicillin and 0.01% (w/v) streptomycin (Invitrogen, Saint Aubin, France), 0.1 mM norepinephrine (Sigma-Aldrich, Germany), and 2 mM L-glutamine (EMD Millipore, Germany).^[28,54] The chip surface was coated at 37 °C for 1 h with 0.02% w/v gelatine (EMD Millipore, Germany) and 0.1% w/v fibronectin (F-1141, Sigma-Aldrich, German). Cells were seeded as 50 000 cells/chip and electrophysiological recordings were performed 6 days later at confluency.

Islet Isolation and Cell Culture: Islets from adult male C57Bl/6J mice (10–15 weeks of age) were obtained as described.^[5,35,36] Chip surfaces were coated with Matrigel (2% v/v; BD Biosciences, San Diego, CA, USA) and 100–200 islets were seeded at 37 °C (5% CO₂, >90% relative humidity) in RPMI medium (11 mM glucose, Thermo Fisher Scientific, Waltham, MA, USA) for 5–6 days on OECTs as entire or as partially dissociated islet-cell clusters (>10 cells per cluster). All experimental procedures were approved by the Ministry of Education and Research (no. 04236.01). To cultivate islets in a small volume, a homemade microfluidic approach was developed using a polydimethylsiloxane (PDMS) microwell, 3 mm in diameter and 3 mm high. The PDMS was cross-linked at 10% and baked for 1 h at 100 °C before attaching it to the vOECT.

This chip consisted of a polydimethylsiloxane (PDMS) microwell 3 mm in diameter and 3 mm high. The PDMS was cross-linked at 10% and baked for 1 h at 100 °C before attaching it to the vOECT.

Extracellular Recording Setup: All measurements were performed at 37 °C with an Ag/AgCl wire as a pseudo-reference electrode in solution. For HL-1 cells, the culture medium on the devices was replaced 30 min before recordings by physiological buffered salt solution. For islets, extracellular recordings were performed as described.^[5,35–37] The experimental setup is composed of two multichannel and tunable electronic boards designed to characterize the transistor as well as to measure and monitor the biological signals. The first board (termed ROKKAKU) bridges the non-standard connector of the sensor device to the second board (termed CHOSEI), which controls polarization and signal conditioning. The polarization circuits in CHOSEI allow via potentiometers for the adjustment of the transistor drain bias to the same value. I/V converter circuits passively convert the drain current signals into voltage signals using 560 Ω resistors connected to the 12 OECT drains. The output connector gives access to all measured signals from both electrodes and OECTs. Multichannel analogue data were acquired using an INTAN system (INTAN RHD2132 Amplifier Board and controller INTAN RHD2000 USB Interface Board; parallel 24 channel signal sampling at 10 kHz/channel, amplifier bandwidth 0.1 to 3000 Hz). Boards were carefully designed to limit electromagnetic interferences and all recordings were performed inside a grounded Faraday cage. Data were analyzed with MATLAB (MathWorks, Cambridge, UK) and Spike2 software (Cambridge Electronic Design Limited, Cambridge, UK).

Event Frequency Quantification and Filter Analysis: A 10–100 Hz second-order Butterworth digital filter was used to extract representative traces of HL-1 signals and to quantify AP frequencies and SNR. For islets, SPs were extracted using a 0.2–4 Hz band-pass filter, detected using the peak and threshold module of Spike2 (dead time 200 ms); APs were extracted using a 20–700 Hz band-pass filter, detected using the threshold module of Spike2 (dead time 10 ms).

Parametric analysis of event detection was conducted for AP and SP, where the cut-off frequencies varied within the range of interest for the given event (20–700 Hz for APs, 0.2–4 Hz for SPs); the orders varied between 1 and 4, and the detection threshold varied according to signal-dependent properties (adaptive threshold ranging from -6σ to $+6\sigma$ for APs, where σ is the signal's standard deviation, and absolute threshold ranging from 0.1% to 100% of the signal's peak-peak amplitude for SPs). For each filter, the threshold-dependent average event count was traced. A plateau in the average event count indicates a region of confidence where event detection is robust. The filter was chosen to maximize the width of the confidence region.

An alternative method for the estimation of AP frequency was developed taking advantage of the regularity of APs in HL-1 cells. For a given electrode, all interspike intervals (ISI) were computed and plotted on a

histogram. A Gaussian curve was fitted to the histogram (truncated between 0.6–1.2 s, where the average ISI is expected for HL-1 cells) using non-linear least squares fitting solved by the Levenberg–Marquardt algorithm. Although maximum likelihood estimation on a normal distribution would have been best suited in ideal conditions, AP detection in poor SNR conditions results in extraneous ISI peaks near 0 s and at multiples of the average ISI that render maximum likelihood estimation unsuitable. All fits with a coefficient of determination $R^2 < 0.5$ were discarded. The average ISI was estimated from the fitted Gaussian curve and inverted to derive the average frequency.

Signal Propagation Analysis: Signals were down-sampled to 1 kHz, and AP waveforms were isolated using a narrow 5–20 Hz band-pass Butterworth filter to minimize noise. APs were then transformed into waveform-independent spikes using a 100 ms moving RMS filter. Rolling window analysis (10 s window, 75% overlap) of cross-correlation between all pairs of signals was then performed to extract the time delay between trains of spikes (defined as the time offset where cross-correlation is maximum, provided correlation at this point was greater than 0.7). The earliest spiking electrode in each window, or “leader”, was identified, and the sequence of the following trains of spikes was determined by sorting the time delays relative to the leader.

Statistics: Results are presented as means and SEM. Following normality tests, Student's *t*-test was used for paired data. ANOVA with Tukey as a post hoc test were used for comparisons between more than two groups.

Supporting Information

Supporting Information is available from the Wiley Online Library or from the author.

Acknowledgements

The authors thank Michael Gramlich (Universitätsklinikum, RWTH Aachen, Germany) for kindly providing HL-1 cells. They gratefully acknowledge Georges Malliaras (University of Cambridge) for many helpful discussions and suggestions as well as the input from the other senior investigators of the MULTISPOT consortium (Eric Cloutet and Alexander Kuhn, Bordeaux). This work was financed by ANR MULTISPOT (ANR-17-CE09-0015) (to J.L., Eric Cloutet, Alexander Kuhn, and R.O.), ANR DIABLO (ANR-18-CE17-0005) (to J.L. and S.R.), LabEx AMADEUS-0042 with the help of the French government “Initiative d'excellence” (to S.R. and J.L.) and by the French Ministry of Education (to J.L.).

Conflict of Interest

The authors declare no conflict of interest.

Author Contributions

M.A. and A.P. contributed equally. Conceptualization: J.L. and S.R.; Data curation: J.L. and S.R.; Formal analysis: M.A., A.P., D.M., G.N., M.R., and J.L.; Funding acquisition: S.R. and J.L.; Investigation: M.A., A.P., M.J.D., D.M., E.P., M.R., G.N., and GP; Project administration: J.L.; Supervision: J.L., S.R., R.O., and M.J.D.; Software: A.P.; Writing – original draft: M.A., D.M., A.P., and J.L.; reviewed by all authors.

Data Availability Statement

The data that support the findings of this study are available from the corresponding author upon reasonable request.

Keywords

biosensor, cardiomyocytes, diabetes, electrophysiology, insulin, organic electrochemical transistors, pancreatic islets

Received: November 13, 2021
Published online:

- [1] L. Bai, C. G. Elósegui, W. Li, P. Yu, J. Fei, L. Mao, *Front. Chem.* **2019**, *7*, 313.
- [2] S. Lee, B. Ozlu, T. Eom, D. C. Martin, B. S. Shim, *Biosens. Bioelectron.* **2020**, *170*, 112620.
- [3] G. Buzsáki, C. A. Anastassiou, C. Koch, *Nat. Rev. Neurosci.* **2012**, *13*, 407.
- [4] B. Pesaran, M. Vinck, G. T. Einevoll, A. Sirota, P. Fries, M. Siegel, W. Truccolo, C. E. Schroeder, R. Srinivasan, *Nat. Neurosci.* **2018**, *21*, 903.
- [5] M. Jaffredo, E. Bertin, A. Pirog, S. Oucherif, F. Lebreton, D. Bosco, B. Catargi, D. Cattaert, S. Renaud, J. Lang, M. Raoux, *Diabetes* **2021**, *70*, 878.
- [6] J. Vangindertael, R. Camacho, W. Sempels, H. Mizuno, P. Dedecker, K. P. F. Janssen, *Methods Appl. Fluoresc.* **2018**, *6*, 022003.
- [7] P. Rorsman, F. M. Ashcroft, *Physiol. Rev.* **2018**, *98*, 117.
- [8] D. A. Koutsouras, R. Perrier, A. Villarreal Marquez, A. Pirog, E. Pedraza, E. Cloutet, S. Renaud, M. Raoux, G. G. Malliaras, J. Lang, *Mater. Sci. Eng.: C* **2017**, *81*, 84.
- [9] G. P. Kittlesen, H. S. White, M. S. Wrighton, *J. Am. Chem. Soc.* **1984**, *106*, 7389.
- [10] J. Rivnay, S. Inal, A. Salleo, R. M. Owens, M. Berggren, G. G. Malliaras, *Nat. Rev. Mater* **2018**, *3*, 17086.
- [11] J. Rivnay, P. Leleux, M. Ferro, M. Sessolo, A. Williamson, D. A. Koutsouras, D. Khodagholy, M. Ramuz, X. Strakosas, R. M. Owens, C. Benar, J. M. Badier, C. Bernard, G. G. Malliaras, *Sci. Adv.* **2015**, *1*, e1400251.
- [12] M. J. Donahue, A. Williamson, X. Strakosas, J. T. Friedlein, R. R. McLeod, H. Gleskova, G. G. Malliaras, *Adv. Mater.* **2018**, *30*, 1705031.
- [13] D. T. Simon, E. O. Gabrielsson, K. Tybrandt, M. Berggren, *Chem. Rev.* **2016**, *116*, 13009.
- [14] D. Khodagholy, T. Doublet, P. Quilichini, M. Gurfinkel, P. Leleux, A. Ghestem, E. Ismailova, T. Herve, S. Sanaur, C. Bernard, G. G. Malliaras, *Nat. Commun.* **2013**, *4*, 1575.
- [15] A. Williamson, M. Ferro, P. Leleux, E. Ismailova, A. Kaszas, T. Doublet, P. Quilichini, J. Rivnay, B. Rozsa, G. Katona, C. Bernard, G. G. Malliaras, *Adv. Mater.* **2015**, *27*, 4405.
- [16] X. Gu, C. Yao, Y. Liu, I. M. Hsing, *Adv. Healthcare Mater.* **2016**, *5*, 2345.
- [17] X. Gu, S. Y. Yeung, A. Chadda, E. N. Y. Poon, K. R. Boheler, I. M. Hsing, *Adv. Biosyst.* **2019**, *3*, 1800248.
- [18] F. Hempel, J. K. Law, T. C. Nguyen, W. Munief, X. Lu, V. Pachauri, A. Susloparova, X. T. Vu, S. Ingebrandt, *Biosens. Bioelectron.* **2017**, *93*, 132.
- [19] A. Kyndiah, F. Leonardi, C. Tarantino, T. Cramer, R. Millan-Solsona, E. Garreta, N. Montserrat, M. Mas-Torrent, G. Gomila, *Biosens. Bioelectron.* **2020**, *150*, 111844.
- [20] Y. Liang, M. Ernst, F. Brings, D. Kireev, V. Maybeck, A. Offenhausser, D. Mayer, *Adv. Healthcare Mater.* **2018**, *7*, e1800304.
- [21] A. Spanu, S. Lai, P. Cosseddu, M. Tedesco, S. Martinoia, A. Bonfiglio, *Sci. Rep.* **2015**, *5*, 8807.
- [22] C. Yao, Q. Li, J. Guo, F. Yan, I. M. Hsing, *Adv. Healthcare Mater.* **2015**, *4*, 528.
- [23] A. Giovannitti, C. B. Nielsen, D. T. Sbircea, S. Inal, M. Donahue, M. R. Niazi, D. A. Hanifi, A. Amassian, G. G. Malliaras, J. Rivnay, I. McCulloch, *Nat. Commun.* **2016**, *7*, 13066.
- [24] A. F. Paterson, A. Savva, S. Wustoni, L. Tsetseris, B. D. Paulsen, H. Faber, A. H. Emwas, X. Chen, G. Nikiforidis, T. C. Hidalgo, M. Moser, I. P. Maria, J. Rivnay, I. McCulloch, T. D. Anthopoulos, S. Inal, *Nat. Commun.* **2020**, *11*, 3004.
- [25] C. M. Moysidou, C. Pitsalidis, M. Al-Sharabi, A. M. Withers, J. A. Zeitler, R. M. Owens, *Adv. Biol.* **2021**, *5*, 2000306.
- [26] J. E. Campbell, C. B. Newgard, *Nat. Rev. Mol. Cell Biol.* **2021**, *22*, 142.
- [27] N. H. Cho, J. E. Shaw, S. Karuranga, Y. Huang, J. D. da Rocha Fernandes, A. W. Ohlrogge, B. Malanda, *Diabetes Res. Clin. Pract.* **2018**, *138*, 271.
- [28] W. C. Claycomb, N. A. Lanson Jr., B. S. Stallworth, D. B. Egeland, J. B. Delcarpio, A. Bahinski, N. J. Izzo Jr., *Proc. Natl. Acad. Sci. U. S. A.* **1998**, *95*, 2979.
- [29] S. Caserta, M. Barra, G. Manganelli, G. Tomaiuolo, S. Filosa, A. Cassinese, S. Guido, *Int. J. Artif. Organs* **2013**, *36*, 426.
- [30] S. M. White, P. E. Constantin, W. C. Claycomb, *Am. J. Physiol.* **2004**, *286*, H823.
- [31] I. Giaever, C. R. Keese, *Proc. Natl. Acad. Sci. U. S. A.* **1984**, *81*, 3761.
- [32] M. Ramuz, K. Margita, A. Hama, P. Leleux, J. Rivnay, I. Bazin, R. M. Owens, *ChemPhysChem* **2015**, *16*, 1210.
- [33] J. Rivnay, P. Leleux, A. Hama, M. Ramuz, M. Huerta, G. G. Malliaras, R. M. Owens, *Sci. Rep.* **2015**, *5*, 11613.
- [34] K. Benson, S. Cramer, H. J. Galla, *Fluids Barriers CNS* **2013**, *10*, 5.
- [35] M. Abarkan, J. Gaitan, F. Lebreton, R. Perrier, M. Jaffredo, C. Mulle, C. Magnan, M. Raoux, J. Lang, *Mol. Metab.* **2019**, *30*, 152.
- [36] F. Lebreton, A. Pirog, I. Belouah, D. Bosco, T. Berney, P. Meda, Y. Bornat, B. Catargi, S. Renaud, M. Raoux, J. Lang, *Diabetologia* **2015**, *58*, 1291.
- [37] M. Raoux, Y. Bornat, A. Quotb, B. Catargi, S. Renaud, J. Lang, *J. Physiol.* **2012**, *590*, 1085.
- [38] N. A. Steinmetz, C. Koch, K. D. Harris, M. Carandini, *Curr. Opin. Neurobiol.* **2018**, *50*, 92.
- [39] J. Muller, M. Ballini, P. Livi, Y. Chen, M. Radivojevic, A. Shadmani, V. Viswam, I. L. Jones, M. Fiscella, R. Diggelmann, A. Stettler, U. Frey, D. J. Bakkum, A. Hierlemann, *Lab Chip* **2015**, *15*, 2767.
- [40] X. Strakosas, M. Bongo, R. M. Owens, *J. Appl. Polym. Sci.* **2015**, *132*, 41735.
- [41] A. Villarreal Marquez, G. Salinas, M. Abarkan, M. Idir, C. Brochon, G. Hadziioannou, M. Raoux, A. Kuhn, J. Lang, E. Cloutet, *Macromol. Rapid Commun.* **2020**, *41*, e2000134.
- [42] A. Kalmykov, C. Huang, J. Bliley, D. Shiwerski, J. Tashman, A. Abdullah, S. K. Rastogi, S. Shukla, E. Mataev, A. W. Feinberg, K. J. Hsia, T. Cohen-Karni, *Sci. Adv.* **2019**, *5*, eaax0729.
- [43] R. Perrier, A. Pirog, M. Jaffredo, J. Gaitan, B. Catargi, S. Renaud, M. Raoux, J. Lang, *Biosens. Bioelectron.* **2018**, *117*, 253.
- [44] L. Olcomendy, A. Pirog, F. Lebreton, M. Jaffredo, L. Cassany, D. Gucik Derigny, J. Cieslak, D. Henry, J. Lang, B. Catargi, M. Raoux, Y. Bornat, S. Renaud, *IEEE. Trans. Biomed. Eng.* **2021**, *1*.
- [45] V. F. Curto, B. Marchiori, A. Hama, A. M. Pappa, M. P. Ferro, M. Braendlein, J. Rivnay, M. Fioocchi, G. G. Malliaras, M. Ramuz, R. M. Owens, *Microsyst. Nanoeng.* **2017**, *3*, 17028.
- [46] S. Jalili-Firoozinezhad, C. C. Miranda, J. M. S. Cabral, *Trends Biotechnol.* **2021**, *39*, 838.
- [47] K. Xiao, C. Wan, L. Jiang, X. Chen, M. Antonietti, *Adv. Mater.* **2020**, *32*, 2000218.
- [48] A. E. Rochford, A. Carnicer-Lombarte, V. F. Curto, G. G. Malliaras, D. G. Barone, *Adv. Mater.* **2020**, *32*, 1903182.
- [49] E. Zeglio, A. L. Rutz, T. E. Winkler, G. G. Malliaras, A. Herland, *Adv. Mater.* **2019**, *31*, 1806712.
- [50] J. Rogers, G. Malliaras, T. Someya, *Sci. Adv.* **2018**, *4*, eaav1889.
- [51] S. Renaud, B. Catargi, J. Lang, *IEEE Pulse* **2014**, *5*, 30.
- [52] R. Feiner, T. Dvir, *iScience* **2020**, *23*, 100833.
- [53] E. Pedraza, A. Karajic, M. Raoux, R. Perrier, A. Pirog, F. Lebreton, S. Arbault, J. Gaitan, S. Renaud, A. Kuhn, J. Lang, *Lab Chip* **2015**, *15*, 3880.
- [54] J. K. Hahn, B. Neupane, K. Pradhan, Q. Zhou, L. Testa, L. Pelzl, C. Maleck, M. Gawaz, M. Gramlich, *J. Mol. Cell. Cardiol.* **2019**, *131*, 12.

Supporting Information

for *Adv. Sci.*, DOI: 10.1002/advs.202105211

Vertical Organic Electrochemical Transistor Tuning for Low Amplitude Micro-Organ Signals

*Myriam Abarkan, Antoine Pirog, Donnie Mafilaza, Gaurav Pathak, Gilles N’Kaoua, Emilie Puginier, Rod O’Connor, Matthieu Raoux, Mary J. Donahue, Sylvie Renaud, Jochen Lang**

Supporting Information

Vertical Organic Electrochemical Transistor Tuning for Low Amplitude Micro-Organic Signals

*Myriam Abarkan, Antoine Pirog, Donnie Mafilaza, Gaurav Pathak, Gilles N’Kaoua, Emilie Puginier, Rod O’Connor, Matthieu Raoux, Mary J. Donahue, Sylvie Renaud, Jochen Lang**

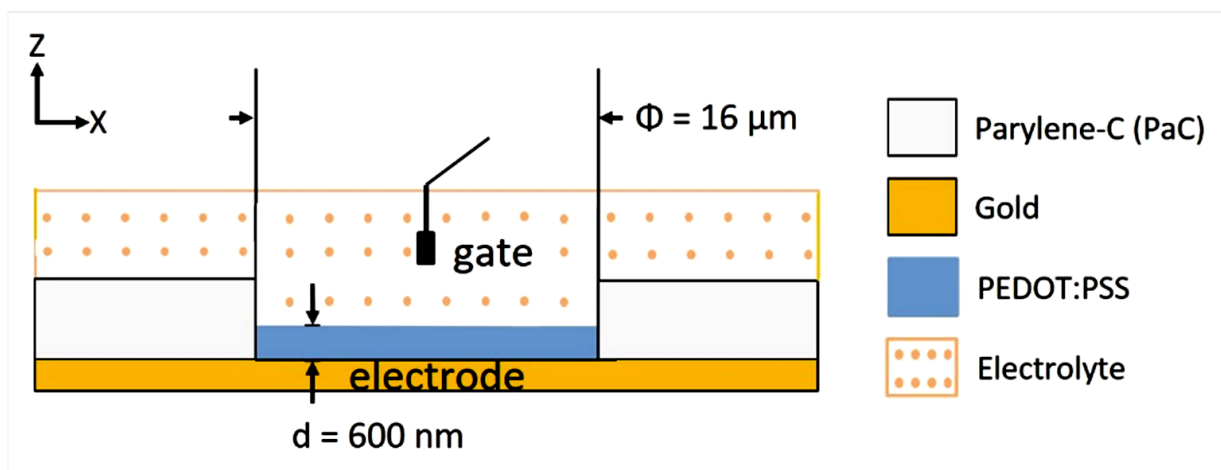


Figure S1. Cross-sectional layout of an electrode and layer dimensions. d , PEDOT:PSS thickness; Φ , electrode dimension. An Ag/AgCl gate electrode is used in characterization and during experiments.

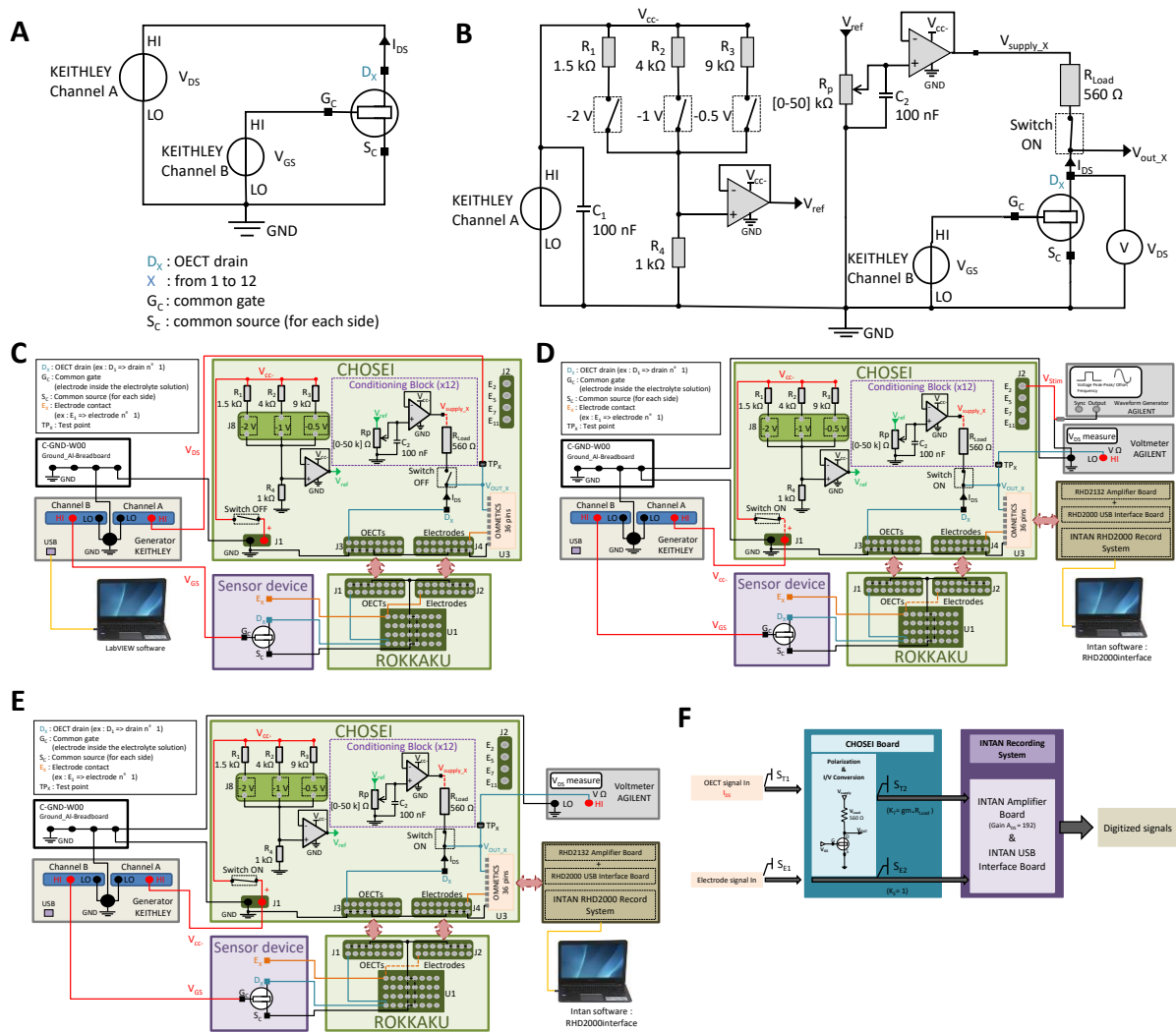


Figure S2. Electronic boards developed for characterization and recording experiments. **A, B.** Scheme of electronic circuits developed for vOECT characterization and recordings. The drain-source and gate-source voltages are respectively applied to the drain and gate contacts directly. **C.** Setup used for vOECT and electrode characterization experiments. vOECTs and electrodes are connected to the CHOSEI board via the connection board (ROKKAKU). The drain-source bias and gate-source bias from a KEITHLEY source-meter are directly applied to the transistors. Note that biasing circuits and I/V converter circuits were not required for this kind of experiment. Output characteristics and transfer curves were measured using a KEITHLEY source-meter and custom LabVIEW program that also plots the data. **D.** Setup for biological signal simulations and validating experiments. An Agilent waveform generator generates standard waveforms (sine, square, pulse) inside the electrolyte bath through one electrode of the device. Input signals are detected by vOECTs before being converted and recorded. **E.** Setup used for electrophysiological experiments with a voltage amplifier and polarization adjustment circuits. The drain-source current is converted into a voltage signal via an I/V

converter circuit while the conditioning circuit adapts the drain-source bias. The source-meter KEITHLEY is used as a DC generator providing gate-source voltage and the power supply voltage for the polarization circuit and the I/V converter blocks. Signals from electrodes and/or vOECTs are conditioned by the voltage amplifier circuit and recorded via an INTAN RHD2000 System (RHD2132 Amplifier Board and RHD2000 USB Interface Board for real-time observation of the signals). The drain-source voltage is continuously monitored by an Agilent voltmeter. **F.** Experimental set up gain and amplification factor. The sensor device contains both vOECTs and PEDOT:PSS coated metal electrodes to compare recordings by the two different technologies.

The signal S_{E1} measured by electrodes is not conditioned by CHOSEI. As a result, the signal collected at the CHOSEI output connector is: $S_{E2} = S_{E1} \times K_E$, with a unitary gain $K_E = 1$. In contrast, voltages S_{T1} sensed by vOECTs generate a current dependent of the vOECT's transconductance (g_m). These signals undergo a I/V conversion resulting in voltages $S_{T2} = S_{T1} \times K_T$ where $K_T = g_m \times R_{Load}$ (where $R_{Load} = 560 \Omega$ is the load resistor of the I/V conversion circuit). For a typical transconductance value of 10 mS, $K_T = 5.6$. All signals are then digitized by the INTAN RHD2132 board (with an on-board gain of 192). They are finally transferred via SPI to the INTAN RHD2000 interface board, where they are made available for recording via USB.

Table S1. Specifications of the CHOSEI board.

Specifications of CHOSEI				
Name	Description	Value		Unit
Voltages specifications				
V_{cc-}	Power supply voltage	Operating voltage		V
		-5	Max -15	
V_{ref}	AOP input voltage	Available voltages ($V_{cc-} = -5$ V)		
		-0.5	-1	-2
V_{supply_X}	OECT polarization voltage	[0 – V_{ref}]		V
Used components				
U4/U5/U6/U8	Operational Amplifiers (TL08xx) as voltage followers	Operating voltage		V
		Max		
		V_{cc-}		
		5	-15	
		V_{cc+}		
		0 (ground)		
R_p	Voltage adjustment potentiometer (conditioning block (x12))	[0-50 k]		Ω
R_{Load}	Load resistance (I/V converter circuits)	560		Ω
TP_x	Test point for OECT's V_{DS} voltage	12		
J2	Terminal block (inputs : stimulating electrodes)	4 positions		
J3	Header test male (inputs : OECTs signals)	2 x 8 positions		
J4	Header test male (inputs : Electrodes signals)	2 x 8 positions		
U3	OMNETICS connector (outputs signals: OECTs + Electrodes)	2 x 18 positions		

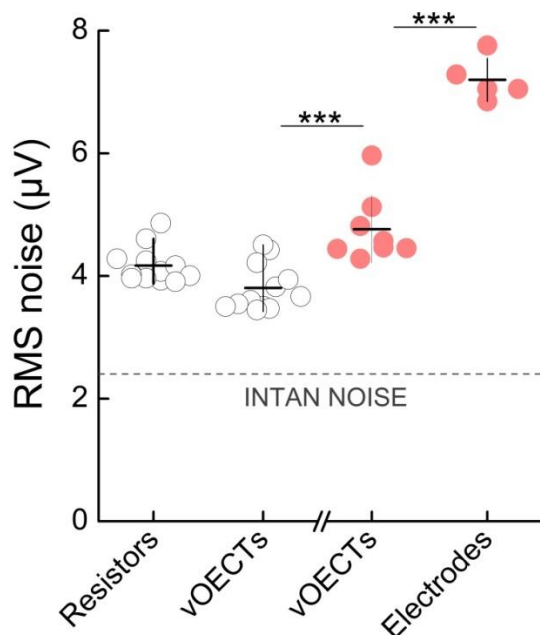


Figure S3. Electronic noise of the set-up. Noise was measured either (left-hand side, open symbols) with resistors of values equivalent to the drain-source junction of the vOECTs and compared with dry vOECTs or with wet setup (right-hand side, closed symbols) of vOECTs or electrodes seeded with HL-1 cells and measured in buffer. The Intan RHD2132 preamplifier's announced input-referred noise is also indicated. The equivalent resistance of every vOECT channel was evaluated by sweeping the drain-source voltage V_{ds} from 0 V to -0.4 V by steps of -0.05 V and measuring the resulting drain current I_{ds} . The equivalent resistance $R_{eq} = V_{ds}/I_{ds}$ was derived through least squares regression for every channel. Resistors of equivalent values were put together by associating up to three through-hole silicon resistors in series to minimize error. These were then connected between the common source and the drain connector of their corresponding recording channel to model the drain-source junction of the vOECTs. The "drain-source" voltage was adjusted to -0.2 V for each resistor individually as is the case for biological recordings. All 12 channels were recorded simultaneously for 300 s. All resistors were removed and the actual vOECTs were connected in their place using their dedicated connector. The drain-source voltage was adjusted to -0.2 V for each vOECT individually and again, all channels were recorded simultaneously for 300 s.

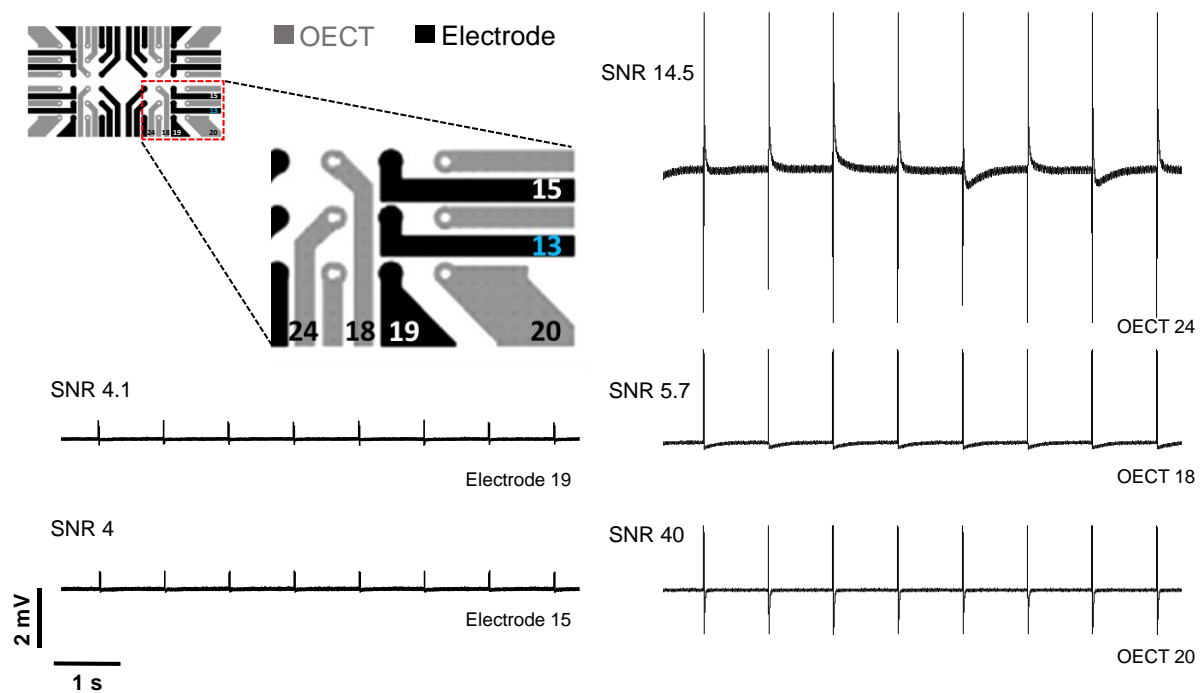


Figure S4. Signal simulation for validation of the setup. The layout of the vOECT/MEA CHIP is shown (upper left) and recorded signals with corresponding numbers of OECT channels or electrodes as well as calculated SNRs. Electrical signals (200 mV, 10 ms, 1 Hz) were applied via electrode 13.

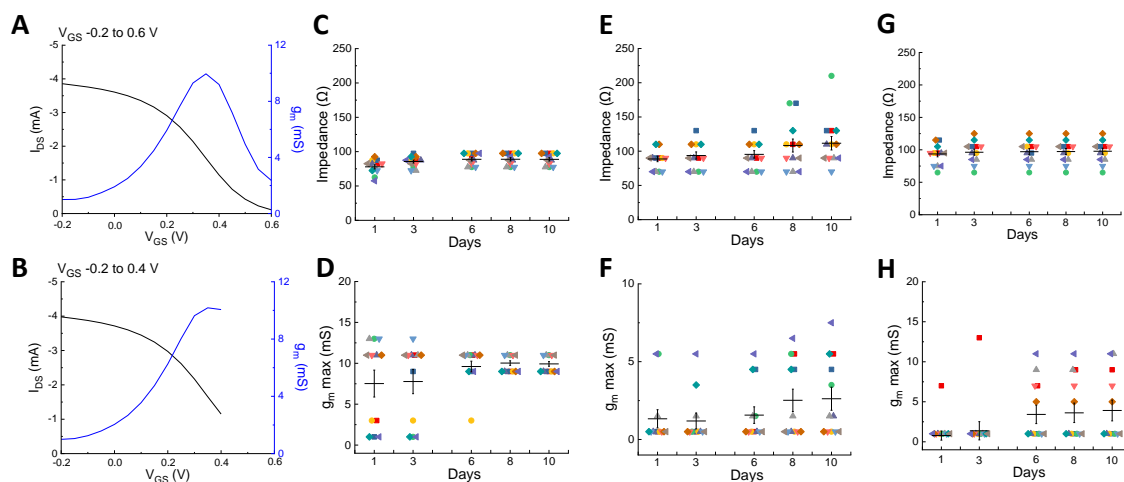


Figure S5. Stability of vOECT performance. Transfer curves and resulting transconductance at $V_{DS} = -0.4$ V in 0.1 M KCl for V_{GS} (A) varying from -0.2 V to 0.6 V or (B) varying from -0.2 V to 0.4. Impedance (C-G) and $g_{m,max}$ (D-H) during repetitive short measurements over days (V_{GS} -0.2 V to 0.4, sufficient to determine $g_{m,max}$, and without polarization in between measurements). vOECTs were kept in physiological buffered salt solution (C,D), in culture medium at 37°C (E,F) or in culture medium after coating of vOECTs with cell adhesion matrix (Matrigel; G,H) as used in recordings of attached cells. Measurements in C-H performed on each vOECT channel are given by different symbols and colors. Statistics did not indicate any significant differences.

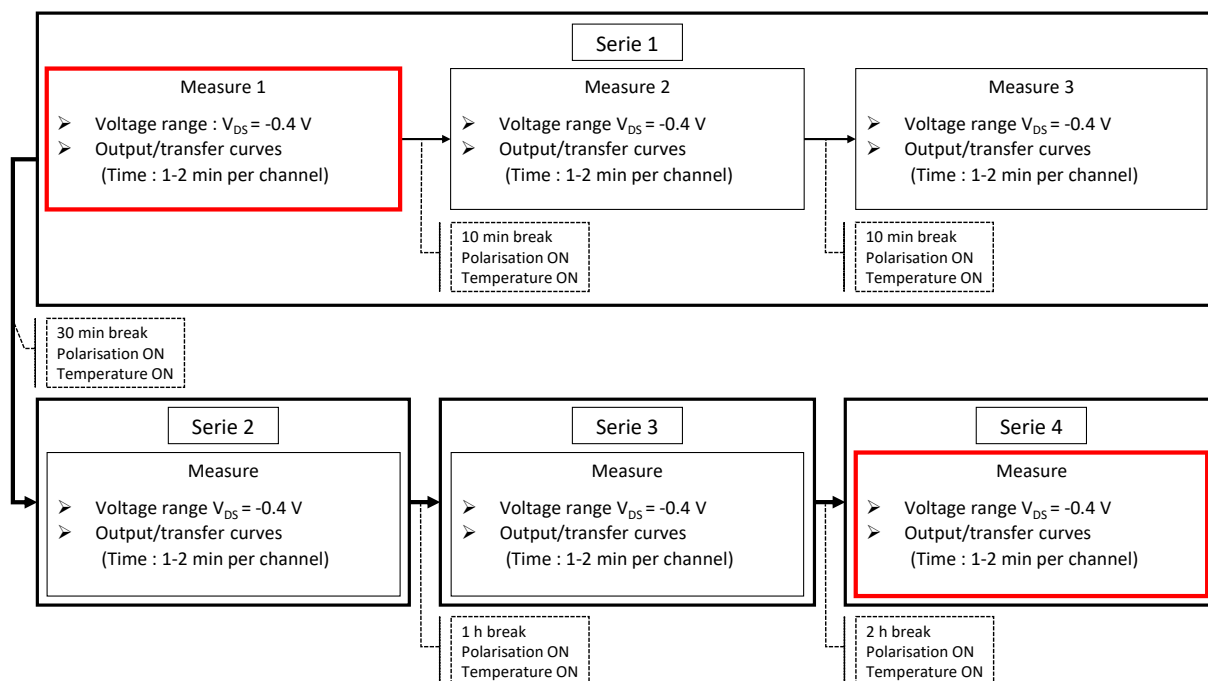


Figure S6. Experimental scheme of measurements given in Fig. 3. 1st and 2nd measurements in Figure 3 correspond to “Measure 1” and “Measure 2”; t_0 corresponds to “Serie 1, Measure 1” and t_4 h to “Serie 4”. For the sake of clarity only these points are depicted in Fig. 3.

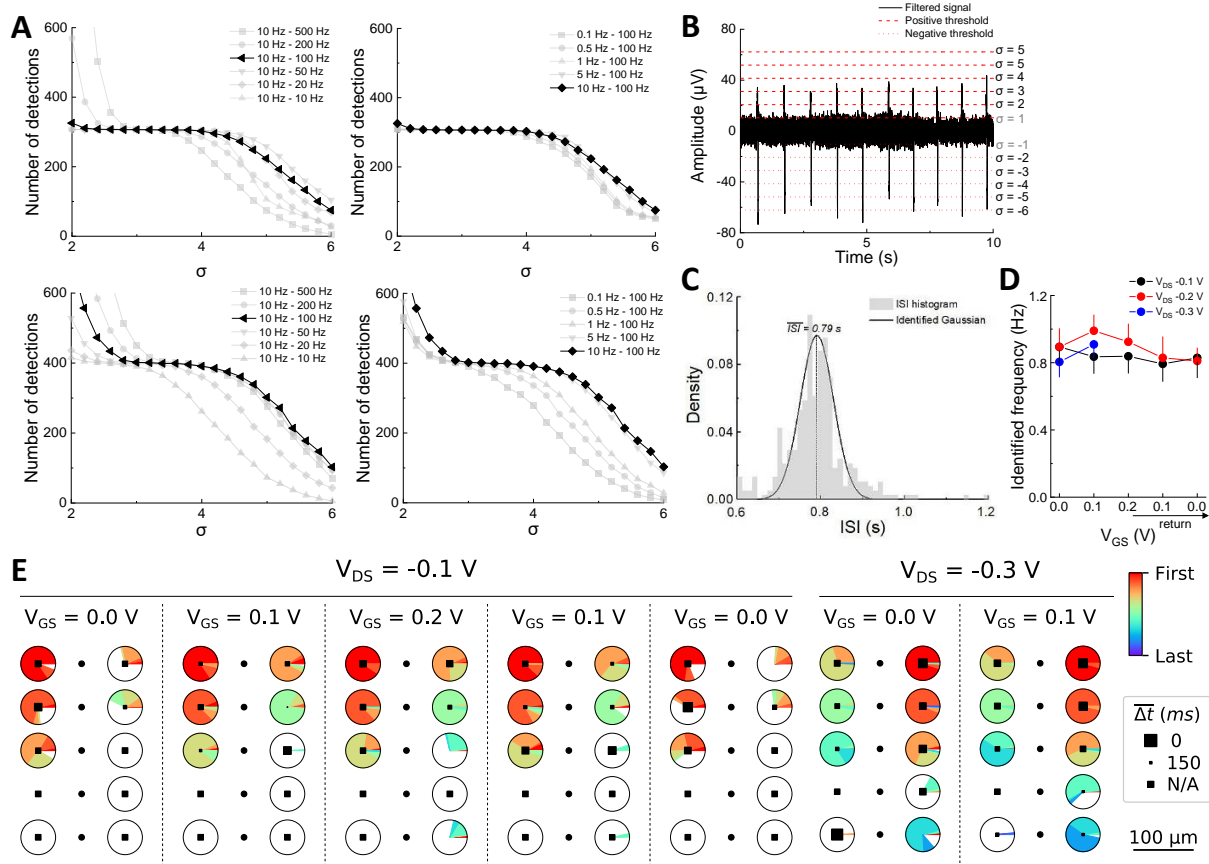


Figure S7. Analysis of signals recorded from HL-1 cardiomyocytes. **A.** Parametric analysis of filters used to detect and extract action potentials recorded by metal electrodes (top) or by vOECTs (bottom). Detections by the combination of a high pass filter of 1 Hz and low pass filter of 100 Hz is given in black, was stable corresponding to a large span of the adaptive threshold σ and was used for all results shown; other combinations are depicted in grey. **B.** Representative trace of several adaptive thresholds σ for action potential detection. $\sigma = -1$ or 1 are not adapted because they are too close to the baseline thus picking false positives. **C.** Frequency evaluation method via the interspike interval ISI. The identified Gaussian shows a stable ISI during the recordings. **D.** Frequencies, identified using the ISI method (in D), are stable throughout the electrical conditions. **E.** Action potential propagation across the surface of the chip. Circle symbols represent electrodes, and square symbols represent vOECTs. Solid symbols indicate that the OECT or electrode recorded action potential activity. For each electrode, a pie chart indicates the distribution of spiking order in all measurement windows, and the size of the marker indicates the average delay of spiking relative to the leader.

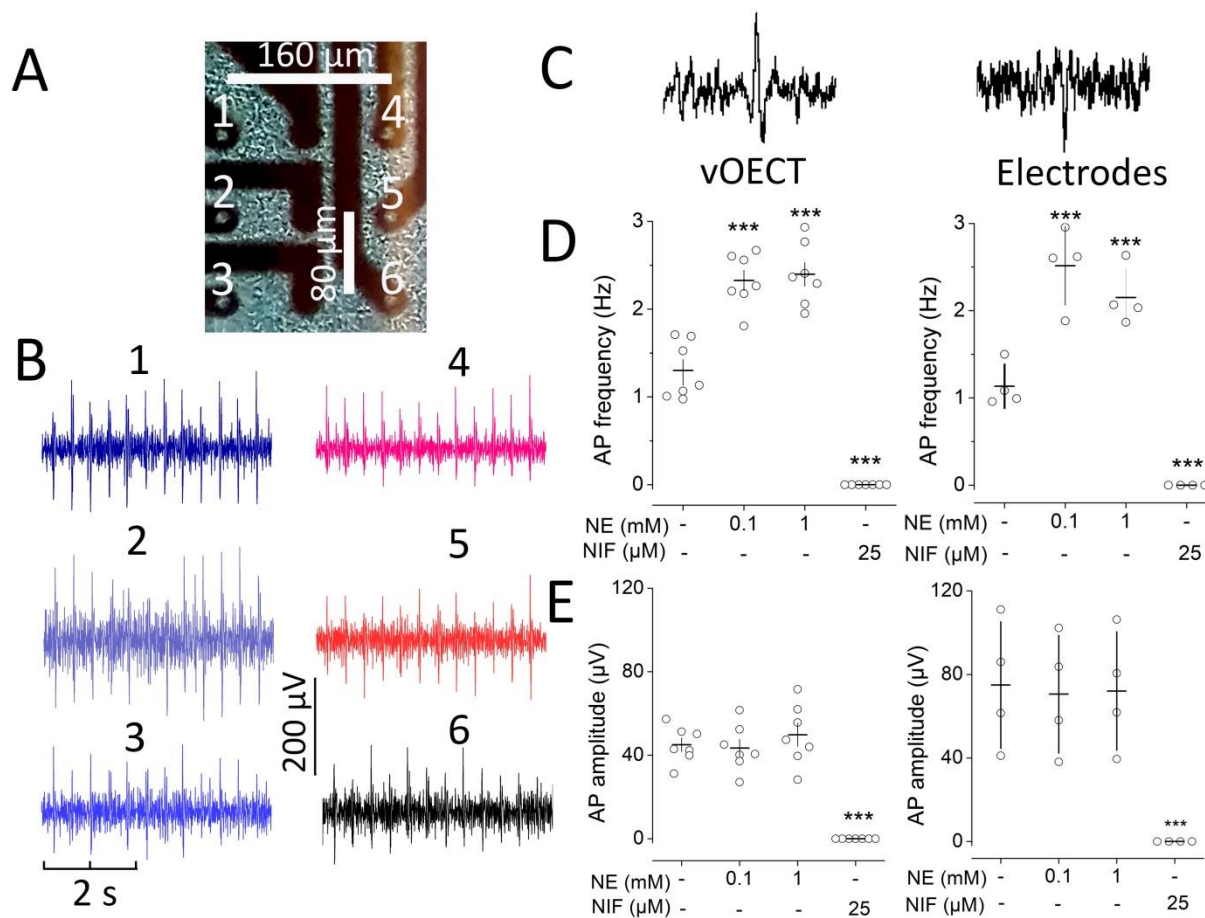


Figure S8. Rhythmicity of clonal HL-1 cardiomyocytes and their regulation by norepinephrine and calcium channel blocker. **A:** Detail and geometry of an OECT with 6 channels. **B:** Recording of HL-1 cells in the presence of 1 mM norepinephrine, channel numbers correspond to those in **A**. **C:** representative traces of recording via vOECT channels or via electrodes on the same chip. **D and E:** Action potential frequency (**D**) and amplitude (**E**) of vOECT (left panels) and MEA recordings (right panels). NE, norepinephrine, NIF, calcium channels blocker nifedipine, given are means and SEM; ***, $2p < 0.001$ (Tukey post-hoc) vs. absence of drugs.

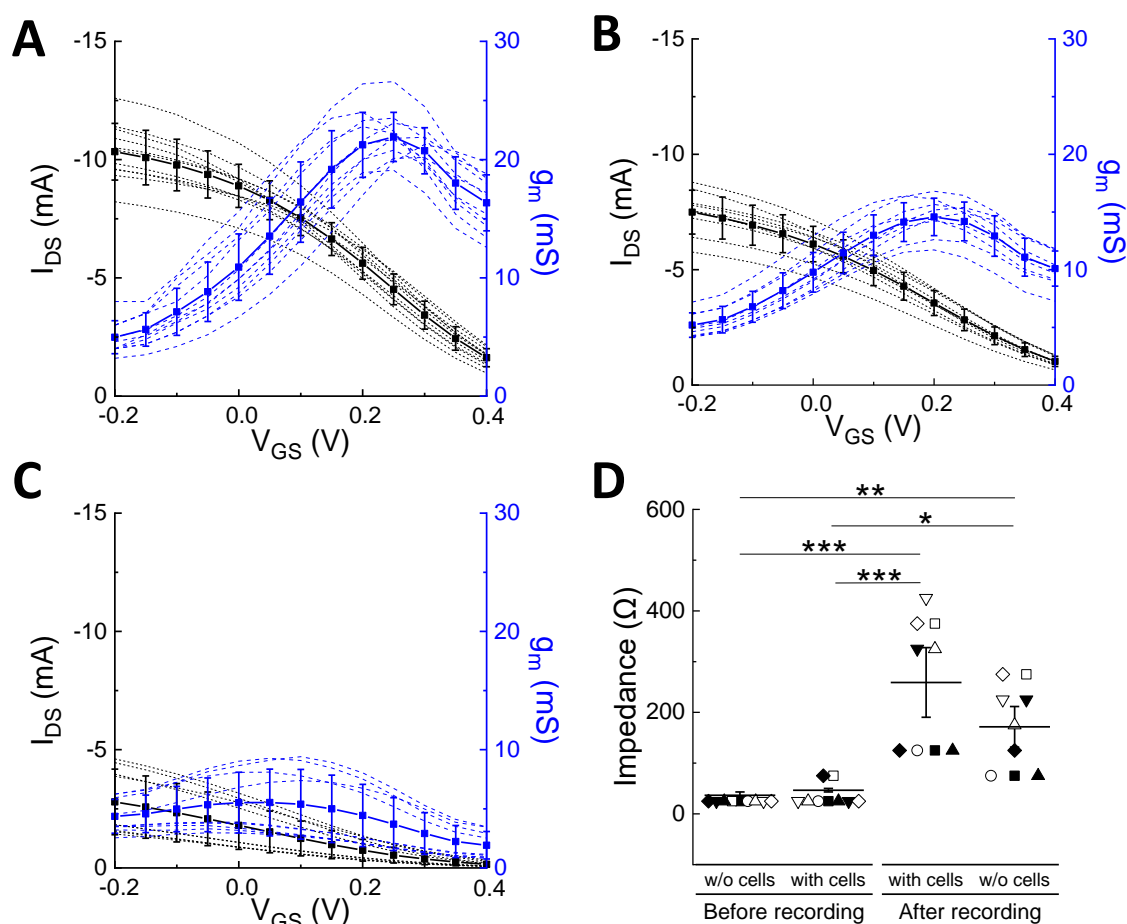


Figure S9. Performance of vOECTs before, during and after islet cell experiments. **A.** Transfer curves and resulting transconductances at V_{DS} -0.4 V, for V_{GS} varying from -0.2 V to 0.4 V in physiological buffered salt solution before seeding islet cells on the vOECTs array, means \pm SEM, N = 11, **B.** same as A but with islet cells seeded in culture medium on vOECTs array, means \pm SEM, N = 9, **C** same as B but after removal of cells and vOECTs kept in physiological buffered salt solution, means \pm SEM, N = 9. **D.** Impedance before recording without cells (buffer, as in A), with cell seeded (culture medium, as in B), directly after recording with cells in culture medium or after removal of cells and addition of physiological buffered salt solution (as in C). Means \pm SEM; ANOVA and Tukey's post-hoc analysis; * $2p < 0.05$, ** $2p < 0.01$, *** $2p < 0.001$; N = 9-11.

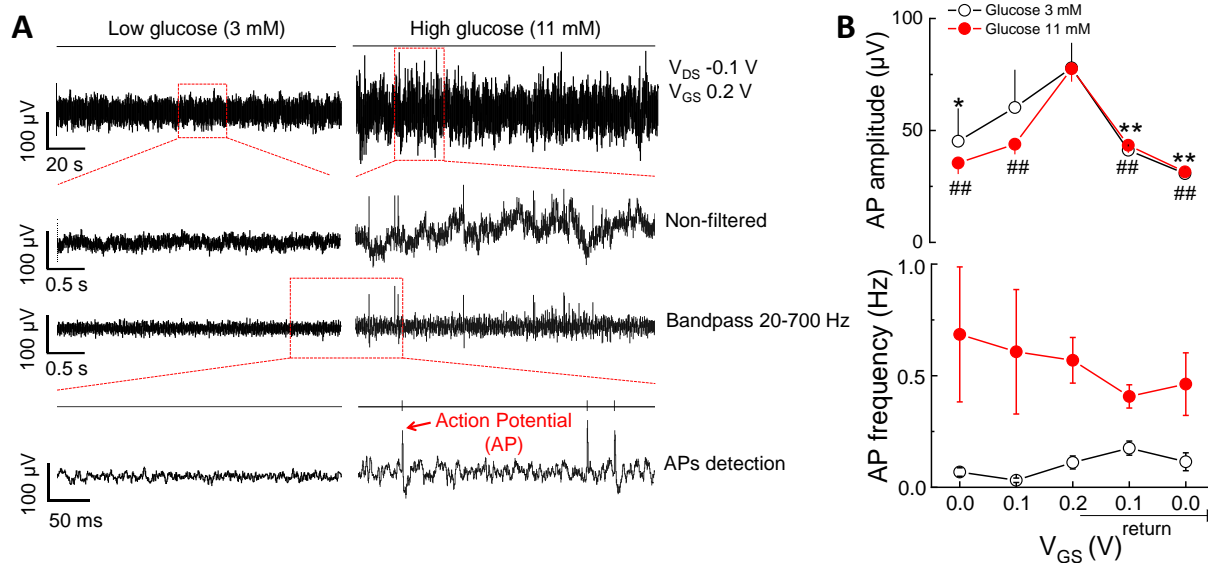


Figure S10. Analysis of signals recorded from pancreatic islets. **A.** Representative raw and filtered recordings of islets at low glucose (non-stimulatory, 3 mM) and high glucose (stimulatory, 11 mM) in physiological buffered ion solution at $V_{DS} = -0.1 V$ and $V_{GS} = 0.2 V$. Given are different time scales as well as non-filtered and band pass filtered traces (20-700 Hz). **B.** Action potential amplitudes and frequencies at $V_{DS} = -0.1 V$ and indicated V_{GS} sweep. Islets on vOECTs were exposed to low (3mM) glucose or stimulatory concentrations (11 mM). Means \pm SEM; paired t test; ## (11 mM) or ** (3 mM) $2p < 0.01$ as compared to $V_{GS} = -0.2 V$, * (3 mM) $2p < 0.05$ as compared to $V_{GS} = -0.2 V$; $N = 7$. Note that no significant differences in frequencies were observed between all measurements at 3 mM glucose or between all measurements at 11 mM glucose (ANOVA).

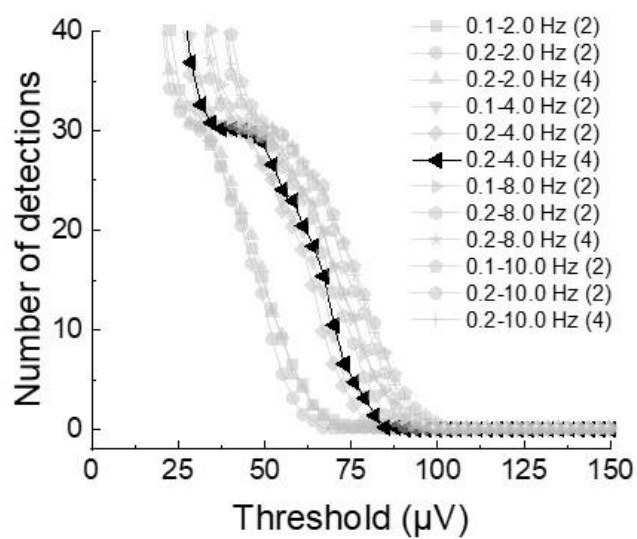


Figure S11. Analysis of signals recorded from pancreatic islets. Parametric analysis of filters used to detect and extract slow potential recorded by transistors. The detection of slow potential is robust at the combination of a 0.2 Hz high pass filter (1st order) and a 4 Hz low pass filter (4th order), given in black, corresponding to a large range of thresholds ranging from 30 µV to 50 µV. This combination was used for analysis; other combinations are given in grey.

Acquisition of biological data for in silico simulation: Manuscript n°6

In diabetes mellitus (DM) treatment, continuous glucose monitoring (CGM) linked to insulin delivery becomes a major therapeutic tool to improve therapeutic outcomes and quality of patients' lives. However, blood glucose (BG) regulation with CGM is still hampered by limitations of algorithms and glucose sensors. Regarding sensor technology, current electrochemical glucose sensors do not capture the full spectrum of other nutrients or physiological signals, i.e., lipids, amino acids or hormones, relaying the general body status. Regarding algorithms, variability between and within patients remains the main challenge for optimal BG regulation in closed-loop therapies.

In the present work, we focus on the management of inter- and intra-patient variability in T1D treatment. We intend here to highlight the benefits of numerical simulations with the UVA/Padova T1DMS to address this issue and establish *in-silico* proofs of concept for the DIABLO project. That simulator is approved by the US Food and Drug Administration (FDA) as an alternative for pre-clinical testing of new devices and closed-loop algorithms. In particular, we propose a method to define meal scenarios based on patients' body weight to better account for the inter-patient variability in energy requirements and define more realistic meal scenarios. With a CGM sensor, we propose a meal size-independent bolus strategy, slightly individualised by integrating the Carbohydrate-to-Insulin Ratio (CIR) in the bolus calculator rule. The objective here is to alleviate patient's workload and anxiety, while keeping him involved in the therapy management, i.e., the patient still has to announce sizeable glucose intakes (meals). To overcome the limitation of standard glucose sensors leading to meal announcements, the concept of an islet-based biosensor, which could integrate multiple physiological signals through electrical activity measurement, is also assessed here in a closed-loop insulin therapy. From an analysis of the *in-silico* results, we will finally discuss the proposal of a new AP paradigm where the dissimilarity between a commercial CGM sensor and our biosensor could be used advantageously, to better handle inter- and intra-patient variability in diabetes treatment and care.

Towards the integration of an islet-based biosensor in closed-loop therapies for patients with Type 1 Diabetes

Loïc Olçomendy¹, Louis Cassany¹, Antoine Pirog¹, Roberto Franco², Emilie Puginier³, Manon Jaffredo³, David Gucik-Derigny¹, Héctor Ríos^{2,4}, Alejandra Ferreira de Loza^{4,5}, Julien Gaitan³, Matthieu Raoux³, Yannick Bornat¹, Bogdan Catargi^{3,6}, Jochen Lang³, David Henry¹, Sylvie Renaud¹, Jérôme Cieslak^{1*}

¹Univ. Bordeaux, CNRS, Bordeaux INP, IMS, UMR 5218, Talence, France

²Tecnológico Nacional de México/I.T. La Laguna, C.P. 27000, Torreón, Coahuila, México

³Univ. Bordeaux, CNRS, CBMN, UMR 5248, Pessac, France

⁴Cátedras CONACYT, C.P. 03940, Ciudad de México, México

⁵Instituto Politécnico Nacional-CITEDI, C.P. 22435, Tijuana, Baja California, México

⁶Bordeaux Hospitals, Endocrinology and Metabolic Diseases Unit, Bordeaux, France

* Correspondence:

Corresponding Author

jerome.cieslak@ims-bordeaux.fr

Keywords: Type 1 Diabetes, Artificial Pancreas, Closed-loop simulation, Insulin therapy, Pancreatic islets, Micro-Electrode Array, Biosensor.

Abstract

In diabetes mellitus (DM) treatment, Continuous Glucose Monitoring (CGM) linked with insulin delivery becomes the main strategy to improve therapeutic outcomes and quality of patients' lives. However, Blood Glucose (BG) regulation with CGM is still hampered by limitations of algorithms and glucose sensors. Regarding sensor technology, current electrochemical glucose sensors do not capture the full spectrum of other physiological signals, *i.e.*, lipids, amino acids or hormones, relaying the general body status. Regarding algorithms, variability between and within patients remains the main challenge for optimal BG regulation in closed-loop therapies. This work highlights the simulation benefits to test new sensing and control paradigms which address the previous shortcomings for Type 1 Diabetes (T1D) closed-loop therapies. The UVA/Padova T1DM Simulator is the core element here, which is a computer model of the human metabolic system based on glucose-insulin dynamics in T1D patients. That simulator is approved by the US Food and Drug Administration (FDA) as an alternative for pre-clinical testing of new devices and closed-loop algorithms. To overcome the limitation of standard glucose sensors, the concept of an islet-based biosensor, which could integrate multiple physiological signals through electrical activity measurement, is assessed here in a closed-loop insulin therapy. This investigation has been addressed by an interdisciplinary consortium, from endocrinology to biology, electrophysiology, bio-electronics and control theory. In parallel to the development of an islet-based closed-loop, it also investigates the benefits of robust control theory against the natural variability within a patient population. [Using 4 meal scenarios, numerous simulation campaigns were conducted. The analysis of their results then introduces a discussion on the potential](#)

Towards the integration of an islet-based biosensor in closed-loop therapies for patients with Type 1 Diabetes

benefits of an Artificial Pancreas (AP) system associating the islet-based biosensor with robust algorithms.

1. Introduction

Destruction of pancreatic β -cells leads to absolute insulin deficiency in Type 1 Diabetes (T1D) and concerns 5 to 10% of the estimated 463 million cases of diabetes worldwide in 2019, expected to rise to 700 million by 2045 according to the International Diabetes Federation (1). In this context, the development of Artificial Pancreas (AP) systems, composed of a Continuous Glucose Monitoring (CGM) sensor fitted with a pump to deliver insulin, is becoming the standard for T1D treatment (2,3). CGM relies on subcutaneous glucose measurement via electrochemical electrodes and algorithms are used to control the pump and safely manage the insulin delivery (Figure 1).

In spite of improvements relative to hypoglycaemia prevention (4) and hyperglycaemia mitigation (5,6), Blood Glucose (BG) regulation with the AP is still biased by the limitations of algorithms (7) and technologies used in commercial glucose sensors (8). Current electrochemical approaches in glucose sensors do not consider the whole spectrum of nutrients and do not respond to all physiological situations (e.g., contribution of intestinal hormones to insulin secretion after a meal, physical activity, stress), which all modulate insulin requirements. Regarding algorithms, variability between and within patients, also referred to as inter- and inpatient variability, remains the main challenge for optimal glycaemia regulation with closed-loop therapies. As a consequence, only partially automated closed-loop systems are currently accepted for therapy in the US and Europe, *i.e.*, the T1D patient still has to announce meals and calculates carbohydrate intake to command himself the bolus insulin injections (9). Alleviating some of these issues, specifically in the case of unstable diabetes, would lower the barriers to closed-loop therapy for patients, with a mitigation of patient's workload and anxiety.

To overcome the shortcomings of enzymatic sensors, our initiative aimed at developing a biosensor which integrates a Micro Electrode Array (MEA) containing a few murine or human islets

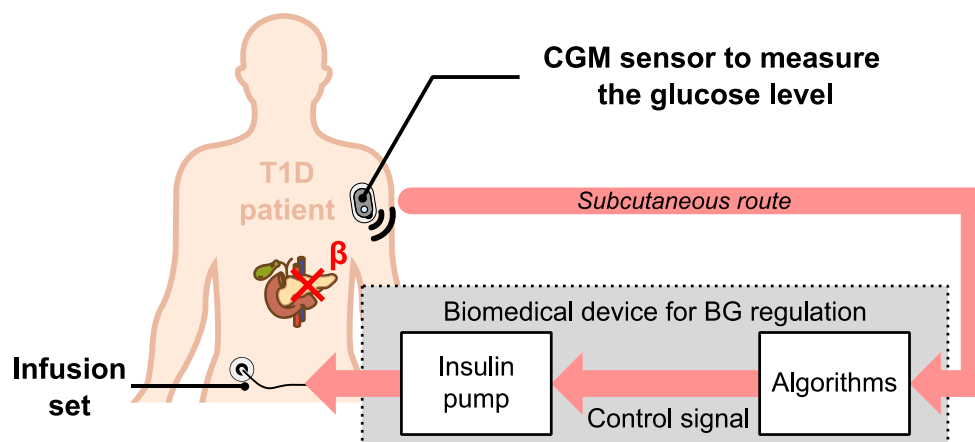


Figure 1: Principle of the Artificial Pancreas for T1D treatment. An electrochemical CGM sensor continuously measures subcutaneous glucose concentrations, which reflect blood glucose concentration. This information is then processed by algorithms (controller, bolus calculator, alarms ...), connected to an insulin pump to deliver the appropriate amounts of insulin.

Towards the integration of an islet-based biosensor in closed-loop therapies for patients with Type 1 Diabetes

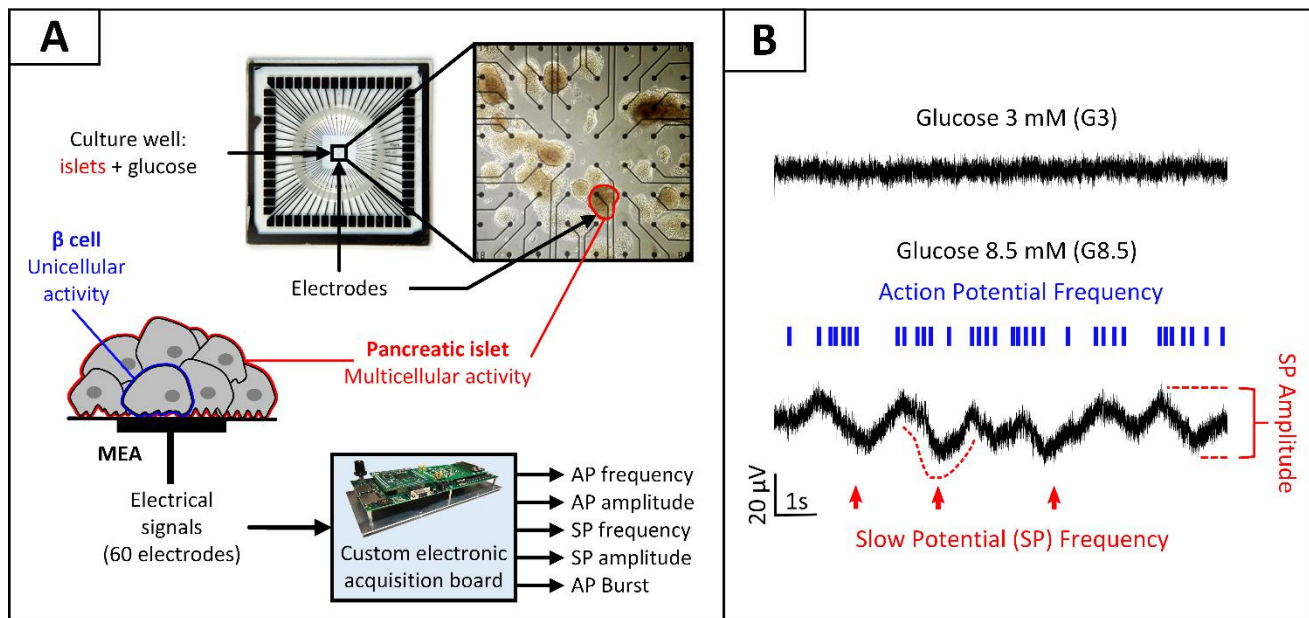


Figure 2: Biosensor principle: acquisition and processing of electrical biosignals generated by pancreatic islets cultured on MEAs and stimulated by increasing glucose levels. A) Pancreatic islets cultured on MEAs. Glucose can be introduced in the culture chamber to stimulate the cells. Each electrode in the MEA captures a combination of uni- and multicellular activity generated by the neighbouring islets. A custom electronic board performs online digital signal processing on the recorded biosignals to extract features of interest for each electrode. B) The electrical activity is modulated by glucose concentration. Low glucose inhibits activity and high glucose induces two signals of interest generated by β -cells, representative of uni- and multicellular activity: action potentials and SPs. Action potentials are mainly characterized by their frequency and organisation in bursts, and SPs by both their frequency and amplitude. (From (23))

linked to real-time/online signal processing (10–13). Pancreatic islets are the “in-born” sensors and actuators, optimally shaped by evolution, to ensure regulation of glucose homeostasis under various natural circumstances and lifestyles. The goal is to design a sensor capable of “seeing” the whole-body physiological interactions, as opposed to the classical glucose-only sensors. Islets, composed of several (hundreds of) excitable cells, display continuous oscillations, reflecting its orchestrated behaviour. Action potentials and slow oscillations – named Slow Potentials (SP) - can be recorded extracellularly using MEAs (Figure 2). Islets SPs have amplitudes in the range of few tens of microvolts, frequency components ranging between 0.2 and 2 Hz (12), and their characteristics are closely correlated to insulin secretion dynamics (14). Signal treatment raises challenges when processing it online and in real-time for *in vivo* applications. Decoding information from the recorded signals requires analogue pre-processing by amplifiers and filters, followed by digital processing with statistical, frequency, or temporal analysis to perform feature extraction and produce relevant metrics (15). Furthermore, adaptive decoding is essential to take into account variations in signal and electrode properties, particularly for chronic recordings (16). This sensor technology has been patented in 2013 (17).

Building on promising results of the previously developed and patented glucose bio-device, which integrates multiple physiological signal information (17,18), a consortium has been created in 2019 to assess the possibility to integrate this islet-based biosensor in closed-loop therapies for patients with T1D. This consortium started the collaboration in a national project named DIABLO, supported by the French National Agency for Research (ANR). Preliminary work (19) provided guidelines for the controller tuning with an *in silico* methodology based on clinically-relevant criterion: a meta-heuristic method (genetic algorithm (GA)-based optimization technique) is used with the BG risk index

Towards the integration of an islet-based biosensor in closed-loop therapies for patients with Type 1 Diabetes

(20). The core element of the GA-based protocol is the UVA/Padova T1DM Simulator (T1DMS - v3.2) (21). This computer model of the human metabolic system simulates the glucose-insulin dynamics in T1D patients, and is approved by the US Food and Drug Administration (FDA) as an alternative for pre-clinical testing of insulin therapies, including closed-loop algorithms (22). Using the T1D adult cohort of the simulator, a first comparison between two AP systems (a biosensor-based one and a CGM-based one) was presented in (23). Thanks to individualised controller parameters, satisfactory performance was achieved with the biosensor-based AP system, even with a simple proportional-derivative controller associated to continuous basal infusion (PD_{BASAL}). This regulation scheme was as efficient as standard treatments with unannounced meals (no bolus strategy was implemented).

Another objective of the DIABLO project lies in the use of control theory to tackle the variability observed between and within patients in a real T1D population. For that purpose, it is necessary to have a relevant model capable of accurately capturing glucose-insulin dynamics. This topic has received a great attention in the last decade, with different type of models: from Linear Time Invariant (LTI) (24,25) to Linear Parameter Varying (LPV) ones (26–28). In the DIABLO project, it has been proposed to derive a family of LTI models of thirteen-order from the UVA/Padova simulator to capture the dynamics from the subcutaneous insulin to the subcutaneous glucose in T1D patients. This set of LTI models is composed of a nominal LTI model fitted with an uncertainty block and it can be used for design and analysis purpose. Based on this modelling, a unique and robust Proportional-Integral-Derivative (PID) has been designed for the T1DMS adult cohort in (29). Results reported in (29) showed that BG regulation fitted with a basic bolus strategy of 2 units of insulin applied during the meal announcement, provided quite similar performances with respect to the individualised PID controllers of (30). These results motivated the use of a unique and robust controller to generate a continuous basal insulin injection. With the current technology of CGM sensors, it appears, however, necessary to couple this basal delivery with a bolus insulin injection protocol to improve the time in the so-called normo-glycaemic range ($70\text{mg/dl} < \text{BG} < 180\text{mg/dl}$) for counteracting the meal intakes. From (9,31), this strategy has been adopted by the current commercial AP systems on the market like MiniMed 780G (CE and FDA approval), Diabeloop (CE approval), Tandem t:slim X2 (FDA approval, CE approval in progress) and Omnipod Horizon (FDA approval in progress) where the bolus strategy involves assistance from the T1D patient, *i.e.* the patient has to calculate carbohydrate intake to precisely dose insulin boluses.

In the present work, we intend to highlight the benefits of numerical simulation (with the UVA/Padova T1DMS) to address this issue and establish *in silico* proofs of concept for the DIABLO project. In particular, we propose a method to define meal scenarios based on patients' body weight to better account for the interpatient variability in energy requirements and define more realistic meal scenarios. These scenarios are then used to assess the two different closed-loop solutions we already mentioned: the first one uses a GA-based controller tuning method (19,23) and the other one based on a robust control theory approach (29,32). With this second approach, we also propose a meal size-independent bolus strategy, slightly individualised by integrating the Carbohydrate-to-Insulin Ratio (CIR) in the bolus calculator rule. The objective here is to alleviate patient's workload and anxiety, while keeping him involved in the therapy management, *i.e.*, the patient still has to announce sizeable glucose intakes (meals). From an analysis of the *in silico* results, we will finally discuss the proposal of an original AP paradigm where the dissimilarity between a commercial CGM sensor and our biosensor could be used advantageously, to better handle inter- and inpatient variability in diabetes treatment and care.

Towards the integration of an islet-based biosensor in closed-loop therapies for patients with Type 1 Diabetes

2. Materials and Methods

2.1. UVA/Padova simulator

Simulators of human metabolic system based on the glucose-insulin dynamics, have been shown to be useful in developing diabetes treatment solutions (33). Such testing environments give the opportunity to assess the performance of algorithms with costs and time savings, and avoid ethical questions. In particular, the UVA/Padova T1DMS is the only simulation tool, approved by the US Food and Drug Administration (FDA), as an alternative for pre-clinical testing of closed-loop algorithms (22,34). T1DMS includes mathematical models of glucose-insulin dynamics, and several types of CGM sensors with realistic imperfections on the glucose measurement, insulin pumps and a simulation block dedicated to algorithm assessment. We used here the latest commercial version (v3.2) based on the equations given in Dalla Man *et al.* (21). This version includes a cohort of 33 T1D patients (11 adults, 11 adolescents, and 11 children). Hence, it is possible to simulate the effect of realistic meal scenarios on various virtual patients treated with the proposed closed-loop insulin solutions. However, it has to be noted that the considered version (v3.2) of the T1DMS involves the following working assumption:

Assumption 1: The glucose-insulin dynamics are not modulated by the circadian variability of insulin sensitivity.

The authors are aware that such assumption can limit the significance of multi-meal simulations. This choice has been made to not question or alter the human metabolic model approved by the FDA. A deeper analysis of this topic will be given in the discussion section.

2.2. A meta-heuristic method to design an islet-based closed-loop therapy

In real T1D populations, a large inter-patient variability is observed in terms of sensitivity to insulin, body weight, and T1D duration. This variability is a serious issue in designing easily adjustable AP systems as the amount of insulin required to mitigate postprandial hyperglycaemia greatly varies among patients. To account for this variability as well as to ensure reliability and stability of the closed-loop system, a fine tuning of the AP controller's parameters is necessary.

Controller tuning

In the first part of this work, a GA¹-based optimization technique is used to tune a PD_{BASAL} controller for each adult patient of the T1DMS cohort with respect to a clinically-relevant objective metric: the Blood Glucose Index (BGI) (Figure 3). This metric is a known indicator of the clinical risk associated with a given blood glucose level (20). The BGI risk function is defined as follows:

$$\text{BGI}(G) = 10 \times (1.509 \times (\ln(G))^{1.084} - 5.381))^2 \quad (1)$$

where G is the glucose level measured in mg/dl. By minimizing the mean BGI over a series of single meal scenarios, our GA-based algorithm can find controller parameters, which minimizes the clinical risk associated with the closed-loop regulation of the patient's glycaemia.

¹ GA = Genetic Algorithm

Towards the integration of an islet-based biosensor in closed-loop therapies for patients with Type 1 Diabetes

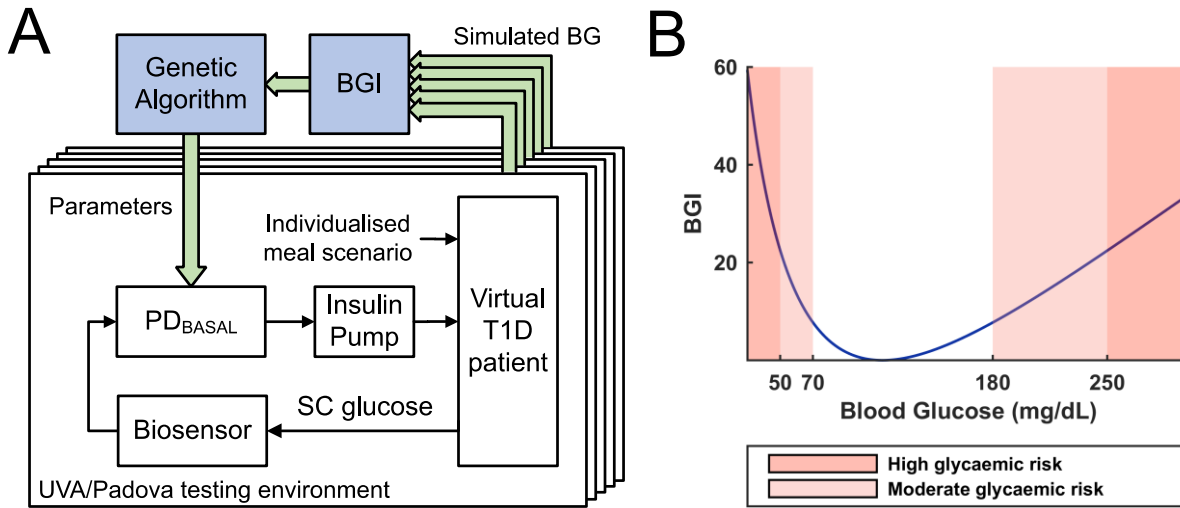


Figure 3: (A) Working principle of the Genetic Algorithm-based controller tuning method. 5 single meal scenarios are simulated for various controller parameter combinations. The closed-loop performance of each combination (averaged on the 5 scenarios) is assessed with a BGI-based cost function to iteratively tune the parameters of a PD_{BASAL} controller. SC glucose denotes the subcutaneous glucose concentration (B) Blood Glucose Index (BGI) risk unction plot.

Controller design

As a first step, this method was applied to the tuning of simple Proportional-Integral-Derivative (PID) controllers to handle the diffusion delays induced by subcutaneous glucose measurement and insulin infusion. Prior to (19), many variants of the traditional PID architecture were tested and a PD architecture associated with a subject specific basal infusion of insulin (PD_{BASAL}) was finally selected. This controller architecture provided good performance and allowed us to reduce the number of parameters to tune to 2, thus increasing the GA convergence speed. The corresponding discrete-time controller is represented by:

$$C(z) = K_p \left(1 + \frac{T_d}{T_s} \times \frac{z-1}{z} \right) \quad (2)$$

where $T_s = 5$ min is the sampling period of the PD_{BASAL} controller, T_d its derivative time constant, and K_p its proportional gain. A constant patient-specific basal insulin infusion rate provided by the T1DMS for each patient, is then summed to the controller output. More details about the islet-based sensor and its integration in a BG regulation closed-loop are given in (23); more details about the controller tuning methodology are given in (19,23).

Body weight-dependent meal scenario definition

The tuning method presented above has already proven its efficiency to individually tune the controller parameters of a CGM-AP for the 11 virtual T1D adults of the T1DMS patient cohort (19). The method was then refined to better handle the CGM sensor noise and applied to the tuning of our biosensor-based AP (Bios-AP) controller (23).

Towards the integration of an islet-based biosensor in closed-loop therapies for patients with Type 1 Diabetes

Real T1D patients have specific energy needs related to their individual metabolisms, ages, sexes and lifestyles. Using a unique meal scenario to evaluate the performance of closed-loop systems on a T1D population (either in vivo or in silico) therefore seems inadequate as most of the patients would receive either an under- or overstimulation by the unique meal scenario relative to their specific needs. To address this issue, and thus better account for the interpatient variability of energy requirements, we propose here a method to individualise the meal scenarios. To keep it simple, individualisation was performed using a single parameter. Among the patient's parameters provided by the T1DMS we chose the body-weight as it is the parameter which best represents patient's singularity, i.e., age, sex, metabolism, and lifestyle. To achieve meal scenario individualisation, each glucose intake of the user-defined scenario is divided by the average body weight of the 11 adults to obtain a meal scenario whose glucose intakes are defined in grams of glucose per kilogram (of body weight). The individualised scenarios which are actually simulated are then generated proportionally to each patient's body weight, see Figure 4. This method is implemented as a MATLAB function which seamlessly integrates the simulator execution flow. The function reads the user-defined meal scenario and generates individualised scenarios, while ensuring that the average daily glucose intake computed on all generated scenarios is the daily glucose intake of the user-defined scenario. In our previous work (23), validation scenarios were designed to match the daily glucose intake reported in the literature for American T1D adults (235 grams of glucose in average) (35). The main advantage of this method is that it maintains, by design, this realism as the scenario defined by the user serves to set the average scenario on the whole adult population. Note that such "normalization" to the body weight is also commonly used for animal *in vivo* glucose tolerance tests to avoid inter-individual bias (36).

Using the GA-method presented in (19,23) with individualised scenarios, a new set of controller parameters was generated for the Bios-AP, and for the 10 virtual T1D patients of the T1DMS (the 11th adult#average patient was not used in this study).

2.3. Simulation benefits for robust control problem formulation

In parallel to the development of an islet-based closed-loop architecture for BG regulation, we also attempted to formulate a control problem compliant with a robust solution. For that purpose, it has been proposed to derive a family of LTI models of thirteen-order from the UVA/Padova simulator able to capture the interpatient variability in the glucose-insulin dynamics. These models were then used to design a unique feedback controller $K(s)$, for a population of T1D patients, which delivers a control signal called insulin basal. To quickly react to food intake, a meal announcement feature was implemented in this second part to trigger the delivery of meal boluses. Contrary to more standard meal bolus features involving a patient-provided estimation of the quantity of ingested carbohydrates (37),

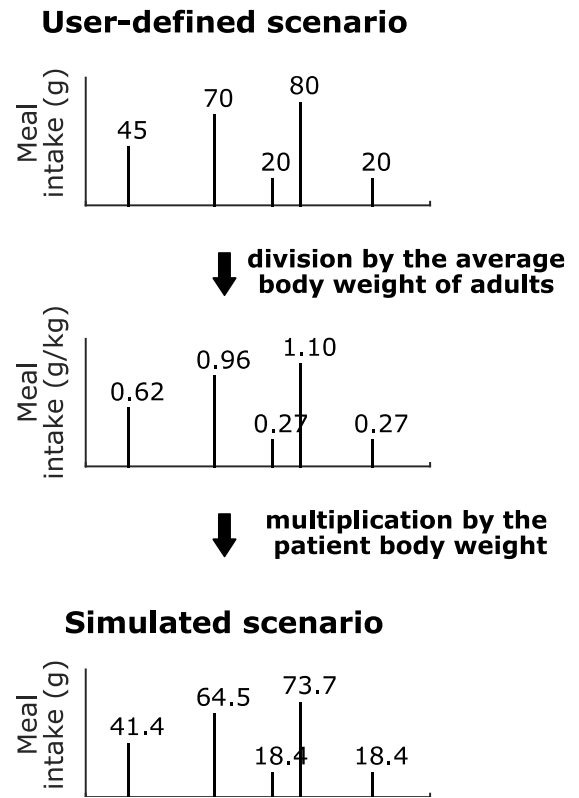


Figure 4: Body weight-dependent definition of the glucose intake scenarios. Example for adult#005 of the T1DMS.

Towards the integration of an islet-based biosensor in closed-loop therapies for patients with Type 1 Diabetes

we developed a bolus strategy which diminish patient's workload and anxiety by only requesting a meal announcement, *i.e.*, a constant insulin bolus is delivered for each sizeable meal (breakfast, lunch and dinner). This meal-independent bolus feature was individualised by integrating the patient CIR² knowledge of the clinician in charge of the T1D patient. The control algorithm, proposed in this subsection, thus delivers the following insulin signal $u(t)$:

$$u(t) = \begin{cases} K(r(t) - SG(t)) + u_{\text{bolus}} & \text{for one minute at meal announcement} \\ K(r(t) - SG(t)) & \text{otherwise} \end{cases} \quad (3)$$

where $SG(t)$ is the subcutaneous glucose signal delivered by a CGM sensor. $r(t)$ is the glucose target. With a duration of one minute after a sizeable meal announcement, the signal u_{bolus} is given by the following mathematical expression:

$$u_{\text{bolus}} = 12000L(\text{CIR}), \quad L(\text{CIR}) = \begin{cases} 1 & \text{if CIR} > 15 \text{ g/U} \\ 2 & \text{if CIR} \leq 15 \text{ g/U} \end{cases} \quad (4)$$

where the value of 12000 pmol/min (2 unities of fast insulin) has been chosen to be compliant with the requirements of (30). This magnitude can be adapted by considering the CIR of the T1D patient to schedule the adaptive gain L , see equation (4). Hence, the retained closed-loop insulin setup in this sub-part obeys to the architecture shown in Figure 5.

In the following subsection, we first provide guidelines showing how it is possible to derive a family of linear models for the considered population of T1D patients. Next, a robust control technique was used for control design purpose.

Getting a family of linear models of T1D patient population

From (21), the nonlinear dynamical model of a T1D patient can be written according to :

$$\begin{cases} \dot{x}(t) = f(x(t), u(t), \theta(t)) \\ y(t) = C_0 x(t) \end{cases} \quad (5)$$

where $C_0 = (0_{1 \times 12} V_G^{-1} \quad 0_{1 \times 5})$ with $x(t) \in \mathbb{R}^{18}$, $u(t) \in \mathbb{R}^3$, $\theta(t) \in \mathbb{R}^9$ and $y(t) \in \mathbb{R}$ are respectively the model state, input, time-varying parameter and output vectors, with the functional $f: \mathbb{R}^{18} \times \mathbb{R}^3 \times \mathbb{R}^9 \rightarrow \mathbb{R}^{18}$. All time-varying parameters and the physiological parameter V_G are defined in (21). As we

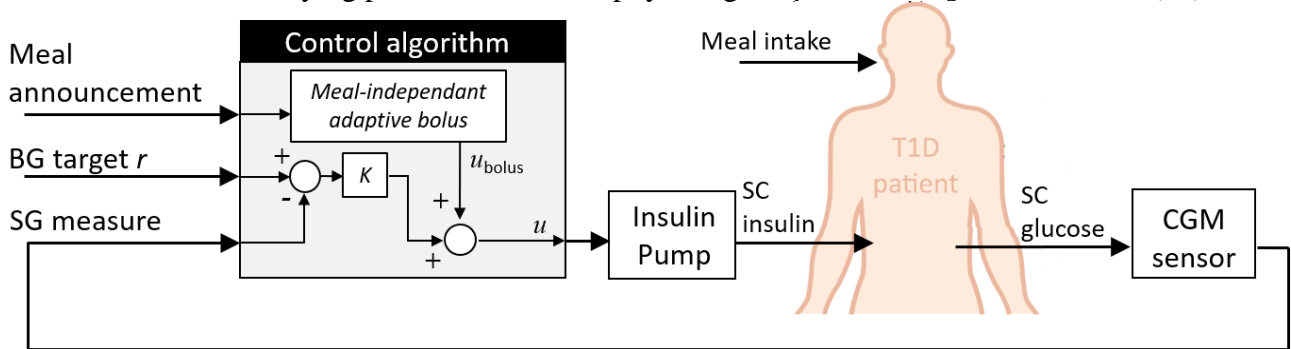


Figure 5: Standard setup for closed-loop insulin therapy. In this work, the controller K is a unique robust controller for the whole T1D patient population. Personalization is deported in the bolus calculator rule.

²CIR : Carbohydrate-to-Insulin Ratio

Towards the integration of an islet-based biosensor in closed-loop therapies for patients with Type 1 Diabetes

were considering closed-loop insulin systems, the model given by equation (5) was reduced to a state vector of 13 states by taking out the contribution of the last 5 states $(x_{14}, x_{15}, \dots, x_{18})$ relative to the glucagon dynamics. Hence, the reduced model became

$$\begin{cases} \dot{x}_r(t) = f_r(x_r(t), u_r(t), \theta_r(t)) \\ y(t) = Cx_r(t) \end{cases} \quad (6)$$

where $C = (0_{1 \times 12} \ V_G^{-1})$ with $x_r(t) \in \mathbb{R}^{13}$, $u_r(t) \in \mathbb{R}^2$, $\theta_r(t) \in \mathbb{R}^7$ and $f_r: \mathbb{R}^{13} \times \mathbb{R}^2 \times \mathbb{R}^7 \rightarrow \mathbb{R}^{13}$. $u_r(t) = (u_1(t) \ u_2(t))^T$ where u_1 refers to the carbohydrate intake (*i.e.* the meal) and u_2 corresponds to the insulin infusion rate, which is delivered to the patient through an insulin pump.

To obtain a family of linear models able to fit the nonlinear model equation (6), the set of operating points (x_r^*, u_r^*) had to be chosen judiciously, *i.e.*, the time-varying parameters θ_r were constant on a time interval described later. For each operating point (x_r^*, u_r^*) , a first-order Taylor approximation was thus performed and the nonlinear model equation (6) were reformulated as follows:

$$\begin{cases} \delta \dot{x}_r(t) = A(x_r^*, u_r^*) \delta x_r(t) + B(x_r^*, u_r^*) \delta u_r(t) \\ \delta y(t) = C \delta x_r(t) \end{cases} \quad (7)$$

where $\delta x_r(t) = x_r(t) - x_r^*$ and $\delta u_r(t) = u_r(t) - u_r^*$. $\delta y(t)$ is the variation of the output with respect to the fasting basal glucose G_b and A, B are the Jacobian matrices of vector field f_r with respect to x_r and u_r , evaluated at (x_r^*, u_r^*) . The key element was then to define a set of values (x_r^*, u_r^*) sufficiently dense to obtain an accurate approximation of equation (6) with (7). To proceed, the nonlinear model of the T1DMS was used to simulate a single meal scenario with basal insulin input ($u_2 = I_b$). The meal corresponded to 50 g of carbohydrates, ingested during 15 min (*i.e.* $u_1 = 3333$ mg/min). The basal insulin I_b is the proper quantity of insulin that allows to reach a steady-state condition during fasting periods (38). For the considered population of adult T1D patients, we have $94.6 \text{ pmol/min} \leq I_b \leq 150.0 \text{ pmol/min}$. From this simulation, the spatial discretization is achieved on x_r and u_r in order to produce a set of adequate values for (x_r^*, u_r^*) such that time-varying parameters θ_r are constant on the considered interval, *i.e.* let the simulation time horizon $[0, T]$ be divided into subintervals as follows: $0 = t_0 < t_1 < \dots < t_n = T$. The set $\lambda = (\lambda_0, \lambda_1, \dots, \lambda_k, \lambda_n)$ is defined such as:

$$\begin{cases} \lambda_0 \in [t_0, \frac{t_1}{2}] \\ \lambda_k \in [\frac{t_k + t_{k-1}}{2}, \frac{t_{k+1} + t_k}{2}] \text{ for } 1 \leq k < n \\ \lambda_n \in [\frac{t_n + t_{n-1}}{2}, t_n] \end{cases} \quad (8)$$

On each subinterval, $t \in \lambda_k$ for $k \in \{0, \dots, n\}$, a linear model for each patient denoted with patient index $i = \{1, \dots, 11\}$ is deduced as

$$\begin{cases} \delta \dot{x}_r^i(t) = A_k^i \delta x_r^i(t) + B_k^i \delta u_r^i(t) \\ \delta y^i(t) = C_k^i \delta x_r^i(t) \end{cases} \quad (9)$$

where $B_k^i = (B_{1_k}^i \ B_{2_k}^i)$ with $B_{1_k}^i, B_{2_k}^i \in \mathbb{R}^{13 \times 1}$. Figure 6A shows the spatial discretization for the considered scenario. This protocol was thus repeated several times (a total of $n = 222$ models per patient) in order to have a family of linear models able to guarantee a good approximation of the nonlinear model equation (6), see (29) for more details.

Towards the integration of an islet-based biosensor in closed-loop therapies for patients with Type 1 Diabetes

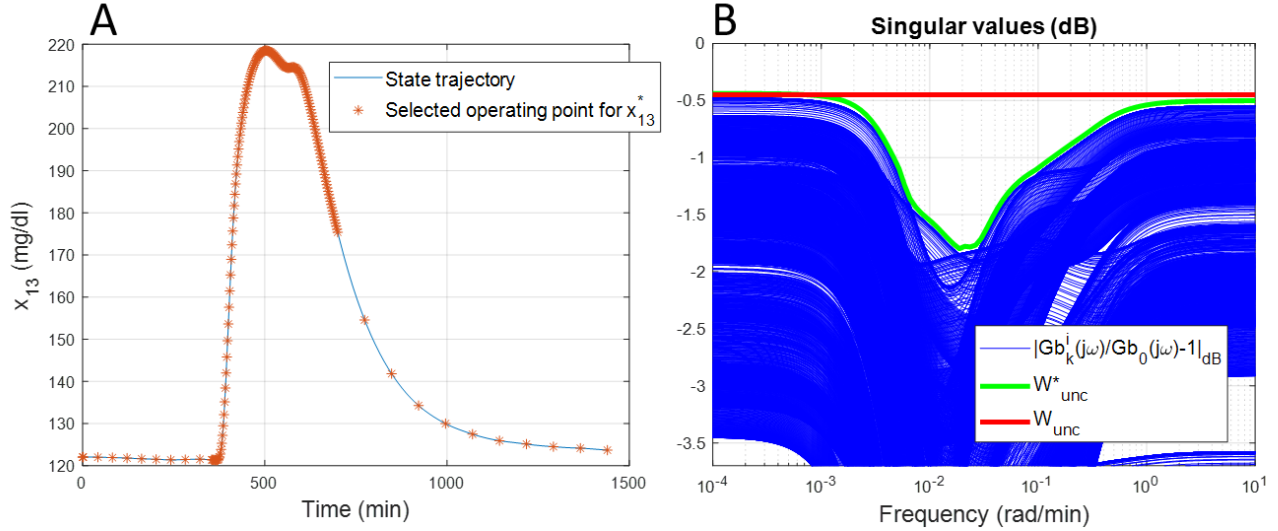


Figure 6: Use of the T1DMS for modelling purpose: two important steps (A) Spatial discretization for the considered single meal scenario on the 13th states of the nonlinear model in UVA/Padova simulator for the patient adult#001 of T1DMS. (B) Results of the constructive solution to obtain the upper LFT of the entire family of linear models. In blue, it is the frequency behaviour of $|G_k^i(j\omega)/G_0(j\omega) - 1|_{dB}$. The optimal solution W_{unc}^* is plotted in green and the retained value W_{unc} for this study case is plotted in red.

Before formulating the control design problem, two sources of uncertainty must be considered: *i*) the inter- and intra-patient variability within a T1D population due to patient's characteristics (*e.g.*, fasting basal, total daily insulin need, weight) and *ii*) the dynamics of the glucose diffusion from the intravascular space to the subcutaneous one. Note that the output of model equation (9) gives information on the 13th model state corresponding to the level of subcutaneous glucose ($SG(t)$). To have information of BG level, it is necessary to refer to the 4th model state.

Regarding the uncertainty of patient's characteristics, the so-called unstructured multiplicative uncertainty form (39) is used to derive the family of linear models (Equation 9), which can be rewritten by using the Linear Fractional Transformation (LFT) representation according to:

$$\begin{aligned} Gb_k^i(s) &= \underline{C}_k^i(sI - A_k^i)^{-1}B_{2k}^i \quad \forall i, k \\ &= Gb_0(s)(1 + W_{unc}(s)\Delta_b(s)) = \mathcal{F}_u(P_b(s), \Delta_b(s)) \end{aligned} \quad (10)$$

where the matrix \underline{C}_k^i is used to refer to the 4th state of equation (9). \mathcal{F}_u is the upper LFT defined as $\mathcal{F}_u(M, N) = M_{22} + M_{21}N(I - M_{11}N)^{-1}M_{12}$. $W_{unc}(s)$ is a weighting function used to normalize the uncertainty Δ_b , $\|\Delta_b\|_\infty \leq 1$. Hence, W_{unc} has to guarantee:

$$|W_{unc}(j\omega)| \geq \left| \frac{Gb_k^i(j\omega)}{Gb_0(j\omega)} - 1 \right| \quad \forall i, k, \omega \quad (11)$$

Equation (11) gives a constructive solution to determine the couple (Gb_0, W_{unc}) . To have the smallest conservative LFT, the optimal solution (Gb_0^*, W_{unc}^*) is constructed such that $\|W_{unc}^*\|_\infty$ is minimal. This optimization problem leads to the results given in Figure 6B, where W_{unc}^* is found of order 11 to perfectly fit the upper bound. However, choosing a simple constant for $W_{unc} \approx 0.45$ leads to a LFT $\mathcal{F}_u(P_b(s), \Delta_b(s))$, which is less complex (dimension of Δ_b is one), with a small conservativeness since

Towards the integration of an islet-based biosensor in closed-loop therapies for patients with Type 1 Diabetes

the maximum gap between the optimal solution W_{unc}^* and W_{unc} is inferior to 1.5dB . Towards this end, the constant solution is retained in this study case.

Next, a parametric uncertainty is considered to integrate the time lag variability in T1D patients (between 6.83 and 10.83 min for the adult cohort of T1DMS) of glucose from intravascular to interstitial space (40). A deeper analysis of the equation (4) reveals that this variability is reflected by a gain variation of the transfer between the 4th (BG level) and the 13th (SG level) state. Such variation can be easily captured by an upper LFT so that

$$G_{sc_k}^i(s) = \mathcal{F}_u(P_{sc}(s), \Delta_{sc}), \forall i, k \Delta_{sc} \in \mathbb{R}: \|\Delta_{sc}\|_{\infty} \leq 1 \quad (12)$$

where Δ_{sc} is the uncertainty block used to capture this variability. The input of $G_{sc_k}^i(s)$ must be the BG level and its output corresponds to the SG one.

Design of the unique controller K

We then aimed to design a unique controller $K(s)$ for a population of T1D patients – the adult cohort in this study case – able to maintain the BG level in a specified range despite T1D patient variabilities. For feedback controller design purpose, it is proposed to work on the feedback architecture given in Figure 7. The block $G_{zoh}(s)$ has been introduced to model the digital-analogue converter integrated in the insulin pump, as a delay of $T_s/2$ where T_s is the considered sample time. Here, we modelled $G_{zoh}(s)$ by a Pade approximation of first order. Hence, the unique controller $K(s)$ must be designed to control the augmented system $\tilde{G}_{\Delta}(s)$ shown in Figure 7. In this work, the loop shaping method fitted with an H_{∞} optimization problem was used to guarantee robustness and the closed-loop stability (41). Such robust technique usually involves two main steps, *i*) define a pre-compensator $W_1(s)$ and a post-compensator $W_2(s)$ to enforce the desired open-loop specifications on the shaped plant $\tilde{G}_s(s) = W_2(s)\tilde{G}_{\Delta}(s)W_1(s)$ and *ii*) use the normalized coprime factor (42) to solve an H_{∞} optimization problem according to (41). All theoretical justifications dedicated to the considered Glover-McFarlane H_{∞} normalized coprime factor loop-shaping algorithm are given in (41,42).

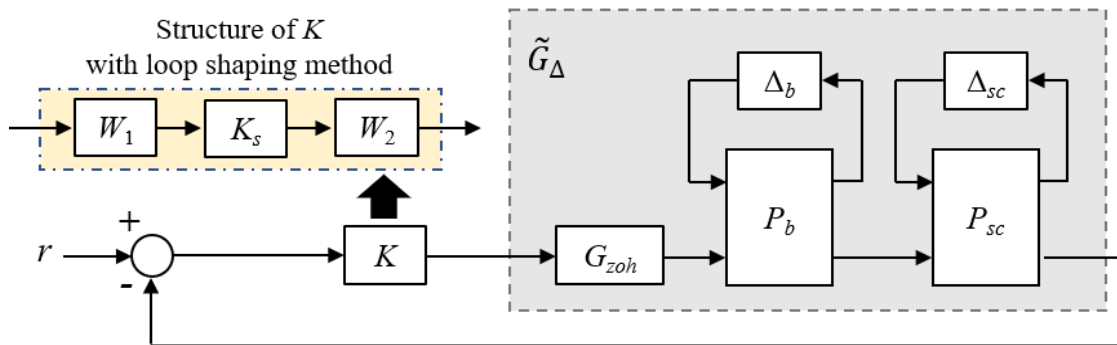


Figure 7: Feedback control setup for design purpose

According to (41), we consider the nominal plant $\tilde{G}_0(s)$ ($\Delta_{sc} = 0$ and $\Delta_b = 0$) for design purpose. Thereby, the constructive solution based on equation (11) becomes a crucial step to obtain the smallest conservative LFT. To design a controller $K_s(s)$ able to stabilize a family of systems of the nominal

Towards the integration of an islet-based biosensor in closed-loop therapies for patients with Type 1 Diabetes

shaped plant $\tilde{G}_{s0}(s) = W_2(s)\tilde{G}_0(s)W_1(s)$, weighting functions $W_1(s)$ and $W_2(s)$ have to be defined. In a preliminary study (29), PID controllers achieved acceptable performance and the worst-case performance was observed for the patient 8 of the adult cohort. Thus, we selected $W_2 = 1$ and chose the continuous state-space representation of the individualised Proportional-Integral-Derivative (PID) controller dedicated to the eighth T1D patient for $W_1(s)$. Interested reader can refer to (30) to have the guidelines for PID tuning with two physiological parameters: the body weight and the total daily insulin dose. The last optimization step can be applied to improve worst-case results and be robust against the uncertainty ball in the normalized coprime factors. With the following H_∞ cost function:

$$\gamma(K_s(s)) = \left\| \left[\begin{array}{c} 1 \\ K_s(s) \end{array} \right] (1 - \tilde{G}_{s0}(s)K_s(s)) \left[1 \quad \tilde{G}_{s0}(s) \right] \right\|_\infty \quad (13)$$

the optimal performance is obtained by minimizing the following cost:

$$\gamma := \min_{K_s} \gamma(K_s(s)) \quad (14)$$

γ is linked with the normalized coprime stability margin. In the range $1 < \gamma < 3$, stability margins are judged satisfactory to be robust against the considered unstructured uncertainties. In our case, we are in this expected range ($\gamma = 1.69$). Hence, the unique robust feedback controller $K(s)$ for a population of T1D patients is finally built by combining the H_∞ controller $K_s(s)$ designed on the worst-case results, with the shaping functions $W_1(s)$ and $W_2(s)$ according to $K(s) = W_1(s)K_s(s)W_2(s)$.

Note that the authors are aware that a μ -analysis should be required to know if the resulting controller is able to theoretically satisfy the control specifications for all uncertainties Δ_{sc} and Δ_b . Due to the scope of the journal, it is proposed here to only perform several simulations in the result section to assess this requirement. Interested readers can however consider the preliminary works (29,32) to know how this concern can be theoretically addressed.

2.4. Metrics for closed-loop therapy assessment

In this study, eight of the metrics recommended in (43–45), *i.e.* the Time Below Range (TBR) with too different levels, the Time In Range (TIR), the Time Above Range (TAR) with also two different levels, the Low Blood Glucose Index (LBGI), the High Blood Glucose Index (HBGI), and the mean BG, were used for performance assessment. In addition, we also considered the Total Daily Insulin (TDI). For the time spent in the different glycaemic ranges the targets recommended in (46) for normal T1D adult patients were used. Definitions of these metrics and recommended targets are provided as Supplementary Material. Note that there is no official recommended value or target for the TDI metric. Indeed, the insulin need is highly dependent on the physiological status (e.g., stress, physical activity) and characteristics of the patients. This metric was therefore used to monitor the aggressiveness of the studied closed-loop solutions, and for comparison purpose.

2.5. Statistical analysis

To complete the performance analysis, normality of datasets was tested using the Shapiro-Wilk test and statistical significance was then assessed using either the two-sided paired sample t-test or the two-sided Wilcoxon signed rank test. P-values lower than 0.01 were considered significant.

Towards the integration of an islet-based biosensor in closed-loop therapies for patients with Type 1 Diabetes

3. Results

As mentioned above, the objective of this work is to present and assess two different manners to handle the interpatient variability, which still challenges AP systems. The first subsection presents the results of a highly individualised approach with the islet-based closed-loop (Figure 3). In contrast, the second subsection presents the results obtained with a more common CGM-based AP system where a unique controller is tuned, for the whole adult cohort of the T1DMS, using a robust control theory approach (Figure 5). The results presented in both subsections are based on meal scenarios individualised with the method presented in subsection 2.2. Two realistic 48-hour scenarios, where the same meal pattern is repeated on two consecutive days, are simulated. The first pattern, referred to as the “standard scenario”, consists in five carbohydrate intakes, 0.62, 0.96, 0.27, 1.10 and 0.27 grams of glucose per kilogram of body weight respectively at time $t = 180, 480, 720, 900,$ and 1080 minutes (corresponding, on average, to 45, 70, 20, 80 and 20 grams of glucose over the whole adult population, see section 2.2). The second pattern, referred to as the “challenging scenario”, consists in three large carbohydrate intakes, 0.89, 1.24, and 1.10 grams per kilogram of body weight respectively at time $t = 180, 480,$ and 960 minutes (corresponding to 65, 90 and 80 grams on average). The default meal duration of 15 minutes was used for all meals.

3.1. Islet-based closed-loop therapy assessment

Our GA-based tuning method was used to tune the parameters of a PD_{BASAL} controller for each adult patient of the T1DMS cohort. Contrary to our previously published works, the controllers are tuned here using individualised single meal scenarios (see Methods section). These controllers are associated with the biosensor model presented in (23) to form the islet-based closed loop. To assess

Table 1: Performance metrics for the 10 T1D adults treated with the islet-based closed loop and submitted to the “standard scenario”.

Patient	LBGI (-)	HBGI (-)	TDI (U)	Mean BG (mg/dl)
1	0.1	2.3	42.4	131.4
2	0.2	1.6	44.9	124.4
3	0.5	1.2	55.3	122.3
4	0.3	1.5	33.3	125.5
5	0.4	1.6	39.1	123.3
6	0.2	2.8	68.3	134.7
7	0.6	1.6	39.5	120.4
8	0.2	4.1	59.7	146.6
9	0.1	2.4	32.0	132.4
10	0.1	1.6	44.8	125.2

The metrics extracted for this analysis are the Low Blood Glucose Index (LBGI) (unitless), the High Blood Glucose Index (HBGI) (unitless), the Total Daily Insulin (TDI) units injected, and the mean BG level (Mean BG).

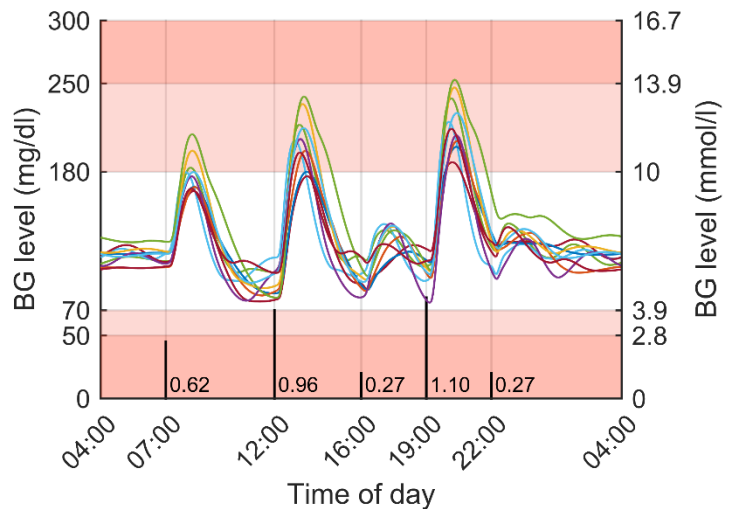


Figure 8: Simulation results for the ten T1D adults submitted to a 48-hour, 3-meal 2-snack scenario (last 24 hours are displayed) and treated with the islet-based closed-loop therapy (via subcutaneous routes). Meal intakes are labelled in g/kg and marked with black vertical bars on the chart. Regions with no glycemic risk, moderate glycemic risk and high glycemic risk are color-coded, respectively in white, pink and red.

Towards the integration of an islet-based biosensor in closed-loop therapies for patients with Type 1 Diabetes

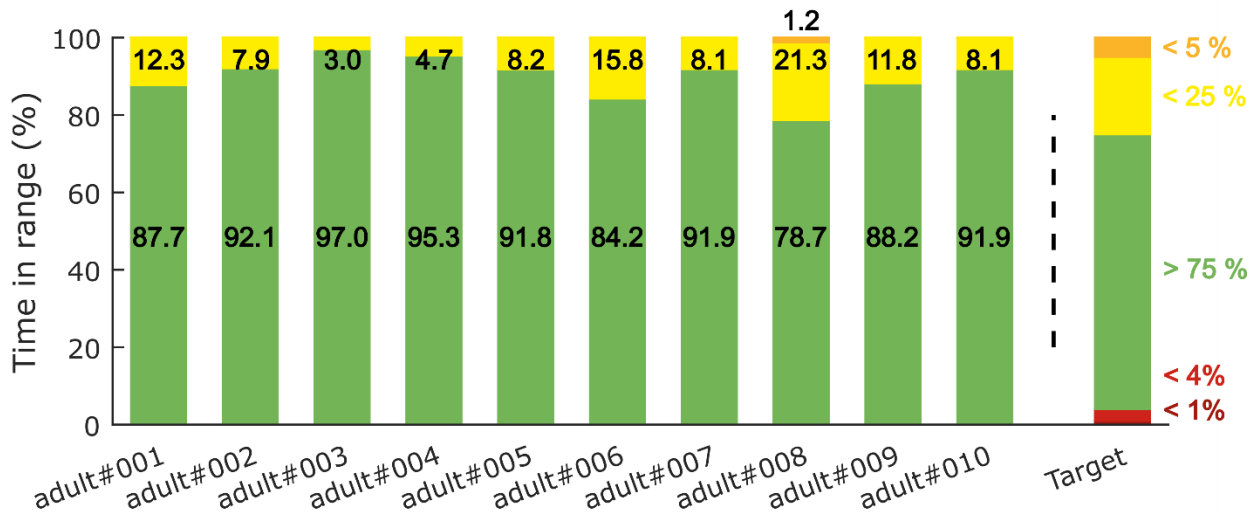


Figure 9: Time spent in the different glycaemic ranges for the ten adults of the T1DMS treated with the islet-based BG regulation closed loop and submitted to the “standard scenario”. The recommended targets (see Battelino et al. (43)) are plotted on the right side of the chart.

the performance of this system, the ten T1D adults were submitted to the “standard scenario”. Figure 8 presents the BG profiles obtained for each patient during the last 24 hours of this realistic 3-meal 2-snack scenario. For every patient, the BG regulation system provided satisfactory performance with limited postprandial hyperglycaemia and no hypoglycaemic event during the 48 hours. To complete the assessment of our islet-based closed-loop system, we computed the performance metrics detailed in the Methods section. Concerning the time spent in the 5 glycaemic ranges defined by Danne and colleagues (45), the islet-based closed loop permitted to all patients to reach the recommended targets (46). Excellent results were obtained for all the patients (TIR ranging from 78.7% to 97.0%) with a particularly satisfactory mitigation of the hypoglycaemic risk (TBR = 0% for every patient), see Figure 9. According to the T1DMS User Manual, the mean LBG and HBG are minimal for all patients (see Table 1). Concerning the mean BG, most patients present levels below 140 mg/dl, which allow them to achieve the recommended HbA1c³ target level of 6.5%⁴.

3.2. Assessment of the robust closed-loop therapy

We integrated the unique robust controller K and the bolus calculator rule (4) (both described in the Methods section) in the UVA/Padova T1DMS according to the setup shown in Figure 5. Closed-loop was assessed with respect to standard recommendations introduced previously. A standard CGM sensor model was used for these simulations. Ten T1D adults were submitted to two multi-meal scenarios: the first one is the “standard scenario” mentioned above (a 3-meal 2-snack pattern repeated on two consecutive days) and the second is the “challenging scenario” (three heavy meals daily for 48 hours). Scenarios were also individualised using the patient body weight. As for the islet-based closed-loop, the performance assessment was made on the last 24 hours (second day). In addition, scenarios were repeated 25 times to account for the random inaccuracies of the CGM sensor (47).

³ HbA1c = glycosylated hemoglobin A1c

⁴ The conversion was computed using the online eAG/A1C Conversion Calculator provided by the American Diabetes Association.

Towards the integration of an islet-based biosensor in closed-loop therapies for patients with Type 1 Diabetes

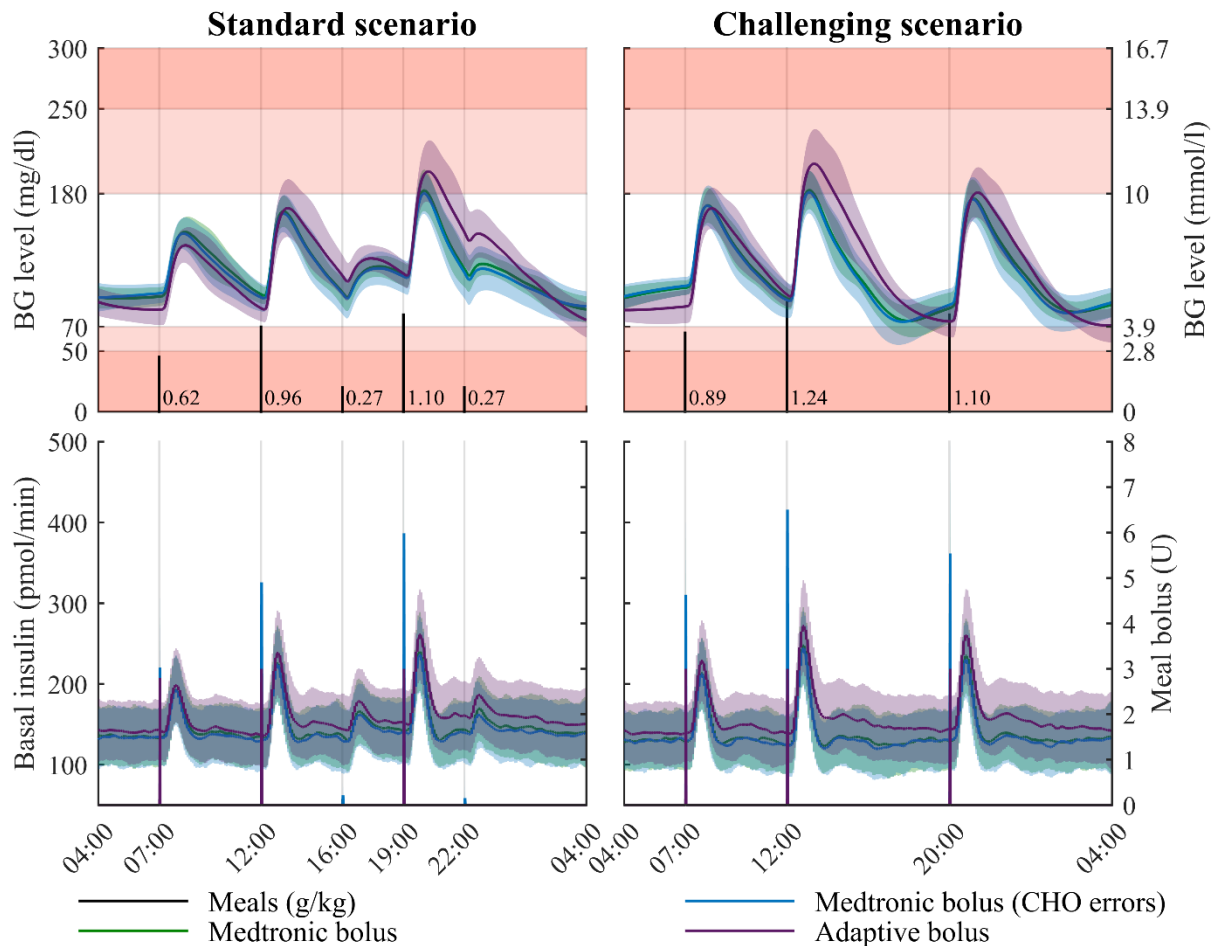


Figure 10: Simulation results for two realistic 48-hour multi-meal scenarios in adults (last 24 hours are displayed), for three closed-loop therapies. The proposed robust controller is assessed with three different meal bolus solutions: the Medtronic bolus, the Medtronic bolus with errors introduced in the patient-provided carbohydrate (CHO) counting, and the proposed adaptive bolus. Mean glucose profile (curve) and standard deviation (coloured patches) are displayed on the top panels. Regions with no glycaemic risk, moderate glycaemic risk and high glycaemic risk are color-coded, respectively in white, pink and red. Bottom panels display the basal and bolus insulin infusion for the three evaluated closed-loop (left axis for the basal and right axis for the bolus).

For both scenarios, three closed-loop therapies were evaluated. In all cases, the unique robust controller designed in subsection 2.3 was used. The changes only concern the insulin bolus delivery triggered by the announcement of a sizeable meal. First, we considered the standard of Medtronic’s bolus rule (see for instance the equation (6) of (47)) with a perfect estimate of carbohydrate (CHO) intakes, *i.e.* the patient enters, to the nearest gram, the exact carbohydrate content of the meal into the AP device. Since it has been reported that errors in carbohydrate counting by patients can range from -30% to +40% (48), a second series of simulations is performed with the same therapy, but with random CHO estimation errors. Finally, the third closed-loop therapy evaluated here, integrates the proposed meal bolus solution called “adaptive bolus”, and whose bolus rule is given in the equation (4). Figure 10 and Table 2 show the simulation results and the corresponding performance metrics.

For the “standard scenario” (left plots of Figure 10), the BG levels remained mostly in the TIR interval without snack bolus. The same trend occurred for the “challenging scenario” reported on the right side of Figure 10. For the so-called “standard scenario”, the three assessed closed-loop insulin

Towards the integration of an islet-based biosensor in closed-loop therapies for patients with Type 1 Diabetes

Table 2: Metrics for closed-loop therapy assessment - Robust control laws - Adult cohort

Standard scenario									
Category	TBR 2 (%)	TBR 1 (%)	TIR (%)	TAR 1 (%)	TAR 2 (%)	LBGI (.)	HBGI (.)	Mean BG (mg/dl)	TDI (U)
MED	0.0 (0.1)	0.5 (1.6)	97.1 (3.5)	2.4 (3.2)	0.0 (0.0)	0.6 (0.4)	1.0 (0.5)	117.9 (5.6)	48.4 (12.3)
MED-ERR	0.5 (2.1)	1.8 (4.0)	95.8 (5.6)	2.4 (3.3)	0.0 (0.0)	0.9 (1.0)*	1.0 (0.5)	116.3 (6.5)*	48.8 (12.8)*
ADAPT	0.2 (0.8)	3.0 (4.4)	90.6 (10.1)	6.4 (7.6)	0.6 (1.8)	1.1 (0.7)*	1.7 (1.3)	121.5 (9.8)	46.8 (10.7)*†
Challenging scenario									
Category	TBR 2 (%)	TBR 1 (%)	TIR (%)	TAR 1 (%)	TAR 2 (%)	LBGI (.)	HBGI (.)	Mean BG (mg/dl)	TDI (U)
MED	0.5 (1.7)	4.6 (6.4)	90.5 (11.3)	4.8 (6.3)	0.0 (0.0)	1.6 (0.9)	1.3 (0.6)	113.7 (3.5)	48.9 (12.7)
MED-ERR	1.9 (4.1)	8.0 (7.5)*	86.9 (10.8)	5.0 (5.7)	0.0 (0.0)	2.2 (1.7)*	1.3 (0.6)	112.6 (5.8)	49.5 (13.1)*
APAPT	1.1 (3.0)	6.5 (8.9)	84.1 (16.4)*	9.4 (9.5)*†	0.8 (2.4)	2.0 (1.3)*	2.2 (1.5)	119.2 (8.5)*†	46.6 (10.7)*†

Simulation results were obtained with the 10 adult patients of the T1DMS. Three closed-loop strategies are compared: the unique robust controller K fitted with the bolus calculator of Medtronic without (MED) and with CHO counting errors (MED-ERR), and the proposed meal-independent adaptive bolus rule associated to the unique robust controller K (ADAPT) shown in Figure 5. Standard and challenging individualised meal scenarios consider realistic daily glucose intakes of a five-meal intakes (45g, 70g, 20g, 80g and 20g) and three heavy meals (65g, 90g, 80g). The metrics extracted for this comparison are the Time Below Range (TBR) (level 1 and 2), Time In Range (TIR), Time Above Range (TAR) (level 1 and 2), the Low- and High- Blood Glucose Index (LBGI and HBGI), mean Blood Glucose (Mean BG) concentration in mg/dl, and the Total Daily Insulin (TDI) in units of insulin. Standard Deviations (SD) are displayed for all metrics, see values into the parentheses. Symbol * indicates statistical significance ($p < 0.01$) with respect to MED and symbol † indicates statistical significance ($p < 0.01$) with respect to MED-ERR.

therapies presented a mean TIR above 90% (see Table 2). Moreover, the unique controller fitted with the adaptive meal-independent bolus rule possessed the smallest TDI, causing *de facto* a small increase of TAR1, TAR2 and HBGI metrics. Nevertheless, all metrics followed the recommended values, see Supplementary Material. These data motivated the use of a unique robust controller designed according to the protocol introduced in section 2.3. As one would expect, the best TIR (97.1%) was obtained with the standard rule of Medtronic bolus delivery, without CHO errors. Removing the CHO estimation in the bolus calculator (*i.e.*, using the adaptive bolus) caused a performance drop of 6.5% for the TIR. An equivalent gap (6.4%) can be observed with the second scenario. However, this gap was attenuated when the CHO counting errors were considered: the drop decreased to 5.2% between the Medtronic bolus with CHO errors and the adaptive one in the standard scenario, and was further reduced to 2.8% in the challenging one. In other words, when realistic CHO counting is considered, the price to pay to mitigate the patient’s workload and anxiety is a deterioration of the time spent in the TIR of 2.8% on the last 24 hours, with slightly better results for the TBR2, TBR1 and LBGI metrics.

3.3. Comparison with other works

During the last decade, many algorithms have been proposed for the Artificial Pancreas controller and tested with the UVA/Padova T1DMS (49–52). Varying levels of closed-loop performance have been achieved *in silico* depending on the complexity of the control algorithm and

Towards the integration of an islet-based biosensor in closed-loop therapies for patients with Type 1 Diabetes

on the degree of user input (meal and exercise announcement). To compare our results to the literature, we selected recent works, published by Gondhalekar et al. (51) and Colmegna et al. (52), for their similarities with our work and their use of the same simulator version, which enables a fair comparison. The meal scenarios used in these works were simulated 25 times for each adult of the T1DMS cohort (note that the individualisation function presented in section 2.2 was not used here). In (51), a MPC law which uses a discrete-time LTI model of glucose-insulin dynamics is proposed. The control algorithm integrates two main features: a velocity-weighting to mitigate controller-induced hypoglycaemia and a velocity-penalty to correct postprandial hyperglycaemia. For this comparison, our unique controller K was associated with the Medtronic bolus rule. The 27-h meal scenario consisted in three large glucose intakes of 90 grams each. Contrasting results were obtained as the TIR increased by 8.8% with our controller but with a poorer mitigation of the hypoglycaemic risk (2.53% vs 0.07% - see Table 3). Of note, this comparison presents two limitations lying in the number of patients used (the full cohort of 111 patients was used in (51)) and the different premeal bolus strategies. In (52), Colmegna and colleagues proposes a control strategy based on hyperglycaemia detection to switch between two controllers of varying aggressiveness, both designed using an LPV model of the glucose-insulin dynamics and the H_∞ framework. This second comparison permitted to assess the performance of our unique robust controller alone, *i.e.*, without premeal bolus. The 28-h meal scenario consisted in 3 glucose intakes of 40, 70 and 60 grams of glucose. Here, our controller was outperformed by the switching controller which permitted both a lower TBR (respectively 2.96 % vs 0.00 %) and a better TIR (88.0 % vs 73.4 %). This result did not come as a surprise since the design of a unique controller for the whole adult cohort (our work), compared to two individualised controllers per patient in (52), induces reduced closed-loop performance due to an increased conservatism.

Table 3: Performance indicators for the comparison with literature

Ref.	Controller	Premeal Bolus	Mean BG [mg/dl]	TBR 2 [%]	TBR 1 [%]	TIR [%]	TAR 1 [%]	TAR 2 [%]	Risk index	
									LBG1	HGI
This work ^a (51) ^b	H_∞	Yes	119.7	0.09	2.53	88.1	9.33	0.00	1.11	1.77
	MPC	Yes	N/A	0.00	0.07	80.8	19.2	1.80	0.12	3.63
This work ^a (52) ^a	H_∞	No	145.2	1.33	2.96	73.4	23.7	2.91	1.00	4.59
	Switched H_∞	No	133.2	0.00	0.00	88.0	12.0	N/A	0.32	2.49

a. Simulated in T1DMS S2013 with 10 adult patients

b. Simulated in T1DMS S2013 with 111 adult patients

Towards the integration of an islet-based biosensor in closed-loop therapies for patients with Type 1 Diabetes

4. Discussion

Modelling the biological diversity to improve simulation realism

Variability in diabetes takes many forms, which can be classified as inter- and intra-patient variabilities. Intra-patient variability is linked to the evolution, over time, of the general body status and physiological features for each T1D patient. Interpatient variability corresponds to the variation of body characteristics between patients, by genetic differences and environmental factors, since past and present lifestyles shape the body and its response to nutrient intake. These variabilities result in a very specific response to meal intake which, paired with the individual response to insulin therapy, still constitute major hurdles to the development of fully automated Artificial Pancreas systems able to truly restore glucose homeostasis. In this context, numerical simulation tools are now commonly used to assess control algorithms with respect to different sources of variability in a cost-effective manner. In particular, the UVA/Padova T1DM Simulator accurately models the interpatient variability observed in response to meal intake in real T1D patients (53).

Concerning the inpatient variability, we are aware that one limitation of the version 3.2 of the UVA/Padova T1DMS (the version used in this work), is the time-invariant definition of some important physiological parameters, e.g., Insulin Sensitivity (IS), which has been clearly stated in the Assumption 1. This limitation led the US FDA to approve the simulator for single-meal simulations only (21). Several methods were proposed to address this issue (54–56). In particular, Visentin *et al.* proposed in (56) an upgrade of the T1DMS where a time-varying definition of the model parameters k_{p3} and V_{mx} is used to account for the intraday and interpatient variabilities of IS. This version of the T1DMS is however not commercially available yet.

In the context of the DIABLO project, other limitations of the T1DMS were highlighted in a precedent *in silico* work, where the simulator was used to validate the concept of an islet-based closed-loop therapy (23). The current metabolic model of the UVA/Padova T1DMS cannot model the dynamics of lipids, amino acids and hormone concentrations in blood, besides insulin and glucagon, which all reflect the general body status. As we already demonstrated *in vitro* that our biosensor properly captures the modulation of islet responses induced by GLP-1, adrenaline, and amino acids (12,14), it is impossible to fully assess *in silico* the potential of our biosensor with the current metabolic model of the T1DMS. The secretion of GLP-1 by intestinal cells is closely related to nutrient intake (57). GLP-1 concentration variations could thus be extrapolated from variables already modelled in the simulator, e.g., glucose mass in intestine, rate constant of intestinal absorption. However, it appears more complicated to include adrenaline, fatty acids or amino acids concentration variations to the T1DMS metabolic model without new clinical data. Despite the above-mentioned limitations, the version 3.2 of the UVA/Padova T1DMS still is a powerful tool to assess different approaches to handle interpatient variability and compare control strategies towards the integration of our islet-based biosensor in an AP system.

Result analysis and learnt lessons for interpatient variability management

To elaborate further on the modelling of interpatient variability, we developed a method which accounts for the specific energy need of each T1D patient by individualising meal scenarios based on patient body weight. Our meal scenario individualisation method is not a built-in feature of the T1DMS, and therefore needs to be discussed further. To ascertain that the method yields realistic glucose intake distributions for T1D adults, we computed the daily energy intakes corresponding to the daily glucose intakes outputted by the individualisation function. We considered three hypotheses

Towards the integration of an islet-based biosensor in closed-loop therapies for patients with Type 1 Diabetes

regarding the proportion of daily energy intake provided by carbohydrates: 45%, 55% and 65%. These hypotheses are in line with the American Diabetes Association recommendation for T1D adults: 45-60% of energy requirements covered by carbohydrates (58). The corresponding daily energy intakes are plotted in Figure 11 for each hypothesis. Unsurprisingly, the total energy intake increased when the proportion of carbohydrates decreased, and fell between 1300 to 2800 kcal/day depending on the carbohydrate proportion hypothesis. As this result is consistent with the range of daily energy intakes reported in the literature for T1D adults (35,59), we can conclude that the weight-dependent definition of meal scenarios is functional for adult patients, and does not yield aberrant results.

Furthermore, the benefits of numerical simulation were exploited to assess two different approaches to handle interpatient variability. First, controllers highly individualised using our GA-based optimisation method and individualised meal scenarios were used to define the best performance that could be achieved with a biosensor-based closed loop and unannounced meals. In so doing, we intended to investigate the relative contribution of controller individualisation and control algorithm complexity. The results obtained with these highly individualised controller parameters were satisfactory as excellent regulation performance was observed without meal announcement. Compared to our previous work (23), the weight-dependant definition of our “standard scenario” resulted in a TIR improved by 1.0% on average (88.1% in (23) vs 89.1% here) with a similar standard deviation (5.4% vs 5.0%), thanks to a better mitigation of the hypoglycaemic risk, - 1.3% on average (1.6% vs 0.3%). In both cases, the adult cohort was submitted to a very similar 3-meal 2-snack scenario with an average daily glucose intake of 235 grams. As there is no other obvious reason why our controller tuning methodology would yield better performing controllers in the second case, we conclude that the use of a unique scenario for all patients could introduce a bias when assessing closed-loop systems with the T1DMS.

As the level of individualisation obtained with the GA could not realistically be achieved *in vivo*, controllers need to be tuned more conservatively. Through the DIABLO project, we thus investigated a second approach based on the design of a unique H_∞ robust controller tuned for all virtual T1D adults and the infusion of a bolus to reduce postprandial hyperglycaemia. Note that we firstly developed this approach with a traditional CGM sensor. The advantage of this approach is that it could theoretically handle both intra- and interpatient variabilities. To manage trade-offs of control requirements, H_∞ control theory is known as a powerful tool. Among the pioneering works, Kienitz *et al.* (60) addressed for the first time the BG regulation with H_∞ control theory to manage the considerable amount of model uncertainty. This work has been followed by (61) where a sensitivity analysis provides the three-parameter set having the most significant effect on insulin and glucose dynamics. In spite of advances in the H_∞ framework, it is important to underline that an efficient robust

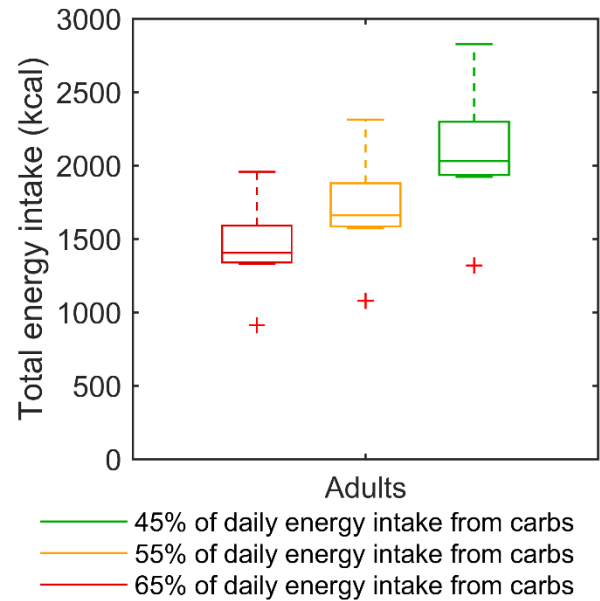


Figure 11: Boxplots of the daily energy intake corresponding to the individualised “standard scenario” of each virtual adult. Three hypotheses are considered for the proportion of energy intake covered by carbohydrates: 45%, 55%, and 65%. For each box, the central mark and the edges of the box are respectively the median and the 25th and 75th percentiles. Data points, without outliers, are delimited by the whiskers, and outliers are plotted individually as red crosses.

Towards the integration of an islet-based biosensor in closed-loop therapies for patients with Type 1 Diabetes

control solution can be obtained if and only if it is designed on an accurate model able to capture all variabilities. In this context, the work reported in (24) highlights the benefits of simulation by providing control-relevant nonparametric models identified from the UVA/Padova simulator. Based on the structure of LTI models, the authors proposed to model glucose-insulin dynamics by a unique LTI model of third order. This work encouraged us to develop the methodology introduced in section 2.3 where a family of thirteen-order linear models is derived by using mathematical formalisms like the unstructured multiplicative uncertainty and the LFT representation. From the results obtained with the proposed closed-loop architecture (Figure 5), acceptable performances (TIR above 90%) were reached thanks to the announcement of sizeable meals. The price to pay to be robust (or as insensitive as possible) against variabilities within a population of T1D patients with a standard CGM sensor (the default sensor configuration of T1DMS (21), with a sampling time of 5 min), is to include the patient in the loop.

To better assess the performance of our unique controller, we compared its performance to two control laws published recently: the velocity-weighting and velocity-penalty MPC law proposed by Gondhalekar et al. (51) and the switching LPV approach proposed by Colmegna et al. (52). The first conclusion of these comparisons introduced in section 3.3 is that safety features to prevent hypoglycaemia are necessary (an Insulin-On-Board (IOB) limitation in the control algorithm is implemented in both cases), even when meal announcement lessen the constraint on the controller. The second conclusion is that the need to include the patient in the loop could be relaxed by individualising the H_∞ controller using the patient's previous therapy parameters (e.g., the Total Daily Insulin as in (25)). In addition, control-oriented models have to be designed to capture other physiological factors than the ones included in the v3.2 of T1DMS. This statement motivated other investigators to develop LPV models capable to integrate the variability of insulin sensitivity in models used for control design purpose (28).

Bridging model-based control theory and the islet-based biosensor

As previously mentioned, the overall objective of the DIABLO project is to gather the sensing capabilities of pancreatic islets and the benefits of robust control theory in a biosensor-based AP system. Thanks to its sensitivity to other insulin secretion modulators, the biosensor could alleviate the patients' burden by reducing the need for meal and physical activity announcement, while providing a new insight on the very specific response of each patient to nutrients. By providing a finer image of the patient's physiological status and multiple signals, we hope that this sensor could also help solving the well-known problem of unstable diabetes. The different simulation campaigns presented in this paper allowed us to highlight the relative contribution of algorithms to the overall closed-loop performance of AP systems. From the first conclusion of the comparison study, hypoglycaemia-prevention features, such as IOB, seem to be necessary. In addition, modern hybrid closed-loop systems frequently integrate a hypoglycaemic alarm to trigger the suspension of basal insulin delivery, referred to as Low Glucose Suspend (LGS). Although the biosensor response presents a natural glucose-dependent hysteresis protecting from hypoglycaemia (12,62), it may have a shortcoming that is worth mentioning: β -cell activity at low glucose, *i.e.*, the SP frequency, is not yet fully explored and the biosensor output may eventually not suffice, when the patient BG level is below the islet glucose stimulation threshold, to trigger such hypoglycaemia-prevention feature. The co-integration of a CGM technology and our biosensing one into a single device, may thus be necessary. This proposal appears reasonable from a technological standpoint as a glucose-oxidase electrode could be placed on the same MEA as the pancreatic islets embedded in the biosensor, and meets the recommendation expressed in (2) to integrate new signals for algorithm improvement. The combined use of multiple input signals

Towards the integration of an islet-based biosensor in closed-loop therapies for patients with Type 1 Diabetes

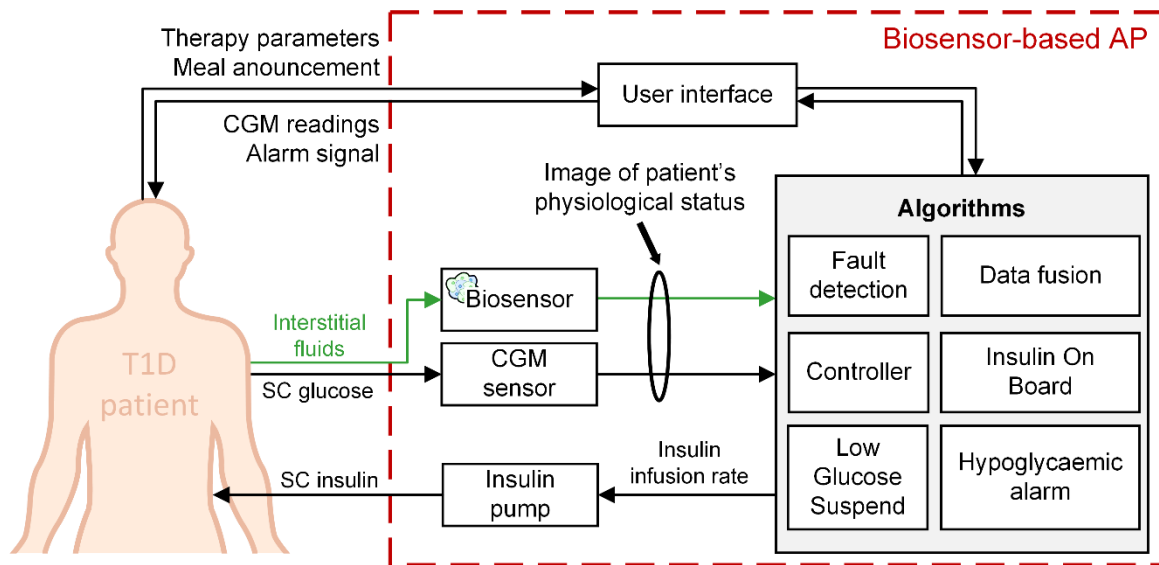


Figure 12: An Artificial Pancreas system based on two dissimilar sensors for insulin therapy of T1D patients

with an LPV formalism to capture other physiological factors (see the second conclusion of the comparative study), would also further highlight the benefits of H_∞ robust control theory for the regulation of T1D patient's BG level. In particular, this method could permit the development of a Multi-Input Single-Output (MISO) controller, involving a better dimensioning of the control problem and a possible improvement to manage variability.

At our current state of knowledge and advance of the biosensor, we thus propose the following setup for a realistic biosensor-based Artificial Pancreas (Figure 12). The integration of this two-sensor device could provide multiple signals to improve the performance of control algorithms (*e.g.*, controller, bolus calculator, Insulin-On-Board estimation, fault detection). A data fusion algorithm could also be developed, to improve the real-time monitoring of patient's physiological state, like in aeronautical systems (63). Such a system would be perfectly in line with the conclusions DCCT-EDIC study (64) concerning the need to mitigate hypoglycaemia in intensive insulin therapy and the recommendations formulated in (2) to integrate new signals to the Artificial Pancreas. Depending on our ongoing research, the set-up may in the long-term be simplified to a pure biosensor capable of detecting hypoglycaemic states by fully using the multiple inborn detection capacity of pancreatic islet sensors.

References

1. Williams R, Karuranga S, Malanda B, Saeedi P, Basit A, Besançon S, et al. Global and regional estimates and projections of diabetes-related health expenditure: Results from the International Diabetes Federation Diabetes Atlas, 9th edition. *Diabetes Res Clin Pract.* 2020;162.
2. Boughton CK, Hovorka R. New closed-loop insulin systems [Internet]. Vol. 64, *Diabetologia*. Springer; 2021 [cited 2021 Sep 16]. p. 1007–15. Available from: <https://link.springer.com/article/10.1007/s00125-021-05391-w>
3. Hartnell S, Fuchs J, Boughton CK, Hovorka R. Closed-loop technology: a practical guide. *Pract Diabetes.* 2021 Jul 1;38(4):33–9.

Towards the integration of an islet-based biosensor in closed-loop therapies for patients with Type 1 Diabetes

4. Magdelaine N, Rivadeneira PS, Chaillous L, Fournier-Guilloux AL, Krempf M, MohammadRidha T, et al. Hypoglycaemia-free artificial pancreas project. *IET Syst Biol*. 2020;14(1):16–23.
5. Toschi E, Wolpert H. Utility of Continuous Glucose Monitoring in Type 1 and Type 2 Diabetes [Internet]. Vol. 45, *Endocrinology and Metabolism Clinics of North America*. 2016 [cited 2021 Sep 16]. p. 895–904. Available from: [https://www.endo.theclinics.com/article/S0889-8529\(16\)30061-5/abstract](https://www.endo.theclinics.com/article/S0889-8529(16)30061-5/abstract)
6. Kropff J, DeVries JH. Continuous Glucose Monitoring, Future Products, and Update on Worldwide Artificial Pancreas Projects. *Diabetes Technol Ther* [Internet]. 2016 Feb 1 [cited 2020 Oct 20];18(S2):S253–63. Available from: <https://www.liebertpub.com/doi/abs/10.1089/dia.2015.0345>
7. Christiansen SC, Fougner AL, Stavadahl Ø, Kölle K, Ellingsen R, Carlsen SM. A Review of the Current Challenges Associated with the Development of an Artificial Pancreas by a Double Subcutaneous Approach [Internet]. Vol. 8, *Diabetes Therapy*. Springer; 2017 [cited 2021 Sep 16]. p. 489–506. Available from: </pmc/articles/PMC5446388/>
8. Cappon G, Vettoretti M, Sparacino G, Facchinetti A. Continuous glucose monitoring sensors for diabetes management: A review of technologies and applications. *Diabetes Metab J* [Internet]. 2019 [cited 2021 Sep 16];43(4):383–97. Available from: <https://synapse.koreamed.org/articles/1142375>
9. Hartnell S, Fuchs J, Boughton CK, Hovorka R. Closed-loop technology: a practical guide. *Pract Diabetes*. 2021 Jul;38(4):33–9.
10. Koutsouras DA, Perrier R, Villarroel Marquez A, Pirog A, Pedraza E, Cloutet E, et al. Simultaneous monitoring of single cell and of micro-organ activity by PEDOT:PSS covered multi-electrode arrays. *Mater Sci Eng C* [Internet]. 2017;81(May):84–9. Available from: <http://dx.doi.org/10.1016/j.msec.2017.07.028>
11. Pedraza E, Karajić A, Raoux M, Perrier R, Pirog A, Lebreton F, et al. Guiding pancreatic beta cells to target electrodes in a whole-cell biosensor for diabetes. *Lab Chip*. 2015;15(19):3880–90.
12. Lebreton F, Pirog A, Belouah I, Bosco D, Berney T, Meda P, et al. Slow potentials encode intercellular coupling and insulin demand in pancreatic beta cells. *Diabetologia*. 2015;58(6):1291–9.
13. Raoux M, Bornat Y, Quotb A, Catargi B, Renaud S, Lang J. Non-invasive long-term and real-time analysis of endocrine cells on micro-electrode arrays. *J Physiol*. 2012;590(5):1085–91.
14. Jaffredo M, Bertin E, Pirog A, Puginier E, Gaitan J, Oucherif S, et al. Dynamic Uni- and Multicellular Patterns Encode Biphasic Activity in Pancreatic Islets. *Diabetes* [Internet]. 2021 Apr 1 [cited 2021 Sep 13];70(4):878–88. Available from: <https://diabetes.diabetesjournals.org/content/70/4/878>
15. Pirog A, Bornat Y, Perrier R, Raoux M, Jaffredo M, Quotb A, et al. Multimed: An integrated,

Towards the integration of an islet-based biosensor in closed-loop therapies for patients with Type 1 Diabetes

- multi-application platform for the real-time recording and sub-millisecond processing of biosignals. *Sensors* (Switzerland) [Internet]. 2018 Jun 30 [cited 2020 Dec 10];18(7):2099. Available from: <http://www.mdpi.com/1424-8220/18/7/2099>
16. Fee MS, Mitra PP, Kleinfeld D. Variability of extracellular spike waveforms of cortical neurons. *J Neurophysiol.* 1996;76(6):3823–33.
 17. Lang J, Catargi B, Renaud S, Raoux M, Charpentier G. SENSOR FOR MEASURING THE ACTIVITY OF BETA-PANCREATIC CELLS OR OF ISLETS OF LANGERHANS, MANUFACTURE AND USE OF SUCH A SENSOR PATENT US2013030271A1. 2013.
 18. Perrier R, Pirog A, Jaffredo M, Gaitan J, Catargi B, Renaud S, et al. Bioelectronic organ-based sensor for microfluidic real-time analysis of the demand in insulin. *Biosens Bioelectron.* 2018;117:253–9.
 19. Olçomendy L, Pirog A, Bornat YB, Cieslak J, Gucik-Derigny D, David H, et al. Tuning of an artificial pancreas controller: an in silico methodology based on clinically-relevant criteria. In: IEEE, editor. 42nd Annual International Conference of the IEEE Engineering in Medicine and Biology Society (EMBC) [Internet]. Montréal, Canada: IEEE; 2020. Available from: <https://hal.archives-ouvertes.fr/hal-02908200>
 20. Kovatchev BP, Clarke WL, Breton M, Brayman K, McCall A. Quantifying temporal glucose variability in diabetes via continuous glucose monitoring: Mathematical methods and clinical application. *Diabetes Technol Ther.* 2005;7(6):849–62.
 21. Dalla Man C, Micheletto F, Lv D, Breton M, Kovatchev B, Cobelli C. The UVA/PADOVA type 1 diabetes simulator: New features. *J Diabetes Sci Technol.* 2014;8(1):26–34.
 22. Kovatchev BP, Breton M, Dalla Man C, Cobelli C. In silico preclinical trials: A proof of concept in closed-loop control of type 1 diabetes. *J Diabetes Sci Technol.* 2009;3(1):44–55.
 23. Olcomendy L, Pirog A, Lebreton F, Jaffredo M, Cassany L, Gucik Derigny D, et al. Integrating an Islet-Based Biosensor in the Artificial Pancreas: In Silico Proof-of-Concept. *IEEE Trans Biomed Eng.* 2021;1–1.
 24. Van Heusden K, Dassau E, Zisser HC, Seborg DE, Doyle FJ. Control-relevant models for glucose control using a priori patient characteristics. *IEEE Trans Biomed Eng.* 2012;59(7):1839–49.
 25. Colmegna P, Sánchez Peña RS, Gondhalekar R, Dassau E, Doyle FJ. Reducing risks in type 1 diabetes using H_{∞} Control. *IEEE Trans Biomed Eng.* 2014;61(12):2939–47.
 26. Colmegna P, Sánchez-Peña RS, Gondhalekar R. Linear parameter-varying model to design control laws for an artificial pancreas. *Biomed Signal Process Control.* 2018;40:204–13.
 27. Bianchi FD, Moscoso-Vásquez M, Colmegna P, Sánchez-Peña RS. Invalidation and low-order model set for artificial pancreas robust control design. *J Process Control.* 2019;76:133–40.
 28. Moscoso-Vasquez M, Colmegna P, Rosales N, Garelli F, Sanchez-Pena R. Control-Oriented Model with Intra-Patient Variations for an Artificial Pancreas. *IEEE J Biomed Heal*

Towards the integration of an islet-based biosensor in closed-loop therapies for patients with Type 1 Diabetes

- Informatics. 2020;24(9):2681–9.
29. Cassany L, Gucik-Derigny D, Cieslak J, Henry D, Franco R, de Loza A, et al. A Robust Control solution for Glycaemia Regulation of Type-1 Diabetes Mellitus. In: IEEE European Control Conference. Rotterdam, Netherlands: IEEE; 2021. p. 327–32. (IEEE European Control Conference).
 30. Steil GM, Palerm CC, Kurtz N, Voskanyan G, Roy A, Paz S, et al. The effect of insulin feedback on closed loop glucose control. *J Clin Endocrinol Metab.* 2011;96(5):1402–8.
 31. Tubiana-Rufi N, Schaepelynck P, Franc S, Chaillous L, Joubert M, Renard E, et al. Practical implementation of automated closed-loop insulin delivery: A French position statement. *Diabetes Metab.* 2021 May 1;47(3):101206.
 32. Cassany L, Gucik-Derigny D, Cieslak J, Henry D, Franco R, de Loza A, et al. A Robust H_{∞} Control Approach for Blood Glucose Regulation in Type-1 Diabetes. In: 11th IFAC Symposium on Biological and Medical Systems. Ghent, Belgium: IFAC; 2021. (11th IFAC Symposium on Biological and Medical Systems).
 33. Fritzen K, Heinemann L, Schnell O. Modeling of diabetes and its clinical impact. *J Diabetes Sci Technol.* 2018;12(5):976–84.
 34. Dalla Man C, Rizza RA, Cobelli C. Meal Simulation of Glucose-Insulin System. *Ieee Trans Biomed Eng.* 2007;54(10):1–33.
 35. Oza-Frank R, Cheng YJ, Narayan KMV, Gregg EW. Trends in nutrient intake among adults with diabetes in the United States: 1988–2004. *J Am Diet Assoc [Internet].* 2009;109(7):1173–8. Available from: <http://dx.doi.org/10.1016/j.jada.2009.04.007>
 36. Benedé-Ubieto R, Estévez-Vázquez O, Ramadori P, Cubero FJ, Nevzorova YA. Guidelines and considerations for metabolic tolerance tests in mice [Internet]. Vol. 13, Diabetes, Metabolic Syndrome and Obesity: Targets and Therapy. *Diabetes Metab Syndr Obes;* 2020 [cited 2021 Oct 12]. p. 439–50. Available from: <https://pubmed.ncbi.nlm.nih.gov/32110077/>
 37. Schmidt S, Norgaard K. Bolus calculators. Vol. 8, *Journal of Diabetes Science and Technology.* 2014. p. 1035–41.
 38. Soru P, De Nicolao G, Toffanin C, Dalla Man C, Cobelli C, Magni L. MPC-based artificial pancreas: Strategies for individualization and meal compensation [Internet]. Vol. 15, *Diabetes Technology and Therapeutics.* 2013 [cited 2021 Sep 16]. Available from: <https://www.sciencedirect.com/science/article/pii/S1367578812000107>
 39. Zhou K, Doyle JC. Essentials of robust control. 1998;411.
 40. Basu A, Dube S, Veetil S, Slama M, Kudva YC, Peyser T, et al. Time lag of glucose from intravascular to interstitial compartment in type 1 Diabetes. *J Diabetes Sci Technol.* 2015;9(1):63–8.
 41. Glover K. A Loop Shaping Design Procedure Using Ha Synthesis. *IEEE Trans Automat Contr [Internet].* 1992 [cited 2021 Sep 16];37(6):759–69. Available from:

Towards the integration of an islet-based biosensor in closed-loop therapies for patients with Type 1 Diabetes

https://scholar.google.com/scholar?hl=en&as_sdt=0%2C5&q=A+Loop+Shaping+Design+Procedure+using+Synthesis&btnG=

42. Glover K, Mcfarlane D. Robust Stabilization of Normalized Coprime Factor Plant Descriptions with H_∞ -Bounded Uncertainty. *IEEE Trans Automat Contr* [Internet]. 1989 [cited 2021 Sep 16];34(8):821–30. Available from: <https://ieeexplore.ieee.org/abstract/document/29424/>
43. Agiostratidou G, Anhalt H, Ball D, Blonde L, Gourgari E, Harriman KN, et al. Standardizing clinically meaningful outcome measures beyond HbA1c for type 1 diabetes: A consensus report of the American Association of Clinical Endocrinologists, the American Association of Diabetes Educators, the American Diabetes Association, the Endo. *Diabetes Care* [Internet]. 2017 [cited 2020 Apr 3];40(12):1622–30. Available from: <http://care.diabetesjournals.org/lookup/suppl/doi:10.2337/dc17-1624/-/DC1>.
44. Petrie JR, Peters AL, Bergenstal RM, Holl RW, Fleming GA, Heinemann L. Improving the clinical value and utility of CGM systems: issues and recommendations: A joint statement of the European Association for the Study of Diabetes and the American Diabetes Association Diabetes Technology Working Group. Vol. 60, *Diabetologia*. 2017. p. 2319–28.
45. Danne T, Nimri R, Battelino T, Bergenstal RM, Close KL, DeVries JH, et al. International consensus on use of continuous glucose monitoring. *Diabetes Care* [Internet]. 2017 [cited 2020 Apr 3];40(12):1631–40. Available from: <https://doi.org/10.2337/dc17-1600>
46. Battelino T, Danne T, Bergenstal RM, Amiel SA, Beck R, Biester T, et al. Clinical targets for continuous glucose monitoring data interpretation: Recommendations from the international consensus on time in range. *Diabetes Care*. 2019;42(8):1593–603.
47. Deichmann J, Bachmann S, Burckhardt M-A, Szinnai G, Kaltenbach H-M. Simulation-Based Evaluation of Treatment Adjustment to Exercise in Type 1 Diabetes. *Front Endocrinol (Lausanne)*. 2021;12(August):1–15.
48. Brazeau AS, Mircescu H, Desjardins K, Leroux C, Strychar I, Ekoé JM, et al. Carbohydrate counting accuracy and blood glucose variability in adults with type 1 diabetes. *Diabetes Res Clin Pract* [Internet]. 2013 Jan [cited 2020 Dec 30];99(1):19–23. Available from: <https://pubmed.ncbi.nlm.nih.gov/23146371/>
49. Herrero P, Bondia J, Oliver N, Georgiou P. A coordinated control strategy for insulin and glucagon delivery in type 1 diabetes. *Comput Methods Biomech Biomed Engin*. 2017;20(13):1474–82.
50. Toffanin C, Visentin R, Messori M, Palma F Di, Magni L, Cobelli C. Toward a Run-to-Run Adaptive Artificial Pancreas: In Silico Results. *IEEE Trans Biomed Eng*. 2018;65(3):479–88.
51. Gondhalekar R, Dassau E, Doyle FJ. Velocity-weighting & velocity-penalty MPC of an artificial pancreas: Improved safety & performance. *Automatica*. 2018;91:105–17.
52. Colmegna PH, Bianchi FD, Sanchez-Pena RS. Automatic Glucose Control during Meals and Exercise in Type 1 Diabetes: Proof-of-Concept in Silico Tests Using a Switched LPV Approach. *IEEE Control Syst Lett*. 2021 Nov 1;5(5):1489–94.

Towards the integration of an islet-based biosensor in closed-loop therapies for patients with Type 1 Diabetes

53. Visentin R, Dalla Man C, Kovatchev B, Cobelli C. The university of virginia/padova type 1 diabetes simulator matches the glucose traces of a clinical trial. *Diabetes Technol Ther.* 2014;16(7):428–34.
54. Toffanin C, Zisser H, Doyle FJ, Dassau E. Dynamic insulin on board: Incorporation of circadian insulin sensitivity variation. *J Diabetes Sci Technol.* 2013;7(4):928–40.
55. Herrero P, Bondia J, Adewuyi O, Pesl P, El-Sharkawy M, Reddy M, et al. Enhancing automatic closed-loop glucose control in type 1 diabetes with an adaptive meal bolus calculator – in silico evaluation under intra-day variability. *Comput Methods Programs Biomed.* 2017;146(June):125–31.
56. Visentin R, Campos-Náñez E, Schiavon M, Lv D, Vettoretti M, Breton M, et al. The UVA/Padova Type 1 Diabetes Simulator Goes From Single Meal to Single Day. *J Diabetes Sci Technol.* 2018;12(2):273–81.
57. Meier JJ, Nauck MA. Glucagon-like peptide 1 (GLP-1) in biology and pathology. *Diabetes Metab Res Rev.* 2005;21(2):91–117.
58. Scott SN, Anderson L, Morton JP, Wagenmakers AJM, Riddell MC. Carbohydrate restriction in type 1 diabetes: A realistic therapy for improved glycaemic control and athletic performance? [Internet]. Vol. 11, *Nutrients*. MDPI AG; 2019 [cited 2021 Jun 11]. Available from: [/pmc/articles/PMC6566372/](https://pmc/articles/PMC6566372/)
59. Ahola AJ, Mikkilä V, Mäkimattila S, Forsblom C, Freese R, Groop PH. Energy and nutrient intakes and adherence to dietary guidelines among Finnish adults with type 1 diabetes. *Ann Med* [Internet]. 2012 Feb [cited 2021 Jun 20];44(1):73–81. Available from: <https://www.tandfonline.com/action/journalInformation?journalCode=iann20>
60. Kienitz KH, Yoneyama T. A Robust Controller for Insulin Pumps Based on H-Infinity Theory. *IEEE Trans Biomed Eng* [Internet]. 1993 [cited 2021 Oct 5];40(11):1133–7. Available from: <https://ieeexplore.ieee.org/abstract/document/245631/>
61. Parker RS, Doyle FJ, Ward JH, Peppas NA. Robust H_{∞} glucose control in diabetes using a physiological model. *AIChE J* [Internet]. 2000 [cited 2021 Oct 5];46(12):2537–49. Available from: https://aiche.onlinelibrary.wiley.com/doi/abs/10.1002/aic.690461220?casa_token=laRtAGsUiF8AAAAA:JkG-Th7mLLonQt5SlQPumad0i1Ri_htvmYFVedq93vT4P1VkkKnOuZ2QtbvHIQdLkgPig4WSB73qZzQ
62. Keenan DM, Basu R, Liu Y, Basu A, Bock G, Veldhuis JD. Logistic model of glucose-regulated C-peptide secretion: Hysteresis pathway disruption in impaired fasting glycemia. *Am J Physiol - Endocrinol Metab* [Internet]. 2012 [cited 2021 May 14];303(3):397–409. Available from: <http://www.ajpendo.org>
63. Berdjag D, Cieslak J, Zolghadri A. Fault diagnosis and monitoring of oscillatory failure case in aircraft inertial system. *Control Eng Pract* [Internet]. 2012 [cited 2021 Oct 5];20(12):1410–25. Available from:

Towards the integration of an islet-based biosensor in closed-loop therapies for patients with Type 1 Diabetes

https://www.sciencedirect.com/science/article/pii/S0967066112001682?casa_token=SOYV5XS3xX0AAAAA:wcYIO8MVIIJvCQYMPfkKrbktRgrU3RVASBWCGiwlYzyHzDte9fUIN4cgEwxQ4VuB362yZ22tg

64. Group TDC and CTR. The Effect of Intensive Treatment of Diabetes on the Development and Progression of Long-Term Complications in Insulin-Dependent Diabetes Mellitus. *N Engl J Med* [Internet]. 1993 Sep 30 [cited 2020 Sep 2];329(14):977–86. Available from: <http://www.nejm.org/doi/abs/10.1056/NEJM199309303291401>

Conflict of Interest

The authors declare that the research was conducted in the absence of any commercial or financial relationships that could be construed as a potential conflict of interest.

Author Contributions

L.O. performed the simulation work, contributed to model development and wrote much of the manuscript. A.P. analysed the experimental data and developed the model. L.C., R.F., D.G-D., H.R., A.F-L., J.C. and D.H. developed codes for robust control strategies in MATLAB. F.L. and M.R. provided the experimental data. All the authors contributed to the discussions. All authors contributed to manuscript writing and approved the submitted version. S.R., J.L., D.H., J.C., A.F-L and B.C. secured funding.

Funding

The authors wish to thank various Funding agencies. ANR (HyBiopacs to JL and SR, Isletchip to BC, JL and SR, DIABLO to SR, JL, BC and HD), Région d'Aquitaine (to BC, SR and JL), French Ministry of Research (to MR). More precisely, this work has been supported by the French National Agency for Research (DIABLO ANR-18-CE17-0005-01), ECOSNord (M18M01) and SEP-CONACYT-ECOS-ANUIES under Grant 296692.

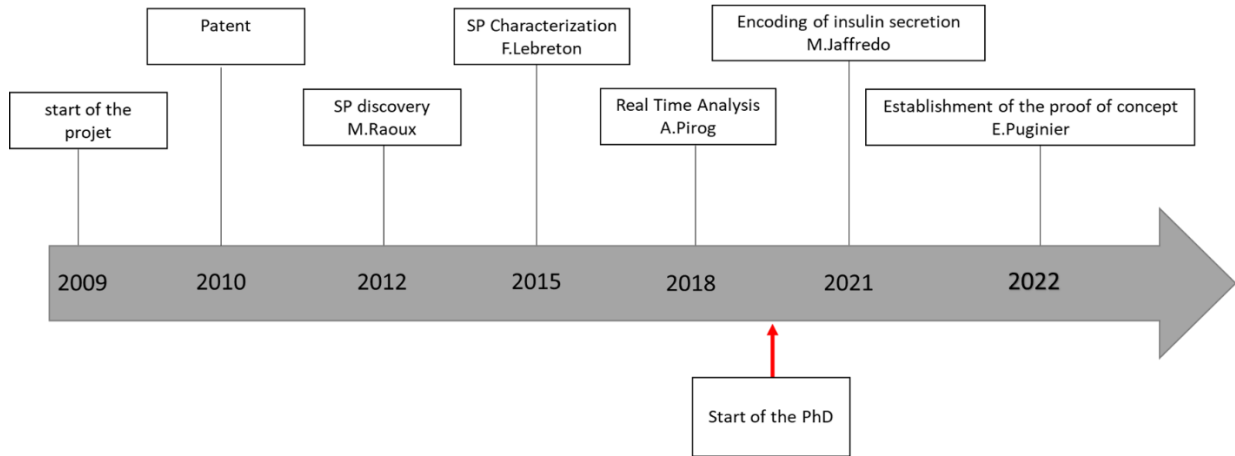
Acknowledgments

Authors acknowledge the French National Agency for Research (DIABLO ANR-18-CE17-0005-01), ECOSNord (M18M01) and SEP-CONACYT-ECOS-ANUIES under Grant 296692. This research has also been supported by the Fonds Européen de Développement Régional (FEDER) under the grant agreement DIAGLYC N°3538519.

Conclusion and perspectives

Conclusion and perspectives:

Development of the project



Conclusion biological substrate

Through the recent years we have been able to make progress on the development of a biosensor based on the electrical activity of the islets of Langerhans. First, we have searched the most suitable biological substrate to serve as a biosensor within our device. We studied two clonal cell lines, INS and EndoC β H1, which we seeded on MEA as a monolayer or after spheroid formation. EndoC- β H1 spheroids provide a model to test the effect of different variables on physiological cell-cell coupling by MEA analysis in line with the advocated utility in drug testing. In the same vein CX-36 transduced cells may be suitable, but obviously restricted to rodents. Electrical signals, in these cell lines are significantly lower than that of native islets from primary cultures. For the development of our biosensor, a strong electrical signal in terms of frequency and amplitude is essential. Native islets are optimal glucose sensors, and their cellular complexity, as well as the richness of the interactions between the different cell types present in this natural organoid, give it a great advantage as a blood glucose sensor. It is not only sensitive to glucose, but also to lipids, amino acids and hormones. This natural ability has not been found within the cell lines and there are also difficulties within the clonal cell lines due to the fact that they are often homotypic in terms of hormone secretion as mentioned in the literature (Masur et al. 2005; Nakashima et al. 2009).

Perspectives biological substrate

A future solution should guarantee homogeneous biological material allowing the production of a standardised medical device. Dissociated/reassociated human islets from InSphero (location) could therefore be one possibility for optimising the system in an industrial development strategy. However, the cost of these organoids is relatively high. Another possibility may be given by the most recently described derivative of ENDO- β H1, ie ENDO- β H5, which have been shown an improved glucose sensitivity.

Conclusion development of a microfluidic device

Another essential step in the development of the islet-based biosensor was the design, fabrication and experimental validation of a microfluidic device adapted to the various technical constraints (loading of the islets, culture, dead volumes during experimentation). We tested two strategies: a complex design, allowing the recording of the electrical activity of islets trapped on an electrode independently, and a simple design allowing the loading of the islets and a static culture in an incubator before the connection to the microfluidic device on the day of the experiment.

The first strategy employed was not compatible with long experiments because of various problems of loading the chip with islets, of islet detachment during the experiment, but also and above all of nucleation problems leading to the formation of bubbles blocking the entire system. The second strategy of using a simple design allowed us to obtain results and to carry out long experiments, compatible with the dead volumes and constraints imposed by the use of a microdialysis system as a pressure pump as well as the anaesthesia times imposed on the animal.

Perspectives development of a microfluidic device

Among the perspectives considered, there is first of all the standardisation of the manufacturing of these chips with a simple linear design. Indeed, at the beginning we used on the moulding of pieces of syringe in PDMS. I designed and launched the manufacture of a Siu-8 wafer in order to manufacture a large quantity of standardised chips per batch. The use of polymers other than PDMS could also be an important step in the development of the manufacturing process, with a view to standardising and optimising the service life of the

chips. Finally, the design could be made more complex in order to reduce the number of islets required within the chip.

More broadly, in the field of organ on chip, another thesis project is currently underway in the team, that of developing a multi-organ on chip platform, in order to study the complex metabolic relationships between the liver, the muscles and the pancreas. The work on islets on chip will have served as a starting point for the development of this project.

Validation of the proof of concept in rodent

We were able to establish the proof of concept in vivo on rodents. Further validation of the assembly of the various constituent elements of the islet-based biosensor allows us to envisage two possible development paths. Firstly, further development and validation in the clinic was planned in the ANR project. However, it turned out that non-human material cannot be introduced in the Bordeaux CHU.

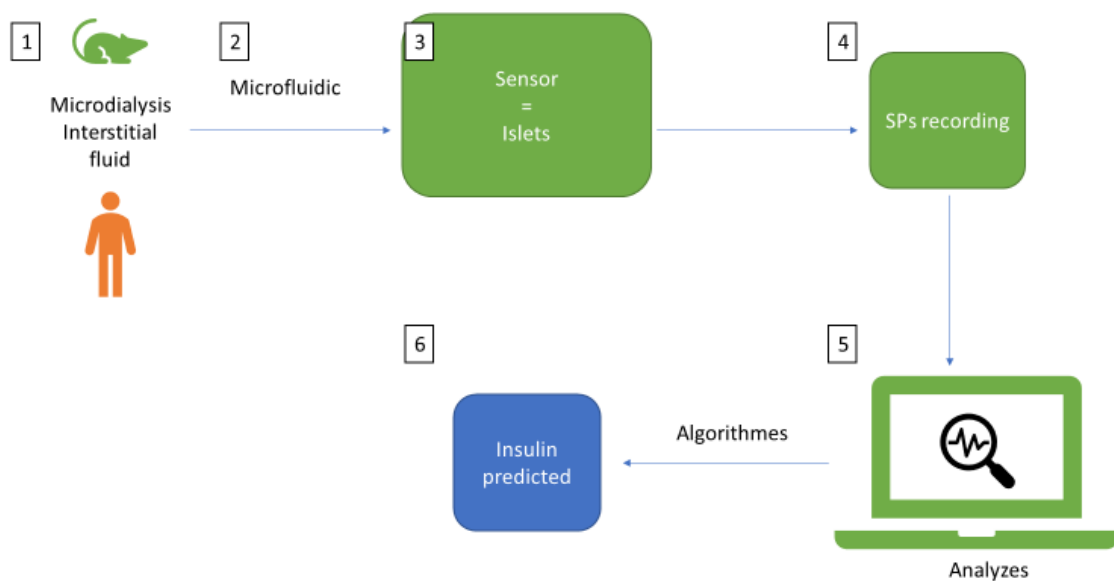


Figure 35: Diagram of the components of the islet-based biosensor. In green: elements validated during the thesis project. In orange: elements still to be validated. In blue: commercial insulin pump

An alternative would be static off-line testing of samples taken from the patient This step is simple to implement and does not face the constraints imposed by clinical protocols or the

entry of murine islets into the biosensor within the hospital. However, the workload and stress on the device would increase considerably with 48 consecutive pipetting steps and around 48h hands-on time to replace some 4h on-line testing. We are not certain that the device will support this recurrent manipulation at the actual stage and also wonder how to normalize between these discontinuous measurements.

To reach the stage of clinical trials allowing a complete validation of the system including microdialysis, microfluidics linked to the patient and connected to the electrophysiological recording device in real time, it seems necessary to involve industrial partners in order to optimise and standardise each element according to the ISO standards for medical devices. In spite of this complexity of development to carry out the validation in clinic, the simulations according to various patient scenarios in silico within the UVA-PADOVA simulator carried out by the electronic and automation partners of the ANR allow us to be confident as for the advantage of an islet-based biosensor over the CGMs currently present on the market.

The second area of development is for use in fundamental research. Indeed, this system can be used as an in vivo study platform to address different pharmacological and biological questions. Current bioassay systems allow to address more and more precise questions, such as ELISA or mass spectrometry, but these techniques are cut off from physiology and are performed after the in vivo experiment that gave rise to the collection of the samples of interest. With our device, we can simultaneously perform electrophysiological and optical monitoring and assays of different metabolites in the dialysate before or after the microfluidic chip without losing the physiological study aspect of the in vivo system.

General conclusion and perspectives

In conclusion, we have succeeded in developing a proof of concept for a new glucose sensor based on the electrical activity of the islets of Langerhans and have demonstrated the advantages of such a biosensor over the CGMs currently on the market. In the future, we can envisage testing different biological substrates by adapting the microfluidic chip to the structure of the substrates studied (pancreas slice, potentially bio-printed vascularised islets) or replacing commercial MEAs by transistors currently developed by various collaborations of the team. The use of transistors could allow the acquisition of an even richer electrical signal, notably by recording slow potentials but also action potentials. The prospect of ion-specific

transistors, particularly for zinc, could also enable us to enrich our platform and to study the secretory activity of insulin islets in an even more precise manner.

This work therefore opens up multiple perspectives both on the clinical and fundamental levels for the study and characterisation of islets.

What would be the next step for another thesis?

Several lines of research could be developed on the time scale of another thesis. Indeed, it would be interesting to focus on one of the axes of the biosensor for three full years. For the biological substrate part, it could be interesting to work with stem cells in order to study the behaviour of beta-like cells in the device. Once a system such as the one mentioned in the microfluidic studies section is available, it would be interesting to work with stem cells, to differentiate and form organoids under microfluidic conditions within the device and to link the system to the animal by characterising the electrical activities of these cells. Indeed, we have worked on anaesthetised animals, and perfecting the protocols for habituating animals to restraint devices could be a continuation of the development in order to follow the activity of the islets in response to the dialysate of the vigorous rat. We have also performed intraperitoneal glucose tolerance protocols; however, this in vivo platform has many possibilities and could allow testing the effect of hormones such as adrenaline or drugs such as sulfonyl ureas and thus characterise the system under these experimental conditions.

To conclude this manuscript, we tried to imagine what the Dia^βSENSOR would look like once industrialisation is complete.

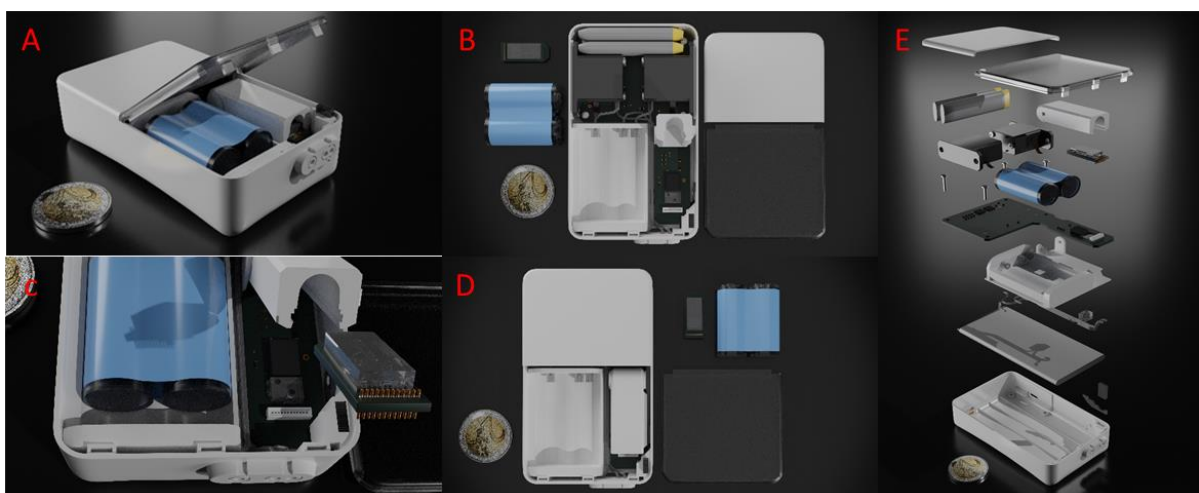


Figure 36: prototyping of the Dia ^{β} SENSOR after industrialisation. A: View of the open device scaled to a 2 euros coin. B: view of the device without the cover, insulin/dialysate reservoir in blue. C: detail of the insulin/dialysate reservoir in blue and the microfluidic MEA removed. D: top view of the biosensor housing, insulin/dialysate reservoir removed. E: exploded view of the biosensor allowing visualization of the components. *Drawing by A. Pirog*

Oral presentations:

E. Puginier, F.Poulletier de Gannes, A.Pirog, J.Gaitan, A.Hurtier, Y.Bornat, C.Cruciani-Guglielmacci, C.Magnan, B.Catargi, M.Raoux, S.Renaud, J.Lang, Extracorporeal islet-based continuous glucose monitoring sensor in rodents. EASD 2021

M. Abarkan, M. Jaffredo, E. Puginier, D. Mafilaza, G. Pathak, N. Krentz, A. Pirog, G. N'Kaoua, N. L. Beer, R. O'Connor, A. L. Gloyn⁴, M. J. Donahue, A. Gloyn⁵, S. Renaud, B.Hastoy, M. Raoux, J. Lang, Microelectrode arrays and organic electrochemical transistors for non-invasive on-line analysis of native and surrogate islets. Keystone Santa Fe 2020

E. Puginier, K. Leal Fischer, J. Gaitan, E. Malyshev, B. Charlot, M. Raoux, J. Lang, Electrical coupling in primary or clonal islet cell spheroids. EASD Barcelone 2019

Previous works:

Di Giovanni G, Bharatiya R, Puginier E, Ramos M, De Deurwaerdère S, Chagraoui A, De Deurwaerdère P. Lorcaserin Alters Serotonin and Noradrenaline Tissue Content and Their Interaction With Dopamine in the Rat Brain Front Pharmacol. 2020 Jun 30;11:962

De Deurwaerdère P, Ramos M, Bharatiya R, Puginier E, Chagraoui A, Manem J, Cuboni E, Pierucci M, Deidda G, Casarrubea M, Di Giovanni G. Lorcaserin bidirectionally regulates dopaminergic function site-dependently and disrupts dopamine brain area correlations in rats. Neuropharmacology. 2019;17;166:107915.

Puginier E, Bharatiya R, Chagraoui A, Manem J, Cho YH, Garret M, De Deurwaerdère P. Early neurochemical modifications of monoaminergic systems in the R6/1 mouse model of Huntington's disease. Neurochem Int. 2019; 128:186-195.

Di Giovanni G, Chagraoui A, Puginier E, Galati S, De Deurwaerdère P. Reciprocal interaction between monoaminergic systems and the pedunculo pontine nucleus: Implication in the mechanism of L-DOPA. Neurobiol Dis.; 2019 128:9-18.

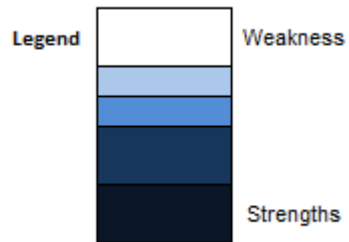
Demany L, Bayle Y, Puginier E, Semal C Detecting temporal changes in acoustic scenes: The variable benefit of selective attention Hearing Research 2017;353:17-25.

Chagraoui A, Puginier E, De Deurwaerdère P. Motivation and motivational aspects of Parkinson's disease. The Neuroscience of Parkinson's Disease, book 2 (Genetic, Neurology, behavior and diet), part 3. Elsevier

Annexes

Annexe 1 : Table 1 : Methods of islets analyses

		Environnement physiologique préservé	Non invasive for cells/islets	Temporal resolution	Spatial resolution	Several islets studied in parallel	Several cells studied in parallel	Ion channel study	Measurement of secretion	Network analysis	Longterm	Reusable	Simplicity of the technique	Simplicity of the analysis
RIA/ELISA	Islets	Strengths	Weakness	Weakness	Weakness				Strengths		Strengths		Weakness	Strengths
	Perfused pancreas	Strengths	Strengths	Weakness					Strengths		Strengths		Weakness	Strengths
	<i>In vivo</i>	Strengths	Strengths						Strengths		Strengths	Strengths	Weakness	Strengths
Optical methods	islets, intracellular probe	Strengths	Strengths	Strengths	Strengths		Strengths	Weakness		Strengths	Strengths		Strengths	Weakness
	islets TIRF	Strengths	Strengths	Strengths	Strengths		Strengths	Strengths	Strengths	Strengths	Strengths		Strengths	Weakness
	Pancreatic slice	Strengths	Weakness	Strengths	Strengths		Strengths	Weakness	Strengths	Strengths	Strengths		Weakness	Weakness
	<i>In vivo</i>	Strengths	Strengths	Strengths	Strengths	Strengths	Strengths	Weakness		Strengths	Strengths		Weakness	Weakness
Intracellular electrophysiology	Sharp microelectrode	Strengths		Strengths	Strengths			Strengths			Weakness		Weakness	Strengths
	patch clamp	Strengths		Strengths	Strengths			Strengths					Weakness	Strengths
	Perforated patch clamp	Strengths	Weakness	Strengths	Strengths			Strengths			Weakness		Weakness	Strengths
Extracellular electrophysiology	Suction microelectrode	Strengths	Strengths	Strengths	Strengths			Strengths			Strengths		Weakness	Weakness
	MEA	Strengths	Strengths	Strengths	Strengths	Strengths	Strengths	Strengths		Strengths	Strengths	Strengths	Strengths	Weakness
	OECT	Strengths	Strengths	Strengths	Strengths	Strengths	Strengths	Strengths		Strengths	Strengths	Strengths	Strengths	Weakness



Annexe 2 : Table 2: CGMs features and limitations

Industry	Name of the sensor	Accuracy (MARD)%	Calibration	Lifetime (Day)	Features	Limitations
Medtronic	Enlite sensor	13.6	12hr	6	Trend arrows, rate-of-change alerts, hypo/hyperglycemic alarms, integration with Medtronic's pumps	Approved only as an adjunctive device, acetaminophen interference
	Guardian sensor 3	10.6	12hr	7	Trend arrows, rate-of-change alerts, hypo/hyperglycemic alarms, integration with Medtronic's pumps	Approved only as an adjunctive device, acetaminophen interference
Abbott	Freestyle Navigator II	14.5	2, 10, 24, 72 hr after insertion	5	Trend arrows, rate-of-change alerts, hypo/hyperglycemic alarms	Approved only in some European countries as adjunctive device
	Freestyle libre	11.4	No	14	Trend arrows	Sensor need to be scanned, not recommended for patient with hypoglycemic unawareness, confirmatory SMBG still recommended
	Freestyle libre 2	No data	No	14	Trend arrows, rate-of-change alerts, hypo/hyperglycemic alarms, remote monitoring	Sensor need to be scanned, not recommended for patient with hypoglycemic unawareness, confirmatory SMBG still recommended
Dexcom	G4 Platinum	9	12 hr	7	Trend arrows, rate-of-change alerts, hypo/hyperglycemic alarms, remote monitoring	Approved only as an adjunctive device
	G5 mobile	9	12hr	7	Trend arrows, rate-of-change alerts, hypo/hyperglycemic alarms, remote monitoring, wireless communication with up to 5 devices	Confirmatory SMBG still recommended when specific episodes occur, acetaminophen interference
	G6	10	No	10	Trend arrows, rate-of-change alerts, hypo/hyperglycemic alarms, remote monitoring, wireless communication with up to 5 devices	Confirmatory SMBG still recommended when specific episodes occur
Senseonics	Eversense	11.4	No	90	Trend arrows, rate-of-change alerts, hypo/hyperglycemic alarms	The sensor needs to be inserted and removed in doctor's office, approved as adjunctive device in Europe only

Annexe 3 : Table 3: Non invasive methods for glucose monitoring

Technology Employed	Company	Device	Target Site	Advantages	Disadvantages
Reverse iontophoresis	Animas Technologies (Cygnus Inc.)	Glucowatch® G2 Biographer	Wrist skin	CE and FDA approved; takes into account skin temperature and perspiration fluctuations; alarm and trend indicators for rapid changes in glucose readings; event marking, data download, software analysis, and data-storage capacity	Expensive; requires 2-3 hour warm-up period, calibration using a standard blood glucose meter and replacement of disposable pad every 12 h; difficulty in calibration; inaccuracy due to subject's movement, exercising, sweating or rapid temperature changes; cannot be used in water; skin irritation was the main drawback; it shuts down automatically in cases of sweating, works better at high glucose levels and does not reliably detect hypoglycemia
Bioimpedance spectroscopy	Biovotion AG (Solianis Monitoring AG; Pendragon)	Glucotrack™	Wrist skin	CE approved; data downloading via USB, data analysis, software, data-storage capacity and long-lasting battery; alerts for rapid changes in glucose concentration and hypoglycemia; self-correction for changes in impedance due to variations in temperature.	Glucose readings vary in individuals; requires additional calibration for differences in skin and underlying tissues among individuals; difficulty in calibration; Pendra tape needs to be changed every 24 h; device needs to be reattached at the same spot where it was calibrated followed by 1-hour equilibrium time; poor correlation of only 35 % with glucose meters; Clark Error Grid Analysis indicated 4.3 % readings in error zone E; patient must rest for 60 min for equilibration before the reading; it cannot be used in many subjects whose skin types and basic skin impedances are unsuitable for the device; poor accuracy in post-marketing validation study
Ultrasound, electromagnetic and heat capacity	integrity Applications Ltd	Glucotrack™	Ear lobe skin	High precision and accuracy as it employs various Ni-CGM techniques; easy calibration procedure; calibration is valid for one month; USB and IR connectivity, alerts for hypo- and hyperglycemia, multi-user support, data-storage capacity, and software for data analysis; readings were unaffected by daily routine activities; high accuracy in clinical trials; good correlation with glucose meters and glucose analyzers; compact and lightweight device with large LCD screen	Requires individual calibration against invasive basal and post-prandial blood glucose references before it can be used for glucose measurements; needs improvements in calibration procedure and algorithm for data processing
Occlusion NIR spectroscopy	OrSense Ltd	OrSense NBM-200G	Fingertip skin	CE approved; allows noninvasive measurement of glucose as well as hemoglobin and oxygen saturation; portable, easy-to-use and measures glucose in less than a minute; data-storage capacity, alarm alerts, trend data analysis and integrated wireless telemetry; does not require frequent calibrations; easy calibration procedure; measures glucose continuously for 24 h; good accuracy in clinical trials that was similar to glucose meters	Not mentioned

References

References:

- Aamodt, Kristie I., et Alvin C. Powers. 2017. « Signals in the Pancreatic Islet Microenvironment Influence β -Cell Proliferation ». *Diabetes, Obesity & Metabolism* 19 Suppl 1 (septembre): 124-36. <https://doi.org/10.1111/dom.13031>.
- Abarkan, Myriam, Antoine Pirog, Donnie Mafilaza, Gaurav Pathak, Gilles N’Kaoua, Emilie Puginier, Rodney O’Connor, et al. 2022. « Vertical Organic Electrochemical Transistors and Electronics for Low Amplitude Micro-Organ Signals ». *Advanced Science (Weinheim, Baden-Wurttemberg, Germany)*, janvier, e2105211. <https://doi.org/10.1002/advs.202105211>.
- Abbes, Ilham Ben, Pierre-Yves Richard, Marie-Anne Lefebvre, Isabelle Guilhem, et Jean-Yves Poirier. 2013. « A Closed-Loop Artificial Pancreas Using a Proportional Integral Derivative with Double Phase Lead Controller Based on a New Nonlinear Model of Glucose Metabolism ». *Journal of Diabetes Science and Technology* 7 (3): 699-707. <https://doi.org/10.1177/193229681300700315>.
- Acciaroli, Giada, Martina Vettoretti, Andrea Facchinetti, et Giovanni Sparacino. 2018. « Calibration of Minimally Invasive Continuous Glucose Monitoring Sensors: State-of-The-Art and Current Perspectives ». *Biosensors* 8 (1): E24. <https://doi.org/10.3390/bios8010024>.
- Achenbach, Peter, Katharina Warncke, Jürgen Reiter, Heike E. Naserke, Alistair J. K. Williams, Polly J. Bingley, Ezio Bonifacio, et Anette-G. Ziegler. 2004. « Stratification of Type 1 Diabetes Risk on the Basis of Islet Autoantibody Characteristics ». *Diabetes* 53 (2): 384-92. <https://doi.org/10.2337/diabetes.53.2.384>.
- Adeva-Andany, María M., Noemi Pérez-Felpete, Carlos Fernández-Fernández, Cristóbal Donapetry-García, et Cristina Pazos-García. 2016. « Liver glucose metabolism in humans ». *Bioscience Reports* 36 (6): e00416. <https://doi.org/10.1042/BSR20160385>.
- Ahlqvist, Emma, Rashmi B. Prasad, et Leif Groop. 2020. « Subtypes of Type 2 Diabetes Determined From Clinical Parameters ». *Diabetes* 69 (10): 2086-93. <https://doi.org/10.2337/dbi20-0001>.
- Ahmed, Awad M. 2002. « History of Diabetes Mellitus ». *Saudi Medical Journal* 23 (4): 373-78.
- Ahrén, B. 2000. « Autonomic Regulation of Islet Hormone Secretion--Implications for Health and Disease ». *Diabetologia* 43 (4): 393-410. <https://doi.org/10.1007/s001250051322>.
- Ainscow, E. K., et M. D. Brand. 1999. « Internal Regulation of ATP Turnover, Glycolysis and Oxidative Phosphorylation in Rat Hepatocytes ». *European Journal of Biochemistry* 266 (3): 737-49. <https://doi.org/10.1046/j.1432-1327.1999.00856.x>.

Alev, Cantas, Stephanie Urschel, Stephan Sonntag, Georg Zoidl, Alfredo G. Fort, Thorsten Höher, Mamoru Matsubara, Klaus Willecke, David C. Spray, et Rolf Dermietzel. 2008. « The Neuronal Connexin36 Interacts with and Is Phosphorylated by CaMKII in a Way Similar to CaMKII Interaction with Glutamate Receptors ». *Proceedings of the National Academy of Sciences of the United States of America* 105 (52): 20964-69. <https://doi.org/10.1073/pnas.0805408105>.

Alvarsson, Alexandra, Maria Jimenez-Gonzalez, Rosemary Li, Carolina Rosselot, Nikolaos Tzavaras, Zhuhao Wu, Andrew F. Stewart, Adolfo Garcia-Ocaña, et Sarah A. Stanley. 2020. « A 3D Atlas of the Dynamic and Regional Variation of Pancreatic Innervation in Diabetes ». *Science Advances* 6 (41): eaaz9124. <https://doi.org/10.1126/sciadv.aaz9124>.

Andralojc, K. M., A. Mercalli, K. W. Nowak, L. Albarello, R. Calcagno, L. Luzi, E. Bonifacio, C. Doglioni, et L. Piemonti. 2009. « Ghrelin-Producing Epsilon Cells in the Developing and Adult Human Pancreas ». *Diabetologia* 52 (3): 486-93. <https://doi.org/10.1007/s00125-008-1238-y>.

Aragón, F., M. Karaca, A. Novials, R. Maldonado, P. Maechler, et B. Rubí. 2015. « Pancreatic Polypeptide Regulates Glucagon Release through PPYR1 Receptors Expressed in Mouse and Human Alpha-Cells ». *Biochimica Et Biophysica Acta* 1850 (2): 343-51. <https://doi.org/10.1016/j.bbagen.2014.11.005>.

Arda, H. Efsun, Cecil M. Benitez, et Seung K. Kim. 2013. « Gene Regulatory Networks Governing Pancreas Development ». *Developmental Cell* 25 (1): 5-13. <https://doi.org/10.1016/j.devcel.2013.03.016>.

Arimura, A., H. Sato, A. Dupont, N. Nishi, et A. V. Schally. 1975. « Somatostatin: Abundance of Immunoreactive Hormone in Rat Stomach and Pancreas ». *Science (New York, N.Y.)* 189 (4207): 1007-9. <https://doi.org/10.1126/science.56779>.

Ascaso, Francisco J., et Valentín Huerva. 2016. « Noninvasive Continuous Monitoring of Tear Glucose Using Glucose-Sensing Contact Lenses ». *Optometry and Vision Science: Official Publication of the American Academy of Optometry* 93 (4): 426-34. <https://doi.org/10.1097/OPX.0000000000000698>.

Asfari, M., D. Janjic, P. Meda, G. Li, P. A. Halban, et C. B. Wollheim. 1992. « Establishment of 2-Mercaptoethanol-Dependent Differentiated Insulin-Secreting Cell Lines ». *Endocrinology* 130 (1): 167-78. <https://doi.org/10.1210/endo.130.1.1370150>.

Ashcroft, F. M., et P. Rorsman. 1989. « Electrophysiology of the Pancreatic Beta-Cell ». *Progress in Biophysics and Molecular Biology* 54 (2): 87-143. [https://doi.org/10.1016/0079-6107\(89\)90013-8](https://doi.org/10.1016/0079-6107(89)90013-8).

Ashcroft, Frances M., et Patrik Rorsman. 2013. « K(ATP) Channels and Islet Hormone Secretion: New Insights and Controversies ». *Nature Reviews. Endocrinology* 9 (11): 660-69. <https://doi.org/10.1038/nrendo.2013.166>.

Assady, S., G. Maor, M. Amit, J. Itskovitz-Eldor, K. L. Skorecki, et M. Tzukerman. 2001. « Insulin Production by Human Embryonic Stem Cells ». *Diabetes* 50 (8): 1691-97. <https://doi.org/10.2337/diabetes.50.8.1691>.

Atkinson, Mark A., George S. Eisenbarth, et Aaron W. Michels. 2014. « Type 1 Diabetes ». *Lancet (London, England)* 383 (9911): 69-82. [https://doi.org/10.1016/S0140-6736\(13\)60591-7](https://doi.org/10.1016/S0140-6736(13)60591-7).

Atwater, I., B. Ribalet, et E. Rojas. 1978. « Cyclic Changes in Potential and Resistance of the Beta-Cell Membrane Induced by Glucose in Islets of Langerhans from Mouse ». *The Journal of Physiology* 278 (mai): 117-39. <https://doi.org/10.1113/jphysiol.1978.sp012296>.

Auner, Alexander W., Kazi M. Tasneem, Dmitry A. Markov, Lisa J. McCawley, et M. Shane Hutson. 2019. « Chemical-PDMS Binding Kinetics and Implications for Bioavailability in Microfluidic Devices ». *Lab on a Chip* 19 (5): 864-74. <https://doi.org/10.1039/c8lc00796a>.

Aussedat, B., M. Dupire-Angel, R. Gifford, J. Klein, G. S. Wilson, et G. Reach. 2000. « Interstitial glucose concentration and glycemia: implications for continuous subcutaneous glucose monitoring. » *American journal of physiology. Endocrinology and metabolism*. <https://doi.org/10.1152/AJPENDO.2000.278.4.E716>.

Azizipour, Neda, Rahi Avazpour, Derek H. Rosenzweig, Mohamad Sawan, et Abdellah Aji. 2020. « Evolution of Biochip Technology: A Review from Lab-on-a-Chip to Organ-on-a-Chip ». *Micromachines* 11 (6): 599. <https://doi.org/10.3390/mi11060599>.

Badugu, Ramachandram, Joseph R. Lakowicz, et Chris D. Geddes. 2003. « A Glucose Sensing Contact Lens: A Non-Invasive Technique for Continuous Physiological Glucose Monitoring ». *Journal of Fluorescence* 13 (5): 371-74. <https://doi.org/10.1023/A:1026103804104>.

Baekkeskov, S., G. Warnock, M. Christie, R. V. Rajotte, P. M. Larsen, et S. Fey. 1989. « Revelation of Specificity of 64K Autoantibodies in IDDM Serums by High-Resolution 2-D Gel Electrophoresis. Unambiguous Identification of 64K Target Antigen ». *Diabetes* 38 (9): 1133-41. <https://doi.org/10.2337/diab.38.9.1133>.

Baeyens, L., S. De Breuck, J. Lardon, J. K. Mfopou, I. Rooman, et L. Bouwens. 2005. « In Vitro Generation of Insulin-Producing Beta Cells from Adult Exocrine Pancreatic Cells ». *Diabetologia* 48 (1): 49-57. <https://doi.org/10.1007/s00125-004-1606-1>.

Baggio, Laurie L., et Daniel J. Drucker. 2007. « Biology of Incretins: GLP-1 and GIP ». *Gastroenterology* 132 (6): 2131-57. <https://doi.org/10.1053/j.gastro.2007.03.054>.

Bailey, Timothy, Bruce W. Bode, Mark P. Christiansen, Leslie J. Klaff, et Shridhara Alva. 2015. « The Performance and Usability of a Factory-Calibrated Flash Glucose Monitoring System ». *Diabetes Technology & Therapeutics* 17 (11): 787-94. <https://doi.org/10.1089/dia.2014.0378>.

Bailey, Timothy S. 2017. « Clinical Implications of Accuracy Measurements of Continuous Glucose Sensors ». *Diabetes Technology & Therapeutics* 19 (Suppl 2): S-51-S-54. <https://doi.org/10.1089/dia.2017.0050>.

Bailey, Timothy S., Andrew Ahmann, Ronald Brazg, Mark Christiansen, Satish Garg, Elaine Watkins, John B. Welsh, et Scott W. Lee. 2014. « Accuracy and Acceptability of the 6-Day Enlite Continuous Subcutaneous Glucose Sensor ». *Diabetes Technology & Therapeutics* 16 (5): 277-83. <https://doi.org/10.1089/dia.2013.0222>.

Bailey, Timothy S., Anna Chang, et Mark Christiansen. 2014. « Clinical Accuracy of a Continuous Glucose Monitoring System With an Advanced Algorithm ». *Journal of Diabetes Science and Technology* 9 (2): 209-14. <https://doi.org/10.1177/1932296814559746>.

Ball, Andrew J., Annelie E. Abrahamsson, Björn Tyrberg, Pamela Itkin-Ansari, et Fred Levine. 2007. « HES6 Reverses Nuclear Reprogramming of Insulin-Producing Cells Following Cell Fusion ». *Biochemical and Biophysical Research Communications* 355 (2): 331-37. <https://doi.org/10.1016/j.bbrc.2007.01.153>.

Banting FG, Best CH, Collip JB, Campell WR, Fletcher AA (1922). The James Lind Library. 26 mai 2010. <https://www.jameslindlibrary.org/banting-fg-best-ch-collip-jb-campell-wr-fletcher-aa-1922/>.

Bantle, John P, et William Thomas. 1997. « Glucose Measurement in Patients with Diabetes Mellitus with Dermal Interstitial Fluid ». *Journal of Laboratory and Clinical Medicine* 130 (4): 436-41. [https://doi.org/10.1016/S0022-2143\(97\)90044-5](https://doi.org/10.1016/S0022-2143(97)90044-5).

Barbieux, Charlotte, Géraldine Parnaud, Vanessa Lavallard, Estelle Brioude, Jérémy Meyer, Mohamed Alibashe Ahmed, Ekaterine Berishvili, Thierry Berney, et Domenico Bosco. 2016. « Asymmetrical Distribution of δ and PP Cells in Human Pancreatic Islets ». *Journal of Endocrinology* 229 (2): 123-32. <https://doi.org/10.1530/JOE-15-0542>.

Barg, S., J. Galvanovskis, S. O. Göpel, P. Rorsman, et L. Eliasson. 2000. « Tight Coupling between Electrical Activity and Exocytosis in Mouse Glucagon-Secreting Alpha-Cells ». *Diabetes* 49 (9): 1500-1510. <https://doi.org/10.2337/diabetes.49.9.1500>.

Barnett, D. W., D. M. Pressel, et S. Mislér. 1995. « Voltage-Dependent Na⁺ and Ca²⁺ Currents in Human Pancreatic Islet Beta-Cells: Evidence for Roles in the Generation of Action Potentials and Insulin Secretion ». *Pflugers Archiv: European Journal of Physiology* 431 (2): 272-82. <https://doi.org/10.1007/BF00410201>.

Bar-Nur, Ori, Holger A. Russ, Shimon Efrat, et Nissim Benvenisty. 2011. « Epigenetic Memory and Preferential Lineage-Specific Differentiation in Induced Pluripotent Stem Cells Derived from Human Pancreatic Islet Beta Cells ». *Cell Stem Cell* 9 (1): 17-23. <https://doi.org/10.1016/j.stem.2011.06.007>.

Bastos, M. 1989. « [Hypoglycemia: prevention and treatment] ». *Acta Medica Portuguesa Suppl* 1 (septembre): 27S-28S.

Battelino, Tadej, Revital Nimri, Klemen Dovc, Moshe Phillip, et Natasa Bratina. 2017. « Prevention of Hypoglycemia With Predictive Low Glucose Insulin Suspension in Children

With Type 1 Diabetes: A Randomized Controlled Trial ». *Diabetes Care* 40 (6): 764-70. <https://doi.org/10.2337/dc16-2584>.

Battelino, Tadej, Moshe Phillip, Natasa Bratina, Revital Nimri, Per Oskarsson, et Jan Bolinder. 2011. « Effect of Continuous Glucose Monitoring on Hypoglycemia in Type 1 Diabetes ». *Diabetes Care* 34 (4): 795-800. <https://doi.org/10.2337/dc10-1989>.

Batterham, R. L., C. W. Le Roux, M. A. Cohen, A. J. Park, S. M. Ellis, M. Patterson, G. S. Frost, M. A. Ghatei, et S. R. Bloom. 2003. « Pancreatic Polypeptide Reduces Appetite and Food Intake in Humans ». *The Journal of Clinical Endocrinology and Metabolism* 88 (8): 3989-92. <https://doi.org/10.1210/jc.2003-030630>.

Baumann, Katrine Y., Martin K. Church, Geraldine F. Clough, Sven Roy Quist, Martin Schmelz, Per Stahl Skov, Chris D. Anderson, et al. 2019. « Skin microdialysis: methods, applications and future opportunities—an EAACI position paper ». *Clinical and Translational Allergy* 9 (avril): 24. <https://doi.org/10.1186/s13601-019-0262-y>.

Becker, Lillian C., Wilma F. Bergfeld, Donald V. Belsito, Ronald A. Hill, Curtis D. Klaassen, Daniel C. Liebler, James G. Marks, et al. 2014. « Safety Assessment of Dimethicone Crosspolymers as Used in Cosmetics ». *International Journal of Toxicology* 33 (2 suppl): 65S-115S. <https://doi.org/10.1177/1091581814524963>.

Bell, G. I., S. Horita, et J. H. Karam. 1984. « A Polymorphic Locus near the Human Insulin Gene Is Associated with Insulin-Dependent Diabetes Mellitus ». *Diabetes* 33 (2): 176-83. <https://doi.org/10.2337/diab.33.2.176>.

Bennett, S. T., A. M. Lucassen, S. C. Gough, E. E. Powell, D. E. Undlien, L. E. Pritchard, M. E. Merriman, Y. Kawaguchi, M. J. Dronsfield, et F. Pociot. 1995. « Susceptibility to Human Type 1 Diabetes at IDDM2 Is Determined by Tandem Repeat Variation at the Insulin Gene Minisatellite Locus ». *Nature Genetics* 9 (3): 284-92. <https://doi.org/10.1038/ng0395-284>.

Benninger, R. K. P., W. Steven Head, Min Zhang, Leslie S. Satin, et David W. Piston. 2011. « Gap Junctions and Other Mechanisms of Cell-Cell Communication Regulate Basal Insulin Secretion in the Pancreatic Islet ». *The Journal of Physiology* 589 (Pt 22): 5453-66. <https://doi.org/10.1113/jphysiol.2011.218909>.

Berchtold, Lukas A., Michela Miani, Thi A. Diep, Andreas N. Madsen, Valentina Cigliola, Maikel Colli, Jelena M. Krivokapic, et al. 2017. « Pannexin-2-Deficiency Sensitizes Pancreatic β -Cells to Cytokine-Induced Apoptosis in Vitro and Impairs Glucose Tolerance in Vivo ». *Molecular and Cellular Endocrinology* 448 (juin): 108-21. <https://doi.org/10.1016/j.mce.2017.04.001>.

Berg, Jeremy M., John L. Tymoczko, Lubert Stryer, Jeremy M. Berg, John L. Tymoczko, et Lubert Stryer. 2002. *Biochemistry*. 5th éd. W H Freeman.

Berger, Constantin, et Daniela Zdzieblo. 2020. « Glucose Transporters in Pancreatic Islets ». *Pflügers Archiv: European Journal of Physiology* 472 (9): 1249-72. <https://doi.org/10.1007/s00424-020-02383-4>.

Berhan, Yonas, Ingeborg Waernbaum, Torbjörn Lind, Anna Möllsten, et Gisela Dahlquist. 2011. « Thirty Years of Prospective Nationwide Incidence of Childhood Type 1 Diabetes ». *Diabetes* 60 (2): 577-81. <https://doi.org/10.2337/db10-0813>.

Berthod, Alain, Mike Rodriguez, Marco Girod, et Daniel Armstrong. 2002. « Use of microbubbles in capillary electrophoresis for sample segregation when focusing microbial samples ». *Journal of Separation Science - J SEP SCI* 25 : 988-95. [https://doi.org/10.1002/1615-9314\(20021101\)25:15/17<988::AID-JSSC988>3.0.CO;2-I](https://doi.org/10.1002/1615-9314(20021101)25:15/17<988::AID-JSSC988>3.0.CO;2-I).

Bhatia, Sangeeta N., et Donald E. Ingber. 2014. « Microfluidic Organs-on-Chips ». *Nature Biotechnology* 32 (8): 760-72. <https://doi.org/10.1038/nbt.2989>.

Bingley, P. J., E. Bonifacio, A. J. Williams, S. Genovese, G. F. Bottazzo, et E. A. Gale. 1997. « Prediction of IDDM in the General Population: Strategies Based on Combinations of Autoantibody Markers ». *Diabetes* 46 (11): 1701-10. <https://doi.org/10.2337/diab.46.11.1701>.

Bingley, P. J., A. J. Williams, et E. A. Gale. 1999. « Optimized Autoantibody-Based Risk Assessment in Family Members. Implications for Future Intervention Trials ». *Diabetes Care* 22 (11): 1796-1801. <https://doi.org/10.2337/diacare.22.11.1796>.

Bm, Jensen, Bjerring P, Christiansen Js, et Orskov H. 1995. « Glucose Content in Human Skin: Relationship with Blood Glucose Levels ». *Scandinavian Journal of Clinical and Laboratory Investigation* 55 (5). <https://doi.org/10.3109/00365519509104982>.

Bokvist, K., M. Hoy, K. Buschard, J. J. Holst, M. K. Thomsen, et J. Gromada. 1999. « Selectivity of Prandial Glucose Regulators: Nateglinide, but Not Repaglinide, Accelerates Exocytosis in Rat Pancreatic A-Cells ». *European Journal of Pharmacology* 386 (1): 105-11. [https://doi.org/10.1016/s0014-2999\(99\)00754-2](https://doi.org/10.1016/s0014-2999(99)00754-2).

Bonner-Weir, S., et L. Orci. 1982. « New Perspectives on the Microvasculature of the Islets of Langerhans in the Rat ». *Diabetes* 31 (10): 883-89. <https://doi.org/10.2337/diab.31.10.883>.

Bonnevie-Nielsen, V., M. W. Steffes, et A. Lernmark. 1981. « A Major Loss in Islet Mass and B-Cell Function Precedes Hyperglycemia in Mice given Multiple Low Doses of Streptozotocin ». *Diabetes* 30 (5): 424-29. <https://doi.org/10.2337/diab.30.5.424>.

Bornat, Yannick, Matthieu Raoux, Youssef Boutaib, Fabrice Morin, Gilles Charpentier, Jochen Lang, et Sylvie Renaud. 2010. « Detection of Electrical Activity of Pancreatic Beta-cells Using Micro-electrode Arrays ». In *Proceedings of the 2010 Fifth IEEE International Symposium on Electronic Design, Test & Applications*, 233-36. DELTA '10. USA: IEEE Computer Society. <https://doi.org/10.1109/DELTA.2010.60>.

Boujard, Daniel, Bruno Anselme, et Christophe Cullin. 2015. *Biologie cellulaire et moléculaire - Tout le cours en fiches : 200 fiches de cours, 400 schémas, 160 QCM et site compagnon Ed. 2*. Dunod. <https://u-bordeaux-scholarvox-com.docelec.u-bordeaux.fr/book/88828472>.

Bracken, Michael B. 2009. « Why Animal Studies Are Often Poor Predictors of Human Reactions to Exposure ». *Journal of the Royal Society of Medicine* 102 (3): 120-22. <https://doi.org/10.1258/jrsm.2008.08k033>.

Brereton, Melissa F., Elisa Vergari, Quan Zhang, et Anne Clark. 2015. « Alpha-, Delta- and PP-Cells: Are They the Architectural Cornerstones of Islet Structure and Co-Ordination? » *The Journal of Histochemistry and Cytochemistry*: 63 (8): 575-91. <https://doi.org/10.1369/0022155415583535>.

Briant, L. J. B., T. M. Reinbothe, I. Spiliotis, C. Miranda, B. Rodriguez, et P. Rorsman. 2018. « δ -Cells and β -Cells Are Electrically Coupled and Regulate α -Cell Activity via Somatostatin ». *The Journal of Physiology* 596 (2): 197-215. <https://doi.org/10.1113/JP274581>.

Briant, Linford J. B., Quan Zhang, Elisa Vergari, Joely A. Kellard, Blanca Rodriguez, Frances M. Ashcroft, et Patrik Rorsman. 2017. « Functional Identification of Islet Cell Types by Electrophysiological Fingerprinting ». *Interface* 14 (128): 20160999. <https://doi.org/10.1098/rsif.2016.0999>.

Brissova, Marcela, et Alvin C. Powers. 2008. « Architecture of Pancreatic Islets ». In *Pancreatic Beta Cell in Health and Disease*, édité par Susumu Seino et Graeme I. Bell, 3-11. Tokyo: Springer Japan. https://doi.org/10.1007/978-4-431-75452-7_1.

Brown, Sue A., Boris P. Kovatchev, Dan Raghinaru, John W. Lum, Bruce A. Buckingham, Yogish C. Kudva, Lori M. Laffel, et al. 2019. « Six-Month Randomized, Multicenter Trial of Closed-Loop Control in Type 1 Diabetes ». *New England Journal of Medicine* 381 (18): 1707-17. <https://doi.org/10.1056/NEJMoa1907863>.

Browning, Kirsteen N. 2013. « Modulation of Gastrointestinal Vagal Neurocircuits by Hyperglycemia ». *Frontiers in Neuroscience* 7: 217. <https://doi.org/10.3389/fnins.2013.00217>.
Brun, Matthias A., Kui-Thong Tan, Rudolf Griss, Anna Kielkowska, Luc Reymond, et Kai Johnsson. 2012. « A Semisynthetic Fluorescent Sensor Protein for Glutamate ». *Journal of the American Chemical Society* 134 (18): 7676-78. <https://doi.org/10.1021/ja3002277>.

Brunicardi, F. C., D. M. Shavelle, et D. K. Andersen. 1995. « Neural Regulation of the Endocrine Pancreas ». *Official Journal of the International Association of Pancreatology* 18 (3): 177-95. <https://doi.org/10.1007/BF02784941>.

Bruno, Graziella, Milena Maule, Annibale Biggeri, Alessia Ledda, Carla Mannu, Franco Merletti, et Marco Songini. 2013. « More Than 20 Years of Registration of Type 1 Diabetes in Sardinian Children ». *Diabetes* 62 (10): 3542-46. <https://doi.org/10.2337/db12-1771>.

Buchan, A. M., J. M. Polak, C. Capella, E. Solcia, et A. G. Pearse. 1978. « Electronimmunocytochemical Evidence for the K Cell Localization of Gastric Inhibitory Polypeptide (GIP) in Man ». *Histochemistry* 56 (1): 37-44. <https://doi.org/10.1007/BF00492251>.

Bunn, H. F., D. N. Haney, K. H. Gabbay, et P. M. Gallop. 1975. « Further Identification of the Nature and Linkage of the Carbohydrate in Hemoglobin A1c ». *Biochemical and Biophysical Research Communications* 67 (1): 103-9. [https://doi.org/10.1016/0006-291x\(75\)90289-2](https://doi.org/10.1016/0006-291x(75)90289-2).

Buzsáki, György, Costas A. Anastassiou, et Christof Koch. 2012. « The Origin of Extracellular Fields and Currents--EEG, ECoG, LFP and Spikes ». *Nature Reviews Neuroscience* 13 (6): 407-20. <https://doi.org/10.1038/nrn3241>.

Cabrera, Over, Dora M. Berman, Norma S. Kenyon, Camillo Ricordi, Per-Olof Berggren, et Alejandro Caicedo. 2006. « The Unique Cytoarchitecture of Human Pancreatic Islets Has Implications for Islet Cell Function ». *Proceedings of the National Academy of Sciences* 103 (7): 2334-39. <https://doi.org/10.1073/pnas.0510790103>.

Cadwell, Cathryn R., Federico Scala, Shuang Li, Giulia Livrizzi, Shan Shen, Rickard Sandberg, Xiaolong Jiang, et Andreas S. Tolias. 2017. « Multimodal Profiling of Single-Cell Morphology, Electrophysiology, and Gene Expression Using Patch-Seq ». *Nature Protocols* 12 (12): 2531-53. <https://doi.org/10.1038/nprot.2017.120>.

Caicedo, Alejandro. 2013. « Paracrine and Autocrine Interactions in the Human Islet: More than Meets the Eye ». *Seminars in Cell & Developmental Biology* 24 (1): 11-21. <https://doi.org/10.1016/j.semcdb.2012.09.007>.

Caillat-Zucman, S, H J Garchon, J Timsit, R Assan, C Boitard, I Djilali-Saiah, P Bougnères, et J F Bach. 1992. « Age-dependent HLA genetic heterogeneity of type 1 insulin-dependent diabetes mellitus. ». *Journal of Clinical Investigation* 90 (6): 2242-50.

Cambronne, Xiaolu A., Melissa L. Stewart, DongHo Kim, Amber M. Jones-Brunette, Rory K. Morgan, David L. Farrens, Michael S. Cohen, et Richard H. Goodman. 2016. « Biosensor Reveals Multiple Sources for Mitochondrial NAD⁺ ». *Science* 352 (6292): 1474-77. <https://doi.org/10.1126/science.aad5168>.

Cappon, Giacomo, Martina Vettoretti, Giovanni Sparacino, et Andrea Facchinetti. 2019. « Continuous Glucose Monitoring Sensors for Diabetes Management: A Review of Technologies and Applications ». *Diabetes & Metabolism Journal* 43 (4): 383-97. <https://doi.org/10.4093/dmj.2019.0121>.

Carey, Andrew, Gregory Steinberg, Stuart Macaulay, Walter Thomas, Anna Holmes, Georg Ramm, Oja Prelovsek, et al. 2006. « Interleukin-6 Increases Insulin-Stimulated Glucose Disposal in Humans and Glucose Uptake and Fatty Acid Oxidation In Vitro via AMP-Activated Protein Kinase ». *Diabetes* 55 : 2688-97. <https://doi.org/10.2337/db05-1404>.

Carvalho, C. P. F., R. B. Oliveira, A. Britan, J. C. Santos-Silva, A. C. Boschero, P. Meda, et C. B. Collares-Buzato. 2012. « Impaired β -Cell- β -Cell Coupling Mediated by Cx36 Gap Junctions in Prediabetic Mice ». *American Journal of Physiology. Endocrinology and Metabolism* 303 (1): E144-151. <https://doi.org/10.1152/ajpendo.00489.2011>.

Castaing, M., A. Guerci, J. Mallet, P. Czernichow, P. Ravassard, et R. Scharfmann. 2005. « Efficient Restricted Gene Expression in Beta Cells by Lentivirus-Mediated Gene Transfer into Pancreatic Stem/Progenitor Cells ». *Diabetologia* 48 (4): 709-19. <https://doi.org/10.1007/s00125-005-1694-6>.

Castaing, M., B. Péault, A. Basmaciogullari, I. Casal, P. Czernichow, et R. Scharfmann. 2001. « Blood Glucose Normalization upon Transplantation of Human Embryonic Pancreas into Beta-Cell-Deficient SCID Mice ». *Diabetologia* 44 (11): 2066-76. <https://doi.org/10.1007/s001250100012>.

Castaing, Muriel, Bertrand Duvillié, Eric Quemeneur, Annie Basmaciogullari, et Raphael Scharfmann. 2005. « Ex Vivo Analysis of Acinar and Endocrine Cell Development in the Human Embryonic Pancreas ». *Developmental Dynamics* 234 (2): 339-45. <https://doi.org/10.1002/dvdy.20547>.

Castle, Jessica R., Julia M. Engle, Joseph El Youssef, Ryan G. Massoud, Kevin C. J. Yuen, Ryland Kagan, et W. Kenneth Ward. 2010. « Novel Use of Glucagon in a Closed-Loop System for Prevention of Hypoglycemia in Type 1 Diabetes ». *Diabetes Care* 33 (6): 1282-87. <https://doi.org/10.2337/dc09-2254>.

Cena, Hellas, et Philip C. Calder. 2020. « Defining a Healthy Diet: Evidence for the Role of Contemporary Dietary Patterns in Health and Disease ». *Nutrients* 12 (2): 334. <https://doi.org/10.3390/nu12020334>.

Cépède, Michel, et Maurice Langellé. 1964. *L'économie de l'alimentation*. Vol. 639. Que sais je ? PUF.

Cersosimo, Eugenio, Xiaojing Xu, Sikarin Upala, Curtis Triplitt, et Nicolas Musi. 2014. « Acute insulin resistance stimulates and insulin sensitization attenuates vascular smooth muscle cell migration and proliferation ». *Physiological Reports* 2 (8): e12123. <https://doi.org/10.14814/phy2.12123>.

Chan, C P, D F Bowen-Pope, R Ross, et E G Krebs. 1987. « Regulation of Glycogen Synthase Activity by Growth Factors. Relationship between Synthase Activation and Receptor Occupancy. » *Journal of Biological Chemistry* 262 (1): 276-81. [https://doi.org/10.1016/S0021-9258\(19\)75923-7](https://doi.org/10.1016/S0021-9258(19)75923-7).

Charpentier, E., J. Cancela, et P. Meda. 2007. « Beta Cells Preferentially Exchange Cationic Molecules via Connexin 36 Gap Junction Channels ». *Diabetologia* 50 (11): 2332-41. <https://doi.org/10.1007/s00125-007-0807-9>.

Cheatham, B., et C. R. Kahn. 1995. « Insulin Action and the Insulin Signaling Network ». *Endocrine Reviews* 16 (2): 117-42. <https://doi.org/10.1210/edrv-16-2-117>.

Chefer, Vladimir I., Alexis C. Thompson, Agustin Zapata, et Toni S. Shippenberg. 2009. « Overview of Brain Microdialysis ». *Current protocols in neuroscience / editorial board, Jacqueline N. Crawley ... [et al.]* CHAPTER (avril): Unit7.1. <https://doi.org/10.1002/0471142301.ns0701s47>.

Chen, Cheng, Xue-Ling Zhao, Zhan-Hong Li, Zhi-Gang Zhu, Shao-Hong Qian, et Andrew J. Flewitt. 2017. « Current and Emerging Technology for Continuous Glucose Monitoring ». *Sensors (Basel, Switzerland)* 17 (1): 182. <https://doi.org/10.3390/s17010182>.

Cheng, Hao-Bin, et Yen-Wen Lu. 2014. « Applications of Textured Surfaces on Bubble Trapping and Degassing for Microfluidic Devices ». *Microfluidics and Nanofluidics* 17 (5): 855-62. <https://doi.org/10.1007/s10404-014-1368-0>.

Chera, Simona, Delphine Baronnier, Luiza Ghila, Valentina Cigliola, Jan N. Jensen, Guoqiang Gu, Kenichiro Furuyama, et al. 2014. « Diabetes Recovery by Age-Dependent Conversion of Pancreatic δ -Cells into Insulin Producers ». *Nature* 514 (7523): 503-7. <https://doi.org/10.1038/nature13633>.

Chetty, Sundari, Felicia Walton Pagliuca, Christian Honore, Anastasie Kweudjeu, Alireza Rezaia, et Douglas A. Melton. 2013. « A Simple Tool to Improve Pluripotent Stem Cell Differentiation ». *Nature Methods* 10 (6): 553-56. <https://doi.org/10.1038/nmeth.2442>.

Chia, Chee W., Juliana O. Odetunde, Wook Kim, Olga D. Carlson, Luigi Ferrucci, et Josephine M. Egan. 2014. « GIP Contributes to Islet Trihormonal Abnormalities in Type 2 Diabetes ». *The Journal of Clinical Endocrinology and Metabolism* 99 (7): 2477-85. <https://doi.org/10.1210/jc.2013-3994>.

Chick, W. L., S. Warren, R. N. Chute, A. A. Like, V. Lauris, et K. C. Kitchen. 1977. « A Transplantable Insulinoma in the Rat ». *Proceedings of the National Academy of Sciences of the United States of America* 74 (2): 628-32. <https://doi.org/10.1073/pnas.74.2.628>.

Chiu, Y.-C., T.-E. Hua, Y.-Y. Fu, P. J. Pasricha, et S.-C. Tang. 2012. « 3-D Imaging and Illustration of the Perfusive Mouse Islet Sympathetic Innervation and Its Remodelling in Injury ». *Diabetologia* 55 (12): 3252-61. <https://doi.org/10.1007/s00125-012-2699-6>.

Choy, C. K., P. Cho, W. Y. Chung, et I. F. Benzie. 2001. « Water-Soluble Antioxidants in Human Tears: Effect of the Collection Method ». *Investigative Ophthalmology & Visual Science* 42 (13): 3130-34.

Christiansen, Mark, Timothy Bailey, Elaine Watkins, David Liljenquist, David Price, Katherine Nakamura, Robert Boock, et Thomas Peyser. 2013. « A New-Generation Continuous Glucose Monitoring System: Improved Accuracy and Reliability Compared with a Previous-Generation System ». *Diabetes Technology & Therapeutics* 15 (10): 881-88. <https://doi.org/10.1089/dia.2013.0077>.

Christiansen, Mark P., Satish K. Garg, Ronald Brazg, Bruce W. Bode, Timothy S. Bailey, Robert H. Slover, Ashley Sullivan, et al. 2017. « Accuracy of a Fourth-Generation Subcutaneous Continuous Glucose Sensor ». *Diabetes Technology & Therapeutics* 19 (8): 446-56. <https://doi.org/10.1089/dia.2017.0087>.

Chruściak, Anna, Kate Kauter, Eliza Whiteside, et Louisa Windus. 2021. *Fundamentals of Anatomy and Physiology*. Australian Edition. Place of publication not identified: University of Southern Queensland. <https://open.umn.edu/opentextbooks/textbooks/974>.

Colom, Cristina, Anna Rull, José Luis Sanchez-Quesada, et Antonio Pérez. 2021. « Cardiovascular Disease in Type 1 Diabetes Mellitus: Epidemiology and Management of Cardiovascular Risk ». *Journal of Clinical Medicine* 10 (8): 1798. <https://doi.org/10.3390/jcm10081798>.

Conde, Silvia V., Joana F. Sacramento, et Maria P. Guarino. 2018. « Carotid Body: A Metabolic Sensor Implicated in Insulin Resistance ». *Physiological Genomics* 50 (3): 208-14. <https://doi.org/10.1152/physiolgenomics.00121.2017>.

Corssmit, E. P., J. A. Romijn, et H. P. Sauerwein. 2001. « Review Article: Regulation of Glucose Production with Special Attention to Nonclassical Regulatory Mechanisms: A Review ». *Metabolism: Clinical and Experimental* 50 (7): 742-55. <https://doi.org/10.1053/meta.2001.24195>.

Craig, Tim J., Frances M. Ashcroft, et Peter Proks. 2008. « How ATP Inhibits the Open KATP Channel ». *The Journal of General Physiology* 132 (1): 131-44. <https://doi.org/10.1085/jgp.200709874>.

Cudworth, A. G., et J. C. Woodrow. 1975. « HL-A System and Diabetes Mellitus ». *Diabetes* 24 (4): 345-49. <https://doi.org/10.2337/diab.24.4.345>.

Dalla Man, Chiara, Davide M. Raimondo, Robert A. Rizza, et Claudio Cobelli. 2007. « GIM, Simulation Software of Meal Glucose—Insulin Model ». *Journal of Diabetes Science and Technology* 1 (3): 323-30. <https://doi.org/10.1177/193229680700100303>.

D'Amour, Kevin A., Anne G. Bang, Susan Eliazar, Olivia G. Kelly, Alan D. Agulnick, Nora G. Smart, Mark A. Moorman, Evert Kroon, Melissa K. Carpenter, et Emmanuel E. Baetge. 2006. « Production of Pancreatic Hormone-Expressing Endocrine Cells from Human Embryonic Stem Cells ». *Nature Biotechnology* 24 (11): 1392-1401. <https://doi.org/10.1038/nbt1259>.

Danne, Thomas, Revital Nimri, Tadej Battelino, Richard M. Bergenstal, Kelly L. Close, J. Hans DeVries, Satish Garg, et al. 2017. « International Consensus on Use of Continuous Glucose Monitoring ». *Diabetes Care* 40 (12): 1631-40. <https://doi.org/10.2337/dc17-1600>.

Date, Y., M. Kojima, H. Hosoda, A. Sawaguchi, M. S. Mondal, T. Suganuma, S. Matsukura, K. Kangawa, et M. Nakazato. 2000. « Ghrelin, a Novel Growth Hormone-Releasing Acylated Peptide, Is Synthesized in a Distinct Endocrine Cell Type in the Gastrointestinal Tracts of Rats and Humans ». *Endocrinology* 141 (11): 4255-61. <https://doi.org/10.1210/endo.141.11.7757>.

DeBoer, Mark D., Daniel R. Cherňavsky, Katarina Topchyan, Boris P. Kovatchev, Gary L. Francis, et Marc D. Breton. 2017. « Heart Rate Informed Artificial Pancreas System Enhances Glycemic Control during Exercise in Adolescents with T1D ». *Pediatric Diabetes* 18 (7): 540-46. <https://doi.org/10.1111/pedi.12454>.

Decochez, K., I. Truyen, B. van der Auwera, I. Weets, E. Vandemeulebroucke, I. H. de Leeuw, B. Keymeulen, et al. 2005. « Combined Positivity for HLA DQ2/DQ8 and IA-2 Antibodies Defines Population at High Risk of Developing Type 1 Diabetes ». *Diabetologia* 48 (4): 687-94. <https://doi.org/10.1007/s00125-005-1702-x>.

Dehennis, Andrew, Mark A. Mortellaro, et Sorin Ioacara. 2015. « Multisite Study of an Implanted Continuous Glucose Sensor Over 90 Days in Patients With Diabetes Mellitus ». *Journal of Diabetes Science and Technology* 9 (5): 951-56. <https://doi.org/10.1177/1932296815596760>.

Del Favero, Simone, Daniela Bruttomesso, Federico Di Palma, Giordano Lanzola, Roberto Visentin, Alessio Filippi, Rachele Scotton, et al. 2014. « First Use of Model Predictive Control in Outpatient Wearable Artificial Pancreas ». *Diabetes Care* 37 (5): 1212-15. <https://doi.org/10.2337/dc13-1631>.

Del Guercio, M. J., B. di Natale, L. Gargantini, C. Garlaschi, et G. Chiumello. 1976. « Effect of Somatostatin on Blood Sugar, Plasma Growth Hormone, and Glucagon Levels in Diabetic Children ». *Diabetes* 25 (7): 550-53. <https://doi.org/10.2337/diab.25.7.550>.

Del Prato, S. 2003. « Loss of Early Insulin Secretion Leads to Postprandial Hyperglycaemia ». *Diabetologia* 46 Suppl 1 : M2-8. <https://doi.org/10.1007/s00125-002-0930-6>.

Desai, Tejal, et Lonnie D. Shea. 2017. « Advances in Islet Encapsulation Technologies ». *Nature Reviews. Drug Discovery* 16 (5): 338-50. <https://doi.org/10.1038/nrd.2016.232>.

Devendra, Devasenan, et George S. Eisenbarth. 2003. « 17. Immunologic Endocrine Disorders ». *The Journal of Allergy and Clinical Immunology* 111 (2 Suppl): S624-636. <https://doi.org/10.1067/mai.2003.81>.

DiGruccio, Michael R., Alex M. Mawla, Cynthia J. Donaldson, Glyn M. Noguchi, Joan Vaughan, Christopher Cowing-Zitron, Talitha van der Meulen, et Mark O. Huising. 2016. « Comprehensive Alpha, Beta and Delta Cell Transcriptomes Reveal That Ghrelin Selectively Activates Delta Cells and Promotes Somatostatin Release from Pancreatic Islets ». *Molecular Metabolism* 5 (7): 449-58. <https://doi.org/10.1016/j.molmet.2016.04.007>.

DiMeglio, Linda A, Carmella Evans-Molina, et Richard A Oram. 2018. « Type 1 Diabetes ». *The Lancet* 391 (10138): 2449-62. [https://doi.org/10.1016/S0140-6736\(18\)31320-5](https://doi.org/10.1016/S0140-6736(18)31320-5).

Doke, Sonali K., et Shashikant C. Dhawale. 2015. « Alternatives to Animal Testing: A Review ». *Saudi Pharmaceutical Journal* 23 (3): 223-29. <https://doi.org/10.1016/j.jsps.2013.11.002>.

Dolenšek, Jurij, Marjan Slak Rupnik, et Andraž Stožer. 2015. « Structural Similarities and Differences between the Human and the Mouse Pancreas ». *Islets* 7 (1): e1024405. <https://doi.org/10.1080/19382014.2015.1024405>.

DRUCKER, D. J., J. PHILIPPE, et S. MOJISOV. 1988. « Proglucagon Gene Expression and Posttranslational Processing in a Hamster Islet Cell Line ». *Endocrinology* 123 (4): 1861-67. <https://doi.org/10.1210/endo-123-4-1861>.

Düfer, Martina. 2012. « Determination of Beta-Cell Function: Ion Channel Function in Beta Cells ». *Methods in Molecular Biology (Clifton, N.J.)* 933: 203-17. https://doi.org/10.1007/978-1-62703-068-7_13.

Duffy, D. C., J. C. McDonald, O. J. Schueller, et G. M. Whitesides. 1998. « Rapid Prototyping of Microfluidic Systems in Poly(Dimethylsiloxane) ». *Analytical Chemistry* 70 (23): 4974-84. <https://doi.org/10.1021/ac980656z>.

Dunlop, John, Mark Bowlby, Ravikumar Peri, Dmytro Vasilyev, et Robert Arias. 2008. « High-Throughput Electrophysiology: An Emerging Paradigm for Ion-Channel Screening and Physiology ». *Nature Reviews. Drug Discovery* 7 (4): 358-68. <https://doi.org/10.1038/nrd2552>.

Dybala, Michael P., et Manami Hara. 2019. « Heterogeneity of the Human Pancreatic Islet ». *Diabetes* 68 (6): 1230-39. <https://doi.org/10.2337/db19-0072>.

Efrat, S., G. Teitelman, M. Anwar, D. Ruggiero, et D. Hanahan. 1988. « Glucagon Gene Regulatory Region Directs Oncoprotein Expression to Neurons and Pancreatic Alpha Cells ». *Neuron* 1 (7): 605-13. [https://doi.org/10.1016/0896-6273\(88\)90110-9](https://doi.org/10.1016/0896-6273(88)90110-9).

Eizirik, Décio L., Michael Sammeth, Thomas Bouckenoghe, Guy Bottu, Giorgia Sisino, Mariana Igoillo-Esteve, Fernanda Ortis, et al. 2012. « The Human Pancreatic Islet Transcriptome: Expression of Candidate Genes for Type 1 Diabetes and the Impact of pro-Inflammatory Cytokines ». *PLoS Genetics* 8 (3): e1002552. <https://doi.org/10.1371/journal.pgen.1002552>.

El, Kimberley, Megan E. Capozzi, et Jonathan E. Campbell. 2020. « Repositioning the Alpha Cell in Postprandial Metabolism ». *Endocrinology* 161 (11): bqaa169. <https://doi.org/10.1210/endo/bqaa169>.

El-Khatib, Firas H, Courtney Balliro, Mallory A Hillard, Kendra L Magyar, Laya Ekhlaspour, Manasi Sinha, Debbie Mondesir, et al. 2017. « Home Use of a Bihormonal Bionic Pancreas versus Insulin Pump Therapy in Adults with Type 1 Diabetes: A Multicentre Randomised Crossover Trial ». *The Lancet* 389 (10067): 369-80. [https://doi.org/10.1016/S0140-6736\(16\)32567-3](https://doi.org/10.1016/S0140-6736(16)32567-3).

Elrick, H., L. Stimmler, C. J. Hlad, et Y. Arai. 1964. « Plasma insulin response to oral and intravenous glucose administration ». *The Journal of Clinical Endocrinology and Metabolism* 24 (octobre): 1076-82. <https://doi.org/10.1210/jcem-24-10-1076>.

« Enquête statistique sur l'utilisation des animaux à des fins scientifiques ». s.d. enseignementsup-recherche.gouv.fr. Consulté le 4 janvier 2022. <https://www.enseignementsup-recherche.gouv.fr/fr/enquete-statistique-sur-l-utilisation-des-animaux-des-fins-scientifiques-46270>.

Evans, Mark, Antonio Ceriello, Thomas Danne, Christophe De Block, J. Hans DeVries, Marcus Lind, Chantal Mathieu, Kirsten Nørgaard, Eric Renard, et Emma G. Wilmot. 2019. « Use of Fast-

Acting Insulin Aspart in Insulin Pump Therapy in Clinical Practice ». *Diabetes, Obesity & Metabolism* 21 (9): 2039-47. <https://doi.org/10.1111/dom.13798>.

Evans-Molina, Carmella, James C. Garmey, Robert Ketchum, Kenneth L. Brayman, Shaoping Deng, et Raghavendra G. Mirmira. 2007. « Glucose Regulation of Insulin Gene Transcription and Pre-mRNA Processing in Human Islets ». *Diabetes* 56 (3): 827-35. <https://doi.org/10.2337/db06-1440>.

Ezcurra, Marina, Frank Reimann, Fiona M. Gribble, et Edward Emery. 2013. « Molecular Mechanisms of Incretin Hormone Secretion ». *Current Opinion in Pharmacology* 13 (6): 922-27. <https://doi.org/10.1016/j.coph.2013.08.013>.

Facchinetti, Andrea. 2016. « Continuous Glucose Monitoring Sensors: Past, Present and Future Algorithmic Challenges ». *Sensors (Basel, Switzerland)* 16 (12): 2093. <https://doi.org/10.3390/s16122093>.

Falkmer, S. 1979. « Immunocytochemical Studies of the Evolution of Islet Hormones ». *The Journal of Histochemistry and Cytochemistry* 27 (9): 1281-82. <https://doi.org/10.1177/27.9.383830>.

Faris, Patricia L., Randall D. Hofbauer, Randall Daughters, Erin Vandenlangenberg, Lauren Iversen, Robert L. Goodale, Robert Maxwell, Elke D. Eckert, et Boyd K. Hartman. 2008. « De-Stabilization of the Positive Vago-Vagal Reflex in Bulimia Nervosa ». *Physiology & Behavior* 94 (1): 136-53. <https://doi.org/10.1016/j.physbeh.2007.11.036>.

Farnsworth, Nikki L., Rachele L. Walter, Alireza Hemmati, Matthew J. Westacott, et Richard K. P. Benninger. 2016. « Low Level Pro-Inflammatory Cytokines Decrease Connexin36 Gap Junction Coupling in Mouse and Human Islets through Nitric Oxide-Mediated Protein Kinase C δ ». *The Journal of Biological Chemistry* 291 (7): 3184-96. <https://doi.org/10.1074/jbc.M115.679506>.

Ferber, S., A. Halkin, H. Cohen, I. Ber, Y. Einav, I. Goldberg, I. Barshack, et al. 2000. « Pancreatic and Duodenal Homeobox Gene 1 Induces Expression of Insulin Genes in Liver and Ameliorates Streptozotocin-Induced Hyperglycemia ». *Nature Medicine* 6 (5): 568-72. <https://doi.org/10.1038/75050>.

Field, Benjamin C. T., Owais B. Chaudhri, et Stephen R. Bloom. 2010. « Bowels Control Brain: Gut Hormones and Obesity ». *Nature Reviews. Endocrinology* 6 (8): 444-53. <https://doi.org/10.1038/nrendo.2010.93>.

Folli, Franco, Stefano La Rosa, Giovanna Finzi, Alberto M. Davalli, Alessandra Galli, Edward J. Dick, Carla Perego, et Rodolfo Guardado Mendoza. 2018. « Pancreatic Islet of Langerhans' Cytoarchitecture and Ultrastructure in Normal Glucose Tolerance and in Type 2 Diabetes Mellitus ». *Diabetes, Obesity & Metabolism* 20 Suppl 2 (septembre): 137-44. <https://doi.org/10.1111/dom.13380>.

Foulis, A. K., M. McGill, et M. A. Farquharson. 1991. « Insulitis in Type 1 (Insulin-Dependent) Diabetes Mellitus in Man--Macrophages, Lymphocytes, and Interferon-Gamma Containing Cells ». *The Journal of Pathology* 165 (2): 97-103. <https://doi.org/10.1002/path.1711650203>.

Fourlanos, Spiros, Michael D. Varney, Brian D. Tait, Grant Morahan, Margo C. Honeyman, Peter G. Colman, et Leonard C. Harrison. 2008. « The Rising Incidence of Type 1 Diabetes Is Accounted for by Cases with Lower-Risk Human Leukocyte Antigen Genotypes ». *Diabetes Care* 31 (8): 1546-49. <https://doi.org/10.2337/dc08-0239>.

Frank, James A., Johannes Broichhagen, Dmytro A. Yushchenko, Dirk Trauner, Carsten Schultz, et David J. Hodson. 2018. « Optical Tools for Understanding the Complexity of β -Cell Signalling and Insulin Release ». *Nature Reviews. Endocrinology* 14 (12): 721-37. <https://doi.org/10.1038/s41574-018-0105-2>.

Frayn, Keith N. 2013. *Metabolic Regulation: A Human Perspective*. John Wiley & Sons.

Freeland, A. C., et R. Bonnecaze. 2004. « Inference of Blood Glucose Concentrations from Subcutaneous Glucose Concentrations: Applications to Glucose Biosensors ». *Annals of Biomedical Engineering*. <https://doi.org/10.1114/1.196>.

Fridlyand, Leonid E., David A. Jacobson, et L. H. Philipson. 2013. « Ion Channels and Regulation of Insulin Secretion in Human β -Cells: A Computational Systems Analysis ». *Islets* 5 (1): 1-15. <https://doi.org/10.4161/isl.24166>.

Fridlyand, Leonid E, et Louis H Philipson. 2011. « Mechanisms of glucose sensing in the pancreatic β -cell ». *Islets* 3 (5): 224-30. <https://doi.org/10.4161/isl.3.5.16409>.

Fronczak, Carolyn M., Anna E. Barón, H. Peter Chase, Colleen Ross, Heather L. Brady, Michelle Hoffman, George S. Eisenbarth, Marian Rewers, et Jill M. Norris. 2003. « In Utero Dietary Exposures and Risk of Islet Autoimmunity in Children ». *Diabetes Care* 26 (12): 3237-42. <https://doi.org/10.2337/diacare.26.12.3237>.

Gall, D., J. Gromada, I. Susa, P. Rorsman, A. Herchuelz, et K. Bokvist. 1999. « Significance of Na/Ca Exchange for Ca^{2+} Buffering and Electrical Activity in Mouse Pancreatic Beta-Cells ». *Biophysical Journal* 76 (4): 2018-28. [https://doi.org/10.1016/S0006-3495\(99\)77359-5](https://doi.org/10.1016/S0006-3495(99)77359-5).

Gautam, Dinesh, Sung-Jun Han, Fadi F. Hamdan, Jongrye Jeon, Bo Li, Jian Hua Li, Yinghong Cui, et al. 2006. « A Critical Role for Beta Cell M3 Muscarinic Acetylcholine Receptors in Regulating Insulin Release and Blood Glucose Homeostasis in Vivo ». *Cell Metabolism* 3 (6): 449-61. <https://doi.org/10.1016/j.cmet.2006.04.009>.

Gazdar, A. F., W. L. Chick, H. K. Oie, H. L. Sims, D. L. King, G. C. Weir, et V. Lauris. 1980. « Continuous, Clonal, Insulin- and Somatostatin-Secreting Cell Lines Established from a Transplantable Rat Islet Cell Tumor ». *Proceedings of the National Academy of Sciences of the United States of America* 77 (6): 3519-23. <https://doi.org/10.1073/pnas.77.6.3519>.

Geoffrey, McGarraugh, Ronald Brazg, et Weinstein Richard. 2011. « FreeStyle Navigator Continuous Glucose Monitoring System with TRUstart Algorithm, a 1-Hour Warm-up Time ».

Journal of Diabetes Science and Technology 5 (1): 99-106.
<https://doi.org/10.1177/193229681100500114>.

Gerich, John. 2013. « Pathogenesis and Management of Postprandial Hyperglycemia: Role of Incretin-Based Therapies ». *International Journal of General Medicine* 6 (décembre): 877-95.
<https://doi.org/10.2147/IJGM.S51665>.

Gerich, John E., Christian Meyer, Hans J. Woerle, et Michael Stumvoll. 2001. « Renal Gluconeogenesis: Its Importance in Human Glucose Homeostasis ». *Diabetes Care* 24 (2): 382-91. <https://doi.org/10.2337/diacare.24.2.382>.

Gerritsen, M. 2000. « Problems Associated with Subcutaneously Implanted Glucose Sensors ». *Diabetes Care* 23 (2): 143-45. <https://doi.org/10.2337/diacare.23.2.143>.

Gershengorn, Marvin C., Anandwardhan A. Hardikar, Chiju Wei, Elizabeth Geras-Raaka, Bernice Marcus-Samuels, et Bruce M. Raaka. 2004. « Epithelial-to-Mesenchymal Transition Generates Proliferative Human Islet Precursor Cells ». *Science (New York, N.Y.)* 306 (5705): 2261-64. <https://doi.org/10.1126/science.1101968>.

Gillespie, Kathleen M. 2006. « Type 1 Diabetes: Pathogenesis and Prevention ». *Canadian Medical Association Journal* 175 (2): 165-70. <https://doi.org/10.1503/cmaj.060244>.

Gillespie, Kathleen M., Steven C. Bain, Anthony H. Barnett, Polly J. Bingley, Michael R. Christie, Geoffrey V. Gill, et Edwin A. M. Gale. 2004. « The Rising Incidence of Childhood Type 1 Diabetes and Reduced Contribution of High-Risk HLA Haplotypes ». *Lancet* 364 (9446): 1699-1700. [https://doi.org/10.1016/S0140-6736\(04\)17357-1](https://doi.org/10.1016/S0140-6736(04)17357-1).

Gilligan, B.J., M.C. Shults, B. Rhodes, Peter Jacobs, James Brauker, Thomas Pintar, et Stuart Updike. 2004. « Feasibility of Continuous Long-Term Glucose Monitoring from a Subcutaneous Glucose Sensor in Humans ». *Diabetes Technology and Therapeutics*: 378-86. <https://doi.org/10.1089/152091504774198089>.

Gilon, P., J. C. Jonas, et J. C. Henquin. 1994. « Culture Duration and Conditions Affect the Oscillations of Cytoplasmic Calcium Concentration Induced by Glucose in Mouse Pancreatic Islets ». *Diabetologia* 37 (10): 1007-14. <https://doi.org/10.1007/BF00400464>.

Gloyn, Anna L., Ewan R. Pearson, Jennifer F. Antcliff, Peter Proks, G. Jan Bruining, Annabelle S. Slingerland, Neville Howard, et al. 2004. « Activating Mutations in the Gene Encoding the ATP-Sensitive Potassium-Channel Subunit Kir6.2 and Permanent Neonatal Diabetes ». *The New England Journal of Medicine* 350 (18): 1838-49. <https://doi.org/10.1056/NEJMoa032922>.

Good, Miranda E., Tasha K. Nelson, Alexander M. Simon, et Janis M. Burt. 2011. « A Functional Channel Is Necessary for Growth Suppression by Cx37 ». *Journal of Cell Science* 124 (Pt 14): 2448-56. <https://doi.org/10.1242/jcs.081695>.

Göpel, S., T. Kanno, S. Barg, J. Galvanovskis, et P. Rorsman. 1999. « Voltage-Gated and Resting Membrane Currents Recorded from B-Cells in Intact Mouse Pancreatic Islets ». *The Journal of Physiology* 521 Pt 3: 717-28. <https://doi.org/10.1111/j.1469-7793.1999.00717.x>.

Göpel, S. O., T. Kanno, S. Barg, et P. Rorsman. 2000. « Patch-Clamp Characterisation of Somatostatin-Secreting -Cells in Intact Mouse Pancreatic Islets ». *The Journal of Physiology* 528 (Pt 3): 497-507. <https://doi.org/10.1111/j.1469-7793.2000.00497.x>.

Göpel, Sven, Quan Zhang, Lena Eliasson, Xiao-Song Ma, Juris Galvanovskis, Takahiro Kanno, Albert Salehi, et Patrik Rorsman. 2004. « Capacitance Measurements of Exocytosis in Mouse Pancreatic Alpha-, Beta- and Delta-Cells within Intact Islets of Langerhans ». *The Journal of Physiology* 556 (Pt 3): 711-26. <https://doi.org/10.1113/jphysiol.2003.059675>.

Gosak, Marko, Rene Markovič, Jurij Dolenšek, Marjan Slak Rupnik, Marko Marhl, Andraž Stožer, et Matjaž Perc. 2018. « Network Science of Biological Systems at Different Scales: A Review ». *Physics of Life Reviews* 24 (mars): 118-35. <https://doi.org/10.1016/j.plrev.2017.11.003>.

Graf, R., et C. Klessen. 1981. « Glycogen in Pancreatic Islets of Steroid Diabetic Rats ». *Histochemistry* 73 (2): 225-32. <https://doi.org/10.1007/BF00493022>.

Groenendaal, Willemijn, Golo von Basum, Kristiane A. Schmidt, Peter A. J. Hilbers, et Natal A. W. van Riel. 2010. « Quantifying the Composition of Human Skin for Glucose Sensor Development ». *Journal of Diabetes Science and Technology* 4 (5): 1032-40. <https://doi.org/10.1177/193229681000400502>.

Gromada, Jesper, Marianne Høy, Karsten Buschard, Albert Salehi, et Patrik Rorsman. 2001. « Somatostatin inhibits exocytosis in rat pancreatic α -cells by Gi2-dependent activation of calcineurin and depriming of secretory granules ». *The Journal of Physiology* 535 (Pt 2): 519-32. <https://doi.org/10.1111/j.1469-7793.2001.00519.x>.

Groop, L. C., K. Ratheiser, L. Luzi, A. Melander, D. C. Simonson, A. Petrides, R. C. Bonadonna, E. Widén, et R. A. DeFronzo. 1991. « Effect of Sulphonylurea on Glucose-Stimulated Insulin Secretion in Healthy and Non-Insulin Dependent Diabetic Subjects: A Dose-Response Study ». *Acta Diabetologica* 28 (2): 162-68. <https://doi.org/10.1007/BF00579720>.

Gylfe, Erik, et Patrick Gilon. 2014. « Glucose Regulation of Glucagon Secretion ». *Diabetes Research and Clinical Practice* 103 (1): 1-10. <https://doi.org/10.1016/j.diabres.2013.11.019>.
Haidar, Ahmad, Mohamed Raef Smaoui, Laurent Legault, et Rémi Rabasa-Lhoret. 2016. « The Role of Glucagon in the Artificial Pancreas ». *The Lancet. Diabetes & Endocrinology* 4 (6): 476-79. [https://doi.org/10.1016/S2213-8587\(16\)30006-7](https://doi.org/10.1016/S2213-8587(16)30006-7).

Hammarlund-Udenaes, Margareta. 2017. « Microdialysis as an Important Technique in Systems Pharmacology-a Historical and Methodological Review ». *The AAPS Journal* 19 (5): 1294-1303. <https://doi.org/10.1208/s12248-017-0108-2>.

Han, Sanggil, Shunsuke Yamamoto, Anastasios G. Polyravas, et George G. Malliaras. 2020. « Microfabricated Ion-Selective Transistors with Fast and Super-Nernstian Response ». *Advanced Materials* 32 (48): e2004790. <https://doi.org/10.1002/adma.202004790>.

Hanahan, D. 1985. « Heritable Formation of Pancreatic Beta-Cell Tumours in Transgenic Mice Expressing Recombinant Insulin/Simian Virus 40 Oncogenes ». *Nature* 315 (6015): 115-22. <https://doi.org/10.1038/315115a0>.

Hariri, Ali. 2011. « Identification, state estimation, and adaptive control of type i diabetic patients ». *Wayne State University Dissertations*, janvier. https://digitalcommons.wayne.edu/oa_dissertations/412.

Hastoy, Benoit, Anne Clark, Patrik Rorsman, et Jochen Lang. 2017. « Fusion Pore in Exocytosis: More than an Exit Gate? A β -Cell Perspective ». *Cell Calcium* 68: 45-61. <https://doi.org/10.1016/j.ceca.2017.10.005>.

Hauge-Evans, Astrid C., Aileen J. King, Danielle Carmignac, Carolyn C. Richardson, Iain C. A. F. Robinson, Malcolm J. Low, Michael R. Christie, Shanta J. Persaud, et Peter M. Jones. 2009. « Somatostatin Secreted by Islet Delta-Cells Fulfills Multiple Roles as a Paracrine Regulator of Islet Function ». *Diabetes* 58 (2): 403-11. <https://doi.org/10.2337/db08-0792>.

Haynes, Aveni, Max K. Bulsara, Carol Bower, Timothy W. Jones, et Elizabeth A. Davis. 2015. « Regular Peaks and Troughs in the Australian Incidence of Childhood Type 1 Diabetes Mellitus (2000–2011) ». *Diabetologia* 58 (11): 2513-16. <https://doi.org/10.1007/s00125-015-3709-2>.

He, Xiao, Binshuai Wang, Jingxin Meng, Shudong Zhang, et Shutao Wang. 2021. « How to Prevent Bubbles in Microfluidic Channels ». *Langmuir* 37 (6): 2187-94. <https://doi.org/10.1021/acs.langmuir.0c03514>.

Heinemann, Lutz. 2003. « Continuous Glucose Monitoring by Means of the Microdialysis Technique: Underlying Fundamental Aspects ». *Diabetes Technology & Therapeutics* 5 (4): 545-61. <https://doi.org/10.1089/152091503322250578>.

Heinemann, Lutz, et Douglas B. Muchmore. 2012. « Ultrafast-Acting Insulins: State of the Art ». *Journal of Diabetes Science and Technology* 6 (4): 728-42. <https://doi.org/10.1177/193229681200600402>.

Helman, Aharon, et Douglas A. Melton. 2021. « A Stem Cell Approach to Cure Type 1 Diabetes ». *Cold Spring Harbor Perspectives in Biology* 13 (1): a035741. <https://doi.org/10.1101/cshperspect.a035741>.

Henquin, J. C. 2000. « Triggering and Amplifying Pathways of Regulation of Insulin Secretion by Glucose ». *Diabetes* 49 (11): 1751-60. <https://doi.org/10.2337/diabetes.49.11.1751>.

Henquin, J. C., et H. P. Meissner. 1981. « Effects of Amino Acids on Membrane Potential and 86Rb^+ Fluxes in Pancreatic Beta-Cells ». *The American Journal of Physiology* 240 (3): E245-252. <https://doi.org/10.1152/ajpendo.1981.240.3.E245>.

Henquin, J. C. 1984. « Significance of Ionic Fluxes and Changes in Membrane Potential for Stimulus-Secretion Coupling in Pancreatic B-Cells ». *Experientia* 40 (10): 1043-52. <https://doi.org/10.1007/BF01971450>.

Henquin, Jean-Claude. 2019. « The Challenge of Correctly Reporting Hormones Content and Secretion in Isolated Human Islets ». *Molecular Metabolism* 30: 230-39. <https://doi.org/10.1016/j.molmet.2019.10.003>.

Henquin, J. C. 2021. « Paracrine and Autocrine Control of Insulin Secretion in Human Islets: Evidence and Pending Questions ». *American Journal of Physiology. Endocrinology and Metabolism* 320 (1): E78-86. <https://doi.org/10.1152/ajpendo.00485.2020>.

Henquin, Jean-Claude, Myriam Nenquin, Patrick Stiernet, et Bo Ahren. 2006. « In Vivo and in Vitro Glucose-Induced Biphasic Insulin Secretion in the Mouse: Pattern and Role of Cytoplasmic Ca²⁺ and Amplification Signals in Beta-Cells ». *Diabetes* 55 (2): 441-51. <https://doi.org/10.2337/diabetes.55.02.06.db05-1051>.

Heptulla, Rubina A., Luisa M. Rodriguez, Lisa Bomgaars, et Morey W. Haymond. 2005. « The Role of Amylin and Glucagon in the Dampening of Glycemic Excursions in Children with Type 1 Diabetes ». *Diabetes* 54 (4): 1100-1107. <https://doi.org/10.2337/diabetes.54.4.1100>.

Hermann, R., M. Knip, R. Veijola, O. Simell, A.-P. Laine, H. K. Akerblom, P.-H. Groop, et al. 2003. « Temporal Changes in the Frequencies of HLA Genotypes in Patients with Type 1 Diabetes-- Indication of an Increased Environmental Pressure? » *Diabetologia* 46 (3): 420-25. <https://doi.org/10.1007/s00125-003-1045-4>.

Hermans, M. P., W. Schmeer, et J. C. Henquin. 1987. « Modulation of the Effect of Acetylcholine on Insulin Release by the Membrane Potential of B Cells ». *Endocrinology* 120 (5): 1765-73. <https://doi.org/10.1210/endo-120-5-1765>.

Hervé, Jean-Claude, et Mickaël Derangeon. 2013. « Gap-Junction-Mediated Cell-to-Cell Communication ». *Cell and Tissue Research* 352 (1): 21-31. <https://doi.org/10.1007/s00441-012-1485-6>.

Hicks, Caitlin W., Shalini Selvarajah, Nestoras Mathioudakis, Ronald L. Sherman, Kathryn F. Hines, James H. Black, et Christopher J. Abularrage. 2016. « Burden of Infected Diabetic Foot Ulcers on Hospital Admissions and Costs ». *Annals of vascular surgery* 33 (mai): 149-58. <https://doi.org/10.1016/j.avsg.2015.11.025>.

Hoang, Danh-Tai, Hitomi Matsunari, Masaki Nagaya, Hiroshi Nagashima, J. Michael Millis, Piotr Witkowski, Vipul Periwal, Manami Hara, et Junghyo Jo. 2014. « A Conserved Rule for Pancreatic Islet Organization ». *PLOS ONE* 9 (10): e110384. <https://doi.org/10.1371/journal.pone.0110384>.

Hohmeier, Hans E., et Christopher B. Newgard. 2005. « Islets for All? » *Nature Biotechnology* 23 (10): 1231-32. <https://doi.org/10.1038/nbt1005-1231>.

Hökfelt, T., S. Efendić, C. Hellerström, O. Johansson, R. Luft, et A. Arimura. 1975. « Cellular Localization of Somatostatin in Endocrine-like Cells and Neurons of the Rat with Special References to the A1-Cells of the Pancreatic Islets and to the Hypothalamus ». *Acta Endocrinologica. Suppl* 200: 5-41.

Holst, J. J. 2006. « Glucagon-like Peptide-1: From Extract to Agent. The Claude Bernard Lecture, 2005 ». *Diabetologia* 49 (2): 253-60. <https://doi.org/10.1007/s00125-005-0107-1>.

Holzer, Peter, Florian Reichmann, et Aitak Farzi. 2012. « Neuropeptide Y, Peptide YY and Pancreatic Polypeptide in the Gut-Brain Axis ». *Neuropeptides* 46 (6): 261-74. <https://doi.org/10.1016/j.npep.2012.08.005>.

Honeyman, M. C., B. S. Coulson, N. L. Stone, S. A. Gellert, P. N. Goldwater, C. E. Steele, J. J. Couper, B. D. Tait, P. G. Colman, et L. C. Harrison. 2000. « Association between Rotavirus Infection and Pancreatic Islet Autoimmunity in Children at Risk of Developing Type 1 Diabetes ». *Diabetes* 49 (8): 1319-24. <https://doi.org/10.2337/diabetes.49.8.1319>.

Hopkins, D. F., et G. Williams. 1997. « Insulin Receptors Are Widely Distributed in Human Brain and Bind Human and Porcine Insulin with Equal Affinity ». *Diabetic Medicine: A Journal of the British Diabetic Association* 14 (12): 1044-50. [https://doi.org/10.1002/\(SICI\)1096-9136\(199712\)14:12<1044::AID-DIA508>3.0.CO;2-F](https://doi.org/10.1002/(SICI)1096-9136(199712)14:12<1044::AID-DIA508>3.0.CO;2-F).

Huang, L., H. Shen, M. A. Atkinson, et R. T. Kennedy. 1995. « Detection of Exocytosis at Individual Pancreatic Beta Cells by Amperometry at a Chemically Modified Microelectrode ». *Proceedings of the National Academy of Sciences of the United States of America* 92 (21): 9608-12. <https://doi.org/10.1073/pnas.92.21.9608>.

Hyöty, Heikki. 2002. « Enterovirus Infections and Type 1 Diabetes ». *Annals of Medicine* 34 (3): 138-47.

Hyppönen, E., E. Läärä, A. Reunanen, M. R. Jarvelin, et S. M. Virtanen. 2001. « Intake of Vitamin D and Risk of Type 1 Diabetes: A Birth-Cohort Study ». *Lancet (London, England)* 358 (9292): 1500-1503. [https://doi.org/10.1016/S0140-6736\(01\)06580-1](https://doi.org/10.1016/S0140-6736(01)06580-1).

« IDF Atlas 9th Edition and Other Resources ». s. d. Consulté le 29 juin 2021. <https://www.diabetesatlas.org/en/resources/>.

« Indications for islet or pancreatic transplantation: Statement of the TREPID working group on behalf of the Société francophone du diabète (SFD), Société française d'endocrinologie (SFE), Société francophone de transplantation (SFT) and Société française de néphrologie - dialyse - transplantation (SFNDT) - PubMed ». s. d. Consulté le 9 février 2022. <https://pubmed.ncbi.nlm.nih.gov/30223084/>.

Ishihara, H., H. Wang, L. R. Drewes, et C. B. Wollheim. 1999. « Overexpression of Monocarboxylate Transporter and Lactate Dehydrogenase Alters Insulin Secretory Responses to Pyruvate and Lactate in Beta Cells ». *The Journal of Clinical Investigation* 104 (11): 1621-29. <https://doi.org/10.1172/JCI7515>.

Islam, Md Shahidul. 2020. « Stimulus-Secretion Coupling in Beta-Cells: From Basic to Bedside ». *Advances in Experimental Medicine and Biology* 1131: 943-63. https://doi.org/10.1007/978-3-030-12457-1_37.

Jacobson, David A., Andrey Kuznetsov, James P. Lopez, Shera Kash, Carina E. Ammälä, et Louis H. Philipson. 2007. « Kv2.1 Ablation Alters Glucose-Induced Islet Electrical Activity, Enhancing Insulin Secretion ». *Cell Metabolism* 6 (3): 229-35. <https://doi.org/10.1016/j.cmet.2007.07.010>.

Jaffredo, Manon, Eléonore Bertin, Antoine Pirog, Emilie Puginier, Julien Gaitan, Sandra Oucherif, Fanny Lebreton, et al. 2021. « Dynamic Uni- and Multicellular Patterns Encode Biphasic Activity in Pancreatic Islets ». *Diabetes* 70 (4): 878-88. <https://doi.org/10.2337/db20-0214>.

Jansson, Leif, et Per-Ola Carlsson. 2019. « Pancreatic Blood Flow with Special Emphasis on Blood Perfusion of the Islets of Langerhans ». *Comprehensive Physiology* 9 (2): 799-837. <https://doi.org/10.1002/cphy.c160050>.

Jaques, Fabienne, Hélène Jousset, Alejandra Tomas, Anne-Lise Prost, Claes B. Wollheim, Jean-Claude Irminger, Nicolas Demaurex, et Philippe A. Halban. 2008. « Dual Effect of Cell-Cell Contact Disruption on Cytosolic Calcium and Insulin Secretion ». *Endocrinology* 149 (5): 2494-2505. <https://doi.org/10.1210/en.2007-0974>.

Jin, Byung-Ju, et A. S. Verkman. 2017. « Microfluidic Platform for Rapid Measurement of Transepithelial Water Transport ». *Lab on a Chip* 17 (5): 887-95. <https://doi.org/10.1039/c6lc01456a>.

Jin, Jonghwa, Jungeun Park, Kyunggon Kim, Yup Kang, Sang Gyu Park, Jae Hyeon Kim, Kyong Soo Park, Heesook Jun, et Youngsoo Kim. 2009. « Detection of Differential Proteomes of Human Beta-Cells during Islet-like Differentiation Using ITRAQ Labeling ». *Journal of Proteome Research* 8 (3): 1393-1403. <https://doi.org/10.1021/pr800765t>.

Jing, Xingjun, Dai-Qing Li, Charlotta S. Olofsson, Albert Salehi, Vikas V. Surve, José Caballero, Rosita Ivarsson, et al. 2005. « CaV2.3 Calcium Channels Control Second-Phase Insulin Release ». *The Journal of Clinical Investigation* 115 (1): 146-54. <https://doi.org/10.1172/JCI22518>.

Jurcovicova, J. 2014. « Glucose Transport in Brain - Effect of Inflammation ». *Endocrine Regulations* 48 (1): 35-48. https://doi.org/10.4149/endo_2014_01_35.

K, Rebrin, Steil Gm, van Antwerp Wp, et Mastrototaro Jj. 1999. « Subcutaneous Glucose Predicts Plasma Glucose Independent of Insulin: Implications for Continuous Monitoring ». *The American Journal of Physiology* 277 (3). <https://doi.org/10.1152/ajpendo.1999.277.3.E561>.

Kadish, A. H. 1963. « Automation Control of Blood Sugar a Servomechanism for Glucose Monitoring and Control ». *Transactions - American Society for Artificial Internal Organs* 9: 363-67.

Kahn, A. 2000. « Converting Hepatocytes to Beta-Cells--a New Approach for Diabetes? » *Nature Medicine* 6 (5): 505-6. <https://doi.org/10.1038/74980>.

Kamohara, S., R. Burcelin, J. L. Halaas, J. M. Friedman, et M. J. Charron. 1997. « Acute Stimulation of Glucose Metabolism in Mice by Leptin Treatment ». *Nature* 389 (6649): 374-77. <https://doi.org/10.1038/38717>.

Kaneto, Hideaki, Yoshihisa Nakatani, Takeshi Miyatsuka, Taka-aki Matsuoka, Munehide Matsuhisa, Masatsugu Hori, et Yoshimitsu Yamasaki. 2005. « PDX-1/VP16 Fusion Protein, Together with NeuroD or Ngn3, Markedly Induces Insulin Gene Transcription and Ameliorates Glucose Tolerance ». *Diabetes* 54 (4): 1009-22. <https://doi.org/10.2337/diabetes.54.4.1009>.

Kang, Chen, Litao Xie, Susheel K. Gunasekar, Anil Mishra, Yanhui Zhang, Saachi Pai, Yiwen Gao, et al. 2018. « SWELL1 Is a Glucose Sensor Regulating β -Cell Excitability and Systemic Glycaemia ». *Nature Communications* 9 (1): 367. <https://doi.org/10.1038/s41467-017-02664-0>.

Kawahara, T., T. Kin, S. Kashkoush, B. Gala-Lopez, D. L. Bigam, N. M. Kneteman, A. Koh, P. A. Senior, et A. M. J. Shapiro. 2011. « Portal Vein Thrombosis Is a Potentially Preventable Complication in Clinical Islet Transplantation ». *American Journal of Transplantation* 11 (12): 2700-2707. <https://doi.org/10.1111/j.1600-6143.2011.03717.x>.

Keenan, D. Barry, John J. Mastrototaro, Gayane Voskanyan, et Garry M. Steil. 2009. « Delays in Minimally Invasive Continuous Glucose Monitoring Devices: A Review of Current Technology ». *Journal of Diabetes Science and Technology* 3 (5): 1207-14. <https://doi.org/10.1177/193229680900300528>.

Keenan, Daniel, Rita Basu, Yan Liu, Ananda Basu, Gerlies TREIBER (Bock), et Johannes Veldhuis. 2012. « Logistic model of glucose-regulated C-peptide secretion: Hysteresis pathway disruption in impaired fasting glycemia ». *American Journal of Physiology. Endocrinology and metabolism* 303 (juin): E397-409. <https://doi.org/10.1152/ajpendo.00494.2011>.

Khan, F., A. Pharo, J. K. Lindstad, T. E. Mollnes, T. I. Tønnessen, et S. E. Pischke. 2015. « Effect of Perfusion Fluids on Recovery of Inflammatory Mediators in Microdialysis ». *Scandinavian Journal of Immunology* 82 (5): 467-75. <https://doi.org/10.1111/sji.12332>.

Kho, Chun Min, Siti Kartini Enche Ab Rahim, Zainal Arifin Ahmad, et Norazharuddin Shah Abdullah. 2017. « A Review on Microdialysis Calibration Methods: The Theory and Current Related Efforts ». *Molecular Neurobiology* 54 (5): 3506-27. <https://doi.org/10.1007/s12035-016-9929-8>.

Khodagholy, Dion, Vincenzo Curto, Kevin Fraser, Moshe Gurfinkel, Robert Byrne, Dermot Diamond, George Malliaras, Fernando Benito-Lopez, et Roisin Owens. 2012. « Organic electrochemical transistor incorporating an ionogel as solid state electrolyte for lactate sensing ». *Journal of Materials Chemistry* 22 (janvier): 4440-43. <https://doi.org/10.1039/c2jm15716k>.

Kieffer, T. J., et J. F. Habener. 2000. « The Adipoinular Axis: Effects of Leptin on Pancreatic Beta-Cells ». *American Journal of Physiology. Endocrinology and Metabolism* 278 (1): E1-14. <https://doi.org/10.1152/ajpendo.2000.278.1.E1>.

King, Kathryn M., et Greg Rubin. 2003. « A History of Diabetes: From Antiquity to Discovering Insulin ». *British Journal of Nursing* 12 (18): 1091-95. <https://doi.org/10.12968/bjon.2003.12.18.11775>.

Kit Lee, Maxwell Kim. 2013. « Crosstalk the Microdialysis in Scientific Research: From Principle to Its Applications ». *Pharmaceutica Analytica Acta* 05 (01). <https://doi.org/10.4172/2153-2435.1000276>.

Klauk, H. 2010. « Organic thin-film transistors. » *Chemical Society Reviews*. <https://doi.org/10.1039/b909902f>.

Kleiner, Israel S. 1919. « The action of intravenous injections of pancreas emulsions in experimental diabetes ». *Journal of Biological Chemistry* 40 (1): 153-70. [https://doi.org/10.1016/S0021-9258\(18\)87274-X](https://doi.org/10.1016/S0021-9258(18)87274-X).

Knaack, D., D. M. Fiore, M. Surana, M. Leiser, M. Laurance, D. Fusco-DeMane, O. D. Hegre, N. Fleischer, et S. Efrat. 1994. « Clonal Insulinoma Cell Line That Stably Maintains Correct Glucose Responsiveness ». *Diabetes* 43 (12): 1413-17. <https://doi.org/10.2337/diab.43.12.1413>.

Koh, Duk-Su, Jung-Hwa Cho, et Liangyi Chen. 2012. « Paracrine Interactions within Islets of Langerhans ». *Journal of Molecular Neuroscience* 48 (2): 429-40. <https://doi.org/10.1007/s12031-012-9752-2>.

Kola, Ismail, et John Landis. 2004. « Can the Pharmaceutical Industry Reduce Attrition Rates? » *Nature Reviews Drug Discovery* 3 (8): 711-16. <https://doi.org/10.1038/nrd1470>.

Konwarh, Rocktotpal, Prerak Gupta, et Biman B. Mandal. 2016. « Silk-Microfluidics for Advanced Biotechnological Applications: A Progressive Review ». *Biotechnology Advances* 34 (5): 845-58. <https://doi.org/10.1016/j.biotechadv.2016.05.001>.

Korsgren, O., L. Jansson, D. Eizirik, et A. Andersson. 1991. « Functional and Morphological Differentiation of Fetal Porcine Islet-like Cell Clusters after Transplantation into Nude Mice ». *Diabetologia* 34 (6): 379-86. <https://doi.org/10.1007/BF00403174>.

Koster, Joseph C., Maria S. Remedi, Crystal Dao, et Colin G. Nichols. 2005. « ATP and Sulfonylurea Sensitivity of Mutant ATP-Sensitive K⁺ Channels in Neonatal Diabetes: Implications for Pharmacogenomic Therapy ». *Diabetes* 54 (9): 2645-54. <https://doi.org/10.2337/diabetes.54.9.2645>.

Koutsouras, Dimitrios A. 2017. « Simultaneous Monitoring of Single Cell and of Micro-Organ Activity by PEDOT_PSS Covered Multi-Electrode Arrays ». *Materials Science*, 6.

Kovacs, G.T.A., N.I. Maluf, et K.E. Petersen. 1998. « Bulk micromachining of silicon ». *Proceedings of the IEEE* 86 (8): 1536-51. <https://doi.org/10.1109/5.704259>.

Kovács, Levente, Balázs Kulcsár, Balázs Benyó, et Zoltán Benyó. 2009. « Induced L2-Norm Minimization of Glucose-Insulin System for Type I Diabetic Patients ». *IFAC Proceedings*

Volumes, 7th IFAC Symposium on Modelling and Control in Biomedical Systems, 42 (12): 55-60. <https://doi.org/10.3182/20090812-3-DK-2006.0068>.

Kovatchev, Boris. 2019. « A Century of Diabetes Technology: Signals, Models, and Artificial Pancreas Control ». *Trends in Endocrinology and Metabolism: TEM* 30 (7): 432-44. <https://doi.org/10.1016/j.tem.2019.04.008>.

Kravarusic, Jelena, et Grazia Aleppo. 2020. « Diabetes Technology Use in Adults with Type 1 and Type 2 Diabetes ». *Endocrinology and Metabolism Clinics of North America* 49 (1): 37-55. <https://doi.org/10.1016/j.ecl.2019.10.006>.

Kravets, Vira, et Richard K. P. Benninger. 2020. « From the Transcriptome to Electrophysiology: Searching for the Underlying Cause of Diabetes ». *Cell Metabolism* 31 (5): 888-89. <https://doi.org/10.1016/j.cmet.2020.04.012>.

Kroon, Evert, Laura A. Martinson, Kuniko Kadoya, Anne G. Bang, Olivia G. Kelly, Susan Eliazer, Holly Young, et al. 2008. « Pancreatic Endoderm Derived from Human Embryonic Stem Cells Generates Glucose-Responsive Insulin-Secreting Cells in Vivo ». *Nature Biotechnology* 26 (4): 443-52. <https://doi.org/10.1038/nbt1393>.

Kropff, Jort, et J. Hans DeVries. 2016. « Continuous Glucose Monitoring, Future Products, and Update on Worldwide Artificial Pancreas Projects ». *Diabetes Technology & Therapeutics* 18 (S2): S2-53-S2-63. <https://doi.org/10.1089/dia.2015.0345>.

Kuhadiya, Nitesh D., Husam Ghanim, Aditya Mehta, Manisha Garg, Salman Khan, Jeanne Hejna, Barrett Torre, et al. 2016. « Dapagliflozin as Additional Treatment to Liraglutide and Insulin in Patients With Type 1 Diabetes ». *The Journal of Clinical Endocrinology and Metabolism* 101 (9): 3506-15. <https://doi.org/10.1210/jc.2016-1451>.

Kühl, C., P. J. Hornnes, S. L. Jensen, et K. B. Lauritsen. 1980. « Gastric Inhibitory Polypeptide and Insulin: Response to Intraduodenal and Intravenous Glucose Infusions in Fetal and Neonatal Pigs ». *Endocrinology* 107 (5): 1446-50. <https://doi.org/10.1210/endo-107-5-1446>.

Kulcu, E., J. A. Tamada, G. Reach, R. O. Potts, et M. J. Lesho. 2003. « Physiological Differences Between Interstitial Glucose and Blood Glucose Measured in Human Subjects ». *Diabetes Care* 26 (8): 2405-9. <https://doi.org/10.2337/diacare.26.8.2405>.

Kulkarni, Rohit N., Ernesto-Bernal Mizrachi, Adolfo Garcia Ocana, et Andrew F. Stewart. 2012. « Human β -Cell Proliferation and Intracellular Signaling: Driving in the Dark without a Road Map ». *Diabetes* 61 (9): 2205-13. <https://doi.org/10.2337/db12-0018>.

Kulkarni, Rohit N., et Andrew F. Stewart. 2014. « Summary of the Keystone Islet Workshop (April 2014): The Increasing Demand for Human Islet Availability in Diabetes Research ». *Diabetes* 63 (12): 3979-81. <https://doi.org/10.2337/db14-1303>.

Kuo, Taiyi, Allison McQueen, Tzu-Chieh Chen, et Jen-Chywan Wang. 2015. « Regulation of Glucose Homeostasis by Glucocorticoids ». *Advances in Experimental Medicine and Biology* 872: 99-126. https://doi.org/10.1007/978-1-4939-2895-8_5.

L, Schaupp, Ellmerer M, Brunner Ga, Wutte A, Sendlhofer G, Trajanoski Z, Skrabal F, Pieber Tr, et Wach P. 1999. « Direct Access to Interstitial Fluid in Adipose Tissue in Humans by Use of Open-Flow Microperfusion ». *The American Journal of Physiology* 276 (2). <https://doi.org/10.1152/ajpendo.1999.276.2.E401>.

Lablanche, Sandrine, Sophie Borot, Anne Wojtuszczyz, Francois Bayle, Rachel Tétaz, Lionel Badet, Charles Thivolet, et al. 2015. « Five-Year Metabolic, Functional, and Safety Results of Patients With Type 1 Diabetes Transplanted With Allogenic Islets Within the Swiss-French GRAGIL Network ». *Diabetes Care* 38 (9): 1714-22. <https://doi.org/10.2337/dc15-0094>.

Lablanche, Sandrine, Sandra David-Tchouda, Jennifer Margier, Edith Schir, Anne Wojtuszczyz, Sophie Borot, Laurence Kessler, et al. 2017. « Randomised, prospective, medico-economic nationwide French study of islet transplantation in patients with severely unstable type 1 diabetes: the STABILOT study protocol ». *BMJ Open* 7 (2): e013434. <https://doi.org/10.1136/bmjopen-2016-013434>.

Lammert, E., O. Cleaver, et D. Melton. 2001. « Induction of Pancreatic Differentiation by Signals from Blood Vessels ». *Science* 294 (5542): 564-67. <https://doi.org/10.1126/science.1064344>.

Lan, M. S., C. Wasserfall, N. K. Maclaren, et A. L. Notkins. 1996. « IA-2, a Transmembrane Protein of the Protein Tyrosine Phosphatase Family, Is a Major Autoantigen in Insulin-Dependent Diabetes Mellitus ». *Proceedings of the National Academy of Sciences of the United States of America* 93 (13): 6367-70. <https://doi.org/10.1073/pnas.93.13.6367>.

Lang Lehrskov, Louise, Mark Preben Lyngbaek, Line Soederlund, Grit Elster Legaard, Jan Adam Ehses, Sarah Elizabeth Heywood, Nicolai Jacob Wewer Albrechtsen, et al. 2018. « Interleukin-6 Delays Gastric Emptying in Humans with Direct Effects on Glycemic Control ». *Cell Metabolism* 27 (6): 1201-1211.e3. <https://doi.org/10.1016/j.cmet.2018.04.008>.

Lange, E. C. de, A. G. de Boer, et D. D. Breimer. 2000. « Methodological Issues in Microdialysis Sampling for Pharmacokinetic Studies ». *Advanced Drug Delivery Reviews* 45 (2-3): 125-48. [https://doi.org/10.1016/s0169-409x\(00\)00107-1](https://doi.org/10.1016/s0169-409x(00)00107-1).

Langerhans, Paul. 1869. *Beiträge zur mikroskopischen Anatomie der Bauchspeicheldrüse : Inaugural-Dissertation, zur Erlangung der Doctorwürde in der Medicine und Chirurgie vorgelegt der Medicinischen Facultät der Friedrich-Wilhelms-Universität zu Berlin und öffentlich zu vertheidigen am 18. Februar 1869 /*. Berlin : Buchdruckerei von Gustav Lange,.

Latres, Esther, Daniel A. Finan, Julia L. Greenstein, Aaron Kowalski, et Timothy J. Kieffer. 2019. « Navigating Two Roads to Glucose Normalization in Diabetes: Automated Insulin Delivery Devices and Cell Therapy ». *Cell Metabolism* 29 (3): 545-63. <https://doi.org/10.1016/j.cmet.2019.02.007>.

Lau, E., A. Salem, J. C. N. Chan, W. Y. So, A. Kong, M. Lamotte, et A. Luk. 2019. « Insulin Glargine Compared to Neutral Protamine Hagedorn (NPH) Insulin in Patients with Type-2 Diabetes Uncontrolled with Oral Anti-Diabetic Agents Alone in Hong Kong: A Cost-Effectiveness Analysis ». *Cost Effectiveness and Resource Allocation*: 13. <https://doi.org/10.1186/s12962-019-0180-9>.

Lauri, Chiara, Antonio Leone, Marco Cavallini, Alberto Signore, Laura Giurato, et Luigi Uccioli. 2020. « Diabetic Foot Infections: The Diagnostic Challenges ». *Journal of Clinical Medicine* 9 (6): 1779. <https://doi.org/10.3390/jcm9061779>.

Lebreton, Fanny, Antoine Pirog, Isma Belouah, Domenico Bosco, Thierry Berney, Paolo Meda, Yannick Bornat, et al. 2015. « Slow Potentials Encode Intercellular Coupling and Insulin Demand in Pancreatic Beta Cells ». *Diabetologia* 58 (6): 1291-99. <https://doi.org/10.1007/s00125-015-3558-z>.

Leech, Colin A., Igor Dzhura, Oleg G. Chepurny, Guoxin Kang, Frank Schwede, Hans-G. Genieser, et George G. Holz. 2011. « Molecular Physiology of Glucagon-like Peptide-1 Insulin Secretagogue Action in Pancreatic β Cells ». *Progress in Biophysics and Molecular Biology* 107 (2): 236-47. <https://doi.org/10.1016/j.pbiomolbio.2011.07.005>.

Leibiger, B., T. Moede, T. Schwarz, G. R. Brown, M. Köhler, I. B. Leibiger, et P. O. Berggren. 1998. « Short-Term Regulation of Insulin Gene Transcription by Glucose ». *Proceedings of the National Academy of Sciences of the United States of America* 95 (16): 9307-12. <https://doi.org/10.1073/pnas.95.16.9307>.

Leiter, Lawrence A., Antonio Ceriello, Jaime A. Davidson, Markolf Hanefeld, Louis Monnier, David R. Owens, Naoko Tajima, Jaakko Tuomilehto, et International Prandial Glucose Regulation Study Group. 2005. « Postprandial Glucose Regulation: New Data and New Implications ». *Clinical Therapeutics* 27 Suppl B: S42-56. <https://doi.org/10.1016/j.clinthera.2005.11.020>.

Lenzen, Sigurd. 2014. « A Fresh View of Glycolysis and Glucokinase Regulation: History and Current Status ». *The Journal of Biological Chemistry* 289 (18): 12189-94. <https://doi.org/10.1074/jbc.R114.557314>.

Levin, Barry E., Christophe Magnan, Ambrose Dunn-Meynell, et Christelle Le Foll. 2011. « Metabolic Sensing and the Brain: Who, What, Where, and How? » *Endocrinology* 152 (7): 2552-57. <https://doi.org/10.1210/en.2011-0194>.

Li, Daliang, Shihwei Chen, Elisa A. Bellomo, Andrei I. Tarasov, Callan Kaut, Guy A. Rutter, et Wen-hong Li. 2011. « Imaging Dynamic Insulin Release Using a Fluorescent Zinc Indicator for Monitoring Induced Exocytotic Release (ZIMIR) ». *Proceedings of the National Academy of Sciences of the United States of America* 108 (52): 21063-68. <https://doi.org/10.1073/pnas.1109773109>.

Lilla, Valérie, Gene Webb, Katharina Rickenbach, Andres Maturana, Donald F. Steiner, Philippe A. Halban, et Jean-Claude Irminger. 2003. « Differential Gene Expression in Well-Regulated and Dysregulated Pancreatic Beta-Cell (MIN6) Sublines ». *Endocrinology* 144 (4): 1368-79. <https://doi.org/10.1210/en.2002-220916>.

Lin, Lin, et Chen-Kuei Chung. 2021. « PDMS Microfabrication and Design for Microfluidics and Sustainable Energy Application: Review ». *Micromachines* 12 (11): 1350. <https://doi.org/10.3390/mi12111350>.

Lindqvist, A., L. Shcherbina, R. B. Prasad, M. G. Miskelly, M. Abels, J. A. Martínez-Lopéz, R. G. Fred, et al. 2020. « Ghrelin Suppresses Insulin Secretion in Human Islets and Type 2 Diabetes Patients Have Diminished Islet Ghrelin Cell Number and Lower Plasma Ghrelin Levels ». *Molecular and Cellular Endocrinology* 511 (juillet): 110835. <https://doi.org/10.1016/j.mce.2020.110835>.

Linhares, M., et P. Kissinger. 1992. « Capillary ultrafiltration: in vivo sampling probes for small molecules. » *Analytical chemistry*. <https://doi.org/10.1021/AC00046A029>.

Liu, Min-tsai, Susumu Seino, et Annette L. Kirchgessner. 1999. « Identification and Characterization of Glucoreponsive Neurons in the Enteric Nervous System ». *Journal of Neuroscience* 19 (23): 10305-17. <https://doi.org/10.1523/JNEUROSCI.19-23-10305.1999>.

Lj, Petersen. 1999. « Interstitial Lactate Levels in Human Skin at Rest and during an Oral Glucose Load: A Microdialysis Study ». *Clinical Physiology* 19 (3). <https://doi.org/10.1046/j.1365-2281.1999.00174.x>.

Lochovsky, Conrad, Sanjesh Yasotharan, et Axel Günther. 2012. « Bubbles No More: In-Plane Trapping and Removal of Bubbles in Microfluidic Devices ». *Lab on a Chip* 12 (3): 595-601. <https://doi.org/10.1039/c1lc20817a>.

Lönnroth, P., et U. Smith. 1990. « Microdialysis--a Novel Technique for Clinical Investigations ». *Journal of Internal Medicine* 227 (5): 295-300. <https://doi.org/10.1111/j.1365-2796.1990.tb00163.x>.

Lukowiak, B., B. Vandewalle, R. Riachy, J. Kerr-Conte, V. Gmyr, S. Belaich, J. Lefebvre, et F. Pattou. 2001. « Identification and Purification of Functional Human Beta-Cells by a New Specific Zinc-Fluorescent Probe ». *The Journal of Histochemistry and Cytochemistry* 49 (4): 519-28. <https://doi.org/10.1177/002215540104900412>.

Lundquist, I., et L. E. Ericson. 1978. « β -Adrenergic Insulin Release and Adrenergic Innervation of Mouse Pancreatic Islets ». *Cell and Tissue Research* 193 (1): 73-85. <https://doi.org/10.1007/BF00221602>.

MacDonald, Patrick E., Yang Zhang De Marinis, Reshma Ramracheya, Albert Salehi, Xiaosong Ma, Paul R. V. Johnson, Roger Cox, Lena Eliasson, et Patrik Rorsman. 2007. « A K_{ATP} Channel-Dependent Pathway within Alpha Cells Regulates Glucagon Release from Both Rodent and

Human Islets of Langerhans ». *PLoS Biology* 5 (6): e143. <https://doi.org/10.1371/journal.pbio.0050143>.

MacLean, D. A., L. I. Sinoway, et U. Leuenberger. 1998. « Systemic Hypoxia Elevates Skeletal Muscle Interstitial Adenosine Levels in Humans ». *Circulation* 98 (19): 1990-92. <https://doi.org/10.1161/01.cir.98.19.1990>.

Magnan, Christophe, et A.A. Ktorza. 2005. « Production et sécrétion de l'insuline par la cellule β pancréatique ». *EMC - Endocrinologie* 10: 241-64. <https://doi.org/10.1016/j.emcend.2005.07.001>.

Maschmeyer, Ilka, et Sofia Kakava. 2020. « Organ-on-a-Chip ». *Advances in Biochemical Engineering/Biotechnology*. https://doi.org/10.1007/10_2020_135.

Mason, M. J., A. K. Simpson, M. P. Mahaut-Smith, et H. P. C. Robinson. 2005. « The Interpretation of Current-Clamp Recordings in the Cell-Attached Patch-Clamp Configuration ». *Biophysical Journal* 88 (1): 739-50. <https://doi.org/10.1529/biophysj.104.049866>.

Mata, A., A. Fleischman, et Shuvo Roy. 2005. « Characterization of Polydimethylsiloxane (PDMS) Properties for Biomedical Micro/Nanosystems ». <https://www.semanticscholar.org/paper/Surface-micromachining-of-polydimethylsiloxane-for-Hill-Qian/183b0425dc6d82e04f13506f71da12c03ffe0811>.

Mathew, Thomas K., et Prasanna Tadi. 2021. « Blood Glucose Monitoring ». In *StatPearls*. Treasure Island (FL): StatPearls Publishing. <http://www.ncbi.nlm.nih.gov/books/NBK555976/>.
Mathieu, Chantal, et Klaus Badenhoop. 2005. « Vitamin D and Type 1 Diabetes Mellitus: State of the Art ». *Trends in Endocrinology and Metabolism: TEM* 16 (6): 261-66. <https://doi.org/10.1016/j.tem.2005.06.004>.

Matschinsky, Franz M., et David F. Wilson. 2019. « The Central Role of Glucokinase in Glucose Homeostasis: A Perspective 50 Years After Demonstrating the Presence of the Enzyme in Islets of Langerhans ». *Frontiers in Physiology* 10: 148. <https://doi.org/10.3389/fphys.2019.00148>.

Matsumoto, Shinichi. 2010. « Islet Cell Transplantation for Type 1 Diabetes ». *Journal of Diabetes* 2 (1): 16-22. <https://doi.org/10.1111/j.1753-0407.2009.00048.x>.

Maughan, R. J., J. Fallah, et E. F. Coyle. 2010. « The Effects of Fasting on Metabolism and Performance ». *British Journal of Sports Medicine* 44 (7): 490-94. <https://doi.org/10.1136/bjism.2010.072181>.

McCluskey, Jane T., Muhajir Hamid, Hong Guo-Parke, Neville H. McClenaghan, Ramon Gomis, et Peter R. Flatt. 2011. « Development and Functional Characterization of Insulin-Releasing Human Pancreatic Beta Cell Lines Produced by Electrofusion ». *The Journal of Biological Chemistry* 286 (25): 21982-92. <https://doi.org/10.1074/jbc.M111.226795>.

McCulloch, Laura J., Martijn van de Bunt, Matthias Braun, Keith N. Frayn, Anne Clark, et Anna L. Gloyn. 2011. « GLUT2 (SLC2A2) Is Not the Principal Glucose Transporter in Human

Pancreatic Beta Cells: Implications for Understanding Genetic Association Signals at This Locus ». *Molecular Genetics and Metabolism* 104 (4): 648-53. <https://doi.org/10.1016/j.ymgme.2011.08.026>.

Meda, P., M. Amherdt, A. Perrelet, et L. Orci. 1981. « Metabolic Coupling between Cultured Pancreatic B-Cells ». *Experimental Cell Research* 133 (2): 421-30. [https://doi.org/10.1016/0014-4827\(81\)90335-9](https://doi.org/10.1016/0014-4827(81)90335-9).

Meier, Juris J., et Michael A. Nauck. 2005. « Glucagon-like Peptide 1 (GLP-1) in Biology and Pathology ». *Diabetes/Metabolism Research and Reviews* 21 (2): 91-117. <https://doi.org/10.1002/dmrr.538>.

Mergenthaler, Philipp, Ute Lindauer, Gerald A. Dienel, et Andreas Meisel. 2013. « Sugar for the brain: the role of glucose in physiological and pathological brain function ». *Trends in neurosciences* 36 (10): 587-97. <https://doi.org/10.1016/j.tins.2013.07.001>.

Mering, J. v., et O. Minkowski. 1890. « Diabetes mellitus nach Pankreasextirpation ». *Archiv für experimentelle Pathologie und Pharmakologie* 26 (5): 371-87. <https://doi.org/10.1007/BF01831214>.

Metwaly, Ahmed M., Mohammed M. Ghoneim, Ibrahim H. Eissa, Islam A. Elsehemy, Ahmad E. Mostafa, Mostafa M. Hegazy, Wael M. Afifi, et Deqiang Dou. 2021. « Traditional Ancient Egyptian Medicine: A Review ». *Saudi Journal of Biological Sciences* 28 (10): 5823-32. <https://doi.org/10.1016/j.sjbs.2021.06.044>.

Meulen, Talitha van der, Alex M. Mawla, Michael R. DiGrucchio, Michael W. Adams, Vera Nies, Sophie Dölleman, Siming Liu, et al. 2017. « Virgin Beta Cells Persist throughout Life at a Neogenic Niche within Pancreatic Islets ». *Cell Metabolism* 25 (4): 911-926.e6. <https://doi.org/10.1016/j.cmet.2017.03.017>.

Min, Kho Chun, Zainal Arifin Ahmad, Siti Kartini Enche Ab Rahim, et Norazharuddin Shah Abdullah. 2016. « Mass Transport Analysis in Linear Microdialysis Probes Utilizing Structural Characterization Technique ». *Procedia Chemistry* 19. <https://cyberleninka.org/article/n/959151>.

Miranda, Caroline, Manisha Begum, Elisa Vergari, et Linford J. B. Briant. 2021. « Gap Junction Coupling and Islet Delta-Cell Function in Health and Disease ». *Peptides*, 170704. <https://doi.org/10.1016/j.peptides.2021.170704>.

Mithieux, Gilles, et Amandine Gautier-Stein. 2014. « Intestinal Glucose Metabolism Revisited ». *Diabetes Research and Clinical Practice* 105 (3): 295-301. <https://doi.org/10.1016/j.diabres.2014.04.008>.

Miyazaki, J., K. Araki, E. Yamato, H. Ikegami, T. Asano, Y. Shibasaki, Y. Oka, et K. Yamamura. 1990. « Establishment of a Pancreatic Beta Cell Line That Retains Glucose-Inducible Insulin Secretion: Special Reference to Expression of Glucose Transporter Isoforms ». *Endocrinology* 127 (1): 126-32. <https://doi.org/10.1210/endo-127-1-126>.

- Molina, Judith, Rayner Rodriguez-Diaz, Alberto Fachado, M. Caroline Jacques-Silva, Per-Olof Berggren, et Alejandro Caicedo. 2014. « Control of Insulin Secretion by Cholinergic Signaling in the Human Pancreatic Islet ». *Diabetes* 63 (8): 2714-26. <https://doi.org/10.2337/db13-1371>.
- Monnier, L., et C. Colette. 2019. « Définitions et classifications des états diabétiques ». In *Diabetologie*, 37-49. Elsevier. <https://doi.org/10.1016/B978-2-294-75889-8.00003-8>.
- Monnier, Louis, Claude Colette, Gareth J. Dunseath, et David R. Owens. 2007. « The Loss of Postprandial Glycemic Control Precedes Stepwise Deterioration of Fasting With Worsening Diabetes ». *Diabetes Care* 30 (2): 263-69. <https://doi.org/10.2337/dc06-1612>.
- Monson, J P, G Koios, G C Toms, P G Kopelman, B J Boucher, S J W Evans, et W L Alexander. 1986. « Relationship between Retinopathy and Glycaemic Control in Insulin-Dependent and Non-Insulin-Dependent Diabetes ». *Journal of the Royal Society of Medicine* 79 (5): 274-76. <https://doi.org/10.1177/014107688607900506>.
- Moullé, V.-S., A. Picard, C. Le Foll, B.-E. Levin, et C. Magnan. 2014. « Lipid Sensing in the Brain and Regulation of Energy Balance ». *Diabetes & Metabolism* 40 (1): 29-33. <https://doi.org/10.1016/j.diabet.2013.10.001>.
- Müller, Markus. 2002. « Science, Medicine, and the Future: Microdialysis ». *BMJ* 324 (7337): 588-91. <https://doi.org/10.1136/bmj.324.7337.588>.
- Murakami, T., T. Miyake, M. Tsubouchi, Y. Tsubouchi, A. Ohtsuka, et T. Fujita. 1997. « Blood Flow Patterns in the Rat Pancreas: A Simulative Demonstration by Injection Replication and Scanning Electron Microscopy ». *Microscopy Research and Technique* 37 (5-6): 497-508. [https://doi.org/10.1002/\(SICI\)1097-0029\(19970601\)37:5/6<497::AID-JEMT12>3.0.CO;2-L](https://doi.org/10.1002/(SICI)1097-0029(19970601)37:5/6<497::AID-JEMT12>3.0.CO;2-L).
- Murtaugh, L. Charles, et Douglas A. Melton. 2003. « Genes, Signals, and Lineages in Pancreas Development ». *Annual Review of Cell and Developmental Biology* 19: 71-89. <https://doi.org/10.1146/annurev.cellbio.19.111301.144752>.
- Muthyala, Sudhakar, Susan Safley, Kereen Gordan, Graham Barber, Collin Weber, et Athanassios Sambanis. 2017. « The Effect of Hypoxia on Free and Encapsulated Adult Porcine Islets-an in Vitro Study ». *Xenotransplantation* 24 (1). <https://doi.org/10.1111/xen.12275>.
- Nair, Gopika G., Emmanuel S. Tzanakakis, et Matthias Hebrok. 2020. « Emerging Routes to the Generation of Functional β -Cells for Diabetes Mellitus Cell Therapy ». *Nature Reviews. Endocrinology* 16 (9): 506-18. <https://doi.org/10.1038/s41574-020-0375-3>.
- Narushima, Michiki, Naoya Kobayashi, Teru Okitsu, Yoshihito Tanaka, Shun-Ai Li, Yong Chen, Atsushi Miki, et al. 2005. « A Human Beta-Cell Line for Transplantation Therapy to Control Type 1 Diabetes ». *Nature Biotechnology* 23 (10): 1274-82. <https://doi.org/10.1038/nbt1145>.
- Nauck, M. A., E. Homberger, E. G. Siegel, R. C. Allen, R. P. Eaton, R. Ebert, et W. Creutzfeldt. 1986. « Incretin Effects of Increasing Glucose Loads in Man Calculated from Venous Insulin

and C-Peptide Responses ». *The Journal of Clinical Endocrinology and Metabolism* 63 (2): 492-98. <https://doi.org/10.1210/jcem-63-2-492>.

Navale, Archana M., et Archana N. Paranjape. 2016. « Glucose Transporters: Physiological and Pathological Roles ». *Biophysical Reviews* 8 (1): 5-9. <https://doi.org/10.1007/s12551-015-0186-2>.

Neher, E., et B. Sakmann. 1976. « Single-Channel Currents Recorded from Membrane of Denervated Frog Muscle Fibres ». *Nature* 260 (5554): 799-802. <https://doi.org/10.1038/260799a0>.

Nerup, J., P. Platz, O. O. Andersen, M. Christy, J. Lyngsoe, J. E. Poulsen, L. P. Ryder, L. S. Nielsen, M. Thomsen, et A. Svejgaard. 1974. « HL-A Antigens and Diabetes Mellitus ». *Lancet* 2 (7885): 864-66. [https://doi.org/10.1016/s0140-6736\(74\)91201-x](https://doi.org/10.1016/s0140-6736(74)91201-x).

Ng, Natasha Hui Jin, Wei Xuan Tan, Ye Xin Koh, et Adrian Teo. 2019. « Human Islet Isolation and Distribution Efforts for Clinical and Basic Research ». *OBM Transplantation* 3 : 1-1. <https://doi.org/10.21926/obm.transplant.1902068>.

Niiijima, Akira, Kunio Torii, et Hisayuki Uneyama. 2005. « Role Played by Vagal Chemical Sensors in the Hepato-portal Region and Duodeno-intestinal Canal: An Electrophysiological Study ». *Chemical Senses* 30 (suppl_1): i178-79. <https://doi.org/10.1093/chemse/bjh172>.

Nikolova, Ganka, Boris Strilic, et Eckhard Lammert. 2007. « The Vascular Niche and Its Basement Membrane ». *Trends in Cell Biology* 17 (1): 19-25. <https://doi.org/10.1016/j.tcb.2006.11.005>.

Niwa, T., Y. Matsukawa, T. Senda, Y. Nimura, H. Hidaka, et I. Niki. 1998. « Acetylcholine Activates Intracellular Movement of Insulin Granules in Pancreatic Beta-Cells via Inositol Trisphosphate-Dependent [Correction of Triphosphate-Dependent] Mobilization of Intracellular Ca^{2+} ». *Diabetes* 47 (11): 1699-1706. <https://doi.org/10.2337/diabetes.47.11.1699>.

Noguchi, Glyn M., et Mark O. Huising. 2019. « Integrating the Inputs That Shape Pancreatic Islet Hormone Release ». *Nature Metabolism* 1 (12): 1189-1201. <https://doi.org/10.1038/s42255-019-0148-2>.

Nolan, Christopher J., et Marc Prentki. 2008. « The Islet Beta-Cell: Fuel Responsive and Vulnerable ». *Trends in Endocrinology and Metabolism*:19 (8): 285-91. <https://doi.org/10.1016/j.tem.2008.07.006>.

Novodvorsky, Peter, Alan Bernjak, Elaine Chow, Ahmed Iqbal, Lianne Sellors, Scott Williams, Robert A. Fawdry, et al. 2017. « Diurnal Differences in Risk of Cardiac Arrhythmias During Spontaneous Hypoglycemia in Young People With Type 1 Diabetes ». *Diabetes Care* 40 (5): 655-62. <https://doi.org/10.2337/dc16-2177>.

Nunemaker, Craig S., David H. Wasserman, Owen P. McGuinness, Ian R. Sweet, Jeanette C. Teague, et Leslie S. Satin. 2006. « Insulin Secretion in the Conscious Mouse Is Biphasic and

Pulsatile ». *American Journal of Physiology. Endocrinology and Metabolism* 290 (3): E523-529. <https://doi.org/10.1152/ajpendo.00392.2005>.

Obici, S, et P.J Martins. 2010. « The role of brain in glucose homeostasis. Principles of Diabetes Mellitus. », 2010, Springer édition.

O'Connor, Elizabeth A., Corinne V. Evans, Megan C. Rushkin, Nadia Redmond, et Jennifer S. Lin. 2020. « Behavioral Counseling to Promote a Healthy Diet and Physical Activity for Cardiovascular Disease Prevention in Adults With Cardiovascular Risk Factors: Updated Evidence Report and Systematic Review for the US Preventive Services Task Force ». *JAMA* 324 (20): 2076-94. <https://doi.org/10.1001/jama.2020.17108>.

O'Dowd, Jacqueline F. 2009. « The Isolation and Purification of Rodent Pancreatic Islets of Langerhans ». *Methods in Molecular Biology* 560: 37-42. https://doi.org/10.1007/978-1-59745-448-3_3.

Olcomendy, Loic, Antoine Pirog, Yannick Bornat, Jerome Cieslak, David Gucik-Derigny, David Henry, Bogdan Catargi, et Sylvie Renaud. 2020. « Tuning of an Artificial Pancreas Controller: An in Silico Methodology Based on Clinically-Relevant Criteria ». *Annual International Conference of the IEEE Engineering in Medicine and Biology Society. IEEE Engineering in Medicine and Biology Society. Annual International Conference 2020* (juillet): 2544-47. <https://doi.org/10.1109/EMBC44109.2020.9175292>.

Olofsson, Charlotta S., Stephan Collins, Martin Bengtsson, Lena Eliasson, Albert Salehi, Kenju Shimomura, Andrei Tarasov, Cecilia Holm, Frances Ashcroft, et Patrik Rorsman. 2007. « Long-Term Exposure to Glucose and Lipids Inhibits Glucose-Induced Insulin Secretion Downstream of Granule Fusion with Plasma Membrane ». *Diabetes* 56 (7): 1888-97. <https://doi.org/10.2337/db06-1150>.

Olson, L. K., J. B. Redmon, H. C. Towle, et R. P. Robertson. 1993. « Chronic Exposure of HIT Cells to High Glucose Concentrations Paradoxically Decreases Insulin Gene Transcription and Alters Binding of Insulin Gene Regulatory Protein ». *The Journal of Clinical Investigation* 92 (1): 514-19. <https://doi.org/10.1172/JCI116596>.

Oomura, Y., T. Nakamura, M. Sugimori, et Y. Yamada. 1975. « Effect of Free Fatty Acid on the Rat Lateral Hypothalamic Neurons ». *Physiology & Behavior* 14 (04): 483-86. [https://doi.org/10.1016/0031-9384\(75\)90015-3](https://doi.org/10.1016/0031-9384(75)90015-3).

Opie, Eugene L. 1901. « THE RELATION OF DIABETES MELLITUS TO LESIONS OF THE PANCREAS. HYALINE DEGENERATION OF THE ISLANDS OF LANGERHANS ». *Journal of Experimental Medicine* 5 (5): 527-40. <https://doi.org/10.1084/jem.5.5.527>.

Orci, L., J. D. Vassalli, et A. Perrelet. 1988. « The Insulin Factory ». *Scientific American* 259 (3): 85-94. <https://doi.org/10.1038/scientificamerican0988-85>.

Ottosson-Laakso, Emilia, Ulrika Krus, Petter Storm, Rashmi B. Prasad, Nikolay Oskolkov, Emma Ahlqvist, João Fadista, Ola Hansson, Leif Groop, et Petter Vikman. 2017. « Glucose-Induced

Changes in Gene Expression in Human Pancreatic Islets: Causes or Consequences of Chronic Hyperglycemia ». *Diabetes* 66 (12): 3013-28. <https://doi.org/10.2337/db17-0311>.

Pagliuca, Felicia W., Jeffrey R. Millman, Mads Gürtler, Michael Segel, Alana Van Dervort, Jennifer Hyoje Ryu, Quinn P. Peterson, Dale Greiner, et Douglas A. Melton. 2014. « Generation of Functional Human Pancreatic β Cells In Vitro ». *Cell* 159 (2): 428-39. <https://doi.org/10.1016/j.cell.2014.09.040>.

Palmer, J. P. 1987. « Insulin Autoantibodies: Their Role in the Pathogenesis of IDDM ». *Diabetes/Metabolism Reviews* 3 (4): 1005-15. <https://doi.org/10.1002/dmr.5610030409>.

Palti, Y., G. B. David, E. Lachov, Y. H. Mida, et R. Schatzberger. 1996. « Islets of Langerhans Generate Wavelike Electric Activity Modulated by Glucose Concentration ». *Diabetes* 45 (5): 595-601. <https://doi.org/10.2337/diab.45.5.595>.

Pammolli, Fabio, Lorenzo Righetto, Sergio Abrignani, Luca Pani, Pier Giuseppe Pelicci, et Emanuele Rabosio. 2020. « The endless frontier? The recent increase of R&D productivity in pharmaceuticals ». *Journal of Translational Medicine* 18 (1): 162. <https://doi.org/10.1186/s12967-020-02313-z>.

Pappa, Anna Maria, David Ohayon, Alexander Giovannitti, Iuliana Petruta Maria, Achilleas Savva, Ilke Uguz, Jonathan Rivnay, Iain McCulloch, Róisín M. Owens, et Sahika Inal. 2018. « Direct Metabolite Detection with an N-Type Accumulation Mode Organic Electrochemical Transistor ». *Science Advances* 4 (6): eaat0911. <https://doi.org/10.1126/sciadv.aat0911>.

Paredes, R. Madelaine, Julie C. Etzler, Lora Talley Watts, Wei Zheng, et James D. Lechleiter. 2008. « Chemical Calcium Indicators ». *Methods* 46 (3): 143-51. <https://doi.org/10.1016/j.ymeth.2008.09.025>.

Park, Sunghye Estelle, Andrei Georgescu, et Dongeun Huh. 2019. « Organoids-on-a-Chip ». *Science (New York, N.Y.)* 364 (6444): 960-65. <https://doi.org/10.1126/science.aaw7894>.

Parlak, Onur, Scott Keene, Andrew Marais, Vincenzo Curto, et Alberto Salleo. 2018. « Molecularly selective nanoporous membrane-based wearable organic electrochemical device for noninvasive cortisol sensing ». *Science Advances* 4eaar2904. <https://doi.org/10.1126/sciadv.aar2904>.

Parnaud, G., D. Bosco, T. Berney, F. Pattou, J. Kerr-Conte, M. Y. Donath, C. Bruun, T. Mandrup-Poulsen, N. Billestrup, et P. A. Halban. 2008. « Proliferation of Sorted Human and Rat Beta Cells ». *Diabetologia* 51 (1): 91-100. <https://doi.org/10.1007/s00125-007-0855-1>.

Pedraza, Eileen, Aleksandar Karaji, Antoine Pirog, Fanny Lebreton, Stéphane Arbault, Julien Gaitan, Sylvie Renaud, Alexander Kuhn, et Jochen Lang. 2015. « Guiding Pancreatic Beta Cells to Target Electrodes in a Whole-Cell Biosensor for Diabetes ». *Lab on a Chip*, 19.

Pereiro, Iago, Anna Fomitcheva Khartchenko, Lorenzo Petrini, et Govind V. Kaigala. 2019. « Nip the Bubble in the Bud: A Guide to Avoid Gas Nucleation in Microfluidics ». *Lab on a Chip* 19 (14): 2296-2314. <https://doi.org/10.1039/c9lc00211a>.

Perrier, R., Pirog A, Jaffredo M, Gaitan J, Catargi B, Renaud S, Raoux M, Lang J2018. « Bioelectronic Organ-Based Sensor for Microfluidic Real-Time Analysis of the Demand in Insulin ». *Biosensors and Bioelectronics*, 7. <https://doi.org/10.1016/j.bios.2018.06.015>

Petersen, K. F., T. Price, G. W. Cline, D. L. Rothman, et G. I. Shulman. 1996. « Contribution of Net Hepatic Glycogenolysis to Glucose Production during the Early Postprandial Period ». *The American Journal of Physiology* 270 (1 Pt 1): E186-191. <https://doi.org/10.1152/ajpendo.1996.270.1.E186>.

Petersen, Max C., et Gerald I. Shulman. 2018. « Mechanisms of Insulin Action and Insulin Resistance ». *Physiological Reviews* 98 (4): 2133-2223. <https://doi.org/10.1152/physrev.00063.2017>.

Pettus, Jeremy, David A. Price, et Steven V. Edelman. 2015. «How patients with type 1 diabetes translate continuous glucose monitoring data into diabetes management decisions ». *Endocrine Practice: Official Journal of the American College of Endocrinology and the American Association of Clinical Endocrinologists* 21 (6): 613-20. <https://doi.org/10.4158/EP14520.OR>.

Pfützner, A., A. Caduff, M. Larbig, T. Schrepfer, et T. Forst. 2004. « Impact of posture and fixation technique on impedance spectroscopy used for continuous and noninvasive glucose monitoring. » *Diabetes Technology & Therapeutics*. <https://doi.org/10.1089/1520915041705839>.

Pigeyre, Marie, Sibylle Hess, Maria F. Gomez, Olof Asplund, Leif Groop, Guillaume Paré, et Hertzfel Gerstein. 2022. « Validation of the Classification for Type 2 Diabetes into Five Subgroups: A Report from the ORIGIN Trial ». *Diabetologia* 65 (1): 206-15. <https://doi.org/10.1007/s00125-021-05567-4>.

Pinsker, Jordan E., Joon Bok Lee, Eyal Dassau, Dale E. Seborg, Paige K. Bradley, Ravi Gondhalekar, Wendy C. Bevier, Lauren Huyett, Howard C. Zisser, et Francis J. Doyle III. 2016. « Randomized Crossover Comparison of Personalized MPC and PID Control Algorithms for the Artificial Pancreas ». *Diabetes Care* 39 (7): 1135-42. <https://doi.org/10.2337/dc15-2344>.

Pirog, Antoine, Yannick Bornat, Romain Perrier, Matthieu Raoux, Manon Jaffredo, Adam Quotb, Jochen Lang, Noëlle Lewis, et Sylvie Renaud. 2018. « Multimed: An Integrated, Multi-Application Platform for the Real-Time Recording and Sub-Millisecond Processing of Biosignals ». *Sensors (Basel, Switzerland)* 18 (7): E2099. <https://doi.org/10.3390/s18072099>.

Plock, Nele, et Charlotte Kloft. 2005. « Microdialysis—Theoretical Background and Recent Implementation in Applied Life-Sciences ». *European Journal of Pharmaceutical Sciences* 25 (1): 1-24. <https://doi.org/10.1016/j.ejps.2005.01.017>.

PMC, Europe. 1971. « The Structure and Biology of Insulin. » *Biochemical Journal* 125 (3): 50P. <https://doi.org/10.1042/bj1250050p>.

Pocock, G., et C. Richards. 2006. *Human Physiology: The Basis of Medicine*. Oxford: Oxford University Press. <https://repository.canterbury.ac.uk/item/86235/human-physiology-the-basis-of-medicine>.

Poenie, M., J. Alderton, R. Steinhardt, et R. Tsien. 1986. « Calcium Rises Abruptly and Briefly throughout the Cell at the Onset of Anaphase ». *Science* 233 (4766): 886-89. <https://doi.org/10.1126/science.3755550>.

Polakof, Sergio, Thomas P. Mommsen, et José L. Soengas. 2011. « Glucosensing and Glucose Homeostasis: From Fish to Mammals ». *Comparative Biochemistry and Physiology. Part B*, 160 (4): 123-49. <https://doi.org/10.1016/j.cbpb.2011.07.006>.

Polonsky, Kenneth S., Bruce D. Given, Laurence J. Hirsch, Hartmut Tillil, E. Timothy Shapiro, Christine Beebe, Bruce H. Frank, John A. Galloway, et Eve Van Cauter. 1988. « Abnormal Patterns of Insulin Secretion in Non-Insulin-Dependent Diabetes Mellitus ». *New England Journal of Medicine* 318 (19): 1231-39. <https://doi.org/10.1056/NEJM198805123181903>.

Popkin, B. M., et P. Gordon-Larsen. 2004. « The Nutrition Transition: Worldwide Obesity Dynamics and Their Determinants ». *International Journal of Obesity* 28 (3): S2-9. <https://doi.org/10.1038/sj.ijo.0802804>.

Power, Michael L., et Jay Schulkin. 2011. « Anticipatory Physiological Regulation in Feeding Biology ». In *Handbook of Behavior, Food and Nutrition*, édité par Victor R. Preedy, Ronald Ross Watson, et Colin R. Martin, 829-44. New York, NY: Springer. https://doi.org/10.1007/978-0-387-92271-3_55.

Powers, A. C., S. Efrat, S. Mojsov, D. Spector, J. F. Habener, et D. Hanahan. 1990. « Proglucagon Processing Similar to Normal Islets in Pancreatic Alpha-like Cell Line Derived from Transgenic Mouse Tumor ». *Diabetes* 39 (4): 406-14. <https://doi.org/10.2337/diab.39.4.406>.

Prabhakar, Nanduri R., et Michael J. Joyner. 2015. « Tasting arterial blood: what do the carotid chemoreceptors sense? » *Frontiers in Physiology* 5: 524. <https://doi.org/10.3389/fphys.2014.00524>.

Prasad, Rashmi B., Olof Asplund, Sharvari R. Shukla, Rucha Wagh, Pooja Kunte, Dattatrey Bhat, Malay Parekh, et al. 2022. « Subgroups of Patients with Young-Onset Type 2 Diabetes in India Reveal Insulin Deficiency as a Major Driver ». *Diabetologia* 65 (1): 65-78. <https://doi.org/10.1007/s00125-021-05543-y>.

Pugliese, A., M. Zeller, A. Fernandez, L. J. Zalcberg, R. J. Bartlett, C. Ricordi, M. Pietropaolo, G. S. Eisenbarth, S. T. Bennett, et D. D. Patel. 1997. « The Insulin Gene Is Transcribed in the Human Thymus and Transcription Levels Correlated with Allelic Variation at the INS VNTR-IDDM2 Susceptibility Locus for Type 1 Diabetes ». *Nature Genetics* 15 (3): 293-97. <https://doi.org/10.1038/ng0397-293>.

Pun, Sirjana, Li Cai Haney, et Riccardo Barrile. 2021. « Modelling Human Physiology on-Chip: Historical Perspectives and Future Directions ». *Micromachines* 12 (10): 1250. <https://doi.org/10.3390/mi12101250>.

Quemerais, Marie Aude, Maeva Doron, Florent Dutrech, Vincent Melki, Sylvia Franc, Michel Antonakios, Guillaume Charpentier, Helene Hanaire, et Pierre Yves Benhamou. 2014. « Preliminary Evaluation of a New Semi-Closed-Loop Insulin Therapy System Over the Prandial Period in Adult Patients With Type 1 Diabetes: The WP6.0 Diabeloop Study ». *Journal of Diabetes Science and Technology* 8 (6): 1177-84. <https://doi.org/10.1177/1932296814545668>.

Quesada, Ivan, Eva Tudurí, Cristina Ripoll, et Angel Nadal. 2008. « Physiology of the Pancreatic Alpha-Cell and Glucagon Secretion: Role in Glucose Homeostasis and Diabetes ». *The Journal of Endocrinology* 199 (1): 5-19. <https://doi.org/10.1677/JOE-08-0290>.

Ramracheya, Reshma, Caroline Ward, Makoto Shigeto, Jonathan N. Walker, Stefan Amisten, Quan Zhang, Paul R. Johnson, Patrik Rorsman, et Matthias Braun. 2010. « Membrane Potential-Dependent Inactivation of Voltage-Gated Ion Channels in Alpha-Cells Inhibits Glucagon Secretion from Human Islets ». *Diabetes* 59 (9): 2198-2208. <https://doi.org/10.2337/db09-1505>.

Randle, P. J. 1964. « The Interrelationships of Hormones, Fatty Acid and Glucose in the Provision of Energy ». *Postgraduate Medical Journal* 40 (466): 457-63. <https://doi.org/10.1136/pgmj.40.466.457>.

Raoux, Matthieu, Yannick Bornat, Adam Quotb, Bogdan Catargi, Sylvie Renaud, et Jochen Lang. 2012a. « Non-Invasive Long-Term and Real-Time Analysis of Endocrine Cells on Micro-Electrode Arrays ». *The Journal of Physiology* 590 (5): 1085-91. <https://doi.org/10.1113/jphysiol.2011.220038>.

Raoux, M . 2012b. « Non-Invasive Long-Term and Real-Time Analysis of Endocrine Cells on Micro-Electrode Arrays ». *The Journal of Physiology* 590 (5): 1085-91. <https://doi.org/10.1113/jphysiol.2011.220038>.

Ratner, Buddy. 2007. « A paradigm shift: Biomaterials that heal ». *Polymer International* 56 : 1183-85. <https://doi.org/10.1002/pi.2319>.

Ravassard, Philippe, Yasmine Hazhouz, Séverine Pechberty, Emilie Bricout-Neveu, Mathieu Armanet, Paul Czernichow, et Raphael Scharfmann. 2011. « A genetically engineered human pancreatic β cell line exhibiting glucose-inducible insulin secretion ». *The Journal of Clinical Investigation* 121 (9): 3589-97. <https://doi.org/10.1172/JCI58447>.

Ravier, Magalie A., Myriam Nenquin, Takashi Miki, Susumu Seino, et Jean-Claude Henquin. 2009. « Glucose Controls Cytosolic Ca²⁺ and Insulin Secretion in Mouse Islets Lacking Adenosine Triphosphate-Sensitive K⁺ Channels Owing to a Knockout of the Pore-Forming Subunit Kir6.2 ». *Endocrinology* 150 (1): 33-45. <https://doi.org/10.1210/en.2008-0617>.

Raybould, Helen E. 2007. « Sensing of Glucose in the Gastrointestinal Tract ». *Autonomic Neuroscience: Basic and Clinical* 133 (1): 86-90. <https://doi.org/10.1016/j.autneu.2007.01.006>.

Rebrin, Kerstin, et Garry Steil. 2000. « Can Interstitial Glucose Assessment Replace Blood Glucose Measurements? » *Diabetes Technology & Therapeutics* 2 (février): 461-72. <https://doi.org/10.1089/15209150050194332>.

Redondo, Maria J, Andrea K Steck, et Alberto Pugliese. 2018. « Genetics of Type 1 Diabetes ». *Pediatric Diabetes* 19 (3): 346-53. <https://doi.org/10.1111/pedi.12597>.

Renaud, Sylvie, Bogdan Catargi, et Jochen Lang. 2014. « Biosensors in Diabetes : How to Get the Most out of Evolution and Transpose It into a Signal ». *IEEE Pulse* 5 (3): 30-34. <https://doi.org/10.1109/MPUL.2014.2309577>.

Rezania, Alireza, Jennifer E. Bruin, Payal Arora, Allison Rubin, Irina Batushansky, Ali Asadi, Shannon O'Dwyer, et al. 2014. « Reversal of Diabetes with Insulin-Producing Cells Derived in Vitro from Human Pluripotent Stem Cells ». *Nature Biotechnology* 32 (11): 1121-33. <https://doi.org/10.1038/nbt.3033>.

Ricci, Francesco, Felice Caprio, Alessandro Poscia, Francesco Valgimigli, Dimitri Messeri, Elena Lepori, Giorgio Dall'Oglio, Giuseppe Palleschi, et Danila Moscone. 2007. « Toward Continuous Glucose Monitoring with Planar Modified Biosensors and Microdialysis: Study of Temperature, Oxygen Dependence and in Vivo Experiment ». *Biosensors and Bioelectronics*, Selected Papers from the Ninth World Congress On Biosensors. 10 - 12 May 2006, 22 (9): 2032-39. <https://doi.org/10.1016/j.bios.2006.08.041>.

Rice, Mark J., Douglas B. Coursin, et Bruno Riou. 2012. « Continuous Measurement of Glucose: Facts and Challenges ». *Anesthesiology* 116 (1): 199-204. <https://doi.org/10.1097/ALN.0b013e318236abf6>.

Rickels, Michael R., Peter G. Stock, Eelco J. P. de Koning, Lorenzo Piemonti, Johann Pratschke, Rodolfo Alejandro, Melena D. Bellin, et al. 2018. « Defining Outcomes for β -Cell Replacement Therapy in the Treatment of Diabetes: A Consensus Report on the Igl's Criteria From the IPITA/EPITA Opinion Leaders Workshop ». *Transplantation* 102 (9): 1479-86. <https://doi.org/10.1097/TP.0000000000002158>.

Rieck, Sebastian, Jia Zhang, Zhaoyu Li, Chengyang Liu, Ali Naji, Karen K. Takane, Nathalie M. Fiaschi-Taesch, Andrew F. Stewart, Jake A. Kushner, et Klaus H. Kaestner. 2012. « Overexpression of Hepatocyte Nuclear Factor-4 α Initiates Cell Cycle Entry, but Is Not Sufficient to Promote β -Cell Expansion in Human Islets ». *Molecular Endocrinology* 26 (9): 1590-1602. <https://doi.org/10.1210/me.2012-1019>.

Risch, N. 1987. « Assessing the Role of HLA-Linked and Unlinked Determinants of Disease ». *American Journal of Human Genetics* 40 (1): 1-14.

Rivnay, Jonathan, Huiliang Wang, Lief Fenno, Karl Deisseroth, et George G. Malliaras. 2017. « Next-Generation Probes, Particles, and Proteins for Neural Interfacing ». *Science Advances* 3 (6): e1601649. <https://doi.org/10.1126/sciadv.1601649>.

Röder, Pia V., Bingbing Wu, Yixian Liu, et Weiping Han. 2016. « Pancreatic Regulation of Glucose Homeostasis ». *Experimental & Molecular Medicine* 48 (mars): e219. <https://doi.org/10.1038/emm.2016.6>.

Rodríguez-Comas, Júlia, et Javier Ramón-Azcón. 2021. « Islet-on-a-Chip for the Study of Pancreatic β -Cell Function ». *In Vitro Models*, décembre. <https://doi.org/10.1007/s44164-021-00005-6>.

Rodriguez-Diaz, Rayner, Midhat H. Abdulreda, Alexander L. Formoso, Itai Gans, Camillo Ricordi, Per-Olof Berggren, et Alejandro Caicedo. 2011. « Innervation Patterns of Autonomic Axons in the Human Endocrine Pancreas ». *Cell Metabolism* 14 (1): 45-54. <https://doi.org/10.1016/j.cmet.2011.05.008>.

Rodriguez-Diaz, Rayner, et Alejandro Caicedo. 2014. « Neural Control of the Endocrine Pancreas ». *Best Practice & Research. Clinical Endocrinology & Metabolism* 28 (5): 745-56. <https://doi.org/10.1016/j.beem.2014.05.002>.

Rodriguez-Diaz, Rayner, Robin Dando, M. Caroline Jacques-Silva, Alberto Fachado, Judith Molina, Midhat H. Abdulreda, Camillo Ricordi, Stephen D. Roper, Per-Olof Berggren, et Alejandro Caicedo. 2011. « Alpha Cells Secrete Acetylcholine as a Non-Neuronal Paracrine Signal Priming Beta Cell Function in Humans ». *Nature Medicine* 17 (7): 888-92. <https://doi.org/10.1038/nm.2371>.

Rodriguez-Diaz, Rayner, R. Damaris Molano, Jonathan R. Weitz, Midhat H. Abdulreda, Dora M. Berman, Barbara Leibiger, Ingo B. Leibiger, et al. 2018. « Paracrine Interactions within the Pancreatic Islet Determine the Glycemic Set Point ». *Cell Metabolism* 27 (3): 549-558.e4. <https://doi.org/10.1016/j.cmet.2018.01.015>.

Rohner-Jeanrenaud, F., et B. Jeanrenaud. 1980. « Consequences of Ventromedial Hypothalamic Lesions upon Insulin and Glucagon Secretion by Subsequently Isolated Perfused Pancreases in the Rat ». *The Journal of Clinical Investigation* 65 (4): 902-10. <https://doi.org/10.1172/JCI109744>.

Rorsman, P., et G. Trube. 1986. « Calcium and Delayed Potassium Currents in Mouse Pancreatic Beta-Cells under Voltage-Clamp Conditions ». *The Journal of Physiology* 374 (mai): 531-50. <https://doi.org/10.1113/jphysiol.1986.sp016096>.

Rorsman, Patrik, et Frances M. Ashcroft. 2018b. « Pancreatic β -Cell Electrical Activity and Insulin Secretion: Of Mice and Men ». *Physiological Reviews* 98 (1): 117-214. <https://doi.org/10.1152/physrev.00008.2017>.

Rorsman, Patrik, et Matthias Braun. 2013. « Regulation of Insulin Secretion in Human Pancreatic Islets ». *Annual Review of Physiology* 75: 155-79. <https://doi.org/10.1146/annurev-physiol-030212-183754>.

Rorsman, Patrik, Matthias Braun, et Quan Zhang. 2012. « Regulation of Calcium in Pancreatic α - and β -Cells in Health and Disease ». *Cell Calcium* 51 (3-4): 300-308. <https://doi.org/10.1016/j.ceca.2011.11.006>.

Rorsman, Patrik, Lena Eliasson, Takahiro Kanno, Quan Zhang, et Sven Gopel. 2011. « Electrophysiology of Pancreatic β -Cells in Intact Mouse Islets of Langerhans ». *Progress in Biophysics and Molecular Biology* 107 (2): 224-35. <https://doi.org/10.1016/j.pbiomolbio.2011.06.009>.

Rorsman, Patrik, et Mark O. Huising. 2018. « The Somatostatin-Secreting Pancreatic δ -Cell in Health and Disease ». *Nature Reviews. Endocrinology* 14 (7): 404-14. <https://doi.org/10.1038/s41574-018-0020-6>.

Rosati, B., P. Marchetti, O. Crociani, M. Lecchi, R. Lupi, A. Arcangeli, M. Olivotto, et E. Wanke. 2000. « Glucose- and Arginine-Induced Insulin Secretion by Human Pancreatic Beta-Cells: The Role of HERG K^+ Channels in Firing and Release ». *FASEB Journal* 14 (15): 2601-10. <https://doi.org/10.1096/fj.00-0077com>.

Rosen, Evan D., et Bruce M. Spiegelman. 2006. « Adipocytes as Regulators of Energy Balance and Glucose Homeostasis ». *Nature* 444 (7121): 847-53. <https://doi.org/10.1038/nature05483>.

Rothberg, Leon, Ty Lees, Roderick Clifton-Bligh, et Sara Lal. 2016. « Association Between Heart Rate Variability Measures and Blood Glucose Levels: Implications for Noninvasive Glucose Monitoring for Diabetes ». *Diabetes Technology & Therapeutics* 18 (juin): 366-76. <https://doi.org/10.1089/dia.2016.0010>.

Routh, Vanessa H., Lihong Hao, Ammy M. Santiago, Zhenyu Sheng, et Chunxue Zhou. 2014. « Hypothalamic glucose sensing: making ends meet ». *Frontiers in Systems Neuroscience* 8: 236. <https://doi.org/10.3389/fnsys.2014.00236>.

Ruiz, Jessica L., Jennifer L. Sherr, Eda Cengiz, Lori Carria, Anirban Roy, Gayane Voskanyan, William V. Tamborlane, et Stuart A. Weinzimer. 2012. « Effect of Insulin Feedback on Closed-Loop Glucose Control: A Crossover Study ». *Journal of Diabetes Science and Technology* 6 (5): 1123-30. <https://doi.org/10.1177/193229681200600517>.

Russ, Holger A., Yael Bar, Philippe Ravassard, et Shimon Efrat. 2008. « In Vitro Proliferation of Cells Derived from Adult Human Beta-Cells Revealed by Cell-Lineage Tracing ». *Diabetes* 57 (6): 1575-83. <https://doi.org/10.2337/db07-1283>.

Russ, Holger A., Elad Sintov, Leeat Anker-Kitai, Orr Friedman, Ayelet Lenz, Ginat Toren, Chen Farhy, et al. 2011. « Insulin-Producing Cells Generated from Dedifferentiated Human Pancreatic Beta Cells Expanded in Vitro ». *PloS One* 6 (9): e25566. <https://doi.org/10.1371/journal.pone.0025566>.

Sacks, David A., David R. Hadden, Michael Maresh, Chaicharn Deerochanawong, Alan R. Dyer, Boyd E. Metzger, Lynn P. Lowe, et al. 2012. « Frequency of Gestational Diabetes Mellitus at Collaborating Centers Based on IADPSG Consensus Panel-Recommended Criteria: The Hyperglycemia and Adverse Pregnancy Outcome (HAPO) Study ». *Diabetes Care* 35 (3): 526-28. <https://doi.org/10.2337/dc11-1641>.

Salinas, Gerardo, Ariana Villarroel Marquez, Maël Idir, Shekhar Shinde, Bernardo A Frontana-Urbe, Matthieu Raoux, Jochen Lang, Eric Cloutet, et Alexander Kuhn. 2020. « Na⁺ ion selectivity study of a crown ether functionalized PEDOT analog ». *ChemElectroChem* 7 (13): 2826-30. <https://doi.org/10.1002/celec.202000693>.

Samols, E., et J. I. Stagner. 1988. « Intra-Islet Regulation ». *The American Journal of Medicine* 85 (5A): 31-35. [https://doi.org/10.1016/0002-9343\(88\)90395-6](https://doi.org/10.1016/0002-9343(88)90395-6).

Samols, E., J. I. Stagner, R. B. Ewart, et V. Marks. 1988. « The Order of Islet Microvascular Cellular Perfusion Is B---A---D in the Perfused Rat Pancreas ». *The Journal of Clinical Investigation* 82 (1): 350-53. <https://doi.org/10.1172/JCI113593>.

Sánchez-Andrés, J. V., A. Gomis, et M. Valdeolmillos. 1995. « The Electrical Activity of Mouse Pancreatic Beta-Cells Recorded in Vivo Shows Glucose-Dependent Oscillations ». *The Journal of Physiology* 486 (Pt 1) (juillet): 223-28. <https://doi.org/10.1113/jphysiol.1995.sp020804>.

Sanders, Francis W. B., et Julian L. Griffin. 2016. « De Novo Lipogenesis in the Liver in Health and Disease: More than Just a Shunting Yard for Glucose ». *Biological Reviews* 91 (2): 452-68. <https://doi.org/10.1111/brv.12178>.

Sanger, F., et E. O. P. Thompson. 1953. « The amino-acid sequence in the glycol chain of insulin. 2. The investigation of peptides from enzymic hydrolysates ». *Biochemical Journal* 53 (3): 366-74. <https://doi.org/10.1042/bj0530366>.

Santerre, R. F., R. A. Cook, R. M. Crisel, J. D. Sharp, R. J. Schmidt, D. C. Williams, et C. P. Wilson. 1981. « Insulin Synthesis in a Clonal Cell Line of Simian Virus 40-Transformed Hamster Pancreatic Beta Cells ». *Proceedings of the National Academy of Sciences of the United States of America* 78 (7): 4339-43. <https://doi.org/10.1073/pnas.78.7.4339>.

Sapir, Tamar, Keren Shternhall, Irit Meivar-Levy, Tamar Blumenfeld, Hamutal Cohen, Ehud Skutelsky, Smadar Eventov-Friedman, et al. 2005. « Cell-Replacement Therapy for Diabetes: Generating Functional Insulin-Producing Tissue from Adult Human Liver Cells ». *Proceedings of the National Academy of Sciences of the United States of America* 102 (22): 7964-69. <https://doi.org/10.1073/pnas.0405277102>.

Scharfmann, Raphael, Latif Rachdi, et Philippe Ravassard. 2013. « Concise Review: In Search of Unlimited Sources of Functional Human Pancreatic Beta Cells ». *Stem Cells Translational Medicine* 2 (1): 61-67. <https://doi.org/10.5966/sctm.2012-0120>.

Schmidt, M.A. 1998. « Wafer-to-wafer bonding for microstructure formation ». *Proceedings of the IEEE* 86 (8): 1575-85. <https://doi.org/10.1109/5.704262>.

Schmidtke, David W., Angela C. Freeland, Adam Heller, et Roger T. Bonnecaze. 1998. « Measurement and Modeling of the Transient Difference between Blood and Subcutaneous Glucose Concentrations in the Rat after Injection of Insulin ». *Proceedings of the National Academy of Sciences* 95 (1): 294-99. <https://doi.org/10.1073/pnas.95.1.294>.

Schuit, F. C., P. Huypens, H. Heimberg, et D. G. Pipeleers. 2001. « Glucose Sensing in Pancreatic Beta-Cells: A Model for the Study of Other Glucose-Regulated Cells in Gut, Pancreas, and Hypothalamus ». *Diabetes* 50 (1): 1-11. <https://doi.org/10.2337/diabetes.50.1.1>.

Schulz, Nadja, Ka-Cheuk Liu, Jérémie Charbord, Charlotte L. Mattsson, Lingjie Tao, Dominika Tworus, et Olov Andersson. 2016. « Critical Role for Adenosine Receptor A2a in β -Cell Proliferation ». *Molecular Metabolism* 5 (11): 1138-46. <https://doi.org/10.1016/j.molmet.2016.09.006>.

Schwartz, M. W., S. C. Woods, D. Porte, R. J. Seeley, et D. G. Baskin. 2000. « Central Nervous System Control of Food Intake ». *Nature* 404 (6778): 661-71. <https://doi.org/10.1038/35007534>.

Schweicher, Julien, Crystal Nyitray, et Tejal A. Desai. 2014. « Membranes to achieve immunoprotection of transplanted islets ». *Frontiers in bioscience* 19 : 49-76.

Scott, R. V., et S. R. Bloom. 2018. « Problem or Solution: The Strange Story of Glucagon ». *Peptides* 100 (février): 36-41. <https://doi.org/10.1016/j.peptides.2017.11.013>.

Scuffi, Cosimo et Scientist, Scientific and Technology Affairs Department, A. Menarini Diagnostics, Florence, Italy. 2010. « Interstitium versus Blood Equilibrium in Glucose Concentration and Its Impact on Subcutaneous Continuous Glucose Monitoring Systems ». *European Endocrinology* 10 (1): 36. <https://doi.org/10.17925/EE.2014.10.01.36>.

Sebeková, Katarína, et Veronika Somoza. 2007. « Dietary Advanced Glycation Endproducts (AGEs) and Their Health Effects--PRO ». *Molecular Nutrition & Food Research* 51 (9): 1079-84. <https://doi.org/10.1002/mnfr.200700035>.

Seino, Susumu, Kenji Sugawara, Norihide Yokoi, et Harumi Takahashi. 2017. « β -Cell Signalling and Insulin Secretagogues: A Path for Improved Diabetes Therapy ». *Diabetes, Obesity and Metabolism* 19 (S1): 22-29. <https://doi.org/10.1111/dom.12995>.

Sekine, N., V. Cirulli, R. Regazzi, L. J. Brown, E. Gine, J. Tamarit-Rodriguez, M. Girotti, S. Marie, M. J. MacDonald, et C. B. Wollheim. 1994. « Low Lactate Dehydrogenase and High Mitochondrial Glycerol Phosphate Dehydrogenase in Pancreatic Beta-Cells. Potential Role in Nutrient Sensing ». *The Journal of Biological Chemistry* 269 (7): 4895-4902.

Serre-Beinier, Véronique, Domenico Bosco, Laurence Zulianello, Anne Charollais, Dorothée Caille, Eric Charpantier, Benoit R. Gauthier, et al. 2009. « Cx36 Makes Channels Coupling

Human Pancreatic Beta-Cells, and Correlates with Insulin Expression ». *Human Molecular Genetics* 18 (3): 428-39. <https://doi.org/10.1093/hmg/ddn370>.

Severinsen, Mai Charlotte Krogh, et Bente Klarlund Pedersen. 2020. « Muscle-Organ Crosstalk: The Emerging Roles of Myokines ». *Endocrine Reviews* 41 (4): bnaa016. <https://doi.org/10.1210/endrev/bnaa016>.

Shapiro, A. M. James, Marta Pokrywczynska, et Camillo Ricordi. 2017. « Clinical Pancreatic Islet Transplantation ». *Nature Reviews. Endocrinology* 13 (5): 268-77. <https://doi.org/10.1038/nrendo.2016.178>.

Shen, Yixiao, Witoon Prinyawiwatkul, et Zhimin Xu. 2019. « Insulin: A Review of Analytical Methods ». *Analyst* 144 (14): 4139-48. <https://doi.org/10.1039/C9AN00112C>.

Shigeto, Makoto, Reshma Ramracheya, Andrei I. Tarasov, Chae Young Cha, Margarita V. Chibalina, Benoit Hastoy, Koenraad Philippaert, et al. 2015. « GLP-1 Stimulates Insulin Secretion by PKC-Dependent TRPM4 and TRPM5 Activation ». *The Journal of Clinical Investigation* 125 (12): 4714-28. <https://doi.org/10.1172/JCI81975>.

Shrayyef, Muhammad Z., et John E. Gerich. 2010. « Normal Glucose Homeostasis ». In *Principles of Diabetes Mellitus*, édité par Leonid Poretsky, 19-35. Boston, MA: Springer US. https://doi.org/10.1007/978-0-387-09841-8_2.

Simeone, Jason C, Surbhi Shah, Michael L Ganz, Sean Sullivan, Anne Koralova, Jackie LeGrand, et Jesse Bushman. 2020. « Healthcare resource utilization and cost among patients with type 1 diabetes in the United States ». *Journal of Managed Care & Specialty Pharmacy* 26 (11): 1399-1410. <https://doi.org/10.18553/jmcp.2020.26.11.1399>.

Sirringhaus, H. 2009. « Reliability of Organic Field-Effect Transistors ». *Advanced material* <https://doi.org/10.1002/ADMA.200901136>.

Skelin Klemen, Maša, Jurij Dolenšek, Marjan Slak Rupnik, et Andraž Stožer. 2017. « The triggering pathway to insulin secretion: Functional similarities and differences between the human and the mouse β cells and their translational relevance ». *Islets* 9 (6): 109-39. <https://doi.org/10.1080/19382014.2017.1342022>.

Sladek, Rob. 2018. « The many faces of diabetes: Addressing heterogeneity of a complex disease ». *The Lancet Diabetes & Endocrinology* 6. [https://doi.org/10.1016/S2213-8587\(18\)30070-6](https://doi.org/10.1016/S2213-8587(18)30070-6).

Sneddon, Julie B., Qizhi Tang, Peter Stock, Jeffrey A. Bluestone, Shuvo Roy, Tejal Desai, et Matthias Hebrok. 2018. « Stem Cell Therapies for Treating Diabetes: Progress and Remaining Challenges ». *Cell Stem Cell* 22 (6): 810-23. <https://doi.org/10.1016/j.stem.2018.05.016>.

Snyder, Kate L., Colleen E. Nathan, Andrew Yee, et Julie A. Stenken. 2001. « Diffusion and Calibration Properties of Microdialysis Sampling Membranes in Biological Media ». *Analyst* 126 (8): 1261-68. <https://doi.org/10.1039/B102488B>.

Sosa-Pineda, B., K. Chowdhury, M. Torres, G. Oliver, et P. Gruss. 1997. « The Pax4 Gene Is Essential for Differentiation of Insulin-Producing Beta Cells in the Mammalian Pancreas ». *Nature* 386 (6623): 399-402. <https://doi.org/10.1038/386399a0>.

Spargo, E., O. E. Pratt, et P. M. Daniel. 1979. « Metabolic Functions of Skeletal Muscles of Man, Mammals, Birds and Fishes: A Review ». *Journal of the Royal Society of Medicine* 72 (12): 921-25.

Steil, G. M., J. Richey, J. K. Kim, J. K. Wi, K. Rebrin, R. N. Bergman, et J. H. Youn. 1996. « Extracellular glucose distribution is not altered by insulin: analysis of plasma and interstitial L-glucose kinetics ». *American Journal of Physiology-Endocrinology and Metabolism* 271 (5): E855-64. <https://doi.org/10.1152/ajpendo.1996.271.5.E855>.

Stipanuk, Martha H., et Marie A. Caudill. 2018. *Biochemical, Physiological, and Molecular Aspects of Human Nutrition - E-Book*. Elsevier Health Sciences.

Strakosas, Xenofon, Manuelle Bongo, et Róisín M. Owens. 2015. « The Organic Electrochemical Transistor for Biological Applications ». *Journal of Applied Polymer Science* 132 (15). <https://doi.org/10.1002/app.41735>.

Strowski, M. Z., R. M. Parmar, A. D. Blake, et J. M. Schaeffer. 2000. « Somatostatin Inhibits Insulin and Glucagon Secretion via Two Receptors Subtypes: An in Vitro Study of Pancreatic Islets from Somatostatin Receptor 2 Knockout Mice ». *Endocrinology* 141 (1): 111-17. <https://doi.org/10.1210/endo.141.1.7263>.

Stuhlmann, Till, Rosa Planells-Cases, et Thomas J. Jentsch. 2018. « LRRC8/VRAC Anion Channels Enhance β -Cell Glucose Sensing and Insulin Secretion ». *Nature Communications* 9 (1): 1974. <https://doi.org/10.1038/s41467-018-04353-y>.

Sun, Jennifer K., Hillary A. Keenan, Jerry D. Cavallerano, Bela F. Asztalos, Ernst J. Schaefer, David R. Sell, Christopher M. Strauch, et al. 2011. « Protection From Retinopathy and Other Complications in Patients With Type 1 Diabetes of Extreme Duration: The Joslin 50-Year Medalist Study ». *Diabetes Care* 34 (4): 968-74. <https://doi.org/10.2337/dc10-1675>.

Sung, Jong Hwan, et Michael L. Shuler. 2009. « Prevention of Air Bubble Formation in a Microfluidic Perfusion Cell Culture System Using a Microscale Bubble Trap ». *Biomedical Microdevices* 11 (4): 731-38. <https://doi.org/10.1007/s10544-009-9286-8>.

Sussman, K. E., G. D. Vaughan, et R. F. Timmer. 1966. « An in Vitro Method for Studying Insulin Secretion in the Perfused Isolated Rat Pancreas ». *Metabolism: Clinical and Experimental* 15 (5): 466-76. [https://doi.org/10.1016/0026-0495\(66\)90089-8](https://doi.org/10.1016/0026-0495(66)90089-8).

Tabeling, Patrick. 2003. *Introduction à la microfluidique*. Échelles. Belin.

Takaki, R., J. Ono, M. Nakamura, Y. Yokogawa, S. Kumae, T. Hiraoka, K. Yamaguchi, K. Hamaguchi, et S. Uchida. 1986. « Isolation of Glucagon-Secreting Cell Lines by Cloning

Insulinoma Cells ». *In Vitro Cellular & Developmental Biology: Journal of the Tissue Culture Association* 22 (3 Pt 1): 120-26. <https://doi.org/10.1007/BF02623498>.

Tang, Liu, Shwu Jen Chang, Ching-Jung Chen, et Jen-Tsai Liu. 2020. « Non-Invasive Blood Glucose Monitoring Technology: A Review ». *Sensors (Basel, Switzerland)* 20 (23): 6925. <https://doi.org/10.3390/s20236925>.

Tang, Shiue-Cheng, Luc Baeyens, Chia-Ning Shen, Shih-Jung Peng, Hung-Jen Chien, David W. Scheel, Chester E. Chamberlain, et Michael S. German. 2018. « Human Pancreatic Neuro-Insular Network in Health and Fatty Infiltration ». *Diabetologia* 61 (1): 168-81. <https://doi.org/10.1007/s00125-017-4409-x>.

Tateishi, Keisuke, Jin He, Olena Taranova, Gaoyang Liang, Ana C. D'Alessio, et Yi Zhang. 2008. « Generation of Insulin-Secreting Islet-like Clusters from Human Skin Fibroblasts ». *The Journal of Biological Chemistry* 283 (46): 31601-7. <https://doi.org/10.1074/jbc.M806597200>.

Tauschmann, Martin, et Roman Hovorka. 2018. « Technology in the Management of Type 1 Diabetes Mellitus - Current Status and Future Prospects ». *Nature Reviews. Endocrinology* 14 (8): 464-75. <https://doi.org/10.1038/s41574-018-0044-y>.

Teff, Karen L. 2011. « How Neural Mediation of Anticipatory and Compensatory Insulin Release Helps Us Tolerate Food ». *Physiology & Behavior* 103 (1): 44-50. <https://doi.org/10.1016/j.physbeh.2011.01.012>.

Teo, Adrian K. K., Rebecca Windmueller, Bente B. Johansson, Ercument Dirice, Pal R. Njolstad, Erling Tjora, Helge Raeder, et Rohit N. Kulkarni. 2013. « Derivation of Human Induced Pluripotent Stem Cells from Patients with Maturity Onset Diabetes of the Young ». *The Journal of Biological Chemistry* 288 (8): 5353-56. <https://doi.org/10.1074/jbc.C112.428979>.

« Texts Adopted - Plans and Actions to Accelerate a Transition to Innovation without the Use of Animals in Research, Regulatory Testing and Education - Thursday, 16 September 2021 ». s. d. Consulté le 4 janvier 2022. https://www.europarl.europa.eu/doceo/document/TA-9-2021-0387_EN.html.

Thomé-Duret, V., G. Reach, M. Gangnerau, F. Lemonnier, J. Klein, Y. Zhang, Y. Hu, et G. S. Wilson. 1996. « Use of a subcutaneous glucose sensor to detect decreases in glucose concentration prior to observation in blood. » *Analytical chemistry*. <https://doi.org/10.1021/AC960069I>.

Thomson, J. A., J. Itskovitz-Eldor, S. S. Shapiro, M. A. Waknitz, J. J. Swiergiel, V. S. Marshall, et J. M. Jones. 1998. « Embryonic Stem Cell Lines Derived from Human Blastocysts ». *Science* 282 (5391): 1145-47. <https://doi.org/10.1126/science.282.5391.1145>.

Thorens, B. 2004. « Mechanisms of Glucose Sensing and Multiplicity of Glucose Sensors ». *Annales d'Endocrinologie, La glycémie, l'insuline et les autres (Klotz 2004)*, 65 (1): 9-12. [https://doi.org/10.1016/S0003-4266\(04\)95624-7](https://doi.org/10.1016/S0003-4266(04)95624-7).

- Thorens, B. 2008. « Glucose Sensing and the Pathogenesis of Obesity and Type 2 Diabetes ». *International Journal of Obesity (2005)* 32 Suppl 6: S62-71. <https://doi.org/10.1038/ijo.2008.208>.
- Thorens, B., D. Accili, B. Ahrén, E. Cerasi, S. Seino, et C. Boitard. 2015. « The Islet and Metabolism Keep Time ». *Diabetes, Obesity and Metabolism* 17 (S1): 3-5. <https://doi.org/10.1111/dom.12547>.
- Thorens, Bernard, et Mike Mueckler. 2010. « Glucose transporters in the 21st Century ». *American Journal of Physiology - Endocrinology and Metabolism* 298 (2): E141-45. <https://doi.org/10.1152/ajpendo.00712.2009>.
- Todd, J. A. 1995. « Genetic Analysis of Type 1 Diabetes Using Whole Genome Approaches ». *Proceedings of the National Academy of Sciences of the United States of America* 92 (19): 8560-65. <https://doi.org/10.1073/pnas.92.19.8560>.
- Tokarz, Victoria L., Patrick E. MacDonald, et Amira Klip. 2018. « The Cell Biology of Systemic Insulin Function ». *The Journal of Cell Biology* 217 (7): 2273-89. <https://doi.org/10.1083/jcb.201802095>.
- Torekov, Signe S., Eva Iepsen, Michael Christiansen, Allan Linneberg, Oluf Pedersen, Jens J. Holst, Jørgen K. Kanters, et Torben Hansen. 2014. « KCNQ1 Long QT Syndrome Patients Have Hyperinsulinemia and Symptomatic Hypoglycemia ». *Diabetes* 63 (4): 1315-25. <https://doi.org/10.2337/db13-1454>.
- Totland, Max, Nikoline Rasmussen, Lars Knudsen, et Edward Leithe. 2020. « Regulation of gap junction intercellular communication by connexin ubiquitination: physiological and pathophysiological implications ». *Cellular and Molecular Life Sciences* 77. <https://doi.org/10.1007/s00018-019-03285-0>.
- Tour, D. de la, T. Halvorsen, C. Demeterco, B. Tyrberg, P. Itkin-Ansari, M. Loy, S. J. Yoo, E. Hao, S. Bossie, et F. Levine. 2001. « Beta-Cell Differentiation from a Human Pancreatic Cell Line in Vitro and in Vivo ». *Molecular Endocrinology (Baltimore, Md.)* 15 (3): 476-83. <https://doi.org/10.1210/mend.15.3.0604>.
- Tsien, R. Y. 1989. « Fluorescent Indicators of Ion Concentrations ». *Methods in Cell Biology* 30: 127-56. [https://doi.org/10.1016/s0091-679x\(08\)60978-4](https://doi.org/10.1016/s0091-679x(08)60978-4).
- Tsien, R. Y., et S. B. Hladky. 1978. « A Quantitative Resolution of the Spectra of a Membrane Potential Indicator, DiS-C3-(5), Bound to Cell Components and to Red Blood Cells ». *The Journal of Membrane Biology* 38 (1-2): 73-97. <https://doi.org/10.1007/BF01875163>.
- Turner, R. C., M. A. Phillips, et E. A. Ward. 1983. « Ultralente Based Insulin Regimens--Clinical Applications, Advantages and Disadvantages ». *Acta Medica Scandinavica. Supplementum* 671: 75-86. <https://doi.org/10.1111/j.0954-6820.1983.tb08551.x>.

« Ueber Versuche einer Specifischen Fermenttherapie des Diabetes | The Discovery and Early Development of Insulin ». s. d. Consulté le 4 janvier 2022. <https://insulin.library.utoronto.ca/islandora/object/insulin%3AT10184>.

Ullsten, Sara, Joey Lau, et Per-Ola Carlsson. 2015. « Vascular Heterogeneity between Native Rat Pancreatic Islets Is Responsible for Differences in Survival and Revascularisation Post Transplantation ». *Diabetologia* 58 (1): 132-39. <https://doi.org/10.1007/s00125-014-3385-7>.
Ungerstedt, U. 1991. « Microdialysis--Principles and Applications for Studies in Animals and Man ». *Journal of Internal Medicine* 230 (4): 365-73. <https://doi.org/10.1111/j.1365-2796.1991.tb00459.x>.

[Ungerstedt](#), U. 1997. « Microdialysis--a New Technique for Monitoring Local Tissue Events in the Clinic ». *Acta Anaesthesiologica Scandinavica. Supplementum* 110: 123. <https://doi.org/10.1111/j.1399-6576.1997.tb05527.x>.

Vaddiraju, Santhisagar, Diane J Burgess, Ioannis Tomazos, Faquir C Jain, et Fotios Papadimitrakopoulos. 2010. « Technologies for Continuous Glucose Monitoring: Current Problems and Future Promises ». *Journal of Diabetes Science and Technology* 4 (6): 1540-62.
Vafiadis, P., S. T. Bennett, J. A. Todd, J. Nadeau, R. Grabs, C. G. Goodyer, S. Wickramasinghe, E. Colle, et C. Polychronakos. 1997. « Insulin Expression in Human Thymus Is Modulated by INS VNTR Alleles at the IDDM2 Locus ». *Nature Genetics* 15 (3): 289-92. <https://doi.org/10.1038/ng0397-289>.

Vantighem, Marie-Christine, Eelco J. P. de Koning, François Pattou, et Michael R. Rickels. 2019. « Advances in β -Cell Replacement Therapy for the Treatment of Type 1 Diabetes ». *Lancet* 394 (10205): 1274-85. [https://doi.org/10.1016/S0140-6736\(19\)31334-0](https://doi.org/10.1016/S0140-6736(19)31334-0).

Varhue, Walter B., Linda Langman, Molly Kelly-Goss, Morgan Lataillade, Kenneth L. Brayman, Shayn Peirce-Cottler, et Nathan S. Swami. 2017. « Deformability-Based Microfluidic Separation of Pancreatic Islets from Exocrine Acinar Tissue for Transplant Applications ». *Lab on a Chip* 17 (21): 3682-91. <https://doi.org/10.1039/c7lc00890b>.

Vashist, Sandeep Kumar. 2012. « Non-Invasive Glucose Monitoring Technology in Diabetes Management: A Review ». *Analytica Chimica Acta* 750: 16-27. <https://doi.org/10.1016/j.aca.2012.03.043>.

Vedula, Else M., José Luis Alonso, M. Amin Arnaut, et Joseph L. Charest. 2017. « A Microfluidic Renal Proximal Tubule with Active Reabsorptive Function ». *PloS One* 12 (10): e0184330. <https://doi.org/10.1371/journal.pone.0184330>.

Velve-Casquillas, Guilhem, Maël Le Berre, Matthieu Piel, et Phong T. Tran. 2010. « Microfluidic Tools for Cell Biological Research ». *Nano Today* 5 (1): 28-47. <https://doi.org/10.1016/j.nantod.2009.12.001>.

Verberne, A J M, W S Korim, A Sabetghadam, et I J Llewellyn-Smith. 2016. « Adrenaline: insights into its metabolic roles in hypoglycaemia and diabetes ». *British Journal of Pharmacology* 173 (9): 1425-37. <https://doi.org/10.1111/bph.13458>.

Vetrani, Claudia, Ilaria Calabrese, Luisa Cavagnuolo, Daniela Pacella, Elsa Napolano, Silvia Di Rienzo, Gabriele Riccardi, Angela A. Rivellese, Giovanni Annuzzi, et Lutgarda Bozzetto. 2022. « Dietary Determinants of Postprandial Blood Glucose Control in Adults with Type 1 Diabetes on a Hybrid Closed-Loop System ». *Diabetologia* 65 (1): 79-87. <https://doi.org/10.1007/s00125-021-05587-0>.

Vettoretti, Martina, Giacomo Cappon, Giada Acciaroli, Andrea Facchinetti, et Giovanni Sparacino. 2018. « Continuous Glucose Monitoring: Current Use in Diabetes Management and Possible Future Applications ». *Journal of Diabetes Science and Technology* 12 (5): 1064-71. <https://doi.org/10.1177/1932296818774078>.

Villarroel Marquez, Ariana, Gerardo Salinas, Myriam Abarkan, Maël Idir, Cyril Brochon, Georges Hadziioannou, Matthieu Raoux, Alexander Kuhn, Jochen Lang, et Eric Cloutet. 2020. « Design of Potassium-Selective Mixed Ion/Electron Conducting Polymers ». *Macromolecular Rapid Communications* 41 (12): e2000134. <https://doi.org/10.1002/marc.202000134>.

Villiger, M., R. Stoop, T. Vetsch, E. Hohenauer, M. Pini, P. Clarys, F. Pereira, et R. Clijsen. 2018. « Evaluation and Review of Body Fluids Saliva, Sweat and Tear Compared to Biochemical Hydration Assessment Markers within Blood and Urine ». *European Journal of Clinical Nutrition* 72 (1): 69-76. <https://doi.org/10.1038/ejcn.2017.136>.

Viswam, Vijay, Marie Engelen J. Obien, Felix Franke, Urs Frey, et Andreas Hierlemann. 2019. « Optimal Electrode Size for Multi-Scale Extracellular-Potential Recording From Neuronal Assemblies ». *Frontiers in Neuroscience* 13: 385. <https://doi.org/10.3389/fnins.2019.00385>.

Voldman, Joel. 2003. « Building with Cells ». *Nature Materials* 2 (7): 433-34. <https://doi.org/10.1038/nmat936>.

Walker, Edward B., et Chase S. Naisbitt. 2019. « Direct Analysis of Dimethicone in Aqueous Emulsions by Infrared Spectroscopy ». *Journal of Cosmetic Science* 70 (4): 209-16.

Wang, Hui-Chen, et An-Rong Lee. 2015. « Recent Developments in Blood Glucose Sensors ». *Journal of Food and Drug Analysis* 23 (2): 191-200. <https://doi.org/10.1016/j.jfda.2014.12.001>.

Wang, Joseph. 2008. « Electrochemical Glucose Biosensors ». *Chemical Reviews* 108 (2): 814-25. <https://doi.org/10.1021/cr068123a>.

Wang, S., G. M. Beattie, M. I. Mally, V. Cirulli, P. Itkin-Ansari, A. D. Lopez, A. Hayek, et F. Levine. 1997. « Isolation and Characterization of a Cell Line from the Epithelial Cells of the Human Fetal Pancreas ». *Cell Transplantation* 6 (1): 59-67. [https://doi.org/10.1016/s0963-6897\(96\)00120-0](https://doi.org/10.1016/s0963-6897(96)00120-0).

Wang, S., G. M. Beattie, M. I. Mally, A. D. Lopez, A. Hayek, et F. Levine. 1997. « Analysis of a Human Fetal Pancreatic Islet Cell Line ». *Transplantation Proceedings* 29 (4): 2219. [https://doi.org/10.1016/s0041-1345\(97\)00306-0](https://doi.org/10.1016/s0041-1345(97)00306-0).

Wang, Yong, Joe F. Lo, Joshua E. Mendoza-Elias, Adeola F. Adewola, Tricia A. Harvat, Katie P. Kinzer, Dongyoung Lee, Meirigeng Qi, David T. Eddington, et José Oberholzer. 2010. « Application of Microfluidic Technology to Pancreatic Islet Research: First Decade of Endeavor ». *Bioanalysis* 2 (10): 1729-44. <https://doi.org/10.4155/bio.10.131>.

Wargent, Edward T. 2009. « The Measurement of Insulin Secretion Using Pancreas Perfusion in the Rodent ». In *Type 2 Diabetes: Methods and Protocols*, édité par Claire Stocker, 203-19. Methods in Molecular Biology. Totowa, NJ: Humana Press. https://doi.org/10.1007/978-1-59745-448-3_14.

Wémeau, J. -L. 2014. « Chapitre 47 - Métabolisme glucidique ». In *Endocrinologie, Diabète, Métabolisme et Nutrition pour le Praticien*, édité par J. -L. Wémeau, 459-63. Paris: Elsevier Masson. <https://doi.org/10.1016/B978-2-294-71584-6.00047-7>.

Wentholt, Iris M., Marit A. Vollebregt, Augustus A. Hart, Joost B. Hoekstra, et J. Hans DeVries. 2005. « Comparison of a Needle-Type and a Microdialysis Continuous Glucose Monitor in Type 1 Diabetic Patients ». *Diabetes Care* 28 (12): 2871-76. <https://doi.org/10.2337/diacare.28.12.2871>.

Wheelock, Kevin M., Jian Cai, Helen C. Looker, Michael L. Merchant, Robert G. Nelson, Gudeta D. Fufaa, E. Jennifer Weil, et al. 2017. « Plasma bradykinin and early diabetic nephropathy lesions in type 1 diabetes mellitus ». *PLoS ONE* 12 (7): e0180964. <https://doi.org/10.1371/journal.pone.0180964>.

Whitesides, George M. 2006. « The Origins and the Future of Microfluidics ». *Nature* 442 (7101): 368-73. <https://doi.org/10.1038/nature05058>.

Wiedemann, Sophia J., Leila Rachid, Ben Illigens, Marianne Böni-Schnetzler, et Marc Y. Donath. 2020. « Evidence for Cephalic Phase Insulin Release in Humans: A Systematic Review and Meta-Analysis ». *Appetite* 155: 104792. <https://doi.org/10.1016/j.appet.2020.104792>.

Willecke, Klaus, Jürgen Eiberger, Joachim Degen, Dominik Eckardt, Alessandro Romualdi, Martin Güldenagel, Urban Deutsch, et Goran Söhl. 2002. « Structural and Functional Diversity of Connexin Genes in the Mouse and Human Genome ». *Biological Chemistry* 383 (5): 725-37. <https://doi.org/10.1515/BC.2002.076>.

Xia, Ying, Zhiguo Xie, Gan Huang, et Zhiguang Zhou. 2019. « Incidence and Trend of Type 1 Diabetes and the Underlying Environmental Determinants ». *Diabetes/Metabolism Research and Reviews* 35 (1): e3075. <https://doi.org/10.1002/dmrr.3075>.

Yach, Derek, Marissa Kellogg, et Janet Voute. 2005. « Chronic Diseases: An Increasing Challenge in Developing Countries ». *Transactions of the Royal Society of Tropical Medicine and Hygiene* 99 (5): 321-24. <https://doi.org/10.1016/j.trstmh.2005.02.001>.

Yamamoto-Honda, Ritsuko, Kazuyuki Tobe, Yasushi Kaburagi, Kohjiro Ueki, Shoji Asai, Makoto Yachi, Mikako Shirouzu, et al. 1995. « Upstream Mechanisms of Glycogen Synthase Activation by Insulin and Insulin-like Growth Factor-I: Glycogen synthase activation is antagonized by

wortmannin or Ly294002 but not by rapamycin or by inhibiting P21ras(*) ». *Journal of Biological Chemistry* 270 (6): 2729-34. <https://doi.org/10.1074/jbc.270.6.2729>.

Yang, Jinzeng. 2014. « Enhanced Skeletal Muscle for Effective Glucose Homeostasis ». *Progress in Molecular Biology and Translational Science* 121: 133-63. <https://doi.org/10.1016/B978-0-12-800101-1.00005-3>.

Yang, Kunlong, Sijian Yuan, Yuxiang Huan, Jiao Wang, Li Tu, Jiawei Xu, Zhuo Zou, Yiqiang Zhan, Lirong Zheng, et Fernando Seoane. 2018. « Tunable Flexible Artificial Synapses: A New Path toward a Wearable Electronic System ». *Npj Flexible Electronics* 2 (1): 1-9. <https://doi.org/10.1038/s41528-018-0033-1>.

Yao, Chunlei, Changyan Xie, Peng Lin, Feng Yan, Pingbo Huang, et I.-Ming Hsing. 2013. « Organic Electrochemical Transistor Array for Recording Transepithelial Ion Transport of Human Airway Epithelial Cells ». *Advanced Materials* 25 (45): 6575-80. <https://doi.org/10.1002/adma.201302615>.

Yoshimatsu, Hironobu, Akira Niiijima, Yutaka Oomura, Kazutoshi Yamabe, et Toshihiko Katafuchi. 1984. « Effects of hypothalamic lesion on pancreatic autonomic nerve activity in the rat ». *Molecular Brain Research* 303 (1): 147-52. [https://doi.org/10.1016/0006-8993\(84\)90222-1](https://doi.org/10.1016/0006-8993(84)90222-1).

Yoshitomi, Hideyuki, et Kenneth S. Zaret. 2004. « Endothelial Cell Interactions Initiate Dorsal Pancreas Development by Selectively Inducing the Transcription Factor Ptf1a ». *Development* 131 (4): 807-17. <https://doi.org/10.1242/dev.00960>.

Youson, J. H., et A. A. Al-Mahrouki. 1999. « Ontogenetic and Phylogenetic Development of the Endocrine Pancreas (Islet Organ) in Fish ». *General and Comparative Endocrinology* 116 (3): 303-35. <https://doi.org/10.1006/gcen.1999.7376>.

Zalzman, Michal, Leeat Anker-Kitai, et Shimon Efrat. 2005. « Differentiation of Human Liver-Derived, Insulin-Producing Cells toward the Beta-Cell Phenotype ». *Diabetes* 54 (9): 2568-75. <https://doi.org/10.2337/diabetes.54.9.2568>.

Zhang, Lijun, Guiheng Wang, Di Wu, Can Xiong, Lei Zheng, Yunsheng Ding, Hongbo Lu, Guobing Zhang, et Longzhen Qiu. 2018. « Highly Selective and Sensitive Sensor Based on an Organic Electrochemical Transistor for the Detection of Ascorbic Acid ». *Biosensors & Bioelectronics* 100 : 235-41. <https://doi.org/10.1016/j.bios.2017.09.006>.

Zhang, Quan, Martin Bengtsson, Chris Partridge, Albert Salehi, Matthias Braun, Roger Cox, Lena Eliasson, et al. 2007. « R-Type Ca²⁺-Channel-Evoked CICR Regulates Glucose-Induced Somatostatin Secretion ». *Nature Cell Biology* 9 (4): 453-60. <https://doi.org/10.1038/ncb1563>.

Zhang, Quan, Margarita V. Chibalina, Martin Bengtsson, Lukas N. Groschner, Reshma Ramracheya, Nils J. G. Rorsman, Veronika Leiss, et al. 2014. « Na⁺ Current Properties in Islet α - and β -Cells Reflect Cell-Specific Scn3a and Scn9a Expression ». *The Journal of Physiology* 592 (21): 4677-96. <https://doi.org/10.1113/jphysiol.2014.274209>.

Zheng, Wenfu, Zhuo Wang, Wei Zhang, et Xingyu Jiang. 2010. « A Simple PDMS-Based Microfluidic Channel Design That Removes Bubbles for Long-Term on-Chip Culture of Mammalian Cells ». *Lab on a Chip* 10 (21): 2906. <https://doi.org/10.1039/c005274d>.

Zhou, Qiao, et Douglas A. Melton. 2018. « Pancreas Regeneration ». *Nature* 557 (7705): 351-58. <https://doi.org/10.1038/s41586-018-0088-0>.

Ziegler, A. G., M. Hummel, M. Schenker, et E. Bonifacio. 1999. « Autoantibody Appearance and Risk for Development of Childhood Diabetes in Offspring of Parents with Type 1 Diabetes: The 2-Year Analysis of the German BABYDIAB Study ». *Diabetes* 48 (3): 460-68. <https://doi.org/10.2337/diabetes.48.3.460>.

Zimmet, P. 2000. « Globalization, Coca-Colonization and the Chronic Disease Epidemic: Can the Doomsday Scenario Be Averted? » *Journal of Internal Medicine* 247 (3): 301-10. <https://doi.org/10.1046/j.1365-2796.2000.00625.x>.

Zisman, A, O D Peroni, E D Abel, M D Michael, F Mauvais-Jarvis, B B Lowell, J F Wojtaszewski, et al. 2000. « Targeted Disruption of the Glucose Transporter 4 Selectively in Muscle Causes Insulin Resistance and Glucose Intolerance ». *Nature Medicine* 6 (8): 924-28. <https://doi.org/10.1038/78693>.

Titre : CAPTEURS BIO-ÉLECTRONIQUES POUR LE CONTRÔLE DE LA GLYCÉMIE EN BOUCLE OUVERTE ET FERMÉE

Résumé :

Les technologies de mesure continue de la glycémie (CGM) et d'insulinothérapie révolutionnent le traitement du diabète mellitus (DM). Les capteurs sont toutefois limités à la mesure de glucose et les algorithmes d'insulinothérapie sont améliorables. DIABLO rassemble des diabétologues et des spécialistes de la biologie des îlots, de la microélectronique et de l'automatique, pour développer un nouvel outil de CGM. DIABLO propose: (i) des techniques de mesure et un capteur bio-électronique haute résolution pour décoder les algorithmes endogènes des îlots; (ii) de nouveaux algorithmes de contrôle robustes et tolérants aux fautes, inspirés par l'avionique ; (iii) la démonstration in vivo de la capacité du capteur bio-électronique à maintenir l'homéostasie du glucose. DIABLO aura un impact sur le traitement du DM et le développement de pancréas artificiels, et facilitera aussi les approches thérapeutiques à base de cellules souches en permettant leur caractérisation fine in situ.

Mots clés : Diabète, CGM, Biocapteur, Îlots de Langerhans, Glycémie

Title : BIOSENSORS FOR OPEN AND CLOSED-LOOP GLYCEMIA CONTROL

Abstract :

In diabetes mellitus (DM), continuous glucose monitoring (CGM) linked to insulin delivery presents a major advance but is still limited by current algorithms and the nature of glucose sensors. DIABLO is a multidisciplinary project from diabetology, islet biology, and microelectronics to automation control, with the objective to establish a new model of CGM (i) by high-resolution techniques to decipher and model islet's endogenous algorithms, (ii) by design of novel control algorithms inspired by aeronautics and (iii) by the proof of concept of maintaining glucose homeostasis by this hybrid biosensor. DIABLO will impact research by multi-physics system modelling and healthcare technology as well as life quality in DM by novel algorithms and an innovative module for the artificial pancreas. The project will also advance for DM and other chronic diseases monitoring of stem-cell derived therapeutic means and the development of Organs-on-Chip.

Keywords : Diabete, CGM, Biosensor, Islets of Langerhans, Glycemia

UMR 5248

CBMN, Allée Geoffroy Saint Hilaire, Bât B14, 33600 Pessac

